frontiers | Research Topics

Biology of myxobacteria

Edited by
Honghui Zhu, Li Zhoukun, David Edward Whitworth and David Cole Stevens

Coordinated by
Jingjing Wang

Published in
Frontiers in Microbiology

ISSN 1664-8714
ISBN 978-2-8325-5177-6
DOI 10.3389/978-2-8325-5177-6

About Frontiers

Frontiers is more than just an open access publisher of scholarly articles: it is a pioneering approach to the world of academia, radically improving the way scholarly research is managed. The grand vision of Frontiers is a world where all people have an equal opportunity to seek, share and generate knowledge. Frontiers provides immediate and permanent online open access to all its publications, but this alone is not enough to realize our grand goals.

Frontiers journal series

The Frontiers journal series is a multi-tier and interdisciplinary set of open-access, online journals, promising a paradigm shift from the current review, selection and dissemination processes in academic publishing. All Frontiers journals are driven by researchers for researchers; therefore, they constitute a service to the scholarly community. At the same time, the *Frontiers journal series* operates on a revolutionary invention, the tiered publishing system, initially addressing specific communities of scholars, and gradually climbing up to broader public understanding, thus serving the interests of the lay society, too.

Dedication to quality

Each Frontiers article is a landmark of the highest quality, thanks to genuinely collaborative interactions between authors and review editors, who include some of the world's best academicians. Research must be certified by peers before entering a stream of knowledge that may eventually reach the public - and shape society; therefore, Frontiers only applies the most rigorous and unbiased reviews. Frontiers revolutionizes research publishing by freely delivering the most outstanding research, evaluated with no bias from both the academic and social point of view. By applying the most advanced information technologies, Frontiers is catapulting scholarly publishing into a new generation.

What are Frontiers Research Topics?

Frontiers Research Topics are very popular trademarks of the *Frontiers journals series*: they are collections of at least ten articles, all centered on a particular subject. With their unique mix of varied contributions from Original Research to Review Articles, Frontiers Research Topics unify the most influential researchers, the latest key findings and historical advances in a hot research area.

Find out more on how to host your own Frontiers Research Topic or contribute to one as an author by contacting the Frontiers editorial office: frontiersin.org/about/contact

Biology of myxobacteria

Topic editors
Honghui Zhu — Guangdong Institute of Microbiology, Guangdong Academy of Science, China
Li Zhoukun — Nanjing Agricultural University, China
David Edward Whitworth — Aberystwyth University, United Kingdom
David Cole Stevens — University of Mississippi, United States

Topic coordinator
Jingjing Wang — Shandong University, China

Citation
Zhu, H., Zhoukun, L., Whitworth, D. E., Stevens, D. C., Wang, J., eds. (2024). *Biology of myxobacteria*. Lausanne: Frontiers Media SA. doi: 10.3389/978-2-8325-5177-6

Table of contents

frontiers | Frontiers in Microbiology

TYPE Editorial
PUBLISHED 05 July 2024
DOI 10.3389/fmicb.2024.1450345

OPEN ACCESS

EDITED AND REVIEWED BY
Ulrike Kappler,
The University of Queensland, Australia

*CORRESPONDENCE
David E. Whitworth
✉ dew@aber.ac.uk

RECEIVED 17 June 2024
ACCEPTED 26 June 2024
PUBLISHED 05 July 2024

CITATION
Li Z, Zhu H, Whitworth DE and Stevens DC (2024) Editorial: Biology of myxobacteria. *Front. Microbiol.* 15:1450345. doi: 10.3389/fmicb.2024.1450345

Editorial: Biology of myxobacteria

Zhoukun Li[1], Honghui Zhu[2], David E. Whitworth[3]* and David C. Stevens[4]

[1]Department of Microbiology and College of Life Sciences, Nanjing Agricultural University, Nanjing, China, [2]Guangdong Institute of Microbiology, Guangdong Academy of Science, Guangzhou, China, [3]Department of Life Sciences, Aberystwyth University, Aberystwyth, United Kingdom, [4]Department of BioMolecular Sciences, School of Pharmacy, University of Mississippi, Oxford, MS, United States

KEYWORDS

developmental biology, predation biology, fruiting body, bacterial communication, biological control, soil ecosystems

Editorial on the Research Topic
Biology of myxobacteria

Myxobacteria are fascinating, soil-dwelling organisms which exhibit several noteworthy biological features. Despite being "lowly" Gram-negative bacteria, cells within a myxobacterial colony are able to communicate with each other in a sophisticated fashion, orchestrating population-wide changes in motility and gene expression. Myxobacteria are micropredators and can acquire nutrients by killing and consuming a broad range of prey organisms, including other bacteria, fungi and oomycetes. They have a profound influence on the composition of microbial communities and are considered apex bacterial predators and keystone taxa in soil ecosystems. When prey nutrients are scarce, cells of a sufficiently large myxobacterial population aggregate together to form multicellular fruiting bodies, within which a complex regulatory network causes cells to differentiate into spores. To achieve such coordinated motion, myxobacteria possess two mechanistically distinct motors for swarming motility. They are also prolific producers of secondary metabolites, many of which have useful biological activities. Myxobacterial natural products have seen use in the clinic, and intact organisms are now also being used to prey upon pathogens, acting as biological control agents for protecting crops.

Over the past few decades, myxobacteria have primarily been investigated as model organisms, providing fundamental insights into specific biological processes such as motility and development. With time, researchers have increasingly investigated how those processes overlap and inter-depend on each other—for instance, motility is a pre-requisite for predation and multicellular development, while secondary metabolite production is required for predation. Fundamental research has also increasingly overlapped with applied research into potential exploitation of myxobacterial behaviors and biomolecules. The intention of this Research Topic was to bring together research articles and reviews spanning the breadth of myxobacterial biology, with special emphasis placed on the application of myxobacteria and their products as biological resources, as well as the overlap between developmental biology, predation biology, and myxobacterial ecology.

The Research Topic has successfully drawn together 14 submissions, including 12 Original Research articles and two Reviews. Some authors have focused on providing fundamental insights into specific aspects of myxobacterial biology, while others have addressed broader Research Topics which draw on overlapping subject areas. Several articles demonstrate how fundamental knowledge can be leveraged to inform potential

applications to benefit humankind, while the two Review articles provide valuable contextualization of important myxobacterial behaviors.

Multicellular development is arguably the most distinctive feature of myxobacteria biology. A key regulator of development is the MrpC DNA-binding protein, which sequentially triggers distinct aspects of the developmental process at different levels of expression. Induction of *mrpC* expression is complicated, involving several regulatory proteins/pathways, while MrpC also acts as a negative autoregulator, down-regulating its own expression. Negative autoregulation (NAR) is a mode of feedback which typically suppresses transcriptional noise during gene expression. In their Original Research article, McLaughlin and Higgs investigated MrpC NAR by disrupting the MrpC-binding sites in the *mrpC* promoter region, which caused cells to lose their synchronicity, with subsets of cells swarming out of nascent cellular aggregates as "developmental swarms" rather than completing the developmental programme. Myxobacterial cells are rod-shaped and move along their long axes, periodically reversing their direction of travel (reversals are suppressed during development). Using mathematical modeling of experimental data, Chen et al. propose in their Original Research article that reversal frequency is affected by mechanical cues (such as the stiffness of the substrate over which the cell is moving, or cell-cell contact), which are directly and indirectly sensed by the motility machineries of the cell. Testable hypotheses are proposed by the authors, which will be invaluable in further deciphering the molecular mechanisms underlying the regulation of motility.

An increasingly studied myxobacterial behavior is their predation of other microbes. The Review article by Contreras-Moreno et al. provides a wonderful summary of a rapidly growing body of literature. Focusing on *Myxococcus xanthus*, the authors explain the importance of synergism between motility and the various (diverse) mechanisms of killing prey organisms, which include contact-dependent intoxification of prey, and the generalized secretion of toxic enzymes and chemicals, including redox-active metals. Predation can be resisted by prey organisms, and Müller et al. have shown in their Original Research article that the production of thiocillins by strains of *Bacillus cereus* helps them resist predation by *M. xanthus* and even fight back. The secretion of specialized antimicrobial metabolites by both "predator" and "prey" is clearly a key determinant of the outcome of microbial competition in the soil. Another determinant of predatory success is the production of flagella by prey. In their Original Research article, Zhang N. et al. have shown that a non-flagellated mutant of *Escherichia coli* is relatively resistant to predation by *M. xanthus* and that an *E. coli* dihydrouridine synthase B, *dusB,* mutant is more resistant to the *M. xanthus* antibiotic myxovirescin. Such studies also allude to the likely uniqueness of predator-prey interactions between different species/strains.

The Original Research article by Han et al. showcases the potential for harnessing myxobacterial predatory activity by applying them as crop protection agents. In their study they showed a strain of *Myxococcus fulvus* (and its protein secretions) could kill the causative agent of fireblight (*Erwinia amylovora*) *in vitro*, and could protect pear explants and seedlings from disease. The article eloquently supports the premise of the Review article by Zhang L. et al. in which they highlight the activity of myxobacteria against plant pathogens. The molecular mechanisms myxobacteria employ to kill prey organisms are summarized, and the article anticipates increasing applications for myxobacteria in the context of biological control, particularly in crop protection. Future applications of myxobacteria in the field will need to consider the impact of myxobacteria on natural microbial communities. The Original Research article by Yang et al. assessed the *in vitro* predatory activity of a myxobacterium against >60 typical soil bacteria. They also investigated the impact of this myxobacterium on the diversity of a soil microcosm, finding that the myxobacterium drove large shifts in population structure. Nevertheless, some organisms (e.g., *Streptomyces* spp.) were relatively unaffected by myxobacterial addition, and some potential "prey" were able to coexist stably with the myxobacterium.

In addition to the Review by Zhang L. et al., several Original Research articles have focused on the production of hydrolytic exoenzymes by myxobacteria. In their study, Zhou X. et al. investigated glycoside hydrolases of *Corallococcus silvisoli* using differential proteomics of the secreted proteomes of cells grown in the presence/absence of cellulose and chitin. Phylogenetic analysis of differentially expressed GH19 family glycoside hydrolases identified features which may confer substrate specificity on the enzymes. Similarly, but starting with a genomic approach, the study by Yuan et al. identified predicted lipolytic enzymes in the genomes of 13 *Sorangium cellulosum* strains. A novel carboxylesterase, LipB, was characterized experimentally, and shown to have activity against a variety of ester substrates, including the antibiotic nitrocefin. Another novel lipase was shown by Zhou Y. et al. to be able to kill pathogenic prey organisms such as *E. coli* and *Staphylococcus aureus*. The ArEstA lipase was originally identified in the genome of a novel species of myxobacterium, *Archangium lipolyticum*, which was isolated from pig farm soil. Expression and purification of the lipase showed it was able to lyse drug-resistant *E. coli*, as was the parental organism.

Novel myxobacterial species are also described in two further articles. The Original Research article by Zang et al. describes how they discovered a novel species, *Hyalangium ruber*, in soil from a wetland park. The isolate was found to produce a variety of secondary metabolites, one of which exhibited moderate cytotoxicity against human cell lines—an uncommon but potentially useful activity exhibited by some myxobacteria. Using rhizospheric soil samples, Ahearne et al. were able to isolate type strains for nine novel myxobacterial species from seven different genera (*Archangium, Myxococcus, Nannocystis, Polyangium, Pyxidicoccus, Sorangium*, and *Stigmatella*). Genome sequence analysis of the novel strains allowed the authors to identify large biosynthetic gene clusters (BGCs) which typically encode enzymes for the production of secondary metabolites. The observation of clusters of hybrid BGCs in the genomes led to the proposal that proximal BGCs contribute to the metabolic diversity and adaptability of myxobacteria by promoting duplication and deletion of homologous modules between BGCs. In their Original Research article, Liu et al. isolated a novel halotolerant *Myxococcus* sp. strain MxC21 from forest soil. Genome sequencing revealed that the strain carried a plasmid, which is very unusual—MxC21 is only the second myxobacterial strain ever found to have contained a

plasmid, and such plasmids can be extremely useful in expanding the genetic toolbox available to myxobacteria researchers.

In conclusion, new studies such as those included in this Research Topic on *Biology of myxobacteria* continue to expand our understanding of myxobacterial ecology and evolution, while providing us with strains and natural products for application in diverse arenas of human endeavor.

Author contributions

ZL: Writing – original draft, Writing – review & editing. HZ: Writing – original draft, Writing – review & editing. DW: Writing – original draft, Writing – review & editing. DS: Writing – original draft, Writing – review & editing.

Funding

The author(s) declare that no financial support was received for the research, authorship, and/or publication of this article.

Acknowledgments

The Research Topic editors thank the authors of all the manuscripts for contributing them to the Research Topic and also thank the expert reviewers for providing constructive evaluations of each submission.

Conflict of interest

The authors declare that the research was conducted in the absence of any commercial or financial relationships that could be construed as a potential conflict of interest.

The author(s) declared that they were an editorial board member of Frontiers, at the time of submission. This had no impact on the peer review process and the final decision.

Publisher's note

frontiers | Frontiers in Microbiology

TYPE Original Research
PUBLISHED 12 June 2023
DOI 10.3389/fmicb.2023.1211756

OPEN ACCESS

EDITED BY
Li Zhoukun,
Nanjing Agricultural University, China

REVIEWED BY
David Cole Stevens,
University of Mississippi, United States
Huirong Liu,
Inner Mongolia Agricultural University, China

*CORRESPONDENCE
Wenhui Wang
✉ wangwenhui@ahau.edu.cn

RECEIVED 25 April 2023
ACCEPTED 22 May 2023
PUBLISHED 12 June 2023

CITATION
Yang Y, Tao H, Ma W, Wang N, Chen X and Wang W (2023) Lysis profile and preference of *Myxococcus* sp. PT13 for typical soil bacteria. *Front. Microbiol.* 14:1211756. doi: 10.3389/fmicb.2023.1211756

Lysis profile and preference of *Myxococcus* sp. PT13 for typical soil bacteria

Yi Yang, Hong Tao, Wenwen Ma, Nana Wang, Xiaolin Chen and Wenhui Wang*

School of Life Sciences, Anhui Agricultural University, Hefei, Anhui, China

Introduction: *Myxococcus* sp. PT13 is a wild strain with multiple predatory properties that prey on multiple model microorganisms preserved in the laboratory. However, the lysis spectrum of PT13 on typical soil bacteria and its driving effect on soil microecosystems are still unclear.

Methods: In this study, the lawn predation method was used to determine the predation diameter of 62 typical soil bacteria by myxobacteria PT13 and analyze their lysis spectra.

Results and Discussion: The results showed that PT13 had a predation diameter greater than 15mm against typical soil microorganisms such as *Aeromonas*, *Bacillus, Brevibacterium*, *Fictibacillus*, *Glutamicibacter*, *Herbaspirillum,* and *Leifsonia* and had an outstanding lysis effect but a significant preference (p <0.05). Absolute high-throughput sequencing results showed that PT13 predation drove the microcosmic system composed of 16 bacterial genera, with a significant decrease in the Shannon index by 11.8% (CK=2.04, D =1.80) and a significant increase in the Simpson index by 45.0% (CK=0.20, D =0.29). The results of principal coordinate analysis (PCoA) showed that myxobacterial addition significantly disturbed the microcosmic microbial community structure (ANOSIM, p <0.05). LEfSe analysis showed that the relative and absolute abundances (copy numbers) of *Bacillus*, *Pedobacter*, *Staphylococcus*, *Streptomyces* and *Fictibacillus* decreased significantly very likely due to myxobacterial predation (p <0.05). However, the predatory effect of PT13 also increased the relative or absolute abundances of some species, such as *Sphingobacterium*, *Paenarthrobacter*, *Microbacterium,* and *Leifsonia*. It can be concluded that PT13 has a broad-spectrum lysis spectrum but poor cleavage ability for *Streptomyces*, and the interaction between complex microorganisms limits the predation effect of PT13 on some prey bacteria. This in turn allows some prey to coexist with myxobacteria. This paper will lay a theoretical foundation for the regulation of soil microecology dominated by myxobacteria.

KEYWORDS

myxobacteria, prey bacteria, predation diameter, microcosmic system, bacterial community structure

Introduction

Myxobacteria are typical indigenous predatory bacteria that are species-rich, globally distributed and inhabit a wide range of natural environments, such as soils. They prefer to inhabit non-saline soils and sediments, some prefer saline environments and rarely occur in host-associated environments (Wang et al., 2021). Myxobacteria are difficult to isolate and purify due

to their intrinsic characteristics, and currently, prey-baiting isolation is an important method to obtain myxobacteria (Yi et al., 2021). Mostly gram-negative bacteria, but also some gram-positive bacteria, can induce myxobacteria fruiting bodies well to achieve myxobacteria strain isolation (Zhou et al., 2020). Among the known bacterial groups, myxobacteria has the largest known genome (some reaching 13–14 Mb), packed with numerous specialized metabolite biosynthetic gene clusters (BGCs) (Phillips et al., 2022). They are considered to be a rich source of secondary metabolites, mainly antibiotics and lytic enzymes with bacterial lysis and cellulolytic properties. Based on this feature, myxobacteria often have great potential for the production of novel drugs (Bhat et al., 2021).

Myxobacteria can feed on living microbial cells or other biomolecules to obtain nutrients. Most strains form fruiting bodies through directed cell movement after nutrient depletion. The fruiting body contains a large number of stress-resistant myxospores, allowing them to survive in harsh environments (Liu et al., 2019). Thus, myxobacteria have a complex life history and growth metabolism regulation process and good environmental adaptability (Li et al., 2021). They mostly adopt collaborative predation, also known as the "wolf pack attack" strategy, in which they lyse prey with antibiotics and hydrolytic enzymes (Pérez et al., 2016). The predation process may be regulated by the motor system, chemotaxis system, secretion of proteases and antimicrobial substances, and intercellular signaling system (Berleman and Kirby, 2009). They can find prey by recognizing *in vitro* acyl homoserine lactones (AHLs) secreted by prey and hunt efficiently through adventure and social movements (Lloyd and Whitworth, 2017; Whitworth and Zwarycz, 2020; Shukria et al., 2021).

Predation is a key process in building ecosystem communities and maintaining biodiversity, and predators can exert an important influence on ecosystems. Studies have shown that myxobacteria are common soil predators and may even be dominant (Petters et al., 2021). Their body size is more similar to the size of prey bacterial cells, making it more convenient to prey on bacteria (Petters et al., 2021). Myxobacteria prey on other soil bacteria and fungi, driving the proportion of bacteria in the soil. They are also new biocontrol microorganisms that prevent and control plant pathogenic fungi and bacteria (Bull et al., 2002; Ye et al., 2020; Li et al., 2022). A study in which the authors of this paper participated showed that the predation ability of *Corallococcus* sp. strain EGB on 9 different prey bacteria was significantly different. The volume of EGB added in simple artificial microcosmic systems is a major factor in the change in microbial community structure (Dai et al., 2020).

Soil is the base camp of microorganisms, and myxobacteria are considered to be indigenous bacteria with broad-spectrum predation ability in soil. *Myxococcus* sp. PT13 is a wild strain isolated from yellow-brown soil collected from Huangshan City, Anhui Province, China, using *Escherichia coli* as bait (Yi et al., 2021), and the soil samples used for PT13 isolation were consistent with the soil samples in the material method. It can prey on many strains of bacteria and fungi preserved in the laboratory, but the preference of PT13 to prey on indigenous prey bacteria and its driving effect on soil microecosystems are unclear. Therefore, this study mainly aimed to (1) clarify the predation preference of PT13 for indigenous bacteria and explore its potential for restoring soil biodiversity and ecological functions; (2) build a research system based on predation by myxobacteria to provide a model reference for further ecological function research; and (3) enrich the knowledge and understanding of predatory myxobacteria in soil systems and provide theoretical and technical support for their application in agriculture and medicine.

Materials and methods

Soil sampling and isolation of prey bacteria

The soil samples used for this experiment were collected from yellow–brown soil in Huangshan City, Anhui Province, China (30°23′N, 118°12′E), which belongs to the subtropical monsoon climate with an average annual temperature of 15–16°C, an average annual rainfall of 1,670 mm and a frost-free period of 236 days. Five kilograms of soil was collected at a depth of 20 cm and sieved (1 cm × 1 cm) to remove plant and other debris. The collected soil samples were stored in a refrigerator at 4°C. Then, 10 g of fresh soil sample was weighed and shaken in a sterile conical flask containing 90 mL of sterile water and glass beads at 180 rpm on a shaker for 2 h. The gradient dilution plate method (Liu et al., 2021) was used to coat the soil suspension to LB (Tryptone 1 g, Yeast extract 0.5 g, NaCl 1 g, Agar 2 g, H_2O 100 ml) and Gao's No.1 (Soluble Starch 2 g, KNO_3 0.1 g, K_2HPO_4•$3H_2O$ 0.05 g, $MgSO_4$•$7H_2O$ 0.05 g, NaCl 0.05 g, $FeSO_4$•$7H_2O$ 0.001 g, Agar 2 g, H_2O 100 ml) plates, and plates were incubated at 37, 30, or 25°C.

Single colonies of different colors and morphologies were selected on solid medium where the bacterial colonies were grown and inoculated into the same medium using plate streaking. DNA from the above bacterial colonies was extracted and the 16S rRNA gene was amplified by PCR. Amplification product sequencing was performed by Tsingke Biotechnology Co., Ltd., and BLAST was performed on NCBI to obtain taxonomic information. The phylogenetic tree was constructed using MEGA 7.0[1] from the amplification sequences and visualized by Interactive Tree of Life (iTOL, version 4.3.2) (Letunic and Bork, 2016).

Predation experiments

PT13 was inoculated into CYE liquid medium (1 g casein peptone, 0.5 g yeast extract, 0.1 g $MgSO_4$•$7H_2O$, 100 ml H_2O) and incubated at 30°C for 1 ~ 2 days. The prey bacterial strains were inoculated into LB or Gao's No. 1 medium and incubated at 37°C or 30°C for 1 ~ 2 days. Bacteria were harvested by centrifugation, and the cell pellet was washed twice with TPM [10 mM Tris–HCl (pH 7.6), 1 mM KH_2PO_4, 8 mM $MgSO_4$, 1% agarose] medium. Prey bacterial cultures were resuspended in TPM medium to 1×10^9 cells/ml, and the myxobacterial cells were concentrated to a final cell density of 1×10^{10} cells/ml. The lawn predation method was used to determine the predation ability of PT13 against various soil bacteria (Mendes-Soares and Velicer, 2013; Li et al., 2018; Arend et al., 2021). Myxobacterial and prey bacterial cultures were resuspended in TPM medium [10 mM Tris–HCl (pH 7.6), 1 mM KH_2PO_4, 8 mM $MgSO_4$, 1% agarose], and 200 µl of prey bacteria was spotted onto TPM solid medium. When the prey bacteria were air-dried to form lawns, 2 µl of PT13 was inoculated in the center of the lawn. Three sets of biological replicates were set up per experiment and incubated at 30°C for 4 days.

1 https://www.megasoftware.net/home

TABLE 1 Related information of 16 strains of prey bacteria and the concentration of diluted bacterial solution.

Type of strain	Number	Taxonomy	OD_{600}	CFU/ml
Pseudomonas resinovorans	TB	*Bacteria; Proteobacteria; Gammaproteobacteria; Pseudomonadales; Pseudomonadaceae; Pseudomonas*	O.626A	6.0×10^{7}
Comamonas sediminis	TE	*Bacteria; Proteobacteria; Betaproteobacteria; Burkholderiales; Comamonadaceae; Comamonas*	0.592A	8.5×10^{8}
Brevundimonas diminuta	TG	*Bacteria; Proteobacteria; Alphaproteobacteria; Caulobacterales; Caulobacteraceae; Brevundimonas*	0.647A	5.6×10^{8}
Sphingobacterium mizutaii	TJ	*Bacteria; Bacteroidetes; Sphingobacteriia; Sphingobacteriales; Sphingobacteriaceae; Sphingobacterium*	0.588A	7.8×10^{8}
Bacillus aerius	TM	*Bacteria; Firmicutes; Bacilli; Caryophanales; Bacillaceae; Bacillus*	0.699A	2.2×10^{8}
Stenotrophomonas bentonitica	TQ	*Bacteria; Proteobacteria; Gammaproteobacteria; Lysobacterales; Lysobacteraceae; Stenotrophomonas*	0.646A	7.7×10^{8}
Mitsuaria chitosomitabida	TU	*Bacteria; Proteobacteria; Betaproteobacteria; Burkholderiales; Comamonadaceae; Mitsuaria*	0.631A	6.72×10^{9}
Fictibacillus phosphorivorans	TX	*Bacteria; Firmicutes; Bacilli; Bacillales; Bacillaceae; Fictibacillus*	0.678A	1.3×10^{7}
Staphylococcus aureus	YC	*Bacteria; Firmicutes; Bacilli; Caryophanales; Staphylococcaceae; Staphylococcus*	0.669A	2.03×10^{9}
Pedobacter rhizosphaerae	MA	*Bacteria; Bacteroidetes; Sphingobacteriia; Sphingobacteriales; Sphingobacteriaceae; Pedobacter*	0.617A	4.2×10^{8}
Delftia tsuruhatensis	MK	*Bacteria; Proteobacteria; Betaproteobacteria; Burkholderiales; Comamonadaceae; Delftia*	0.695A	5.8×10^{8}
Brevibacterium sanguinis	FD	*Bacteria; Actinobacteria; Actinobacteria; Micrococcales; Brevibacteriaceae; Brevibacterium*	0.670A	2.1×10^{8}
Paenarthrobacter nicotinovorans	FI	*Bacteria; Actinobacteria; Actinomycetia; Micrococcales; Micrococcaceae; Paenarthrobacter*	0.510A	7.71×10^{9}
Leifsonia soli	FN	*Bacteria; Actinobacteria; Actinomycetia; Micrococcales; Microbacteriaceae; Leifsonia*	0.694A	2.3×10^{8}
Glutamicibacter arilaitensis	FP	*Bacteria; Actinobacteria; Actinomycetia; Micrococcales; Micrococcaceae; Glutamicibacter*	0.572A	1.0×10^{7}
Streptomyces cinnamonensis	FS	*Bacteria; Actinobacteria; Actinomycetia; Streptomycetales; Streptomycetaceae; Streptomyces*	0.625A	8.08×10^{7}#

#Representative qPCR result. CFU, colony-forming unit.

Construction of the prey bacterium microcosm system

Prey strains in the logarithmic growth stage were centrifuged at 7000 rpm for 5 min. The bacterial body was retained and washed with TPM liquid medium and resuspended. The concentration of each bacterial solution was determined by the dilution gradient coating plate method or real-time quantitative PCR, as shown in Table 1. Then, 100 mL of each prey bacterial solution resuspended by the above 16 strains was added to a sterile 3 L blue cap bottle and allowed to stand at 30°C for 24 h to construct a prey bacteria mixture. PT13 in the logarithmic growth phase were treated in the same way as the predator. These prey bacteria mixture and predator constructed a 100 ml microcosmic system. In a microcosmic system, 80 ml of the above prey bacteria mixture was added to a sterile Erlenmeyer flask. Then, 0 mL (CK), 1 mL (A), 5 mL (B), 10 mL (C), and 20 mL (D) PT13 were added to different groups of Erlenmeyer flask, respectively. Finally, the volume was brought up to 100 ml with TPM liquid medium; four parallel replicates were conducted per group.

Extraction and sequencing of sample DNA

After 12 h (T1) and 24 h (T2) of incubation, 1 ml of sample was added to a centrifuge tube and stored at −80°C for sequencing, and then 1 ml of sample was taken to determine its OD_{600} value. DNA was extracted using the FastDNA® SPIN Kit for soil (MP Biomedicals, Santa Ana, CA) according to the instructions and stored at −80°C. The V4-V5 region of the 16S rRNA gene (Primer F: GTGCCAGCMGCCGCGG, Primer R: CCGTCAATTCMTTTRAGTTT) was the target for absolute high-throughput sequencing by Shanghai Tianhao Biotechnology Co., Ltd. using the Illumina MiSeq PE250 (Wang et al., 2020b). These sequence data have been submitted to the GenBank database under accession number PRJNA953930.

Statistical analyses

Quality control and bioinformatics analysis were performed using the DADA2 plug-in for QIIME2. Gene copy number was estimated for each amplicon sequence variant (ASV) based on the rrnDB database (version V5.6) (Stoddard et al., 2015). Species annotation of ASV sequences was performed using QIIME2 software (cutoff = 0.8). Principal coordinate analysis (PCoA) and analysis of similarities (ANOSIM) based on Bray–Curtis dissimilarities were performed using R (Version 4.1.0, vegan package) to assess the statistically significant effects of treatment processes on bacterial communities (Anderson and Walsh, 2013; Krych et al., 2013). Then, LEfSe was used to find specialized indicator bacterial groups within the different treatments of samples (Segata et al., 2011). All statistical analyses were performed by the R *stats* package (Version 4.1.0).

Results

Isolation of typical soil bacteria

A total of 62 indigenous bacterial strains belonging to 21 different genera were isolated and purified from the soil samples (Supplementary Table S1). Among them were *Streptomyces* (22 strains),

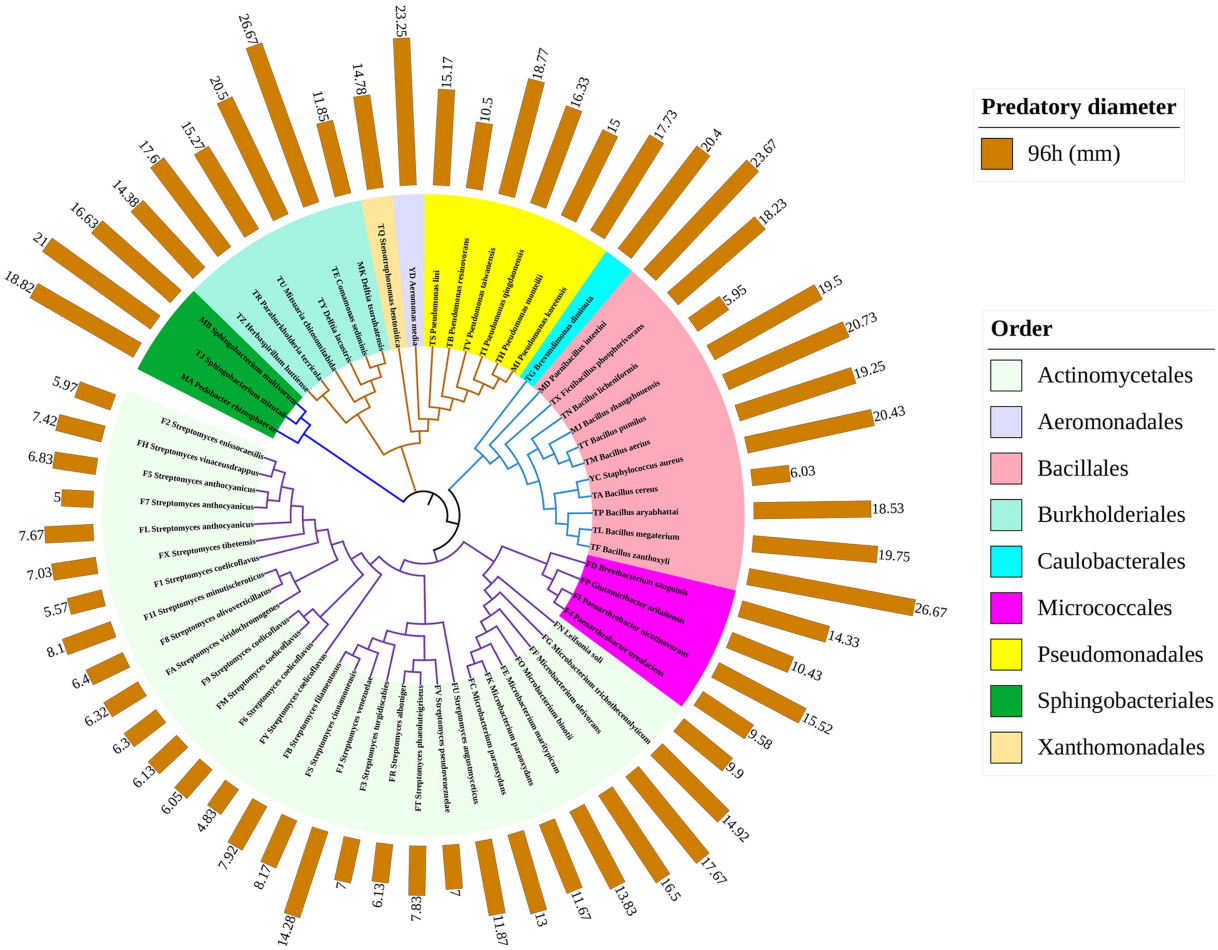

FIGURE 1
Phylogenetic tree based on the 16S rRNA gene sequences of 62 isolates. Phylogenetic tree branches are colored according to the bacterial order to which the species belongs. The outer orange bars represent the predation diameter (mm) of each strain at 96h.

Bacillus (8), *Pseudomonas* (6), *Microbacterium* (6), *Paenarthrobacter* (2), *Sphingobacterium* (2), *and Delftia* (2). One strain was isolated from each of the following genera: *Comamonas*, *Brevundimonas*, *Stenotrophomonas*, *Paraburkholderia*, *Mitsuaria*, *Pedobacter*, *Herbaspirillum*, *Paenibacillus*, *Fictibacillus*, *Staphylococcus*, *Aeromonas*, *Brevibacterium*, *Glutamicibacter*, and *Leifsonia*. A phylogenetic tree was constructed based on the 16S rRNA sequences of the above 62 strains. These 62 strains belong to the phyla Actinomycetes (33), Proteomycetes (15), Firmicutes (11) and Bacteroides (3), all of which are the dominant bacterial phyla in soil microorganisms (Figure 1).

Predation experiments

In TPM medium, which contains a lawn of prey bacteria as the only nutrient source, PT13 had a predatory effect on all 62 strains. The predation diameter of PT13 on prey bacteria increased with predation time. Some strains had prey diameters up to 20 mm at 96 h, such as *Aeromonas* and *Bacillus* (Figure 2A). However, there was a significant difference in predation diameter between the eight *Bacillus* strains in the same genus. The diameter of *Bacillus* sp. TF preyed upon by PT13 was 26.7 mm, which was significantly higher than that of the other seven *Bacillus* strains ($p < 0.05$). *Delftia* sp. TY and MK also had significantly different predation diameters of 20.5 and 11.9 mm, respectively (Figure 2B, $p < 0.05$). Significant differences in predation diameter between strains of the same genus were also observed in *Microbacterium*, *Paenarthrobacter,* and *Pseudomonas* (Figures 2C,D, $p < 0.05$).

Predation diameters varied more significantly between different bacterial genera. *Comamonas* sp. TE, *Brevundimonas* sp. TG and *Delftia* sp. TY all had predation diameters significantly larger than those of *Brevibacterium*, *Fictibacillus*, *Glutamicibacter*, *Herbaspirillum*, and *Leifsonia,* with a diameter at predation greater than 20 mm (Figure 1B, $p < 0.05$). Microorganisms with predation diameters greater than 15 mm mainly included *Paenibacillus*, *Paraburkholderia*, *Pedobacter*, *Sphingobacterium*, and *Staphylococcus* (Figures 2C–E).

In contrast, for 22 strains of *Streptomyces*, PT13 showed only a weak lytic capacity. The predation diameter of all *Streptomyces* spp. at 24, 48, and 72 h was less than 8 mm, except that the diameter of FJ was 11.2 mm at 72 h (Figures 1, 2). At 96 h, *Streptomyces* sp. FJ and FU had predation diameters of 14.3 mm and 11.9 mm, respectively, but those of the other 20 *Streptomyces* spp. were only 4–8 mm (Figures 1, 2). These results showed that PT13 had obvious predatory effects on the above indigenous bacteria, but its predation preference was directly related to the bacterial species.

10.3389/fmicb.2023.1211756

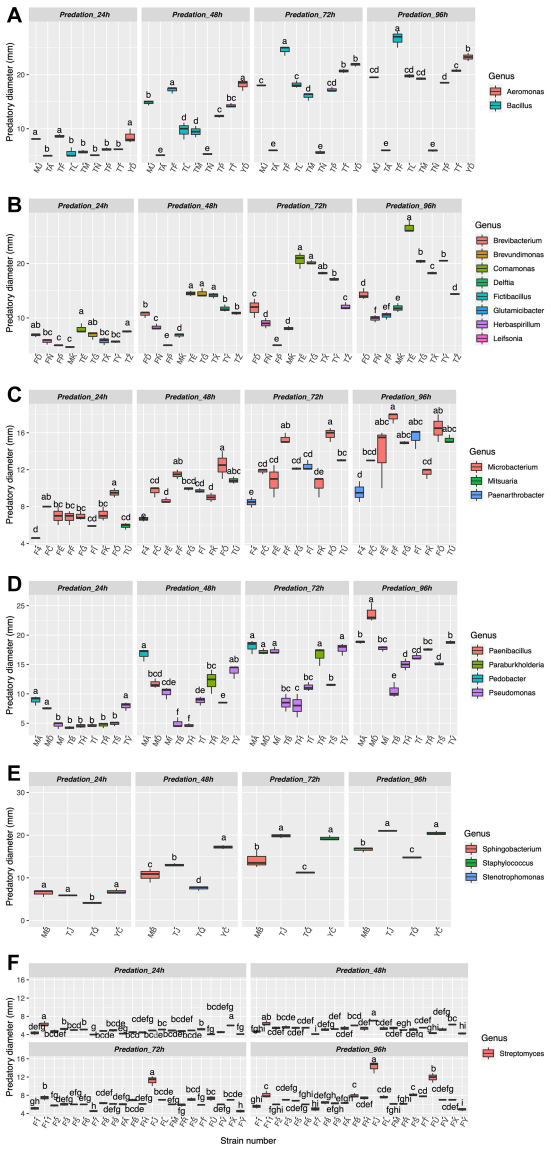

FIGURE 2
Myxobacteria PT13 predation on 62 strains of prey bacteria. The abscissa of the boxplot represents different strain number, and the ordinate represents the predation diameter at different culture times. Bacteria of different genera are distinguished by different colors, and **(A–F)** diagrams are made according to the alphabetical order of bacterial names. Different letters in the same diagram indicate a significant difference (ANOVA, $n = 3$, $p < 0.05$).

Microcosmic systems under predation by myxobacteria

In a microcosmic system with PT13 as its predator, different myxobacteria volumes significantly altered bacterial community structure α and β diversity (Supplementary Figures S1, S2 and Figure 3). Increased or decreased sequentially with the addition of PT13. At 12 h, the Shannon index of each group was 2.04, 2.04, 1.92, 1.84, and 1.80, decreasing sequentially with the addition of PT13 (ANOVA, $p < 0.01$). The Simpson index increased sequentially to 0.20, 0.21, 0.25, 0.28, and 0.29 ($p < 0.01$). The changes in the Shannon and Simpson indices at 24 h were similar to those at 12 h ($p < 0.01$). There were no significant differences between groups in the Chao1 and ACE indices ($p < 0.01$), indicating that predation of PT13 had no significant effect on species number at either incubation time.

PCoA demonstrated that 75.9 and 14.2% of the total community variation in relative abundance and 63.0 and 20.9% of the total community variation in absolute abundance was explained by PCoA1 and PCoA2, respectively. Figure 3A shows the difference between treatments with added myxobacteria (B, C and D) and CK in the direction of the PC1 axis, and Figure 3B shows the difference in the PC2 axis (Tables 2, 3, ANOSIM, Bray–Curtis, $p < 0.01$). This difference increased with the addition of PT13, indicating that the predation of myxobacteria PT13 was the main factor driving the composition of bacterial communities in the microcosmic system.

In the microcosmic system, *Sphingobacterium*, *Comamonas*, *Pedobacter*, *Delftia*, *Bacillus*, *Stenotrophomonas*, *Ochrobactrum*, *Brevundimonas*, *Paenarthrobacter*, and *Staphylococcus* were the 10 bacterial genera with the highest relative abundances. The relative abundances of *Myxococcus*, *Pseudomonas,* and *Fictibacillus* were lower. In the T1CK and T2CK treatments without myxobacteria, the abundance ratios of these genera did not change significantly between 12 and 24 h (Figure 4A). However, predation by PT13 drove community changes in the microcosm system, particularly at high volumes of D treatments. The abundance of *Sphingobacterium* increased significantly to 52.2 and 53.8% in the T1D and T2D groups, which increased by 30.8 and 31.5% compared with T1CK (39.9%) and T2CK (40.9%). The average abundance of PT13 in T1D and T2D was 4.2 and 4.4%, respectively. There was also a significant decrease in the abundance of *Pedobacter*, *Bacillus*, *Ochrobactrum,* and *Staphylococcus* in these groups.

The results of absolute abundance (copy number) were similar to the results of relative abundance. However, some samples did not show a significant decrease in total bacterial copy number with myxobacterial predation, such as T1C and T2C (Figure 4B). Under the predation of PT13, the absolute copy number of *Sphingobacterium* increased significantly, while that of *Pedobacter*, *Bacillus*, *Ochrobactrum,* and *Staphylococcus* decreased significantly. This indicated that the predation of PT13 caused the death of some bacteria but also nourished other types of bacteria, causing fluctuations in the total copy number of bacteria.

Iconic species under the predation of myxobacteria

LEfSe analysis (Figure 5) was used to distinguish iconic species with significant differences in abundance or copies between the above treatments. The relative abundance results (Figure 5A) showed that a total of 42 bacterial taxa were detected, including four genera (*Bacillus, Pedobacter, Staphylococcus* and *Streptomyces*) in T1CK; four genera in T2CK (*Ochrobactrum, Comamonas, Delftia* and *Brevibacterium*); two genera (*Fictibacillus* and *Pseudomonas*) in T1A; two genera (*Sphingobacterium* and *Paenarthrobacter*) in T2B; one genus (*Brevundimonas*) in T2C; and three genera (*Myxococcus*, *Microbacterium,* and *Leifsonia*) in T2D. A total of 13 genera were detected as iconic microorganisms (Figure 5A, $p < 0.05$). The absolute abundance results (Figure 5B) showed 29 bacterial taxa, including five genera (*Pedobacter*, *Bacillus*, *Staphylococcus*, *Fictibacillus,* and *Streptomyces*) in the T1CK; two genera (*Ochrobactrum* and

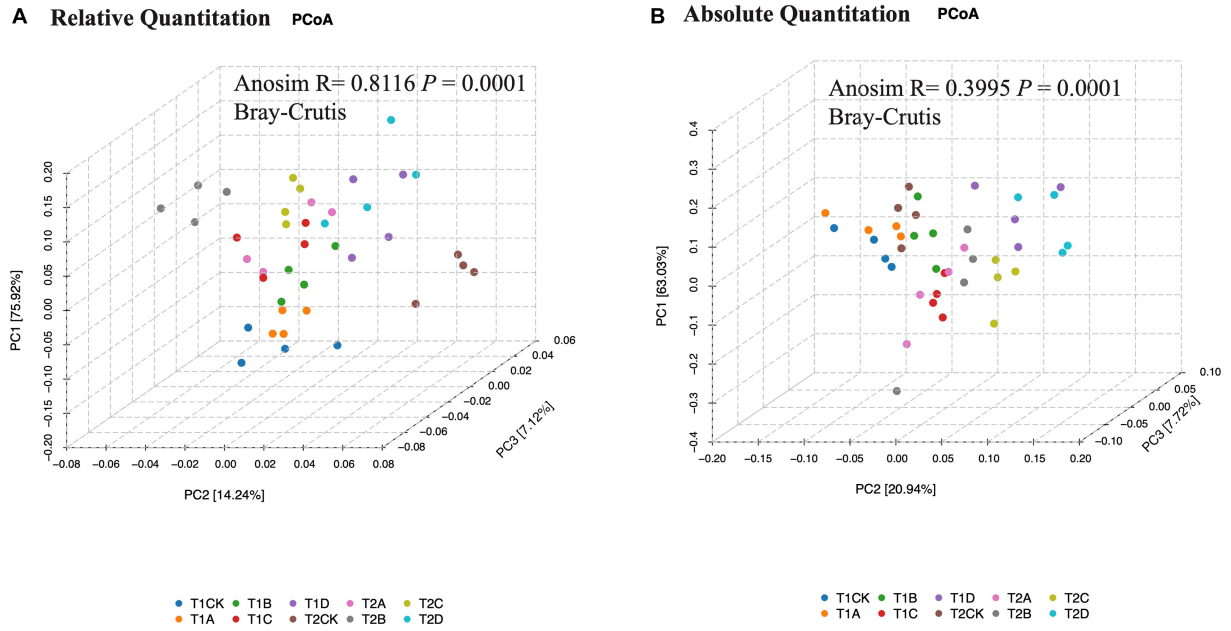

FIGURE 3
Effects of different volumes of myxobacteria treatment on the β diversity of bacterial community abundance **(A)** and copy number **(B)**. PCoA (Bray–Curtis distance index) plots allowing visualization of the differences in the bacterial community structure between samples (based on OTU information). The color of the sample points indicates the 10 treatments. The different sample numbers indicate the incubation time and the amount of PT13 added. T1: 12h; T2: 24h; CK: 0ml of PT13; A: 1ml; B: 5ml; C: 10ml; D: 20ml.

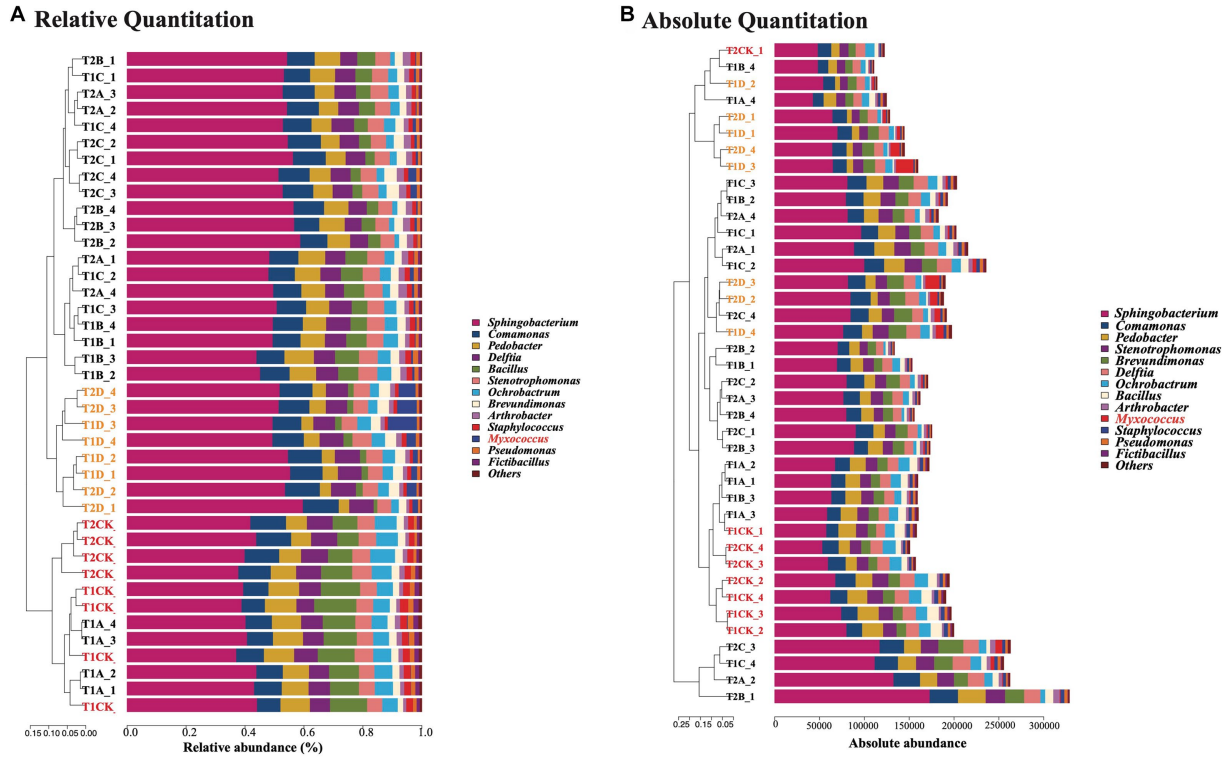

FIGURE 4
Relative **(A)** and absolute **(B)** abundance (copy number) of each genus under different volumes of myxobacteria. The different sample numbers indicate the incubation time and the volume of PT13 added. T1: 12h; T2: 24h; CK: 0ml of PT13; A: 1ml; B: 5ml; C: 10ml; D: 20ml. The sample font of the control group (CK) is marked in red; the D group is labeled orange.

TABLE 2 ANOSIM analysis between five experimental treatments at 12h.

	CK		A		B		C		D	
	R	*p*	*R*	*p*	*R*	*p*	*R*	*p*	*R*	*p*
CK			**0.438**	**0.091**	**0.979**	**0.032***	**1.000**	**0.028***	**1.000**	**0.028***
A	0.240	0.091			**0.844**	**0.029***	**1.000**	**0.030***	**1.000**	**0.030***
B	0.375	0.061	0.052	0.424			**0.26**	**0.145**	**0.854**	**0.029***
C	0.833	0.027*	0.917	0.027*	0.490	0.026*			**0.729**	**0.029***
D	0.781	0.031*	0.604	0.029*	0.010	0.483	0.708	0.030*		

Analysis of similarity was calculated between all treatments based on OTUs tables relative (bold font) and absolute abundance (regular font) Bray–Curtis distance matrices. Each pairwise comparison of two groups was performed using 999 permutations. *R* values > 0.75 are generally interpreted as clearly separated. *R* > 0.5 as separated and *R* < 0.25 as groups hardly separated (Krych et al., 2013). CK: 0 ml of PT13; A: 1 ml; B: 5 ml; C: 10 ml; D: 20 ml. *$p < 0.05$.

TABLE 3 ANOSIM analysis between five experimental treatments at 24h.

	CK		A		B		C		D	
	R	*p*	*R*	*p*	*R*	*p*	*R*	*p*	*R*	*p*
CK			**1.000**	**0.032***	**1.000**	**0.028***	**1.000**	**0.030***	**1.000**	**0.027***
A	0.490	0.057			**0.750**	**0.030***	**0.531**	**0.031***	**0.865**	**0.030***
B	0.458	0.025*	0.010	0.430			**0.844**	**0.028***	**0.938**	**0.028***
C	0.688	0.029*	0.010	0.403	0.021	0.371			**0.604**	**0.030***
D	0.677	0.029*	0.354	0.030*	0.188	0.145	0.188	0.181		

Analysis of similarity was calculated between all treatments based on OTUs tables relative (bold font) and absolute abundance (regular font) Bray–Curtis distance matrices. Each pairwise comparison of two groups was performed using 999 permutations. *R* values > 0.75 are generally interpreted as clearly separated, *R* > 0.5 as separated and *R* < 0.25 as groups hardly separated (Krych et al., 2013). CK: 0 ml of PT13; A: 1 ml; B: 5 ml; C: 10 ml; D: 20 ml. *$p < 0.05$.

Brevibacterium) in the T2CK; one genus (*Sphingobacterium*) in the T2B; two genera (*Pseudomonas* and *Paenarthrobacter*) in the T1C and T2C treatments; and one genus (*Myxococcus*) in the T2D. A total of 11 iconic genera were detected between these treatments (Figure 5B, $p < 0.05$).

Combining the differential iconic species data for relative and absolute abundance, 13 and 11 iconic genera were disturbed by PT13, respectively. *Myxococcus* sp. PT13 significantly reduced the relative abundance of eight genera and increased the absolute abundance of seven genera ($p < 0.05$) but also increased the relative or absolute abundance of some species, such as *Sphingobacterium*, *Paenarthrobacter*, *Microbacterium*, and *Leifsonia* (Figure 5A).

Discussion

Myxobacteria are the most common predatory bacteria in agricultural soils, and their good motility and sociological behavior have attracted attention from researchers (Thiery and Kaimer, 2020; Wang et al., 2020a). *Myxococcus* sp. PT13, a wild myxobacteria strain isolated from yellow-brown soils, was chosen for its good bacterial lysing ability and motility. The lysis spectrum of PT13 was determined by measuring the predation diameter of 62 typical soil strains, including *Aeromonas*, *Bacillus*, *Brevibacterium*, *Fictibacillus*, *Glutamicibacter*, *Herbaspirillum*, and *Leifsonia*. Gram positivity or negativity does not directly affect its lysis effect, and the above conclusions are similar to the results of Dai et al. (2020). In addition, our study measured multiple strains of the same genus, such as the diameter of *Bacillus* sp. TF was preyed upon up to 26.7 mm, whereas *Bacillus* sp. TA and TN were largely not predated. This suggests that strain differences directly influence predation diameter (efficiency). Similar results were shown for *Microbacterium*, *Paenarthrobacter*, and *Pseudomonas* (Figure 1).

Bacillus licheniformis TN can significantly resist the predation of PT13 (Figure 1). The findings also afford additional evidence that *Bacillus licheniformis* escapes from *M. xanthus* predation by deactivating myxovirescin A through enzymatic glucosylation (Wang et al., 2019). There is also evidence that bacillaene inhibits *M. xanthus* predation and sporulation protects *Bacillus subtilis* from predation by *M. xanthus* (Müller et al., 2014). In addition, *Bacillus subtilis* can produce an extracellular matrix and biofilm to defend against *M. xanthus* (Susanne et al., 2015). Akbar et al. observed some surviving *Pseudomonas* phenotypes able to elude *M. xanthus* predation. Increased pyoverdine production, mucoid conversion, and antibiotic resistance observed from survivor *Pseudomonas putida* associated with avoidance of the *M. xanthus* predation (Akbar and Stevens, 2021). *Sinorhizobium meliloti* utilizes secreted Galactoglucan protects cells from *M. xanthus* (Pérez et al., 2014). In addition, there are many factors related to the predator avoidance of prey bacteria, including quorum sensing (Sun et al., 2013; Shukria et al., 2021), increasing the amount of mucus and reducing the movement speed of myxobacteria (Nair et al., 2019), toxin production functional genomics (Weitere et al., 2010; Akbar and Stevens, 2021), type III and type VI secretion systems (Coulthurst, 2019; Le et al., 2021) and antibiotic resistance-associated efflux pumps (Ana et al., 2017). We speculate that these factors may be related to the characteristics of the strain itself, resulting in the difference in the predation efficiency of PT13 on the prey strains of the same genus.

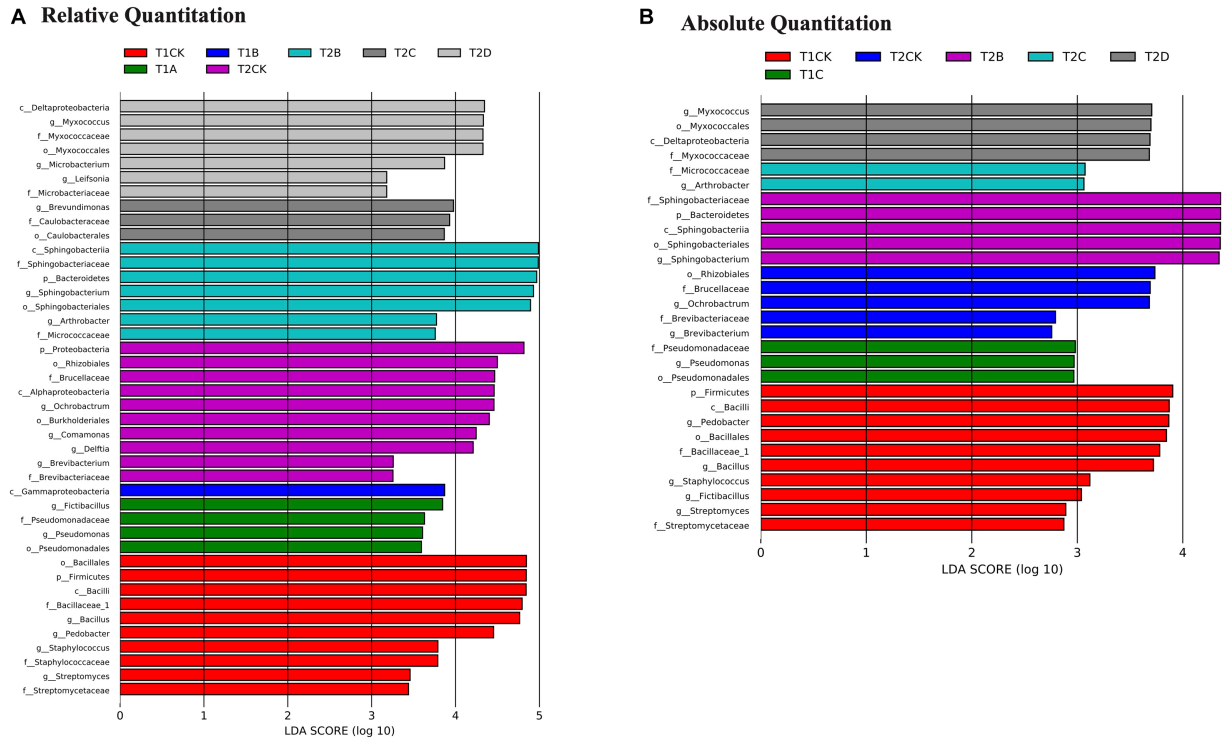

FIGURE 5
LEfSe plots showing bacterial abundance **(A)** and copies **(B)** enriched in the different treatments. Histograms of different colors stand for taxa which were abundant in the corresponding treatment sample (p <0.05). The different sample numbers indicate the incubation time and the amount of PT13 added. T1: 12h; T2: 24h; CK: 0ml of PT13; A: 1ml; B: 5ml; C: 10ml; D: 20ml.

However, the present results do not support the idea that myxobacteria have a greater preference for predation on gram-negative prey bacteria (Morgan et al., 2010; Mendes-Soares and Velicer, 2013; Livingstone et al., 2017; Petters et al., 2021). However, the 20 strains of *Streptomyces* spp. that were gram-positive significantly restricted the motility and lysis of PT13 (Figure 1). This may be related to the fact that both are important medicinal microorganisms. Myxobacteria are another important drug-derived microbial group after *Streptomyces* (actinomycetes), which can produce abundant secondary metabolites (Iizuka et al., 2013). There is also evidence that *Streptomyces coelicolor* M45 resists predation by *M. xanthus* DK1622 through aerial mycelia and antimicrobial substances (Pérez et al., 2011, 2016). Lee et al. (2020) found that iron competition triggered antibiotic biosynthesis in *Streptomyces coelicolor* during coculture with *M. xanthus*. In the soil, both *Myxococcus* and *Streptomyces* coexist and there is evidence of horizontal gene (*celA* gene) transfer between *Streptomyces* and *Myxococcus* ancestors (Quillet et al., 1995; Pérez et al., 2011). In conclusion, *Myxococcus* PT13 has a significant lytic effect on typical agricultural soil bacteria, but its preference is linked to the strain itself, and *Streptomyces* can effectively inhibit the lysis of PT13.

A microcosmic system composed of 16 indigenous bacteria was constructed, and myxobacteria PT13 could prey on these bacteria in the microcosmic system and eventually colonize. This result showed that the interaction of multiple prey bacteria cannot completely resist predation by PT13. However, there was a preference for lysing these prey bacteria by PT13, e.g., the relative and absolute abundances (copy numbers) of *Bacillus*, *Pedobacter*, *Staphylococcus*, *Streptomyces* and *Fictibacillus* were significantly reduced for PT13 addition. In particular, *Streptomyces* was significantly antagonistic to lysis by PT13 under one-to-one predation but was significantly lysed under this microcosmic system. This may be related to the culture environment (solid plates, liquid shake flasks) in which they were incubated or to the interaction of several microorganisms.

Myxobacteria are generally considered to be the apex predators of these groups. The nutrients released by the prey of myxobacteria not only maintain the growth of myxobacteria but also increase the absolute copy number of other bacteria, which is manifested in *Sphingobacterium*, *Pseudomonas* and *Paenarthrobacter*. However, the increase in relative abundance in the study of Dai et al. was only manifested in the genus *Burkholderia*. This paper further elaborates the above results from the perspective of absolute copy number and reconfirmed that myxobacteria does not significantly reduce the bacterial community richness indices (ACE and Chao1).

In complex microcosmic systems, bacterial community assembly processes often have multiple mechanisms, such as heterogeneous selection (HeS), homogeneous selection (HoS), dispersal limitation (DL), homogenizing dispersal (HD), and drift (DR) (Ning et al., 2020). In addition, some scholars suggest that priority effects by the initially inoculated community reduce the establishment success of taxa from the later arriving community (Svoboda et al., 2018). The predation of PT13 is likely involved in the community assembly process of bacteria but not necessarily, population drift and other mechanisms have potential effects on this system.

Myxobacteria are generally considered to be microbial predators with broad-spectrum lysis capabilities in soil. Notably, there are many factors in the soil environment that limit their habitat. Examples include excessive use of nitrogen fertilizers, incompatibility between individuals of different myxobacteria (potential inhibition), and

inhibition of other predatory microorganisms (*Streptomyces* spp. etc.) (Wang et al., 2020b). We noticed a study on *Bdellovibrio* (obligate predatory bacteria), where they constructed prey landscapes including periplasmic or epibiotic predators including two types of decoy under a large range of initial decoy:prey ratio, and mixed cultures containing multiple predators and prey (Sathyamoorthy et al., 2021). They believe that in complex prey landscapes, such as multiple predator and prey cultures, less preferred prey appears to act as decoy (Sathyamoorthy et al., 2021). This study partly explains the coexistence of PT13 with some microorganisms in the microcosmic system. This paper adopted a microcosmic system to confirm the predation preference of myxobacteria under complex microbial interactions. This predation preference preserves other potential prey bacteria and is an important factor in the coexistence of some prey bacteria and myxobacteria.

Conclusion

In this study, we explored the lysis spectrum of *Myxococcus* sp. PT13 on different typical soil bacteria and clarified the disturbance of the bacterial community structure in the microcosmic system by myxobacteria predation. PT13 has a preference for predation of soil bacteria and a significant lysis effect on the genera *Bacillus, Brevibacterium*, *Herbaspirillum,* and *Leifsonia* but poor lysis effect on 20 *Streptomyces* spp. In the microcosmic system constructed by 16 indigenous prey bacteria, the predation of PT13 was likely the main factor driving the bacterial communities. The added volume of PT13 was also an important factor affecting the bacterial community composition. However, there are many factors affecting the predation of myxobacteria in the actual soil environment, and this paper adopts a simplified microcosmic system to focus on the interaction between microorganisms, thereby ignoring the influence of other factors, which is somewhat insufficient. However, this study further enriches the knowledge and understanding of predatory myxobacteria in soil habitats and lays a theoretical foundation for the study of the regulation of soil microecology by myxobacteria.

Data availability statement

The datasets presented in this study can be found in online repositories. The names of the repository/repositories and accession number(s) can be found in the article/Supplementary material.

Author contributions

YY, HT, and WM performed all the experiments and coordinated the data analyses. WW prepared the manuscript, experimental design, and formal analysis. WW and YY contributed to the preparation of the manuscript and data analyses. WW and XC conceived the research. XC revised the manuscript. WW and NW supervised the entire study. All authors contributed to the article and approved the submitted version.

Funding

This work was financially supported by Anhui Provincial Natural Science Foundation, China (2108085QC89), the Natural Science Research Project of Anhui Educational Committee, China (2022AH050870), and the Anhui Postdoctoral Science Foundation, China (2020B410).

Acknowledgments

We thank Ranxiang Lan for assistance in bioinformatics analysis.

Conflict of interest

The authors declare that the research was conducted in the absence of any commercial or financial relationships that could be construed as a potential conflict of interest.

Publisher's note

Supplementary material

The Supplementary material for this article can be found online at: https://www.frontiersin.org/articles/10.3389/fmicb.2023.1211756/full#supplementary-material

SUPPLEMENTARY FIGURE S1
Effect of myxobacteria addition on microcosmic bacterial community diversity indices.

SUPPLEMENTARY FIGURE S2
Absorbance of microcosmic systems with different incubation times.

SUPPLEMENTARY TABLE S1
16S rRNA sequence information of 62 soil bacteria.

References

Akbar, S., and Stevens, D. C. (2021). Functional genomics study of *Pseudomonas putida* to determine traits associated with avoidance of a myxobacterial predator. *Sci. Rep.* 11:16445. doi: 10.1038/s41598-021-96046-8

Ana, V., Amritha, R., Alan, M. S., and Andrey, V. K. (2017). CmeABC multidrug efflux pump contributes to antibiotic resistance and promotes *Campylobacter jejuni* survival and multiplication in *Acanthamoeba polyphaga*. *Appl. Environ. Microbiol.* 83:e01600-17. doi: 10.1128/AEM.01600-17

Anderson, M. J., and Walsh, D. C. I. (2013). PERMANOVA, ANOSIM, and the mantel test in the face of heterogeneous dispersions: what null hypothesis are you testing? *Ecol. Monogr.* 83, 557–574. doi: 10.1890/12-2010.1

Arend, K. I., Schmidt, J. J., Bentler, T., Lüchtefeld, C., Eggerichs, D., Hexamer, H. M., et al. (2021). *Myxococcus xanthus* predation of gram-positive or gram-negative bacteria is mediated by different bacteriolytic mechanisms. *Appl. Environ. Microbiol.* 87, e02382–e02320. doi: 10.1128/AEM.02382-20

Berleman, J. E., and Kirby, J. R. (2009). Deciphering the hunting strategy of a bacterial wolfpack. *FEMS Microbiol. Rev.* 33, 942–957. doi: 10.1111/j.1574-6976.2009.00185.x

Bhat, M. A., Mishra, A. K., Bhat, M. A., Banday, M. I., Bashir, O., Rather, I. A., et al. (2021). Myxobacteria as a source of new bioactive compounds: a perspective study. *Pharmaceutics* 13:1265. doi: 10.3390/pharmaceutics13081265

Bull, C. T., Shetty, K. G., and Subbarao, K. V. (2002). Interactions between Myxobacteria, plant pathogenic fungi, and biocontrol agents. *Plant Dis.* 86, 889–896. doi: 10.1094/PDIS.2002.86.8.889

Coulthurst, S. (2019). The type VI secretion system: a versatile bacterial weapon. *Microbiology* 165, 503–515. doi: 10.1099/mic.0.000789

Dai, W., Jiu, M., Wang, W., Cui, Z., and Wang, H. (2020). Effects of myxobacteria predation on microbial community structure of artificial microcosm. *Acta Microbiol Sin.* 60, 452–463.

Iizuka, T., Jojima, Y., Hayakawa, A., Fujii, T., Yamanaka, S., and Fudou, R. (2013). *Pseudenhygromyxa salsuginis* gen. Nov., sp. nov., a myxobacterium isolated from an estuarine marsh. *Int. J. Syst. Evol. Microbiol.* 63, 1360–1369. doi: 10.1099/ijs.0.040501-0

Krych, L., Hansen, C. H., Hansen, A. K., Van Den Berg, F. W., and Nielsen, D. S. (2013). Quantitatively different, yet qualitatively alike: a meta-analysis of the mouse core gut microbiome with a view towards the human gut microbiome. *PLoS One* 8:e62578. doi: 10.1371/journal.pone.0062578

Le, N. H., Pinedo, V., Lopez, J., Cava, F., and Feldman, M. F. (2021). Killing of gram-negative and gram-positive bacteria by a bifunctional cell wall-targeting T6SS effector. *Natl. Acad. Sci.* 118:e2106555118. doi: 10.1073/pnas.2106555118

Lee, N., Kim, W., Chung, J., Lee, Y., Cho, S., Jang, K. S., et al. (2020). Iron competition triggers antibiotic biosynthesis in *Streptomyces coelicolor* during coculture with *Myxococcus xanthus*. *ISME J.* 14, 1111–1124. doi: 10.1038/s41396-020-0594-6

Letunic, I., and Bork, P. (2016). Interactive tree of life (iTOL) v3: an online tool for the display and annotation of phylogenetic and other trees. *Nucleic Acids Res.* 44, W242–W245. doi: 10.1093/nar/gkw290

Li, Z., Wang, T., Luo, X., Li, X., Xia, C., Zhao, Y., et al. (2018). Biocontrol potential of *Myxococcus* sp. strain BS against bacterial soft rot of calla lily caused by *Pectobacterium carotovorum*. *Biol. Control* 126, 36–44. doi: 10.1016/j.biocontrol.2018.07.004

Li, Z., Ye, X., Yang, F., Huang, Y., Fan, J., Wang, H., et al. (2021). The predation biology of myxobacteria and its application in agricultural field. *J. Nanjing Agric. Univ.* 44, 208–216. doi: 10.7685/jnau.202010034

Li, Y., Zhou, X., Zhang, X., Xu, Z., Dong, H., Yu, G., et al. (2022). A myxobacterial GH19 lysozyme with bacteriolytic activity on both gram-positive and negative phytopathogens. *AMB Express* 12:54. doi: 10.1186/s13568-022-01393-y

Liu, Y. H., Liu, B. B., and Li, W. J. (2021). Isolation and preservation of microorganisms in salty Lake. *Microbiome Protocols eBook*. Bio-101:e2003811. doi: 10.21769/BioProtoc.2003811

Liu, Y., Yao, Q., and Zhu, H. (2019). Meta-16S rRNA gene phylogenetic reconstruction reveals the astonishing diversity of cosmopolitan Myxobacteria. *Microorganisms* 7:551. doi: 10.3390/microorganisms7110551

Livingstone, P. G., Morphew, R. M., and Whitworth, D. E. (2017). Myxobacteria are able to prey broadly upon clinically-relevant pathogens, exhibiting a prey range which cannot be explained by phylogeny. *Front. Microbiol.* 8:1593. doi: 10.3389/fmicb.2017.01593

Lloyd, D. G., and Whitworth, D. E. (2017). The myxobacterium *Myxococcus xanthus* can sense and respond to the quorum signals secreted by potential prey organisms. *Front. Microbiol.* 8:439. doi: 10.3389/fmicb.2017.00439

Mendes-Soares, H., and Velicer, G. J. (2013). Decomposing predation: testing for parameters that correlate with predatory performance by a social bacterium. *Microb. Ecol.* 65, 415–423. doi: 10.1007/s00248-012-0135-6

Morgan, A. D., MacLean, R. C., Hillesland, K. L., and Velicer, G. J. (2010). Comparative analysis of Myxococcus predation on soil Bacteria. *Appl. Environ. Microbiol.* 76, 6920–6927. doi: 10.1128/AEM.00414-10

Müller, S., Strack, S. N., Hoefler, B. C., Straight, P. D., Kearns, D. B., and Kirby, J. R. (2014). Bacillaene and sporulation protect *Bacillus subtilis* from predation by *Myxococcus xanthus*. *Appl. Environ. Microbiol.* 80, 5603–5610. doi: 10.1128/aem.01621-14

Nair, R. R., Vasse, M., Wielgoss, S., Sun, L., Yu, Y.-T. N., and Velicer, G. J. (2019). Bacterial predator-prey coevolution accelerates genome evolution and selects on virulence-associated prey defences. *Nat. Commun.* 10:4301. doi: 10.1038/s41467-019-12140-6

Ning, D., Yuan, M., Wu, L., Zhang, Y., Guo, X., Zhou, X., et al. (2020). A quantitative framework reveals ecological drivers of grassland microbial community assembly in response to warming. *Nat. Commun.* 11:4717. doi: 10.1038/s41467-020-18560-z

Pérez, J., Jiménez-Zurdo, J. I., Martínez-Abarca, F., Millán, V., Shimkets, L. J., and Muñoz-Dorado, J. (2014). Rhizobial galactoglucan determines the predatory pattern of *Myxococcus xanthus* and protects *Sinorhizobium meliloti* from predation. *Environ. Microbiol.* 16, 2341–2350. doi: 10.1111/1462-2920.12477

Pérez, J., Moraleda-Muñoz, A., Marcos-Torres, F. J., and Muñoz-Dorado, J. (2016). Bacterial predation: 75 years and counting! *Environ. Microbiol.* 18, 766–779. doi: 10.1111/1462-2920.13171

Pérez, J., Muñoz-Dorado, J., Braña, A. F., Shimkets, L. J., Sevillano, L., and Santamaría, R. I. (2011). *Myxococcus xanthus* induces actinorhodin overproduction and aerial mycelium formation by *Streptomyces coelicolor*. *Microb. Biotechnol.* 4, 175–183. doi: 10.1111/j.1751-7915.2010.00208.x

Petters, S., Groß, V., Söllinger, A., Pichler, M., Reinhard, A., Bengtsson, M. M., et al. (2021). The soil microbial food web revisited: predatory myxobacteria as keystone taxa? *ISME J.* 15, 2665–2675. doi: 10.1038/s41396-021-00958-2

Phillips, K. E., Akbar, S., and Stevens, D. C. (2022). Concepts and conjectures concerning predatory performance of myxobacteria. *Front. Microbiol.* 13:1031346. doi: 10.3389/fmicb.2022.1031346

Quillet, L., Barray, S., Labedan, B., Petit, F., and Guespin-Michel, J. (1995). The gene encoding the β-1,4-endoglucanase (CelA) from *Myxococcus xanthus*: evidence for independent acquisition by horizontal transfer of binding and catalytic domains from actinomycetes. *Gene* 158, 23–29. doi: 10.1016/0378-1119(95)00091-J

Sathyamoorthy, R., Huppert, A., Kadouri, D. E., and Jurkevitch, E. (2021). Effects of the prey landscape on the fitness of the bacterial predators Bdellovibrio and like organisms. *FEMS Microbiol. Ecol.* 97:fiab047. doi: 10.1093/femsec/fiab047

Segata, N., Izard, J., Waldron, L., Gevers, D., Miropolsky, L., Garrett, W. S., et al. (2011). Metagenomic biomarker discovery and explanation. *Genome Biol.* 12:R60. doi: 10.1186/gb-2011-12-6-r60

Shukria, A., Sandeep, K. M., Joshua, S. S., and Stevens, D. C. (2021). Differential response to prey quorum signals indicates predatory range of myxobacteria. *bioRxiv*:2021.2006.2004.447097. doi: 10.1101/2021.06.04.447097

Stoddard, S. F., Smith, B. J., Hein, R., Roller, B. R., and Schmidt, T. M. (2015). rrnDB: improved tools for interpreting rRNA gene abundance in bacteria and archaea and a new foundation for future development. *Nucleic Acids Res.* 43, D593–D598. doi: 10.1093/nar/gku1201

Sun, S., Kjelleberg, S., and McDougald, D. (2013). Relative contributions of Vibrio polysaccharide and quorum sensing to the resistance of *Vibrio cholerae* to predation by heterotrophic Protists. *PLoS One* 8:e56338. doi: 10.1371/journal.pone.0056338

Susanne, M., Sarah, N. S., Sarah, E. R., Daniel, B. K., and John, R. K. (2015). Predation by *Myxococcus xanthus* induces *Bacillus subtilis* to form spore-filled megastructures. *Appl. Environ. Microbiol.* 81, 203–10. doi: 10.1128/AEM.02448-14

Svoboda, P., Lindström, E. S., Ahmed Osman, O., and Langenheder, S. (2018). Dispersal timing determines the importance of priority effects in bacterial communities. *ISME J.* 12, 644–646. doi: 10.1038/ismej.2017.180

Thiery, S., and Kaimer, C. (2020). The predation strategy of *Myxococcus xanthus*. *Front. Microbiol.* 11:2. doi: 10.3389/fmicb.2020.00002

Wang, C., Liu, X., Zhang, P., Wang, Y., Li, Z., Li, X., et al. (2019). *Bacillus licheniformis* escapes from *Myxococcus xanthus* predation by deactivating myxovirescin a through enzymatic glucosylation. *Environ. Microbiol.* 21, 4755–4772. doi: 10.1111/1462-2920.14817

Wang, W., Luo, X., Ye, X., Chen, Y., Wang, H., Wang, L., et al. (2020a). Predatory Myxococcales are widely distributed in and closely correlated with the bacterial community structure of agricultural land. *Appl. Soil Ecol.* 146:103365. doi: 10.1016/j.apsoil.2019.103365

Wang, W., Wang, N., Dang, K., Dai, W., Guan, L., Wang, B., et al. (2020b). Long-term nitrogen application decreases the abundance and copy number of predatory myxobacteria and alters the myxobacterial community structure in the soil. *Sci. Total Environ.* 708:135114. doi: 10.1016/j.scitotenv.2019.135114

Wang, J., Wang, J., Wu, S., Zhang, Z., and Li, Y. (2021). Global geographic diversity and distribution of the Myxobacteria. *Microbiol. Spectr.* 9, e0001221–e0000021. doi: 10.1128/Spectrum.00012-21

Weitere, M., Bergfeld, T., Rice, S. A., Matz, C., and Kjelleberg, S. (2010). Grazing resistance of *Pseudomonas aeruginosa* biofilms depends on type of protective mechanism, developmental stage and protozoan feeding mode. *Environ. Microbiol.* 7, 1593–1601. doi: 10.1111/j.1462-2920.2005.00851.x

Whitworth, D. E., and Zwarycz, A. (2020). A genomic survey of signalling in the Myxococcaceae. *Microorganisms* 8:1739. doi: 10.3390/microorganisms8111739

Ye, X., Li, Z., Luo, X., Wang, W., Li, Y., Li, R., et al. (2020). A predatory myxobacterium controls cucumber fusarium wilt by regulating the soil microbial community. *Microbiome* 8:49. doi: 10.1186/s40168-020-00824-x

Yi, S., Zhou, Y., Zhang, X., Yao, Q., Li, H., and Zhu, H. (2021). Effects of different methods on the formation of fruiting bodies and isolation of myxobacteria. *Acta Microbiol. Sin.* 61, 923–934.

Zhou, Y., Yi, S., Zhang, X., Yao, Q., and Honghui, Z. (2020). Isolation of soil myxobacteria based on bacterial co-occurrence network. *Biotic Resour.* 42, 531–539. doi: 10.14188/j.ajsh.2020.05.007

frontiers | Frontiers in Microbiology

TYPE Original Research
PUBLISHED 03 August 2023
DOI 10.3389/fmicb.2023.1227206

OPEN ACCESS

EDITED BY
Veronica Godoy,
Northeastern University, United States

REVIEWED BY
David Edward Whitworth,
Aberystwyth University, United Kingdom
Bertrand Aigle,
Université de Lorraine, France

*CORRESPONDENCE
David Cole Stevens
✉ stevens@olemiss.edu

†These authors have contributed equally to this work

RECEIVED 22 May 2023
ACCEPTED 11 July 2023
PUBLISHED 03 August 2023

CITATION
Ahearne A, Phillips KE, Knehans T, Hoing M, Dowd SE and Stevens DC (2023) Chromosomal organization of biosynthetic gene clusters, including those of nine novel species, suggests plasticity of myxobacterial specialized metabolism. *Front. Microbiol.* 14:1227206. doi: 10.3389/fmicb.2023.1227206

Chromosomal organization of biosynthetic gene clusters, including those of nine novel species, suggests plasticity of myxobacterial specialized metabolism

Andrew Ahearne[1†], Kayleigh E. Phillips[1†], Thomas Knehans[1], Miranda Hoing[1], Scot E. Dowd[2] and David Cole Stevens[1*]

[1]Department of BioMolecular Sciences, School of Pharmacy, University of Mississippi, Oxford, MS, United States, [2]Molecular Research LP (MR DNA), Shallowater, TX, United States

Introduction: Natural products discovered from bacteria provide critically needed therapeutic leads for drug discovery, and myxobacteria are an established source for metabolites with unique chemical scaffolds and biological activities. Myxobacterial genomes accommodate an exceptional number and variety of biosynthetic gene clusters (BGCs) which encode for features involved in specialized metabolism.

Methods: In this study, we describe the collection, sequencing, and genome mining of 20 myxobacteria isolated from rhizospheric soil samples collected in North America.

Results: Nine isolates were determined to be novel species of myxobacteria including representatives from the genera *Archangium*, *Myxococcus*, *Nannocystis*, *Polyangium*, *Pyxidicoccus*, *Sorangium*, and *Stigmatella*. Growth profiles, biochemical assays, and descriptions were provided for all proposed novel species. We assess the BGC content of all isolates and observe differences between Myxococcia and Polyangiia clusters.

Discussion: Continued discovery and sequencing of novel myxobacteria from the environment provide BGCs for the genome mining pipeline. Utilizing complete or near-complete genome sequences, we compare the chromosomal organization of BGCs of related myxobacteria from various genera and suggest that the spatial proximity of hybrid, modular clusters contributes to the metabolic adaptability of myxobacteria.

KEYWORDS

myxobacteria, specialized metabolism, genome mining, biosynthetic gene clusters, *Nannocystis*

Introduction

Myxobacteria are metabolically "gifted" bacteria with large genomes accommodating an exceptional number of biosynthetic gene clusters (BGCs) and the potential to produce highly diverse specialized metabolites (Baltz, 2017, 2021; Herrmann et al., 2017; Bader et al., 2020). Excellent reservoirs of candidate therapeutics, over 100 unique metabolite scaffolds have been discovered from myxobacteria (Herrmann et al., 2017).

Extensive metabolomic analysis of ~2,300 myxobacterial extracts revealed a correlation between detected metabolites and taxonomic distance with genus-level hierarchical clustering of metabolite profiles (Hoffmann et al., 2018). Although limited to the metabolic profiles of axenically grown myxobacteria, this observation suggests that the investigation of lesser-studied genera within the phylum Myxococcota might increase the likelihood of metabolite discovery. Ongoing natural product discoveries from novel species of myxobacteria reinforce the need for continued isolation and characterization of environmental myxobacteria (Bader et al., 2022; Haack et al., 2022; Okoth et al., 2022; Zeng et al., 2022). The most recently described Myxococcota belong to the genera *Corallococcus*, *Myxococcus*, and *Pyxidicoccus* (Chambers et al., 2020; Livingstone et al., 2020; Babadi et al., 2022; Inoue et al., 2022; Wang et al., 2022), and comparatively fewer members of lesser-studied myxobacterial taxa have been reported over the last decade (Mohr et al., 2018a; Wang et al., 2021). For example, no new type of strain *Stigmatella* has been reported since 2007. In this study, we report the isolation and genome sequencing of 20 environmental myxobacteria including representatives from the less well-studied *Archangium*, *Nannocystis*, and *Polyangium*. Complete and near-complete genome data enabled a thorough assessment of BGC content, which revealed (1) significant differences in cluster sizes of Myxococcia and Polyangiia, (2) unique biosynthetic capacity of *Nannocystis*, and (3) chromosomal organization of myxobacterial BGCs.

Results

Isolation and genomic comparison of 20 isolated myxobacteria

Rhizospheric soil samples collected from shrubs and trees were screened for bacterial swarms using standard prey-baiting and filter paper degradation methods (Mohr et al., 2016, 2017; Mohr, 2018) to isolate environmental myxobacteria (Supplementary Figure 1) (Adaikpoh et al., 2020). Morphology screening of visible swarms facilitated the isolation of myxobacteria from multiple genera with a specific focus on lesser-studied myxobacteria. A total of 20 environmental isolates of putative myxobacteria including 8 agarolytic isolates were obtained as monocultures (Figure 1). Lesser-studied myxobacteria include genera with agarolytic phenotypes such as *Nannocystis, Polyangium,* and *Sorangium*, hence numerous agarolytic isolates with similar morphologies were advanced for genome sequencing (Mohr, 2018). We have previously discussed 4 of the 20 environmental isolates (SCHIC03, SCPEA02, NCCRE02, and NCSPR01) (Ahearne et al., 2021). Genome sequencing of all isolates provided five complete genomes, seven draft genomes with ≤3 contigs, three draft genomes with 5–8 contigs, and five lower-quality genome assemblies with ≤44 contigs (Table 1). Genome sizes ranged from 9,459,689 to 13,831,693 Mb, and GC content varied from 68.1 to 71.5%. High-quality assemblies enabled subsequent whole-genome comparison approaches for phylogenetic analysis and assessment of biosynthetic gene cluster content and organization.

Phylogenetic relationships of isolated myxobacteria

Initial phylogenetic analysis using 16S rRNA sequences of type strain myxobacteria [obtained from the List of Prokaryotic names with Standing in Nomenclature (LPSN)] suggested the environmental isolates included 1 *Archangium*, 5 *Corallococcus*, 3 *Myxococcus*, 6 *Nannocystis*, 1 *Polyangium*, 2 *Pyxidicoccus*, 1 *Sorangium*, and 1 *Stigmatella* (Supplementary Figure 2). Utilizing genome data from isolates and the type strain of myxobacteria, sequence similarities were determined using average nucleotide identity (ANI) and digital DNA–DNA hybridization values (dDDH) according to the established methods for the taxonomic assignment of myxobacteria (Chambers et al., 2020; Livingstone et al., 2020). Resulting ANI and dDDH values indicated 10 of the 20 environmental isolates to be novel species with values below the respective cutoffs of 95% and 70% when compared to most similar type strains (Figure 2 and Supplementary Table 1). Isolate MIWBW is most phylogenetically similar to *Archangium gephyra* DSM2261^T and *A. gephyra* Cbvi76 [previously referred to as *Cystobacter violaceus* Cbvi76 (Stevens et al., 2014)] (Figure 2A). Of the four published type strain of *Archangium*, *A. gephyra* DSM2261^T is currently the only representative sufficiently sequenced for comparative genomic analysis. More rigorous analysis comparing sequenced representatives of closely related *Cystobacter* and *Melittangium* reinforced MIWBW as a novel species. This analysis also revealed *Cystobacter gracilis* DSM 14753^T to be an outlier within the three genera with ANI values below 77.5 for all included representatives. Isolate SCHIC03 is most phylogenetically similar to *Myxococcus stipitatus* DSM 14675^T when compared to eight *Myxococcus*-type strains (Figure 2B). As observed by Chambers et al. (2020) the ANI value between the established type strain species *Myxococcus xanthus* DSM 16526^T and *Myxococcus virescens* DSM 2260^T is above the threshold for novel species. Initial 16S rRNA analysis suggested that environmental isolates RBIL2, FL3, BB15-2, and NCELM were all novel *Nannocystis* species. However, of the three *Nannocystis*-type strains, there was no genome data for *Nannocystis pusilla* DSM 14622^T (also referred to as *N. pusilla* Na p29^T). Subsequent sequencing of *N. pusilla* DSM 14622^T and comparison including our genome data for *N. pusilla* DSM 14622^T revealed RBIL2 to be a subspecies of *N. pusilla* that is slightly above the novel species threshold (Figure 2E). Isolates BB15-2, FL3, and NCELM are most phylogenetically similar to *Nannocystis exedens* DSM 71^T and are significantly distinct from each other. Our proposed addition of three *Nannocystis* doubles the current member total. Isolate RJM3 is most phylogenetically similar to *Polyangium fumosum* DSM 14688^T (Figure 2C). However, only 3 of 10 *Polyangium*-type strains have sufficient 16S rRNA and genome sequence data suitable for thorough analysis (Lang and Reichenbach, 2013; Wang et al., 2021). Isolate SCPEA02 is most phylogenetically similar to *Pyxidicoccus caerfyrddinensis* CA032A^T (Figure 2G) (Chambers et al., 2020). The proposed addition to *Pyxidicoccus* will make SCPEA02 only the fourth type of *Pyxidicoccus* strain. Isolate WIWO2 is most phylogenetically similar to *Sorangium cellulosum* Soce56, but no type strain of *Sorangium* has been sufficiently sequenced for comparative genomics (Figure 2D). Alternatively, 16S RNA

10.3389/fmicb.2023.1227206

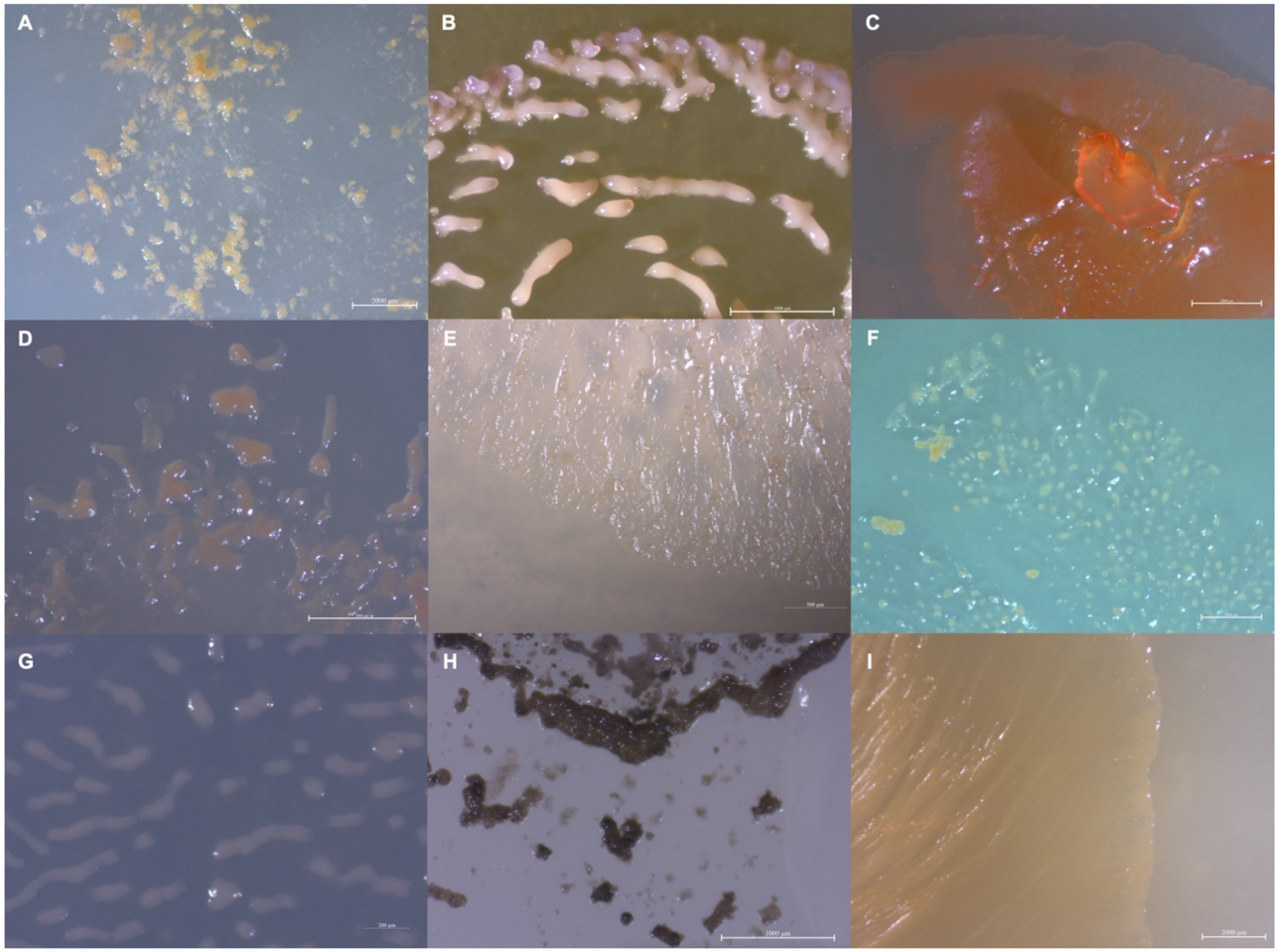

FIGURE 1
Images depicting the observed variety in isolate morphology **(A)** MIWBW, **(B)** SCHIC03, **(C)** BB15-2, **(D)** FL3, **(E)** NCELM, **(F)** RJM3, **(G)** SCPEA02, **(H)** WIWO2, and **(I)** NCWAL01.

analysis suggests that WIWO2 is most phylogenetically similar to *Sorangium kenyense* Soce 375^T (Supplementary Figure 2). Isolate NCWAL01 is most phylogenetically similar to *Stigmatella aurantiaca* DSM17044^T and *St. aurantiaca* DW4_3-1. Interestingly, our analysis indicates ANI values above the threshold for novel species for all three *Stigmatella*-type strains (Figure 2F).

Environmental isolates NCSPR01 and NCRR are highly similar subspecies of *Corallococcus coralloides* DSM 2259^T (Supplementary Table 1 and Supplementary Figure 3A). As previously suggested by Ahearne et al. (2021), isolate NCCRE02 is a subspecies of *Corallococcus exiguus* DSM 14696^T (Supplementary Table 1 and Supplementary Figure 3A). Isolate BB12-1 is likely a subspecies of *Corallococcus terminator* CA054A^T, and isolate BB11-1 is potentially a novel species of *Corallococcus* (Supplementary Table 1 and Supplementary Figure 3B). However, fragmented genome assemblies for BB11-1 and BB12-1 limited our confidence in precise taxonomic placement. Isolate MISCRS is a subspecies of *Myxococcus fulvus* DSM 16525^T, and isolate NMCA is a subspecies of *M. xanthus* DSM 16526^T (Supplementary Table 1 and Supplementary Figure 3C). Isolate MSG2 is a subspecies of *Py. caerfyrddinensis* CA032A^T (Supplementary Table 1 and Supplementary Figure 3D). Isolate SCPEA04 is a *Nannocystis* highly similar to NCELM, and isolates RBIL2 and ILAH1 are both subspecies of *N. pusilla* DSM 14622^T (Supplementary Table 1 and Supplementary Figure 3E).

Physiological and biochemical analyses of nine novel genomospecies

All isolated strains swarmed on VY/2 media, and growth characteristics at various pH values and temperatures were analyzed for all nine novel species (Table 2). All nine strains grew at 25–30°C, and SCPEA02 grew at temperatures up to 40°C. Growth at pH 7 was observed in all strains, and SCHIC03, NCELM, and SCPEA02 all grew at pH 6–9. Agarolytic strains include BB15-2, WIWO2, FL3, NCELM, and RJM3. Metabolic activity was assessed for all strains (Table 3), and none were able to reduce nitrate or metabolize arginine, glucose, or urea. All strains were able to hydrolyze esculin, and all except FL3 and WIWO2 hydrolyzed

10.3389/fmicb.2023.1227206

TABLE 1 Genome assembly data for sequenced isolates with proposed novel species bolded.

Isolate	Size (bp)	CDS	GC%	N50	L50	Contigs
MIWBW	13,831,693	11,592	68.1	13,758,192	1	2
SCHIC03*	10,367,529	8,339	68.6	-	1	1
BB15-2	11,048,555	9,803	71.5	3,033,751	2	5
FL3	13,228,663	12,183	71.5	-	1	1
NCELM	12,940,226	11,412	71.2	791,632	7	29
RBIL	12,529,437	11,262	71.4	6,343,246	1	3
RJM3	13,254,631	11,155	68.6	13,235,919	1	2
SCPEA02*	13,211,253	10,588	69.6	-	1	1
WIWO2	13,472,481	11,616	71.1	2,525,385	2	7
NCWAL01	10,951,030	8,884	66.9	941,459	1	2
NCSPR01*	9,785,177	8,033	70.1	9,343,940	1	3
NCCRE02*	10,538,407	8,589	69.7	3,024,381	2	8
MSG2	13,340,839	10,353	70.3	13,193,640	1	2
NCRR	9,787,125	8,044	70.2	-	1	1
MISCRS	10,873,373	8,896	70.2	10,790,239	1	2
SCPEA4	12,461,442	11,002	71.3	1,797,159	3	22
BB11-1	9,459,689	7,665	70.6	427,033	7	44
BB12-1	10,337,840	8,427	69.6	593,731	6	38
ILAH1	12,844,680	11,575	71.2	573,330	8	41
NMCA1	9,502,182	8,152	69	-	1	1

Asterisks denote previously reported isolates.

gelatin. SCPEA02 and SCHIC03 were the only strains that did not exhibit alkaline phosphatase activity. MIWBW was the only strain to demonstrate both trypsin and a-chymotrypsin activity and possessed overlapping characteristics with *A. gephyra* (Lang et al., 2015). The growth and activity of SCHIC03 were most similar to *M. stipitatus* and *M. fulvus* (Chambers et al., 2020). The growth profiles and biochemical activities of BB15-2, FL3, and NCELM were similar to those of other *Nannocystis;* however, all three demonstrated comparatively limited pH-dependent growth (Mohr et al., 2018a). Unlike *Nannocystis konarekensis*, *N. exedens,* and *N. pusilla*, none of the *Nannocystis* strains grew at pH 10. Temperature and pH-dependent growth ranges for RJM3 were notably different from those of other *Polyangium,* which all grow at temperatures above 30°C and pH ranges of 6–8.5 (Wang et al., 2021). The growth profile and biochemical activity of SCPEA02 were closely aligned with the reported activities of *Py. caerfyrddinensis* (Chambers et al., 2020). The growth profile and biochemical activity of WIWO2 overlapped somewhat with those of the recently described *Sorangium* species (Mohr et al., 2018b). The characterization and description of all *Stigmatella*-type strains pre-date the present description methodology; however, *St. aurantiac*a and NCELM have similar growth and biochemical profiles (Kleinig and Reichenbach, 1969; Reichenbach et al., 1969).

Biosynthetic potential of myxobacterial isolates

AntiSMASH analysis of BGCs in all sequenced isolates provided notable differences in BGC contents, sizes, and similarities with previously characterized clusters (Medema et al., 2011; Blin et al., 2021b). A total of 735 BGCs were predicted from 20 genome assemblies, and only 36 were identified by antiSMASH to be fragmented clusters (~5%) with the vast majority of fragmented BGCs included in sequenced *Corallococcus* strains (20 fragmented BGCs). Genome data from sequenced *Archangium*, *Myxococcus*, *Polyangium*, *Pyxidicoccus*, *Sorangium*, and *Stigmatella* provided three or fewer fragmented BGCs total from each genus. Of our isolated strains, MIWBW had the most predicted BGCs with 52 total (zero fragmented), and NMCA1 had the least with 23 total (zero fragmented). The average length of BGCs from all 20 sequenced isolates was ~56 kb. Clusters from *Nannocystis* strains were significantly shorter (average size ~30 kb) than *Corallococcus*, *Myxococcus*, and *Pyxidicoccus* clusters (Figure 3A). Clusters from *Pyxidicoccus* strains were significantly longer than those from *Archangium*, *Nannocystis*, *Polyangium*, and *Sorangium* clusters. Interestingly, Myxococcia clusters were significantly longer than Polyangiia BGCs (Figure 3B).

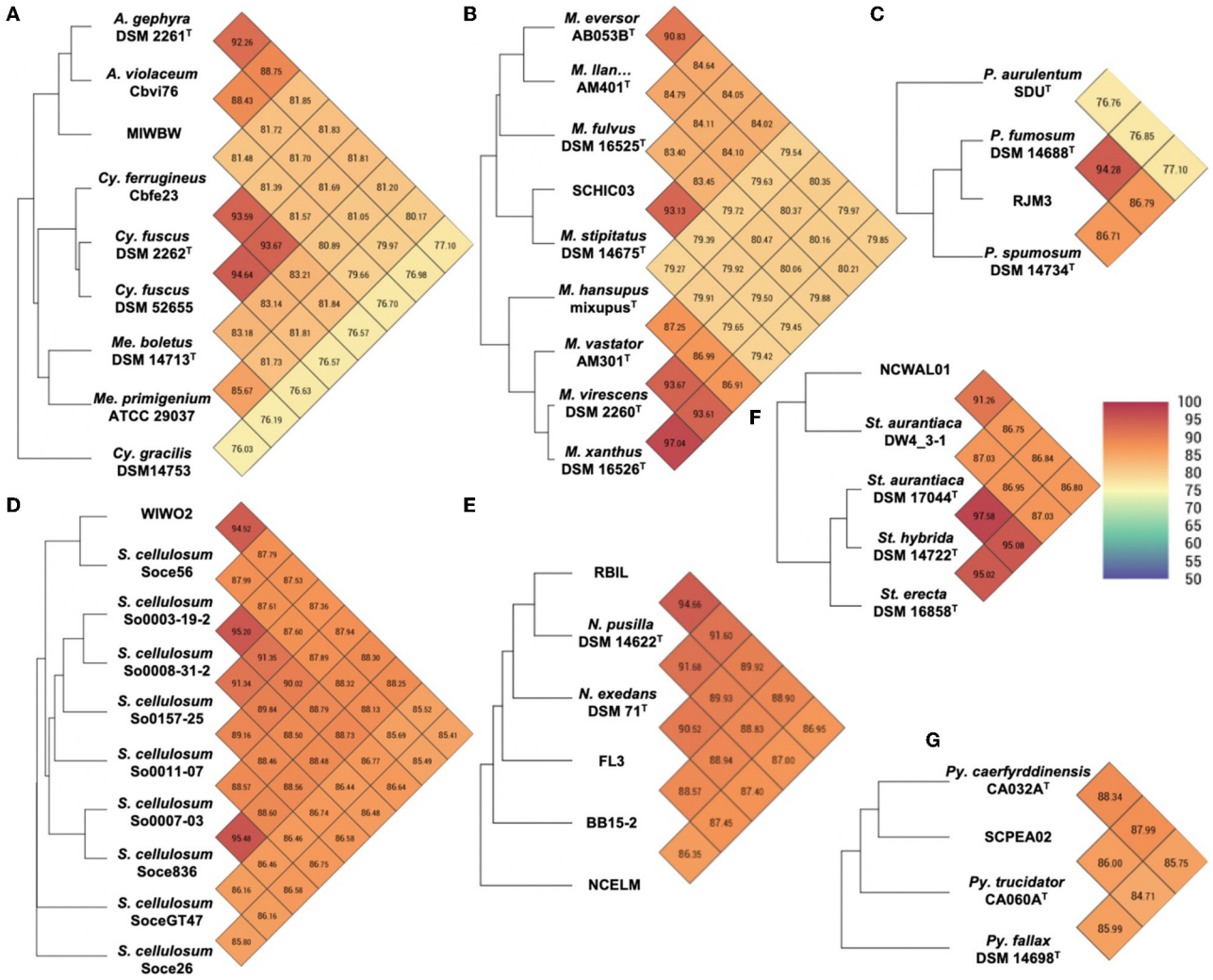

FIGURE 2
Heatmaps generated from OrthoANI values calculated using OAT for **(A)** MIWBW and sequenced strains of *Archangium*, *Cystobacter*, and *Melittangium* **(B)** SCHIC03 and type strain *Myxococcus*, **(C)** RJM3 and type strain *Polyangium*, **(D)** WIWO2 and sequenced *Sorangium*, **(E)** RBIL2, FL3, BB15-2, NCELM, and sequenced *Nannocystis*, **(F)** NCWAL01 and sequenced *Stigmatella*, and **(G)** SCPEA02 and type strain *Pyxidicoccus*. The established cutoff for new species designation is <95%. "*M. llan...*" is an abbreviation of *Myxococcus llanfairpwllgwyngyllgogerychwyrndrobwllllantysiliogogogochensis* AM401^T.

All identified BGCs were compared with the 1,225,071 BGCs and 29,955 gene cluster families (GCFs) included in the BiG-FAM database (Kautsar et al., 2021a,b). Utilizing a previously established clustering threshold (T = 900) to determine distance from database GCFs, we evaluated our 735 BGCs for similarity with BiG-FAM BGCs. Clusters below the arbitrary threshold have similarities with BiG-FAM GCFs and are likely less novel than clusters above the threshold (Kautsar et al., 2021a; Waschulin et al., 2022). Clusters from *Pyxidicoccus* strains (SCPEA02 and MSG2) had the highest average distance (1165), and somewhat predictably *Myxococcus* strains had the lowest (824) with an average distance below the threshold (Figure 3C). Average distance of *Pyxidicoccus* BGCs was significantly higher than the average distances of *Corallococcus, Myxococcus*, and *Nannocystis* clusters. Although *Nannocystis* and *Polyangium* are lesser-studied myxobacteria, the average distances of clusters from members of each genus were just above the threshold for novelty (923 and 924, respectively). No significant difference was observed between the average distances of Myxococcia and Polyangiia clusters (Figure 3D).

Of the 735 predicted BGCs, 384 clusters (~50%) had distances above the threshold. The removal of clusters below the threshold revealed differences in the remaining cluster types across genera (Figure 4). Subsequent comparison of these 384 BGCs with cluster similarities identified during antiSMASH analysis revealed that 52 clusters were either highly homologous to characterized clusters deposited in the MiBIG database (Kautsar et al., 2020) or included embedded clusters with high similarity to known clusters. For example, the myxochelin BGC was found to be embedded in 10 clusters that scored above the BiG-FAM threshold (Gaitatzis et al., 2001; Li et al., 2008). Although co-clustering likely impedes the analysis of novelty and similarity to BiG-FAM GCFs, we suggest that

10.3389/fmicb.2023.1227206

TABLE 2 Growth characteristics for isolates proposed to be novel species.

Temperature (°C)	WIWO2	BB15-2	FL3	RJM3	NCWAL01	SCHIC03	NCELM	SCPEA02	MIWBW
20	-	++	+	+	+++	++	-	+	++
25	+	+++	+++	+++	+++	+++	++	+++	+++
30	+++	++	+++	+++	+++	++	+++	+++	+++
35	+	-	+++	-	+	+++	-	+++	+++
40	-	-	-	-	-	-	-	+++	-
pH									
5	-	-	-	-	-	-	-	-	-
6	+	-	+	-	++	+++	++	++	+
7	+++	+++	+++	+++	+++	+++	+++	+++	+++
8	-	+++	+++	-	+++	++	+++	+	+++
9	-	-	-	-	-	+	+	+	-
10	-	-	-	-	-	++	-	-	-

Symbols indicate growth using percent increase in swarm diameters over 10 days with "-" as no growth, "+" low growth (≤39% swarm diameter), "++" moderate growth (40–75% swarm diameter), and "+ + +" high growth (76–100% swarm diameter).

such co-clustering does not necessarily preclude the uniqueness of proximal clusters. This analysis also identified clusters that likely produce known metabolites including: 2-methylisoborneol (FL3), alkylpyrone 407/393 (BB11-1 and BB12-1), aurafuron A (NCWAL01), carotenoid (RJM3), chloromyxamide (MSG2), dawenol (BB12-1 and SCHIC03), dkxanthene (MISCRS, NMCA1, and SCHIC03), geosmin (BB12-1, NCRR, and NCSPR01), myxoprincomide (MSG2), nannocystin A (FL3), phenalamide A2 (SCHIC03), pyrronazol B (RBIL2), rhizopodin (NCWAL01 and SCHIC03), ripostatin A/B/C (WIWO2), and VEPE/AEPE/TG-1 (BB11-1, BB12-1, CRE02, MIWBW, MSG2, and NCRR) clusters (Botella et al., 1995; Frank et al., 2007; Jiang et al., 2007; Oliynyk et al., 2007; Meiser et al., 2008; Cortina et al., 2012; Pistorius and Muller, 2012; Bhat et al., 2014; Lorenzen et al., 2014; Osswald et al., 2014; Krastel et al., 2015; Park et al., 2016; Fu et al., 2017; Witte et al., 2017; Gorges et al., 2018; Hug et al., 2019). Modular clusters with high homology but differing organization that likely produce analogs of known metabolites were also identified, including the 2-methylisoborneol (NCELM), fulvuthiacene A/B (MISCRS), lyngbyatoxin A (NCELM and SCPEA04), myxoprincomide (MISCRS, SCPEA02, SCHIC03, and MIWBW), pyrronazol B (BB15-2 and ILAH1), and violacein (SCHIC03) clusters (Cardellina et al., 1979; Edwards and Gerwick, 2004; Jiang et al., 2007; Hoshino, 2011; Cortina et al., 2012; Witte et al., 2017; Panter et al., 2019). Additional cluster similarity was identified across the eight sequenced *Nannocystis* strains. For example, strain SCPEA04 contained no unique clusters that were not also present in the other seven *Nannocystis* genomes, and no strain had more than five unique clusters. Five intriguing novel phosphonate clusters from four *Nannocystis* strains (BB15-2, NCELM, SCPEA04, and RBIL2) and WIWO2 highlight the potential for novel metabolite discovery from the lesser-studied myxobacteria (Supplementary Figure 4). Typically discovered from *Streptomyces* and *Pseudomonas* spp. (Rogers and Birnbaum, 1974; Olivares et al., 2017), no phosphonate metabolites have previously been discovered from a myxobacterium. Further differences between Myxococcia and Polyangiia cluster content were revealed with subsequent analysis of BGC relatedness between isolates and sequenced myxobacteria deposited in the antiSMASH database using BiG-SCAPE (Supplementary Figures 5, 6). The resulting gene cluster families included connectivities between clusters of various Myxococcia suggesting an inherited overlap in specialized metabolism. However, all *Nannocystis* and *Sorangium* gene cluster families with two or more clusters were exclusively genus-specific, and all BGCs from *Polyangium* sp. strain RJM3 were present in singleton gene cluster families.

Additional analysis of myxobacterial BGCs that encode metabolites with reported ecological utility unveiled notable differences and similarities among genera. The myxochelin cluster is present in all sequenced strains, excluding WIWO2 and *Nannocystis* strains (Figure 5). Myxochelin has been discovered in numerous myxobacteria and functions as a siderophore during iron starvation conditions (Silakowski et al., 2000). One or more alternative siderophore clusters are present in all *Nannocystis* strains. Carotenoid and VEPE/AEPE/TG-1 clusters were present in all analyzed Myxococcia and notably absent in all Polyangiia. Geosmin serves as a small molecule deterrent or "warning signal" to dissuade predatory nematodes, and the geosmin cluster is present in all strains (Zaroubi et al., 2022). Myxovirescin (Xiao et al., 2011, 2012) and myxoprincomide (Muller et al., 2016) benefit *M. xanthus* predation on Gram-negative and Gram-positive prey, respectively (Phillips et al., 2022). Myxovirescin has been found to significantly benefit *M. xanthus* predation on *E. coli* (Xiao et al., 2011; Ellis et al., 2019). However, none of the investigated strains including the *M. xanthus* strain NMCA1 possessed a cluster with similarity to the myxovirescin BGC. Aside from the absence of a myxovirescin cluster, NMCA1 and *M. xanthus* DK1622 share incredible similarity in BGC content including high similarity surrounding the myxovirescin BGC in *M. xanthus* DK1622 (Supplementary Figure 7). The myxoprincomide cluster

10.3389/fmicb.2023.1227206

TABLE 3 Enzymatic activity data for isolates proposed to be novel species.

Assay	MIWBW	FL3	BB15-2	NCELM	NCWAL01	RJM3	SCPEA02	WIWO2	SCHIC03
Alkaline phosphatase	+	+	+	+	+	+	-	+	-
Esterase (C4)	+	+	+	+	+	+	+	+	+
Esterase Lipase (C8)	+	+	+	+	+	+/-	+	+	+
Lipase (C14)	+	+/-	-	-	+	-	-	-	+/-
Leucine arylamidase	+	+	+	+	+	+	+	+	+
Valine arylamidase	+	+	-	+	+	+/-	+/-	+	+/-
Cysteine arylamidase	+/-	+	-	+/-	-	-	+/-	-	-
Trypsin	+/-	-	-	-	-	-	-	-	-
α-chymotrypsin	+/-	-	+	-	-	+	-	-	-
Acid phosphatase	+	+	+	+	+	+	+	+/-	+
Naphthol-AS-BI-phosphohydrolase	+	+	+	+	+	+/-	+	+	+/-
α-galactosidase	-	-	-	-	-	-	-	-	-
β-galactosidase	-	-	-	-	-	-	-	-	-
β-glucuronidase	-	-	-	-	-	-	-	-	-
α-glucosidase	-	-	-	-	+/-	-	-	-	-
β-glucosidase	-	+/-	-	+	+	-	-	+	-
N-acetyl-β-glucosaminidase	+/-	-	-	-	+/-	-	-	-	-
α-mannosidase	-	-	-	-	-	-	-	-	-
α-fucosidase	-	-	-	-	-	-	-	-	-
Nitrate reduction	-/-	-/-	-/-	-/-	-/-	-/-	-/-	-/-	-/-
Indole production	-	-	-	-	-	-	-	-	-
Glucose acidification	-	-	-	-	-	-	-	-	-
Arginine dihydrolase	-	-	-	-	-	-	-	-	-
Urease	-	-	-	-	-	-	-	-	-
Esculin hydrolysis	+	+	+	+/-	+	+	+	+	+
Gelatin hydrolysis	+	-	+/-	+	+	+	+	-	+
p-Nitrophenyl-beta-D-galactopyranosidase	-	-	-	-	-	-	+/-	+	-

Symbols indicate "-" no activity, "+/-" low activity, and "+" high activity.

or a cluster with high similarity to it is present in all strains excluding members of the class Polyangiia and NCWAL01.

Genomic organization of BGCs

AntiSMASH analysis of complete or near-complete genome data from FL3, MIWBW, MSG2, NCRR, NCSPR03, NMCA1, SCHIC03, and SCPEA02 provided contiguous sequence data sufficient to observe the genome organization of BGCs. Cluster data from related myxobacteria and complete genome data from the antiSMASH database were used to compare BGC organization between related strains (Figures 6, 7). Similarities between BGC content and genome organization were observed between subspecies (Figures 6A, B) and related strains within the same genus (Figures 6C, 7). Biosynthetic gene clusters were dispersed throughout all genomes, and cluster-dense genomic segments were observed during the comparison of BGC organization. Notably, cluster-dense segments include hybrid-type clusters such as PKS-NRPS clusters or clusters including more than one cluster type. The myxochelin and myxoprincomide BGCs are located within a cluster-dense region in all sequenced environmental Myxococcia (Supplementary Figure 8). Clusters highly similar to carotenoid, geosmin, and VEPE/AEPE/TG-1 BGCs are often located in less-dense segments of analyzed chromosomes. Chromosomal segments with increased adjacency of hybrid and modular clusters were observed for all analyzed myxobacteria albeit less apparent in FL3 and *N. exedens* DSM 71^T (Figure 7C). Other than small differences in cluster content between analyzed subspecies, such as the absence of the myxovirescin BGC from

10.3389/fmicb.2023.1227206

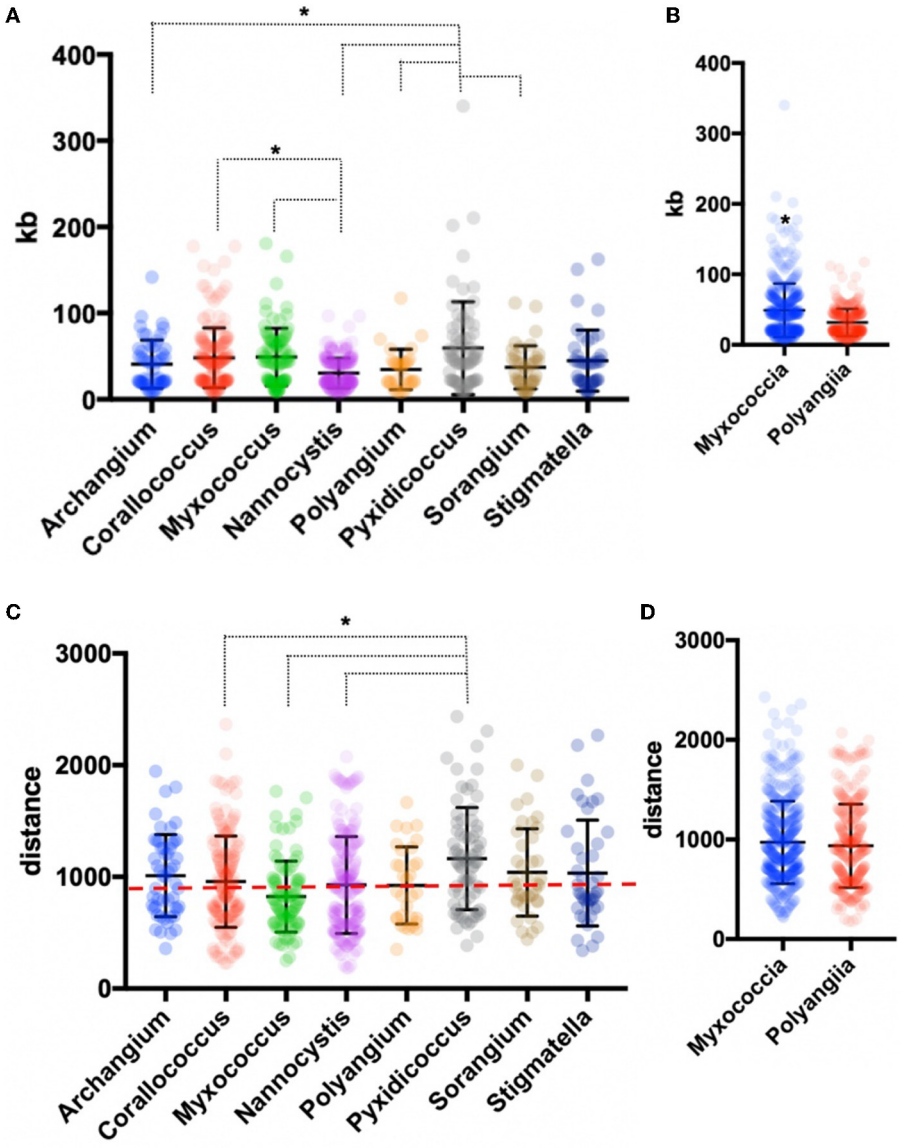

FIGURE 3
Genus-level analysis of BGCs and BiG-FAM distances. **(A)** Genus- and **(B)** class-level comparison of BGC size. **(C)** Genus- and **(D)** class-level comparison of BiG-FAM distances of BGCs with the red, dashed line indicating $d = 900$. Ordinary one-way ANOVA with multiple comparisons was used to determine the significance of genus-level analysis, and Welch's t-test was used to determine the significance of class-level analysis (for genus-level analysis *Archangium* $n = 52$, *Corallococcus* $n = 176$, *Myxococcus* $n = 91$, *Nannocystis* $n = 212$, *Polyangium* $n = 32$, *Pyxidicoccus* $n = 73$, *Sorangium* $n = 39$, *Stigmatella* $n = 42$; $p < 0.05$ and class-level analysis Myxococcia $n = 434$, Polyangiia $n = 283$; $p < 0.0001$). Asterisks indicate the associated p values included in the figure descriptions.

NMCA1 (Figure 6A), numerous inversions of clusters resulting in changes in cluster organization were observed. Apparent BGC inversions were predominantly located within or near cluster-dense regions, and inversions were often relegated to core biosynthetic genes of single clusters with proximal genes unchanged between strains (Supplementary Figure 9). Additional synteny analysis of strains with observed BGC inversions using a set of 10 homologous housekeeping genes revealed highly similar genome organization with no observed inversions (Supplementary Figures 10, 11) (Veltri et al., 2016).

Proposal of nine novel species from the seven genera of Myxococcota

We propose nine candidate strains to represent novel species in the genera *Archangium*, *Myxococcus*, *Nannocystis*, *Polyangium*, *Pyxidicoccus*, *Sorangium*, and *Stigmatella*. Comparative genomics including differences in genome content, phylogeny, and biosynthetic capacities, as well as physiological and biochemical analyses support the following distinctions: *Archangium lansinium* sp. nov. (MIWBW^T), *Myxococcus landrumus* sp. nov. (SCHIC03^T), *Nannocystis bainbridge* sp. nov. (BB15-2^T), *Nannocystis poenicansa*

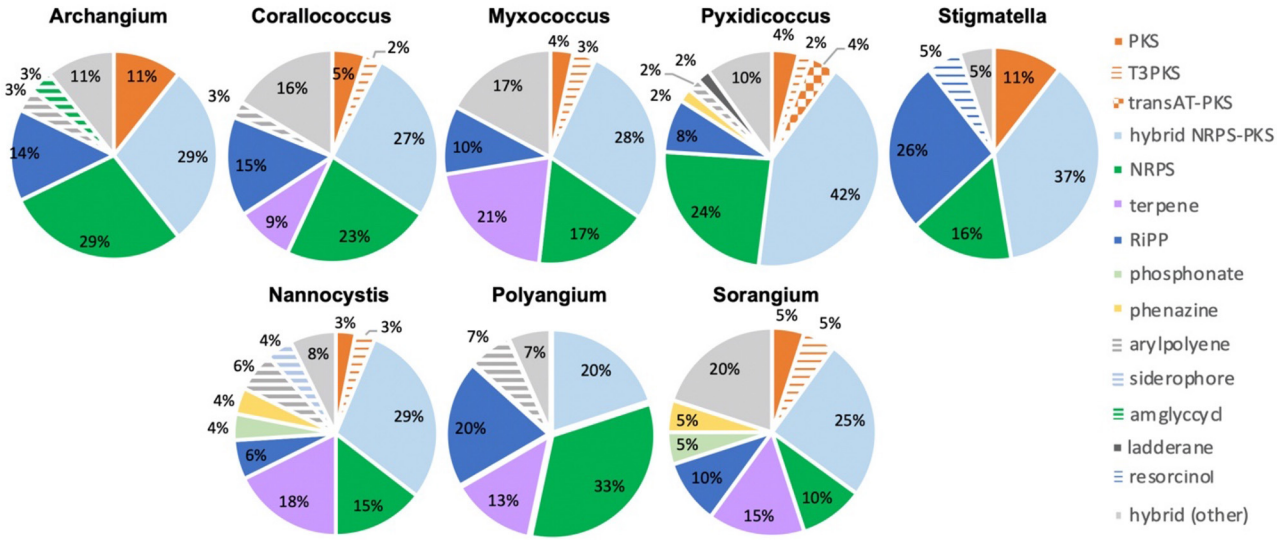

FIGURE 4
Genus-level distribution of likely novel BGCs by cluster type with cluster novelty assumed for BGCs with distances below the BiG-FAM threshold (d = 900). Cluster type designations provided by antiSMASH analysis.

sp. nov. (FL3^T), *Nannocystis radixulma* sp. nov. (NCELM^T), *Polyangium mundeleinium* sp. nov. (RJM3^T), *Pyxidicoccus parkwaysis* sp. nov. (SCPEA02^T), *Sorangium aterium* sp. nov. (WIWO2^T), and *Stigmatella ashevillena* sp. nov. (NCWAL01^T). Corresponding species descriptions for each candidate strain are provided below.

Discussion

Myxococcota taxonomy

Myxobacteria are excellent resources for the discovery of therapeutics and are suggested to be keystone taxa influencing polymicrobial community structure in soil (Herrmann et al., 2017; Baltz, 2019; Bader et al., 2020; Perez et al., 2020; Petters et al., 2021). Recent discoveries of novel *Corallococcus*, *Myxococcus*, and *Pyxidicoccus* species as well as species from lesser-studied genera indicate an abundance of uncharacterized myxobacteria (Mohr et al., 2012, 2018a,b; Iizuka et al., 2013; Garcia et al., 2014, 2016; Yamamoto et al., 2014; Sood et al., 2015; Awal et al., 2016, 2017; Moradi et al., 2017; Garcia and Muller, 2018; Chambers et al., 2020; Livingstone et al., 2020; Wang et al., 2021, 2022; Zhou et al., 2021; Babadi et al., 2022). Our investigation of rhizospheric soil samples provided 20 environmental myxobacteria including 9 proposed novel species. As an initial attempt to isolate myxobacteria from the soil, we were surprised by the effectiveness of morphology screening to enable the discovery of myxobacteria from a variety of genera. We suspect that improved genome data will clarify the observed discrepancies in type strain differentiation and recommend that high-quality genome data be provided for all newly described type strain myxobacteria. We demonstrate that established comparative genome analysis thresholds for the designation of novel species indicate that *M. xanthus* DSM 16526^T and *M. virescens* DSM 2260^T, *St. aurantiaca* DSM 17044^T, *Stigmatella erecta* DSM 16858^T, and *Stigmatella hybrida* DSM 14722^T are not different species. Data from sequenced *Myxococcus* and *Pyxidicoccus* strains align with the previously recommended consideration of *Myxococcus/Pyxidicoccus* as a single genus (Chambers et al., 2020; Wang et al., 2022). However, we note the significant differences in BGC content between *Myxococcus* and *Pyxidicoccus* strains included in this analysis. Overall, our phylogenetic analysis provides further support for comparative genomic approaches to identify and classify myxobacteria. The primary limitation is the absence of quality genome data for established type strains within genera such as *Archangium, Polyangium*, and *Sorangium*.

Expansion of the genus *Nannocystis*

The current type strain *Nannocystis* includes *N. exedens* DSM 71^T, *N. konarekensis* DSM 104509^T, and *N. pusilla* DSM 14622^T. Our investigation resulted in the discovery of an additional three proposed type strains doubling the current total of *Nannocystis* (Mohr et al., 2018a). We also report genome data for all three proposed type strain species as well as three *Nannocystis* subspecies and *N. pusilla* DSM 14622^T. When compared to other myxobacteria, the analysis of all sequenced *Nannocystis* and our isolates provided notable differences in BGC content, such as the absence of a cluster similar to the myxochelin BGC, the presence of multiple siderophore and phosphonate cluster types, and smaller cluster sizes. The resulting genome data for an additional eight *Nannocystis* will improve future efforts to characterize and describe the members of this underexplored genus of myxobacteria.

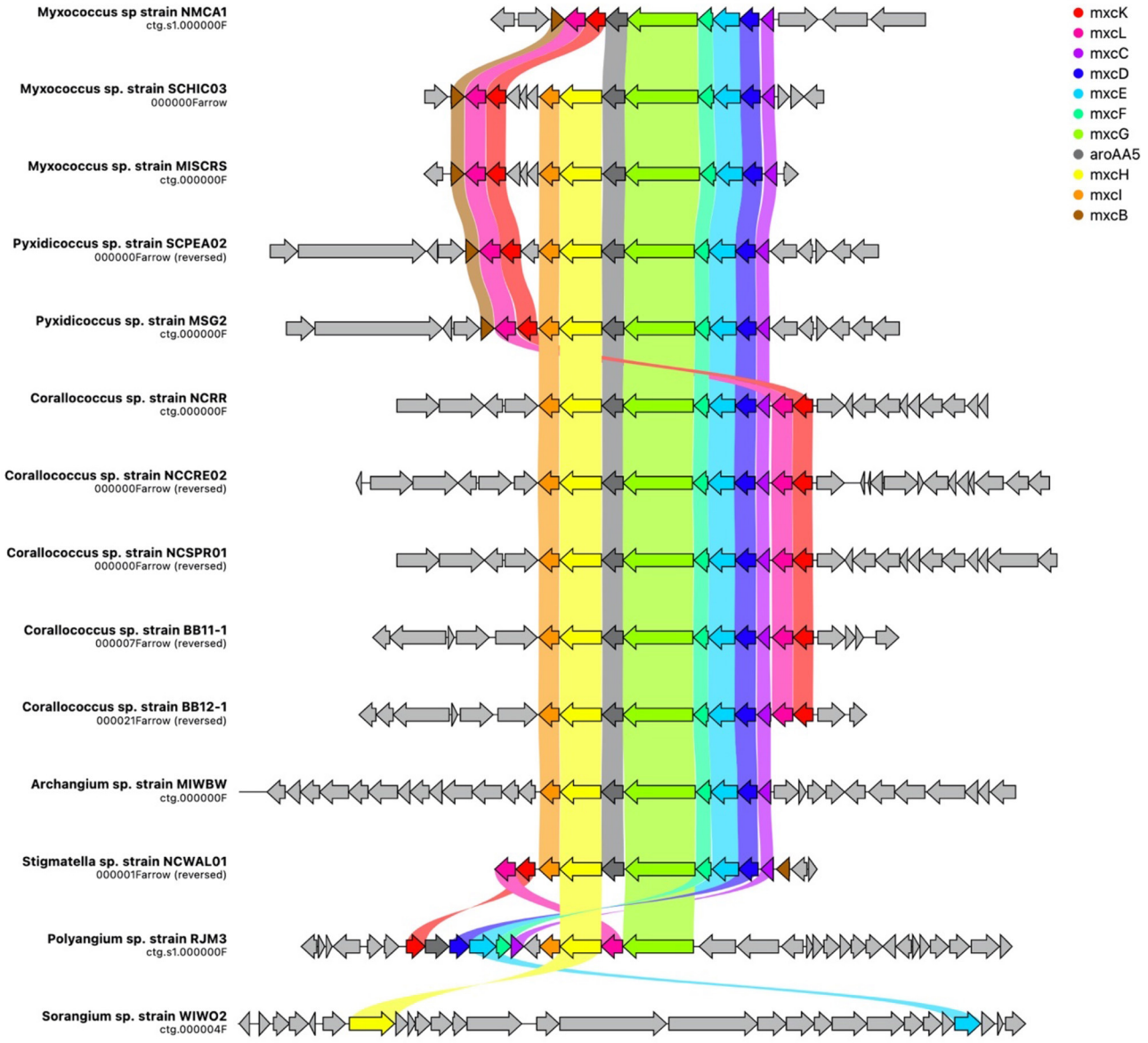

FIGURE 5
Spatial organization of the myxochelin BGC across all isolates with cluster homology. Gene names assigned by homology to the mxyochelin BGC deposited in the MiBIG database (BGC0001345), and ribbons indicate shared gene identity between clusters. Image generated using CAGECAT (version 1.0) using an identity threshold of 0.49 (van den Belt et al., 2023).

Genomic organization of BGCs and adaptability of specialized metabolism

Afforded complete or near-complete genome sequence data, we report the first comparative analysis of spatial organization of myxobacterial BGCs. Dissimilar from *Streptomyces* localization of BGCs in the extremities of linear genomes (Karoonuthaisiri et al., 2005; Lioy et al., 2021), clusters were distributed throughout the circular genomes of myxobacteria. Observed cluster-rich regions replete with modular BGCs, and noted inversions of biosynthetic genes could, however, contribute to metabolic differentiation similar to how terminal compartments of *Streptomyces* chromosomes enable spatial reorganization and conditional expression of BGCs during metabolic development and sporulation (Lioy et al., 2021). We suggest that BGC-enriched regions may benefit BGC evolution and contribute to the metabolic adaptability of myxobacteria. Compartmentalization of modular-type clusters with highly homologous domains may benefit module duplication and deletion events associated with the evolution of BGCs (Fischbach et al., 2008; Medema et al., 2014; Chevrette et al., 2020). Vertical inheritance of the myxochelin cluster is apparent in all sequenced Myxococcia. Our data also reveal vertical transfer and the likely concerted evolution of myxoprincomide-type clusters across sequenced Myxococcia (Medema et al., 2014). Alternatively, the presence of the myxovirescin trans-AT PKS cluster within a cluster-rich region of the *M. xanthus* DK1622 genome and the

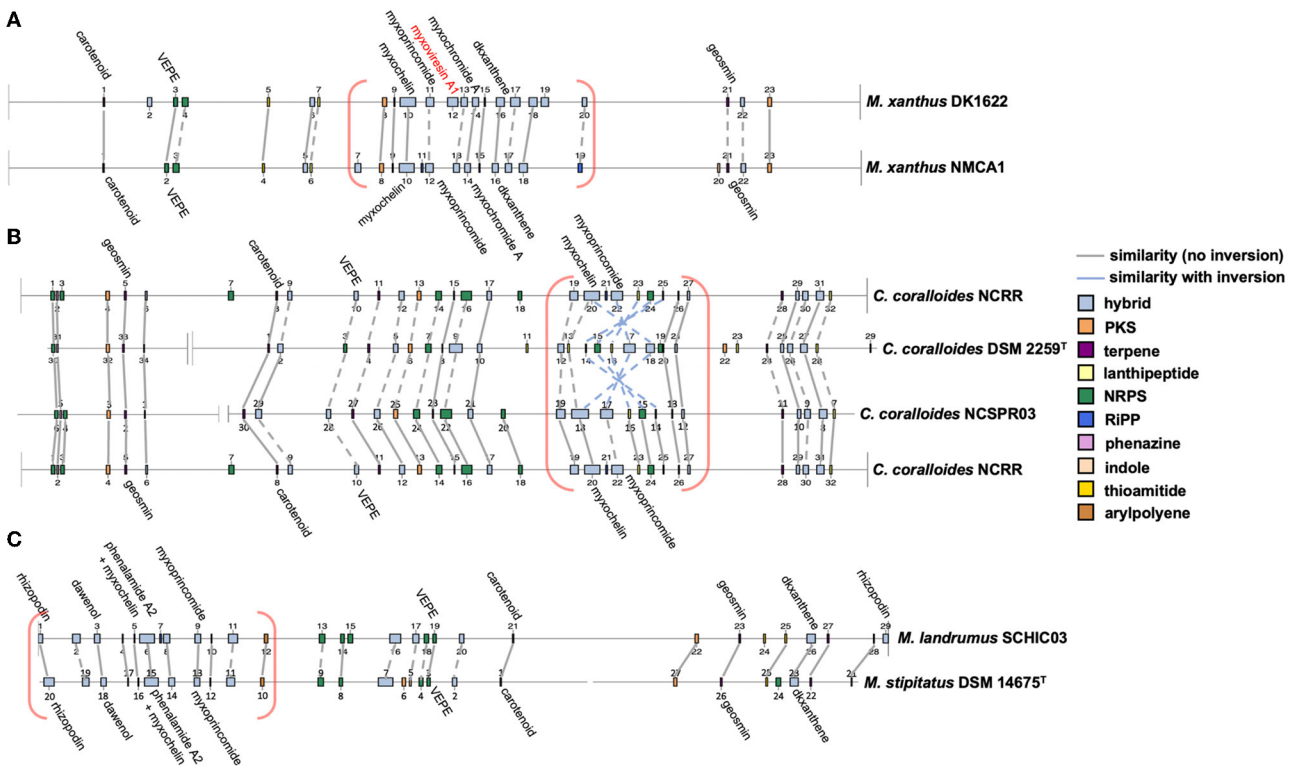

FIGURE 6
Whole-genome comparisons depicting similar BGC organization between subspecies **(A, B)** and species **(C)**. Labeled clusters have high similarity (≥66%) with corresponding myxobacterial BGCs deposited in the MIBiG database as determined by antiSMASH analysis. Myxobacterial clusters with no matching cluster between genomes are labeled with red text. Connecting lines between clusters indicate similar gene organization, and dashed lines indicate minor changes in gene organization or domain content of modular clusters. Cluster-dense chromosomal segments are denoted with red brackets. Inversions defined as the inversion of entire clusters or subclusters within multicluster BGCs. BGC data for *M. xanthus* DK1622, *C. coralloides* DSM 2259^T, and *M. stipitatus* DSM 14675^T obtained from the antiSMASH database (version 3). Numerical labels, BGC coloring (by type), and graphical depictions of genome data taken from antiSMASH (version 6.0) with images altered to depict similarities in cluster organization.

absence of a homologous cluster in NMCA1 indicate horizontal acquisition. Although the absence of the myxovirescin cluster in NMCA1 provides an alternative explanation, the absence of the myxovirescin cluster in all other sequenced *Myxococcus* and Myxococcota members currently deposited in the antiSMASH database supports horizontal acquisition by DK1622. Regardless, the presence of clusters in DK1622 and their absence in other myxobacteria demonstrate metabolic adaptability among myxobacterial genomes with BGC-enriched segments. Further investigation of the chromosomal organization of BGCs in myxobacteria is required to determine functional impacts on metabolic adaptability and cluster evolution.

Species descriptions

Archangium lansinium sp. nov

Archangium lansinium (lan.sin'i.um. N.L. neut. adj. *lansinium* from Lansing, Michigan, USA, referencing the area of isolation).

Vegetative cells glide on solid media. Cells grow as translucent swarms during the early growth phase on VY/4 agar and form non-uniform, clumping fruiting bodies that range from yellow to pale orange over time. Aerobic growth was observed at 20 to 35°C but not at 40°C at a pH range of 6.0 to 8.0. Hydrolyzes gelatin and esculin. Shows an API ZYM positive reaction to alkaline phosphatase, C4 esterase, C8 lipase, C14 lipase, leucine arylamidase, valine arylamidase, cysteine arylamidase, trypsin, α-chymotrypsin, acid phosphatase, napthol-AS-BI-aphosphohydrolase, and *N*-acetyl-β-glucosaminidase, and a negative reaction to α-galactosidase, β-galactosidase, β-glucuronidase, α-glucosidase, β-glucosidase, α-mannosidase, and α-fucosidase. DNA GC content is 68.1%. The genome assembly of the organism is available at NCBI Assembly (ASM2662663v1). The 16S ribosomal RNA gene sequence is available at GenBank (OP852336.1). Phylogenetically most similar to *A. gephyra* DSM 2261^T.

The type strain (MIWBW^T = TSD-326^T = NCCB 100916^T) was isolated from soil collected in Summer 2021 from the roots of a white basswood tree near the city of Lansing, Michigan, USA (42.73°N, 84.48°W).

Myxococcus landrumus sp. nov

Myxococcus landrumus (lan.drum'us. N.L. masc. adj. *landrumus* from Landrum, South Carolina, USA, referencing the area of isolation).

Vegetative cells glide on solid media. Cells grow as slightly orange swarms and develop rounded, stalking fruiting bodies

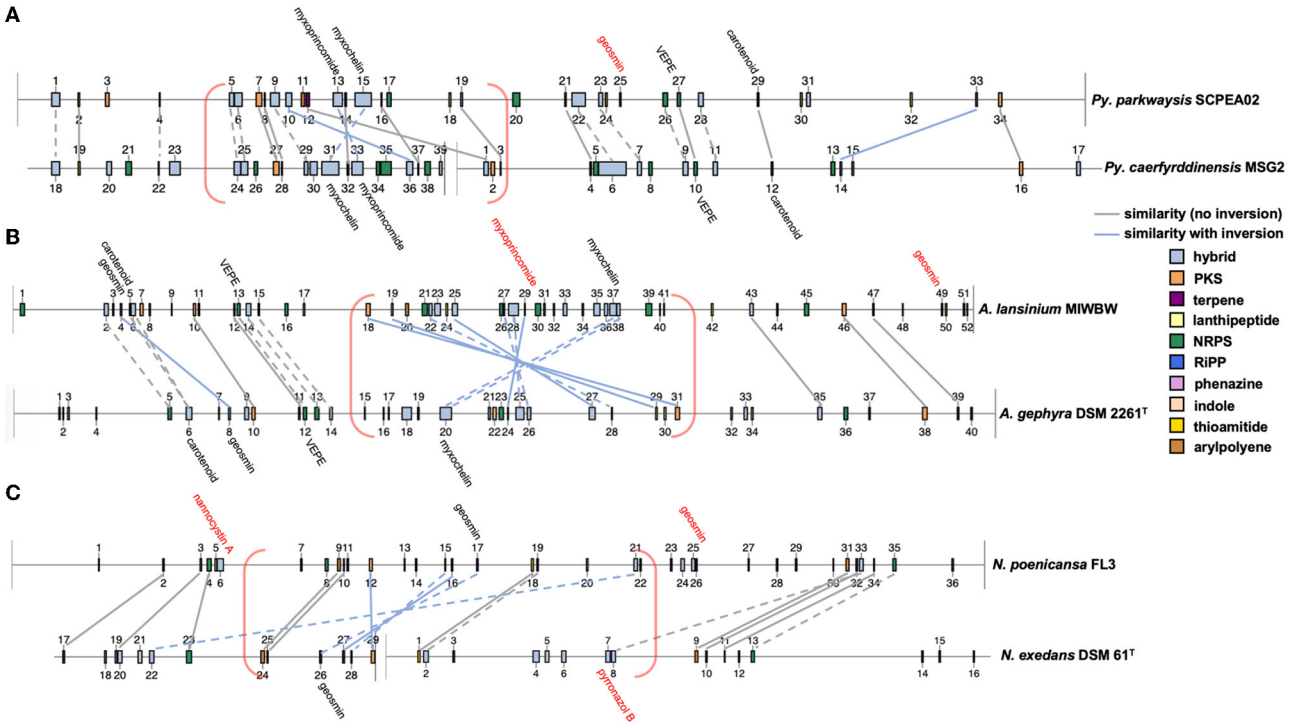

FIGURE 7
Cluster inversions impacting BGC organization between *Pyxidicoccus* **(A)**, *Archangium* **(B)**, and *Nannocystis* **(C)**. Labeled clusters have high similarity (≥66%) with corresponding myxobacterial BGCs deposited in the MiBIG database as determined by antiSMASH analysis. Myxobacterial clusters with no matching cluster between genomes are labeled with red text. Connecting lines between clusters indicate similar gene organization, and dashed lines indicate slight changes in the gene organization or domain content of modular clusters. Cluster-dense chromosomal segments are denoted with red brackets. Inversions defined as the inversion of entire clusters or subclusters within multicluster BGCs. BGC data for *A. gephyra* DSM 2261^T and *N. exedens* DSM 61^T obtained from the antiSMASH database (version 3). Numerical labels, BGC coloring (by type), and graphical depictions of genome data taken from antiSMASH (version 6.0) with images altered to depict similarities in cluster organization.

that range from white to purple on VY/4 media. Aerobic growth was observed at 20 to 35°C but not at 40°C at a pH range of 6.0 to 10.0. Hydrolyzes gelatin and esculin. Shows an API ZYM positive reaction to C4 esterase, C8 lipase, C14 lipase, leucine arylamidase, valine arylamidase, acid phosphatase, and napthol-AS-BI-aphosphohydrolase, and a negative reaction to alkaline phosphatase, cysteine arylamidase, trypsin, α-chymotrypsin, *N*-acetyl-β-glucosaminidase, α-galactosidase, β-galactosidase, β-glucuronidase, α-glucosidase, β-glucosidase, α-mannosidase, and α-fucosidase. DNA GC content is 68.6%. The genome assembly of the organism is available at NCBI Assembly (ASM1730163v1). The 16S ribosomal RNA gene sequence is available at GenBank (OP852328v1). Phylogenetically most similar to *M. stipitatus* DSM 14675^T.

The type strain (SCHIC03^T = TSD-327^T = NRRL B-65669^T = NCCB 100915^T) was isolated from soil collected in Spring 2020 from the roots of a hickory tree near the city of Landrum, South Carolina, USA (35.14°N, -82.16°W).

Nannocystis bainbridge sp. nov

Nannocystis bainbridge (bain'bridg.ea. N.L. fem. adj. *bainbridge* from Bainbridge Island, Washington, USA, referencing the area of isolation).

Vegetative cells glide on solid media. Cells are agarolytic and form deep etches in VY/4 agar, and grow as translucent red swarms and form rounded fruiting bodies. Aerobic growth was observed at 20 to 30°C but not at 35 to 40°C at a pH range of 7.0 to 8.0. Hydrolyzes gelatin and esculin. Shows an API ZYM positive reaction to alkaline phosphatase, C4 esterase, C8 lipase, leucine arylamidase, α-chymotrypsin, acid phosphatase, and napthol-AS-BI-aphosphohydrolase, and a negative reaction to C14 lipase, valine arylamidase, cysteine arylamidase, trypsin, *N*-acetyl-β-glucosaminidase, α-galactosidase, β-galactosidase, β-glucuronidase, α-glucosidase, β-glucosidase, α-mannosidase, and α-fucosidase. DNA GC content is 71.5%. The genome assembly of the organism is available at NCBI Assembly (ASM2696555v1). The 16S ribosomal RNA gene sequence is available at GenBank (OP852329.1). Phylogenetically most similar to *N. exedens* DSM 71^T.

The type strain (BB15-2^T = NCCB 100934^T) was isolated from soil collected in Summer 2020 from the roots of a blueberry bush near the city of Bainbridge Island, Washington, USA (47.65°N, -122.55°W).

Nannocystis poenicansa sp. nov

Nannocystis poenicansa (poe.ni.can'sa. N.L. fem. adj. *poenicansa* the bright red, referencing bright red pigment production).

Vegetative cells glide on solid media. Cells are agarolytic and form deep etches in VY/4 agar. Aerobic growth was observed at 20 to 35°C but not at 40°C at a pH range of 6.0 to 8.0. Hydrolyzes esculin. Shows an API ZYM positive reaction to alkaline phosphatase, C4 esterase, C8 lipase, C14 lipase, leucine arylamidase, cysteine arylamidase, acid phosphatase, napthol-AS-BI-aphosphohydrolase, and β-glucosidase, and a negative reaction to valine arylamidase, trypsin, α-chymotrypsin, *N*-acetyl-β-glucosaminidase, α-galactosidase, β-galactosidase, β-glucuronidase, α-glucosidase, α-mannosidase, and α-fucosidase. DNA GC content is 71.5%. The complete genome sequence of the organism is available at GenBank (CP114040.1). The 16S ribosomal RNA gene sequence is available at GenBank (OP852330.1). Phylogenetically most similar to *N. exedens* DSM 71^T.

The type strain (FL3^T = TSD-332^T = NCCB 100918^T) was isolated from soil collected in Fall 2020 from the roots of a southern live oak near the city of Palm Coast, Florida, USA (29.59°N, −81.21°W).

Nannocystis radixulma sp. nov

Nannocystis radixulma (ra'dix.ul.ma. L. fem. n. *poenicansa* the root of elm, referencing the isolation from an elm tree rhizosphere).

Vegetative cells glide on solid media. Cells are agarolytic and form deep etches in VY/4 agar. Early growth ranges from translucent swarm perimeters to yellow-pigmented swarm centers, and form textured, clumping fruiting bodies that range from yellow to orange on VY/4 agar. Aerobic growth was observed at 25 to 30°C but not at 20°C or 35 to 40°C at a pH range of 6.0 to 9.0. Hydrolyzes gelatin and esculin. Shows an API ZYM positive reaction to alkaline phosphatase, C4 esterase, C8 lipase, leucine arylamidase, cysteine arylamidase, acid phosphatase, napthol-AS-BI-aphosphohydrolase, and β-glucosidase, and a negative reaction to C14 lipase, valine arylamidase, trypsin, α-chymotrypsin, *N*-acetyl-β-glucosaminidase, α-galactosidase, β-galactosidase, β-glucuronidase, α-glucosidase, α-mannosidase, and α-fucosidase. DNA GC content is 71.2%. The genome assembly of the organism is available at NCBI Assembly (ASM2836909v1). The 16S ribosomal RNA gene sequence is available at GenBank (OP852331.1). Phylogenetically most similar to *N. exedens* DSM 71^T.

The type strain (NCELM^T = NCCB 100919^T) was isolated from soil collected in Spring 2020 from the roots of an elm tree near the city of Asheville, North Carolina, USA (35.63°N, −82.55°W).

Polyangium mundeleinium sp. nov

Polyangium mundelenium (mun.del.en'ni.um. N.L. neut. adj. *mundelenium* from Mundelein, Illinois, USA, referencing the area of isolation).

Vegetative cells glide on solid media. Cells grow as translucent swarms and develop dispersed rounded, yellow fruiting bodies on VY/4 media. Aerobic growth was observed at 20 to 30°C but not at 20°C or 35 to 40°C at a pH of 7.0. Hydrolyzes gelatin and esculin. Shows an API ZYM positive reaction to alkaline phosphatase, C4 esterase, C8 lipase, leucine arylamidase, valine arylamidase, α-chymotrypsin, acid phosphatase, and napthol-AS-BI-aphosphohydrolase, and a negative reaction to C14 lipase, cysteine arylamidase, trypsin, *N*-acetyl-β-glucosaminidase, α-galactosidase, β-galactosidase, β-glucuronidase, α-glucosidase, β-glucosidase, α-mannosidase, and α-fucosidase. DNA GC content is 68.6%. The genome assembly of the organism is available at NCBI Assembly (ASM2836910v1). The 16S ribosomal RNA gene sequence is available at GenBank (OP852332.1). Phylogenetically most similar to *P. fumosum* DSM 14688^T.

The type strain (RJM3^T = NCCB 100920^T) was isolated from soil collected in Fall 2020 from the roots of a red Japanese maple near the village of Mundelein, Illinois, USA (42.26°N, −88.0°W).

Pyxidicoccus parkwaysis sp. nov

Pyxidicoccus parkwaysis (park.way.sis. N.L. masc. adj. *parkwaysis* from Parkway Farm in Landrum, South Carolina, USA, referencing the area of isolation).

Vegetative cells glide on solid media. Cells grow as mucoid swarms with a slight pink pigmentation and develop, mounded fruiting bodies after 3 weeks of growth on VY/4 media. Aerobic growth was observed at 20 to 40°C at a pH range of 6.0 to 9.0. Hydrolyzes gelatin and esculin. Shows an API ZYM positive reaction to C4 esterase, C8 lipase, leucine arylamidase, acid phosphatase, and napthol-AS-BI-aphosphohydrolase, and a negative reaction to alkaline phosphatase, C14 lipase, valine arylamidase, cysteine arylamidase, trypsin, α-chymotrypsin, *N*-acetyl-β-glucosaminidase, α-galactosidase, β-galactosidase, β-glucuronidase, α-glucosidase, β-glucosidase, α-mannosidase, and α-fucosidase. DNA GC content is 69.6%. The genome assembly of the organism is available at NCBI Assembly (ASM1730173v1). The 16S ribosomal RNA gene sequence is available at GenBank (OP852333). Phylogenetically most similar to *P. caerfyrddinensis* CA032A^T.

The type strain (SCPEA02^T = TSD-328^T = NRRL B-65670^T = NCCB 100921^T) was isolated from soil collected in Spring 2020 from the roots of a peach tree near Parkway Farm in Landrum, South Carolina, USA (35.14°N, −82.12°W).

Sorangium aterium sp. nov

Sorangium aterium (at'er.i.um. N.L. neut. adj. *aterium* the flat black, referencing black pigment production).

Vegetative cells are Gram-negative and glide on solid media. Degrades and decomposes cellulose filter paper. Cells are pigmented dark brown to black when grown on VY/4 agar. Dark brown to black fruiting bodies form on ST21 media, and similarly pigmented sporangioles form on VY/4 agar. Aerobic growth was observed at 25 to 30°C but not at 20°C or 35 to 40°C at a pH range of 6.0 to 7.0. Hydrolyzes esculin. Shows an API ZYM positive reaction to alkaline phosphatase, C4 esterase, C8 lipase, leucine arylamidase, acid phosphatase, napthol-AS-BI-aphosphohydrolase, and β-glucosidase, and a negative reaction to C14 lipase, valine arylamidase, cysteine arylamidase, trypsin, α-chymotrypsin, *N*-acetyl-β-glucosaminidase, α-galactosidase, β-galactosidase, β-glucuronidase, α-glucosidase, α-mannosidase, and α-fucosidase. DNA GC content is 71.1%. The genome assembly of the organism is available at NCBI Assembly (ASM2836893v1). The 16S ribosomal RNA gene sequence is available at GenBank (OP852334.1). Phylogenetically most similar to *S. cellulosum* Soce56.

The type strain (WIWO2^T = NRRL B-65671^T = NCCB 100922^T) was isolated from soil collected in Fall 2021 from the roots of a white oak near the village of Pleasant Prairie, Wisconsin, USA (42.56°N, −87.94°W).

Stigmatella ashevillena sp. nov

Stigmatella ashevillena (ash'vill.en.a. N.L. fem. adj. from Asheville, North Carolina, USA, referencing the area of isolation).

Vegetative cells are Gram-negative and glide on solid media. Cells are yellow during early growth on VY/4 media and form stalked, orange fruiting bodies over time. Aerobic growth was observed at 25 to 30 °C but not at 20°C or 35 to 40°C at a pH range of 6.0 to 9.0. Hydrolyzes gelatin and esculin. Shows an API ZYM positive reaction to alkaline phosphatase, C4 esterase, C8 lipase, C14 lipase, leucine arylamidase, cysteine arylamidase, acid phosphatase, napthol-AS-BI-aphosphohydrolase, α-glucosidase, β-glucosidase, and *N*-acetyl-β-glucosaminidase, and a negative reaction to valine arylamidase, trypsin, α-chymotrypsin, α-galactosidase, β-galactosidase, β-glucuronidase, α-mannosidase, and α-fucosidase. DNA GC content is 66.9%. The genome assembly of the organism is available at NCBI Assembly (ASM2836897v1). The 16S ribosomal RNA gene sequence is available at GenBank (OP852335.1). Phylogenetically most similar to *S. aurantiaca* DSM17044^T.

The type strain (NCWAL01^T = TSD-329^T = NCCB 100923^T) was isolated from soil collected in Spring 2020 from the roots of a walnut tree near the city of Asheville, North Carolina, USA (35.63°N, −82.55°W).

Materials and methods

Isolation of myxobacteria

Bacteriolytic myxobacteria were isolated by the *Escherichia coli* baiting method (Mohr, 2018). Briefly, an *E. coli* lawn was grown overnight at 37°C and resuspended in 1 mL of an antifungal solution (250 μg/mL of cycloheximide and nystatin). A 300 μl of the solution was spread across a WAT agar (1.5% agar, 0.1% $CaCl_2$) plate and air-dried. Previously air-dried soil was wetted with the antifungal solution to a mud-like consistency, and a pea-sized amount was placed on the dried *E. coli* WAT plate. The plate was incubated at 25°C for up to 4 weeks. After 3 days of incubation, the plates were checked daily for the appearance of lytic zones or fruiting bodies in the *E. coli* lawn. Using a syringe needle, the lytic zones were moved to a plate of VY/4 (Baker's yeast 2.5 g/L, $CaCl_2 \times 2H_2O$ 1.36 g/L, vitamin B_{12} 0.5 mg/L, and agar 15 g/L). The swarm edge was repeatedly used to inoculate a fresh VY/4 plate until pure cultures were obtained. Isolates were cultivated continuously at 25–30°C on VY/4. Isolation of cellulolytic myxobacteria was accomplished using the filter paper method (Mohr, 2018). A small square of autoclaved filter paper was placed in the center of a ST21 agar plate (1 g/L of K_2HPO_4, 20 mg/L of yeast extract, 14 g/L of agar, 1 g/L of KNO_3, 1 g/L of $MgSO_{4\times}$ $7H_2O$, 1 g/L of $CaCl_2 \times 2H_2O$, 0.1 g/L of $MnSO_{4\times}$ $7H_2O$, and 0.2 g/L of $FeCl_3$). A pea-sized amount of soil, wet with the antifungal solution, was placed at the edge of the filter paper. Plates were incubated at 25°C for up to 2 months. After 2 weeks, the plates were checked every 2 days for cellulose degradation and fruiting body formation. Fruiting bodies were moved to a fresh ST21 plate with filter paper repeatedly until pure monocultures were observed. Isolates were cultivated continuously at 25–30°C on VY/4.

Cultivation of isolates

All isolates were maintained on VY/4 media. Growth in liquid cultures was achieved using CYH/2 media (0.75 g/L of casitone, 0.75 g/L of yeast extract, 2g/L of starch, 0.5 g/L of soy flour, 0.5 g/L of glucose, 0.5 g/L of $MgSO_{4\times}$ $7H_2O$, 1 g/L of $CaCl_2 \times 2H_2O$, 6 g/L of HEPES, 8 mg/L of EDTA-Fe, and 0.5 mg/L of vitamin B_{12}).

Sequencing methods

Once pure cultures were obtained, DNA isolation was performed using either the Monarch HMW DNA extraction kit for tissue or the Macherey Nagel NucleoBond HMW DNA extraction kit, following the manufacturer's instructions for Gram-negative bacteria. All novel strains were sequenced using PacBio Sequel or Sequel II with a 10 h movie. De novo assembly of the genome was accomplished using the SMRT Analysis Hierarchical Genome Assembly Process (HGAP; SMRT Link 9.0.0 or SMRT Link 10.1.0). *Nannocystis pusilla* Na p29^T was sequenced using an Oxford Nanopore Minion Flongle R9.4.1. Raw data were processed using Guppy (v6.0.1) (Wick et al., 2019). Reads were trimmed using a porechop (v0.2.4) (Wick et al., 2017). The worst 10% of reads were filtered out using filtong (v0.2.1). Flye assembler (v2.9) was used for de novo assembly using the trimmed and filtered reads (Kolmogorov et al., 2019). The correction of the final assembly was achieved by long-read correction using two iterations of Racon (v1.5) (Vaser et al., 2017), followed by two iterations of Medaka (v1.7.2) (Nicholls et al., 2019). Genome assemblies and complete genome data were deposited at NCBI for the following isolates: *Corallococcus exiguus* strain NCCRE02 (ASM1730297v1), *Corallococcus* sp. strain NCSPR01 (ASM1730913v1), *Corallococcus* sp. strain BB11-1 (ASM2662662v1), *Corallococcus* sp. strain BB12-1 (ASM2662676v1), *Corallococcus* sp. strain NCRR (ASM2696553v1), *Myxococcus* sp. strain MISCRS (ASM2662660v1), *Myxococcus* sp. strain NMCA1 (ASM2681020v1), *Nannocystis* sp. strain SCPEA4 (ASM2662668v1), *Nannocystis* sp. strain ILAH1 (ASM2662658v1), *Nannocystis* sp. strain RBIL2 (ASM2662674v1), and *Pyxidicoccus* sp. strain MSG2 (ASM2662670v1). Genome assembly for *Nannocystis pusilla* Na p29^T was also deposited at NCBI (ASM2662666v1).

Microscopy

A Zeiss stereo discovery.V12 microscope using Axiocam 105 and a Plano Apo S 1.0X objective was used to observe fruiting bodies and swarming patterns.

Comparative genomics

OrthoANI calculations and tree generation were achieved using OAT (orthoANI tool v0.93.1) (Lee et al., 2016). dDDH calculations were performed on the type strain genome server (TYGS) website (Meier-Kolthoff and Goker, 2019). Synteny analysis was performed using SimpleSynteny (v1.6) (Veltri et al., 2016).

Enzymatic assays

Enzymatic activity was assessed for myxobacteria utilizing commercial API ZYM (bioMérieux, France) and API NE (bioMérieux, France) kits. Each isolate strain was suspended in 0.85% NaCl to an OD_{600} of 0.7 and 0.1 for API NE. API ZYM strips were incubated for 4.5 h at 37°C, and API NE strips were incubated for 24 h at 37°C. After incubation, specific reagents were added to the cupule and evaluated according to the manufacturer's instructions.

Growth conditions

For most of the myxobacteria tested, strains were grown on VY/4 (pH 7.2) for 5 to 7 days and resuspended in deionized water to an OD_{600} of 0.5. For the genera *Nannocystis* and *Polyangium,* strains were grown for 5 to 7 days in CYH/2 media, centrifuged, washed, and resuspended in sterile distilled water. The optimal growth temperature was tested by inoculating VY/4 plates with 25 µl of the 0.5 OD_{600} suspension for the given myxobacteria. Plates were incubated at 20, 25, 30, 35, and 40°C for up to 14 days. Optimal pH was assessed by plating the 0.5 OD_{600} solution on VY/4 plates buffered to pH 5, 6, 7, 8, 9, or 10. The pH conditions were buffered at a pH of 5 to 6 with 25 mM MES buffer, 7 to 8 with 25 mM HEPES buffer, and 9 to 10 with 25 mM TRIS buffer in VY/4 plates and incubated at 25°C for 2 weeks. Comparisons of swarm diameters were used to determine optimal growth conditions.

BGC analysis

FASTA files for all sequenced isolates were uploaded for analysis using antiSMASH (version 6.1.1) using relaxed detection strictness with all extra features toggled on (Blin et al., 2021b). Resulting antiSMASH job IDs from analyzed isolates were submitted as queries using the BiG-FAM database v1.0.0 (1,225,071 BGCs and 29,955 GCFs) to assess BGC similarity to database clusters (Kautsar et al., 2021a). All BGCs with >900 distance from model GCFs were subsequently dereplicated manually to remove characterized BGCs not clustered with GCFs within the BiG-FAM database. The antiSMASH database v3.0 (147,571 BGCs) was used to analyze BGCs from myxobacteria (Blin et al., 2021a). BiG-SCAPE v1.1.0 was used to analyze all BGCs.gbk files from sequenced isolates as well as all .gbk files from myxobacteria with sequenced genomes deposited in the antiSMASH database with the "hybrids-off" and "MiBIG" parameters (Kautsar et al., 2020; Navarro-Munoz et al., 2020).

Data availability statement

The datasets presented in this study can be found in online repositories. The names of the repository/repositories and accession number(s) can be found below: https://www.ncbi.nlm.nih.gov/, ASM2662663v1; https://www.ncbi.nlm.nih.gov/, ASM1730163v1; https://www.ncbi.nlm.nih.gov/, ASM2696555v1; https://www.ncbi.nlm.nih.gov/genbank/, CP114040.1; https://www.ncbi.nlm.nih.gov/, ASM2836909v1; https://www.ncbi.nlm.nih.gov/, ASM2836910v1; https://www.ncbi.nlm.nih.gov/, ASM1730173v1; https://www.ncbi.nlm.nih.gov/, ASM2836893v1; https://www.ncbi.nlm.nih.gov/, ASM2836897v1; https://www.ncbi.nlm.nih.gov/, ASM1730297v1; https://www.ncbi.nlm.nih.gov/, ASM1730913v1; https://www.ncbi.nlm.nih.gov/, ASM2662662v1; https://www.ncbi.nlm.nih.gov/, ASM2662676v1; https://www.ncbi.nlm.nih.gov/, ASM2696553v1; https://www.ncbi.nlm.nih.gov/, ASM2662660v1; https://www.ncbi.nlm.nih.gov/, ASM2681020v1; https://www.ncbi.nlm.nih.gov/, ASM2662668v1; https://www.ncbi.nlm.nih.gov/, ASM2662658v1; https://www.ncbi.nlm.nih.gov/, ASM2662674v1; https://www.ncbi.nlm.nih.gov/, ASM2662670v1; and https://www.ncbi.nlm.nih.gov/, ASM2662666v1.

Author contributions

AA, KP, and TK: isolation of environmental myxobacteria. KP, TK, and MH: growth profiles, biochemical assays, and imaging for isolates. AA, KP, and SD: genome sequencing. AA, KP, and DS: BGC analyses, manuscript preparation, and editing. DS: supervision and administration. All authors have read and approved the final manuscript.

Funding

This research was supported by the National Institute of Allergy and Infectious Diseases (1 R15 AI137996) and the National Institute of General Medical Sciences (1 P20 GM130460).

Acknowledgments

The authors would like to thank Mary Williams and Ashlen Ahearne for coordinating the collection and delivery of soil samples analyzed in this project. The authors also appreciate the Glycoscience Center of Research Excellence Imaging Research Core and Computational Chemistry and Bioinformatics Research Core for assistance in imaging the isolates and assembly of the *N. pusilla* Na $p29^T$ draft genome with specific gratitude for the Imaging Research Core manager, Dr. Ruofan Cao.

Conflict of interest

SD was employed by Molecular Research LP (MR DNA).

The remaining authors declare that the research was conducted in the absence of any commercial or financial relationships that could be construed as a potential conflict of interest.

The reviewer DW is currently organizing a Research Topic with the author DS.

Publisher's note

All claims expressed in this article are solely those of the authors and do not necessarily represent those of their affiliated organizations, or those of the publisher, the editors and the reviewers. Any product that may be evaluated in this article, or claim that may be made by its manufacturer, is not guaranteed or endorsed by the publisher.

Supplementary material

The Supplementary Material for this article can be found online at: https://www.frontiersin.org/articles/10.3389/fmicb.2023.1227206/full#supplementary-material

References

Adaikpoh, B. I., Akbar, S., Albataineh, H., Misra, S. K., Sharp, J. S., Stevens, D. C., et al. (2020). Myxobacterial response to methyljasmonate exposure indicates contribution to plant recruitment of micropredators. *Front. Microbiol.* 11, 34. doi: 10.3389/fmicb.2020.00034

Ahearne, A., Albataineh, H., Dowd, S. E., and Stevens, D. C. (2021). Assessment of evolutionary relationships for prioritization of myxobacteria for natural product discovery. *Microorganisms* 9, 1376. doi: 10.3390/microorganisms9071376

Awal, R. P., Garcia, R., Gemperlein, K., Wink, J., Kunwar, B., Parajuli, N., et al. (2017). *Vitiosangium cumulatum gen. nov.,* sp. nov. *and Vitiosangium subalbum* sp. nov., soil myxobacteria, and emended descriptions of the genera Archangium and Angiococcus, and of the family Cystobacteraceae. *Int. J. Syst. Evol. Microbiol.* 67, 1422–1430. doi: 10.1099/ijsem.0.001829

Awal, R. P., Garcia, R., and Muller, R. (2016). *Racemicystis crocea gen. nov.,* sp. nov., a soil myxobacterium in the family Polyangiaceae. *Int. J. Syst. Evol. Microbiol.* 66, 2389–2395. doi: 10.1099/ijsem.0.001045

Babadi, Z. K., Garcia, R., Ebrahimipour, G. H., Risdian, C., Kampfer, P., Jarek, M., et al. (2022). *Corallococcus soli sp. Nov.,* a soil myxobacterium isolated from subtropical climate, chalus county, iran, and its potential to produce secondary metabolites. *Microorganisms* 10, 262. doi: 10.3390/microorganisms10071262

Bader, C. D., Panter, F., Garcia, R., Tchesnokov, E. P., Haid, S., Walt, C., et al. (2022). Sandacrabins - structurally unique antiviral RNA polymerase inhibitors from a rare myxobacterium. *Chemistry* 28, e202104484. doi: 10.1002/chem.202104484

Bader, C. D., Panter, F., and Muller, R. (2020). In depth natural product discovery - Myxobacterial strains that provided multiple secondary metabolites. *Biotechnol. Adv.* 39, 107480. doi: 10.1016/j.biotechadv.2019.107480

Baltz, R. H. (2017). Gifted microbes for genome mining and natural product discovery. *J. Ind. Microbiol. Biotechnol.* 44, 573–588. doi: 10.1007/s10295-016-1815-x

Baltz, R. H. (2019). Natural product drug discovery in the genomic era: realities, conjectures, misconceptions, and opportunities. *J. Ind. Microbiol. Biotechnol.* 46, 281–299. doi: 10.1007/s10295-018-2115-4

Baltz, R. H. (2021). *Genome mining for drug* discovery: progress at the front end. *J. Ind. Microbiol. Biotechnol.* 48, kuab044. doi: 10.1093/jimb/kuab044

Bhat, S., Ahrendt, T., Dauth, C., Bode, H. B., and Shimkets, L. J. (2014). Two lipid signals guide fruiting body development of *Myxococcus xanthus*. *mBio* 5, e00939–13. doi: 10.1128/mBio.00939-13

Blin, K., Shaw, S., Kautsar, S. A., Medema, M. H., and Weber, T. (2021a). The antiSMASH database version 3: increased taxonomic coverage and new query features for modular enzymes. *Nucleic Acids Res.* 49, D639–D643. doi: 10.1093/nar/gkaa978

Blin, K., Shaw, S., Kloosterman, A. M., Charlop-Powers, Z., van Wezel, G. P., Medema, M. H., et al. (2021b). antiSMASH 6, 0. improving cluster detection and comparison capabilities. *Nucleic Acids Res.* 49, W29–W35. doi: 10.1093/nar/gkab335

Botella, J. A., Murillo, F. J., and Ruiz-Vazquez, R. (1995). A cluster of structural and regulatory genes for light-induced carotenogenesis in *Myxococcus xanthus*. *Eur J Biochem* 233, 238–48. doi: 10.1111/j.1432-1033.1995.238_1.x

Cardellina, J. H., Marner, F. J., Moore, R. E. (1979). Seaweed dermatitis: structure of lyngbyatoxin A. *Science* 204, 193–5. doi: 10.1126/science.107586

Chambers, J., Sparks, N., Sydney, N., Livingstone, P. G., Cookson, A. R., Whitworth, D. E., et al. (2020). Comparative genomics and pan-genomics of the myxococcaceae, including a description of five novel species: *Myxococcus eversor* sp. *nov., Myxococcus llanfairpwllgwyngyllgogerychwyrndrobwllllantysiliogogogochensis* sp. nov., *Myxococcus vastator* sp. nov., *Pyxidicoccus caerfyrddinensis* sp. nov., *and Pyxidicoccus trucidator* sp. nov. *Genome Biol. Evol.* 12, 2289–2302. doi: 10.1093/gbe/evaa212

Chevrette, M. G., Gutierrez-Garcia, K., Selem-Mojica, N., Aguilar-Martinez, C., Yanez-Olvera, A., Ramos-Aboites, H. E., et al. (2020). Evolutionary dynamics of natural product biosynthesis in bacteria. *Nat. Prod. Rep.* 37, 566–599. doi: 10.1039/C9NP00048H

Cortina, N. S., Krug, D., Plaza, A., Revermann, O., and Muller, R. (2012). Myxoprincomide: a natural product from *Myxococcus xanthus* discovered by comprehensive analysis of the secondary metabolome. *Angew. Chem. Int. Ed. Engl.* 51, 811–6. doi: 10.1002/anie.201106305

Edwards, D. J., and Gerwick, W. H. (2004). Lyngbyatoxin biosynthesis: sequence of biosynthetic gene cluster and identification of a novel aromatic prenyltransferase. *J. Am. Chem. Soc.* 126, 11432–3. doi: 10.1021/ja047876g

Ellis, B. M., Fischer, C. N., Martin, L. B., Bachmann, B. O., and McLean, J. A. (2019). Spatiochemically profiling microbial interactions with membrane scaffolded desorption electrospray ionization-ion mobility-imaging mass spectrometry and unsupervised segmentation. *Anal. Chem.* 91, 13703–13711. doi: 10.1021/acs.analchem.9b02992

Fischbach, M. A., Walsh, C. T., and Clardy, J. (2008). The evolution of gene collectives: How natural selection drives chemical innovation. *Proc. Natl. Acad. Sci. U. S. A.* 105, 4601–8. doi: 10.1073/pnas.0709132105

Frank, B., Wenzel, S. C., Bode, H. B., Scharfe, M., Blocker, H., Muller, R., et al. (2007). From genetic diversity to metabolic unity: studies on the biosynthesis of aurafurones and aurafuron-like structures in myxobacteria and streptomycetes. *J. Mol. Biol.* 374, 24–38. doi: 10.1016/j.jmb.2007.09.015

Fu, C., Auerbach, D., Li, Y., Scheid, U., Luxenburger, E., Garcia, R., et al. (2017). Solving the puzzle of one-carbon loss in ripostatin biosynthesis. *Angew. Chem. Int. Ed. Engl.* 56, 2192–2197. doi: 10.1002/anie.201609950

Gaitatzis, N., Kunze, B., and Muller, R. (2001). In vitro reconstitution of the myxochelin biosynthetic machinery of *Stigmatella aurantiaca* Sg a15: biochemical characterization of a reductive release mechanism from nonribosomal peptide synthetases. *Proc. Natl. Acad. Sci. U. S. A.* 98, 11136–41. doi: 10.1073/pnas.201167098

Garcia, R., Gemperlein, K., and Muller, R. (2014). *Minicystis rosea* gen. nov., sp. nov., a polyunsaturated fatty acid-rich and steroid-producing soil myxobacterium. *Int. J. Syst. Evol. Microbiol.* 64, 3733–3742. doi: 10.1099/ijs.0.068270-0

Garcia, R., and Muller, R. (2018). *Simulacricoccus ruber gen. nov.,* sp. nov., a microaerotolerant, non-fruiting, myxospore-forming soil myxobacterium and emended description of the family Myxococcaceae. *Int. J. Syst. Evol. Microbiol.* 68, 3101–3110. doi: 10.1099/ijsem.0.002936

Garcia, R., Stadler, M., Gemperlein, K., and Muller, R. (2016). *Aetherobacter fasciculatus gen. nov.,* sp. nov. *and Aetherobacter rufus* sp. nov., *novel myxobacteria with promising biotechnological applications. Int. J. Syst. Evol. Microbiol.* 66, 928–938. doi: 10.1099/ijsem.0.000813

Gorges, J., Panter, F., Kjaerulff, L., Hoffmann, T., Kazmaier, U., Muller, R., et al. (2018). Structure, total synthesis, and biosynthesis of chloromyxamides: myxobacterial tetrapeptides featuring an uncommon 6-chloromethyl-5-methoxypipecolic acid building block. *Angew. Chem. Int. Ed. Engl.* 57, 14270–14275. doi: 10.1002/anie.201808028

Haack, P. A., Harmrolfs, K., Bader, C. D., Garcia, R., Gunesch, A. P., Haid, S., et al. (2022). Thiamyxins: structure and biosynthesis of myxobacterial RNA-virus inhibitors. *Angew. Chem. Int. Ed. Engl.* 61, e202212946. doi: 10.1002/anie.202212946

Herrmann, J., Fayad, A. A., and Muller, R. (2017). Natural products from myxobacteria: novel metabolites and bioactivities. *Nat. Prod. Rep.* 34, 135–160. doi: 10.1039/C6NP00106H

Hoffmann, T., Krug, D., Bozkurt, N., Duddela, S., Jansen, R., Garcia, R., et al. (2018). Correlating chemical diversity with taxonomic distance for discovery of natural products in myxobacteria. *Nat. Commun.* 9, 803. doi: 10.1038/s41467-018-03184-1

Hoshino, T. (2011). Violacein and related tryptophan metabolites produced by Chromobacterium violaceum: biosynthetic mechanism and pathway for

construction of violacein core. *Appl. Microbiol. Biotechnol.* 91, 1463–75. doi: 10.1007/s00253-011-3468-z

Hug, J. J., Panter, F., Krug, D., and Muller, R. (2019). Genome mining reveals uncommon alkylpyrones as type III PKS products from myxobacteria. *J. Ind. Microbiol. Biotechnol.* 46, 319–334. doi: 10.1007/s10295-018-2105-6

Iizuka, T., Jojima, Y., Hayakawa, A., Fujii, T., Yamanaka, S., Fudou, R., et al. (2013). *Pseudenhygromyxa salsuginis gen.* nov., sp. nov., *a myxobacterium* isolated from an estuarine marsh. *Int. J. Syst. Evol. Microbiol.* 63, 1360–1369. doi: 10.1099/ijs.0.040501-0

Inoue, D., Hiroshima, N., Nakamura, S., Ishizawa, H., and Ike, M. (2022). Characterization of Two novel predatory bacteria, bacteriovorax stolpii HI3 and Myxococcus sp. MH1, isolated from a freshwater pond: prey range, and predatory dynamics and efficiency. *Microorganisms* 10, 816. doi: 10.3390/microorganisms10091816

Jiang, J., He, X., and Cane, D. E. (2007). Biosynthesis of the earthy odorant geosmin by a bifunctional *Streptomyces coelicolor* enzyme. *Nat. Chem. Biol.* 3, 711–5. doi: 10.1038/nchembio.2007.29

Karoonuthaisiri, N., Weaver, D., Huang, J., Cohen, S. N., and Kao, C. M. (2005). Regional organization of gene expression in Streptomyces coelicolor. *Gene* 353, 53–66. doi: 10.1016/j.gene.2005.03.042

Kautsar, S. A., Blin, K., Shaw, S., Navarro-Munoz, J. C., Terlouw, B. R., van der Hooft, J. J. J., et al. (2020). MIBiG 2, 0. a repository for biosynthetic gene clusters of known function. *Nucleic Acids Res.* 48, D454–D458. doi: 10.1093/nar/gkz882

Kautsar, S. A., Blin, K., Shaw, S., Weber, T., and Medema, M. H. (2021a). BiG-FAM: the biosynthetic gene cluster families database. *Nucleic Acids Res.* 49, D490–D497. doi: 10.1093/nar/gkaa812

Kautsar, S. A., van der Hooft, J. J. J., de Ridder, D., and Medema, M. H. (2021b). BiG-SLiCE: a highly scalable tool maps the diversity of 1, 2. million biosynthetic gene clusters. *Gigascience* 10, 154. doi: 10.1093/gigascience/giaa154

Kleinig, H., and Reichenbach, H. (1969). Carotenoid pigments of *Stigmatella aurantiaca* (Myxobacterales).I. *The minor carotenoids. Arch. Mikrobiol.* 68, 210–7. doi: 10.1007/BF00409913

Kolmogorov, M., Yuan, J., Lin, Y., and Pevzner, P. A. (2019). Assembly of long, error-prone reads using repeat graphs. *Nat. Biotechnol.* 37, 540–546. doi: 10.1038/s41587-019-0072-8

Krastel, P., Roggo, S., Schirle, M., Ross, N. T., Perruccio, F., Aspesi, P., et al. (2015). Nannocystin A: an elongation factor 1 inhibitor from myxobacteria with differential anti-cancer properties. *Angew. Chem. Int. Ed. Engl.* 54, 10149–54. doi: 10.1002/anie.201505069

Lang, E., and Reichenbach, H. (2013). Designation of type strains for seven species of the order Myxococcales and proposal for neotype strains of *Cystobacter ferrugineus, Cystobacter minus* and *Polyangium fumosum*. *Int. J. Syst. Evol. Microbiol.* 63, 4354–60. doi: 10.1099/ijs.0.056440-0

Lang, E., Schumann, P., Tindall, B. J., Mohr, K. I., and Sproer, C. (2015). Reclassification of *Angiococcus disciformis, Cystobacter minus* and *Cystobacter violaceus* as *Archangium disciforme comb. nov., Archangium minus* comb. nov. and *Archangium violaceum* comb. nov., unification of the families Archangiaceae and Cystobacteraceae, and emended descriptions of the families Myxococcaceae and Archangiaceae. *Int. J. Syst. Evol. Microbiol.* 65, 4032–4042. doi: 10.1099/ijsem.0.000533

Lee, I., Ouk Kim, Y., Park, S. C., and Chun, J. (2016). OrthoANI: an improved algorithm and software for calculating average nucleotide identity. *Int. J. Syst. Evol. Microbiol.* 66, 1100–1103. doi: 10.1099/ijsem.0.000760

Li, Y., Weissman, K. J., and Muller, R. (2008). Myxochelin biosynthesis: direct evidence for two- and four-electron reduction of a carrier protein-bound thioester. *J. Am. Chem. Soc.* 130, 7554–5. doi: 10.1021/ja8025278

Lioy, V. S., Lorenzi, J. N., Najah, S., Poinsignon, T., Leh, H., Saulnier, C., et al. (2021). Dynamics of the compartmentalized Streptomyces chromosome during metabolic differentiation. *Nat. Commun.* 12, 5221. doi: 10.1038/s41467-021-25462-1

Livingstone, P. G., Ingleby, O., Girdwood, S., Cookson, A. R., Morphew, R. M., Whitworth, D. E., et al. (2020). Predatory organisms with untapped biosynthetic potential: descriptions of novel corallococcus species *C. aberystwythensis sp. nov., C. carmarthensis* sp. nov., *C. exercitus* sp. nov., *C. interemptor* sp. nov., *C. llansteffanensis* sp. nov., *C. praedator* sp. nov., *C. sicarius* sp. nov., *and C. terminator* sp. nov. *Appl. Environ. Microbiol.* 86, 19. doi: 10.1128/AEM.01931-19

Lorenzen, W., Ahrendt, T., Bozhuyuk, K. A., and Bode, H. B. (2014). A multifunctional enzyme is involved in bacterial ether lipid biosynthesis. *Nat. Chem. Biol.* 10, 425–7. doi: 10.1038/nchembio.1526

Medema, M. H., Blin, K., Cimermancic, P., de Jager, V., Zakrzewski, P., Fischbach, M. A., et al. (2011). antiSMASH: rapid identification, annotation and analysis of secondary metabolite biosynthesis gene clusters in bacterial and fungal genome sequences. *Nucleic Acids Res.* 39, W339–46. doi: 10.1093/nar/gkr466

Medema, M. H., Cimermancic, P., Sali, A., Takano, E., and Fischbach, M. A. (2014). A systematic computational analysis of biosynthetic gene cluster evolution: lessons for engineering biosynthesis. *PLoS Comput. Biol.* 10, e1004016. doi: 10.1371/journal.pcbi.1004016

Meier-Kolthoff, J. P., and Goker, M. (2019). TYGS is an automated high-throughput platform for state-of-the-art genome-based taxonomy. *Nat. Commun.* 10, 2182. doi: 10.1038/s41467-019-10210-3

Meiser, P., Weissman, K. J., Bode, H. B., Krug, D., Dickschat, J. S., Sandmann, A., et al. (2008). DKxanthene biosynthesis–understanding the basis for diversity-oriented synthesis in myxobacterial secondary metabolism. *Chem. Biol.* 15, 771–81. doi: 10.1016/j.chembiol.2008.06.005

Mohr, K. I. (2018). Diversity of myxobacteria-we only see the tip of the iceberg. *Microorganisms* 6, 84. doi: 10.3390/microorganisms6030084

Mohr, K. I., Garcia, R. O., Gerth, K., Irschik, H., and Muller, R. (2012). *Sandaracinus amylolyticus gen. nov.,* sp. nov., *a starch-degrading soil myxobacterium, and description of Sandaracinaceae fam. nov. Int. J. Syst. Evol. Microbiol.* 62, 1191–1198. doi: 10.1099/ijs.0.033696-0

Mohr, K. I., Moradi, A., Glaeser, S. P., Kampfer, P., Gemperlein, K., Nubel, U., et al. (2018a). *Nannocystis konarekensis* sp. nov., a novel myxobacterium from an Iranian desert. *Int. J. Syst. Evol. Microbiol.* 68, 721–729. doi: 10.1099/ijsem.0.002569

Mohr, K. I., Stechling, M., Wink, J., Wilharm, E., and Stadler, M. (2016). Comparison of myxobacterial diversity and evaluation of isolation success in two niches: Kiritimati Island and German compost. *Microbiologyopen* 5, 268–78. doi: 10.1002/mbo3.325

Mohr, K. I., Wolf, C., Nubel, U., Szafranska, A. K., Steglich, M., Hennessen, F., et al. (2018b). A polyphasic approach leads to seven new species of the cellulose-decomposing genus Sorangium, *Sorangium ambruticinum* sp. nov., *Sorangium arenae* sp. nov., *Sorangium bulgaricum* sp. nov., *Sorangium dawidii* sp. nov., *Sorangium kenyense* sp. nov., *Sorangium orientale* sp. nov. *and Sorangium reichenbachii* sp. nov. *Int. J. Syst. Evol. Microbiol.* 68, 3576–3586. doi: 10.1099/ijsem.0.003034

Mohr, K. I., Zindler, T., Wink, J., Wilharm, E., and Stadler, M. (2017). Myxobacteria in high moor and fen: an astonishing diversity in a neglected extreme habitat. *Microbiologyopen* 6, 1–14. doi: 10.1002/mbo3.464

Moradi, A., Ebrahimipour, G. H., Mohr, K. I., Kampfer, P., Glaeser, S. P., Hennessen, F., et al. (2017). *Racemicystis persica sp. nov., a myxobacterium from soil. Int. J. Syst. Evol. Microbiol.* 67, 472–478. doi: 10.1099/ijsem.0.001655

Muller, S., Strack, S. N., Ryan, S. E., Shawgo, M., Walling, A., Harris, S., et al. (2016). Identification of functions affecting predator-prey interactions between *Myxococcus xanthus* and *Bacillus subtilis. J. Bacteriol.* 198, 3335–3344. doi: 10.1128/JB.00575-16

Navarro-Munoz, J. C., Selem-Mojica, N., Mullowney, M. W., Kautsar, S. A., Tryon, J. H., Parkinson, E. I. (2020). A computational framework to explore large-scale biosynthetic diversity. *Nat. Chem. Biol.* 16, 60–68. doi: 10.1038/s41589-019-0400-9

Nicholls, S. M., Quick, J. C., Tang, S., and Loman, N. J. (2019). Ultra-deep, long-read nanopore sequencing of mock microbial community standards. *Gigascience* 8, giz043. doi: 10.1093/gigascience/giz043

Okoth, D. A., Hug, J. J., Garcia, R., and Muller, R. (2022). Discovery, Biosynthesis and biological activity of a succinylated myxochelin from the myxobacterial strain MSr12020. *Microorganisms* 10, 959. doi: 10.3390/microorganisms10101959

Olivares, P., Ulrich, E. C., Chekan, J. R., van der Donk, W. A., and Nair, S. K. (2017). Characterization of two late-stage enzymes involved in fosfomycin biosynthesis in pseudomonads. *ACS Chem. Biol.* 12, 456–463. doi: 10.1021/acschembio.6b00939

Oliynyk, M., Samborskyy, M., Lester, J. B., Mironenko, T., Scott, N., Dickens, S., et al. (2007). Complete genome sequence of the erythromycin-producing bacterium *Saccharopolyspora erythraea* NRRL23338. *Nat. Biotechnol.* 25, 447–53. doi: 10.1038/nbt1297

Osswald, C., Zaburannyi, N., Burgard, C., Hoffmann, T., Wenzel, S. C., Muller, R., et al. (2014). A highly unusual polyketide synthase directs dawenol polyene biosynthesis in *Stigmatella aurantiaca. J. Biotechnol.* 191, 54–63. doi: 10.1016/j.jbiotec.2014.07.447

Panter, F., Krug, D., and Muller, R. (2019). Novel methoxymethacrylate natural products uncovered by statistics-based mining of the *Myxococcus fulvus* secondary metabolome. *ACS Chem. Biol.* 14, 88–98. doi: 10.1021/acschembio.8b00948

Park, S., Hyun, H., Lee, J. S., and Cho, K. (2016). Identification of the phenalamide biosynthetic gene cluster in *Myxococcus stipitatus* DSM 14675. *J. Microbiol. Biotechnol.* 26, 1636–42. doi: 10.4014/jmb.1603.03023

Perez, J., Contreras-Moreno, F. J., Marcos-Torres, F. J., Moraleda-Munoz, A., and Munoz-Dorado, J. (2020). The antibiotic crisis: how bacterial predators can help. *Comput. Struct. Biotechnol. J.* 18, 2547–2555. doi: 10.1016/j.csbj.2020.09.010

Petters, S., Gross, V., Sollinger, A., Pichler, M., Reinhard, A., Bengtsson, M. M., et al. (2021). The soil microbial food web revisited: predatory myxobacteria as keystone taxa? *ISME J.* doi: 10.1038./s41396-021-00958-2

Phillips, K. E., Akbar, S., and Stevens, D. C. (2022). Concepts and conjectures concerning predatory performance of myxobacteria. *Front. Microbiol.* 13, 1031346. doi: 10.3389/fmicb.2022.1031346

Pistorius, D., and Muller, R. (2012). Discovery of the rhizopodin biosynthetic gene cluster in *Stigmatella aurantiaca* Sg a15 by genome mining. *Chembiochem* 13, 416–26. doi: 10.1002/cbic.201100575

Reichenbach, H., Voelz, H., and Dworkin, M. (1969). Structural changes in *Stigmatella aurantiaca* during myxospore induction. *J. Bacteriol.* 97, 905–11. doi: 10.1128/jb.97.2.905-911.1969

Rogers, T. O., and Birnbaum, J. (1974). Biosynthesis of fosfomycin by *Streptomyces fradiae*. *Antimicrob. Agents Chemother.* 5, 121–32. doi: 10.1128/AAC.5.2.121

Silakowski, B., Kunze, B., Nordsiek, G., Blocker, H., Hofle, G., Muller, R., et al. (2000). The myxochelin iron transport regulon of the myxobacterium *Stigmatella aurantiaca* Sg a15. *Eur. J. Biochem.* 267, 6476–85. doi: 10.1046/j.1432-1327.2000.01740.x

Sood, S., Awal, R. P., Wink, J., Mohr, K. I., Rohde, M., Stadler, M., et al. (2015). *Aggregicoccus edonensis gen.* nov., sp. nov., an unusually aggregating myxobacterium isolated from a soil sample. *Int. J. Syst. Evol. Microbiol.* 65, 745–753. doi: 10.1099/ijs.0.061176-0

Stevens, D. C., Young, J., Carmichael, R., Tan, J., and Taylor, R. E. (2014). Draft genome sequence of gephyronic acid producer cystobacter violaceus strain Cb vi76. *Genome Announc.* 2, 10–128. doi: 10.1128/genomeA.01299-14

van den Belt, M. G., Booth, C., Chooi, T. J., Medema, Y., and Alanjary, M. H. M. (2023). CAGECAT: the comparative gene cluster analysis toolbox for rapid search and visualisation of homologous gene clusters. *BMC Inf.* 24, 1–8. doi: 10.1101/2023.02.08.527634

Vaser, R., Sovic, I., Nagarajan, N., and Sikic, M. (2017). Fast and accurate de novo genome assembly from long uncorrected reads. *Genome Res.* 27, 737–746. doi: 10.1101/gr.214270.116

Veltri, D., Wight, M. M., and Crouch, J. A. (2016). SimpleSynteny: a web-based tool for visualization of microsynteny across multiple species. *Nucleic Acids Res.* 44, W41–W45. doi: 10.1093/nar/gkw330

Wang, C., Lv, Y., Zhou, L., Zhang, Y., Yao, Q., Zhu, H., et al. (2022). Comparative genomics of Myxococcus and Pyxidicoccus, including the description of four novel species: *Myxococcus guangdongensis sp. nov., Myxococcus qinghaiensis* sp. nov., *Myxococcus dinghuensis* sp. nov., *and Pyxidicoccus xibeiensis* sp. nov. *Front. Microbiol.* 13, 995049. doi: 10.3389/fmicb.2022.995049

Wang, J., Ran, Q., Du, X., Wu, S., Wang, J., Sheng, D., et al. (2021). Two new Polyangium species, *P. aurulentum* sp. nov. and *P. jinanense* sp. nov., isolated from a soil sample. *Syst. Appl. Microbiol.* 44, 126274. doi: 10.1016/j.syapm.2021.126274

Waschulin, V., Borsetto, C., James, R., Newsham, K. K., Donadio, S., Corre, C., et al. (2022). Biosynthetic potential of uncultured Antarctic soil bacteria revealed through long-read metagenomic sequencing. *ISME J.* 16, 101–111. doi: 10.1038/s41396-021-01052-3

Wick, R. R., Judd, L. M., Gorrie, C. L., and Holt, K. E. (2017). Completing bacterial genome assemblies with multiplex MinION sequencing. *Microb. Genom.* 3, e000132. doi: 10.1099/mgen.0.000132

Wick, R. R., Judd, L. M., and Holt, K. E. (2019). Performance of neural network basecalling tools for Oxford Nanopore sequencing. *Genome Biol.* 20, 129. doi: 10.1186/s13059-019-1727-y

Witte, S. N. R., Hug, J. J., Geraldy, M. N. E., Muller, R., and Kalesse, M. (2017). Biosynthesis and total synthesis of pyrronazol b: a secondary metabolite from *Nannocystis pusilla*. *Chemistry* 23, 15917–15921. doi: 10.1002/chem.201703782

Xiao, Y., Gerth, K., Muller, R., and Wall, D. (2012). Myxobacterium-produced antibiotic TA (myxovirescin) inhibits type II signal peptidase. *Antimicrob. Agents Chemother.* 56, 2014–21. doi: 10.1128/AAC.06148-11

Xiao, Y., Wei, X., Ebright, R., and Wall, D. (2011). Antibiotic production by myxobacteria plays a role in predation. *J. Bacteriol.* 193, 4626–33. doi: 10.1128/JB.05052-11

Yamamoto, E., Muramatsu, H., and Nagai, K. (2014). *Vulgatibacter incomptus gen. nov.,* sp. nov. *and Labilithrix luteola* gen. nov., sp. nov., two myxobacteria isolated from soil in Yakushima Island, and the description of Vulgatibacteraceae fam. nov., Labilitrichaceae fam. nov. and Anaeromyxobacteraceae fam. nov. *Int. J. Syst. Evol. Microbiol.* 64, 3360–3368. doi: 10.1099/ijs.0.063198-0

Zaroubi, L., Ozugergin, I., Mastronardi, K., Imfeld, A., Law, C., Gelinas, Y., et al. (2022). The ubiquitous soil terpene geosmin acts as a warning chemical. *Appl. Environ. Microbiol.* 88, e0009322. doi: 10.1128/aem.00093-22

Zeng, H., Birkelbach, J., Hoffmann, J., Popoff, A., Volz, C., Muller, R., et al. (2022). Expanding the ajudazol cytotoxin scaffold: insights from genome mining, biosynthetic investigations, and novel derivatives. *J. Nat. Prod.* 85, 2610–2619. doi: 10.1021/acs.jnatprod.2c00637

Zhou, Y., Yi, S., Zang, Y., Yao, Q., and Zhu, H. (2021). The Predatory Myxobacterium *Citreicoccus inhibens gen.* nov. sp. nov. *showed antifungal activity and bacteriolytic property against phytopathogens. Microorganisms* 9, 137. doi: 10.3390/microorganisms9102137

frontiers | Frontiers in Microbiology

TYPE Original Research
PUBLISHED 18 September 2023
DOI 10.3389/fmicb.2023.1250602

OPEN ACCESS

EDITED BY
Masaki Shintani,
Shizuoka University, Japan

REVIEWED BY
Ryosuke Nakai,
National Institute of Advanced Industrial Science and Technology (AIST), Japan
Steven Batinovic,
Yokohama National University, Japan

*CORRESPONDENCE
Gang Hu
✉ hugang@njau.edu.cn
Zhoukun Li
✉ zkl@njau.edu.cn

RECEIVED 30 June 2023
ACCEPTED 28 August 2023
PUBLISHED 18 September 2023

CITATION
Liu L, Xu F, Lei J, Wang P, Zhang L, Wang J, Zhao J, Mao D, Ye X, Huang Y, Hu G, Cui Z and Li Z (2023) Genome analysis of a plasmid-bearing myxobacterim *Myxococcus* sp. strain MxC21 with salt-tolerant property. *Front. Microbiol.* 14:1250602. doi: 10.3389/fmicb.2023.1250602

Genome analysis of a plasmid-bearing myxobacterim *Myxococcus* sp. strain MxC21 with salt-tolerant property

Lin Liu[1], Fengjuan Xu[2], Jinhui Lei[1], Peiwen Wang[1], Lei Zhang[1], Jihong Wang[1], Jingya Zhao[1], Dongmei Mao[2], Xianfeng Ye[1], Yan Huang[1], Gang Hu[2]*, Zhongli Cui[1] and Zhoukun Li[1]*

[1]Key Laboratory of Agricultural Environmental Microbiology, Ministry of Agriculture and Rural Affairs, College of Life Sciences, Nanjing Agricultural University, Nanjing, China, [2]College of Life Sciences, Nanjing Agricultural University, Nanjing, China

Myxobacteria are widely distributed in various habitats of soil and oceanic sediment. However, it is unclear whether soil-dwelling myxobacteria tolerate a saline environment. In this study, a salt-tolerant myxobacterium *Myxococcus* sp. strain MxC21 was isolated from forest soil with NaCl tolerance >2% concentration. Under 1% salt-contained condition, strain MxC21 could kill and consume bacteria prey and exhibited complex social behaviors such as S-motility, biofilm, and fruiting body formation but adopted an asocial living pattern with the presence of 1.5% NaCl. To investigate the genomic basis of stress tolerance, the complete genome of MxC21 was sequenced and analyzed. Strain MxC21 consists of a circular chromosome with a total length of 9.13 Mbp and a circular plasmid of 64.3 kb. Comparative genomic analysis revealed that the genomes of strain MxC21 and *M. xanthus* DK1622 share high genome synteny, while no endogenous plasmid was found in DK1622. Further analysis showed that approximately 21% of its coding genes from the genome of strain MxC21 are predominantly associated with signal transduction, transcriptional regulation, and protein folding involved in diverse niche adaptation such as salt tolerance, which enables social behavior such as gliding motility, sporulation, and predation. Meantime, a high number of genes are also found to be involved in defense against oxidative stress and production of antimicrobial compounds. All of these functional genes may be responsible for the potential salt-toleration. Otherwise, strain MxC21 is the second reported myxobacteria containing indigenous plasmid, while only a small proportion of genes was specific to the circular plasmid of strain MxC21, and most of them were annotated as hypothetical proteins, which may have a direct relationship with the habitat adaptation of strain MxC21 under saline environment. This study provides an inspiration of the adaptive evolution of salt-tolerant myxobacterium and facilitates a potential application in the improvement of saline soil in future.

KEYWORDS

myxobacteria, salt tolerance, social behavior, adaptive evolution, predation

1. Introduction

Myxobacteria are considered unique gram-negative bacteria for their social behavior and complex developmental stages. Up to now, myxobacteria, such as *Myxococcus xanthus*, have emerged as the pre-eminent model system to understand the genetics and molecular mechanisms involved in social behaviors (Kaiser, 2003). As micropredator, myxobacteria are

able to prey on bacteria and fungi and oomycetes in a possible wolf-pack-like manner (Zhang et al., 2023a), while there is accumulating evidence for predatory mechanisms promoting "selfish" behavior during predation as myxobacteria reduce the transport of lytic factors away from the secretor by increasing the size of cell populations without cell cooperation (Berleman et al., 2016). During this process, lytic enzymes, chemical metabolites, and outer membrane vesicles (OMVs) are deduced to be involved in prey killing (Li et al., 2019; Thiery and Kaimer, 2020; Zhang et al., 2023a). Otherwise, myxobacteria are regarded as microbial factories for production of active secondary metabolites and enzymes (Kaur et al., 2018; Li et al., 2022). These characteristics could allow myxobacteria to survive in different condition, which may also find great application in agriculture and biomedicine and environmental protection.

Myxobacteria are globally distributed and prefer non-saline soil and sediments, followed by saline environments, plant rhizospheres and surfaces, and animal secretions, but also minorly appear in host-associated environments (Wang et al., 2021b). Recently, *Myxococcota* species also show predominant roles in activated sludge (Zhang et al., 2023b). This wide distribution enables myxobacteria to play a major role in determining community structures and potential mass circulation (Wang et al., 2021a). However, limited natural species of myxobacteria are explored. It is a common perception that chances for the discovery of resource novelty increase by moving toward rarely screened myxobacteria, such as underexplored species occupying extraordinary habitats or specific ecological niches (Hoffmann et al., 2018). In contrast to isolates from terrestrial soil, saline habitat represents an extreme environment (Zhang et al., 2020), and halophilic or halotolerant myxobacteria from saline habitat are classified as a special myxobacterial group due to their growth characteristics and sociological behavior under saline condition (Zhang et al., 2005).

Up to now, salt-tolerant myxobacteria are mainly isolated from marine samples, such as seawater and sediments, and marine *Myxococcus fulvus* HW-1 has been regarded as a model strain to investigate the adaptation of social behavior of myxobacteria from soil to oceanic conditions (Pan et al., 2010; Li et al., 2011). Investigation of the salt-tolerant mechanism showed that halotolerant myxobacteria are the result of the degenerative adaptation of soil myxobacteria to the marine environment (Zhang et al., 2005), and their salt tolerance is often closely associated with genes of S-motility, two-component system, and outer membrane component (Pan et al., 2009, 2010). The social behavior of marine salt-tolerant myxobacteria under hypersaline environment represents potential evolutional lineage. Compared with marine enviroment, myxobacterial strains from saline–alkaline soil also have been identified with salt tolerance (Zhang et al., 2013), whereas whether the salt-tolerant myxobacteria from terrestrial system adopt the similar adaptation behavior of marine myxobacteria, and similar machanisms are deployed in response to salt remain to be determined.

In the present study, a halotolerant myxobacterium *Myxococcus* sp. strain MxC21 with favorable NaCl tolerance was isolated from forest soil. Strain MxC21 displayed typical social behaviors with the presence of 1% NaCl and also harbored the ability to prey on bacteria. Previous research studies indicated that adenylyl cyclase and Clp/HSP100 family of molecular chaperones (Kimura et al., 2002; Pan et al., 2012), sodium-hydrogen exchange family protein (Bhardwaj et al., 2018), S-motility-related gene locus (Zhang et al., 2007), and two-component system gene Tc105 (Pan et al., 2010) are involved in salt tolerance of myxobacteria, whereas genome-based information is unexplored. To characterize and explore the potential feathers of salt-tolerant strain MxC21, we assembled the chromosome-level genome of strain MxC21, performed a comparative analysis of genomes and functional genes, and highlighted the different metabolic and signal pathways potentially contributing to salt tolerance.

2. Materials and methods

2.1. Myxobacteria isolation and culture condition

The model *M. xanthus* DK1622 was cultured on CTT (1% Casitone, 10 mM Tris-HCl; 0.1 mM PBS; and 8 mM $MgSO_4$, pH 7.6). *Myxococcus* sp. strain MxC21 (GDMCC No:63059) was isolated from saline soil using the rabbit fecal separation method and purified by repeated inoculation onto VY/4 medium (1% yeast cells and 1% $CaCl_2$, w/v, pH 7.0). The obtained isolates were inoculated in LB liquid medium (1% tryptone, 0.5% yeast extract, 0.5% NaCl, and 1% w/v) and cultured overnight at 30°C at 180 rpm. The strain that could grow normally under certain salt concentration was screened and stored at −80°C in glycerol tubes at a final concentration of 16% for further use.

2.2. Isolation and identification of candidate myxobacteria with salt tolerance

Approximately 200 g of soil from Xinjiang province of China was collected from the upper 5–15 cm layer. The samples were air-dried as quickly as possible after collection and stored at room temperature. The myxobacteria isolation with induction of fruiting body formation was performed as described before (Li et al., 2018). In brief, fruiting bodies induced on sterile rabbit dung pellets were transferred to VY/4 medium and incubated at 30°C. The emergence of diffuse colonies was observed after 4–7 days of incubation. The strain from the colony edge was transferred to a new medium, and the procedure was repeated until a pure culture was obtained.

For the phylogenetic analysis, the 16S rRNA gene was amplified using the forward primer 20F (5′-AGAGTTTGATCCTGGCTCAG-3′) and the reverse primer 1500R (5′-GGTACCTTGTTACGACTT-3′). The similarity search of the 16S rRNA gene was performed using BLAST from the NCBI database. Multiple alignments of the sequenced nucleotides were generated, and a neighbor-joining tree was constructed using ClustalX (version 2.0) (Thompson et al., 1997) and MEGA 11 (Kumar et al., 2016).

2.3. Salt tolerance of myxobacterium MxC21

Myxococcus sp. strain MxC21 was cultured in CTT medium at 32°C with the addition of salt when necessary. The effect of sodium chloride (NaCl) on the growth of MxC21 was investigated on CTT agar media with the presence of 0–3% NaCl. Strain MxC21 was cultured on the center of the agar plate and incubated at 30°C for 2 days. Otherwise, strain MxC21 was cultured in CTT liquid medium with 0–2% NaCl at 30°C for 24 h. Due to the clump growth of wild-type myxobacteria in liquid condition, the biomass of strain MxC21 was determined by qRT-PCR. For qPCR, the total DNA of strains from the liquid condition was isolated by liquid nitrogen treatment (AceQ® Universal SYBR qPCR Master Mix, Vazyme Biotech Co., Ltd, China), following the manufacturer's instructions.

2.4. Fruiting body formation and motility assays

Fruiting body formation of strain MxC21 was performed on TPM agar plates (10 mM Tris-HCl, pH 7.6, 1 mM KH_2PO_4, 8 mM $MgSO_4$, and 1.5% Agar), as described before (Skotnicka et al., 2016). In brief, 5 μl of spots containing 5×10^9 cells/ml of strain MxC21 each were placed on TPM agar plates and allowed to develop at 30 °C for 7 days. The fruiting body formation was observed by the formation of aggregates with a stereo microscope (Nikon SMZ1270). Otherwise, 2 μl of spot containing 5×10^9 cells/ml strain MxC21 was spotted onto the CTT plate containing 0.3% agar and 1.5% agar with the presence of 0–1.5% NaCl. The plates were incubated at 32°C for approximately 2–3 days. A- and S-motility were analyzed by observing the colonies for expansion *via* a Nikon SMZ1500 stereo microscope.

2.5. Submerge cultural assay

Cells in CTT liquid medium at the mid-exponential phase were washed with ice-cold MOPS buffer (10 mM 3-(N-morpholino)-propanesulfonic acid, 1 mM $CaCl_2$, 1 mM $MgCl_2$, and pH6.8). The washed cells were resuspended to a final concentration of 5×10^9 cells/ml, and 2 ml of samples were transferred to the 24-well plates with the presence of 0–1.5% NaCl, followed by incubation at 32°C for 4–6 days without shaking, and the aggregations from different treatments were observed (Mironenko et al., 2020).

2.6. Predation assays

After activated growth on an agar plate at 30°C for 2 days, strain MxC21 was cultured in 50 ml CTT liquid medium at 30°C for 16 h. *Escherichia coli* was grown in an LB medium to an OD600 of 1.0. Then, the bacterial cells were collected by centrifugation at 10 000×g for 3 min and washed with TPM buffer three times (10 mM Tris-HCl, pH 7.6, 1 mM KH_2PO_4, and 8 mM $MgSO_4$), followed by resuspending in TPM buffer to an OD_{600} value of 40. To identify the effects of NaCl on the predation of strain MxC21, 2 μl or 200 μl of *E. coli* cells was placed in a TPM plate with the presence of NaCl and allowed to dry. Then, 2 μl of strain MxC21 was placed into the center or the edge of the *E. coli* prey colony. After incubation at 30°C for 2–3 days, spots were harvested with a loop and resuspended in 200 μl of TPM buffer. The number of surviving prey cells was counted by serial dilution on LB agar plates, on which strain EGB did not grow.

2.7. Whole-genome sequencing and functional annotation

The genome of strain MxC21 was sequenced using DNBSEQ and Nanopore platform at the Beijing Genomics Institute (BGI, Shenzhen, China). Short and long reads were obtained using the DNBSEQ (MGI) and the Nanopore platforms, respectively, of which the DNBSEQ (MGI) reads provided 1424.5-fold coverage and the Nanopore reads provided 300.2-fold coverage. The DNBSEQ sequencing generated 1,310 Mb of data, and the Nanopore platform sequencing produced 2.7 Gb of data. The data were subjected to quality control using SOAPnuke (v1.5.6; parameter, -l20-q40% -n10% -d) and Porechop (v0.2.4; default parameters) software. The program Canu (version 1.5 available at https://github.com/marbl/canu/releases; parameter, estn=24, npruseGrid=0corOvlMemory=4) was used for self-correction. Draft genomic unities were assembled using the Canu, a high-quality corrected circular consensus sequence subread set, and they are uncontested groups of fragments. To improve the accuracy of the genome sequence analysis, GATK (version 1.6–13 available at https://www.broadinstitute.org/gatk/; parameter, -cluster 2 -window 5 -stand_call_conf 50 -stand_emit_conf 10.0 -dcov 200 MQ0>=4) was used to make single-base corrections. The complete genome sequence of strain MxC21 was submitted to the NCBI GenBank with the accession number CP123278-CP123279. Gene prediction and functional annotation were performed by the online platform Rapid Annotation using Subsystem Technology (RAST) (Aziz et al., 2008; Sutton et al., 2019). To run the Cluster of Orthologous Group (COG) annotation, only the best blast hit was retained for each protein (Tatusov et al., 2000).

2.8. Quantitative PCR (RT-qPCR)

To evaluate the effects of salt on the growth of strain MxC21 in CTT medium, the gene expression levels of several key genes about the two-component system and phosphotransferase proteins and CRISPR-Cas were determined. The total RNA was extracted from the strains with different treatments using a HiScript III All-in-one RT SuperMix Perfect (Vazyme Biotech Co., Ltd, China). The total RNA was reverse-transcribed into cDNA using HiScript II QRT SuperMix for qPCR (Vazyme Biotech Co., Ltd, China) and used as a template for real-time quantitative reverse transcription-PCR (qRT-PCR) with Power SYBR Green PCR Master Mix (ABI). In total, 2 μl of the obtained cDNA solution was diluted 2-fold and mixed with specific primers (Supplementary Table S1) and AceQ® Universal SYBR qPCR Master Mix (Vazyme Biotech Co., Ltd,

China). The thermal cycling conditions for cDNA amplification involved an initial denaturation step at 95°C for 5 min, 40× (95°C for 10 s and 60°C for 34 s), 95°C for 15 s, and a final melting curve (65–95°C, 0.5°C increment, for 5 s). All real-time quantitative PCR amplifications were run on the Applied Biosystems 7500 Real-Time PCR system. Gene expression values were calculated, relative to the housekeeping gene *rpoB*, by using the $^{\Delta}\Delta$Ct method.

2.9. Comparative genomic analysis

To conduct a comparative genomic analysis of strain MxC21 with the other related myxobacterial species, the genome sequences of 10 species belonging to the genus *Myxococcus* were retrieved from the NCBI database (Supplementary Table S1). Predicted protein sequences for nine species were selected to perform the all-vs.-all blastp analysis with a cutoff value of 1×10^{-5}. Then, blast scores were delivered to the MCL Markov clustering program with an inflation parameter of 2, resulting in rapid clustering of orthologous groups (Gibbons et al., 2015). Core proteome, dispensable proteome, and unique proteome were defined as proteins conserved in all the 9 *Myxococcus* genomes, 2–10 *Myxococcus* genomes, and only exist in the individual genome, respectively.

2.10. Phylogenetic analysis

Whole-genome phylogeny was performed to confirm the taxonomic classification. Based on the clustering results of orthologous proteins, we randomly selected 135 single-copy genes that conserved in all nine species (Edgar, 2004; Zhao et al., 2021). Alignments of the concatenated sequences of 135 single-copy genes were generated by the Muscle algorithm, and then, the phylogenetic tree was constructed by the neighbor joining algorithm with 1,000 bootstrap replicates in MEGA11 (Kumar et al., 2016). The synteny of *Myxococcus* sp. strain MxC21 genome and other bacterial genomes was determined using BLAST and Artemis Comparison Tool (ACT) (Carver et al., 2005). Otherwise, taxonomic annotations of the genomes were conducted with the toolkit GTDB-Tk v.1.4.0, according to the Genome Taxonomy Database (GTDB) (Parks et al., 2022). The average nucleotide identity (ANI) between genomes was counted using OrthoANI software (Yoon et al., 2017). The digital DNA–DNA hybridization (dDDH) values were calculated using the GGDC server with the recommended formula 2 (Meier-Kolthoff et al., 2013).

2.11. Statistical analysis

All experiments in the study were performed in triplicate with similar results, and the statistical significance was performed using Duncan's multiple comparisons test in SPSS 20.0 (IBM Inc., Chicago, IL, USA). The analytic results were expressed as mean values with standard deviations, and differences with $p < 0.05$ were considered statistically significant.

2.12. Data deposition

The whole-genome shotgun project was deposited in the NCBI/DDBJ/EMBL database under the accession number of CP123278-CP123279.

3. Results

3.1. Isolation of myxobacteria MxC21 with salt tolerance

Using rabbit dung as the bait, 15 myxobacteria were isolated from forest soil in Xinjiang province *via* induction of fruiting body formation. The isolated strains were screened for their ability to grow in CTT medium with the presence of 1% NaCl (w/v). Among these isolates, strain MxC21 was selected as a promising salt-tolerant agent. Orange fruiting bodies were observed after induction by sterilized rabbit dung pellets for 3–4 days (Figure 1A). Moreover, strain MxC21 was a gram-negative bacterium with rod-shaped cell lacking flagella. To identify the salt-tolerant growth, strain MxC21 was cultured on the CTT agar plates containing NaCl with different concentrations (0–3%, w/v) (Figure 1B). The results showed that strain MxC21 tolerates NaCl concentrations as high as 1.5%, while growth inhibition of strain MxC21 was observed when the NaCl concentrations increased to 2% (Figure 2B). MxC21 cells clumped substantially in a liquid medium; we failed to determine the cell numbers by serial dilution. Hence, the biomass of strain MxC21 was qualified by qPCR. Strain MxC21 was able to grow in a liquid CTT medium containing 1.5% NaCl with maximal biomass, and limited growth with reduced biomass was identified with 2% NaCl (Figure 1C). This is consistent with the swarming growth of strain MxC21 on the CTT agar plate. These results indicate that wild myxobacterial isolate MxC21 from terrestrial soil can tolerate higher concentrations of NaCl with superior salt tolerance characteristics.

3.2. Social behavior and predation of MxC21 under salt condition

Social behavior of myxobacteria on solid surfaces is strongly affected by the salinity (Zhang et al., 2005), and the effects of NaCl on the development and motility of strain MxC21 were investigated. On the TPM agar plate containing 0.5% NaCl, typical development was observed after 3 days of inoculation. Whereas the number of fruiting bodies decreased, and consequently, few myxospores were produced with the concentration of NaCl increased to 1%. In total, 1.5% NaCl prevented the aggregation and sporulation of strain MxC21 (Figure 2A). Motility observation showed that 1% NaCl exhibits no effects on the A- and S-motility of strain MxC21, while obvious deficiency was observed for the motility of strain MxC21 when the concentration of NaCl increased to 1.5% (Figure 2A). These results are similar to the behavior of salt-tolerant strains HW-1 and DK1622 in response to different concentrations of NaCl or seawater (Pan et al., 2009).

The presence of biofilm surrounding bacterial cells confers protection against stress (Saidi et al., 2022). To determine the

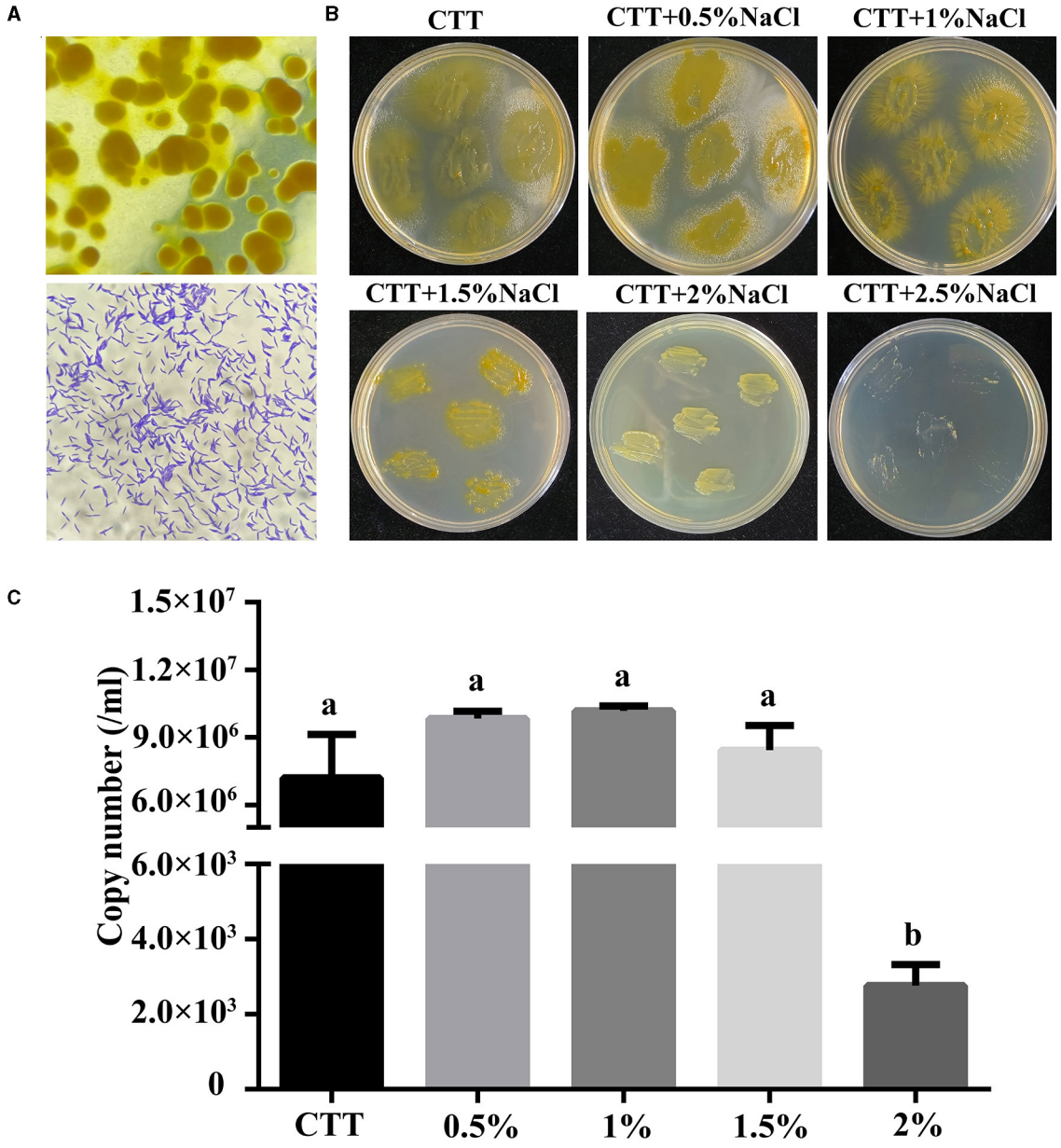

FIGURE 1
Salt-tolerant characteristics of strain MxC21. **(A)** Fruiting body formation and micrograph of strain MxC21 cells (1,000 ×); **(B)** salt-tolerant growth of strain MxC21 on CTT agar plates; **(C)** biomass analysis of strain MxC21 by qPCR. Error bars denote st. dev. (SD), and values with different letters indicate statistically significant differences ($p < 0.05$).

effects of salt on the biofilm formation of strain MxC21, the submerged cultures in 24-well plates were performed. As shown in Figure 2B, after incubation in MOPS buffer, biofilm formation was observed for strain MxC21 with the presence of 0.5–2.5% salt. This result indicates that strain MxC21 reserves the ability to produce extracellular matrix polysaccharide under salt conditions, which may be important for its salt tolerance and social behavior in a saline environment.

The predatory ability of strain MxC21 was also assessed under different salt conditions. Strain MxC21 was incubated onto (Figure 3A) or close to (Figure 3C) the colony of *E. coli* on TPM plates, and the swarming growth of strain MxC21 was obviously observed with prey *E. coli* as the sole nutrition with the presence of NaCl (0.5% and 1%). The predatory performance was assessed by counting the number of surviving cells of prey *E. coli* encountered by the expanding swarm of strain MxC21, which significantly decreased after the swarming predation when strain MxC21 was incubated onto (Figure 3B) and close to (Figure 3D) the colony of prey with the presence of NaCl (0.5 and 1%). These results indicate that strain MxC21 is able to feed on the bacteria prey under a saline environment. However, when the concentration of NaCl increased to 1.5%, strain MxC21 was unable to prey on bacteria (Figure 3), which was consistent with the motility deficiency (Figure 2). We deduced that

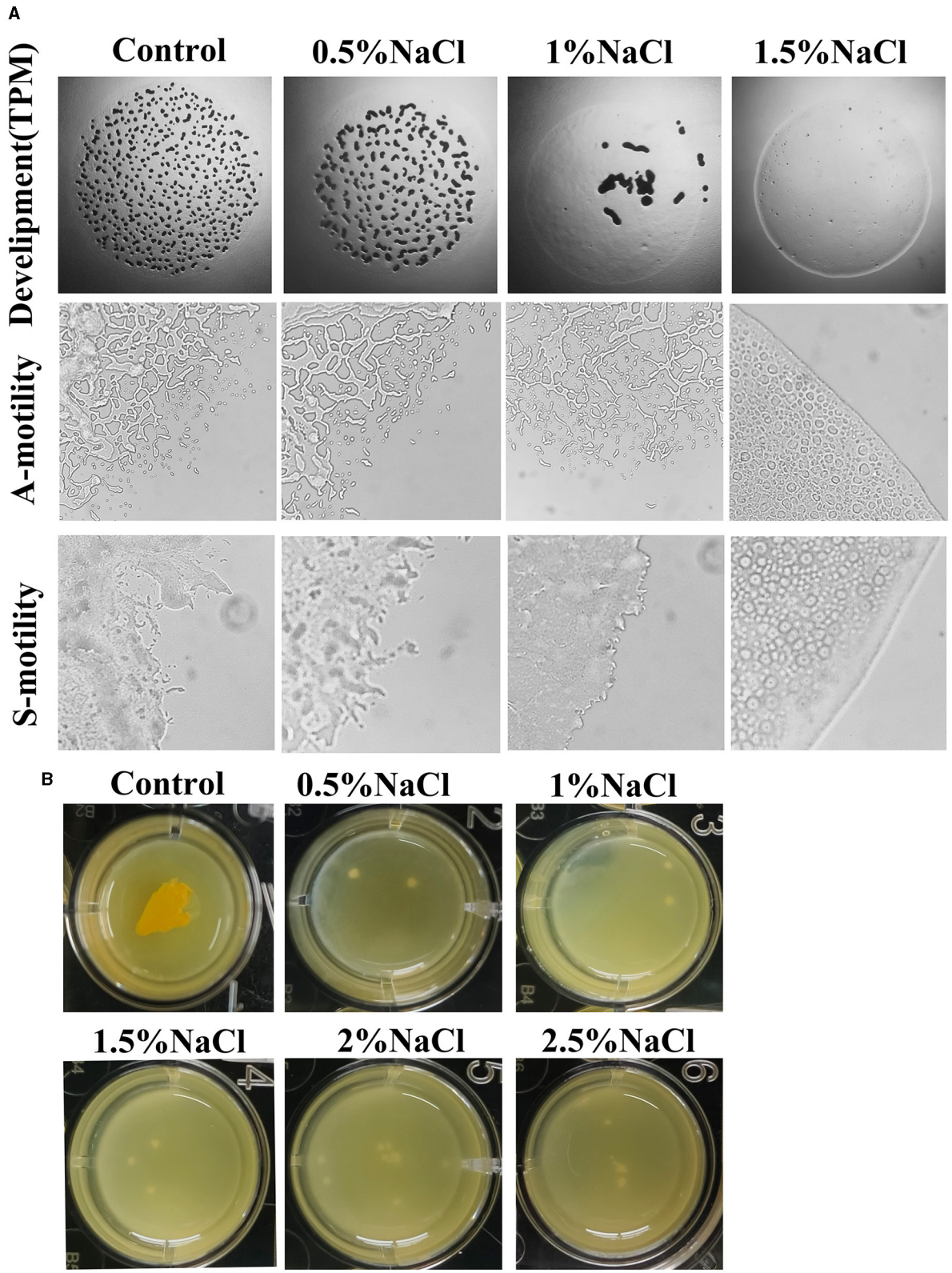

FIGURE 2
Effects of salt on the fruiting body formation and motility **(A)** and biofilm formation **(B)** of strain MxC21. The used concentration of NaCl is 0.5%, 1%, 1.5%, 2%, and 2.5% when necessary, and cultures without NaCl are used as control.

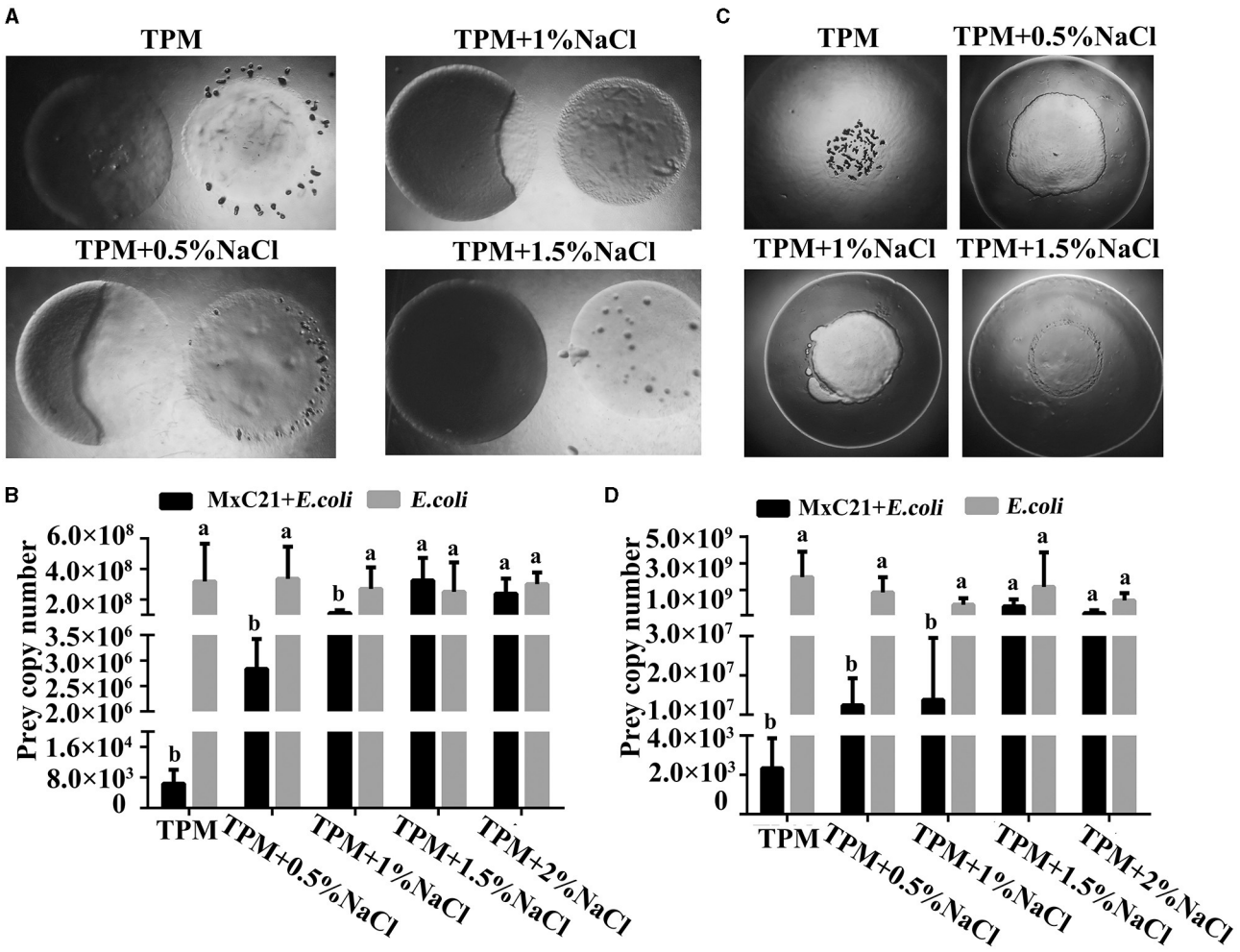

FIGURE 3
Effects of salt on the predation of strain MxC21. Strain MxC21 is cultured onto **(A)** or close to **(C)** the colony of *E. coli* on TPM plates with the presence of 0.5%, 1%, and 1.5% NaCl, and TPM plates without NaCl are used as control. **(B, D)** The viable cells of *E. coli* from the co-cultural assay **(A, C)** are also identified, respectively. The lowercases indicate the statistically significant differences ($p < 0.05$).

strain MxC21 harboring the predatory ability is essential for its environmental adaptation.

3.3. Genome sequence assembly and general features

The genome of strain MxC21 was sequenced using a hybrid strategy that combined sequences from Nanopore long reads and DNBSEQ short reads. The genome was assembled as a single circular chromosome of 9.41 Mbp with a high GC content of 69.13% (Figure 4A), and a circular plasmid of 64.3 kb with a GC content of 65.62% was also identified based on the genome sequence assembly (Figure 4B). Subsequently, RAST-based annotation has identified 9584 coding genes in the strain MxC21 genome, and 50.17% of the proteins were functionally annotated, while the remaining proteins (49.83%) were hypothetical proteins or proteins with unknown function. The identified indigenous plasmids in strain MxC21 were the second reported plasmid from myxobacteria; 68 coding genes in the strain MxC21 plasmid were identified, while 64 proteins were annotated as hypothetical proteins, and other 4 proteins were predicted as serine/threonine protein kinase, chromosome segregation protein, DNA repair protein, and DNA primase (Supplementary Table S3). The detailed functions and their potential relationship with the salt tolerance of strain MxC21 need further research. Otherwise, 31 ncRNAs were identified as clustered regularly interspaced short palindromic repeat (CRISPR) RNA direct repeat elements, which may provide acquired resistance against bacteriophages. These results indicated that the abundance of protein corresponding to signal transduction and regulation is possibly involved in the salt responses in myxobacteria with salt tolerance.

3.4. Taxonomic affiliation

Strain MxC21 was first identified as *Myxococcus* sp. and closely related to *M. xanthus* based on the phylogenetic analysis

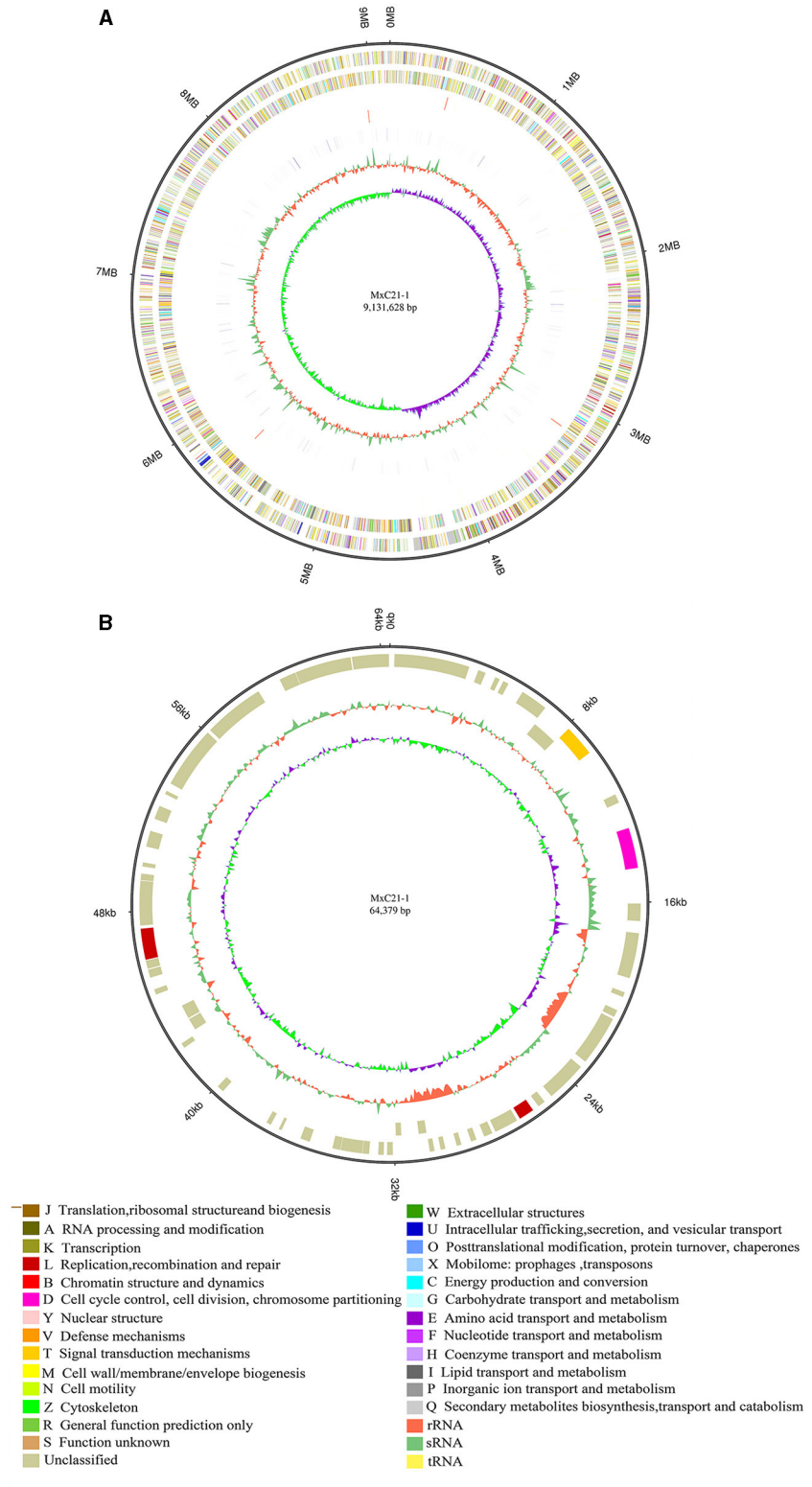

FIGURE 4
Circular representation of the complete genome **(A)** and plasmid **(B)** of strain MxC21. The outermost circle is the coordinate of the genome position. The corresponding circles from outside to the inside represent COG annotation gene distribution of the forwarding strand, COG annotation of the reverse strand, ncRNA distribution of the forwarding strand, and ncRNA distribution of the reverse strand, which depict the GC content and the GC skew, respectively.

of the 16S rRNA gene. However, the polyphyletic nature of myxobacteria taxa makes its classification very difficult, according to the 16S rRNA gene analysis. To further establish the phylogenetic relationship of strain MxC21 with other related *Myxococcus* species, the phylogenetic tree was constructed using the concatenated sequences of 135 single-copy genes, which were conserved in all the analyzed genomes. As shown in Figure 5A, *Myxococcus* species grouped into two major clades, namely groups A and B. Strain MxC21 was located in the clade Group A clustering closely with *M. xanthus* DK1622. DK1622 is a model organism for studying bacterial social behaviors due to the feasible genetic manipulation. Hence, the alignment of three chromosomal sequences of strain MxC21, *M. xanthus* DK1622, and *C. coralloides* DSM 2259 was analyzed using ACT software. As shown in Figure 5B, strain MxC21 exhibited relatively high synteny with *M. xanthus* DK1622 but poor synteny with significant rearrangements from the genome comparison of strains MxC21 and DSM 2259. Meanwhile, the abundance of inverted matching regions was also observed between strains MxC21 and DK1622, although the two strains shared consistent phylogenetic lineage.

As a category of computational analysis, average nucleotide identity (ANI) is commonly used to define species boundaries, along with digital DNA–DNA hybridization (dDDH) (Kim et al., 2014). To further determine the evolutional lineage, the ANI and dDDH values between the above genomes were calculated. As shown in Table 1, all the ANI values ranged from 78.1% to 97% between the *Myxococcus* genomes. Meanwhile, strain MxC21 exhibited 97% ANI values and 73.5% dDDH values with *M. xanthus* DK1622 (Table 1), which was consistent with the phylogenetic relationship (Figure 5A). However, combining the linear genomic comparison and the low dDDH values indicates the possibility of strain MxC21 as a novel species within *Myxococcus* genus. Considering the high genome synteny of the genomes of strains MxC21 and DK1622, we provided a phylogenetically consistent and rank-normalized genome-based taxonomy by GTDB-Tk, according to the Genome Taxonomy Database (GTDB) based on approximately 120 marker genes. The result showed that strains MxC21 and DK1622 share similar evolutionary lines (Supplementary Figure S1). However, whether strain MxC21 belongs to members of *Myxococcus xanthus* needs more evidence.

3.5. Genomic evidence for signal transduction and regulation

In response to high salinity stress, plants and microbes undergo a stress adaptive response and regulate a variety of genes whose products are involved in signal transduction, transcriptional regulation, and induction of stress tolerance by efficient protein folding involved in salt tolerance (Ayaz et al., 2022). Considering the salt tolerance characteristics of strain MxC21, we further analyzed the genes involved in signal transduction and regulation referring to the sequenced genome, as shown in Table 2. Strain MxC21 contains 285 two-component systems, 99 Ser/Thr kinases, 26 one-component systems, 235 transcription factors, and 121 histidine kinases, which mediate dominant response to a wide array of physiological changes, such as salinity stress (Pan et al., 2009). Otherwise, 26 one-component system proteins linking environmental signals to cellular responses were also identified. Otherwise, the genome of strain MxC21 contains 18 phosphotransferase proteins, higher than other *Myxococcus* species. Phosphotransferase proteins are group translocators that catalyze the uptake of hexoses or hexose derivatives and mediate cellular stress tolerance (Jamal et al., 2013). Considering the non-salt tolerance of the other *Myxococcus* species except for *M. xanthus* DK1622 and *M. fulvus*, the abundance of phosphotransferase proteins in strain MxC21 represents a potential function in environmental adoption.

3.6. Gene expression profiles of the signal response to the presence of salt

Adaptation of bacteria to the prevailing environmental stress is often mediated by regulatory proteins, which have essential functions in the sensing of external and self-generated signals in bacteria and the generation of appropriate output responses. The abundance of the two-component system and phosphotransferase proteins in the genome of strain MxC21 indicates the potential function in environmental adoption. To determine the response of these proteins toward salt stress, the expression levels of the representative 6 TCS and 4 phosphotransferase coding genes from strain MxC21 were studied with the presence of 1% NaCl. As shown in Figure 6, the presence of salt increased the gene transcript levels of all the 6 TCSs (Figure 6A) and 4 phosphotransferases (Figure 6B) of strain MxC21. These results indicate that these proteins corresponding to signal transduction and regulation are possibly involved in the salt responses of salt-tolerant myxobacteria. Otherwise, to identify whether CRISPR-Cas is active during growth under a saline environment, the expression levels of the representative 6 CRISPR-Cas genes in strain MxC21 were studied with the presence of 1% NaCl. As shown in Figure 6C, salt concentration promotes the gene transcript levels of all 4 CRISPR-Cas genes, indicating the active states of these genes from strain MxC21 in response to salt.

4. Discussion

Myxobacteria are ubiquitous micropredators that possess the capability to feed on a broad range of soil bacteria and fungi and oomycetes (Livingstone et al., 2017; Li et al., 2019; Zhang et al., 2023b), which are regarded as promising biocontrol agents for biocontrol of plant diseases (Ye et al., 2020; Luo et al., 2022). Myxobacteria have been considered as terrestrial bacteria, and abundant isolates of myxobacteria have been collected from soil environments. However, global geographic distribution showed that myxobacteria are one of the most diverse bacterial groups on earth with preferred appearances in non-saline soil and sediments, followed by saline environments (Wang et al., 2021b), whereas salt-tolerant myxobacteria have received less attention due to the limited resources and their adjustment to saline environments. Up to now, several myxobacteria with salt-tolerant properties have been isolated from seawater and

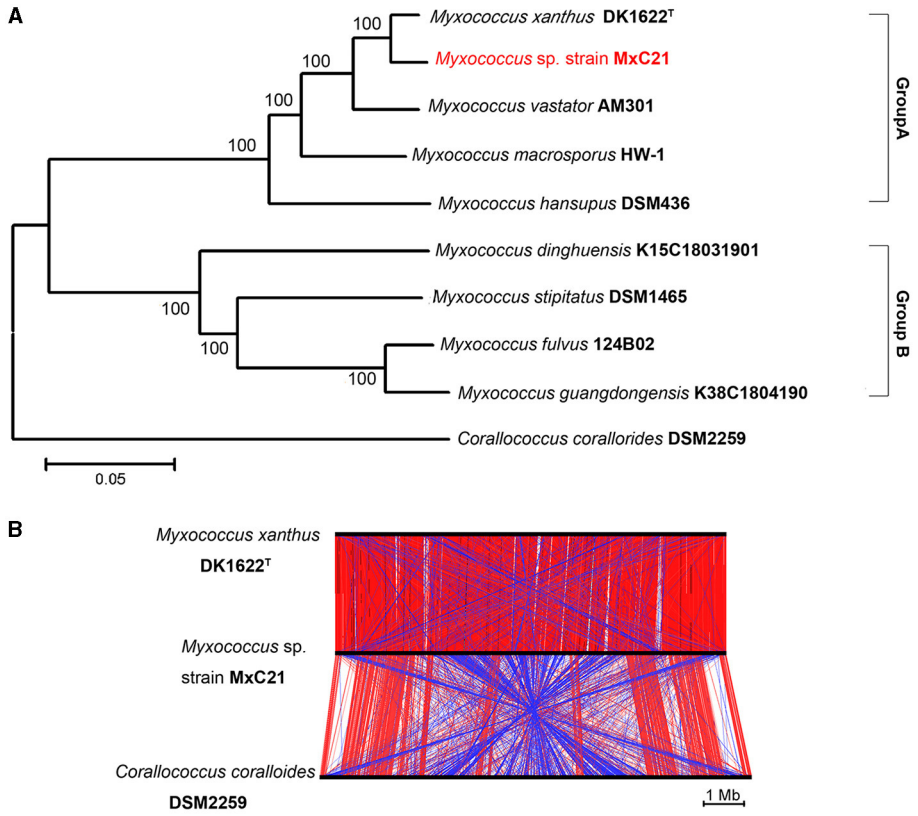

FIGURE 5
Phylogenetic relationships of strain MxC21 and related myxobacteria. **(A)** Construction of phylogenetic tree by the neighbor-joining algorithm with concatenated sequences of 135 single-copy genes. **(B)** Linear genomic comparison of strain MxC21, *M. xanthus* DK1622, and *C. coralloides* DSM 2259. The red lines represent matching regions, and the blue lines denote inverted matching regions.

TABLE 1 ANI and dDDH values for pairwise comparisons between *Myxococcus* species and *C. coralloides* DSM 2259.

dDDH\ANI	MxC21	Mxan	Msti	Mful	Mhan	Mdin	Mgua	Mvas	Ccor
MxC21	100.0	97.0	79.9	80.3	87.2	80.6	80.3	93.6	78.4
Mxan	73.5	100.0	79.8	80.3	87.1	80.5	80.2	93.5	78.2
Msti	22.5	22.3	100.0	83.6	79.7	81.9	83.4	80.2	78.1
Mful	22.9	22.9	26.5	100.0	80.1	82.7	94.1	80.7	78.6
Mhan	32.1	31.9	22.2	22.8	100.0	80.3	80.1	87.3	78.4
Mdin	23.3	23.2	24.6	25.4	23.1	100.0	82.3	80.9	78.9
Mgua	22.8	22.7	26.2	54.8	22.7	25.2	100.0	80.7	78.4
Mvas	52.8	52.8	23.0	23.5	32.9	23.8	23.5	100.0	79.0
Ccor	21.4	21.2	20.9	21.2	21.2	21.7	21.2	21.9	100.0

Average nucleotide identity (ANI) values (above) and digital DNA–DNA hybridization (dDDH) values (below) are present. Mxan, Myxococcus xanthus DK1622 (NC_008095.1); Msti, Myxococcus stipitatus DSM 14675 (NC_020126.1); Mful, Myxococcus fulvus 124B02 (CP006003); Mhan, Myxococcus hansupus strain DSM 436 (NZ_CP012109.1); Mdin, Myxococcus dinghuensis K15C18031901 (NZ_JAKCFB000000000.1); Mgua, Myxococcus guangdongensis K38C18041901 (NZ_JAJVKW000000000.1); Mvas, Myxococcus vastator AM301 (NZ_JAAIYB000000000.1); Ccor, Corallococcus coralloides DSM 2259 (NC_017030.1).

sediments, and their predatory behavior under saline environment is largely unknown. In this study, we identified that a halotolerant *Myxococcus* sp. strain MxC21 isolated from forest soil displays typical social behaviors and predatory ability with the presence of 1% NaCl, and complex metabolic and signal pathways relating to salt tolerance were revealed by comparative genome and functional gene analysis. Salt-tolerant strain MxC21 represents fresh insight into the adaptive evolution of myxobacteria under terrestrial environment.

Salt-tolerant myxobacteria have been screened from marine enviroment, which mainly belong to the genus *Myxococcus* (Wang et al., 2007). Usually, terrestrial myxobacteria are salt

10.3389/fmicb.2023.1250602

TABLE 2 Variability in the numbers of regulatory genes among the *Myxococcus* species.

	MxC21	Mxan	Msti	Mful	Mhan	Mdin	Mgua	Mvas	Ccor
Ser/Thr kinases	99	99	111	100	94	113	108	113	107
Two-component system	285	282	296	322	301	315	329	294	305
Histidine kinase	121	141	153	168	159	167	175	149	162
Phosphotransferase protein	18	4	3	4	2	4	3	7	2
Response regulator	146	137	140	150	140	144	151	138	141
Transcription factor	235	270	372	400	295	378	404	256	351
One-component system	26	40	77	75	55	65	71	38	79
Response regulator	35	49	60	61	54	62	62	43	49
Sigma factors	51	56	67	72	48	63	67	52	56
Transcriptional regulators	123	125	168	192	138	188	204	123	167

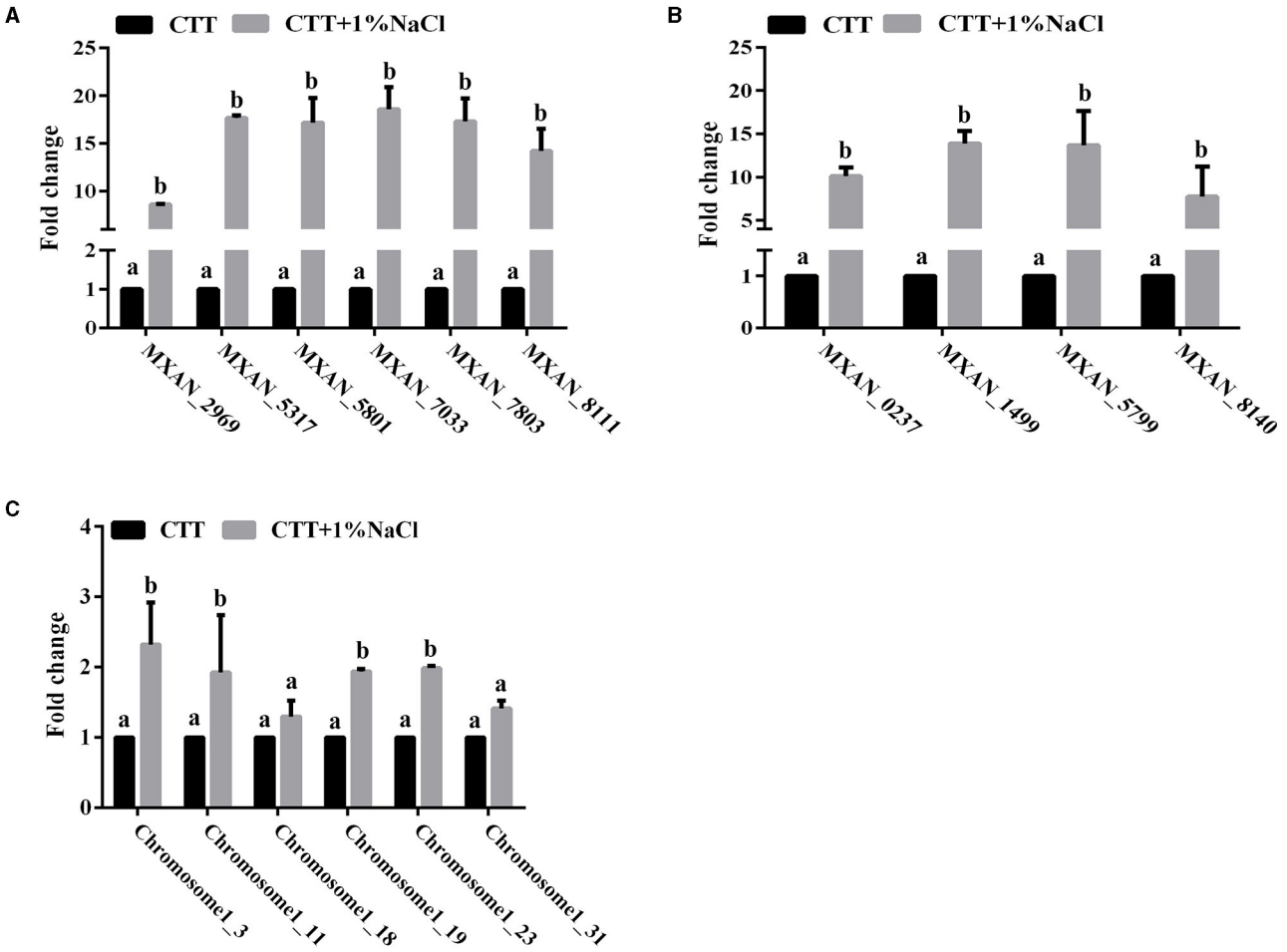

FIGURE 6
Expression profiles of the representative 6 TCS **(A)**, 4 phosphotransferase **(B)**, and 6 CRISPR-Cas **(C)** coding genes from strain MxC21 with the presence of 1% NaCl. The 6 TCS coding genes from strain MxC21 are MXAN_2969, MXAN_5317, MXAN_5801, MXAN_7033, MXAN_7803, and MXAN_8111; the 4 phosphotransferase coding genes from strain MxC21 are MXAN_0237, MXAN_1499, MXAN_5799, and MXAN_8140. The lowercases indicate the statistically significant differences ($p < 0.05$). The locations of the 6 CRISPR-Cas in chromosome of strain MxC21 are 1-3, 1-11, 1-18, 1-19, 1-23, and 1-31.

sensitive and cannot grow at NaCl concentration higher than 1%, while genera of *Myxococcus*, *Cystobacter*, *Corallococcus*, *Sorangium*, *Nannocystis,* and *Polyangium* isolated from saline–alkaline soils also exhibit efficient growth with 1% NaCl (Zhang et al., 2013). *Myxococcus* sp. strain MxC21 isolated from forest soil exhibits favorable salt tolerance with 1.5% NaCl. Meantime, strain MxC21 still displays typical social behaviors such as motility and fruiting body formation with the presence of 1% NaCl. Commonly, colony expansion and development are restricted with increasing salt concentration, while the fruiting body structure of strain MxC21 was still completed under salt condition, but the number of fruiting bodies decreased. This is consistent with wild-type strain DK1622 (Pan et al., 2009). Previous research showed that horizontally transferred gene *Hdsp* is required for social behavior and halotolerance of *Myxococcus* strain during the adaptive evolution from terrestrial environment to liquid habitat (Pan et al., 2010). However, this gene is absent in genomes of strains MxC21 and DK1622, indicating that salt-tolerant soil myxobacteria present different lifestyles compared with marine isolates. Research studies of salt-tolerant myxobacteria indicate the potential adaptive evolution of myxobacteria from the terrestrial environment to liquid habitat, as social behaviors such as development and motility, which are important feathers for soil habitat, are lost in the liquid living environment. However, loss of social behaviors by *M. xanthus* after 1,000 generations of evolution in a liquid habitat is also identified (Velicer et al., 1998), which raises the question of what is the role of salt during the evolution. The social behavior of strain MxC21 with the presence of 1% NaCl may inspire us to perform further study.

Genome sequencing of halotolerant *Myxococcus* is able to get a full picture of the evolutionary trial. In this study, we reported the complete genome sequence and functional annotation of strain MxC21. The phylogenetic tree is constructed based on the 135 single-copy genes, which indicate that strain MxC21 belongs to Group A of *Myxococcus* genus, closer to *M. xanthus* DK1622. However, linear genomic comparison and dDDH and ANI values revealed that strain MxC21 exhibits insufficient genomic similarity with the existing *Myxococcus* species, especially DK1622. Otherwise, HW-1 is a model myxobacterium for investigation of the social behavior from soil to oceanic condition (Pan et al., 2010; Li et al., 2011). Except for AM301 and DSM436, DK1622, HW-1, and MxC21 (Group A) all tolerate 1% NaCl during growth, indicating potential adaptation to salinity soil. Otherwise, biofilm formation is a common mechanism for surviving environmental stress (Kumar et al., 2016), and strain MxC21 reserves the abilities of predation and biofilm formation with the presence of 1% NaCl, which promotes the adaption to different habitats and thereby keeps population competition of myxobacteria.

Circular plasmid pMF1 from *M. fulvus* strain 124B02 is the first reported indigenous autonomously replicating plasmids from myxobacteria (Zhao et al., 2008), which raises the question of whether similar plasmids are present in myxobacteria. In strain MxC21, we found a circular plasmid of 64.3 kb according to genome sequence assembly, whereas strains MxC21 and 124B02 were distributed into different groups, indicating different functions of the plasmids. pMF1 from strain 124B02 has been identified to participate in natural genetic transformation (Zhao et al., 2008), and plasmid-mediated horizontal gene transfer (Li and Zhang, 2023) and pollutant degradation (Qin et al., 2015) were also identified. The appearance of indigenous plasmids in strain MxC21 may encourage us to consider their ecological function during the adaptive evolution of myxobacteria in a specific habitat.

Two-component systems and outer membrane proteins were involved in response to salt tolerance of *Myxococcus* cells (Pan et al., 2009), and adenylyl cyclase and Clp/HSP100 family of molecular chaperones were deduced to function in signal transduction during osmotic stress (Kimura et al., 2002; Pan et al., 2012). Genome analysis showed that the abundance of the two-component system and phosphotransferase proteins distributed in the genome of strain MxC21. In response to salt stress, expression levels of the representative genes encoding 6 TCSs and 4 phosphotransferases from strain MxC21 were significantly upregulated. The multifunctionality of these proteins involving signal transduction may enable myxobacteria to efficiently use cellular resources and acclimate to various environmental conditions.

5. Conclusion

In this study, a salt-tolerant myxobacterium *Myxococcus* sp. MxC21 was isolated from forest soil, which reserved predatory ability and social behaviors with the presence of 1% NaCl. Terrestrial myxobacteria are able to prey on bacteria under salt conditions, and diverse survival strategies enable myxobacteria to keep high environmental abundance. Phylogenomic analysis showed that strain MxC21 exhibits a phylogenetic relationship and diversity compared with other *Myxococcus* species. Strain MxC21 consists of a circular chromosome with a total length of 9.13 Mbp and a circular plasmid of 64.3 kb with abundant hypothetical proteins. Considering the wide distribution of proteins associated with signal transduction, transcriptional regulation, and protein folding, we deduce that strain MxC21 exhibits diverse niche adaptation toward different environments. The present study provides a preliminary inspiration for the social behaviors of salt-tolerant myxobacteria and the recognition of the adaptive evolution of myxobacteria. However, further investigations are required to investigate the underlying mechanisms.

Data availability statement

The data presented in this study are deposited in the NCBI GenBank repository under accession number PRJNA956062.

Author contributions

LL designed the experiments and performed the experiments. FX, PW, and LZ performed the experiments. JW, JZ, DM, XY, and YH analyzed the data. GH and ZC revised the manuscript. ZL wrote the manuscript and was responsible

for the funding support. All authors read and approved the final manuscript.

Funding

This study was supported by the National Natural Science Foundation of China (32270066, 32070027, and 32170123) and the Fundamental Research Funds for the Central Universities (YDZX2023014).

Acknowledgments

The authors would like to thank Assistant Professor Danyu Shen (Nanjing Agricultural University) for the genome analysis.

Conflict of interest

The authors declare that the research was conducted in the absence of any commercial or financial relationships that could be construed as a potential conflict of interest.

Publisher's note

All claims expressed in this article are solely those of the authors and do not necessarily represent those of their affiliated organizations, or those of the publisher, the editors and the reviewers. Any product that may be evaluated in this article, or claim that may be made by its manufacturer, is not guaranteed or endorsed by the publisher.

Supplementary material

The Supplementary Material for this article can be found online at: https://www.frontiersin.org/articles/10.3389/fmicb.2023.1250602/full#supplementary-material

References

Ayaz, M., Ali, Q., Jiang, Q., Wang, R., Wang, Z., Mu, G., et al. (2022). Salt tolerant bacillus strains improve plant growth traits and regulation of phytohormones in wheat under salinity stress. *Plants (Basel).* 11, 2769. doi: 10.3390/plants11202769

Aziz, R. K., Bartels, D., Best, A. A., DeJongh, M., Disz, T., Edwards, R. A., et al. (2008). The RAST Server: rapid annotations using subsystems technology. *BMC Genom.* 9, 75. doi: 10.1186/1471-2164-9-75

Berleman, J. E., Zemla, M., Remis, J. P., Liu, H., Davis, A. E., Worth, A. N., et al. (2016). Exopolysaccharide microchannels direct bacterial motility and organize multicellular behavior. *ISME J.* 10, 2620–2632. doi: 10.1038/ismej.2016.60

Bhardwaj, T., Haque, S., and Somvanshi, P. (2018). In silico identification of molecular mimics involved in the pathogenesis of Clostridium botulinum ATCC 3502 strain. *Microb. Pathog.* 121, 238–244. doi: 10.1016/j.micpath.2018.05.017

Carver, T. J., Rutherford, K. M., Berriman, M., Rajandream, M. A., Barrell, B. G., and Parkhill, J. (2005). ACT: the artemis comparison tool. *Bioinformatics* 21, 3422–3423. doi: 10.1093/bioinformatics/bti553

Edgar, R. C. (2004). MUSCLE: a multiple sequence alignment method with reduced time and space complexity. *BMC Bioinformat.* 5, 113. doi: 10.1186/1471-2105-5-113

Gibbons, T. R., Mount, S. M., Cooper, E. D., and Delwiche, C. F. (2015). Evaluation of BLAST-based edge-weighting metrics used for homology inference with the Markov clustering algorithm. *BMC Bioinformat.* 16, 218. doi: 10.1186/s12859-015-0625-x

Hoffmann, T., Krug, D., Bozkurt, N., Duddela, S., Jansen, R., Garcia, R., et al. (2018). Correlating chemical diversity with taxonomic distance for discovery of natural products in myxobacteria. *Nat Commun.* 9, 803. doi: 10.1038/s41467-018-03184-1

Jamal, Z., Miot-Sertier, C., Thibau, F., Dutilh, L., Lonvaud-Funel, A., Ballestra, P., et al. (2013). Distribution and functions of phosphotransferase system genes in the genome of the lactic acid bacterium *Oenococcus oeni*. *Appl. Environ. Microbiol.* 79, 3371–3379. doi: 10.1128/AEM.00380-13

Kaiser, D. (2003). Coupling cell movement to multicellular development in myxobacteria. *Nat. Rev. Microbiol.* 1, 45–54. doi: 10.1038/nrmicro733

Kaur, R., Kaur, R., Sharma, A., Kumar, V., Sharma, M., Bhardwaj, R., et al. (2018). Microbial production of dicarboxylic acids from edible plants and milk using GC-MS. *J Anal Sci. Technol.* 9, 21. doi: 10.1186/s40543-018-0154-0

Kim, M., Oh, H. S., Park, S. C., and Chun, J. (2014). Towards a taxonomic coherence between average nucleotide identity and 16S rRNA gene sequence similarity for species demarcation of prokaryotes. *Int. J. Syst. Evol. Microbiol.* 64, 346–351. doi: 10.1099/ijs.0.059774-0

Kimura, Y., Mishima, Y., Nakano, H., and Takegawa, K. (2002). An adenylyl cyclase, CyaA, of *Myxococcus xanthus* functions in signal transduction during osmotic stress. *J Bacteriol.* 184, 3578–3585. doi: 10.1128/JB.184.13.3578-3585.2002

Kumar, S., Stecher, G., and Tamura, K. (2016). MEGA7: Molecular evolutionary genetics analysis version 7.0 for bigger datasets. *Mol. Biol. Evol.* 33, 1870–1874. doi: 10.1093/molbev/msw054

Li, L. G., and Zhang, T. (2023). Plasmid-mediated antibiotic resistance gene transfer under environmental stresses: insights from laboratory-based studies. *Sci. Total. Environ.* 887, 163870. doi: 10.1016/j.scitotenv.2023.163870

Li, X., Zhang, L., Jiang, Z., Liu, L., Wang, J., Zhong, L., et al. (2022). A novel cold-active GH8 xylanase from cellulolytic myxobacterium and its application in food industry. *Food Chem.* 393, 133463. doi: 10.1016/j.foodchem.2022.133463

Li, Z., Wang, T., Luo, X., Li, X., Xia, C., Zhao, Y., et al. (2018). Biocontrol potential of *Myxococcus* sp. strain BS against bacterial soft rot of calla lily caused by *Pectobacterium carotovorum*. *Biol. Control* 126, 36–44. doi: 10.1016/j.biocontrol.2018.07.004

Li, Z., Ye, X., Liu, M., Xia, C., Zhang, L., Luo, X., et al. (2019). A novel outer membrane beta-1,6-glucanase is deployed in the predation of fungi by myxobacteria. *ISME J.* 13, 2223–2235. doi: 10.1038/s41396-019-0424-x

Li, Z. F., Li, X., Liu, H., Liu, X., Han, K., Wu, Z. H., et al. (2011). Genome sequence of the halotolerant marine bacterium *Myxococcus fulvus* HW-1. *J. Bacteriol.* 193, 5015–5016. doi: 10.1128/JB.05516-11

Livingstone, P. G., Morphew, R. M., and Whitworth, D. E. (2017). Myxobacteria are able to prey broadly upon clinically-relevant pathogens, exhibiting a prey range which cannot be explained by phylogeny. *Front. Microbiol.* 8, 1593. doi: 10.3389/fmicb.2017.01593

Luo, D., Guan, J., Dong, H., Chen, J., Liang, M., Zhou, C., et al. (2022). Simultaneous determination of twelve mycotoxins in edible oil, soy sauce and bean sauce by PRiME HLB solid phase extraction combined with HPLC-Orbitrap HRMS. *Front. Nutr.* 9, 1001671. doi: 10.3389/fnut.2022.1001671

Meier-Kolthoff, J. P., Auch, A. F., Klenk, H. P., and Göker, M. (2013). Genome sequence-based species delimitation with confidence intervals and improved distance functions. *BMC Bioinformat.* 14, 60. doi: 10.1186/1471-2105-14-60

Mironenko, N. V., Gavrilenko, T. A., Khiutti, A. V., and Afanasenko, O. S. (2020). Quarantine nematode species and pathotypes potentially dangerous for domestic potato production: populations diversity and the genetics of potato resistance. *Vavilovskii Zhurnal Genet Selektsii.* 24, 705–721. doi: 10.18699/VJ20.665

Pan, H., Luan, J., He, X., Lux, R., and Shi, W. (2012). The *clpB* gene is involved in the stress response of *Myxococcus xanthus* during vegetative growth and development. *Microbiology (Reading) 158(Pt* 9), 2336–2343. doi: 10.1099/mic.0.060103-0

Pan, H. W., Liu, H., Liu, T., Li, C. Y., Li, Z. F., Cai, K., et al. (2009). Seawater-regulated genes for two-component systems and outer membrane proteins in *Myxococcus*. *J Bacteriol* 191, 2102–2111. doi: 10.1128/JB.01556-08

Pan, H. W., Tan, Z. G., Liu, H., Li, Z. F., Zhang, C. Y., Li, C. Y., et al. (2010). *Hdsp*, a horizontally transferred gene required for social behavior and halotolerance in salt-tolerant *Myxococcus fulvus* HW-1. *ISME J* 4, 1282–1289. doi: 10.1038/ismej.2010.52

Parks, D. H., Chuvochina, M., Rinke, C., Mussig, A. J., Chaumeil, P. A., and Hugenholtz, P. (2022). GTDB: an ongoing census of bacterial and archaeal diversity through a phylogenetically consistent, rank normalized and complete genome-based taxonomy. *Nucleic Acids Res* 50, D785–D794. doi: 10.1093/nar/gkab776

Qin, H., Dong, Q., Chen, H., Yang, G., and Zhang, X. (2015). Kinetics and mechanism of humic acids degradation by ozone in the presence of CeO2/AC. *Ozone* 37, 371–378. doi: 10.1080/01919512.2015.1006725

Saidi, F., Bitazar, R., Bradette, N. Y., and Islam, S. T. (2022). Bacterial Glycocalyx Integrity Impacts Tolerance of *Myxococcus xanthus* to Antibiotics and Oxidative-Stress Agents. *Biomolecules* 12, 571. doi: 10.3390/biom12040571

Skotnicka, D., Smaldone, G. T., Petters, T., Trampari, E., Liang, J., Kaever, V., et al. (2016). A minimal threshold of c-di-GMP is essential for fruiting body formation and sporulation in *Myxococcus xanthus*. *PLoS Genet.* 12, e1006080. doi: 10.1371/journal.pgen.1006080

Sutton, D., Livingstone, P. G., Furness, E., Swain, M. T., and Whitworth, D. E. (2019). Genome-wide identification of myxobacterial predation genes and demonstration of formaldehyde secretion as a potentially predation-resistant trait of *Pseudomonas aeruginosa*. *Front. Microbiol.* 10, 2650. doi: 10.3389/fmicb.2019.02650

Tatusov, R. L., Galperin, M. Y., Natale, D. A., and Koonin, E. V. (2000). The COG database: a tool for genome-scale analysis of protein functions and evolution. *Nucleic Acids Res.* 28, 33–36. doi: 10.1093/nar/28.1.33

Thiery, S., and Kaimer, C. (2020). The predation strategy of *Myxococcus xanthus*. *Front. Microbiol.* 11, 2. doi: 10.3389/fmicb.2020.00002

Thompson, J. D., Gibson, T. J., Plewniak, F., Jeanmougin, F., and Higgins, D. G. (1997). The CLUSTAL_X windows interface: flexible strategies for multiple sequence alignment aided by quality analysis tools. *Nucleic Acids Res.* 25, 4876–4882. doi: 10.1093/nar/25.24.4876

Velicer, G. J., Kroos, L., and Lenski, R. E. (1998). Loss of social behaviors by *Myxococcus xanthus* during evolution in an unstructured habitat. *P Natl. Acad. Sci. USA*. 95, 12376–12380. doi: 10.1073/pnas.95.21.12376

Wang, B., Hu, W., Liu, H., Zhang, C. Y., Zhao, J. Y., Jiang, D. M., et al. (2007). Adaptation of salt-tolerant *Myxococcus* strains and their motility systems to the ocean conditions. *Microb. Ecol.* 54, 43–51. doi: 10.1007/s00248-006-9169-y

Wang, C., Morrissey, E. M., Mau, R. L., Hayer, M., Pineiro, J., Mack, M. C., et al. (2021a). The temperature sensitivity of soil: microbial biodiversity, growth, and carbon mineralization. *ISME J.* 15, 2738–2747. doi: 10.1038/s41396-021-00959-1

Wang, J., Wang, J., Wu, S., Zhang, Z., and Li, Y. (2021b). Global geographic diversity and distribution of the myxobacteria. *Microbiol. Spectr.* 9, e0001221. doi: 10.1128/Spectrum.00012-21

Ye, X., Li, Z., Luo, X., Wang, W., Li, Y., Li, R., et al. (2020). A predatory myxobacterium controls cucumber Fusarium wilt by regulating the soil microbial community. *Microbiome* 8, 49. doi: 10.1186/s40168-020-00824-x

Yoon, S. H., Ha, S. M., Kwon, S., Lim, J., Kim, Y., Seo, H., et al. (2017). Introducing EzBioCloud: a taxonomically united database of 16S rRNA gene sequences and whole-genome assemblies. *Int. J. Syst. Evol. Microbiol.* 67, 1613–1617. doi: 10.1099/ijsem.0.001755

Zhang, C. Y., Cai, K., Liu, H., Zhang, Y., Pan, H. W., Wang, B., et al. (2007). New locus important for *Myxococcus* social motility and development. *J. Bacteriol.* 189, 7937–7941. doi: 10.1128/JB.00942-07

Zhang, G., Bai, J., Tebbe, C. C., Zhao, Q., Jia, J., Wang, W., et al. (2020). Salinity controls soil microbial community structure and function in coastal estuarine wetlands. *Environ. Microbiol.* 23, 1020–1037. doi: 10.1111/1462-2920.15281

Zhang, L., Dong, C., Wang, J., Liu, M., Wang, J., Hu, J., et al. (2023a). Predation of oomycetes by myxobacteria via a specialized CAZyme system arising from adaptive evolution. *ISME J.* 17, 1089–1103. doi: 10.1038/s41396-023-01423-y

Zhang, L., Huang, X., Zhou, J., and Ju, F. (2023b). Active predation, phylogenetic diversity, and global prevalence of myxobacteria in wastewater treatment plants. *ISME J.* 17, 671–681. doi: 10.1038/s41396-023-01378-0

Zhang, X., Yao, Q., Cai, Z., Xie, X., and Zhu, H. (2013). Isolation and identification of myxobacteria from saline-alkaline soils in Xinjiang, China. *PLoS ONE.* 8, e70466. doi: 10.1371/journal.pone.0070466

Zhang, Y. Q., Li, Y. Z., Wang, B., Wu, Z. H., Zhang, C. Y., Gong, X., et al. (2005). Characteristics and living patterns of marine myxobacterial isolates. *Appl. Environ. Microbiol.* 71, 3331–3336. doi: 10.1128/AEM.71.6.3331-3336.2005

Zhao, J. Y., Zhong, L., Shen, M. J., Xia, Z. J., Cheng, Q. X., Sun, X., et al. (2008). Discovery of the autonomously replicating plasmid pMF1 from *Myxococcus fulvus* and development of a gene cloning system in *Myxococcus xanthus*. *Appl. Environ. Microbiol.* 74, 1980–1987. doi: 10.1128/AEM.02143-07

Zhao, Y., Wang, Y., Xia, C., Li, X., Ye, X., Fan, Q., et al. (2021). Whole-genome sequencing of *Corallococcus sp.* strain EGB reveals the genetic determinants linking taxonomy and predatory behavior. *Genes (Basel).* 12, 1421. doi: 10.3390/genes12091421

frontiers | Frontiers in Microbiology

TYPE Original Research
PUBLISHED 23 November 2023
DOI 10.3389/fmicb.2023.1293966

OPEN ACCESS

EDITED BY
Honghui Zhu,
Guangdong Academy of Science, China

REVIEWED BY
Matthew Culyba,
University of Pittsburgh, United States
Wei Hu,
Shandong University, China

*CORRESPONDENCE
Penelope I. Higgs
✉ pihiggs@wayne.edu

RECEIVED 14 September 2023
ACCEPTED 14 November 2023
PUBLISHED 23 November 2023

CITATION
McLaughlin M and Higgs PI (2023) Mutation of self-binding sites in the promoter of the MrpC transcriptional regulator leads to asynchronous *Myxococcus xanthus* development. *Front. Microbiol.* 14:1293966. doi: 10.3389/fmicb.2023.1293966

Mutation of self-binding sites in the promoter of the MrpC transcriptional regulator leads to asynchronous *Myxococcus xanthus* development

Maeve McLaughlin and Penelope I. Higgs*

Department of Biological Sciences, Wayne State University, Detroit, MI, United States

Introduction: MrpC, a member of the CRP/Fnr transcription factor superfamily, is necessary to induce and control the multicellular developmental program of the bacterium, *Myxococcus xanthus*. During development, certain cells in the population first swarm into haystack-shaped aggregates and then differentiate into environmentally resistant spores to form mature fruiting bodies (a specialized biofilm). *mrpC* transcriptional regulation is controlled by negative autoregulation (NAR).

Methods: Wild type and mutant *mrpC* promoter regions were fused to a fluorescent reporter to examine effects on *mrpC* expression in the population and in single cells *in situ*. Phenotypic consequences of the mutant *mrpC* promoter were assayed by deep convolution neural network analysis of developmental movies, sporulation efficiency assays, and anti-MrpC immunoblot. In situ analysis of single cell MrpC levels in distinct populations were assayed with an MrpC-mNeonGreen reporter.

Results: Disruption of MrpC binding sites within the *mrpC* promoter region led to increased and broadened distribution of *mrpC* expression levels between individual cells in the population. Expression of *mrpC* from the mutant promoter led to a striking phenotype in which cells lose synchronized transition from aggregation to sporulation. Instead, some cells abruptly exit aggregation centers and remain locked in a cohesive swarming state we termed developmental swarms, while the remaining cells transition to spores inside residual fruiting bodies. *In situ* examination of a fluorescent reporter for MrpC levels in developmental subpopulations demonstrated cells locked in the developmental swarms contained MrpC levels that do not reach the levels observed in fruiting bodies.

Discussion: Increased cell-to-cell variation in *mrpC* expression upon disruption of MrpC binding sites within its promoter is consistent with NAR motifs functioning to reducing noise. Noise reduction may be key to synchronized transition of cells in the aggregation state to the sporulation state. We hypothesize a novel subpopulation of cells trapped as developmental swarms arise from intermediate levels of MrpC that are sufficient to promote aggregation but insufficient to trigger sporulation. Failure to transition to higher levels of MrpC necessary to induce sporulation may indicate cells in developmental swarms lack an additional positive feedback signal required to boost MrpC levels.

KEYWORDS

***Myxococcus xanthus*, biofilm, genetic regulatory network, development, negative autoregulation**

1 Introduction

Myxococcus xanthus is a "social" bacterium with a life cycle that is highly dependent on collective behaviors (Munoz-Dorado et al., 2016). During vegetative growth, large groups of *M. xanthus* cells swarm over solid surfaces in search of prey on which they cooperatively predate (Rosenberg et al., 1977; Berleman et al., 2008). Under nutrient limited conditions, *M. xanthus* enters an ~72-h developmental program during which cells form a specialized biofilm and segregate into distinct cell fates (Higgs et al., 2014). Some cells are induced to swarm into aggregation centers to produce mounds of approximately 10^5 cells. Once inside aggregation centers, individual cells slow down and stop moving (Cotter et al., 2017), which prevents them from leaving the aggregation center. These cells are then induced to differentiate into environmentally resistant spores, producing mature multicellular fruiting bodies. Other cells within the developing population remain outside of the fruiting bodies and differentiate into peripheral rods, which are thought of as a persister-like state (O'Connor and Zusman, 1991; Lee et al., 2012). For development to be effective, cells in the population must coordinate their behavior both in time and space. If sporulation were to occur before completion of aggregation, then the benefits conferred by a multicellular fruiting body structure, such as enhanced resistance to environmental stresses or group dispersal, would be lost (Velicer et al., 2014).

MrpC, is a CRP/Fnr superfamily transcriptional regulator that coordinates expression of hundreds of developmental genes (Sun and Shi, 2001b; Robinson et al., 2014). Under standard laboratory developmental conditions, no ligand has been identified to activate MrpC, and purified MrpC binds efficiently to target DNA binding sites *in vitro* (Nariya and Inouye, 2006; Mittal and Kroos, 2009a; McLaughlin et al., 2018). Threshold levels of MrpC appear to drive distinct stages of development: low levels are associated with induction of aggregation onset, higher levels are associated with commitment to sporulation (Lee et al., 2012; Rajagopalan and Kroos, 2014, 2017; Hoang and Kroos, 2018). Peripheral rods contain low levels of MrpC in the wild type *M. xanthus* strain DZ2 (Lee et al., 2012). One immediate target of MrpC is activation of the transcription factor, FruA (Ueki and Inouye, 2003). FruA is essential for development (Ogawa et al., 1996; Ellehauge et al., 1998), and FruA and MrpC coordinately induce expression of multiple downstream genes (Mittal and Kroos, 2009b; Lee et al., 2011; Son et al., 2011).

MrpC is under complex regulation. Shortly after cells sense nutrient limitation, *mrpC* expression is upregulated by MrpB, a bacterial enhancer binding protein (bEBP) (Sun and Shi, 2001a). MrpB binds to two upstream activating sequences (UAS1 and UAS2) 182 bp from the *mrpC* start codon, where it presumably stimulates *mrpC* expression from a sigma^{54}-dependent promoter (Sun and Shi, 2001a; McLaughlin et al., 2018). MrpC directly binds to at least four sites (BS1, 3, 4, and 5) in its own promoter and functions as a negative autoregulator by competing with its transcriptional activator, MrpB, for overlapping UAS1/BS3 and UAS2/BS4 binding sites (McLaughlin et al., 2018). MrpC also positively regulates expression of *mrpB* (Sun and Shi, 2001a) (C. Mataczynski and P.I. Higgs, unpublished results). Finally, early during the developmental program, gradual accumulation of MrpC is achieved because the Esp signaling system induces turnover of MrpC (Higgs et al., 2008; Schramm et al., 2012). Several additional post-transcriptional events modulate MrpC accumulation (and therefore progression through development) in response to changing environmental conditions (Nariya and Inouye, 2005; Rajagopalan and Kroos, 2014, 2017; Marcos-Torres et al., 2020).

NAR is a particularly abundant genetic regulatory network motif (Thieffry et al., 1998; Rosenfeld et al., 2002). Theoretical and experimental data have demonstrated NAR network motifs serve to buffer against transcriptional noise, speed up response times, increase the input dynamic range of a circuit, and optimize fitness (Becskei and Serrano, 2000; Rosenfeld et al., 2002; Camas et al., 2006; Nevozhay et al., 2009; Kozuch et al., 2020). Most of these well-described functions have been investigated synthetic systems or in single-celled organisms; fewer examples of the phenotypic consequences of perturbing network motifs in natural multicellular systems are available.

Here, we set out to investigate the role of MrpC NAR in the context of the multicellular developmental program in *M. xanthus*. We demonstrate that disruption of BS1 and BS5 independently and additively increase *mrpC* reporter expression, consistent with both playing a role in NAR. *mrpC* expressed from a BS1/BS5 mutant promoter was associated with early and increased MrpC accumulation and led to premature aggregation onset, reduced fruiting body organization, and, unexpectedly, reduced sporulation efficiency. Using a method to film strains developing under submerged culture (Glaser and Higgs, 2019), we observed that this strain exhibited striking asynchronous development: after formation of aggregates, some cells suddenly exited aggregation centers as fast-moving swarms, while other cells remained in stationary fruiting bodies. Deep convolution neural network analyzes indicated these developmental swarms displayed trajectories and velocities that were distinct from cells in the mobile aggregate phase. Also consistent with loss of NAR, analysis of single cell *mrpC* expression *in situ* demonstrated that mutated BS1/BS5 resulted in increased cell-to-cell variability of *mrpC* expression. These data suggest that in the context of the multicellular developmental program, MrpC NAR may help to constrain variation in *mrpC* expression within the developing population to facilitate synchronized transition from cells in the aggregation state to the sporulation state. Interestingly, *in situ* analysis of single cell MrpC-reporter accumulation suggested that developmental swarms maintained MrpC levels intermediate between those found in peripheral rods and sporulating cells suggesting distinct MrpC steady-state levels can produce novel group phenotypes.

2 Materials and methods

2.1 Bacterial strains, plasmids, and oligonucleotides

The bacterial strains used in this study are listed in Supplementary Table S1. Plasmids were constructed (Lee et al., 2010) using the oligonucleotide sequences, and construction strategy listed in Supplementary Table S2.

2.2 Growth and developmental conditions

Escherichia coli were grown under standard laboratory conditions in LB media supplemented with 50 μg ml^{-1} of kanamycin and/or

20 μg ml^{-1} of tetracycline, where necessary (Maniatis et al., 1982). *M. xanthus* DZ2 strains were grown under vegetative conditions on CYE agar or in broth, as described previously (Lee et al., 2010); plates were supplemented with 100 μg ml^{-1} of kanamycin and/or oxytetracycline at 10 μg ml^{-1}, where necessary.

M. xanthus strains were induced to develop under submerged culture conditions (Lee et al., 2010). Briefly, vegetative cells were diluted to an absorbance measured at 500 nm (A_{550}) of 0.035 in fresh CYE broth, seeded into petri dishes or tissue culture dishes (as indicated in the relevant methods sections) and allowed to grow to a confluent layer for 24 h at 32°C. We estimate the cells grew to approximately 6×10^5 cells mm^{-1} (Lee et al., 2010). To initiate development, CYE media was removed and replaced with an equivalent volume of MMC buffer [10 mM 4-morpholinepropanesulfonic acid (MOPS) pH 7.6, 4 mM $MgSO_4$, 2 mM $CaCl_2$], followed by continued incubation at 32°C for 72–120 h.

To record static developmental phenotypes, 0.5 mL diluted cells were seeded into 24-well tissue culture plates in triplicate and imaged at the indicated times with a Leica M80 stereomicroscope.

2.3 Analysis of mCherry fluorescence by plate reader

Submerged culture assays were set up using 0.5 mL diluted cells seeded into each well of 24-well tissue culture plates, and population mCherry fluorescence was measured as described previously (McLaughlin et al., 2018). Briefly, developing cells were harvested at the indicated hours post-starvation, dispersed, and 1/10 volume of each sample was assayed for fluorescence at 580 nm in a Typhoon imager scan. Values plotted are the average and associated standard deviation from three independent biological replicates. Similar patterns were observed when fluorescence was first normalized to total protein concentration from each sample at each time point (data not shown).

2.4 Sporulation assay

Developmental sporulation efficiency was determined as described previously from 0.5 mL diluted cells developed in triplicate in 24-well tissue culture plates under submerged culture conditions (Lee et al., 2010). Briefly, heat (50°C for 60 min)- and sonication (60 pulses 30% output)-resistant spores were enumerated in a Helber counting chamber. Sporulation efficiency was calculated as percent of wild type spores at 72 or 120 h as indicated. Values reported are the average and associated standard deviation from triplicate independent biological experiments. Chemical-induced sporulation was triggered by addition of glycerol to 0.5 M to vegetatively growing cells in CYE broth with shaking incubation for 24 h at 32°C (Muller et al., 2010). Spores were isolated and enumerated as indicated above.

2.5 Developmental video analysis

M. xanthus strains were induced to develop under submerged culture using 0.15 mL diluted cells per well in 96-well tissue culture plates. After induction of starvation, plates were incubated in a Tecan Spark10M plate reader preheated to 32°C (Glaser and Higgs, 2019). The center of each well was imaged every 30 min from 0 to 72 h post-starvation and images assembled into movies (6 fps) in ImageJ (Schindelin et al., 2012). For each movie, onset of aggregation (Agg_{ONSET}), maximum aggregates (Agg_{MAX}) and final fruiting bodies (Agg_{FINAL}) were enumerated as described previously (Glaser and Higgs, 2019). The percent of aggregates that transitioned to stationary fruiting bodies was calculated as [Agg_{FINAL}/Agg_{MAX}]. The number of aggregates that were mobile (Agg_{MOBILE}) in each movie was recorded and percent Agg_{MOBILE} was calculated as [Agg_{MOBILE}/Agg_{FINAL}]. For each movie, the first frame ($Mobility_I$) and final frame ($Mobility_F$) in which aggregates were mobile was recorded and mobility duration was calculated as [($Mobility_F$ – $Mobility_I$) × 0.5 h/frame]. Mobility delay was calculated as [$Mobility_I$ – Agg_{ONSET}]. Data were compiled from three biological replicates that contained five technical replicates per strain. Statistical significance was analyzed in Prism (GraphPad) using unpaired *t*-test assuming Gaussian distribution, or otherwise the Mann–Whitney test.

2.6 Neural network training and analysis

For tracking aggregate and swarm mobility, DeepLabCut deep convolution neural network was used (Mathis et al., 2018). To train DeepLabCut, 769 total frames were extracted from 29 developmental movies that contained aggregates and/or developmental swarms, which were manually labeled in every frame in which they were present. Using the labeled frames, the DeepLabCut neural network was trained using a 50-layer residual network (He et al., 2016) on Google Colaboratory (hardware accelerator: GPU) for 340,000 iterations (p-cutoff = 0.1). The trained neural network possessed a training and test error of 1.62 and of 6.66 pixels, respectively. To track movement of aggregates and swarms, 15 videos for each strain (3 biological replicates each with 5 technical replicates) from 25 to 72 h of development were analyzed with the trained neural network. The predicted labels (likelihood > p-cutoff) for each video were then manually processed and any spurious labels were removed. To track mobility of individual swarms and aggregates, videos were cropped to contain only a single aggregate and/or swarm. Swarms and aggregates were only analyzed for mobility if they remained within the frame for the entirety of the recording. To track mobility in an entire well, developmental videos (640 × 510 pixels) were initially cropped into 20 smaller videos (160 × 102 pixels) with ImageJ (Schindelin et al., 2012). Each cropped video was analyzed with the trained neural network as stated previously. Labels from individual videos were then manually stitched together. Displacement between two time points with coordinates (x_i, y_i) and (x_f, y_f) was calculated as [$((x_f - x_i)^2 + (y_f - y_i)^2)^{-2}$ × (1661.5 μm/1280 pixels)]. Total swarm displacement was calculated as the sum of all displacements across all time points. Speed of mobility between two time points (t_i and t_f) was calculated as [displacement/((t_f – t_i) × 60 min/h)].

2.7 Confocal microscopy

For analysis of single cell *mrpC* expression, *M. xanthus* strains bearing P_{van}-*mNeonGreen* and either P_{WT}-*mCherry* (PH1373) or

P_{MUT}-*mCherry* (PH1374) were diluted 1:19 with an unlabeled wild type strain (DZ2) and induced to develop under submerged culture conditions using 2.1 mL diluted cells to seed ibiTreated µ-dishes$^{35\ mm,\ high}$ (Ibidi). Developing cultures were imaged using a Leica TCS SP8 inverted confocal microscope with a 63x objective. Brightfield images were taken with a gain of 230 V and 0.0% offset. mNeonGreen fluorescence was examined using a 488 nm wavelength laser (5% power) for excitation, a 500–540 nm emission spectra, 800 V gain, and 0.0% offset. mCherry fluorescence was examined using a 552 nm wavelength laser (5% power) for excitation, a 585–630 nm emission spectra, 650 V gain, and 0.0% offset. For each replicate of 24 h pre-aggregating cells and 48 h peripheral rods, five images were taken from throughout the plate for each strain (line average: 8, resolution: 1,024 × 1,024). For analysis of the 48 h fruiting bodies, z-stacks of three fruiting bodies were taken for each strain. Each fruiting body was imaged from the base to the interior of the fruiting body (21–37 images; step size: 1 µm, line average: 4, resolution: 1,024 × 1,024). Data were compiled from three independent biological replicates.

Images were subsequently analyzed in ImageJ (Schindelin et al., 2012). For 48 h aggregated populations, images were initially cropped to include only the fruiting body. ROIs were created by thresholding the images from the mNeonGreen channel to contain only pixels that were above the intensity of the unlabeled background strain (pixel threshold: 45), then analyzing particles with area > 0.5 µm^2 and circularity of 0.0–1.0. ROIs were then transferred to the mCherry channel images and the integrated density was measured. The red-green (RG) ratios were plotted and points identified as outliers by Grubb's test ($p < 0.5$) were removed. The coefficient of variation (CV) for each biological replicated was calculated by dividing the standard deviation by the mean. Similar RG ratios and CV values were obtained from random single z-layer images indicating no significant differences in *mrpC* reporter expression were observed in different layers of cells.

For analysis of MrpC-mNeonGreen production in developing cells, *M. xanthus* strain PH1375 was induced to develop as above. Prior to imaging, FM 4-64 was added to 5 µg ml^{-1} final concentration and incubated at 32°C for 60 min (modified from Hoang et al., 2021). At the designated time points, developing cultures were imaged as above, except mNeonGreen fluorescence was recorded with 500 V gain. FM 4-64 fluorescence was detected using 722–762 nm emission spectra and 650 V gain. For analysis of peripheral rod populations, five images for each replicate were taken throughout the plate (line average: 8, resolution: 1,024 × 1,024) and ROIs (identified based on membrane stain) were drawn for 20 rod shaped cells and 20 circular cells representing average sizes. For analysis of aggregated cell populations, 1 µm z-stacks of three fruiting bodies or developmental swarms were recorded. One layer in the z-stack was randomly chosen and ROIs were drawn around 40 circular cells within the fruiting body or 40 rod-shaped cells in the swarms each of which was fully in-plane in the image. The mean fluorescence for each ROI in the mNeonGreen channel was measured and plotted.

To account for the relative proportion of spheres and rods in each peripheral rod population, the number of rod-shaped and circular cells were counted in 30.84 × 30.84 pixel ROI (24 h) or 60.07 × 60.07 pixel ROI (30 and 48 h) and a proportional equivalent of random cells or spheres were chosen for plotting. All images were analyzed with the Leica Application Suite X (LasX) histogram tool.

2.8 Cell lysate preparation and immunoblot analysis

Cell lysates were generated from strains developed under submerged culture using 16 mL diluted cells seeded in 100-mm petri dishes. At the indicated time points, the overlay buffer was removed, the cell layer was resuspended in 1.5 mL ice-cold MMC. Cells were pelleted (17,000 × g, 5 min, 4°C), and pellets were stored at −20°C until further use. 1 mL 13% ice-cold trichloroacetic acid (TCA) and 0.1 mm zirconia/silca beads were added to each pellet and subject bead beating with a FastPrep-24 tissue homogenizer (MP Biomedical) at 6.5 m/s for 45 s at 4°C, six times with 2 min incubation on ice between rounds. Samples were then incubated on ice for at least 15 min. Protein was pelleted as above, washed with 1.0 mL ice-cold Tris buffer [100 mM Tris–HCl (pH 8.0)], then resuspended in 50 µL Tris buffer and 150 µL clear LSB (Schramm et al., 2012), heated at 95°C for 5 min, then stored at −20°C until further use. Protein concentration was determined by Pierce BCA protein assay kit (Thermo Fisher Scientific), samples were diluted to 0.87 µg µl^{-1} in 2 × LSB, and 10 µg protein resolved by denaturing polyacrylamide (10%) gel electrophoresis and transferred (semi-dry) to polyvinylidene difluoride (PVDF) membrane. Membranes were probed with rabbit polyclonal anti-MrpC (1:1,000) or anti-mNeonGreen (1:1,000) (Cell Signaling Technologies), and anti-rabbit IgG secondary antibodies conjugated to horseradish peroxidase (HRP) at 1:20,000 or 1:5,000, respectively. Signal was detected with enhanced chemiluminescence substrate followed by exposure to autoradiography film.

3 Results

3.1 Disruption of MrpC binding sites in the *mrpC* promoter region produces increased *mrpC* expression consistent with perturbed negative autoregulation

mrpC expression is subject to NAR due at least in part to competition between MrpC and its transcriptional activator, MrpB, for overlapping binding sites (McLaughlin et al., 2018) (Figure 1A). MrpC binds to two additional sequences within its promoter (termed BS5 and BS1) (McLaughlin et al., 2018). To examine whether BS5 and BS1 contributed to MrpC NAR, we analyzed *mrpC* reporter constructs bearing either the wild-type promoter or mutant promoters containing substitutions within BS1 (BS1*), a deletion of BS5 (ΔBS5), or both (BS1*ΔBS5). BS1* was generated by substituting the TGT consensus resides to GAA which completely disrupts MrpC binding to BS1 *in vitro* (McLaughlin et al., 2018) (Figure 1A; Supplementary Figure S1B). Each reporter construct was inserted into the Mx8 phage attachment site (*attB*) of wild-type *M. xanthus* strain DZ2, and developmental assays indicated all resulting strains displayed wild-type developmental phenotypes (data not shown). Analysis of the reporters during development demonstrated the ΔBS5 and BS1* mutations resulted in 2.5-fold and 1.8-fold increases in mCherry fluorescence compared to the wild-type reporter at 48 h, respectively (Supplementary Figure S1C). The reporter bearing the BS1* ΔBS5 double disruption yielded a 3.3 fold increase in mCherry fluorescence compared to the wild type

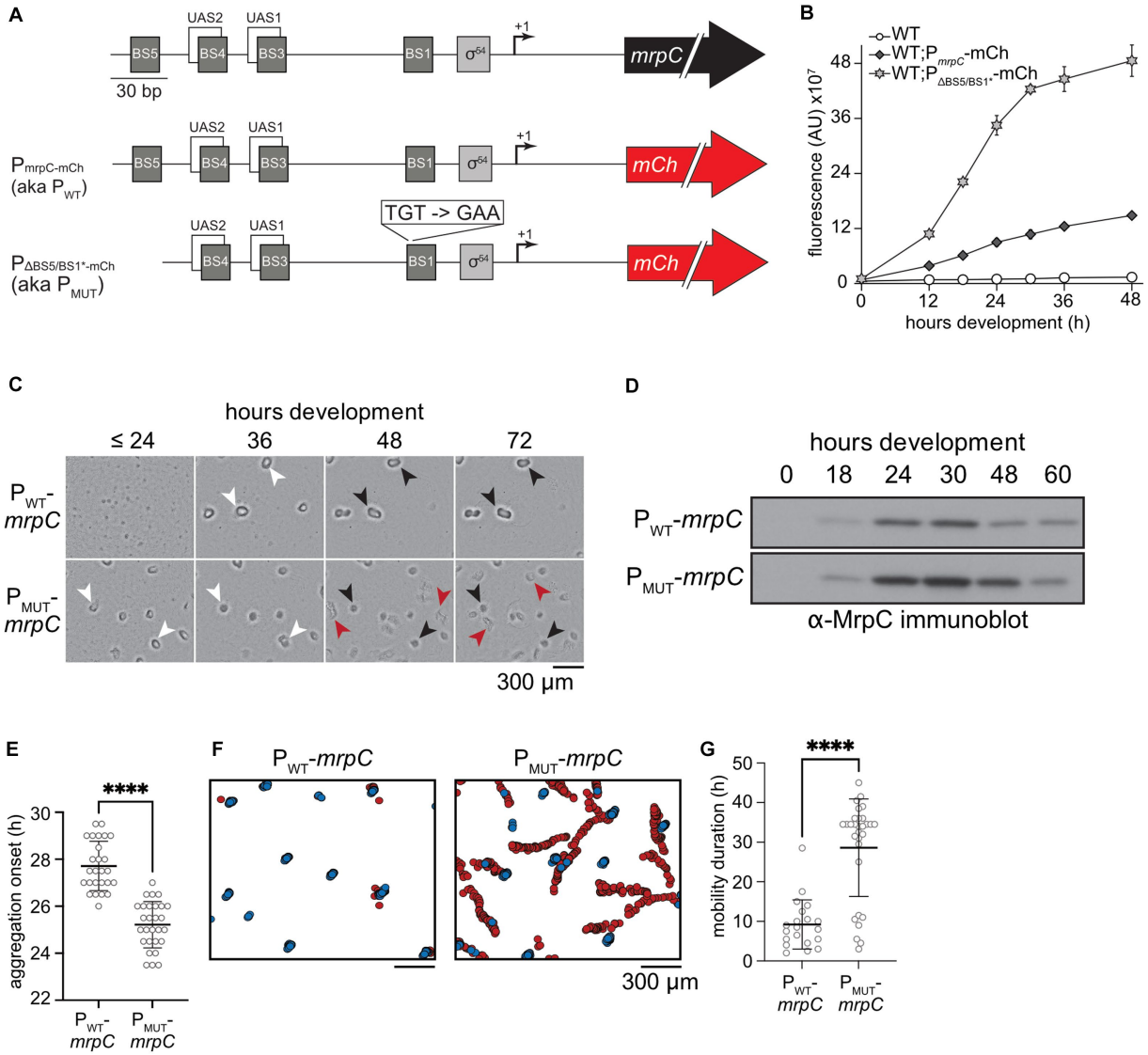

FIGURE 1
Disruption of MrpC binding sites 1 and 5 perturbs MrpC negative autoregulation (NAR) and leads to asynchronous development. **(A)** Top: Schematic of the *mrpC* promoter region. BS: Sequences to which MrpC directly binds; UAS: upstream activating sequences to which MrpB directly binds; σ^{54}: putative sigma^{54}-dependent promoter; +1: transcriptional start site; black arrow: *mrpC* gene. Middle: Schematic of the reporter construct used in **(B)**. P_{mrpC}-mCh: the wild type *mrpC* promoter region was fused to the mCherry fluorescence reporter gene (red arrow). Bottom: Reporter with deletion of BS5 and disruption of BS1 in the *mrpC* promoter. **(B)** *mrpC* expression is increased when binding sites (BS) 5 and 1 are disrupted. Analysis of *mrpC* expression with an mCherry reporter expressed from the wild type *mrpC* (P_{mrpC}-*mCh*) or mutant MrpC binding sites 1 and 5 ($P_{\Delta BS5/BS1*}$-*mCh mrpC*) promoters. Reporters were integrated into wild type cells and mCherry fluorescence was recorded during development under submerged culture. Data plotted is the average and associated standard deviation of three independent biological replicates. **(C)** Disruption of MrpC BS 5 and 1 caused early aggregation and disrupted fruiting bodies. The developmental phenotype observed from Δ*mrpC* cells expressing *mrpC* from its wild type- (P_{WT}-*mrpC*) or $P_{\Delta BS5/BS1*}$- (P_{MUT}-*mrpC*) promoters recorded at the hours post-starvation indicated; >24 indicates images recorded at 0, 12, 18, and 24 h of development were indistinguishable. White arrows: aggregates of ~10^5 cells; black arrows: immobile fruiting bodies; red arrows: developmental swarms. **(D)** Representative anti-MrpC immunoblot of lysates prepared from P_{WT}-*mrpC* or P_{MUT}-*mrpC* cells developing under submerged culture. **(E,G)** Distribution of developmental times at which aggregation centers were first observed (aggregation onset; **E**), or durations of time that aggregates (P_{WT}-*mrpC*) or developmental swarms (P_{MUT}-*mrpC*) traveled (mobility duration; **G**). Mean (bar) and associated standard deviations are indicated. Data was analyzed for statistically significant differences using an unpaired *t* test **(E)** or Mann–Whitney test **(G)**. ****$p < 0.0001$. Strains were developed under submerged culture in 96 well plates and imaged every 30 min for 72 h Data are compiled from three independent biological replicates. $n = 26$ (P_{WT}-*mrpC*) and 28 (P_{MUT}-*mrpC*) **(E)**; $n = 20$ (P_{WT}-*mrpC*) and 30 (P_{MUT}-*mrpC*) **(G)**. **(F)** Identification and tracking of aggregates by a DeepLabCut trained neural network. Stationary aggregates (blue) and developmental swarms (red) identified from movies of cells developing under submerged culture as in **(C)**. Data from one representative assay is shown.

parent, and 1.3-fold increase compared to the single ΔBS5 reporters (Figure 1B; Supplementary Figure S1C). No significant mCherry fluorescence was detected from the $P_{\Delta BS5\text{-}3}$-mCh reporter which lacks the MrpB binding sites UAS1 and 2 as well as MrpC BS3, 4 and 5 (McLaughlin et al., 2018) (Supplementary Figures S1A,C), indicating no other promoter elements contribute to induction of *mrpC* expression. The observation that reporter expression in the Δ*mrpC* strain is dramatically higher early during development (Supplementary Figure S1D) reflects the contribution of MrpC binding to BS3/4 to directly compete with MrpB binding at UAS1/2.

MrpC BS3/4 intimately overlap with MrpB UAS1/2 (McLaughlin et al., 2018), and we could not design mutations which would not also be predicted to perturb MrpB-dependent activation of *mrpC* expression.

3.2 Mutation of MrpC BS1 and BS5 leads to early aggregation and reduced sporulation

To examine how the MrpC BS1 and BS5 mutations affect *M. xanthus* development, we next generated constructs in which the *mrpC* gene was driven from its wild-type promoter or from the ΔBS5/BS1* promoter. These constructs were integrated in the Δ*mrpC* background at the *attB* site, producing Δ*mrpC attB*::P_{WT}-*mrpC* (parent) and Δ*mrpC attB*::$P_{\Delta BS5/BS1*}$-*mrpC* strains (hereafter termed P_{WT}-*mrpC* and P_{MUT}-*mrpC*, respectively). The phenotype of these two strains was compared to the Δ*mrpC* and wild type background strains induced to develop under submerged culture. In this assay, cells are first allowed to grow into a uniform layer that covers the bottom of the well, and development is induced by replacing growth media with starvation buffer. As expected, the Δ*mrpC* strain failed to produce aggregates, whereas the wild-type and P_{WT}-*mrpC* strains produced similar visible aggregation centers between 24 and 36 h that darkened by 72 h post-starvation (Figure 1C; Supplementary Figure S2A), indicating exogenously expressed *mrpC* restores wild type aggregation. In contrast, the P_{MUT}-*mrpC* strain produced aggregates at least 6 h earlier than the parent strain (Figure 1C; Supplementary Figure S2A). Furthermore, while the P_{MUT}-*mrpC* aggregates appeared similar to the parent at 36 h, they subsequently failed to appropriately darken, and by 48–72 h became more disorganized than the parent and wild-type strains (Figure 1C).

To examine sporulation levels in these strains, heat- and sonication-resistant spores were enumerated at 48, 72, and 120 h. After 120 h of development, the wild type had produced $3.1 \pm 0.7 \times 10^7$ spores (recorded as 100 ± 23%), while no spores could be detected from Δ*mrpC* mutant (≤0.07% wild type) (Supplementary Figure S2B). The P_{WT}-*mrpC* strain produced 70 ± 16% of the wild type levels, suggesting exogenous expression of *mrpC* did not fully complement with respect to sporulation efficiency (Supplementary Figure S2B). The P_{MUT}-*mrpC* strain, however, exhibited a striking reduction in sporulation corresponding to 30 ± 17% of the resistant spores produced by the P_{WT}-*mrpC* strain at 72 h of development (Supplementary Figure S2B). To determine if there was an inherent defect in the core sporulation program in the P_{MUT}-*mrpC* mutant, we examined the number of heat- and sonication-resistant spores produced after artificial chemical induction of sporulation in liquid cultures which bypasses the requirement for aggregation (Dworkin and Gibson, 1964). The P_{MUT}-*mrpC* mutant produced a similar number of chemical-induced spores as the wild type, whereas the Δ*mrpC* mutant failed to produce any spores (Supplementary Figure S2C). These results suggested that the inefficient sporulation observed by the P_{MUT}-*mrpC* strain during starvation-induced development was not due to failure to execute spore differentiation *per se*.

Finally, to examine how the observed phenotypes correlated with total MrpC levels, we prepared lysates from P_{WT}-*mrpC* or P_{MUT}-*mrpC* strains at intervals between 0 and 60 h of development and subjected them to anti-MrpC immunoblot. In the P_{WT}-*mrpC* strain, MrpC was absent at the onset of development ($t = 0$), increased between 18 and 30 h of development, and then subsequently decreased after the onset of sporulation (Figure 1D; Supplementary Figure S2B). Relative to the P_{WT}-*mrpC* strain, levels of MrpC in the P_{MUT}-*mrpC* strain were 2-3-fold higher between 18 and 48 h, and eventually decreased to P_{WT}-*mrpC* levels by 60 h (Figure 1D; Supplementary Figure S3B). This pattern of MrpC accumulation in the two strains was similar to *mrpC* expression levels when the relative increase in mCherry production was examined by plotting the change in mCherry fluorescence between n and $n+1$ time points (Supplementary Figure S3). Consistent with previous observations (Higgs et al., 2008; Schramm et al., 2012), elevated MrpC levels at 24 h likely explained the early aggregation onset observed in the P_{MUT}-*mrpC* strain (Figure 1C). However, the reduced sporulation efficiency observed by this strain was surprising given MrpC levels were similar at 60 h of development when sporulation levels were reduced compared to the parent (Supplementary Figure S2B). Together, these results suggested that perturbing the binding of MrpC in its promoter region, and likely interfering in MrpC NAR, resulted in an uncoupling between completion of aggregation and induction of sporulation.

3.3 Perturbation of MrpC NAR leads to asynchronous development

Movies of *M. xanthus* development have demonstrated that prior to the onset of sporulation, aggregates are surprisingly dynamic (Curtis et al., 2007; Xie et al., 2011; Zhang et al., 2011; Bahar et al., 2014; Glaser and Higgs, 2019). Initial aggregates often dissolve or coalesce, and even mature aggregates can be mobile prior to transition to stationary spore-filled fruiting bodies (Glaser and Higgs, 2019). To examine how MrpC NAR affected these transient behaviors, the wild type, P_{WT}-*mrpC* (Supplementary Movie S1), and P_{MUT}-*mrpC* (Supplementary Movie S2) strains were induced to develop under submerged culture conditions, imaged every 30 min from 0 to 72 h in an automated plate reader, and the images assembled into movies. For each movie, the time of aggregation onset, the number of initial vs. mature aggregates, and the duration of mature aggregate mobility was recorded. These analyzes demonstrated that aggregation onset in the P_{MUT}-*mrpC* strain assays was 3 h earlier than the wild type and P_{WT}-*mrpC* strains (25 ± 1 vs. 28 ± 1 and 28 ± 1 h post-starvation, respectively) (Figure 1E; Supplementary Figure S2D; Supplementary Table S3).

Remarkable differences in the behavior of mature aggregates between the strains was detected. In the wild type strain, very few mobile aggregates were observed (5 ± 12%) and the duration of mobility was short (2 ± 1 h) (Supplementary Table S3). In the P_{WT}-*mrpC* strain, 40 ± 30% of the aggregates were mobile for 7 ± 3 h (Figures 1F,G; Supplementary Table S3; Supplementary Movie S1). As the endogenous *mrpC* promoter region is still intact in the Δ*mrpC* background, we speculated that the differences between the wild type and P_{WT}-*mrpC* (i.e., Δ*mrpC attB*::P_{WT}-*mrpC*) strains may result from two copies of the *mrpC* promoter region, which may dilute the NAR activity of the available MrpC. Remarkably, however, in 80 ± 20% of the aggregates produced in the P_{MUT}-*mrpC* strain, a large proportion of cells suddenly exited one side of the aggregate, leaving other cells behind as darkened shallow fruiting bodies (Supplementary Movie S2). The cells that exited the aggregate collectively migrated throughout the plate; we referred to these cells as a developmental swarm. Most of these swarms (70%; 19/27) were still actively moving by the end of the

filming period at 72 h. These observations explained both the disorganized appearance of the late aggregates (Figure 1C) and the reduced sporulation efficiencies (Supplementary Figure S2B) observed in the P_{MUT}-*mrpC* strain.

On average, all three strains produced similar maximum numbers of initial aggregates (between 6 and 8) and final fruiting bodies (between 5 and 6) (Supplementary Table S3). However, in the P_{MUT}-*mrpC* strain, the overall number of aggregates that transitioned into fruiting bodies (60 ± 10%) was significantly reduced ($p = 0.031$; *t*-test) compared to the wild type and P_{WT}-*mrpC* strains (80 ± 16% and 80 ± 19%, respectively) (Supplementary Table S3; Supplementary Figure S4B). Interestingly, although aggregation onset in the P_{MUT}-*mrpC* cells was 3 h earlier than the other strains, there was no significant difference in the time at which fully formed aggregates began to move (mobility onset) in the P_{MUT}-*mrpC* (37 ± 4 h) relative to the P_{WT}-*mrpC* cells (37 ± 4 h) (Supplementary Table S3; Supplementary Figure S4A). Thus, the interval between formation of aggregates and onset of aggregate mobility in the P_{WT}-*mrpC* and P_{MUT}-*mrpC* was 7 ± 3, and 11 ± 3 h, respectively.

To better compare the characteristics of the individual entities produced by the P_{MUT}-*mrpC* and P_{WT}-*mrpC* mobile strains, we employed the DeepLabCut deep convolutional neural network (Mathis et al., 2018) to analyze developing strains. The neural network was trained on manually labeled P_{WT}-*mrpC* or P_{MUT}-*mrpC* developmental images with a 50-layer residual network (ResNet-50) for 340,000 iterations resulting in a training and test error of 1.62 and 6.66 pixels, respectively (Becskei and Serrano, 2000; He et al., 2016). The trained neural network was then used to analyze 15 videos of each strain (3 independent biological replicates each with 5 technical replicates). First, the neural network assigned non-mobile aggregates a median speed of 0.22 μm/min (IQR: 0.12–0.40 μm/min), which was attributed to an artifact from slight shifts in the position of the automated plate reader camera between time points (data not shown). In the P_{WT}-*mrpC* strain, the mobile aggregates traveled at an average speed of 0.3 μm/min (Supplementary Figure S4F), and movement was primarily radial (Figure 1F, Supplementary Figure S4C) such that the average net displacement was within two aggregate diameters of the starting point (Figure 1F, Supplementary Figure S4E). In the P_{MUT}-*mrpC* strain, developmental swarms traveled at an average speed of 0.6 μm/min (Supplementary Figure S4F) and their movement involved long runs, sharp turns, and/or repeated reversals (Figure 1F, Supplementary Figure S4D); the average total displacement was 1,500 ± 400 μm (Supplementary Figure S4E). Unlike with the P_{WT}-*mrpC* strain, almost all mobile aggregates left a shallow immobile fruiting body behind (Figures 1C,F). Thus, developmental swarms displayed speed and trajectory characteristics that were significantly different from the P_{WT}-*mrpC* mobile aggregates, suggesting they did not result from simply increasing the duration of the parent aggregate mobility phase.

3.4 MrpC NAR dampens cell-to-cell variability in *mrpC* expression

Theoretical and experimental analyzes have suggested that NAR motifs function to decrease cell-to-cell variability in gene expression, ensuring that expression is homogenous within a population (Becskei and Serrano, 2000). Since the P_{MUT}-*mrpC* strain appeared to produce subpopulations of cells in different developmental states (i.e., developmental swarms and stationary fruiting bodies; Figure 1F), we hypothesized that MrpC-mediated NAR may be functioning to limit heterogeneity of *mrpC* expression thus ensuring a coordinated developmental process.

To examine population variation in *mrpC* expression, we measured mCherry production from individual wild-type cells bearing the P_{WT}-mCh or P_{MUT}-mCh reporter during *in situ* development under submerged culture. For normalization purposes, these cells also contained a construct that expressed mNeonGreen from an inducible promoter integrated at a second genomic site (1.38 kb::$P_{vanillate}$-*mNeonGreen*). These double labeled strains were each diluted 1:19 into a markerless wild type, and single cell fluorescence was recorded using confocal laser scanning microscopy (CLSM). For each cell, mCherry fluorescence was normalized to mNeonGreen fluorescence, and the distribution of red-to-green (RG) ratios from individual cells from three independent biological experiments was plotted. Variability in single-cell RG ratios among the population was calculated using the coefficient of variation (CV).

In pre-aggregating cells (24 h development) with the wild type reporter, a mean RG ratio of 0.38 ± 0.09 was observed with a narrow distribution in values (Figure 2A) that corresponded to a CV of 23.4 ± 0.3% (Figure 2D). Cells with the P_{MUT}-mCh reporter displayed both 3-fold increased mean reporter expression (RG ratio of 1.2 ± 0.4) and a significantly increased spread in distribution of expression (CV 32 ± 2%) (Figures 2A,D). Similarly, in fruiting bodies, cells bearing the P_{MUT}-mCh reporter displayed 2.5- and 1.3-fold increased mean RG ratio and CV compared to the P_{WT}-mCh fruiting body cells, respectively (Figures 2B,D). This trend was also observed in the peripheral rods (mean RG ratio and CV of 3- and 1.3-fold higher than the P_{WT}-mCh reporter, respectively). These results indicated that MrpC-mediated NAR may function to not only limit the level of expression, but also to limit the cell-to-cell variability in expression. Additionally, these results suggested the increase in variability was not subpopulation specific, indicating that MrpC-mediated NAR was functioning throughout the entire population to limit expression heterogeneity.

3.5 Developmental swarms possess an intermediate level of MrpC

Thus far, we observed that disruption of MrpC BS1/5 led to uncoordinated behavior and increased variability in *mrpC* expression within the population. To examine the MrpC levels in individual cells in the distinct subpopulations, we set out to generate strains producing MrpC fused to a fluorescent marker. Attempts to generate strains producing MrpC with fluorescent proteins or small fluorescent tags fused to either the amino- or carboxy-terminus, expressed either from the endogenous *mrpC* locus or from exogenous sites, resulted in strong developmental phenotypes and/or partial release of MrpC from the fusion proteins (data not shown). One interesting exception was a strain bearing a carboxy-terminal mNeonGreen fusion to MrpC expressed from the native *mrpC* promoter in the Δ*mrpC* background (Δ*mrpC attB*::P_{WT}-*mrpC-mNeonGreen*; hereafter termed *mrpC-mNG*). Surprisingly, this strain exhibited a similar developmental swarm phenotype to that of the P_{MUT}-*mrpC* (Supplementary Figure S5A, Supplementary Movie S3) although aggregation onset was 6 h earlier in

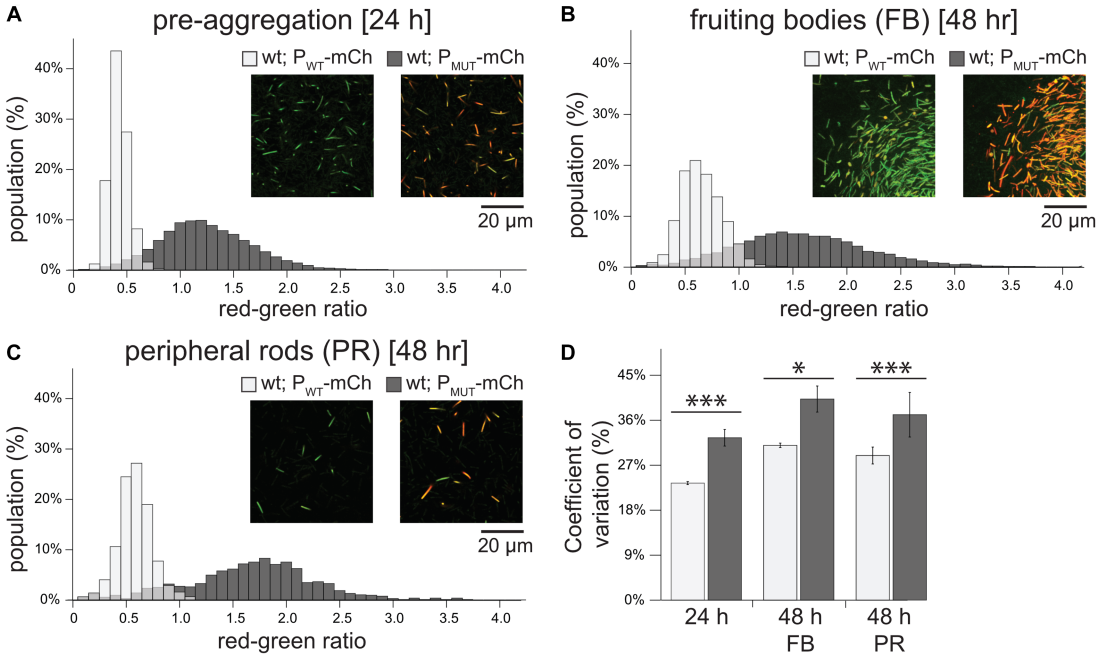

FIGURE 2
Perturbation of MrpC NAR increases the level and population-wide variability of *mrpC* expression. **(A–C)** Histogram of *mrpC* reporter expression in pre-aggregation **(A)**, fruiting body **(B)**, or peripheral rod populations **(C)**. Wild-type cells expressing mCherry from either the wild-type *mrpC* promoter (P_{mrpC}-*mCh*; P_{WT}-*mCh*) or perturbed NAR *mrpC* promoter ($P_{BS5/BS1*}$-*mCh*; P_{MUT}-*mCh*), and mNeonGreen from a constitutive promoter ($P_{vanillate}$-*mNG*). Strains were developed under submerged culture and imaged by confocal microscopy. mCherry (red) and mNeonGreen fluorescence was measured for individual cells and the red-green ratio calculated. Ratios were binned and the percent of the population with the indicated red-green ratio displayed by histogram. For the P_{WT}-mCh strain, n = 8,064 **(A)**, 14,298 **(B)**, and 933 **(C)** cells. For the P_{MUT}-mCh strain, n = 5,835 **(A)**, 11,198 **(B)**, and 850 **(C)** cells. Representative images showing mCherry and mNeonGreen fluorescence overlayed from each population in the indicated strains is shown. Note: the edge of a fruiting body is shown in **(B)**. **(D)** Average coefficient of variation and associated standard deviation was calculated from three independent biological replicates. Light gray: P_{WT}-*mCh*; dark gray: P_{MUT}-*mCh*. Data was analyzed for statistically significant differences using an unequal variances t-test. $*p < 0.05$; $***p < 0.001$.

the *mrpC-mNG* strain than in the P_{MUT}-*mrpC* strain, and there was more variability in the number of mobile aggregates between biological replicates (Supplementary Table S3). These results strongly suggested that fusion of mNeonGreen to the C-terminus of MrpC was interfering in efficient NAR, perhaps because the mNG fusion interferes with cooperative multimeric MrpC interactions required for efficient exclusion of MrpB from the *mrpC* promoter region (McLaughlin et al., 2018). Examination of developing *mrpC-mNG* cells by fluorescence microscopy demonstrated that fluorescence was detected primarily in the center of the cell (Supplementary Figure S5C) likely colocalized with the nucleoid, consistent with the role of MrpC as a global transcriptional regulator. A similar localization was also observed by anti-MrpC immunofluorescence in wild-type developing cells (V. Bhardwaj and P. I. Higgs, unpublished results). Finally, immunoblot analyzes of the developmental *mrpC-mNG* lysates demonstrated no untagged MrpC could be by detected by polyclonal anti-MrpC immunoblot, indicating MrpC-mNG (predicted molecular mass 54 kDa) was the sole version of MrpC in this strain (Supplementary Figure S5B). However, anti-mNG antibodies detected bands corresponding to the 54 kDa MrpC-mNG fusion protein and a 27 kDa mNG monomer (Supplementary Figure S5B). We speculate mNeonGreen was released as a result of normal MrpC turnover (Schramm et al., 2012); importantly, this mNeonGreen should not be localized over the nucleoid and was likely detected as diffuse signal in the cells. Regardless, mNeonGreen fluorescence indicated the level of MrpC that was (at one point) produced. Therefore, we took advantage of the *mrpC-mNG* strain to examine the relative accumulation of MrpC in developing cells in the pre-aggregation, developmental swarm, sporulating fruiting body, and peripheral rod populations *in situ*. For this purpose, the *mrpC-mNG* strain was induced to develop for 24, 30, or 48 h and stained with a membrane dye (FM4-64) for 60 min prior to imaging by CLSM. At the pre-aggregation stage (24 h post-starvation), we observed randomly aligned rod-shaped cells with a mean per cell mNeonGreen fluorescence of 80 ± 20 arbitrary units (AU) (Figures 3A–C). By 30 h, the population divided to produce cells within symmetric round aggregates and peripheral rods remaining between the aggregates with mean per cell fluorescence of 120 ± 20 AU and 60 ± 20 AU, respectively. The observation that mNG fluorescence levels in these two populations correlated with relative levels of MrpC previously observed in peripheral rod populations vs. aggregate populations in *M. xanthus* strain DZ2 (Lee et al., 2012) strongly suggests that mNG fluorescence was also useful for estimating relative levels of MrpC in the developmental swarms. Developmental swarms observed at 48 h contained per cell fluorescence values (70 ± 20 AU) between those observed for cells in the residual fruiting bodies (100 ± 30) and peripheral rods (40 ± 20) (Figures 3A–C). The developmental swarms consisted almost exclusively of rods aligned with their long axis perpendicular to the moving front of the swarm, whereas the fruiting bodies consisted of rods aligned tangential to the edge of the fruiting body or spherical shaped spores (Supplementary Figure S5D). At both 30 and 48 h, the peripheral rods were randomly aligned (Supplementary Figure S5D). These observations

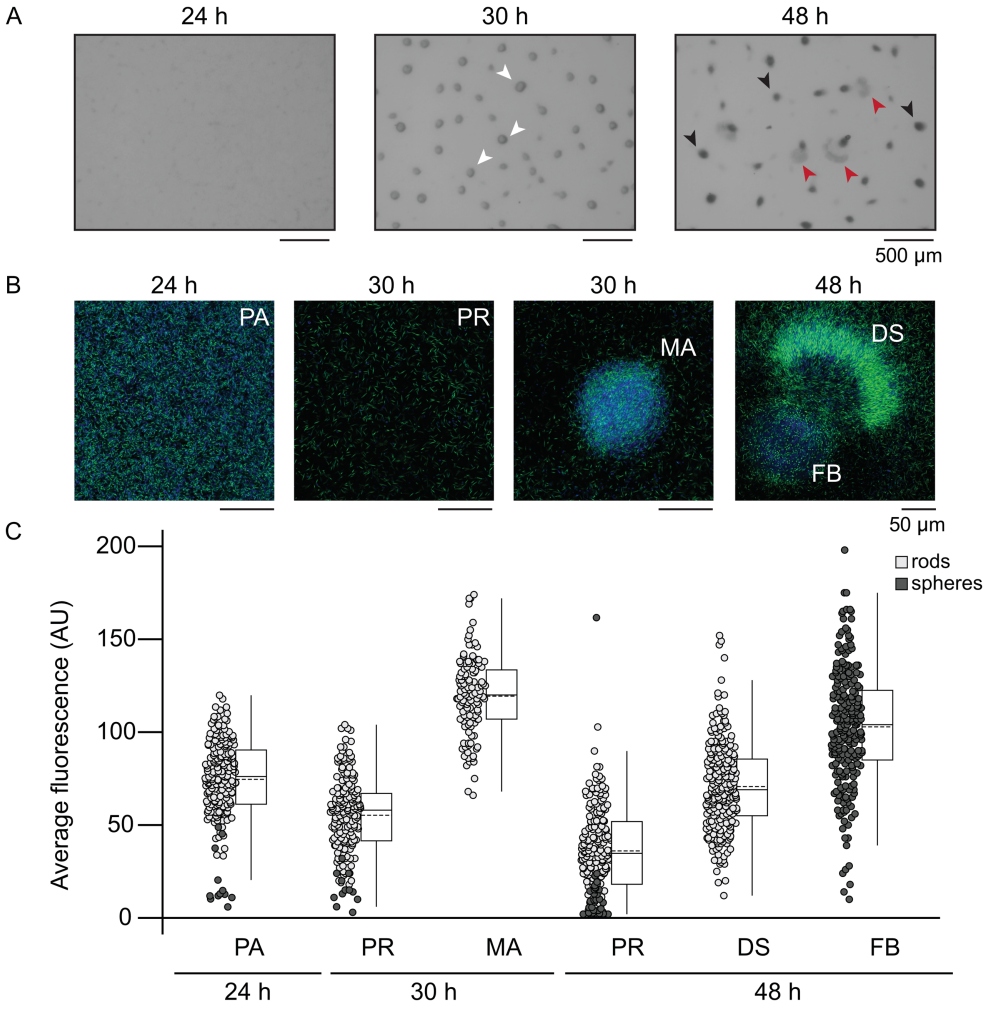

FIGURE 3
Developmental swarms correlate with intermediate MrpC production. **(A)** Developmental phenotype images of the Δ*mrpC* strain expressing *mrpC-mNG* from the wild type *mrpC* promoter integrated at an exogenous locus (P_{WT}-*mrpC-mNG*). **(B)** Fluorescent imaging of P_{WT}-*mrpC-mNG* cells in the indicated stages. Development was induced under submerged culture conditions for the indicated times, treated with FM4-64 membrane stain, and imaged by confocal microscopy. Fluorescence captured from the membrane strain and mNeonGreen is colored blue and green, respectively. **(A,B)** Pre-aggregation cells (PA), mature aggregates (MA, white arrows), developmental swarms (DS, red arrows), and fruiting bodies (FB, black arrows) are indicated. **(C)** Average mNeonGreen fluorescence recorded from individual rod shaped cells (light gray circles) or spherical cells (dark gray circles) in each population. Data distribution is indicated to the right by box plots. Boxes: first quartile-third quartile; whiskers: minimum and maximum; solid line: median; dashed line: mean. Outliers show as distinct dots. Regions of interest (ROIs) were identified based on the membrane stain and the average mNeonGreen fluorescence within the ROI was measured. Results from two independent biological replicates are shown. $n = 200$ cells for PA, 30 h PR and 48 h PR populations. $n = 240$ cells for 30 h MA, 48 h FB, and 48 h DS populations. Circles in the pre-aggregate and peripheral rod populations likely corresponded to end-on cells, rather than spores. Statistical analysis (two-sample unequal variances *t*-test) indicated all populations displayed significantly different average fluorescence intensities ($p < 0.001$), except 48 h DS and 24 h PA ($p = 0.08$).

suggested that developmental swarms arise from cells locked into an intermediate MrpC level. We speculate these intermediate MrpC levels promote cell movement, whereas cells that attained a higher level of MrpC had reduced cell movement and triggered differentiation into non-motile spores forming immobile fruiting bodies.

4 Discussion

MrpC is a key developmental transcriptional regulator of the multicellular developmental program in *M. xanthus*. MrpC accumulation is key to dictate onset of stages (i.e., aggregation and sporulation) within the developmental program, but also likely determines distinct cell fates within the program (Figure 3; Lee et al., 2012). MrpC is subject to negative autoregulation and its promoter region contains at least four MrpC binding sites (McLaughlin et al., 2018). Disruption of either binding site 1 or 5 led to increased *mrpC* expression (Figure 1; Supplementary Figure S1), and disruption of both produced a nearly additive effect. The arrangement of BS1 suggests that MrpC dimers sterically hinder binding of the sigma^{54} factor to its promoter, consistent with DNase foot printing analyzes (Nariya and Inouye, 2006). MrpC binding at BS5 may additionally interfere with MrpB binding to UAS1. We further hypothesize that MrpC bound at BS5 and BS1 may interact to stabilize a DNA loop that further impedes MrpB access to UAS1/2, because deletion of an unusual 25

amino acid N-terminal extension in MrpC has the same effect on the *mrpC* reporter as the Δ*mrpC* deletion strain, but is completely competent for binding at any of BS 1, 3, 4, and 5 *in vitro* (McLaughlin et al., 2018). Thus, the BS1/BS5 mutations likely perturbed MrpC NAR. Consistently, a known attribute of NAR is to constrain variation in gene expression (due to noise reduction), and the BS1/BS5 mutation lead to increased cell-to-cell variation in *mrpC* expression (Figure 2). However, we could not address other known attributes of NAR that have been observed in synthetic systems because we did not isolate MrpC from its additional feedback circuits (examples described below).

One phenotypic consequence of the BS1/BS5 mutations was production of aggregation centers earlier than the parent (Figures 1C,E), likely because MrpC accumulated earlier in this strain (Figure 1D). MrpC levels exhibit similar accumulation patterns in the absence of the Esp signaling system, which induces proteolytic turnover of MrpC (Cho and Zusman, 1999; Schramm et al., 2012). *esp* mutants likewise display early aggregation onset but, in contrast to the P_{MUT}-*mrpC* strain, also result in early and increased sporulation efficiency (Cho and Zusman, 1999; Schramm et al., 2012). The P_{MUT}-*mrpC* strain displayed significantly reduced sporulation efficiency because some cells abruptly exited the aggregation centers and remained locked in a swarming state (Figure 1F; Supplementary Figure S2). This phenomenon can be attributed to increased variability in *mrpC* expression (Figure 2) rather than just increased levels *per se*, because the *esp* mutant does not produce developmental swarms (Schramm et al., 2012) (Supplementary Movie S4). Instead, the *esp* strain skipped the aggregate mobility phase and transitioned into darkened immobile fruiting bodies earlier than the wild type (Supplementary Movie S4).

The increased cell-to-cell variability in *mrpC* expression likely produced a population that simultaneously contains a mixture of cells at different MrpC thresholds (i.e., pre-aggregation, aggregation, or sporulation) (Figure 4). For example, at 30 h of development, the population consisted of cells that had already accumulated higher levels of MrpC and were already in mature aggregates (Figure 3), as well as cells which had not yet accumulated much MrpC and had likely not yet aggregated into these centers. By 48 h, some of these cells had already reached the level of MrpC required to commit to sporulation and thus remained in stationary fruiting bodies (Figure 3). Those at the lower end were in the aggregation phase and collectively exited the aggregation center as a swarm. With the wild-type *mrpC* promoter, MrpC levels are more homogeneous within a given time frame, and the population undergoes a quick, collective transition from aggregation to sporulation (Figure 4). Thus, MrpC negative autoregulation appears to be important in maintaining population synchrony during the *M. xanthus* multicellular developmental program.

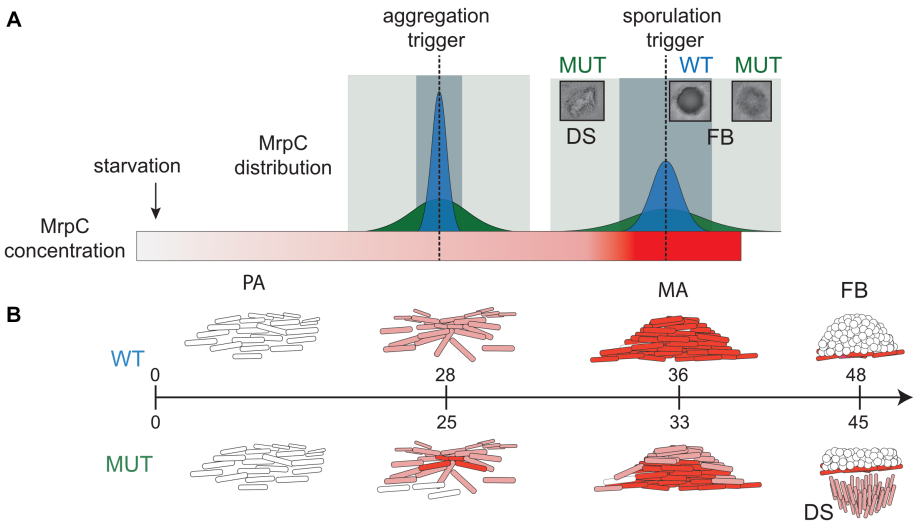

FIGURE 4
Model for role of NAR in synchronized progression through developmental phases. **(A)** Distributions of MrpC in the wild-type (dark blue peak) and perturbed MrpC NAR (dark green peak) strains at trigger points (dotted lines) for aggregation and sporulation. After the onset of starvation, MrpC levels (red gradient rectangle) steadily increase. With appropriate NAR, the distribution of MrpC at the trigger thresholds is constrained which promotes synchronized transition of the population to aggregation and then sporulation phases. The window for population transition to the next stage is short (light blue rectangle). When NAR is perturbed, the distribution of MrpC at the trigger thresholds is broad and cells can contain different threshold levels of MrpC. The window for population transition to the next stage is lengthened (light green rectangle) causing some cells to swarm away from fruiting bodies. **(B)** Schematic of *M. xanthus* developmental stages and associated MrpC levels in individual cells in the wild type (WT; top) and perturbed MrpC NAR mutant (MUT; bottom). WT: Cells (white rods) in the pre-aggregation (PA) stage contain little MrpC. Accumulation of MrpC (light red) triggers aggregation, and cells move into aggregation centers (mounds of cells). Continued accumulation of MrpC (dark red) in mature aggregates (MA) triggers sporulation (white circles) forming fruiting bodies (FB). Mature committed spores contain little MrpC. MUT: Broadened distribution of MrpC results in multiple stages of development at the same time. MAs contain some cells that reached the sporulation threshold. Cells which did not reach the sporulation threshold exit the aggregate as developmental swarms (DS), leaving residual fruiting bodies in place. Peripheral rods are not shown. Aggregation onset is induced on average 3 h earlier than in the wild type.

The swarms that exited the mounds exhibited aberrant behavior because they left the mature aggregates and continued to migrate as a group until at least 72 h post-starvation. How could the P_{MUT}-*mrpC* lead to this novel behavior? One possibility is that cells inside an aggregation center are normally subject to an additional positive feedback loop which is necessary to reinforce transition to sporulation. For example, C-signaling, a contact-dependent signaling system is highly active in aggregated cells and particular in cells transitioning to spores (Sogaard-Andersen and Kaiser, 1996; Hoang et al., 2021), but is presumably inactivated once the cells differentiate into spores. In the P_{MUT}-*mrpC* strain, developmental swarms appear to arise from cells that expressed lower levels of MrpC and arrived at the mature aggregate after the other cells had already sporulated. These late-to-arrive cells may have therefore missed the positive feedback loop necessary to increase MrpC levels to the sporulation threshold (Supplementary Figure S6A), and are instead stuck at intermediate MrpC levels which stimulate aggregation. A second (not mutually exclusive) possibility is that an oscillation motif is triggered in the developmental swarms such that MrpC levels never reach the sporulation threshold but never fall below the aggregation threshold. It is known that oscillations can be generated through a network motif comprised of a composite negative feedback loop coupled to an additional positive feedback loop (Alon, 2007; Stricker et al., 2008). Interestingly, such a motif can be identified for MrpC (Supplementary Figure S6B): MrpC induces expression of *esp* (S. Kasto, A. Schramm and P. I. Higgs, unpublished results), and Esp indirectly induces degradation of MrpC via proteolysis (Schramm et al., 2012). MrpB induces expression of *mrpC*, and MrpC positively regulates expression of *mrpB* (Sun and Shi, 2001a) (C. Mataczynski and P.I. Higgs, unpublished results). Another possibility is that the propagation of these swarms could arise from changes in mechanical forces that govern cell swarms, such as local changes in surfactant or cell–cell adhesion properties (Guzman-Herrera et al., 2020; Islam et al., 2020; Saïdi et al., 2021). The observation that strains that produce the developmental swarms initially produce relatively normal aggregates, is consistent with models suggesting initial aggregates (cell layers) form as a result of physical forces governing self-organization, such as Oswald ripening or active nematic liquid crystal formation (Bahar et al., 2014; Copenhagen et al., 2021). The role of distinct levels of MrpC in strain DZ2 may then be to control the proportions of cells in distinct fates and stabilize transition of aggregates into mature fruiting bodies.

During development in *M. xanthus*, groups of cells organize into a defined pattern (i.e., fruiting bodies) for a designated function (protection and/or collective dispersal), making the developing population akin to a specialized bacterial tissue. While multicellular tissue formation in *M. xanthus* is relatively simple compared to that of higher eukaryotic organisms, many of the same basic regulatory principles still apply. Cells must synchronously progress through development in a defined temporal order to produce a functional structure. This principle is exemplified by the regulation of gastrulation in *Drosophila melanogaster* embryogenesis. Invagination (coordinated cell movement) during gastrulation is largely coordinated by the key regulator, *snail* (Leptin and Grunewald, 1990). Expression of *snail* displays a significant degree of homogeneity and synchronicity, which is crucial for its function (Boettiger and Levine, 2013; Lagha et al., 2013). If synchronicity is perturbed, then multicellular coordination of invagination becomes defective and the severity of the defect strongly correlates with the level of asynchronicity (Lagha et al., 2013). Intriguingly, Snail is proposed to function as a negative autoregulator, which is thought to promote homogeneity of *snail* expression in the population (Boettiger and Levine, 2013); this provides an additional example where the noise reduction attribute of NAR motifs may promote synchronized responses in a multicellular developmental systems.

Our study also illustrates a mechanism for evolution of emergent behaviors. Developmental swarms, a distinct subpopulation of cells stuck in a collective movement state, arose from mutations in MrpC binding sites which likely lead to disruption of MrpC NAR. In general, NAR motifs are thought to contribute to an organism's robustness against mutational perturbations (Marciano et al., 2014). For example, mutations in NAR TF genes are tolerated at a higher rate than in non-NAR TF genes, likely because alterations in NAR TF activity are automatically compensated by changes in the TF self-expression (Marciano et al., 2016). Mutations in a self-promoter, however, can alter the steady state levels of the TF without a corresponding compensation in binding affinity to other target promoters (Kozuch et al., 2020). In a developmental transcriptional network with multiple interconnected regulatory motifs (Supplementary Figure S6C), a perturbed NAR motif leading to increased cell-to-cell variation could lead to subpopulations of cells which trigger or bypass connected regulatory motifs to induce novel cell fate trajectories. Given that *M. xanthus* development is heavily influenced by a number of factors independent of genetic regulatory networks, including physical factors (e.g., surface characteristics) and mechanical properties (e.g., coarsening processes) (Bahar et al., 2014; Liu et al., 2019; Guzman-Herrera et al., 2020; Ramos et al., 2021), it is likely that emerging phenotypes could be drastically different depending on specific environmental conditions or difference in initial population density, leading to eventual selection of beneficial phenotypes perhaps optimized for specific environmental niches.

Data availability statement

The raw data supporting the conclusions of this article will be made available by the authors, without undue reservation.

Author contributions

MM: Conceptualization, Writing – original draft, Writing – review & editing, Investigation. PH: Conceptualization, Writing – original draft, Writing – review & editing, Formal analysis, Funding acquisition, Supervision.

Funding

The author(s) declare financial support was received for the research, authorship, and/or publication of this article. This work was funded by a National Science Foundation grant IOS-1651921 (PIH) and a Rumble Graduate Research Assistantship (MM).

Acknowledgments

The authors gratefully acknowledge Justin Kenney for initial advice on deep convolution neural network analyzes and members of the Higgs and Schrader lab groups for helpful discussions. This manuscript has been submitted as a preprint to bioRxiv (McLaughlin and Higgs, 2019).

Conflict of interest

The authors declare that the research was conducted in the absence of any commercial or financial relationships that could be construed as a potential conflict of interest.

Publisher's note

All claims expressed in this article are solely those of the authors and do not necessarily represent those of their affiliated organizations, or those of the publisher, the editors and the reviewers. Any product that may be evaluated in this article, or claim that may be made by its manufacturer, is not guaranteed or endorsed by the publisher.

Supplementary material

The Supplementary material for this article can be found online at: https://www.frontiersin.org/articles/10.3389/fmicb.2023.1293966/full#supplementary-material

References

Alon, U. (2007). Network motifs: theory and experimental approaches. *Nat. Rev. Genet.* 8, 450–461. doi: 10.1038/nrg2102

Bahar, F., Pratt-Szeliga, P. C., Angus, S., Guo, J., and Welch, R. D. (2014). Describing *Myxococcus xanthus* aggregation using Ostwald ripening equations for thin liquid films. *Sci. Rep.* 4:6376. doi: 10.1038/srep06376

Becskei, A., and Serrano, L. (2000). Engineering stability in gene networks by autoregulation. *Nature* 405, 590–593. doi: 10.1038/35014651

Berleman, J. E., Scott, J., Chumley, T., and Kirby, J. R. (2008). Predataxis behavior in *Myxococcus xanthus*. *Proc. Natl. Acad. Sci. U. S. A.* 105, 17127–17132. doi: 10.1073/pnas.0804387105

Boettiger, A. N., and Levine, M. (2013). Rapid transcription fosters coordinate snail expression in the Drosophila embryo. *Cell Rep.* 3, 8–15. doi: 10.1016/j.celrep.2012.12.015

Camas, F. M., Blázquez, J., and Poyatos, J. F. (2006). Autogenous and nonautogenous control of response in a genetic network. *Proc. Natl. Acad. Sci. U. S. A.* 103, 12718–12723. doi: 10.1073/pnas.0602119103

Cho, K., and Zusman, D. R. (1999). Sporulation timing in *Myxococcus xanthus* is controlled by the espAB locus. *Mol. Microbiol.* 34, 714–725. doi: 10.1046/j.1365-2958.1999.01633.x

Copenhagen, K., Alert, R., Wingreen, N. S., and Shaevitz, J. W. (2021). Topological defects promote layer formation in *Myxococcus xanthus* colonies. *Nat. Phys.* 17, 211–215. doi: 10.1038/s41567-020-01056-4

Cotter, C. R., Schuttler, H. B., Igoshin, O. A., and Shimkets, L. J. (2017). Data-driven modeling reveals cell behaviors controlling self-organization during *Myxococcus xanthus* development. *Proc. Natl. Acad. Sci. U. S. A.* 114, E4592–E4601. doi: 10.1073/pnas.1620981114

Curtis, P. D., Taylor, R. G., Welch, R. D., and Shimkets, L. J. (2007). Spatial organization of *Myxococcus xanthus* during fruiting body formation. *J. Bacteriol.* 189, 9126–9130. doi: 10.1128/JB.01008-07

Dworkin, M., and Gibson, S. M. (1964). A system for studying microbial morphogenesis: rapid formation of microcysts in *Myxococcus Xanthus*. *Science* 146, 243–244. doi: 10.1126/science.146.3641.243

Ellehauge, E., Norregaard-Madsen, M., and Sogaard-Andersen, L. (1998). The FruA signal transduction protein provides a checkpoint for the temporal co-ordination of intercellular signals in *Myxococcus xanthus* development. *Mol. Microbiol.* 30, 807–817. doi: 10.1046/j.1365-2958.1998.01113.x

Glaser, M. M., and Higgs, P. I. (2019). Orphan hybrid histidine protein kinase SinK acts as a signal integrator to fine-tune multicellular behavior in *Myxococcus xanthus*. *J. Bacteriol.* 201:e00561-18. doi: 10.1128/JB.00561-18

Guzman-Herrera, A., Arias Del Angel, J. A., Rivera-Yoshida, N., Benitez, M., and Franci, A. (2020). Dynamical patterning modules and network motifs as joint determinants of development: lessons from an aggregative bacterium. *J. Exp. Zool. B Mol. Dev. Evol.* 336, 300–314. doi: 10.1002/jez.b.22946

He, K., Zhang, X., Ren, S., and Sun, J. (2016). Deep residual learning for image recognition. Proceedings of the IEEE conference on computer vision and pattern, 770–778.

Higgs, P. I., Hartzell, P. L., Holkenbrink, C., and Hoiczyk, E. (2014). "*Myxococcus xanthus* vegetative and developmental cell heterogeneity" in *Myxobacteria: Genomics, cellular and molecular biology*. eds. Z. Yang and P. I. Higgs (Norfolk: Caister Academic Press), 51–77.

Higgs, P. I., Jagadeesan, S., Mann, P., and Zusman, D. R. (2008). EspA, an orphan hybrid histidine protein kinase, regulates the timing of expression of key developmental proteins of *Myxococcus xanthus*. *J. Bacteriol.* 190, 4416–4426. doi: 10.1128/JB.00265-08

Hoang, Y., Franklin, J. L., Dufour, Y. S., and Kroos, L. (2021). Cell density, alignment, and orientation correlate with C-signal-dependent gene expression during *Myxococcus xanthus* development. *Proc. Natl. Acad. Sci. U. S. A.* 118:e2111706118. doi: 10.1073/pnas.2111706118

Hoang, Y., and Kroos, L. (2018). Ultrasensitive response of developing *Myxococcus xanthus* to the addition of nutrient medium correlates with the level of MrpC. *J. Bacteriol.* 200:e00456-18. doi: 10.1128/JB.00456-18

Islam, S. T., Vergara Alvarez, I., Saidi, F., Guiseppi, A., Vinogradov, E., Sharma, G., et al. (2020). Modulation of bacterial multicellularity via spatio-specific polysaccharide secretion. *PLoS Biol.* 18:e3000728. doi: 10.1371/journal.pbio.3000728

Kozuch, B. C., Shaffer, M. G., and Culyba, M. J. (2020). The parameter-fitness landscape of lexA autoregulation in *Escherichia coli*. *mSphere* 5, e00718–e00720. doi: 10.1128/mSphere.00718-20

Lagha, M., Bothma, J. P., Esposito, E., Ng, S., Stefanik, L., Tsui, C., et al. (2013). Paused pol II coordinates tissue morphogenesis in the Drosophila embryo. *Cells* 153, 976–987. doi: 10.1016/j.cell.2013.04.045

Lee, B., Holkenbrink, C., Treuner-Lange, A., and Higgs, P. I. (2012). *Myxococcus xanthus* developmental cell fate production: heterogeneous accumulation of developmental regulatory proteins and reexamination of the role of MazF in developmental lysis. *J. Bacteriol.* 194, 3058–3068. doi: 10.1128/JB.06756-11

Lee, B., Schramm, A., Jagadeesan, S., and Higgs, P. I. (2010). Two-component systems and regulation of developmental progression in *Myxococcus xanthus*. *Methods Enzym.* 471, 253–278. doi: 10.1016/S0076-6879(10)71014-4

Lee, J. S., Son, B., Viswanathan, P., Luethy, P. M., and Kroos, L. (2011). Combinatorial regulation of fmgD by MrpC2 and FruA during *Myxococcus xanthus* development. *J. Bacteriol.* 193, 1681–1689. doi: 10.1128/JB.01541-10

Leptin, M., and Grunewald, B. (1990). Cell shape changes during gastrulation in Drosophila. *Development* 110, 73–84. doi: 10.1242/dev.110.1.73

Liu, G., Patch, A., Bahar, F., Yllanes, D., Welch, R. D., Marchetti, M. C., et al. (2019). Self-driven phase transitions drive *Myxococcus xanthus* fruiting body formation. *Phys. Rev. Lett.* 122:248102. doi: 10.1103/PhysRevLett.122.248102

Maniatis, T., Fritsch, E. F., and Sambrook, J. (1982). *Molecular cloning: A laboratory manual*. Cold Spring Harbor, NY: Cold Spring Harbor Laboratory.

Marciano, D. C., Lua, R. C., Herman, C., and Lichtarge, O. (2016). Cooperativity of negative autoregulation confers increased mutational robustness. *Phys. Rev. Lett.* 116:258104. doi: 10.1103/PhysRevLett.116.258104

Marciano, D. C., Lua, R. C., Katsonis, P., Amin, S. R., Herman, C., and Lichtarge, O. (2014). Negative feedback in genetic circuits confers evolutionary resilience and capacitance. *Cell Rep.* 7, 1789–1795. doi: 10.1016/j.celrep.2014.05.018

Marcos-Torres, F. J., Volz, C., and Muller, R. (2020). An ambruticin-sensing complex modulates *Myxococcus xanthus* development and mediates myxobacterial interspecies communication. *Nat. Commun.* 11:5563. doi: 10.1038/s41467-020-19384-7

Mathis, A., Mamidanna, P., Cury, K. M., Abe, T., Murthy, V. N., Mathis, M. W., et al. (2018). DeepLabCut: markerless pose estimation of user-defined body parts with deep learning. *Nat. Neurosci.* 21, 1281–1289. doi: 10.1038/s41593-018-0209-y

McLaughlin, M., Bhardwaj, V., Feeley, B. E., and Higgs, P. I. (2018). MrpC, a CRP/Fnr homolog, functions as a negative autoregulator during the *Myxococcus xanthus* multicellular developmental program. *Mol. Microbiol.* 109, 245–261. doi: 10.1111/mmi.13982

McLaughlin, M., and Higgs, P. I. (2019). A negative autoregulation network motif is required for synchronized *Myxococcus xanthus* development. *bioRxiv 738716*. doi: 10.1101/738716

Mittal, S., and Kroos, L. (2009a). A combination of unusual transcription factors binds cooperatively to control *Myxococcus xanthus* developmental gene expression. *Proc. Natl. Acad. Sci. U. S. A.* 106, 1965–1970. doi: 10.1073/pnas.0808516106

Mittal, S., and Kroos, L. (2009b). Combinatorial regulation by a novel arrangement of FruA and MrpC2 transcription factors during *Myxococcus xanthus* development. *J. Bacteriol.* 191, 2753–2763. doi: 10.1128/JB.01818-08

Muller, F. D., Treuner-Lange, A., Heider, J., Huntley, S. M., and Higgs, P. I. (2010). Global transcriptome analysis of spore formation in *Myxococcus xanthus* reveals a locus necessary for cell differentiation. *BMC Genomics* 11:264. doi: 10.1186/1471-2164-11-264

Munoz-Dorado, J., Marcos-Torres, F. J., Garcia-Bravo, E., Moraleda-Munoz, A., and Perez, J. (2016). Myxobacteria: moving, killing, feeding, and surviving together. *Front. Microbiol.* 7:781. doi: 10.3389/fmicb.2016.00781

Nariya, H., and Inouye, S. (2005). Identification of a protein Ser/Thr kinase cascade that regulates essential transcriptional activators in *Myxococcus xanthus* development. *Mol. Microbiol.* 58, 367–379. doi: 10.1111/j.1365-2958.2005.04826.x

Nariya, H., and Inouye, S. (2006). A protein Ser/Thr kinase cascade negatively regulates the DNA-binding activity of MrpC, a smaller form of which may be necessary for the *Myxococcus xanthus* development. *Mol. Microbiol.* 60, 1205–1217. doi: 10.1111/j.1365-2958.2006.05178.x

Nevozhay, D., Adams, R. M., Murphy, K. F., Josic, K., and Balazsi, G. (2009). Negative autoregulation linearizes the dose-response and suppresses the heterogeneity of gene expression. *Proc. Natl. Acad. Sci. U. S. A.* 106, 5123–5128. doi: 10.1073/pnas.0809901106

O'Connor, K. A., and Zusman, D. R. (1991). Development in *Myxococcus xanthus* involves differentiation into two cell types, peripheral rods and spores. *J. Bacteriol.* 173, 3318–3333. doi: 10.1128/jb.173.11.3318-3333.1991

Ogawa, M., Fujitani, S., Mao, X., Inouye, S., and Komano, T. (1996). FruA, a putative transcription factor essential for the development of *Myxococcus xanthus*. *Mol. Microbiol.* 22, 757–767. doi: 10.1046/j.1365-2958.1996.d01-1725.x

Rajagopalan, R., and Kroos, L. (2014). Nutrient-regulated proteolysis of MrpC halts expression of genes important for commitment to sporulation during *Myxococcus xanthus* development. *J. Bacteriol.* 196, 2736–2747. doi: 10.1128/JB.01692-14

Rajagopalan, R., and Kroos, L. (2017). The dev operon regulates the timing of sporulation during *Myxococcus xanthus* development. *J. Bacteriol.* 199:e00788-16. doi: 10.1128/JB.00788-16

Ramos, C. H., Rodriguez-Sanchez, E., Del Angel, J. A. A., Arzola, A. V., Benitez, M., Escalante, A. E., et al. (2021). The environment topography alters the way to multicellularity in *Myxococcus xanthus*. *Sci. Adv.* 7:eabh2278. doi: 10.1126/sciadv.abh2278

Robinson, M., Son, B., Kroos, D., and Kroos, L. (2014). Transcription factor MrpC binds to promoter regions of hundreds of developmentally-regulated genes in *Myxococcus xanthus*. *BMC Genomics* 15:1123. doi: 10.1186/1471-2164-15-1123

Rosenberg, E., Keller, K. H., and Dworkin, M. (1977). Cell density-dependent growth of *Myxococcus xanthus* on casein. *J. Bacteriol.* 129, 770–777. doi: 10.1128/jb.129.2.770-777.1977

Rosenfeld, N., Elowitz, M. B., and Alon, U. (2002). Negative autoregulation speeds the response times of transcription networks. *J. Mol. Biol.* 323, 785–793. doi: 10.1016/s0022-2836(02)00994-4

Saïdi, F., Jolivet, N. Y., Lemon, D. J., Nakamura, A., Belgrave, A. M., Garza, A. G., et al. (2021). Bacterial glycocalyx integrity drives multicellular swarm biofilm dynamism. *Mol. Microbiol.* 116, 1151–1172. doi: 10.1111/mmi.14803

Schindelin, J., Arganda-Carreras, I., Frise, E., Kaynig, V., Longair, M., Pietzsch, T., et al. (2012). Fiji: an open-source platform for biological-image analysis. *Nat. Methods* 9, 676–682. doi: 10.1038/nmeth.2019

Schramm, A., Lee, B., and Higgs, P. I. (2012). Intra- and interprotein phosphorylation between two-hybrid histidine kinases controls *Myxococcus xanthus* developmental progression. *J. Biol. Chem.* 287, 25060–25072. doi: 10.1074/jbc.M112.387241

Sogaard-Andersen, L., and Kaiser, D. (1996). C factor, a cell-surface-associated intercellular signaling protein, stimulates the cytoplasmic Frz signal transduction system in *Myxococcus xanthus*. *Proc. Natl. Acad. Sci. U. S. A.* 93, 2675–2679. doi: 10.1073/pnas.93.7.2675

Son, B., Liu, Y., and Kroos, L. (2011). Combinatorial regulation by MrpC2 and FruA involves three sites in the fmgE promoter region during *Myxococcus xanthus* development. *J. Bacteriol.* 193, 2756–2766. doi: 10.1128/JB.00205-11

Stricker, J., Cookson, S., Bennett, M. R., Mather, W. H., Tsimring, L. S., and Hasty, J. (2008). A fast, robust and tunable synthetic gene oscillator. *Nature* 456, 516–519. doi: 10.1038/nature07389

Sun, H., and Shi, W. (2001a). Analyses of mrp genes during *Myxococcus xanthus* development. *J. Bacteriol.* 183, 6733–6739. doi: 10.1128/JB.183.23.6733-6739.2001

Sun, H., and Shi, W. (2001b). Genetic studies of mrp, a locus essential for cellular aggregation and sporulation of *Myxococcus xanthus*. *J. Bacteriol.* 183, 4786–4795. doi: 10.1128/JB.183.16.4786-4795.2001

Thieffry, D., Huerta, A. M., Perez-Rueda, E., and Collado-Vides, J. (1998). From specific gene regulation to genomic networks: a global analysis of transcriptional regulation in *Escherichia coli*. *BioEssays* 20, 433–440. doi: 10.1002/(SICI)1521-1878(199805)20:5<433::AID-BIES10>3.0.CO;2-2

Ueki, T., and Inouye, S. (2003). Identification of an activator protein required for the induction of fruA, a gene essential for fruiting body development in *Myxococcus xanthus*. *Proc. Natl. Acad. Sci. U. S. A.* 100, 8782–8787. doi: 10.1073/pnas.1533026100

Velicer, G. J., Mendes-Soares, H., and Wiegloss, S. (2014). "Whence comes social diversity? Ecological and evolutionary analysis of the Myxobacteria" in *Myxobacteria: Genomics, cellular and molecular biology*. eds. Z. Yang and P. I. Higgs (Norfolk: Caister Academic Press), 1–29.

Xie, C., Zhang, H., Shimkets, L. J., and Igoshin, O. A. (2011). Statistical image analysis reveals features affecting fates of *Myxococcus xanthus* developmental aggregates. *Proc. Natl. Acad. Sci. U. S. A.* 108, 5915–5920. doi: 10.1073/pnas.1018383108

Zhang, H., Angus, S., Tran, M., Xie, C., Igoshin, O. A., and Welch, R. D. (2011). Quantifying aggregation dynamics during *Myxococcus xanthus* development. *J. Bacteriol.* 193, 5164–5170. doi: 10.1128/JB.05188-11

frontiers | Frontiers in Microbiology

TYPE Original Research
PUBLISHED 24 November 2023
DOI 10.3389/fmicb.2023.1295262

OPEN ACCESS

EDITED BY
David Edward Whitworth,
Aberystwyth University, United Kingdom

REVIEWED BY
Volker Siegfried Brozel,
South Dakota State University, United States
Carlos C. Goller,
North Carolina State University, United States

*CORRESPONDENCE
John R. Kirby
jkirby@mcw.edu

†PRESENT ADDRESS
Fatima Saravia,
Research and Innovation Global Oral Care,
Colgate-Palmolive, Piscataway, NJ,
United States

RECEIVED 15 September 2023
ACCEPTED 09 November 2023
PUBLISHED 24 November 2023

CITATION
Müller S, DeLeon O, Atkinson SN, Saravia F, Kellogg S, Shank EA and Kirby JR (2023) Thiocillin contributes to the ecological fitness of *Bacillus cereus* ATCC 14579 during interspecies interactions with *Myxococcus xanthus*.
Front. Microbiol. 14:1295262.
doi: 10.3389/fmicb.2023.1295262

Thiocillin contributes to the ecological fitness of *Bacillus cereus* ATCC 14579 during interspecies interactions with *Myxococcus xanthus*

Susanne Müller[1], Orlando DeLeon[2], Samantha N. Atkinson[1], Fatima Saravia[1†], Stephanie Kellogg[1], Elizabeth A. Shank[3] and John R. Kirby[1*]

[1]Department of Microbiology & Immunology, Medical College of Wisconsin, Milwaukee, WI, United States, [2]Department of Medicine, University of Chicago Pritzker School of Medicine, Chicago, IL, United States, [3]Department of Systems Biology, University of Massachusetts Chan Medical School, Worchester, MA, United States

The soil-dwelling delta-proteobacterium *Myxococcus xanthus* is a model organism to study predation and competition. *M. xanthus* preys on a broad range of bacteria mediated by lytic enzymes, exopolysaccharides, Type-IV pilus-based motility, and specialized metabolites. Competition between *M. xanthus* and prey bacterial strains with various specialized metabolite profiles indicates a range of fitness, suggesting that specialized metabolites contribute to prey survival. To expand our understanding of how specialized metabolites affect predator–prey dynamics, we assessed interspecies interactions between *M. xanthus* and two strains of *Bacillus cereus*. While strain ATCC 14579 resisted predation, strain T was found to be highly sensitive to *M. xanthus* predation. The interaction between *B. cereus* ATCC 14579 and *M. xanthus* appears to be competitive, resulting in population loss for both predator and prey. Genome analysis revealed that ATCC 14579 belongs to a clade that possesses the biosynthetic gene cluster for production of thiocillins, whereas *B. cereus* strain T lacks those genes. Further, purified thiocillin protects *B. cereus* strains unable to produce this specialized metabolite, strengthening the finding that thiocillin protects against predation and contributes to the ecological fitness of *B. cereus* ATCC 14579. Lastly, strains that produce thiocillin appear to confer some level of protection to their own antibiotic by encoding an additional copy of the L11 ribosomal protein, a known target for thiopeptides. This work highlights the importance of specialized metabolites affecting predator–prey dynamics in soil microenvironments.

KEYWORDS

predator–prey interactions, competition, specialized metabolites, *M. xanthus*, *B. cereus*

1 Introduction

Predation is a common form of interspecies interaction in ecosystems. Bacterial predators are important drivers shaping ecological communities: they affect microbial diversity and composition and act as an evolutionary force in bacterial selection (Johnke et al., 2014; Koskella and Brockhurst, 2014; Karakoc et al., 2017; Nair et al., 2019; Wang et al., 2019). Predatory myxobacteria like

Myxococcus xanthus secrete hydrolytic enzymes that degrade prey into consumable molecules (Hart and Zahler, 1966; Sudo and Dworkin, 1972; Munoz-Dorado et al., 2016). *M. xanthus* has a broad prey spectrum ranging from bacteria to yeast and phage, which makes it a major contributor shaping microbial populations in the environment (Morgan et al., 2010; Muller et al., 2014; Livingstone et al., 2018). *M. xanthus* also produces specialized metabolites, two of which have been shown to affect predation (Findlay, 2016; Bader et al., 2020): myxovirescin targets signal peptidase LspA from *Escherichia coli* to enhance predation (Xiao et al., 2012), and myxoprincomide provides protection for *M. xanthus* against *Bacillus subtilis* to promote predation (Muller et al., 2016).

Specialized metabolites are also important for defense and multiple strategies for avoidance have been identified. For example, *Streptomyces coelicolor* produces actinorhodin in response to *M. xanthus* predation, while *Bacillus licheniformis* escapes predation by deactivating myxovirescin (Perez et al., 2011; Wang et al., 2019). Additionally, we have shown that *B. subtilis* NCIB3610 produces bacillaene to delay predation by *M. xanthus* until *B. subtilis* is capable of sporulating within megastructures (Muller et al., 2014). Thus, evidence continues to accumulate that specialized metabolites are part of both predatory and survival mechanisms.

To expand our understanding of *M. xanthus* predator–prey interactions, we conducted a screen to identify susceptible or resistant bacterial strains commonly found in soil. In a companion study (unpublished data), we assayed 5 predatory Myxococcales strains (*M. xanthus*, *Stigmatella aurantiaca, M. flavescens*, *M. virescens*, and *M. fulvus*) for their ability to induce megastructure formation (Muller et al., 2015) in 9 related Bacillales strains (*B. subtilis* 3610, *B. cereus* strains T and ATCC 14579, *B. thuringiensis*, *B. licheniformis*, *B. pumilis*, *Paenibacillus alvei*, and *P. polymyxa* strains ATCC 842 and KCT 3627). From that initial screen, two *B. cereus* stains displayed differential susceptibility to predation: strain ATCC 14579 is resistant to predation whereas strain T is sensitive. We therefore hypothesized that strain ATCC 14579 may produce a specialized metabolite responsible for resistance to predation by *M. xanthus*.

Genome sequencing and analysis revealed that strain T lacks the core components of the biosynthetic gene cluster (BGC) for thiocillins, whereas the predation-resistant 14579 encodes all components for thiocillin biosynthesis. Thiocillins are ribosomally encoded, post-translationally modified, thiazolyl peptide antibiotics and are known to inhibit the interaction between the 23S rRNA and protein L11 within the 50S ribosomal subunit of Gram-positive bacteria (Cameron et al., 2002; Harms et al., 2008). Thiocillin precursors undergo extensive posttranslational modifications on the C-terminus of the pre-peptide, generating a set of eight related antibiotics (Acker et al., 2009; Wieland Brown et al., 2009). Additionally, we performed a phylogenetic analysis of 109 *B. cereus* strains, which revealed that 14579 belongs to a clade possessing the thiocillin BGC while other close relatives do not. Thus, it appears that the thiocillin BGC was horizontally acquired from other bacteria, consistent with previous findings (Grubbs et al., 2017). Furthermore, each thiocillin BGC encodes at least one paralog for L11, providing a potential mechanism for resistance for the producing strains, as previously suggested (Acker et al., 2009; Wieland Brown et al., 2009; Bowers et al., 2010).

Our predation assays here demonstrate that 14579 mutants lacking thiocillin precursor-encoding genes are sensitive to *M. xanthus* predation, while the addition of purified thiocillin rescues these same mutants. Lastly, we observed that viability of *M. xanthus* was strongly affected during competition with 14579 cells in a thiocillin-dependent manner, strongly suggesting that the antimicrobial activity of thiocillins goes beyond Gram-positive bacteria, although the mechanism of action has not been determined. To our knowledge, thiocillin is the first specialized metabolite known to directly affect the fitness of *M. xanthus*. Overall, these findings show that thiocillin provides an advantage for *B. cereus* during competition with a naturally co-occurring predator, *M. xanthus*.

2 Materials and methods

2.1 Bacterial strains and media

Myxococcus xanthus and *Bacillus* strains used in this study are listed in Table 1. *M. xanthus* cultures were grown in liquid CYE media to mid-log phase before processing (Bretscher and Kaiser, 1978). *Bacillus* strains were grown in liquid LB media to a final optical density of about OD_{600nm} of 2.

2.2 Interspecies interaction assays

The *M. xanthus* predator strain DZ2 was washed twice with MMC buffer to remove all nutrients and diluted in MMC buffer (10 mM MOPS [morpholinepropanesulfonic acid; pH 7.6], 4 mM $MgSO_4$, 2 mM $CaCl_2$) to a final concentration of 2×10^9 cells/ml (Muller et al., 2014). Predator and prey cells (*B. cereus* strains at a final concentration of 1×10^{11} cells/ml) were mixed at a ratio of 1:50 and 7 μL were spotted onto CFL starvation media [10 mL 1 M MOPS pH 7.6, 10 mL 0.1 M KH_2PO_4, 10 mL 0.8 M $MgSO_4$, 10 mL 2% $(NH_4)_2SO_4$, 1 mL 20% Sodium Citrate, 0.015 g Casitone, 15 g agar, 959 mL H2O] (Berleman and Kirby, 2007) and incubated at 32°C. As a negative control, MMC buffer alone was used instead of the predator. Predation is displayed in form of lysis of the prey cells compared to the control. To test whether purified thiocillin affects predation, interspecies interaction assays were set up as described above and thiocillin or thiocillin T4V (dissolved in DMSO) were added at a final concentration of 330–990 ng/microliter. As a negative control, DMSO alone, at the same concentration was

TABLE 1 Bacterial strains used in this study.

Bacterial strains	Reference/Source
Myxococcus xanthus DZ2	Muller et al. (2014)
DZ2 *attB8*::pWB200	Muller et al. (2016)
Bacillus cereus strain T	Bacillus genetic stock center
Bacillus cereus ATCC14579	Bacillus genetic stock center
Bacillus cereus ATCC14579 Δ*tclE-H*	Bleich et al. (2015)
Bacillus cereus ATCC14579 *tclE-H*::*tclE* (T4V)	Bleich et al. (2015)
Bacillus cereus ATCC14579 Δ*tclM*	Bleich et al. (2015)
Bacillus cereus ATCC14579 *tclE-H*::*tclE* (A78)	Bleich et al. (2015)
Bacillus cereus ATCC14579 *tclE-H*::*tclE* (C9A)	Bleich et al. (2015)
Bacillus cereus ATCC14579 *tclE-H*::*tclE* (C5A)	Bleich et al. (2015)
Bacillus cereus ATCC14579 *tclE-H*::*tclE* (C7A)	Bleich et al. (2015)
Bacillus cereus ATCC14579 *tclE-H*::*tclE* (C2S)	Bleich et al. (2015)

used instead of the predator. Native thiocillin was purified or obtained from Cayman Chemical or from Albert Bowers (UNC-Chapel Hill, provided to E.A.S.) (Acker et al., 2009; Bowers et al., 2012). Molecules from each source yielded similar results. Purified thiocillin T4V is not commercially available and was obtained from Albert Bowers.

2.3 Microscopy

All assays were monitored by microscopy using a Nikon SMZ10000 dissecting microscope. Images were taken using a QImaging Micropublisher CCD camera and processed with Qcapture software.

2.4 PacBio sequencing and assembly

Bacillus cereus strains T and ATCC 14579 were sequenced at the University of Wisconsin Milwaukee School Freshwater Sciences Great Lakes Genomic Center using the Pacific Biosciences (PacBio) RSII SMRTcell system. Resulting reads were then assembled using Canu v.1.6 (Koren et al., 2017) with default settings except for a corrected error rate of 0.040 and the respective genome size of 5.76 MB for *B. cereus* strains. Circlator v. 1.5.5 (Hunt et al., 2015) was used to circularize the genomes and verified with MUMmer v. 3.23 (Kurtz et al., 2004) to confirm the correct regions were matched. Circularized genomes were then annotated on the RAST server[1] (Aziz et al., 2008; Brettin et al., 2015). The nucleotide sequence for *B. cereus* strain T has been submitted to GenBank under nucleotide accession number CP130491. The nucleotide sequence for *B. cereus* ATCC 14579 is available under nucleotide accession number CP138336, CO138337.

2.5 Pangenomics analysis

Pangenomics analysis of the *B. cereus* strains were performed using the anvio suite (v5.5) (Eren et al., 2015; Delmont and Eren, 2018). FASTA files for the *B. cereus* strains T and ATCC 14579 were annotated for open reading frames (ORFs) using Prodigal under default settings. Subsequent ORF calls were translated and given protein annotations using the PFAMs database (Jones et al., 2014) under "sensitive" settings. Biosynthetic gene clusters (BGCs) were identified using antiSMASHv5 under default settings (Blin et al., 2019). FASTA files were then converted into anvio contigs databases ("anvi-gen-contigs-database") with the ORF calls, PFAM calls, and BGC annotations imported using the "anvi-import". A custom python script was used to parse the antiSMASH outputs to the anvio import format. Single copy genes in each genome were identified using a hidden markov model (hmm) with the Campbell database for reference ("anvi-run-hmms") (Campbell et al., 2013). To perform the pangenomics analysis, a single genomes database file was generated to integrate the two contigs database files for the two strains ("anvi-gen-genomes-storage" using the flag "—external-genomes"). The pangenome analysis was performed under the command "anvi-pan-genome" using the settings "—minbit = 0.5", "—mcl-inflation = 10", and "—use-ncbi-blast". Briefly, NCBI BLASTP was used to generate matches between the translated ORFs of the two strains. The subsequent protein cluster matches were then refined using the minbit heuristic as defined by Benedict et al. (2014). Cluster granularity and sensitivity was further refined by the MCL inflation parameter =10 (high sensitivity, low granularity) as T and ATCC 14579 are strains of the same species and closely related. The resulting protein clusters were then visualized using "anvi-display-pan" and sorted using a "presence or absence" scheme including protein clusters belonging to the thiocillin cluster and other BGCs flagged. Further visual manipulations were performed in Inkscape.

2.6 Phylogenomics analysis

To provide phylogenetic relationships between the *B. cereus* species relative to the presence of the thiocillin BGC, we examined 109 publicly available strains' genomes (from the RefSeq database) including the original ATCC 14579 sequence (accession number AE016877.1). See Supplementary Table S1 for strain names. FASTA files for these genomes, along with those for strain T and ATCC 14579 were annotated and imported into anvio for a pangenomics analysis as described above. All open reading frames were reannotated using Prodigal for consistency and anvio formatting purposes. For phylogenomic comparisons, single-copy genes found to be shared by the 111 strains were called using "anvi-get-sequences-for-hmm-hits" using the flags "--hmm-source Campbell_et_al", "--get-aa-sequences", and "—concatenate" (Campbell et al., 2013). The resulting FASTA file output had a resulting aa sequence of the concatenated single-copy genes for each genome. Sequences were then aligned using MUSCLE (Edgar, 2004) and a tree was generated using an approximately maximum-likelihood method (ML) and exported into Newick (.nwk) format (Edgar, 2004; Price et al., 2010). The resulting tree was midpoint rooted and visualized in FigTree (Rambaut, A., Drummond AJ 2010 FigTree v1.3.1. Institute of Evolutionary Biology, University of Edinburgh, Edinburgh http://tree.bio.ed.ac.uk/software/figtree/).

3 Results

3.1 Production of thiocillin protects *Bacillus cereus* ATCC 14579 from predation by *Myxococcus xanthus*

While *M. xanthus* can prey upon a large variety of bacteria, some strains are resistant to predation (Muller et al., 2014). We conducted a screen that revealed that *B. cereus* strain T is sensitive to *M. xanthus* predation while *B. cereus* ATCC 14579 is resistant. Both predator and prey cells were grown as described in Materials and Methods, washed, mixed and then spotted onto agar plates (See Methods). Predation is visible as clearing of the prey colony relative to the buffer control, while resistance is indicated by a ring of cells at the edge of the original spot (Figure 1). Colonies form a doughnut shape with higher cell density at the outer edge of the spot due to surface tension. After suitable prey is consumed, *M. xanthus* cells undergo fruiting body formation as described previously (Berleman and Kirby, 2007) and is visible as dark aggregates after 48 h (square in Figure 1). The results

1 http://rast.nmpdr.org/

indicate that *B. cereus* strain T is consumed while strain 14579 is largely resistant to predation by *M. xanthus* under the conditions of our assay. In addition, few *M. xanthus* cells appear outside of the original spot of 14579 (Supplementary Figure S1), suggesting that predation or motility may be reduced for *M. xanthus* cells due to an inhibitory factor produced by 14579.

Because specialized metabolites contribute to interspecies interactions, and due to thiocillin's established role as both a killing and signaling molecule, we hypothesized that *B. cereus* ATCC 14579 is resistant to predation by *M. xanthus* due to thiocillin production (Xiao et al., 2012; Muller et al., 2014; Bleich et al., 2015; Muller et al., 2015; Findlay, 2016; Muller et al., 2016). Therefore, we tested various 14579 thiocillin mutant strains for their ability to resist or compete with *M. xanthus*. 14579 mutant cells lacking genes encoding the thiocillin precursor peptide (Δ*tclE-H*) were found to be sensitive to predation by *M. xanthus*, like strain T. Furthermore, we tested various mutant thiocillin strains (T4V, A78, C9A, C5A, C7A, and C2S) each of which lack antimicrobial activity against *B. subtilis* but retain the capacity to induce biofilm formation in *B. subtilis* (Acker et al., 2009; Bleich et al., 2015). We also tested a Δ*tclM* mutant strain that produces a thiocillin derivative with no macrocycle ring. Each *B. cereus* thiocillin mutant strain was sensitive to predation by *M. xanthus* (Figure 1 and Supplementary Figure S2). We conclude that the *B. cereus* wild-type thiocillin confers resistance to *M. xanthus* predation.

3.2 Purified thiocillin protects sensitive *Bacillus cereus* strains from predation by *Myxococcus xanthus*

To further assess the ability for thiocillin to protect against predation, we tested purified thiocillin for its ability to rescue predation-sensitive mutants. We also tested the purified T4V variant of thiocillin, since this molecule was shown to have no antimicrobial activity against *B. subtilis* or *Staphylococcus aureus* (Acker et al., 2009). The purified molecules were dissolved in DMSO to a final concentration up to 1 μg/μl. Assays were performed by mixing *M. xanthus* and *B. cereus* cells with and without purified thiocillin or vehicle alone (see Methods, Figure 2). We tested both *B. cereus* strain T (Figure 2A) and 14579 Δ*tclE-H* mutant cells (Figure 2B). *B. cereus* cells alone show no clearing (Figure 2, columns I and II). When *M. xanthus* is added, the prey cells are consumed resulting in clearing (Figure 2, column III). In contrast, purified thiocillin appears to increase survival of *B. cereus*, which was more pronounced with increasing concentrations of thiocillin (Figure 2,

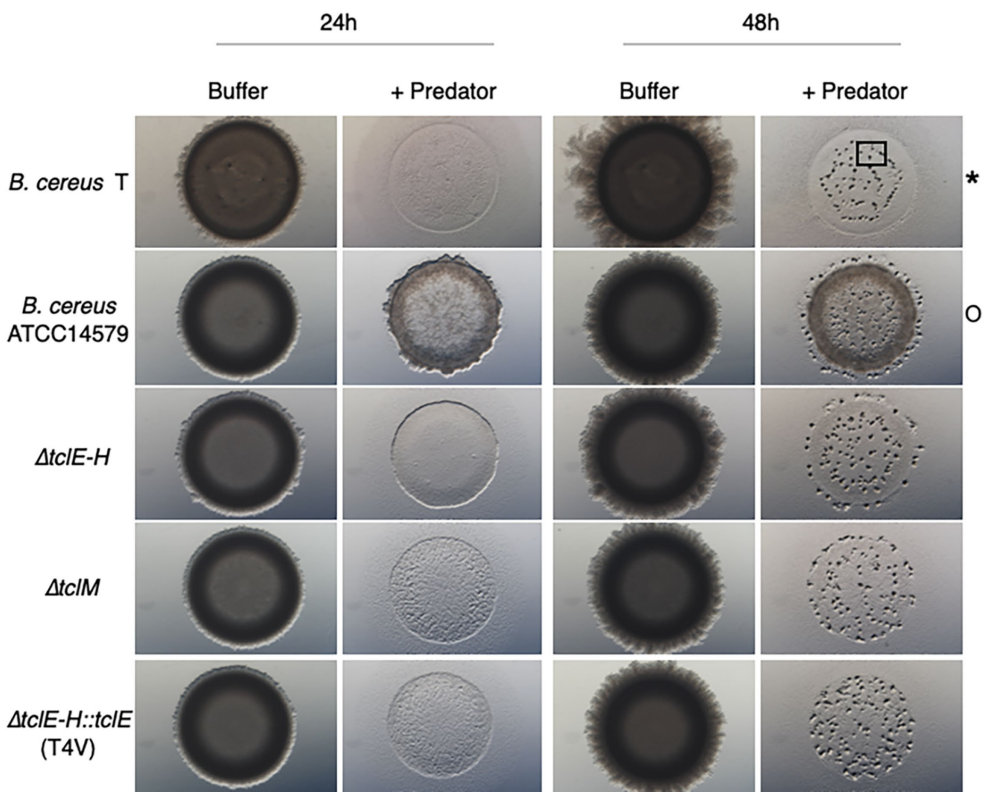

FIGURE 1
Thiocillin protects *B. cereus* ATCC 14579 from predation by *M. xanthus*. *B. cereus* strains (prey) were grown to a certain cell density (see Materials and Methods) and nutrients were removed by washing the cells multiple times. Prey cells were mixed with the predator *M. xanthus* in a ratio of 50:1, spotted on CFL Agar plates and incubated at 32°C. Pictures were taken after different times of incubation at 15x magnification. Predation is visible by cell lysis (*) whereas competition/predation resistance is indicated by minimal loss of cells (O). Fruiting body formation can be seen after 48 h as an indicator that predator *M. xanthus* sensed a drop down in nutrients and is starving (black square). Only *B. cereus* ATCC 14579 resists predation and mutations inhibiting thiocillin production or resulting in modifications of the thiocillin molecule render cells to be predation sensitive. *B. cereus* ATCC 14579 Δ*tclE-H* does not contain the thiocillin prepeptide encoding genes *tclE-H* and does therefore not make thiocillin. *B. cereus* ATCC 14579 Δ*tclE-H::tclE* (T4V) makes a variant of the thiocillin molecule that has lost the antimicrobial function of the molecule but is still able to induce matrix formation in *B. subtilis*. Strain Δ*tclM* produces a thiocillin-like molecule that has no closed ring structure.

10.3389/fmicb.2023.1295262

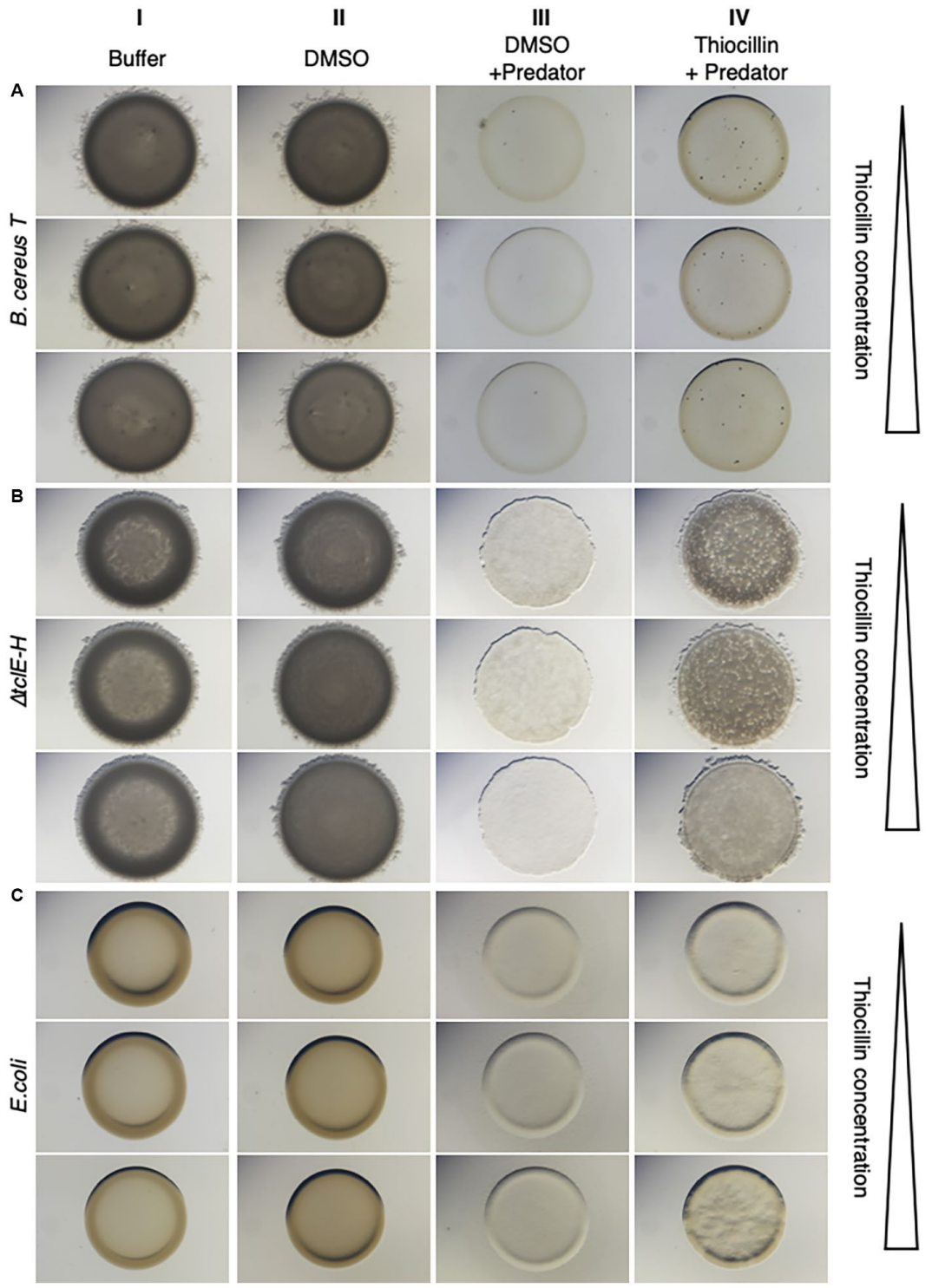

FIGURE 2
Purified Thiocillin rescues sensitive strains from predation by *M. xanthus*. The predation sensitive strains *B. cereus* strain T **(A)**, *B. cereus* ATCC 14579 Δ*tclE-H* **(B)** and *E.coli DH5α* **(C)** were tested in predation assays with the predator *M. xanthus* with and without purified thiocillin (dissolved in DMSO). *B. cereus* ATCC 14579 Δ*tclE-H* is not able to produce thiocillin anymore and *B. cereus* strain T does not contain the thiocillin BSG. All strains are sensitive to predation (comparing column III to I and II). The addition of purified thiocillin protected all sensitive strains from predation (column IV). Increasing concentrations of thiocillin enhanced the predation protective effect. Pictures were taken after 24 h.

column IV). Protection from predation was also visible using *E. coli* and the *B. cereus* 14579 T4V mutant cells supplied with extracellular thiocillin (Figure 2C and Supplementary Figure S3). We also observed *M. xanthus* cells beyond the edge of the original prey spot when thiocillin was present at low concentrations but not at high concentrations, further suggesting an inhibitory role for thiocillin against *M. xanthus* (Supplementary Figure S4). We conducted a parallel set of assays using purified T4V (Supplementary Figure S5). The T4V variant of thiocillin

10.3389/fmicb.2023.1295262

was unable to protect sensitive cells against predation by *M. xanthus*. Together, these results show that exogenous thiocillin can protect sensitive *B. cereus* strains, as well as *E. coli*, from *M. xanthus* predation.

3.3 Thiocillin affects the fitness of *Myxococcus xanthus* in predation assays with *Bacillus cereus* 14579

The above experiments (Figure 1) reveal that thiocillin confers resistance to predation by *M. xanthus* and suggest a potential to inhibit predator cells. To test this possibility, we conducted additional quantitative experiments to assess survival rates for both *M. xanthus* and *B. cereus* in our assays. To conduct these experiments, both wild-type and mutant *B. cereus* strains were mixed with *M. xanthus* cells and incubated as described above. For controls, and to normalize the results, each strain was also incubated alone on agar surfaces. Cells were harvested after 24 h and colony forming units (CFU) were determined on selective media that supported either the growth of *B. cereus* (LB) or *M. xanthus* (CYE with kanamycin). *B. cereus* strains were evaluated at 24 h when no growth of *M. xanthus* was detected. The results were normalized to the starting number of CFUs for each experiment (Figure 3, Methods). In agreement with the visual phenotypic data (Figure 1), *B. cereus* mutants (Δ*tclE-H* and T4V-producing strains) showed survival rates that were below 1%. In contrast, about 23% of the *B. cereus* ATCC 14579 cells survived, indicating that thiocillin provides a distinct advantage against predation by *M. xanthus* (Figure 3A).

Predators typically grow because of the nutrient uptake from killing and consuming prey. This was observed for *M. xanthus*, which displayed growth of ~230% when mixed with *B. cereus* strain Δ*tclE-H* and ~ 150% when mixed with *B. cereus* T4V compared to growth alone. In contrast, only about 12% of *M. xanthus* cells survived the interaction with *B. cereus* 14579 (Figure 3B). Together, these results indicate that production of native thiocillin not only enhances *B. cereus* survival in the presence of *M. xanthus* but also that thiocillin reduces *M. xanthus* survival under the conditions of our assay. We next tested the effect of purified thiocillin directly on *M. xanthus* cells and plated as above to determine CFU. The addition of thiocillin resulted in a ~ 50% decrease in survival of *M. xanthus* when compared to controls (Figure 3C). These results suggest that thiocillin exerts its protective effect by reducing the viability of the predator.

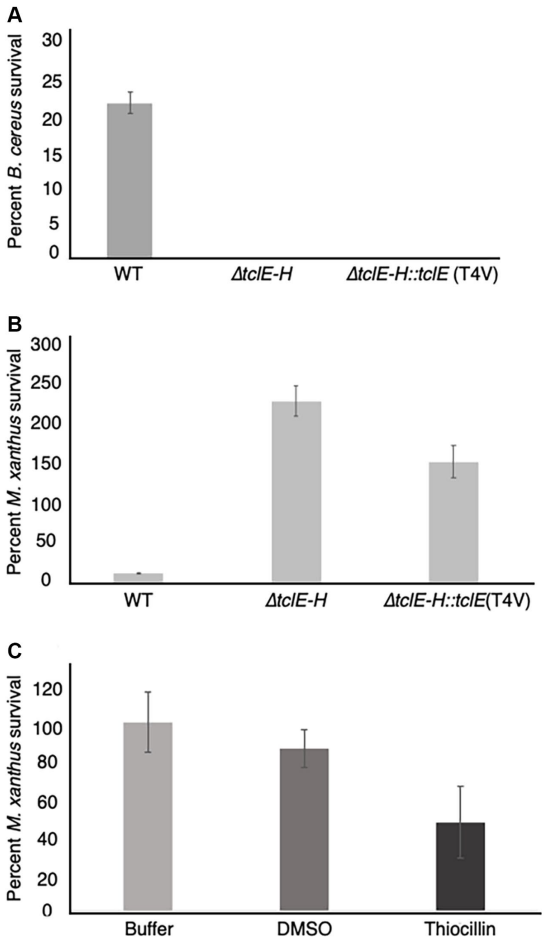

FIGURE 3
Quantification of predator and prey survival reveals strong competition during interspecies interactions between *M. xanthus* and *B. cereus* ATCC 14579. Quantification of prey survival and predator survival/growth. **(A)** Prey *B. cereus* ATCC 14579 and mutant strains *B. cereus* ATCC 14579 Δ*tclE-H* or Δ*tclE-H::tclE* (T4V) were mix in a 50:1 ratio with *M. xanthus* and spotted onto CFL Agar plates. As controls the strains were incubated individually. After incubation at 32°C. for 24 h, cells were removed from the plates and CFU were determined to calculate prey survival calculated relative to controls. The majority of *B. cereus* ATCC 14579 Δ*tclE-H* and Δ*tclE-H::tclE* (T4V) were consumed by the predator *M. xanthus,* whereas about 23.5% of the wild type strain *B. cereus* ATCC 14579 survived. **(B)** *M. xanthus* was able to grow in the presence of *B. cereus* ATCC 14579 Δ*tclE-H* and Δ*tclE-H::tclE* (T4V) but only around 12% of *M. xanthus* could be recovered when mixed with *B. cereus* ATCC 14579 clearly showing this interspecies interaction is of competitive nature effecting the ecological fitness of both strains. **(C)** Purified thiocillin affects predator viability. Percent *M. xanthus* survival after 24 h. *M. xanthus* cells where washed and resuspended to 250 KU. Cells where mixed with either buffer, DMSO or thiocillin (thiocillin 300 ng) and spotted on CFL Agar. Cells were harvested after 24 h and serial dilutions were plates in CYE agar to calculated CFU's.

3.4 Comparative genomics of *Bacillus cereus* strain T and strain ATCC 14579 reveals a difference in the biosynthetic gene cluster responsible for thiocillin production

The above data demonstrate a role for thiocillin in protecting *B. cereus* from *M. xanthus* predation. Furthermore, the phenotypic differences between strain T and 14579 suggest that thiocillin production likely does not occur for strain T. We predicted that these strains would harbor changes in biosynthetic genes required for production or delivery of thiocillin. Thus, we utilized PacBio long-read sequencing to determine genomic content for each strain. The Anvi'o workflow for pangenomics was used to compare both genomes (Figure 4B). Overall, we found 4,656 shared gene clusters between the two strains, 406 gene clusters exclusive to strain T, and 549 gene clusters exclusive to 14579 (Figure 4A). The term "gene cluster" is defined as sequences of one or more predicted open reading frames grouped together based on homology from translated DNA sequences. Gene clusters may contain orthologous or paralogous sequences from one or more genomes analyzed within the pangenome (Delmont and Eren, 2018).

We identified 9 BGCs common to both genomes including 3 non-ribosomal peptide synthases as well as other BGCs required for

10.3389/fmicb.2023.1295262

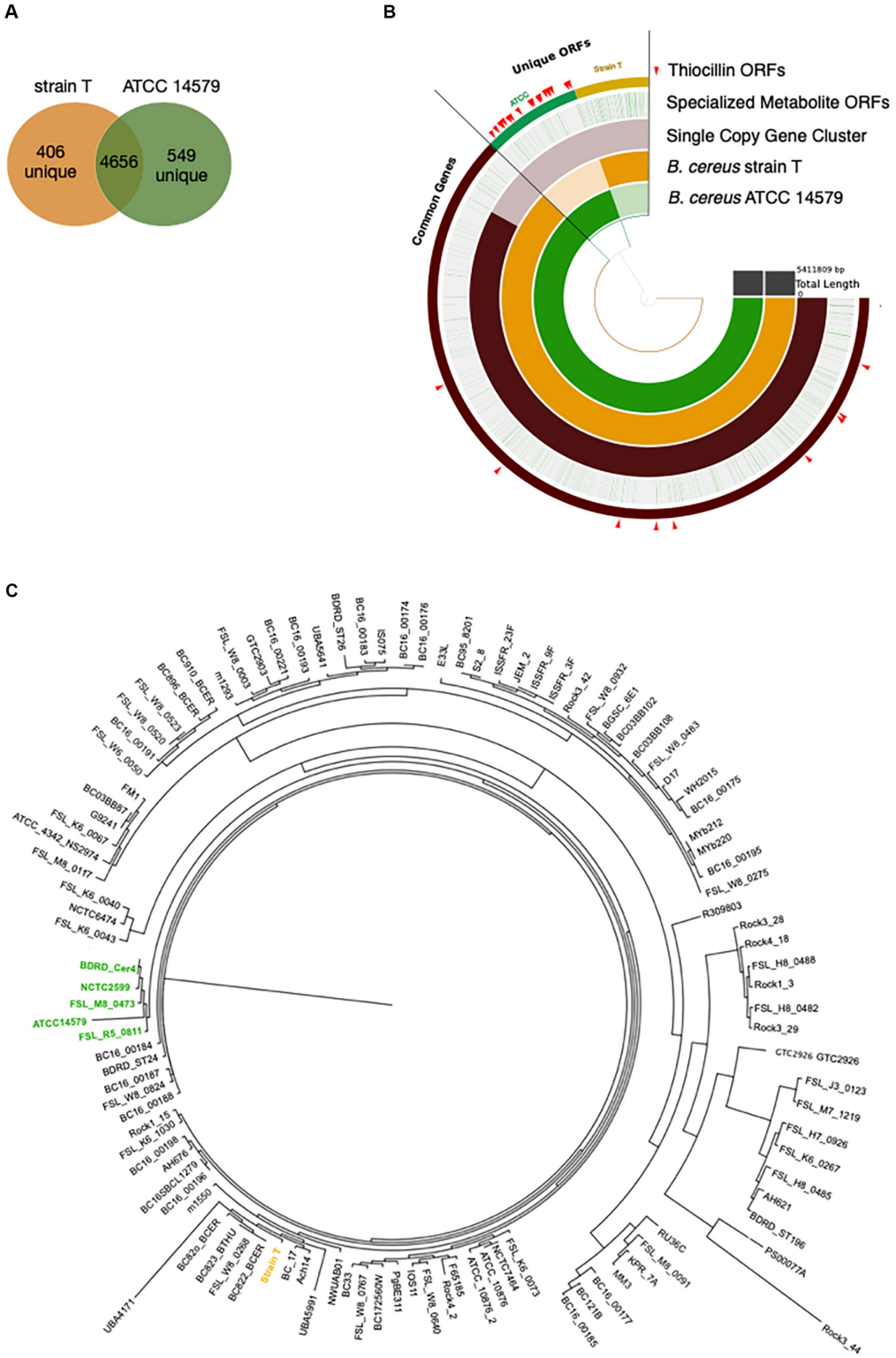

FIGURE 4
Pangenomics of *B. cereus* strain T and ATCC 14579 reveals differences in specialized metabolite gene clusters. **(A)** Venn diagram of the shared genes and unique genes between *B. cereus* strain T and ATCC 14579. **(B)** Anvi'o plot of *B. cereus* strain T and ATCC 14579 genomes. Open reading frames (ORFs) for the two strains were compared using the anvio workflow for pangenomics. ORFs were called using prodigal and annotated using InterproScan for PFAM annotations. ORFs were aligned and compared using blastp and weak matches refined using minbit = 0.5 and MCL inflation parameter of 10. AntiSMASHv5.0 was used to annotate the complete specialized metabolite clusters, including thiocillin. Individual ORFs for all specialized metabolites are shown in green lines (Specialized Metabolite ORFs ring), many of which are specific to ATCC (green) and strain T (gold) as visible in the thiocillin ORFs ring. ORFs comprising the thiocillin operon are marked with red arrows. **(C)** Phylogenetic tree (Maximum Likelihood, midpoint root) based on a multiple sequence alignment of SCGs (single copy genes) using 109 *B. cereus* strains. Five thiocillin producing strains were identified that cluster together (green) indicating that they are closely related. Due to the close phylogenetic relationship of the thiocillin BGC containing strains it is most likely that a single common ancestor did gain the BGC by horizontal gene transfer.

synthesis of 3 bacteriocins, 1 betalactone, 1 siderophore, and 1 terpene. Strain T has 3 additional BGCs not found in 14579 (Table 2) while 14579 has 1 BGC predicted to generate thiocillin, which was not found in strain T (Blin et al., 2019). The thiocillin BGC in 14579 includes the thiocillin-precursor encoding genes *tclE-H* as well as core genes involved in biosynthesis, posttranslational modification, transport, and additional genes (Figure 5). Notably, strain T lacks open reading frames encoding TclA-TclU, which include most of the core functions for production of thiocillin. However, strain T does possess transporter functions common to strain 14579, suggesting either an insertion or deletion of the core biosynthetic genes for thiocillin occurred in a common ancestor. Overall, *B. cereus* strain T appears to be incapable of thiocillin production.

TABLE 2 Comparison of BGCs found in *B. cereus* strain T and ATCC14579.

Type	% Nucleotide similarity of core BGCs ORFs
Similar BGCs	
Bacteriocin	98.13%
Bacteriocin	97.88%
Bacteriocin	91.41%
Betalactone	97.51%
NRPS	98.40%
NRPS	98.31%
NRPS	92.59%
Siderophore	98.42%
Terpene	98.84%
Unique BGCs	
Thiopeptide (thiocillin)	ATCC14579
NRPS/transAT-PKS	strain T
NRPS	strain T
NRPS	strain T

Furthermore, the BGC in 14579 encodes two copies of a paralog of the L11 ribosomal protein encoded by *rplK* located near genes encoding the alpha and beta subunits of RNA polymerase, *rpoA* and *rpoB*, respectively. L11 associates with the 23S rRNA within the 50S subunit of bacterial ribosomes and is the known target for thiocillins (Cameron et al., 2002; Harms et al., 2008). The two paralogs of L11 encoded within the thiocillin BGC for 14579, TclQ and TclT, are identical to each other but distinct from L11 (Supplementary Figure S6). As previously described, the L11 paralogs likely provide protection for thiocillin-producing strains, as suggested previously (Acker et al., 2009; Wieland Brown et al., 2009; Bowers et al., 2010). Whether or not TclQ and TclT can interact directly or indirectly with 23S rRNA or within the 50S subunit has not been determined experimentally.

To address the question of whether the core BGC differences between 14579 and strain T likely resulted from insertion or deletion, we analyzed 109 publicly available *B. cereus* genomes for the presence or absence of 21 core thiocillin biosynthetic genes within the group (Figure 4C). We generated a multiple sequence alignment of all shared proteins between these strains using MUSCLE and examined their phylogenetic relationships using a maximum likelihood tree (Edgar, 2004). We then examined the genomes for each gene within the known thiocillin BGC spanning *tclA-tclX* and utilized antiSMASH to assess each genome for the presence of a thiocillin-encoding BGC. Of the 109 strains, only five contained the biosynthetic gene cluster for thiocillin (strains FSL_R5_0811, FSL_M8_0473, NCTC2599, BDRD_Cer4, and ATCC 14579), consistent with previous reports indicating that only 4% of *B. cereus* strains possess thiocillin-like BGCs (Grubbs et al., 2017).

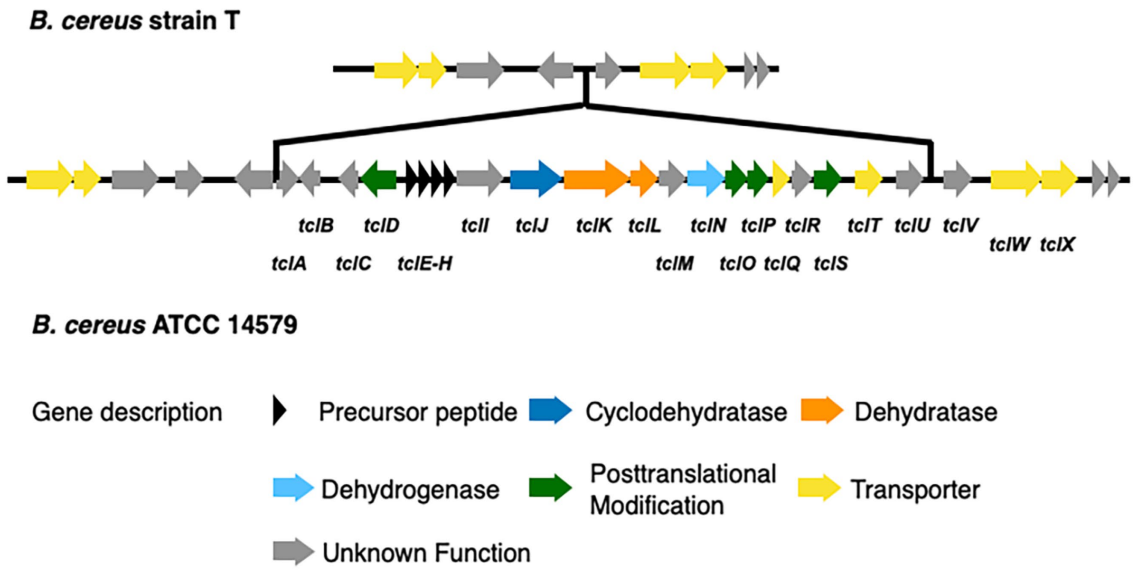

FIGURE 5
Comparison of the thiocillin synthesis gene clusters of *B. cereus* ATCC 14579 and *B. cereus* T. The thiocillin synthesis gene cluster is composed of the precursor peptide encoding genes *tclE-H* (black) as well as biosynthesis genes (blue and orange). Genes encoding proteins functioning in posttranslational modification (green) and transport (yellow) are also part of the thiocillin synthesis gene cluster. Comparison of both *B. cereus* strains revealed that *B. cereus* T does not contain the central components of the thiocillin synthesis gene cluster *tclA-tclU* including the precursor peptide encoding genes *tclE-H*.

Each of these 5 strains encode at least one paralog of the L11 ribosomal protein. Other than the 5 strains listed above, the remaining 104 *B. cereus* genomes lack the core *tclA-tclX* genes based on a BLAST-P cutoff (E < 10e-5) utilized by antiSMASH (Blin et al., 2019). Overall, the close phylogenetic relationship between the thiocillin-BGC-containing *B. cereus* strains identified here indicate that a single common ancestor likely acquired the thiocillin BGC as a gain of function for the clade represented in Figure 4C.

4 Discussion

Competition between different bacterial species is diverse and relies on many different strategies. In this study, we have focused on the use of specialized metabolites to influence predator–prey dynamics thought to occur in soil microenvironments. We show that *Bacillus cereus* protects itself from predation by *Myxococcus xanthus* and that the specialized metabolite, thiocillin, is responsible for the observed protection. We performed assays using a thiocillin mutant strain (Δ*tclE-H*) as well as several strains that produce variant forms of thiocillin (e.g., T4V); the assays reveal that only native thiocillin promotes survival of *B. cereus* in the presence of *M. xanthus*. We also show that purified thiocillin transiently protects non-thiocillin producing strains in a dose-dependent manner, including *E. coli*, from predation by *M. xanthus*. Together, these results indicate that the specialized metabolite, thiocillin, is important for protection from *M. xanthus* predation.

Thiopeptides have not been widely reported to have antimicrobial activity against proteobacteria, although *Pseudomonas aeruginosa* and *Acinetobacter baumannii* were found to be sensitive to thiostrepton (Ranieri et al., 2019), and *P. aeruginosa* is sensitive to thiocillin and micrococcin (Chan and Burrows, 2021). Here we show that thiocillin produced by *B. cereus* ATCC 14579 significantly affects *M. xanthus* survival during predation assays, and that both predator and prey display losses in viability when thiocillin is present. In contrast, the antibiotic-null T4V variant of thiocillin did not protect *B. cereus* from predation and *B. cereus* cells producing the T4V thiocillin variant allowed *M. xanthus* predator cells to grow. To our knowledge, this is the first report of a bacterial specialized metabolite that negatively influences *M. xanthus* viability.

Our analysis of the genomes of 109 *B. cereus* strains leads to the conclusion that a small clade of *B. cereus* acquired the thiocillin BGC, likely through a horizontal gain of function event, enabling this subset of strains to produce this specialized metabolite. PacBio sequencing revealed that *B. cereus* strain T lacks the BGC for thiocillin production while strain 14579 possesses it. Further analysis of publicly available *B. cereus* metagenomes revealed that 5 strains closely related to 14579 also possess the BGC and therefore likely can produce thiocillin whereas no other members of the broader *B. cereus* group possess genes related to thiocillin production. In support of our hypothesis, it is known that other genera, including *Streptomyces*, possess a similar BGC and are capable of thiocillin production. Because these bacteria are also soil inhabitants and live in similar ecological niches as Bacilli, horizontal gene transfer from *Streptomyces* species may account for the observed acquisition of this BGC within the Bacilli (Bleich et al., 2015).

It is known that thiocillin acts to inhibit L11 interactions with 23S rRNA to affect translation (Cameron et al., 2002; Harms et al., 2008). Thus, the identification of two paralogs of L11 supports the proposal that gene dosage may provide a mechanism for immunity from thiocillin that would otherwise inhibit translation for thiocillin producers (Acker et al., 2009; Wieland Brown et al., 2009; Bowers et al., 2010). The paralogs of L11 encoded within the thiocillin BGCs are identical within the clade (Supplementary Figure S6) yet are distinct from the native copy of encoded by *rplK* located near *rpoA* and *rpoB*. The identity and conservation of TclQ and TclT within the thiocillin-producing clade of 5 closely related strains of *B. cereus* is consistent with recent acquisition via horizontal gene transfer. We speculate that *M. xanthus* is inhibited by thiocillin at concentrations suitable to allow for inhibition of protein translation via L11 (Figure 6). Detailed studies of thiocillin entry into *M. xanthus*

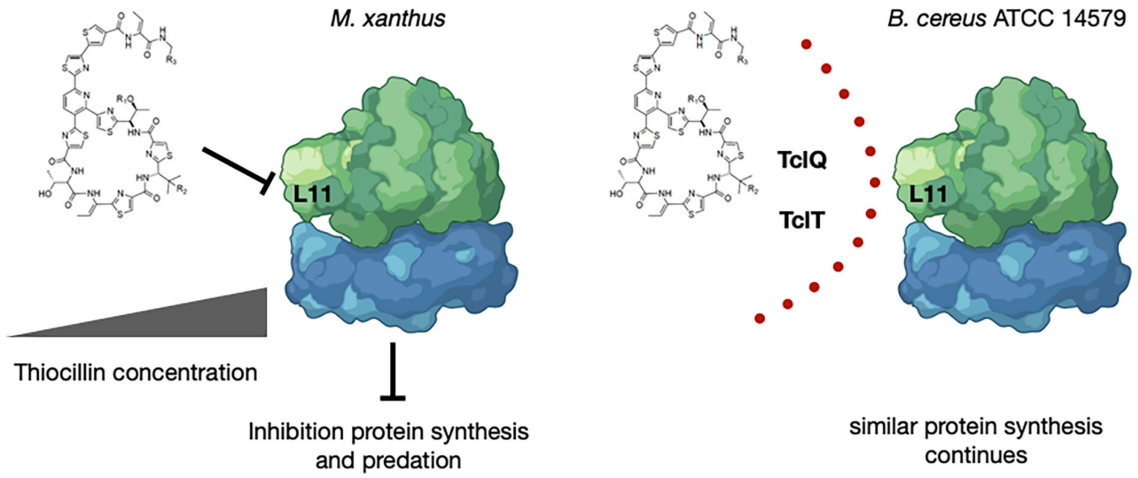

FIGURE 6
Model for Inhibition by and Protection from Thiocillin During Predation. Thiocillin is known to inhibit the L11 interaction with 23S rRNA within the 50S subunit of the ribosome to affect translation. *B. cereus* ATCC 14579, a thiocillin producer, encodes two L11 paralogs, TclQ and TclT, whereas *M. xanthus* and other *B. cereus* strains do not. TclQ and TclT most likely provide a mechanism for immunity from thiocillin within thiocillin-producing *B. cereus* strains. Thiocillin affects the fitness of *M. xanthus* and therefore provides an advantage against predation. "Created with BioRender.com."

cytoplasm and its mechanism of action are ongoing. Overall, this work demonstrates that thiocillin is an important contributor to survival of *B. cereus* ATCC 14579 during interspecies interactions with the predator *M. xanthus*. This specialized metabolite study extends our understanding of the chemical weaponry utilized between organisms known to interact with *M. xanthus*.

Data availability statement

The datasets presented in this study are deposited in the NCBI database under accession numbers CP130491, CP138336, and CO138337.

Author contributions

SM: Conceptualization, Formal analysis, Methodology, Visualization, Writing – original draft, Writing – review & editing, Investigation. OD: Methodology, Software, Visualization, Writing – review & editing. SA: Methodology, Software, Writing – review & editing. FS: Methodology, Software, Writing – review & editing. SK: Writing – review & editing. ES: Conceptualization, Supervision, Writing – review & editing. JK: Conceptualization, Funding acquisition, Project administration, Supervision, Writing – review & editing.

Funding

The author(s) declare financial support was received for the research, authorship, and/or publication of this article. This research was supported by funds provided by the National Institutes of Health (GM145261 to ES and AI108255 to JK), the Susanna & Justin Mortara Innovation Fund (JK), and the Walter Schroeder Endowment (JK).

Acknowledgments

We gratefully acknowledge Albert Bowers, PhD (University of North Carolina, Chapel Hill) for providing native and variant forms of thiocillin. We also thank the School of Freshwater Sciences (University of Wisconsin, Milwaukee) for providing access to PacBio sequencing.

Conflict of interest

The authors declare that the research was conducted in the absence of any commercial or financial relationships that could be construed as a potential conflict of interest.

Publisher's note

Supplementary material

The Supplementary material for this article can be found online at: https://www.frontiersin.org/articles/10.3389/fmicb.2023.1295262/full#supplementary-material

SUPPLEMENTARY FIGURE S1
Thiocillin affects surface spreading of *M. xanthus* cells. Shown are enlarged pictures taken from Figure 1 (24h) to emphasize that only a few *M. xanthus* cells are visible outside of the *B. cereus* ATCC 14579 prey spot compared to sensitive prey strains *B. cereus* T and *ΔtclE-H*. The prey spot location is indicated by a black ring and the distance of *M. xanthus* traveled outside of the prey spot is indicated by a double arrow line. With both sensitive strains (*B. cereus* T and *ΔtclE-H)* we see consumption of the prey spot and *M. xanthus* moving beyond the initial prey spot. For the predation resistant strain ATCC 14579 we see most of the prey spot remaining and only a few *M. xanthus* cells outside of it.

SUPPLEMENTARY FIGURE S2
Thiocillin protects *B. cereus* ATCC 14579 from predation by *M. xanthus*. *B. cereus* strains (prey) were grown to a certain cell density (see Materials and Methods) and nutrients were removed by washing the cells multiple times. Prey cells were mixed with the predator *M. xanthus* in a ratio of 50:1, spotted on CFL Agar plates and incubated at 32°C. Pictures were taken after different times of incubation at 15x magnification. Predation is visible by cell lysis (*) whereas competition/predation resistance is indicated by minimal loss of cells (O). Fruiting body formation can be seen after 48h as an indicator that predator *M. xanthus* sensed a drop down in nutrients and is starving (black square). Strains *ΔtclE-H::tclE (C9A), ΔtclE-H::tclE (C5A), ΔtclE-H::tclE (C7A)* and *ΔtclE-H::tclE (C2S)* represent in frame deletions of the tclE gene that where complement with tclE point mutations leading to amino acid changes in the thiocillin molecule that disrupt the thiazolyl ring. Strain *ΔtclE-H::tclE (A78)* produces a thiocillin variant with a larger thiazolyl ring. All these strains have no known antimicrobial activity against Gram-positive bacteria and do not induce matrix formation in *B. subtilis*.

SUPPLEMENTARY FIGURE S3
Purified Thiocillin rescues sensitive strains from predation by *M. xanthus*. The predation sensitive strains *B. cereus* ATCC 14579 *ΔtclE-H::tclE* (T4V) was tested in predation assays with the predator *M. xanthus* with and without purified thiocillin (dissolved in DMSO). *B. cereus* strain *ΔtclE-H::tclE* (T4V) makes a variant of the thiocillin molecule that has lost the antimicrobial function of the molecule. The strain is sensitive to predation (comparing column III to I and II). The addition of purified thiocillin protected the sensitive strain from predation (column IV). Increasing concentrations of thiocillin enhanced the predation protective effect. Pictures were taken after 24 h.

SUPPLEMENTARY FIGURE S4
Purified Thiocillin affects surface spreading and eating by *M. xanthus*. Shown are enlarged pictures within Figure 2 and Supplementary Figure S3. The pictures on the left show the prey strain mixed with *M. xanthus* and 330ng of purified thiocillin. The right column shows the prey strain mixed with *M. xanthus* and 990ng of purified thiocillin. The black ring indicates the prey spot and the distance traveled by *M. xanthus* outside of the prey spot is indicated by a double arrow line. At low thiocillin concentrations we see *M. xanthus* outside of the prey spots, an indicator of predation. Additionally, we see predation indicated by more lysis of the prey spot (areas marked by black square).

SUPPLEMENTARY FIGURE S5
Thiocillin variant T4V does not protect from predation by *M. xanthus*. The predation sensitive strains and *B. cereus* ATCC 14579 *ΔtclE-H::tclE* (T4V) were tested in predation assays with the predator *M. xanthus* with and without the purified thiocillin TV4 variant molecule (dissolved in DMSO).
B. cereus strain *ΔtclE-H* does not make thiocillin and *ΔtclE-H::tclE* (T4V) makes a variant of the thiocillin molecule that has lost the antimicrobial function of the molecule. All strains are sensitive to predation (comparing column III to I and II). The addition of purified thiocillin protected all sensitive strains from predation (column IV). Increasing concentrations of thiocillin enhanced the predation protective effect. Pictures were taken after 24 h.

SUPPLEMENTARY FIGURE S6
Alignment of L11 homologs TclT and TclQ. Protein sequence Alignment of L11 homologs from strains FSL_M8_0473, FSL_R5_0811, ATCC 14579, NCTC2599 and BDRD_Cer4 (Figure S6 A) and tctT and tclQ (Figure S6 B).

References

Acker, M. G., Bowers, A. A., and Walsh, C. T. (2009). Generation of thiocillin variants by prepeptide gene replacement and in vivo processing by *Bacillus cereus*. *J. Am. Chem. Soc.* 131, 17563–17565. doi: 10.1021/ja908777t

Aziz, R. K., Bartels, D., Best, A. A., Dejongh, M., Disz, T., Edwards, R. A., et al. (2008). The RAST server: rapid annotations using subsystems technology. *BMC Genomics* 9:75. doi: 10.1186/1471-2164-9-75

Bader, C. D., Panter, F., and Muller, R. (2020). In depth natural product discovery – Myxobacterial strains that provided multiple secondary metabolites. *Biotechnol. Adv.* 39:107480. doi: 10.1016/j.biotechadv.2019.107480

Benedict, M. N., Henriksen, J. R., Metcalf, W. W., Whitaker, R. J., and Price, N. D. (2014). ITEP: an integrated toolkit for exploration of microbial pan-genomes. *BMC Genomics* 15:8. doi: 10.1186/1471-2164-15-8

Berleman, J. E., and Kirby, J. R. (2007). Multicellular development in *Myxococcus xanthus* is stimulated by predator-prey interactions. *J. Bacteriol.* 189, 5675–5682. doi: 10.1128/JB.00544-07

Bleich, R., Watrous, J. D., Dorrestein, P. C., Bowers, A. A., and Shank, E. A. (2015). Thiopeptide antibiotics stimulate biofilm formation in *Bacillus subtilis*. *Proc. Natl. Acad. Sci. U. S. A.* 112, 3086–3091. doi: 10.1073/pnas.1414272112

Blin, K., Shaw, S., Steinke, K., Villebro, R., Ziemert, N., Lee, S. Y., et al. (2019). antiSMASH 5.0: updates to the secondary metabolite genome mining pipeline. *Nucleic Acids Res.* 47, W81–W87. doi: 10.1093/nar/gkz310

Bowers, A. A., Acker, M. G., Koglin, A., and Walsh, C. T. (2010). Manipulation of thiocillin variants by prepeptide gene replacement: structure, conformation, and activity of heterocycle substitution mutants. *J. Am. Chem. Soc.* 132, 7519–7527. doi: 10.1021/ja102339q

Bowers, A. A., Acker, M. G., Young, T. S., and Walsh, C. T. (2012). Generation of thiocillin ring size variants by prepeptide gene replacement and in vivo processing by *Bacillus cereus*. *J. Am. Chem. Soc.* 134, 10313–10316. doi: 10.1021/ja302820x

Bretscher, A. P., and Kaiser, D. (1978). Nutrition of *Myxococcus xanthus*, a fruiting myxobacterium. *J. Bacteriol.* 133, 763–768. doi: 10.1128/jb.133.2.763-768.1978

Brettin, T., Davis, J. J., Disz, T., Edwards, R. A., Gerdes, S., Olsen, G. J., et al. (2015). RASTtk: a modular and extensible implementation of the RAST algorithm for building custom annotation pipelines and annotating batches of genomes. *Sci. Rep.* 5:8365. doi: 10.1038/srep08365

Cameron, D. M., Thompson, J., March, P. E., and Dahlberg, A. E. (2002). Initiation factor IF2, thiostrepton and micrococcin prevent the binding of elongation factor G to the *Escherichia coli* ribosome. *J. Mol. Biol.* 319, 27–35. doi: 10.1016/S0022-2836(02)00235-8

Campbell, J. H., O'donoghue, P., Campbell, A. G., Schwientek, P., Sczyrba, A., Woyke, T., et al. (2013). UGA is an additional glycine codon in uncultured SR1 bacteria from the human microbiota. *Proc. Natl. Acad. Sci. U. S. A.* 110, 5540–5545. doi: 10.1073/pnas.1303090110

Chan, D. C. K., and Burrows, L. L. (2021). Thiocillin and micrococcin exploit the ferrioxamine receptor of *Pseudomonas aeruginosa* for uptake. *J. Antimicrob. Chemother.* 76, 2029–2039. doi: 10.1093/jac/dkab124

Delmont, T. O., and Eren, A. M. (2018). Linking pangenomes and metagenomes: the Prochlorococcus metapangenome. *PeerJ* 6:e4320. doi: 10.7717/peerj.4320

Edgar, R. C. (2004). MUSCLE: a multiple sequence alignment method with reduced time and space complexity. *BMC Bioinformatics* 5:113. doi: 10.1186/1471-2105-5-113

Eren, A. M., Esen, O. C., Quince, C., Vineis, J. H., Morrison, H. G., Sogin, M. L., et al. (2015). Anvi'o: an advanced analysis and visualization platform for 'omics data. *PeerJ* 3:e1319. doi: 10.7717/peerj.1319

Findlay, B. L. (2016). The chemical ecology of predatory soil Bacteria. *ACS Chem. Biol.* 11, 1502–1510. doi: 10.1021/acschembio.6b00176

Grubbs, K. J., Bleich, R. M., Santa Maria, K. C., Allen, S. E., Farag, S., Agbiome, T., et al. (2017). Large-scale bioinformatics analysis of Bacillus genomes uncovers conserved roles of natural products in bacterial physiology. *mSystems* 2:e00040-17. doi: 10.1128/mSystems.00040-17

Harms, J. M., Wilson, D. N., Schluenzen, F., Connell, S. R., Stachelhaus, T., Zaborowska, Z., et al. (2008). Translational regulation via L11: molecular switches on the ribosome turned on and off by thiostrepton and micrococcin. *Mol. Cell* 30, 26–38. doi: 10.1016/j.molcel.2008.01.009

Hart, B. A., and Zahler, S. A. (1966). Lytic enzyme produced by *Myxococcus xanthus*. *J. Bacteriol.* 92, 1632–1637. doi: 10.1128/jb.92.6.1632-1637.1966

Hunt, M., Silva, N. D., Otto, T. D., Parkhill, J., Keane, J. A., and Harris, S. R. (2015). Circlator: automated circularization of genome assemblies using long sequencing reads. *Genome Biol.* 16:294. doi: 10.1186/s13059-015-0849-0

Johnke, J., Cohen, Y., De Leeuw, M., Kushmaro, A., Jurkevitch, E., and Chatzinotas, A. (2014). Multiple micro-predators controlling bacterial communities in the environment. *Curr. Opin. Biotechnol.* 27, 185–190. doi: 10.1016/j.copbio.2014.02.003

Jones, P., Binns, D., Chang, H. Y., Fraser, M., Li, W., Mcanulla, C., et al. (2014). InterProScan 5: genome-scale protein function classification. *Bioinformatics* 30, 1236–1240. doi: 10.1093/bioinformatics/btu031

Karakoc, C., Singer, A., Johst, K., Harms, H., and Chatzinotas, A. (2017). Transient recovery dynamics of a predator-prey system under press and pulse disturbances. *BMC Ecol.* 17:13. doi: 10.1186/s12898-017-0123-2

Koren, S., Walenz, B. P., Berlin, K., Miller, J. R., Bergman, N. H., and Phillippy, A. M. (2017). Canu: scalable and accurate long-read assembly via adaptive k-mer weighting and repeat separation. *Genome Res.* 27, 722–736. doi: 10.1101/gr.215087.116

Koskella, B., and Brockhurst, M. A. (2014). Bacteria-phage coevolution as a driver of ecological and evolutionary processes in microbial communities. *FEMS Microbiol. Rev.* 38, 916–931. doi: 10.1111/1574-6976.12072

Kurtz, S., Phillippy, A., Delcher, A. L., Smoot, M., Shumway, M., Antonescu, C., et al. (2004). Versatile and open software for comparing large genomes. *Genome Biol.* 5:R12. doi: 10.1186/gb-2004-5-2-r12

Livingstone, P. G., Millard, A. D., Swain, M. T., and Whitworth, D. E. (2018). Transcriptional changes when *Myxococcus xanthus* preys on *Escherichia coli* suggest myxobacterial predators are constitutively toxic but regulate their feeding. *Microb Genom* 4:e000152. doi: 10.1099/mgen.0.000152

Morgan, A. D., Maclean, R. C., Hillesland, K. L., and Velicer, G. J. (2010). Comparative analysis of myxococcus predation on soil bacteria. *Appl. Environ. Microbiol.* 76, 6920–6927. doi: 10.1128/AEM.00414-10

Muller, S., Strack, S. N., Hoefler, B. C., Straight, P. D., Kearns, D. B., and Kirby, J. R. (2014). Bacillaene and sporulation protect *Bacillus subtilis* from predation by *Myxococcus xanthus*. *Appl. Environ. Microbiol.* 80, 5603–5610. doi: 10.1128/AEM.01621-14

Muller, S., Strack, S. N., Ryan, S. E., Kearns, D. B., and Kirby, J. R. (2015). Predation by *Myxococcus xanthus* induces *Bacillus subtilis* to form spore-filled megastructures. *Appl. Environ. Microbiol.* 81, 203–210. doi: 10.1128/AEM.02448-14

Muller, S., Strack, S. N., Ryan, S. E., Shawgo, M., Walling, A., Harris, S., et al. (2016). Identification of functions affecting predator-prey interactions between Myxococcus xanthus and *Bacillus subtilis*. *J. Bacteriol.* 198, 3335–3344. doi: 10.1128/JB.00575-16

Munoz-Dorado, J., Marcos-Torres, F. J., Garcia-Bravo, E., Moraleda-Munoz, A., and Perez, J. (2016). Myxobacteria: moving, killing, feeding, and surviving together. *Front. Microbiol.* 7:781. doi: 10.3389/fmicb.2016.00781

Nair, R. R., Vasse, M., Wielgoss, S., Sun, L., Yu, Y. N., and Velicer, G. J. (2019). Bacterial predator-prey coevolution accelerates genome evolution and selects on virulence-associated prey defences. *Nat. Commun.* 10:4301. doi: 10.1038/s41467-019-12140-6

Perez, J., Munoz-Dorado, J., Brana, A. F., Shimkets, L. J., Sevillano, L., and Santamaria, R. I. (2011). *Myxococcus xanthus* induces actinorhodin overproduction and aerial mycelium formation by *Streptomyces coelicolor*. *Microb. Biotechnol.* 4, 175–183. doi: 10.1111/j.1751-7915.2010.00208.x

Price, M. N., Dehal, P. S., and Arkin, A. P. (2010). FastTree 2--approximately maximum-likelihood trees for large alignments. *PLoS One* 5:e9490. doi: 10.1371/journal.pone.0009490

Ranieri, M. R. M., Chan, D. C. K., Yaeger, L. N., Rudolph, M., Karabelas-Pittman, S., Abdo, H., et al. (2019). Thiostrepton hijacks Pyoverdine receptors to inhibit growth of *Pseudomonas aeruginosa*. *Antimicrob. Agents Chemother.* 63:e00472-19. doi: 10.1128/AAC.00472-19

Sudo, S., and Dworkin, M. (1972). Bacteriolytic enzymes produced by *Myxococcus xanthus*. *J. Bacteriol.* 110, 236–245. doi: 10.1128/jb.110.1.236-245.1972

Wang, C., Liu, X., Zhang, P., Wang, Y., Li, Z., Li, X., et al. (2019). *Bacillus licheniformis* escapes from *Myxococcus xanthus* predation by deactivating myxovirescin a through enzymatic glucosylation. *Environ. Microbiol.* 21, 4755–4772. doi: 10.1111/1462-2920.14817

Wieland Brown, L. C., Acker, M. G., Clardy, J., Walsh, C. T., and Fischbach, M. A. (2009). Thirteen posttranslational modifications convert a 14-residue peptide into the antibiotic thiocillin. *Proc. Natl. Acad. Sci. U. S. A.* 106, 2549–2553. doi: 10.1073/pnas.0900008106

Xiao, Y., Gerth, K., Muller, R., and Wall, D. (2012). Myxobacterium-produced antibiotic TA (myxovirescin) inhibits type II signal peptidase. *Antimicrob. Agents Chemother.* 56, 2014–2021. doi: 10.1128/AAC.06148-11

frontiers | Frontiers in Microbiology

TYPE Original Research
PUBLISHED 04 December 2023
DOI 10.3389/fmicb.2023.1304233

OPEN ACCESS

EDITED BY
Li Zhoukun,
Nanjing Agricultural University, China

REVIEWED BY
Huirong Liu,
Inner Mongolia Agricultural University, China
Jie Zhou,
Nanjing Tech University, China
Wenhui Wang,
Anhui Agricultural University, China

*CORRESPONDENCE
Xin-Jing Yue
xjy2018@sdu.edu.cn
Yue-Zhong Li
lilab@sdu.edu.cn

RECEIVED 29 September 2023
ACCEPTED 17 November 2023
PUBLISHED 04 December 2023

CITATION
Yuan S-F, Yue X-J, Hu W-F, Wang Y and Li Y-Z (2023) Genome-wide analysis of lipolytic enzymes and characterization of a high-tolerant carboxylesterase from *Sorangium cellulosum*.
Front. Microbiol. 14:1304233.
doi: 10.3389/fmicb.2023.1304233

Genome-wide analysis of lipolytic enzymes and characterization of a high-tolerant carboxylesterase from *Sorangium cellulosum*

Shu-Fei Yuan, Xin-Jing Yue*, Wei-Feng Hu, Ye Wang and Yue-Zhong Li*

State Key Laboratory of Microbial Technology, Institute of Microbial Technology, Shandong University, Qingdao, China

Microorganisms are important sources of lipolytic enzymes with characteristics for wide promising usages in the specific industrial biotechnology. The cellulolytic myxobacterium *Sorangium cellulosum* is rich of lipolytic enzymes in the genome, but little has been investigated. Here, we discerned 406 potential lipolytic enzymes in 13 sequenced *S. cellulosum* genomes. These lipolytic enzymes belonged to 12 families, and most are novel with low identities (14–37%) to those reported. We characterized a new carboxylesterase, LipB, from the alkaline-adaptive So0157-2. This enzyme, belonging to family VIII, hydrolyzed glyceryl tributyrate and *p*-nitrophenyl esters with short chain fatty acids (≤C12), and exhibited the highest activity against *p*-nitrophenyl butyrate. It retained over 50% of the activities in a broad temperature range (from 20°C to 60°C), alkaline conditions (pH 8.0–9.5), and the enzymatic activity was stable with methanol, ethanol and isopropanol, and stimulated significantly in the presence of 5 mM Ni^{2+}. LipB also exhibited β-lactamase activity on nitrocefin, but not ampicillin, cefotaxime and imipenem. The bioinformatic analysis and specific enzymatic characteristics indicate that *S. cellulosum* is a promising resource to explore lipolytic enzymes for industrial adaptations.

KEYWORDS

lipolytic enzymes, family VIII carboxylesterase, β-lactamase, *Sorangium cellulosum*, myxobacteria

1 Introduction

Lipolytic enzymes represent a group of proteins catalyzing the hydrolysis and formation of ester bonds of a structurally diverse array of compounds with no requirement for cofactors (Bornscheuer, 2002). Lipolytic enzymes can be employed for the synthesis of structurally diverse polymeric materials by catalyzing free combinations of diester and diol monomers (Kim and Dordick, 2001; Ning et al., 2022), forming chiral and enantioselective intermediates in the production of agrochemicals, flavoring compounds and pharmaceuticals (Tanaka et al., 2002; Athawale et al., 2003). Lipolytic enzymes are also used to degrade environmental toxic pesticides like pyrethroids, carbamate and organophosphate in an effective and green manner (Diegelmann et al., 2015; Sirajuddin et al., 2020). Significantly, lipolytic enzymes with high-tolerance characteristics, like thermophilic, cold-adaptive, alkaline, salt-tolerant, or stable in organic solvents, could bring higher yields and fewer by-products in the production of foods, detergents, fragrances and pharmaceuticals than those under mesophilic conditions (Priyanka

et al., 2019; Al-Ghanayem and Joseph, 2020; Johan et al., 2021). With the increasing requirement of lipolytic enzymes for industrial biocatalysis, discovering novel lipolytic enzymes or remolding enzymes have attracted a lot of interests. Microbial lipolytic enzymes are widely used in industrial processes because of their potential broad substrate specificity, high region- and stereo-selectivity, and remarkable stability in organic solvents (Jaeger and Eggert, 2002; Panda and Gowrishankar, 2005). Exploring microbial genomic resources provides opportunities for deep excavation of novel lipolytic enzymes (Johan et al., 2021).

The lipolytic enzymes include two types, carboxylesterases (EC 3.1.1.1), hydrolyzing small water-soluble esters or triglycerides with fatty acids shorter than C6, and lipases (EC 3.1.1.3), which hydrolyze triglycerides composed of long-chain fatty acids. Both the carboxylesterase and the lipase belong to the alpha/beta-hydrolase superfamily and are characterized by having a catalytic triad composed of Ser, His and Asp (or Glu) residues and a conserved G-x-S-x-G, G-D-S-L or S-x-x-K motif around the nucleophilic serine at the active site (Holmquist, 2000; Bornscheuer, 2002). The classification system of bacterial lipolytic enzymes was first proposed from 53 enzymatic proteins by Arpigny & Jaeger, and included 8 families defined by the biochemical properties and sequence identities (Arpigny and Jaeger, 1999). With the discovery of more lipolytic enzymes, the bacterial lipolytic enzymes have been expanded to 19 families based on the phylogenetic criterium, conserved motifs and biological characteristics (Kovacic et al., 2018; Johan et al., 2021). Lipases are grouped in family I, including eight subfamilies, while carboxylesterases are reported in the rest of 18 families. Among these lipolytic enzyme families, family VIII carboxylesterases are unique for displaying both esterase and β-lactamase activities (Biver and Vandenbol, 2013; Mokoena et al., 2013; Jeon et al., 2016; Kwon et al., 2019), making them promising in the synthesis and modification of β-lactam antibiotics (Mokoena et al., 2013). The active serine residues of family VIII carboxylesterases are in the S-x-x-K motif, instead of the typical G-x-S-x-G pentapeptide, forming the catalytic triad with lysine and the other conserved tyrosine in the Y-x-x motif, the same as that of β-lactamases (Petersen et al., 2001; Cha et al., 2013).

The cellulolytic myxobacterium *Sorangium cellulosum* is not only extremely attractive in drug screening (Bollag et al., 1995; Gerth et al., 2003), but also exhibits extensive degradation abilities on a wide range of macromolecules, such as lipids and polysaccharides. In recent years, some novel glycoside hydrolases have been reported from this cellulolytic myxobacterium (Wang et al., 2012; Li et al., 2022), but little attention has been paid on lipolytic enzymes. *S. cellulosum* genomes have many ORFs (open reading frames) predicted to encode various hydrolytic enzymes (Schneiker et al., 2007; Han et al., 2013), and four lipolytic enzymes have been characterized (Cheng et al., 2011; Wu et al., 2012; Udatha et al., 2015), including the cold-adapted lipase LipA previously reported in the So0157-2 strain. Studying lipolytic enzymes with promiscuous activities will be helpful for our understanding of the cellulolytic myxobacteria and potential applications of the diverse enzyme resources. In this study, we identified the lipases and carboxylesterases from 13 available sequenced *S. cellulosum* genomes and characterized a novel family VIII carboxylesterase LipB, which was alkali-tolerant, feasible to a wide range of temperature, and especially stimulated by specific alcohols, suggesting potentials in industrial processing associated with alcohols or detergents production. Diverse lipases and carboxylesterases with potential adverse-tolerances from *S. cellulosum* genomes will conduce for the lipolytic enzyme applications in industrial production.

2 Materials and methods

2.1 Strains, plasmids, culture media and chemicals

Strains and plasmids used in this study are listed in Supplementary Table S1. *Escherichia coli* strains DH5α and BL21 (DE3) were used to clone plasmids and express the recombinant protein. *E. coli* strains were grown in Luria-Bertani (LB) broth at 37°C. *Myxococcus xanthus* strains were grown at 30°C in CYE medium [10 g/L casitone, 5 g/L yeast extract, 10 mM 3-(N-morpholino) propanesulfonic acid (MOPS) and 4 mM MgSO4, pH 7.6]. The media were supplemented with 40 μg/mL kanamycin, 30 μg/mL apramycin, or 10 μg/mL tetracycline if required. We employed the plasmids pET-28a and pET-29b as the expression vectors, while pBJ113 and pSWU30 were as the knock-out plasmid and the overexpression plasmid, respectively. Primers used in constructing plasmids are listed in Supplementary Table S2.

The substrates *p*-nitrophenyl (*p*-NP) acetate (C2), butyrate (C4), hexanoate (C6), octanoate (C8), decanoate (C10), laurate (C12), and β-lactam antibiotics of ampicillin, nitrocefin, cefotaxime, imipenem were purchased from Aladdin (Shanghai, China). Other chemicals used in this study were analytical grade unless otherwise specified.

2.2 Bioinformatics analysis of lipolytic enzymes in *Sorangium cellulosum* genomes

Lipolytic enzymes were identified from 13 *S. cellulosum* genomes by PSI-BLAST searches using representative enzymes of the 19 families as queries (num_interactions = 3, E-value cut-off = 10^{-5}). The protein sequences were obtained from GenBank assembly of *S. cellulosum* genomes (Supplementary Table S3). The identified proteins were further filtered by the analysis of characteristic conserved motifs with FIMO[1] and the reserved lipolytic enzymes were classified based on sequence identities with query sequences. The information of query sequences and consensus motifs of each lipolytic enzyme family is listed in Supplementary Table S4.

The sequence similarity network of 406 predicted *S. cellulosum* lipolytic enzymes was constructed with 171 studied lipolytic enzymes by EFI-EST (Oberg et al., 2023), the E-value for BLAST was set to 5 and the alignment score threshold was set at 10. Deductive amino acid sequences of the family VIII carboxylesterases were further aligned by MAFFT online version[2] and embellished with ESPript (Robert and Gouet, 2014). The phylogenetic tree was constructed using the

1 https://meme-suite.org/meme/tools/fimo

2 https://mafft.cbrc.jp/alignment/server/

maximum likelihood method in IQ-TREE 2 (Minh et al., 2020) and modified by iTOL (Letunic and Bork, 2021).

2.3 Three-dimensional structure and docking analysis of LipB

To model the three-dimensional (3D) structure of the LipB protein, we submitted the amino acid sequence to I-TASSER online program based on a threading approach (Yang and Zhang, 2015) and visualized by PyMOL (Lilkova, 2015). AlphaFold2 (Cramer, 2021) was also applied to build the 3D structure of LipB, and models with predicted local-distance difference test (pLDDT) value of major sites above 70 were considered credible (Jumper et al., 2021). The accuracy of predicted structural models was assessed by SAVES v6.0.[3] For molecular docking by AutoDock Vina (Trott and Olson, 2010; Eberhardt et al., 2021), the structure of LipB predicted by AlphaFold2 was employed as the receptor protein, and ligand molecules were downloaded in the mol2 format from the PubChem database.[4] The docking results were visualized using PyMOL.

2.4 Expression and purification of recombinant LipB

Codon-optimized *lipB* sequence (Supplementary Table S5) was synthesized by GENEWIZ (Suzhou, China), amplified with the *lipB* F1/R1 and *lipB* F2/R2 primer pairs and cloned into the expression vectors pET-28a and pET-29b by homologous recombination with ClonExpress® MultiS One Step Cloning Kit (Vazyme, China) to generate recombinant plasmids pET-28a-*lipB* and pET-29b-*lipB*. For expression of the LipB protein, *E. coli* BL21 (DE3) harboring the recombinant plasmid was grown in 50 mL LB medium with 40 μg/mL kanamycin at 37°C to 0.6 of the OD600 value. Then isopropyl-*β*-D-thiogalactoside (IPTG) was added to the culture at a final concentration of 1 mM for additional 6 h incubation at 37°C or 0.1 mM for additional 22 h incubation at 16°C. The cells were collected by centrifugation and resuspended in Lysis buffer (25 mM Tris, 200 mM NaCl, 10% glycerin, pH 8.0), then crushed with an ultrasonic cell disruptor and the cellular supernatant was obtained by centrifugation at 12000 × g and 4°C for 30 min. The expression of the LipB protein was examined by SDS-PAGE.

To prepare the recombinant protein (LipB tagged with maltose-binding protein, MBP-LipB), *E. coli* BL21 (DE3) cells harboring the recombinant vector pET29b-*lipB* were cultured in 3 L of LB broth, and induced with 0.1 mM IPTG incubated at 16°C for 22 h. The supernatant was incubated with amylose affinity column (GE Healthcare, America), which was pre-equilibrated with Lysis buffer, and then eluted with the elution buffer containing 10 mM maltose. The soluble MBP-LipB protein was further purified using gel permeation chromatography to remove non-targeting proteins and finally resuspended in Lysis buffer.

3 https://saves.mbi.ucla.edu/

4 https://pubchem.ncbi.nlm.nih.gov/

2.5 Esterase activity assay of MBP-LipB

To assay the crude enzymatic activity, the *E. coli* BL21 (DE3) cells harboring the recombinant vector pET29b-*lipB* without and with induction of 0.1 mM IPTG at 16°C for 22 h were, respectively, harvested and resuspended with fresh LB broth at the concentration of 10 OD/mL, subsequently inoculated on the plate with glyceryl tributyrate, incubated overnight and observed by Stereo Microscope (Nikon, Japan).

The standard assay for esterase activity was carried out using spectrophotometric method with the reaction mixture containing 1 mM *p*-NP esters, 1 μL (0.67 μg) of purified MBP-LipB and 1% acetonitrile in a total volume of 1 mL of 50 mM Tris–HCl buffer (pH 8.0) (Petersen et al., 2001; Gupta et al., 2002). The reaction mixture was incubated for 10 min and terminated by the addition of 20 μL of 10% SDS. The enzymatic activity was measured by monitoring the changes of absorbance at 405 nm. All measurements were performed in triplicate.

Substrate specificity was detected by using *p*-NP esters with different length of aliphatic side chains, including *p*-NP acetate (C2), *p*-NP butyrate (C4), *p*-NP hexanoate (C6), *p*-NP octanoate (C8), *p*-NP decanoate (C10), and *p*-NP laurate (C12).

The optimal pH value was determined with *p*-NP butyrate as the substrate in the pH range from 3.0 to 10.0. The following buffers (50 mM) with different pH values were used: citrate buffer (pH 3.0–5.0), sodium phosphate buffer (pH 5.0–7.0), Tris–HCl (pH 7.0–9.0) and sodium bicarbonate–NaOH buffer (pH 9.0–10.0).

Similarly, the optimal temperature was determined at the temperatures ranging from 20°C to 70°C. The thermostability was determined by incubating the reaction mixtures at 35°C, 45°C, 55°C for different times until up to 1 h and the residual activity was measured.

Effects of metal ions ($MnCl_2$, $MgCl_2$, $CaCl_2$, $CuCl_2$, $CoCl_2$, $ZnCl_2$ and $NiCl_2$) or organic solvents (methanol, ethanol, acetone, trichloromethane, acetonitrile and isopropanol) on LipB esterase activity were detected by incubating the reaction mixture, respectively, with the metal ions or organic solvents under the reaction condition mentioned above for 1 h, and the residual activity subsequently tested. The concentration of each of the metal ions was 5 mM, and the final concentrations of the organic solvents were 5%, 10% or 15%. The enzymatic activity of the protein without additives was defined as 100%.

2.6 *β*-lactamase activity assay of MBP-LipB

The *β*-lactamase activity of LipB was determined by using nitrocefin as the substrate with the method (O'Callaghan et al., 1972) with small modifications. Briefly, the reaction mixture containing 1 mM nitrocefin, 1 μL purified enzyme (0.67 μg), 500 μL of 200 mM Tris–HCl buffer (pH 7.0) and distillation-distillation water (ddH_2O) in a total 1 mL volume was incubated at 30°C and measured with the spectrophotometric method at 482 nm every 1 h. To exclude the influence of the MBP-tag, we used the MBP protein in the *β*-lactamase activity assay with nitrocefin as the substrate.

Ampicillin, cefotaxime or imipenem was also used as substrate to detect the *β*-lactamase activity of MBP-LipB using the same reaction mixture without nitrocefin and then incubated at 30°C for 24 h. The

concentrations of residual substrates and reaction products were determined by High Performance Liquid Chromatography (HPLC) equipped with a C18 reverse-phase column (Thermo Fisher Scientific, Boston, USA). The elution condition was a constant concentration gradient of phosphate buffer and acetonitrile (HPLC grade) at a flow rate of 0.5 mL/min for 20 min to detect at 230 nm for ampicillin, at a flow rate of 0.8 mL/min for 20 min to detect at 254 nm for cefotaxime, and at a flow rate of 1 mL/min for 15 min to detect at 295 nm for imipenem. The reaction metabolites were identified by comparing the retention time and the UV visible spectra with the negative control using ddH_2O to replace the enzyme.

The optimal temperature and pH for LipB β-lactamase activity were employed. Because nitrocefin was unstable under the thermal (≥55°C) or alkaline (pH ≥8.0) conditions, the detection was conducted at the temperature range from 20°C to 50°C or in the pH range from 3.0 to 7.5.

2.7 Epothilone hydrolase activity assay of MBP-LipB

To analyze the hydrolase activity of MBP-LipB against epothilones, 0.5 mM epothilone A or epothilone B and 2 μg of purified enzyme were added into 50 mM Tris–HCL (pH 9.0) at a final volume of 100 μL and incubated at 30°C for 24 h. An equal volume of ethyl acetate was added to finish the reaction, the mixture was evaporated under reduced pressure and dissolved in 50 μL methanol. The remained epothilone A or epothilone B was determined by HPLC. The elution condition was a programmed concentration gradient of 60% methanol (HPLC grade) and 40% ddH_2O (HPLC grade) at a flow rate of 1 mL/min for 25 min to detect at 249 nm.

Primers *lipB*-up F and *lipB*-up R, *lipB*-down F and *lipB*-down R were used to amplify the up and down homologous arms of *lipB* from *S. cellulosum* So0157-2 genome, respectively. The arms were linked to pBJ113 to obtain knockout plasmid pBJ-*lipB*. The *lipB* gene was amplified with *lipB* F3 and *lipB* R3 primers, digested with KpnI and EcoRI and then cloned into pSWU30-pilA resulting in the overexpression plasmid pSWU30-pilA-*lipB*. The pBJ-*lipB* and pSWU30-pilA-*lipB* were introduced into the epothilone-producing strain ZE9 (Zhu et al., 2015) by electroporation and the positive mutant strains ZE9Δ*lipB* and ZE9 + *lipB* were screened as previously reported (Yue et al., 2017). ZE9 and mutants were cultivated overnight in 50 mL of CYE medium, then inoculated at a ratio of 0.04 OD/mL into 50 mL medium containing 2% of the XAD-16 resin and fermented at 30°C for 7 days. The resin was harvested with strainer and extracted with 3 mL methanol by shaking overnight at room temperature (Gong et al., 2007). The supernatant was examined by HPLC. The yield of epothilones was quantified from the peak area in the UV chromatogram, by reference against a calibration standard.

3 Results

3.1 Identification of lipolytic enzymes in *Sorangium cellulosum*

We searched the 13 available *S. cellulosum* genomes (Supplementary Table S3) by PSI-BLAST with 19 representatives from those identified lipolytic enzymes of different families as query sequences, and discerned 1,084 non-redundant lipolytic enzymes, which belonged to 14 families (Supplementary Table S6). These putative enzymes were filtered with FIMO to determine the existence of the typical motifs conserved in lipolytic enzyme families (Johan et al., 2021). After removing the sequences without the conserved motifs we obtained 406 lipolytic enzymes (Supplementary Table S7). Notably, because the conserved motifs in the families III, VI, XV and XIX, or in the families IV and VII, were closely similar, 61 of the 406 proteins appeared in different families, which were determined of their ascription by the BLASTP similarity values (Supplementary Table S8). Finally, these *S. cellulosum* lipolytic enzymes were classified into 12 families (Figure 1A).

The *S. cellulosum* genomes each contained multiple genes (22–44) encoding lipolytic enzymes (Supplementary Table S9), with varied compositions in different families (Figure 1B). According to the sequence similarity network analysis, the lipolytic enzymes belonging to families I, IV, VII, VIII, and XVII showed high similarities, but many others (up to 60% of the 406 enzymes) exhibited low similarities with those reported representatives (Figure 1C), showing rich novel lipolytic enzymes in *S. cellulosum*.

The family VIII carboxylesterases were the most abundant lipolytic enzymes occurring in *S. cellulosum*. These 74 predicted family VIII carboxylesterases, together with 29 reported ones, could be divided into four groups (Figure 1D). To understand lipolytic enzymes in *S. cellulosum*, we further investigate the sequence and functional characteristics of LipB (AKI82204.1) of the family VIII carboxylesterases in *S. cellulosum* So0157-2, an alkaline epothilone-producing strain with the known largest *S. cellulosum* genome (Han et al., 2013). One more reason for the choice of LipB is that the *lipB* gene is adjacent to the biosynthetic gene cluster of epothilones, and the LipB protein was once predicted to be an esterase responsible for the hydrolysis of epothilones to prevent self-toxicity (Gerth et al., 2002; Zhao et al., 2010; Li et al., 2017).

3.2 Sequence alignment and three-dimensional structure of LipB

So0157-2 contained 34 lipolytic enzymes, and 7 of them belonged to the family VIII carboxylesterases. The *lipB* gene encodes a protein containing 454 amino acid residues with the predicted molecular weight of 48.4 kDa. Multiple amino acid sequence alignment revealed that LipB contained the conserved S-x-x-K motif (at the position of residues of 118–121) and Y-x-x motif (239–241), which are commonly observed in class C β-lactamases, penicillin binding proteins and family VIII carboxylesterases (Figure 2). Besides, the W-x-G motif, conserved in the oxyanion hole of family VIII carboxylesterases (Nan et al., 2019; Park et al., 2020), was also observed in the C-terminal region of LipB (Trp^{407}-Asp^{408}-Gly^{409}). The sequence characteristics suggested that LipB was a dual-functional enzyme with the class C β-lactamase and the family VIII carboxylesterase activities.

We constructed the 3D structure of LipB protein using the I-TASSER online program, and revealed that LipB was structurally close to some carboxylesterases (PDB IDs: 4IVI, 1CI8, and 3ZYT) and several penicillin binding proteins (PDB IDs: 4P6B, 5GKV, and 2QMI) (Supplementary Table S10). The optimal structures predicted by

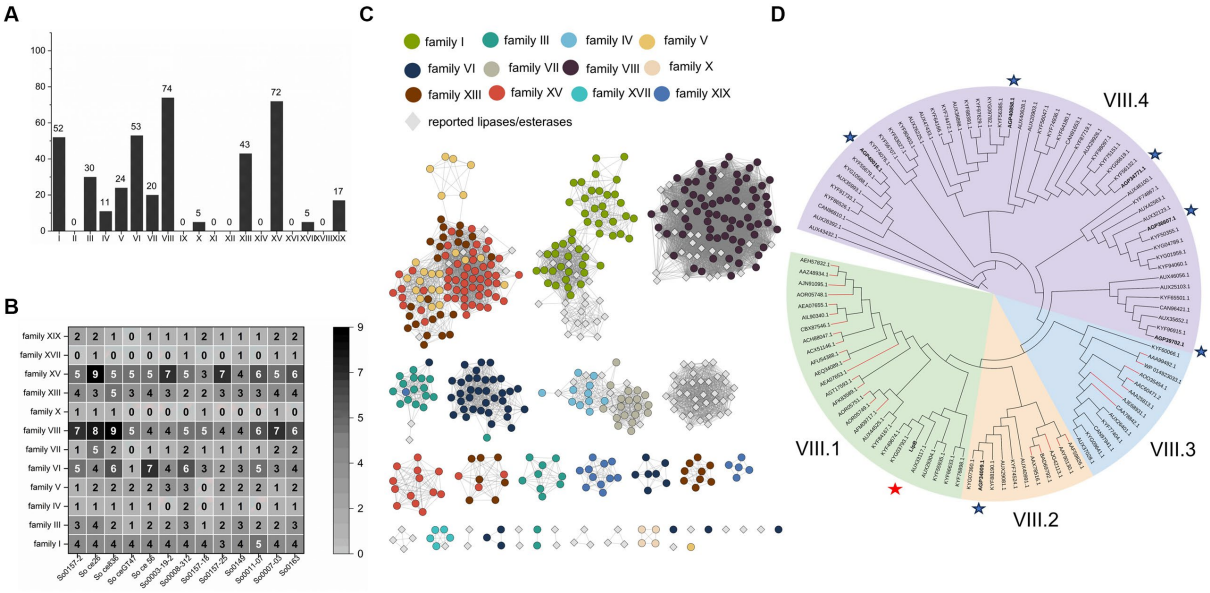

FIGURE 1
Identification and amino acid sequences analysis of lipolytic enzymes from *S. cellulosum*. **(A)** The amount of lipolytic enzymes of each gene family from *S. cellulosum* was plotted with the histogram and labeled on top of each bar. **(B)** The number of each lipolytic enzyme family in various *S. cellulosum* genomes was counted with the heat map. The number larger than or equal to 5 was marked in white, otherwise in black. **(C)** The sequence similarity network constructed by EFI-EST. Dots represent enzymes identified from *S. cellulosum*, of them different enzyme families were exhibited in various colors. Reported enzymes were displayed with gray diamonds. **(D)** The phylogenetic tree of family VIII carboxylesterases established by IQ-TREE. These enzymes were divided into four groups. There were 29 reported family VIII esters, of which the branches were painted red. Seven enzymes from *S. cellulosum* So0157-2 were bold and highlighted with asterisks, and the LipB was highlighted with red asterisk.

I-TASSER and AphaFold2 (model 1 and rank_1) were aligned and matched well with each other (Supplementary Figure S1A), and residues, 65.1% of model 1 and 85.1% of rank_1, revealed by ramachandran plot analysis, were in the most favored regions (Supplementary Figure S1B). According to Verify3D, 68.9% of residues in model 1 have scored ≥0.2 in the 3D-1D profile, while the residues scored ≥0.2 in the rank_1 were 70.9% (Supplementary Figure S1C). Therefore, the rank_1 model estimated by AlphaFold2 (pLDDT:87.3, pTM:0.857) was adopted as the supposed 3D structure of LipB (Figure 3A).

Similar to the class C β-lactamase and family VIII carboxylesterases (Wagner et al., 2002), LipB was composed of two domains, a small helical domain (residues 136–257, painted orange in Figure 3A) and an alpha/beta-domain (residues 1–135 and residues 258–454, painted green). The helical domain consisted of four alpha-helices and a short two-stranded antiparallel beta-sheet. The alpha/beta-domain had five long antiparallel beta-sheets, two pairs of short two-stranded antiparallel beta-sheet and 10 alpha-helices (7 on one side and 3 on the other). These two domains shaped a catalytic active pocket, where three conserved motifs (S-x-x-K, Y-x-x, W-x-G, painted red in surface) were precisely fit (Figure 3B). As shown in Figure 3C, a structure superimposition (root-mean-square deviation (RMSD) of 1.1 Å) was observed between LipB and EstU1 (PDB ID: 4IVI), a characterized family VIII carboxylesterase with the β-lactamase activity on the first-generation cephalosporins, and the key active sites essential for the β-lactam hydrolytic activity overlapped well in LipB (Ser^{118}, Lys^{121} and Tyr^{239}) and EstU1 (Ser^{100}, Lys^{103} and Tyr^{218}). The above bioinformatics analysis further suggested that LipB might display both esterase and β-lactamase activities.

3.3 Expression and purification of recombinant MBP-LipB

To investigate the biological activity of this enzyme, we expressed the recombinant LipB in *E. coli*. The codon optimized *lipB* gene was cloned in different expression vectors and transformed into *E. coli* BL21 (DE3). With the expression plasmid pET28a-*lipB*, the His-LipB recombinant proteins were expressed in an insoluble form, even after optimization of the induction conditions (Supplementary Figure S2A, the band of His-LipB was marked with red arrows). When labeled with the MBP-tag at the N-terminal of LipB, MBP-LipB was solubly expressed in cells harboring pET-29b-*lipB*; more recombinant proteins were obtained with the induction with 0.1 mM IPTG at 16°C for 22 h than that induced by 1 mM IPTG at 37°C for 6 h (Supplementary Figure S2B). The recombinant proteins were purified with amylose affinity chromatography and gel permeation chromatography. Notably, if the MBP-tag was truncated from MBP-LipB, the LipB protein became insoluble. Thus, the recombinant MBP-LipB protein was employed in the following assays.

3.4 Biochemical characterization of LipB as an esterase

To determine the esterase activity of LipB in *E. coli*, the IPTG-induced and uninduced cells harboring pET-29b-*lipB* were inoculated on the plates supplemented with glyceryl tributyrate. After overnight incubation, an obvious transparent zone was observed around the induced colonies, but not the uninduced, indicating that the induced

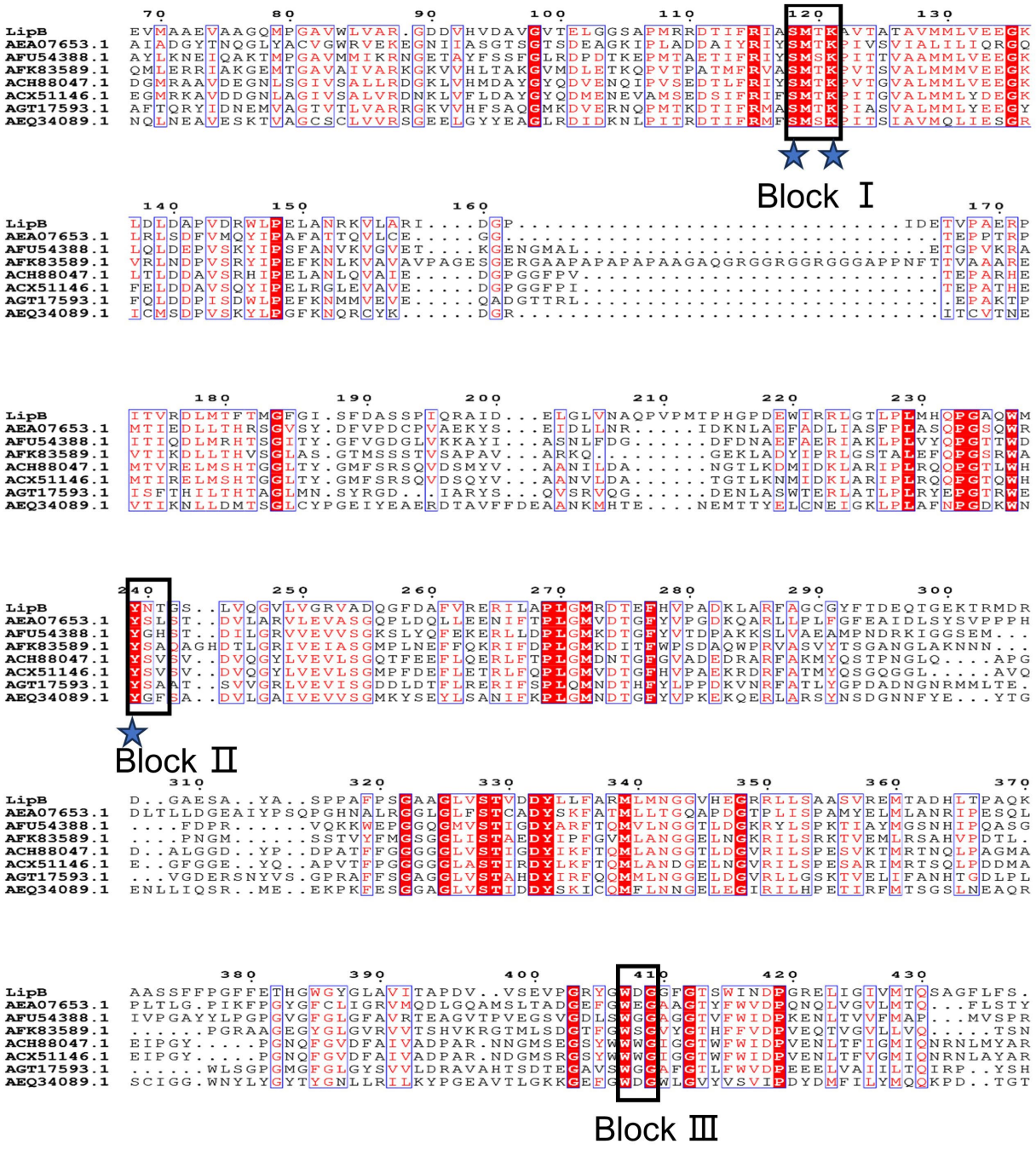

FIGURE 2
Multiple amino acid sequences alignment of LipB and reported homologs. Identical residues are indicated by white text on a red background and similar residues are shown in red text on a white background. Groups of residues with a global similarity score above 0.7 are framed in blue. The pivotal conserved motifs S-x-x-K, Y-x-x, and W-x-G are marked as Block I, Block II and Block III, respectively. The putative catalytic triad (Ser118, Lys121 and Tyr239) is indicated by blue asterisks.

LipB could hydrolyze the glyceryl tributyrate (Figure 4A). Subsequently, we purified the MBP-LipB proteins and assayed the esterase activity with the substrates *p*-NP esters with various chain lengths of fatty acids (from C2 to C12). As shown in Figure 4B, LipB efficiently hydrolyzed *p*-NP esters with short chain fatty acids and exhibited the highest activity toward *p*-NP butyrate (C4). Defining the hydrolytic activity toward *p*-NP butyrate as 100%, LipB maintained more than 70% of activity against *p*-NP esters with acetate (C2) or hexanoate (C6). When *p*-NP esters were with longer chain lengths (C8 and C10), the esterase activities were less than 40%, and dropped to 20% with the *p*-NP laurate (C12) as a substrate. The absorbance of *p*-NP esters incubation showed no activity with the MBP protein, which excluded the influence of MBP-tag in esterase activity of LipB (Supplementary Figure S3A). In addition, the structure modeling also showed that the MBP and LipB fragments formed two separate parts with no significant interactions (Supplementary Figure S3B). Notably,

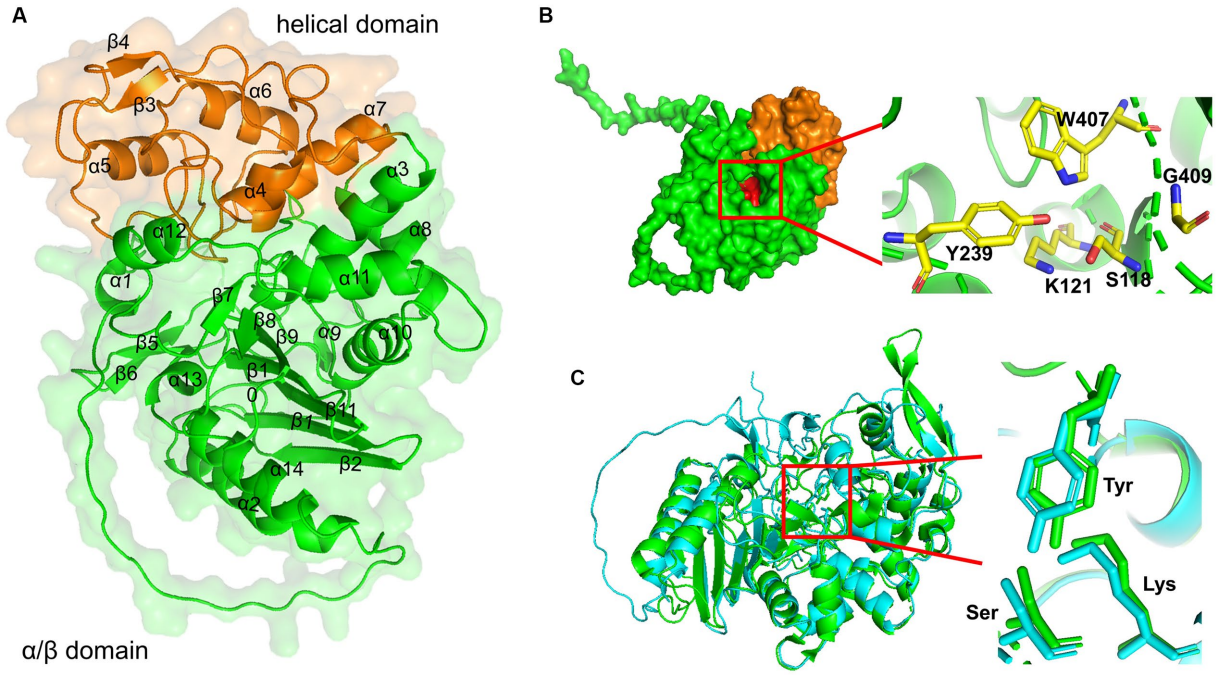

FIGURE 3
3D structure modeling of LipB. **(A)** A ribbon diagram of LipB was shown with the transparent surface structures. The secondary structures were labeled in black. The protein was divided into two domains: an alpha/beta-domain (residues 1–135 and residues 258–454) shown in green and a helical domain (residues 136–257) shown in orange. **(B)** Three conserved motifs were shown in red by the surface drawing. And the key residues (S118 and K121 in S-x-x-K motif, Y239 in Y-x-x motif, W407 and G409 in W-x-G motif) were zoomed clearly and shown as sticks in the ribbon diagram of LipB on the right. **(C)** Alignment of 3D structures of EstU1 and LipB. EstU1 (PDB code: 4IVI) and LipB were colored in green and cyan, respectively. The key residues related to β-lactam hydrolytic activity in catalytic triad were shown in sticks and zoomed at the right.

the activities of LipB were some different from that of LipA of the same strain, which belongs to family XV and exhibited the highest activity toward *p*-NP acetate (C2) under various pH and temperature conditions (Cheng et al., 2011).

Effect of pH on the esterase activity of LipB was measured in a pH range from 3 to 10 with *p*-NP butyrate as the substrate. As shown in Figure 4C, the LipB protein exhibited high activity under an alkaline condition (pH 8.0–9.5) and the maximum activity appeared at pH 9.0, which was corresponding to the natural growing environment of *S. cellulosum* So0157-2 (Han et al., 2013). Under the conditions with pH value lower than 7.0 or higher than 10.0, LipB lost more than 80% of activity.

LipB retained high activity in a broad temperature range (from 20°C to 60°C) and exhibited the maximum activity at 50°C. When the temperature increased to 70°C, the enzyme lost its activity almost completely (Figure 4D). Thus, unlike the cold-adapted lipase LipA identified previously, LipB worked as a thermophilic family VIII carboxylesterase. As to the temperature stability, LipB retained about 60% of activity after an incubation at 35°C or 45°C for 60 min. However, 30-min incubation at 55°C diminished more than 80% of the enzymatic activity (Figure 4E).

The activities of LipB in the presence of different metal ions are shown in Table 1. In general, lipolytic enzymes do not need cofactors in the hydrolyzation of the ester-bond. Nevertheless, it has been reported that activities of lipases and carboxylesterases are also enhanced by some divalent cations such as Ca^{2+}, Zn^{2+}, and Mg^{2+} (Choi et al., 2004; Gao et al., 2016; Araujo et al., 2020). As to LipB, addition of Ca^{2+}, Cu^{2+} or Zn^{2+} reduced the activity approximately in half, whereas the presence of 5 mM of Mg^{2+}, Co^{2+} or Ni^{2+} enhanced LipB esterase activity, and the highest increase to 142.8% was obtained by the addition of Ni^{2+}. As suggested by Araujo et al. (2020), the activity of LipB might be strengthened by the promotion of these divalent cations on a rapid product release or cleaning the enzyme's active sites.

More interestingly, LipB exhibited superior tolerance to organic solvents. The activity of LipB was stimulated 2-fold, 2.7-fold and 1.6-fold by the presence of 15% of methanol, 10% of ethanol or 5% of isopropanol, respectively, but suppressed by acetone, trichloromethane and acetonitrile. 10% of trichloromethane or 15% of acetonitrile inactivated LipB completely (Table 2). The organic solvent stability is an important criterion for industrial esterases (Gorman and Dordick, 1992). The excellent organic solvent stability of LipB implied its potentials in industrial applications for biotransformation and bioremediation associated with organic solvents.

3.5 β-lactamase activity of LipB

According to the β-lactamase activity, family VIII carboxylesterases were classified into three types: having no β-lactamase activity, represented by EstB (Petersen et al., 2001); only active to nitrocefin, represented by EstC (Rashamuse et al., 2009); and having β-lactamase activities toward different β-lactam antibiotics including cephaloridine, cefazolin, cephalothin and nitrocefin, represented by EstU1 (Jeon et al., 2011). We used four β-lactam antibiotics as the substrates for the β-lactamase activity assay: ampicillin, nitrocefin, cefotaxime and imipenem

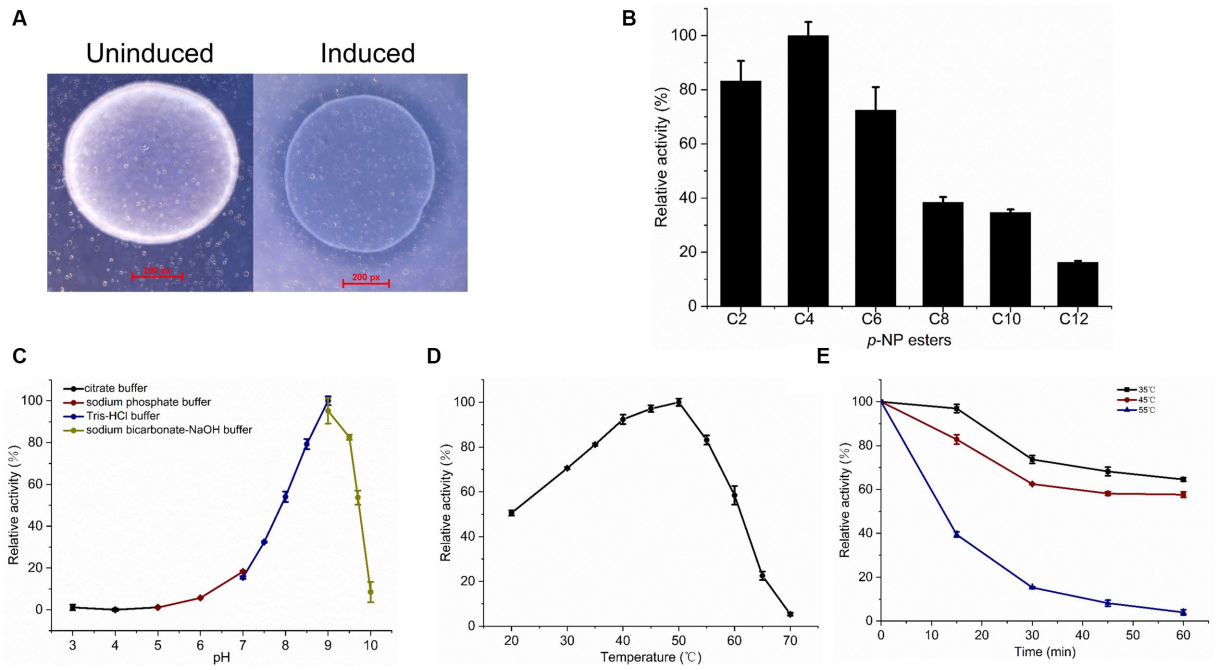

FIGURE 4
Esterase activity assay and biochemical characterization of recombinant LipB. **(A)** Hydrolysis of glyceryl tributyrate by LipB. Transparent zone was observed around the induced colonies. **(B)** Relative activity of LipB at *p*-NP esters with different chain lengths of fatty acids. Substrates used were *p*-NP acetate (C2), *p*-NP butyrate (C4), *p*-NP hexanoate (C6), *p*-NP octanoate (C8), *p*-NP decanoate (C10) and *p*-NP laurate (C12). **(C)** Effect of pH on activity of LipB. Activities under various pH conditions were marked by black (pH 3.0–5.0), wine (pH 5.0–7.0), navy (pH 7.0–9.0), dark yellow (pH 9.0–10.0). **(D)** Effect of temperature on activity of LipB. **(E)** Thermostability of LipB. The enzyme was preincubated at different temperatures for different time quantum, and the residual activity was determined. The residual activities incubated at 35°C, 45°C and 55°C were marked by black, wine and navy, respectively.

TABLE 1 Effects of metal ions on the esterase activity of LipB.

Cations	Relative activity (%) [a]
Control	100
$MnCl_2$	92.6 ± 5.6
$MgCl_2$	112.0 ± 1.3
$CaCl_2$	66.3 ± 5.3
$CuCl_2$	52.4 ± 2.3
$CoCl_2$	117.6 ± 9.2
$ZnCl_2$	50.0 ± 5.1
$NiCl_2$	142.8 ± 1.3

[a] The relative activities are given as a percentage of the activity in the absence of cations.

TABLE 2 Effects of organic solvents on the esterase activity of LipB.

Organic solvents	Relative activity (%) [a] at various solvent concentrations (%) of		
	5	10	15
Control	100	100	100
Methanol	248.6 ± 16.3	227.3 ± 5.6	203.8 ± 7.7
Ethanol	256.7 ± 17.6	272.4 ± 8.5	94.3 ± 5.3
Acetone	78.6 ± 4.7	49.0 ± 7.9	12.2 ± 4.3
Trichloromethane	7.4 ± 8.6	— [b]	—
Isopropanol	156.0 ± 11.6	116.4 ± 3.1	—
Acetonitrile	54.9 ± 4.0	11.3 ± 3.1	—

[a] The relative activities are given as a percentage of the activity in the absence of organic solvents.
[b] — represents the inactive state of enzyme.

(Supplementary Figure S4). As shown in Figure 5A, the absorbance of nitrocefin at 482 nm raised to 1.42 after incubation with MBP-LipB, and the color of solution changed from yellow to red which indicated that LipB could hydrolyze the amide bond of nitrocefin (Lee et al., 2005), and exhibited the maximum β-lactamase activity at 40°C or pH 7.0 (Supplementary Figure S5). The β-lactamase activities against ampicillin, cefotaxime and imipenem by LipB were also analyzed by HPLC, but no novel peaks derived from the substrate hydrolysis were observed (Figure 5B), illustrating that LipB had no β-lactamase activity toward these three antibiotics. Thus, LipB mimicked the β-lactamase activity of EstC, although the structure of LipB was closer to EstU1 (Figure 3C).

It was previously reported that appropriate length of the Ω-loop and the R1 segment (the connecting region between α6 and α8) in EstU1 played a critical role for its substrate hybridity to multiple β-lactam antibiotics, and the long Ω-loop might cover the R1 site and block the access to the catalytic triad (Cha et al., 2013). We aligned the amino acid sequences of LipB, EstU1, EstC and EstB, and found that the Ω-loop of LipB was 7 residues longer than that of EstU1, 4 residues longer than that of EstC, and 9 residues shorter than that of EstB (Figure 5C), which suggested that, compared with EstU1 and EstB, the intermediate length of Ω-loop might prompt LipB to form a conformation that allowed the moderate β-lactamase activity.

In addition, based on the docking model estimated by AutoDock, the nitrocefin was well located in the active pocket without blocking

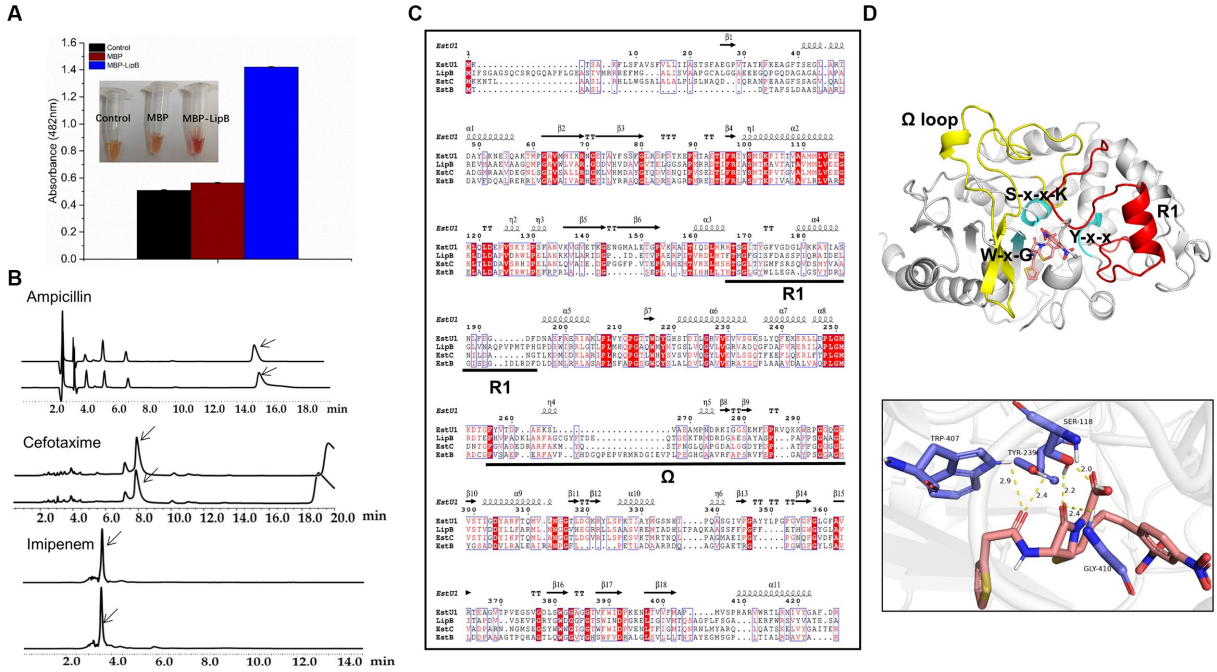

FIGURE 5
Activity of LipB toward β-lactam antibiotics. **(A)** Color change of nitrocefin-containing solution with MBP and MBP-LipB, using reaction mixture without proteins as a blank control. Specific data of absorbance at 482 nm is shown in the histogram form. **(B)** High performance liquid chromatography profiles for β-lactam antibiotics (upper) and β-lactam antibiotics incubated with LipB (nether). The substrate peaks of ampicillin, cefotaxime and imipenem are at 15.4 min, 7.9 min and 3.5 min, which were marked with arrows. **(C)** Sequence alignment among LipB, EstU1 (AFU54388.1), EstC (ACH88047.1) and EstB (AAF59826.1). The secondary structure assignment corresponds to EstU1. Ω represents the Ω loop and R1 represents R1 segment. **(D)** Molecule docking of LipB with the substrate nitrocefin and interactions of key sites. The predicted LipB/nitrocefin complex was shown at the image upper, Ω and R1 represent Ω-loop (yellow, residues 277–325) and R1 segment (red, residues 181–216), respectively. S-x-x-K motif, Y-x-x motif and W-x-G motif are marked by cyan. The potential hydrogen bond interactions of serine, tyrosine, tryptophan and glycine toward nitrocefin was displayed below.

from the moderate Ω-loop of LipB. Serine in the S-x-x-K motif, tyrosine in the Y-x-x motif, and tryptophan in the W-x-G motif formed hydrogen bonds interaction with the ligand nitrocefin, and the carbonyl oxygen in the β-lactam ring of nitrocefin was located at the oxyanion hole derived from Ser118 and Gly410 (Figure 5D). While in the docking model of LipB/ampicillin, the carbonyl oxygen of the opened β-lactam ring of ampicillin was interacted with Ser118 and Tyr239 instead of the oxyanion hole (Supplementary Figure S6A), which may affect the occurrence of the second reaction of hydrolysis. For cefotaxime and imipenem, no key residue in active pocket was linked to the lactam ring of substrates in the docking models with LipB (Supplementary Figures S6B,C), explaining why they could not be hydrolyzed by LipB.

4 Discussion

Diverse microbial lipolytic enzymes exhibited versatile application potentials with their catalytic activities on various substrates under adverse conditions (Bornscheuer, 2002). *S. cellulosum* is an intriguing but unexploited resource for lipolytic enzymes screening. In the 13 sequenced *S. cellulosum*, we discerned hundreds of lipolytic enzymes belonging to 12 families. In addition to the LipA previously reported in *S. cellulosum*, the LipB also exhibited excellent properties potential for specific industrial processing. Hence deep exploration of *S. cellulosum* is promising to provide more novel candidate lipolytic enzymes for the various requirements of industrial biotechnology. Notably, although LipB was once predicted to be responsible for the hydrolysis of epothilones (Gerth et al., 2002; Zhao et al., 2010; Li et al., 2017), our *in vitro* and *in vivo* analyses indicated that the enzyme was unable to hydrolyze epothilones (Supplementary Figure S7).

The broad substrate spectrum and harsh environment tolerance prompt family VIII carboxylesterases to be potentially applied in pharmaceutical, organic synthesis and other industrial productions, but only dozens of enzymes of this family have been investigated so far. Bioinformatics analysis shows that there were normally many family VIII carboxylesterases in *S. cellulosum* genomes, which were deserved for further investigation. Exemplified in this study, we analyzed the sequence and functional characteristics of LipB, a family VIII carboxylesterase. LipB had esterase activity toward glyceryl tributyrate and *p*-NP esters with short length of aliphatic side chains and weak β-lactamase activity against nitrocefin. The enzyme was alkaline and exhibited excellent activities in a wide range of temperature. Moreover, LipB was well tolerant to organic solvents, and even stimulated by methanol, ethanol, and isopropanol, which might indicate potential application in specific industrial processing associated with alcohols solvents. Similarly, several family VIII carboxylesterases were reported to be stimulated by methanol (Rashamuse et al., 2009; Selvin et al., 2012; Ouyang et al., 2013; Lee et al., 2016). It was confirmed by Müller et al. that some methanol-stimulated esterase could catalyze the acylation of methanol and the acyl-enzyme intermediate would be rapidly disassociated to accelerate

the release of *p*-nitrophenol and results in higher hydrolysis activities (Müller et al., 2021).

Family VIII carboxylesterases show different hydrolase activities against different type of β-lactam antibiotics. Although the key active sites (Ser, Lys and Tyr) essential for the β-lactamase activity overlapped well in the three-dimensional structures of LipB and EstU1, LipB catalyzes the hydrolysis of only nitrocefin, but not ampicillin, cefotaxime and imipenem. The spatial adaptation of LipB might be a more essential criterion for β-lactamase activity according to the results of sequence alignment and AutoDock.

5 Conclusion

In this study, we discerned a total of 406 lipolytic enzymes in 13 *S. cellulosum* genomes, and most of them exhibit low sequence similarity with those reported. We characterized a family VIII carboxylesterase LipB, alkaline, feasible to a wide range of temperature, and especially stimulated by organic solvents like methanol, ethanol and isopropanol. We propose that *S. cellulosum* strains are a treasury for digging more novel and promising industrial lipolytic enzymes.

Data availability statement

The original contributions presented in the study are included in the article/Supplementary material, further inquiries can be directed to the corresponding authors.

Author contributions

S-FY: Data curation, Investigation, Methodology, Software, Visualization, Writing – original draft, Writing – review & editing. X-JY: Funding acquisition, Project administration, Resources, Supervision, Writing – review & editing. W-FH: Methodology, Software, Writing – review & editing. YW: Methodology, Software, Writing – review & editing. Y-ZL: Funding acquisition, Project administration, Resources, Supervision, Validation, Writing – review & editing.

Funding

The author(s) declare financial support was received for the research, authorship, and/or publication of this article. This research was funded by the National Key Research and Development Program of China (2018YFA0901704, 2018YFA0900400 and 2021YFC2101000), the Natural Science Foundation of Shandong Province (ZR2019BC041) and National Natural Science Foundation of China (32301220).

Acknowledgments

We thank Zhifeng Li, Jing Zhu, Jingyao Qu, and Guannan Lin from the State Key Laboratory of Microbial Technology of Shandong University for help and guidance with High Performance Liquid Chromatography.

Conflict of interest

The authors declare that the research was conducted in the absence of any commercial or financial relationships that could be construed as a potential conflict of interest.

Publisher's note

Supplementary material

The Supplementary material for this article can be found online at: https://www.frontiersin.org/articles/10.3389/fmicb.2023.1304233/full#supplementary-material

References

Al-Ghanayem, A. A., and Joseph, B. (2020). Current prospective in using cold-active enzymes as eco-friendly detergent additive. *Appl. Microbiol. Biotechnol.* 104, 2871–2882. doi: 10.1007/s00253-020-10429-x

Araujo, F. J., Hissa, D. C., Silva, G. O., Antunes, A., Nogueira, V. L. R., Gonçalves, L. R. B., et al. (2020). A novel bacterial carboxylesterase identified in a metagenome derived-clone from Brazilian mangrove sediments. *Mol. Biol. Rep.* 47, 3919–3928. doi: 10.1007/s11033-020-05484-6

Arpigny, J. L., and Jaeger, K. E. (1999). Bacterial lipolytic enzymes: classification and properties. *Biochem. J.* 343, 177–183. doi: 10.1042/bj3430177

Athawale, V., Manjrekar, N., and Athawale, M. (2003). Effect of reaction parameters on synthesis of citronellyl methacrylate by lipase-catalyzed transesterification. *Biotechnol. Prog.* 19, 298–302. doi: 10.1021/bp0202867

Biver, S., and Vandenbol, M. (2013). Characterization of three new carboxylic ester hydrolases isolated by functional screening of a forest soil metagenomic library. *J. Ind. Microbiol. Biotechnol.* 40, 191–200. doi: 10.1007/s10295-012-1217-7

Bollag, D. M., Mcqueney, P. A., Zhu, J., Hensens, O., Koupal, L., Liesch, J., et al. (1995). Epothilones, a new class of microtubule-stabilizing agents with a taxol-like mechanism of action. *Cancer Res.* 55, 2325–2333.

Bornscheuer, U. T. (2002). Microbial carboxyl esterases: classification, properties and application in biocatalysis. *FEMS Microbiol. Rev.* 26, 73–81. doi: 10.1111/j.1574-6976.2002.tb00599.x

Cha, S. S., An, Y. J., Jeong, C. S., Kim, M. K., Jeon, J. H., Lee, C. M., et al. (2013). Structural basis for the β-lactamase activity of EstU1, a family VIII carboxylesterase. *Proteins* 81, 2045–2051. doi: 10.1002/prot.24334

Cheng, Y. Y., Qian, Y. K., Li, Z. F., Wu, Z. H., Liu, H., and Li, Y. Z. (2011). A novel cold-adapted lipase from *Sorangium cellulosum* strain So0157-2: gene cloning, expression, and enzymatic characterization. *Int. J. Mol. Sci.* 12, 6765–6780. doi: 10.3390/ijms12106765

Choi, Y. J., Miguez, C. B., and Lee, B. H. (2004). Characterization and heterologous gene expression of a novel esterase from *Lactobacillus casei* CL96. *Appl. Environ. Microbiol.* 70, 3213–3221. doi: 10.1128/AEM.70.6.3213-3221.2004

Cramer, P. (2021). AlphaFold2 and the future of structural biology. *Nat. Struct. Mol. Biol.* 28, 704–705. doi: 10.1038/s41594-021-00650-1

Diegelmann, C., Weber, J., Heinzel-Wieland, R., and Kemme, M. (2015). Characterization of a cypermethrin-degrading Methylobacterium sp. strain A-1 and molecular cloning of its carboxylesterase gene. *J. Basic Microbiol.* 55, 1245–1254. doi: 10.1002/jobm.201500186

Eberhardt, J., Santos-Martins, D., Tillack, A. F., and Forli, S. (2021). AutoDock Vina 1.2.0: new docking methods, expanded force field, and Python bindings. *J. Chem. Inf. Model.* 61, 3891–3898. doi: 10.1021/acs.jcim.1c00203

Gao, W., Wu, K., Chen, L., Fan, H., Zhao, Z., Gao, B., et al. (2016). A novel esterase from a marine mud metagenomic library for biocatalytic synthesis of short-chain flavor esters. *Microb. Cell Factories* 15:41. doi: 10.1186/s12934-016-0435-5

Gerth, K., Pradella, S., Perlova, O., Beyer, S., and Müller, R. (2003). Myxobacteria: proficient producers of novel natural products with various biological activities--past and future biotechnological aspects with the focus on the genus Sorangium. *J. Biotechnol.* 106, 233–253. doi: 10.1016/j.jbiotec.2003.07.015

Gerth, K., Steinmetz, H., Höflel, G., and Reichenbach, H. (2002). Studies on the biosynthesis of epothilones: hydroxylation of Epo a and B to epothilones E and F. *J. Antibiot. (Tokyo)* 55, 41–45. doi: 10.7164/antibiotics.55.41

Gong, G. L., Sun, X., Liu, X. L., Hu, W., Cao, W. R., Liu, H., et al. (2007). Mutation and a high-throughput screening method for improving the production of Epothilones of Sorangium. *J. Ind. Microbiol. Biotechnol.* 34, 615–623. doi: 10.1007/s10295-007-0236-2

Gorman, L. A., and Dordick, J. S. (1992). Organic solvents strip water off enzymes. *Biotechnol. Bioeng.* 39, 392–397. doi: 10.1002/bit.260390405

Gupta, N., Rathi, P., and Gupta, R. (2002). Simplified para-nitrophenyl palmitate assay for lipases and esterases. *Anal. Biochem.* 311, 98–99. doi: 10.1016/S0003-2697(02)00379-2

Han, K., Li, Z. F., Peng, R., Zhu, L. P., Zhou, T., Wang, L. G., et al. (2013). Extraordinary expansion of a *Sorangium cellulosum* genome from an alkaline milieu. *Sci. Rep.* 3:2101. doi: 10.1038/srep02101

Holmquist, M. (2000). Alpha/Beta-hydrolase fold enzymes: structures, functions and mechanisms. *Curr. Protein Pept. Sci.* 1, 209–235. doi: 10.2174/1389203003381405

Jaeger, K. E., and Eggert, T. (2002). Lipases for biotechnology. *Curr. Opin. Biotechnol.* 13, 390–397. doi: 10.1016/S0958-1669(02)00341-5

Jeon, J. H., Kim, S. J., Lee, H. S., Cha, S. S., Lee, J. H., Yoon, S. H., et al. (2011). Novel metagenome-derived carboxylesterase that hydrolyzes β-lactam antibiotics. *Appl. Environ. Microbiol.* 77, 7830–7836. doi: 10.1128/AEM.05363-11

Jeon, J. H., Lee, H. S., Lee, J. H., Koo, B. S., Lee, C. M., Lee, S. H., et al. (2016). A novel family VIII carboxylesterase hydrolysing third- and fourth-generation cephalosporins. *Springerplus* 5:525. doi: 10.1186/s40064-016-2172-y

Johan, U. U. M., Rahman, R., Kamarudin, N. H. A., and Ali, M. S. M. (2021). An integrated overview of bacterial carboxylesterase: structure, function and biocatalytic applications. *Colloids Surf. B Biointerfaces* 205:111882. doi: 10.1016/j.colsurfb.2021.111882

Jumper, J., Evans, R., Pritzel, A., Green, T., Figurnov, M., Ronneberger, O., et al. (2021). Highly accurate protein structure prediction with AlphaFold. *Nature* 596, 583–589. doi: 10.1038/s41586-021-03819-2

Kim, D. Y., and Dordick, J. S. (2001). Combinatorial array-based enzymatic polyester synthesis. *Biotechnol. Bioeng.* 76, 200–206. doi: 10.1002/bit.10011

Kovacic, F., Babic, N., Krauss, U., and Jaeger, K.-E. (2018). "Classification of Lipolytic enzymes from Bacteria" in *Aerobic utilization of hydrocarbons, oils and lipids*. ed. F. Rojo (Cham: Springer International Publishing), 1–35.

Kwon, S., Yoo, W., Kim, Y. O., Kim, K. K., and Kim, T. D. (2019). Molecular characterization of a novel family VIII esterase with β-lactamase activity (PsEstA) from Paenibacillus sp. *Biomolecules* 9:786. doi: 10.3390/biom9120786

Lee, M., Hesek, D., and Mobashery, S. (2005). A practical synthesis of nitrocefin. *J. Org. Chem.* 70, 367–369. doi: 10.1021/jo0487395

Lee, H. W., Jung, W. K., Kim, Y. H., Ryu, B. H., Kim, T. D., Kim, J., et al. (2016). Characterization of a novel alkaline family VIII esterase with S-enantiomer preference from a compost metagenomic library. *J. Microbiol. Biotechnol.* 26, 315–325. doi: 10.4014/jmb.1509.09081

Letunic, I., and Bork, P. (2021). Interactive tree of life (iTOL) v5: an online tool for phylogenetic tree display and annotation. *Nucleic Acids Res.* 49, W293–w296. doi: 10.1093/nar/gkab301

Li, X., Zhang, L., Jiang, Z., Liu, L., Wang, J., Zhong, L., et al. (2022). A novel cold-active GH8 xylanase from cellulolytic myxobacterium and its application in food industry. *Food Chem.* 393:133463. doi: 10.1016/j.foodchem.2022.133463

Li, Z. F., Zhu, L. P., Gu, J. Y., Singh, R. P., and Li, Y. Z. (2017). Isolation and characterisation of the epothilone gene cluster with flanks from high alkalotolerant strain *Sorangium cellulosum* (So0157-2). *World J. Microbiol. Biotechnol.* 33:137. doi: 10.1007/s11274-017-2301-y

Lilkova, E. (2015). "*The PyMOL molecular graphics system, version 1.8*". Schrodinger, LLC. New York

Minh, B. Q., Schmidt, H. A., Chernomor, O., Schrempf, D., Woodhams, M. D., Von Haeseler, A., et al. (2020). IQ-TREE 2: new models and efficient methods for phylogenetic inference in the genomic era. *Mol. Biol. Evol.* 37, 1530–1534. doi: 10.1093/molbev/msaa015

Mokoena, N., Mathiba, K., Tsekoa, T., Steenkamp, P., and Rashamuse, K. (2013). Functional characterisation of a metagenome derived family VIII esterase with a deacetylation activity on β-lactam antibiotics. *Biochem. Biophys. Res. Commun.* 437, 342–348. doi: 10.1016/j.bbrc.2013.06.076

Müller, H., Godehard, S. P., Palm, G. J., Berndt, L., Badenhorst, C. P. S., Becker, A. K., et al. (2021). Discovery and Design of Family VIII carboxylesterases as highly efficient acyltransferases. *Angew. Chem. Int. Ed. Engl.* 60, 2013–2017. doi: 10.1002/anie.202014169

Nan, F., Jiang, J., Wu, S., Zhang, Y., Qiu, J., Qiao, B., et al. (2019). A novel VIII carboxylesterase with high hydrolytic activity against ampicillin from a soil metagenomic library. *Mol. Biotechnol.* 61, 892–904. doi: 10.1007/s12033-019-00220-3

Ning, Z., Lang, K., Xia, K., Linhardt, R. J., and Gross, R. A. (2022). Lipase-catalyzed synthesis and characterization of poly (glycerol sebacate). *Biomacromolecules* 23, 398–408. doi: 10.1021/acs.biomac.1c01351

Oberg, N., Zallot, R., and Gerlt, J. A. (2023). EFI-EST, EFI-GNT, and EFI-CGFP: enzyme function initiative (EFI) web resource for genomic enzymology tools. *J. Mol. Biol.* 435:168018. doi: 10.1016/j.jmb.2023.168018

O'callaghan, C. H., Morris, A., Kirby, S. M., and Shingler, A. H. (1972). Novel method for detection of beta-lactamases by using a chromogenic cephalosporin substrate. *Antimicrob. Agents Chemother.* 1, 283–288. doi: 10.1128/AAC.1.4.283

Ouyang, L. M., Liu, J. Y., Qiao, M., and Xu, J. H. (2013). Isolation and biochemical characterization of two novel metagenome-derived esterases. *Appl. Biochem. Biotechnol.* 169, 15–28. doi: 10.1007/s12010-012-9949-4

Panda, T., and Gowrishankar, B. S. (2005). Production and applications of esterases. *Appl. Microbiol. Biotechnol.* 67, 160–169. doi: 10.1007/s00253-004-1840-y

Park, J. M., Won, S. M., Kang, C. H., Park, S., and Yoon, J. H. (2020). Characterization of a novel carboxylesterase belonging to family VIII hydrolyzing β-lactam antibiotics from a compost metagenomic library. *Int. J. Biol. Macromol.* 164, 4650–4661. doi: 10.1016/j.ijbiomac.2020.09.070

Petersen, E. I., Valinger, G., Sölkner, B., Stubenrauch, G., and Schwab, H. (2001). A novel esterase from *Burkholderia gladioli* which shows high deacetylation activity on cephalosporins is related to beta-lactamases and DD-peptidases. *J. Biotechnol.* 89, 11–25. doi: 10.1016/S0168-1656(01)00284-X

Priyanka, P., Tan, Y., Kinsella, G. K., Henehan, G. T., and Ryan, B. J. (2019). Solvent stable microbial lipases: current understanding and biotechnological applications. *Biotechnol. Lett.* 41, 203–220. doi: 10.1007/s10529-018-02633-7

Rashamuse, K., Magomani, V., Ronneburg, T., and Brady, D. (2009). A novel family VIII carboxylesterase derived from a leachate metagenome library exhibits promiscuous beta-lactamase activity on nitrocefin. *Appl. Microbiol. Biotechnol.* 83, 491–500. doi: 10.1007/s00253-009-1895-x

Robert, X., and Gouet, P. (2014). Deciphering key features in protein structures with the new ENDscript server. *Nucleic Acids Res.* 42, W320–W324. doi: 10.1093/nar/gku316

Schneiker, S., Perlova, O., Kaiser, O., Gerth, K., Alici, A., Altmeyer, M. O., et al. (2007). Complete genome sequence of the myxobacterium *Sorangium cellulosum*. *Nat. Biotechnol.* 25, 1281–1289. doi: 10.1038/nbt1354

Selvin, J., Kennedy, J., Lejon, D. P., Kiran, G. S., and Dobson, A. D. (2012). Isolation identification and biochemical characterization of a novel halo-tolerant lipase from the metagenome of the marine sponge *Haliclona simulans*. *Microb. Cell Fact.* 11:72. doi: 10.1186/1475-2859-11-72

Sirajuddin, S., Khan, M. A., Qader, S. A. U., Iqbal, S., Sattar, H., and Ansari, A. (2020). A comparative study on degradation of complex malathion organophosphate using of *Escherichia coli* IES-02 and a novel carboxylesterase. *Int. J. Biol. Macromol.* 145, 445–455. doi: 10.1016/j.ijbiomac.2019.12.192

Tanaka, K., Yoshida, K., Sasaki, C., and Osano, Y. T. (2002). Practical asymmetric synthesis of the herbicide (S)-indanofan via lipase-catalyzed kinetic resolution of a diol and stereoselective acid-catalyzed hydrolysis of a chiral epoxide. *J. Org. Chem.* 67, 3131–3133. doi: 10.1021/jo010816y

Trott, O., and Olson, A. J. (2010). AutoDock Vina: improving the speed and accuracy of docking with a new scoring function, efficient optimization, and multithreading. *J. Comput. Chem.* 31, 455–461. doi: 10.1002/jcc.21334

Udatha, D. B., Madsen, K. M., Panagiotou, G., and Olsson, L. (2015). Multiple nucleophilic elbows leading to multiple active sites in a single module esterase from *Sorangium cellulosum*. *J. Struct. Biol.* 190, 314–327. doi: 10.1016/j.jsb.2015.04.009

Wagner, U. G., Petersen, E. I., Schwab, H., and Kratky, C. (2002). EstB from *Burkholderia gladioli*: a novel esterase with a beta-lactamase fold reveals steric factors to discriminate between esterolytic and beta-lactam cleaving activity. *Protein Sci.* 11, 467–478. doi: 10.1110/ps.33002

Wang, S. Y., Hu, W., Lin, X. Y., Wu, Z. H., and Li, Y. Z. (2012). A novel cold-active xylanase from the cellulolytic myxobacterium *Sorangium cellulosum* So9733-1: gene cloning, expression, and enzymatic characterization. *Appl. Microbiol. Biotechnol.* 93, 1503–1512. doi: 10.1007/s00253-011-3480-3

Wu, M., Abokitse, K., Grosse, S., Leisch, H., and Lau, P. C. (2012). New feruloyl esterases to access phenolic acids from grass biomass. *Appl. Biochem. Biotechnol.* 168, 129–143. doi: 10.1007/s12010-011-9359-z

Yang, J., and Zhang, Y. (2015). I-TASSER server: new development for protein structure and function predictions. *Nucleic Acids Res.* 43, W174–W181. doi: 10.1093/nar/gkv342

Yue, X. J., Cui, X. W., Zhang, Z., Peng, R., Zhang, P., Li, Z. F., et al. (2017). A bacterial negative transcription regulator binding on an inverted repeat in the promoter for epothilone biosynthesis. *Microb. Cell Factories* 16:92. doi: 10.1186/s12934-017-0706-9

Zhao, L., Zhao, B.-B., Lu, C.-H., Li, Y.-Z., and Shen, Y.-M. (2010). Two Epothilones from *Sorangium cellulosum* strain So0157-2. *Chin. J. Nat. Med.* 8, 298–300. doi: 10.1016/S1875-5364(10)60038-6

Zhu, L. P., Yue, X. J., Han, K., Li, Z. F., Zheng, L. S., Yi, X. N., et al. (2015). Allopatric integrations selectively change host transcriptomes, leading to varied expression efficiencies of exotic genes in *Myxococcus xanthus*. *Microb. Cell Fact.* 14:105. doi: 10.1186/s12934-015-0294-5

frontiers | Frontiers in Microbiology

TYPE Original Research
PUBLISHED 05 December 2023
DOI 10.3389/fmicb.2023.1304874

OPEN ACCESS

EDITED BY
Honghui Zhu,
Guangdong Academy of Sciences, China

REVIEWED BY
Jianhua Yin,
Zhejiang University of Technology, China
Volker Siegfried Brozel,
South Dakota State University, United States

*CORRESPONDENCE
Wei Hu
✉ hw_1@sdu.edu.cn
Chuandong Wang
✉ wangchuandong@sdu.edu.cn
Fengyu Zhang
✉ zfengyu@sdu.edu.cn

RECEIVED 30 September 2023
ACCEPTED 13 November 2023
PUBLISHED 05 December 2023

CITATION
Zhang N, Li T, Pan H, Wang Y, Li Q, Luan J, He X, Shi W, Li Y, Wang C, Zhang F and Hu W (2023) Genetic components of *Escherichia coli* involved in its complex prey-predator interaction with *Myxococcus xanthus*. *Front. Microbiol.* 14:1304874. doi: 10.3389/fmicb.2023.1304874

Genetic components of *Escherichia coli* involved in its complex prey-predator interaction with *Myxococcus xanthus*

Ning Zhang[1], Tingyi Li[1], Hongwei Pan[2], Yipeng Wang[1], Qi Li[1], Jia Luan[3], Xuesong He[4,5], Wenyuan Shi[4], Yuezhong Li[1], Chuandong Wang[1]*, Fengyu Zhang[1]* and Wei Hu[1]*

[1]State Key Laboratory of Microbial Technology, Microbial Technology Institute, Shandong University, Qingdao, Shandong, China, [2]Department of Clinical Laboratory, Qilu Hospital of Shandong University, Jinan, Shandong, China, [3]Immunology and Molecular Genetics, University of California, Los Angeles, Los Angeles, CA, United States, [4]Department of Microbiology, The Forsyth Institute, Cambridge, MA, United States, [5]Department of Oral Medicine, Infection and Immunity, Harvard School of Dental Medicine, Boston, MA, United States

Myxococcus xanthus and *Escherichia coli* represent a well-studied microbial predator-prey pair frequently examined in laboratory settings. While significant progress has been made in comprehending the mechanisms governing *M. xanthus* predation, various aspects of the response and defensive mechanisms of *E. coli* as prey remain elusive. In this study, the *E. coli* MG1655 large-scale chromosome deletion library was screened, and a mutant designated as ME5012 was identified to possess significantly reduced susceptibility to predation by *M. xanthus*. Within the deleted region of ME5012 encompassing seven genes, the significance of *dusB* and *fis* genes in driving the observed phenotype became apparent. Specifically, the deletion of *fis* resulted in a notable reduction in flagellum production in *E. coli*, contributing to a certain level of resistance against predation by *M. xanthus*. Meanwhile, the removal of *dusB* in *E. coli* led to diminished inducibility of myxovirescin A production by *M. xanthus*, accompanied by a slight decrease in susceptibility to myxovirescin A. These findings shed light on the molecular mechanisms underlying the complex interaction between *M. xanthus* and *E. coli* in a predatory context.

KEYWORDS

***Myxococcus xanthus*, *Escherichia coli*, predator-prey interaction, *fis* gene, *dusB* gene, flagellum, myxovirescin A**

Introduction

Predatory bacteria are pervasive in the natural environment, employing diverse strategies to prey upon various microorganisms and exerting significant influence on the modulation of microbial population structures and dynamics (Hungate et al., 2021). Notably, *Myxococcus xanthus* stands out as a well-documented predatory species, characterized

by a complex epibiotic predation strategy (Perez et al., 2016; Thiery and Kaimer, 2020; Zwarycz et al., 2023), which infers a wide-ranging prey spectrum encompassing gram-positive and gram-negative bacteria (Livingstone et al., 2017; Arend et al., 2021), as well as certain fungi (Lloyd and Whitworth, 2017). The predation mechanisms employed by *M. xanthus* are multifaceted, operating either independently or synergistically to kill and consume different preys (Thiery and Kaimer, 2020; Sydney et al., 2021; Kaimer et al., 2023). *M. xanthus* cells search and encounter the prey by slowly gliding over surfaces powered by two motility mechanisms (Munoz-Dorado et al., 2016; Rombouts et al., 2023); a single predator cell approaches and dispatches a prey cell in a contact-dependent manner (Zhang W. et al., 2020), involving the concerted action of a tad-like apparatus (Seef et al., 2021) and a type III-like system (T3SS*) (Thiery et al., 2022); the secondary metabolites (Xiao et al., 2011), such as myxovirescin A (also known as antibiotic TA), and secreted hydrolytic enzymes like protease MepA (Berleman et al., 2014), are vital components of the predation arsenal, effectively targeting prey cells with the assistance of outer membrane vesicles (OMVs) (Zwarycz et al., 2020). These intricate procedures necessitate the participation of either individuals or a substantial population of predator cells, potentially eliciting a distinct reaction from the prey (Hungate et al., 2021).

In the context of predatory dynamics, prey organisms may employ defensive strategies in response to the predatory actions of *M. xanthus* (Muller et al., 2014; Perez et al., 2014; Sydney et al., 2021). *Escherichia coli* is one of the most commonly studied prey organisms killed by *M. xanthus* (DePas et al., 2014; Livingstone et al., 2018; Sydney et al., 2021). The development of biofilms, specifically the production of the curli and cellulose matrix, serves as a protective barrier for *E. coli* against the predation efforts of *M. xanthus* (DePas et al., 2014). Reciprocal adaptations have been observed in an artificial evolution experiment involving predator-prey co-cultures of *M. xanthus* and *E. coli*, resulting in the induction of outer-membrane protease OmpT aggregations and mucoidy development in *E. coli* as defensive responses (Nair et al., 2019). The overexpression of *lspA*, encoding the bacterial type II signal peptidase (SPase II), enhances TA resistance in *E. coli* and presents a potential defense mechanism against *M. xanthus* (Xiao and Wall, 2014). Additionally, transcriptomic analysis has revealed that nearly 40% of *E. coli* genes exhibit significant differential expression when co-incubated with *M. xanthus* (Livingstone et al., 2018). Despite the significant advancements in understanding the fundamental mechanisms underlying *M. xanthus* predation and *E. coli* defense, many facets of their interaction remain enigmatic.

In this study, we conducted a systematic screening of the *E. coli* Large-scale Chromosome Deletion Library (National Bioresource Project, NBRP) to reveal potential molecular constituents of *E. coli* involved in its predator-prey interaction with *M. xanthus* as a prey organism. Leveraging the well-established genetic systems of these microorganisms and employing a double-layer agar assay, we identified novel genetic elements within *E. coli* that play a role in its defense against *M. xanthus* predation. The findings from this research provide some insights into the underlying molecular mechanisms of this complex predator-prey interaction.

Materials and methods

Bacterial strains and cultural condition

The bacterial strains used in this study are listed in the **Supplementary Table 1**. All the *M. xanthus* strains were cultured in CYE liquid medium (pH 7.6) or on CYE plates supplemented with 1.5% agar at 30°C (Campos et al., 1978). *E. coli* cells were cultured in liquid Luria-Bertani (LB) medium or M9 medium at 37°C (Zhang F. et al., 2020). A total of 124 ME strains from the *E. coli* Large-scale Chromosome Deletion Library (Kato and Hashimoto, 2008) at the Japan National Institute of Genetics were acquired from Dr. Barry Warner and cultivated following the provided instructions. When needed, kanamycin (Km, 40 μg/mL), ampicillin (Amp, 100 μg/mL), chloramphenicol (Chl 17 μg/mL), or spectinomycin (Spe, 30 μg/mL) was added to the medium.

Double-layered agar assay

The assay was derived from prior studies on bacterial-phage interactions (Moce-Llivina et al., 2004; Santos et al., 2009). Briefly, 5 μL aliquot of *M. xanthus* cell suspension ($OD_{600\ nm}$ = 10) was spotted on CYE plates with 3–5 replicates, incubated at 30°C for 24 h, and 200 μL aliquot of overnight cultured *E. coli* ($OD_{600\ nm}$ = 4) was mixed with 3 mL 0.3% CYE soft agar and overlaid onto CYE plates with *M. xanthus* spots. Comparing reduced inhibition zones around *M. xanthus* spots were assessed to determine predation efficacy after another 24 h co-incubation. For screening, all *E. coli* mutants were sourced from the *E. coli* Large-scale Chromosome Deletion Library of NBRP, stored in the liquid nitrogen, and subsequently re-cultured in LB medium.

Colony-invasion predation assay

Quantified colony-invasion predation assay was conducted as previously described with some modifications (Berleman and Kirby, 2007; Wang et al., 2019). *M. xanthus* and *E. coli* cells were harvested to log phase, and concentrated to $OD_{600\ nm}$ as 35 and 100 with 10 mM MOPS buffer (pH 7.6), respectively. On CFL medium with 1.5% agar, 2.5 μL of *E. coli* suspension was pipetted at a distance of 5 mm from 2.5 μL of *M. xanthus* spots with the assistance of the microscope (Eclipse E400, Nikon, Japan). Plates were incubated at 30°C, and predator-prey colonies were documented and collected for quantification at timescales. The viable *E. coli* cells were quantified through the counting of colony-forming units (CFU) on LB plates by the automatic colony analyzer (Czone G6T, Shineso, China). A minimum of biological triplicates was conducted to ensure accuracy.

Construction of *E. coli* mutants and complement strains

Escherichia coli gene knockout mutants, including in-frame deletion of every gene encompassed by ME5012, Δ*flhDC*, and

Δ*tolC*, were obtained based on the λ-Red recombinase-mediated system assay as previously described (Datsenko and Wanner, 2000; Tas et al., 2015; Zhang F. et al., 2020). The primers and plasmids were detailed in the **Supplementary Table 1**. Kanamycin gene cassettes, bordered by FRT (FLP recognition target) sites, and homologous arms were amplified through polymerase chain reaction (PCR) with templates of plasmid pKD4 or MG1655 DNA, respectively. These amplified sequences were assembled into a single sequence and electroporated into *E. coli* MG1655 harboring plasmid pTKRed for target-gene replacement. Gene deletion mutants were identified through a 2 × T5 Super PCR Mix kit (Tsingke, China), and the resistance marker was further excised through plasmid pCP20 at 42°C.

The p*fis*, p*dusB* and p*dusB-fis* plasmids were constructed using Gibson assembly method (Gibson et al., 2009), and detailed information is provided in **Supplementary Table 1**. The linearized plasmid vector and their genes containing homologous arms were amplified using pTrc99a or *E. coli* MG1655 genome as templates through PCR using corresponding primers (**Supplementary Table 1**). The construction of expression plasmids followed the guidelines of the Gibson assembly kit (New England Biolabs, China). Positive clones were subsequently verified through DNA sequencing. The plasmids were individually introduced into MG1655 Δ*fis*, Δ*dusB* or Δ*dusB-fis* strains to construct complement strains via chemical transformation.

iTRAQ quantitative proteomic analysis

ME5012 and MG1655 were delivered with three replicates for quantitative proteomic analysis through the isobaric tags for relative and absolute quantitation (iTRAQ) methodology (Wang et al., 2016). Initially, cells were lysed to extract proteins, and they were reduced into peptides through trypsin digestion. Peptides sequentially were labeled individually with iTRAQ reagents for 2 h at room temperature. These labeled peptides were pooled and fractionated through strong cation exchange fractionation on high performance liquid chromatography (HPLC, LC-20AB, Shimadzu, Japan). After drying under vacuum, the labeled samples were analyzed using liquid chromatography-tandem mass spectrometry (LC-MS/MS, Thermo Fisher, USA).

The raw MS data were processed and analyzed to identify differentially expressed proteins (DEPs) for mechanisms exploration as previously described (Jeong et al., 2001; von Mering et al., 2005). The statistically significant difference of a protein was considered with fold change (FC) >1.5 in the expression level and FDR q-value < 0.05. The pathway enrichment analysis was obtained based on the Kyoto Encyclopedia of Genes and Genomes (KEGG) database, and top KEGG enrichment results were listed with p-value < 0.05. Protein-protein interaction (PPI) network of DEPs was predicted through String database and was further visualized based on Degree Centrality Analysis using Cytoscape software 3.10.0 (Majeed and Mukhtar, 2023). The mass spectrometry proteomics data have been deposited to the ProteomeXchange Consortium via the PRIDE partner repository with the dataset identifier PXD046017.

TEM observation

Morphologies of *E. coli* mutants were examined using a transmission electron microscopy (TEM) assay (Cujova et al., 2013). Briefly, *E. coli* mutants were absorbed on a carbon-stabilized copper grid for 5 min and subsequentially negative stained with 0.25% aqueous phosphotungstic acid for 10 s. Observations were performed through a STEM microscope (Talos F200X, Thermo Fisher).

Motility assay

The motility assay was conducted as previously described (Teng et al., 2010). *E. coli* mutants were grown in the LB medium and allowed to incubate overnight. A total of 0.5 μL of cell suspension (OD_{600} = 10.0) was spotted onto 0.2% agar LB plates and incubated at 37°C for 5 h. Motility halos were documented and measured by a Czone G6T automatic colony analyzer.

Bacterial tracking and analysis

Sample preparation was as previously described (Zhang W. et al., 2020; Thiery et al., 2022). *M. xanthus* DK1622 and *E. coli* were harvested and mixed at a ratio of 1:10, the mixture (1 μL) was applied to object slides with 1% CFL agar, overlaid with a cover glass, and incubated for 10 min at room temperature. The videos of predation were taken through the BX51 microscope equipped with a 100 × oil objective (Olympus, Japan). Bright-field images, with the dimensions of 133.2 μm × 88.8 μm, were acquired every 2 s, over a period of about 2 h. The bacterial movements were tracked and quantitative analyzed as previously described (Hu et al., 2016; Zhang W. et al., 2020). The primary steps encompass image background subtraction, smoothing processing, binarization processing, bacterial identification, and geometric information extraction. By evaluating kinematic parameters such as mean speed distribution, the rate of approaching prey, and the speed of leaving, the quantitative assessment of the alterations in speed during the predation process of the DK1622 cells was performed.

Real-time quantitative PCR (RT-qPCR)

The RT-qPCR procedure was carried out based on the published methodology (Zhang F. et al., 2020). In brief, total RNA was extracted following the instructions of the MiniBEST universal RNA extraction kit (TaKaRa, China), and qualified by NanoDrop 2000 UV-vis spectrophotometer (Thermo Fisher). cDNA synthesis was conducted by the 5 × HiScript III qRT SuperMix (Vazyme, China). The allocation system of samples was meticulously prepared to employ 2 × AceQ Universal SYBR qPCR Master Mix (Vazyme). Related primers utilized in this process have been cataloged in the **Supplementary Table 1**. The RT-qPCR results were quantified using Quant Studio Design and Analysis Software v1.3.1 (Thermo Fisher). The *gapA* expression was set as the

reference gene to normalize the target gene expression (Li et al., 2017).

MIC measurement

The minimal inhibitory concentrations (MICs) of *E. coli* toward TA were determined following the guidelines from EUCAST (Kassim et al., 2016; Cunrath et al., 2019). The TA was prepared and purified from the fermentative broth of *M. xanthus* DK1622 as previously described (Wang et al., 2019).

Antibiotic TA quantification

The extraction and detection of TA was performed as described previously described (Simunovic et al., 2006; Wang et al., 2019). Extracted fractions that contained TA were detected by HPLC (LC-20AD) with XTerra MS C18 column (5 μm, 2.1 mm × 100 mm, Waters, USA). The test conditions were set as: flow rate is 0.3 mL/min, solvent A is formic acid water solution (0.1%), solvent B is acetonitrile with formic acid (0.1%), and the elution program is 0–2 min with 5% B, 2–10 min to 50% B, 10–27 min to 95% B, 27–40 min maintaining 95% B. TA showed a characteristic UV_{max} absorption at 239 nm and was further confirmed by its mass spectrum. The exact amount of TA was calculated using the relative peak areas produced by the injection of a known amount of standard TA compound.

Efflux pump activity assay

Efflux pump activity was determined by a Nile Red assay with minor modifications (Bohnert et al., 2010; Cunrath et al., 2019). After an overnight incubation within M9 medium at 37°C, *E. coli* cells were collected and washed with PPB buffer, treated with 10 μM carbonyl cyanide m-chlorophenylhydrazone (CCCP) for 15 min. A total of 10 μL 5 mM Nile Red solution was sequentially added, and incubated for 3 h at 37°C, and the mixed samples were rested at room temperature for 1 h. Cells were collected by centrifugation and resuspended with PPB buffer, and 200 μL of samples were transferred to a 96-well plate and measured fluorescence (excitation at 552 nm and emission at 636 nm) for 120 s, then 1 μL of 1 M glucose was added, and the signal was recorded for additional 300 s. The percentage fluorescence decreases and efflux half-time after energization of *E. coli* strains were calculated as previously described (Cunrath et al., 2019).

Statistical analysis

Three biological replicates were conducted for quantitative analysis unless indicated otherwise. The results were expressed as mean ± SD, and One-way ANOVA analysis was employed for group comparisons. Visualization of results was accomplished by GraphPad Prism 9 software (La Jolla, CA, USA) and R packages (Li et al., 2023).

Results

The screening of an *E. coli* large-scale chromosome deletion mutant library to identify its genetic components involved in the predator-prey interaction with *M. xanthus*

A double-layer agar assay (**Figure 1A**-right panel) adapted from prior studies on bacterium-phage interactions (Cormier and Janes, 2014) was employed as an initial screening method to assess the predation efficacy of *M. xanthus* on various *E. coli* strains. To execute this assay, overnight cultured *E. coli* cells were amalgamated with semi-hard CYE agar, which was subsequently poured onto a CYE solid plate that had been previously incubated with *M. xanthus* colonies for a duration of 24 h. The wild-type (WT) *M. xanthus* DK1622 exhibited a clear zone of killing around its colonies after an overnight incubation period (**Figure 1A**-left panel), indicating its capacity for positive predation against WT *E. coli* MG1655. Conversely, *M. xanthus* YL0912 mutant deficient in TA production (Δ*MXAN3936* and *MXAN3938*) and with diminished prey-killing ability, did not display the inhibition zone against MG1655, consistent with earlier findings (Wang et al., 2014).

Subsequently, a comprehensive screening of all strains within the *E. coli* Large-scale Chromosome Deletion Library (NBRP) was conducted to reveal any potential molecular constituents of *E. coli* involved in the predator-prey interaction. Among these strains, an *E. coli* mutant denoted as ME5012 was identified to possess the most significantly reduced sensitivity to predation by DK1622 showing the substantially diminished inhibition zone (**Figure 1A**-left panel). This observation was further corroborated through the colony invasion assay and quantification of the surviving *E. coli* by CFU counting (**Figure 1B**).

The identification of pivotal genes in ME5012 accountable for the reduced susceptibility to *M. xanthus* predation

The deletion fragment located within ME5012 encompasses a cluster of seven genes situated at 73.39 min on the *E. coli* chromosome (**Figure 2A**). To elucidate the specific genes responsible for *E. coli*'s reduced sensitivity to *M. xanthus* predation within this genomic region, we systematically generated in-frame deletion mutants for each of the genes encompassed by ME5012.

As illustrated in the colony invasion assay presented in **Figure 2B**, and further validated through CFU quantification (**Figure 2C**), deletions of the *yhdT*, *panF*, *prmA*, *yhdJ*, and *yhdU* genes did not result in any noticeable alteration in the susceptibility of *E. coli* cells to predation by *M. xanthus* DK1622, which remained comparable to that of the MG1655. In contrast, the deletion of the *dusB* and *fis* genes led to a notable resistant phenotype, and simultaneous deletion of *dusB* and *fis* genes replicated the predation susceptibility observed in ME5012 (**Figure 2** and **Supplementary Figure 1**). The complemented strains of Δ*dusB*, Δ*fis* and Δ*fis-dusB* exhibited a restoration of susceptibility to the WT MG1655 level

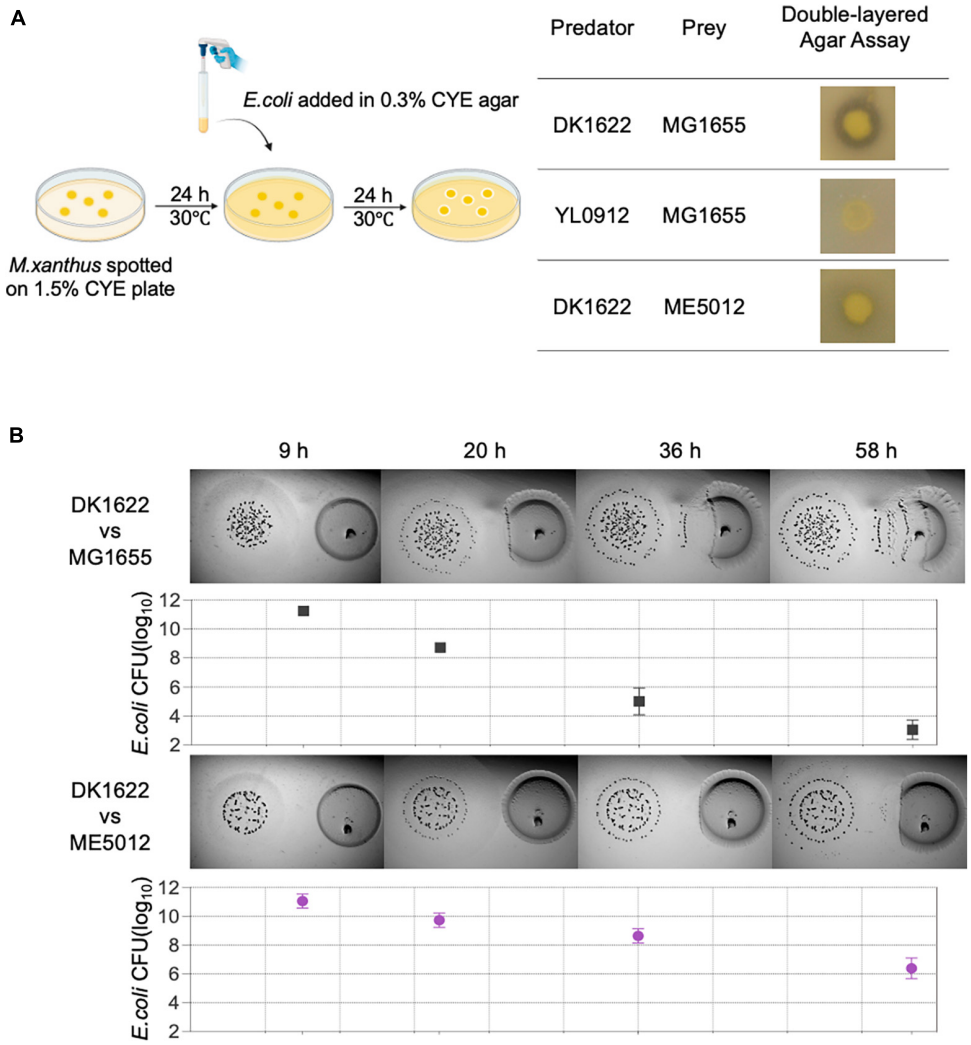

FIGURE 1
The predation efficiency of *M. xanthus* DK1622 on *E. coli* mutant ME5012 compared to wild-type MG1655. **(A)** Left illustration depicts the double-layered agar assay used to assess predator-prey interspecies interaction between *M. xanthus* and *E. coli*, and the representative screening results are shown in the right panel. **(B)** Visualization of colony invasion of *M. xanthus* DK1622 (left) into *E. coli* MG1655 and ME5012 (right), with the distance between the two colonies set at 5 mm. The surviving *E. coli* cells were quantified by CFU determination at set intervals.

(Supplementary Figure 2). Conversely, the deletion combinations of *yhdT-panF-prmA* or *yhdJ-yhdU* had no discernible impact on sensitivity. These results strongly suggest that the *dusB* and *fis* genes are pivotal in driving the observed phenotypic variations exhibited by mutant ME5012.

Quantitative proteomics analysis of *E. coli* ME5012 compared to MG1655

Through literature review, we have noticed that in *E. coli*, the *dusB-fis* operon encodes the global regulator Fis (factor for inversion stimulation), an abundant nucleoid-associated protein (NAP) that undergoes transient expression during the early exponential phase, which serves as an important global regulator of cellular metabolism, coordinating chromosomal DNA topology and ribosomal biosynthesis (Crozat et al., 2010; Gerganova et al., 2015; Kasho et al., 2023). Given that the *dusB-fis* operon regulates a multitude of crucial physiological processes in *E. coli*, establishing a direct causal link between the mutation of the *dusB-fis* operon and the observed defensive phenotype in predation through bioinformatics analysis becomes challenging. Therefore, we conducted a quantitative proteomics analysis of ME5012 in comparison with MG1655. The iTRAQ was used to analyze total cellular proteins obtained from *E. coli* cells. As a result, 22355 peptides and 2358 proteins were identified (filter criteria = 1% FRD). FC > 1.5 and FDR q-value < 0.05 were used as the screening criteria for DEPs. Compared with MG1655, a total of 116 proteins were differentially expressed in the ME5012 (Figure 3A and Supplementary Table 2). Among these DEPs, 43 were upregulated and 73 were downregulated. Then, we conducted the KEGG pathway enrichment analysis to further characterize the biological functions of the identified DEPs (Supplementary Table 3). Five pathways were significantly enriched based on the p-value (Figure 3B), including flagella assembly (ko02040), bacterial chemotaxis (ko02030), two-component systems (ko02020),

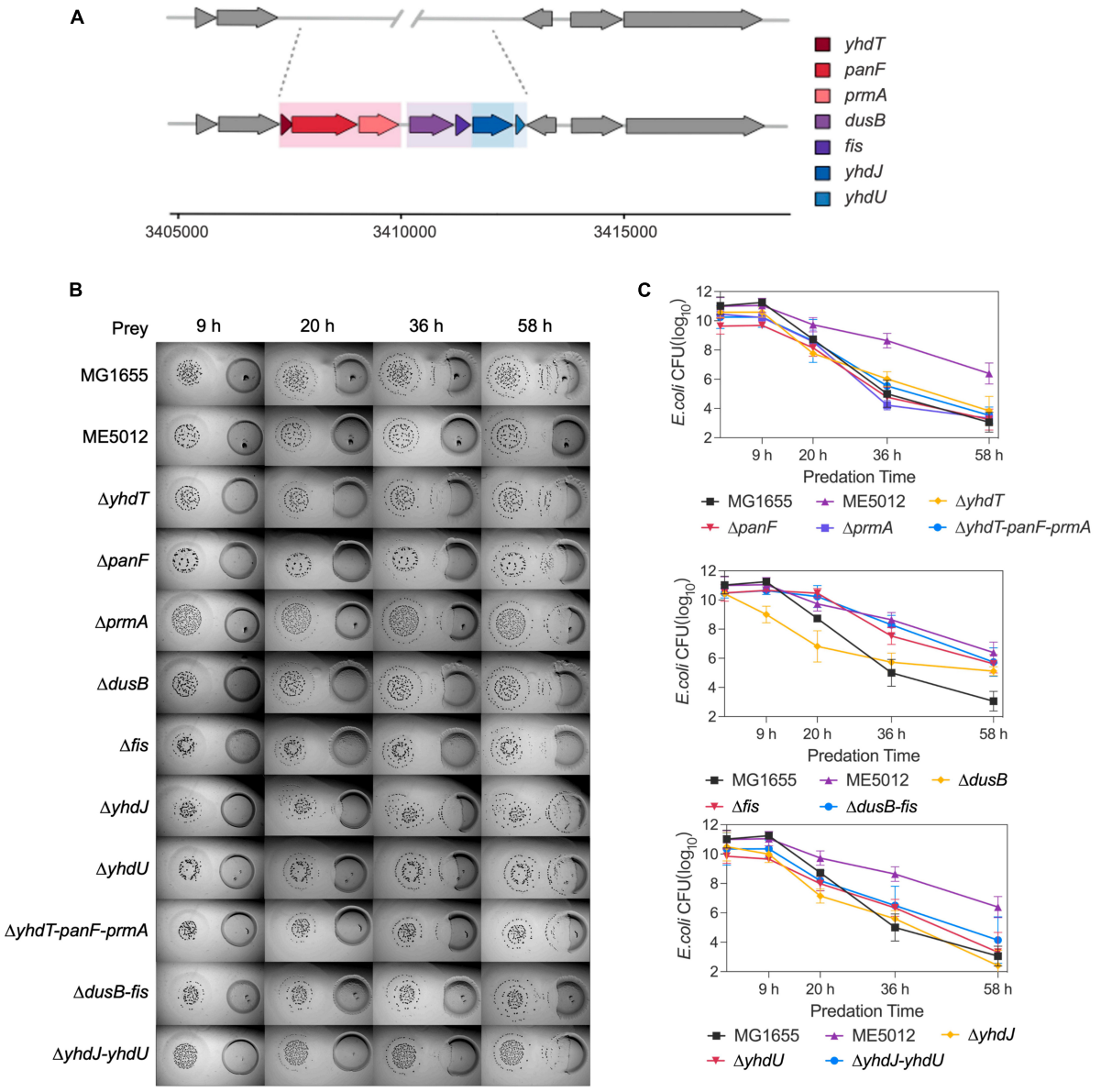

FIGURE 2
The *dusB* and *fis* genes were responsible for the less predation-susceptible phenotypes in ME5012. **(A)** ME5012 is a large-sequence-deletion *E. coli* mutant, involving seven genes, i.e., *yhdT*, *panF*, *prmA*, *dusB*, *fis*, *yhdJ*, and *yhdU*. **(B)** Visualization of colony invasion of *M. xanthus* DK1622 (left) into *E. coli* mutants (right) of all genes covered by ME5012. **(C)** Quantitative analysis of surviving *E. coli* cells during the colony invasion assay [panel **(B)**] facilitated by CFU determination at set intervals.

pyrimidine metabolism (ko00240), and drug metabolism-other enzymes (ko00983). Among these, the most enriched was the flagella assembly pathway including 21 downregulated genes.

The deletion of *fis* significantly reduces flagellum production in *E. coli*, leading to a certain degree of reduced susceptibility to *M. xanthus* predation

Based on the results of proteomic analysis, we initially focused on the flagellar production in strain ME5012. The PPI network of the identified DEPs for flagella assembly was constructed as previously described (Jeong et al., 2001), and the selection standards were based on topological algorithms, including degree, betweenness centrality, and closeness centrality, ensuring a comprehensive and robust selection of hub genes. As shown in Figure 3C, among the seven genes missing in ME5012, only *fis* and *prmA* were identified as potentially part of the regulatory network involved in *E. coli* flagellar synthesis, albeit in relatively peripheral roles.

Next, TEM observations of mutants (Figure 4A) revealed that MG1655 exhibited abundant flagellar structures on its surface, whereas flagellar was largely absent in ME5012, consistently echoing the KEGG analysis of the limited flagella assembly pathway (Figure 3B). The control strain Δ*flhDC* (lacking essential flagellar

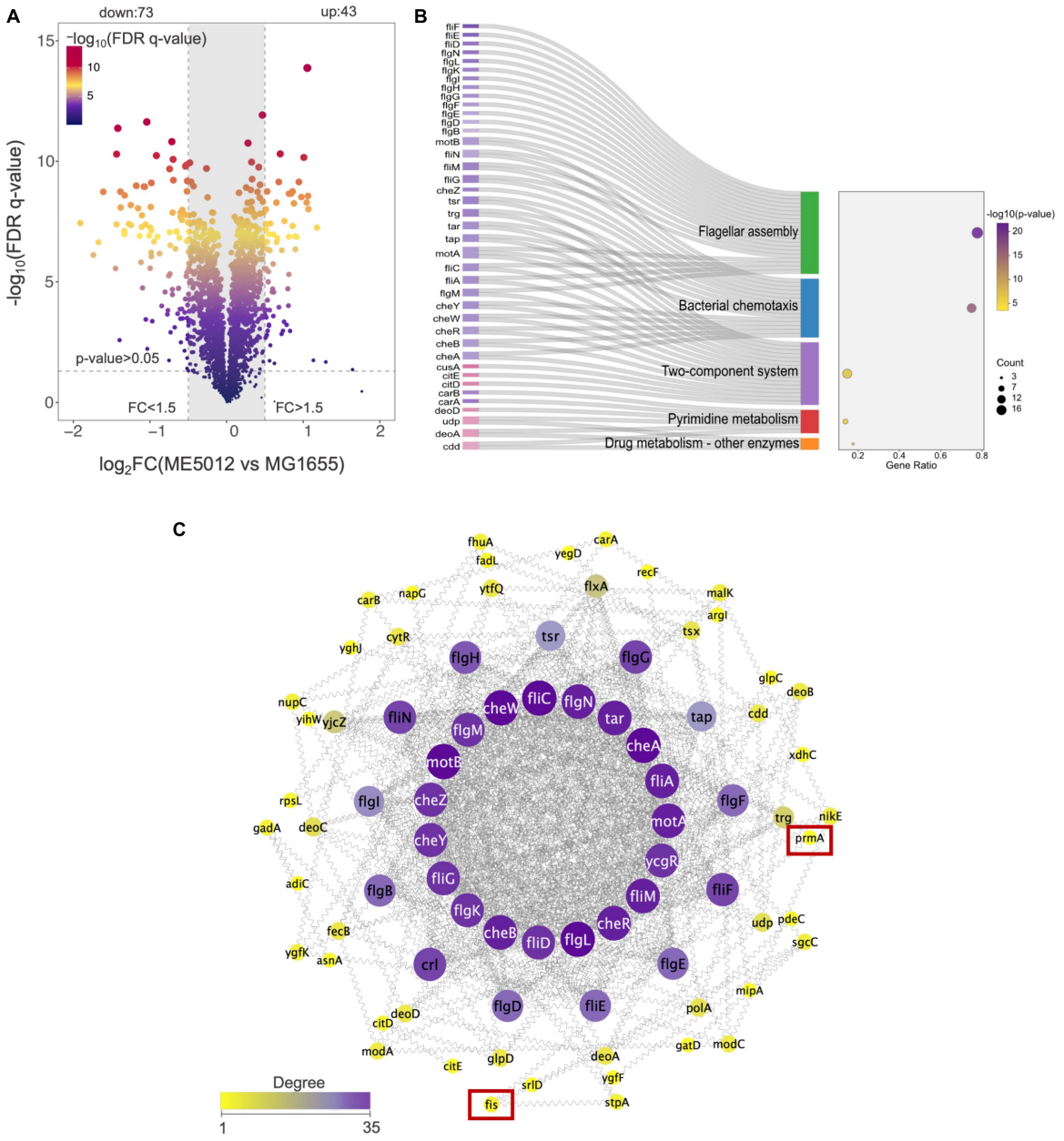

FIGURE 3
Quantitative proteomics analysis of *E. coli* ME5012 compared to MG1655. **(A)** Identification of significantly differentially expressed proteins (DEPs) in ME5012 compared to MG1655. The *X*-axis represents protein difference (log2-transformed fold changes), and the *Y*-axis represents the corresponding log10 transformed FRD *q*-value. Two vertical lines indicate expression fold change (ME5012 vs. MG1655) >1.5 and <-1.5, respectively, and a horizontal line indicates the adjusted *p*-value (FDR *q*-value) of 0.05. The *p*-values were calculated by a two-sided Wilcoxon rank-sum test, the bigger size of the dot infers a smaller FDR *q*-value, and the color of the dot represents the FDR *q*-value levels. The gray panel infers annotated proteins with insignificant differences. There are 43 dots identified as the significantly upregulated proteins, and 73 dots identified as the significantly downregulated proteins in the plot. **(B)** KEGG pathway enrichment of DEPs. The Sankey-dot plot diagram was employed to visualize top 5 enriched KEGG pathways of DEPs (p-value < 0.05). Related genes were listed on the left side of the panel (the pink color refers to upregulated genes, and the purple color refers to downregulated genes). The bubble diagram panel represents fold enrichment, gene count, and *p*-value KEGG pathways. The size of the dot is directly proportional to the gene count. **(C)** The protein-protein interaction (PPI) network construction based on degree centrality analysis. The node sizes represent the degree of centrality, meaning nodes with more interactions appear larger. Purple color refers to a high degree of centrality (>26).

regulatory gene *flhDC*) displayed a complete absence of flagella, which is consistent with previous report (Zhao et al., 2007). The Δ*prmA* and Δ*dusB* mutant strains continued to produce a relatively large number of flagella, while the Δ*fis* and Δ*fis-dusB* mutants nearly approached the flagellar abundance of ME5012. These observations were further confirmed through a motility assay conducted in semi-solid agar (**Figures 4B, C**). A marginal reduction in motility halos was noted in the Δ*prmA* and Δ*dusB* mutants compared to the WT. In contrast, both Δ*fis* and Δ*fis-dusB* strains exhibited significantly reduced motility compared to

the WT, similar to the ME5012. However, their motility did not reach the level of complete loss observed in the Δ*flhDC* mutant. Subsequently, we assessed the predation sensitivity of Δ*flhDC* mutant (**Figure 4D**). As expected, this strain displayed some level of reduced predation susceptibility, albeit higher than that of ME5012. These results suggest a potential role for flagellar structures of *E. coli* during predation by *M. xanthus*.

To further validate this hypothesis, we employed tracking software to automatically record and analyze the movement of *M. xanthus* DK1622 during predation on various live *E. coli* prey cells. The analysis encompassed approximately 12,000 predator cells, and Kernel Density Estimation (KDE) curves were generated from the density functions of each dataset, yielding a smoothed estimate of the speed distribution for each scenario (**Figure 5A**). Simultaneously, we extracted and presented the motion patterns of representative individual DK1622 cells encountering different individual *E. coli* cells (**Figure 5B**). The results corroborate that, in the presence of live WT *E. coli* MG1655, DK1622 exhibits predatory behavior, characterized by the lowest average velocity and the speed distribution (**Figure 5A**), which aligns with prior observations (Zhang W. et al., 2020). Notably, the instantaneous speed of DK1622 cell significantly diminishes when departing from MG1655 cell (**Figure 5B**). When DK1622 encounters Δ*fis* or Δ*flhDC* mutant cells, the average velocity was markedly higher than when encountering MG1655, and a significantly increased instantaneous velocity was recorded when departing from flagellum-deficient *E. coli* cells. Intriguingly, despite ME5012 having flagellar production similar to that of Δ*fis* strain, DK1622 displayed a much lower average velocity when interacting with ME5012 compared to Δ*fis* cells. Additionally, a significantly increased instantaneous velocity was observed when DK1622 departed from ME5012 cells.

The deletion of *dusB* leads to a diminished inducibility of *M. xanthus* TA production and a marginal decrease in susceptibility to TA

It has been previously established that antibiotic TA plays a pivotal role in the inhibition effects when *M. xanthus* preys on live *E. coli* (Xiao et al., 2011). The TA production of *M. xanthus* DK1622 with the presence of various live *E. coli* prey strains was quantified by HPLC. **Figure 6A** demonstrates that when encountering MG1655 cells, DK1622 significantly boosts the secretion of TA, thereby ensuring effective predation. However, this inductive response diminishes considerably when ME5012 and Δ*dusB* cells are used as prey. Strain Δ*fis* exhibits a significantly higher inductive capability than ME5012 and closely resembles the WT strain. To confirm this observation, additional transcriptional analyses of the TA operon were conducted. As the structural gene at the beginning of the TA operon, *taA* was selected for qPCR analysis. As shown in **Figure 6B**, the expression of *taA* was up-regulated approximately 2.3 to 2.6-fold when *M. xanthus* cells were, respectively, mixed with MG1655 and Δ*fis* cells, while ME5012 and Δ*dusB* failed to induce *taA* expression.

Beyond its reduced capacity to induce *M. xanthus* TA production, the mutants less susceptible to the predation may also exhibit enhanced resistance against TA lethality. To investigate this, we determined the MICs of purified TA against four *E. coli* strains (**Figure 6C**). ME5012 and Δ*dusB* displayed a MIC of 8 μg/mL, slightly higher than that of MG1655 and Δ*fis* (4 μg/mL). Previous reports have suggested that some prey cells increase *lspA* expression to acquire resistance to TA (Xiao et al., 2012; Wang et al., 2019). However, qPCR analysis revealed that all *E. coli* mutants exhibited similar *lspA* expression levels compared to WT MG1655 (**Figure 6D**). Furthermore, a re-analysis of our proteomic data unveiled the upregulated expression of some efflux pump proteins in ME5012 compared to MG1655 (**Figure 6E**), which has been shown to provide resistance to a variety of antimicrobial agents in *E. coli* (Borges-Walmsley and Walmsley, 2001; Kobayashi et al., 2001; Nagakubo et al., 2002). In Gram-negative bacteria, series of efflux pump systems rely on TolC to facilitate the translocation of a myriad of substrates, and the genetic ablation of *tolC* markedly attenuates efflux activity and increases in antibiotic susceptibility, while overexpression of *tolC* have been verified to directly proportional to antibiotic resistance (Cunrath et al., 2019). The Nile-red assay was employed to evaluate the efflux activities of *E. coli* cells, which is especially suitable for comparing efflux in diverse isolates (Bohnert et al., 2010; Cunrath et al., 2019). As shown in **Figure 6F**, MG1655 showed rapid energy-dependent efflux, whereas deletion of *tolC* abolished efflux in WT strain, which is consistent with previous observations (Bohnert et al., 2010; Cunrath et al., 2019). In addition to the representative fluorescence curves in Nile-red assay (**Figure 6F**), the statistical analysis of percentage fluorescence decreases and efflux half-times (**Supplementary Figure 3**) demonstrated that both ME5012 and Δ*dusB* strains exhibited slightly higher levels of active efflux activity compared to MG1655. These findings collectively suggest that the deletion of *dusB* in *E. coli* results in reduced inducibility of TA production by *M. xanthus*, and a slight increase in resistance to TA likely due to the overexpression of efflux pumps.

Discussion

Microbial predator-prey relationships have traditionally emphasized the role of the predator, but recent research has illuminated the molecular responses of various prey organisms when confronted with predation by *M. xanthus*, which has revealed that a relatively limited number of overarching resistant strategies are employed by the diversified prey species (Sydney et al., 2021). While considerable attention has been directed toward studying the interaction between *M. xanthus* and *E. coli*, many aspects of *E. coli*'s response and defense mechanisms against predation by *M. xanthus* remain poorly understood, particularly considering that transcriptomic analysis has unveiled significant differential expression in approximately 40% of *E. coli* genes during co-incubation with *M. xanthus* (Livingstone et al., 2018). This knowledge gap persists, even in the face of extensive research, which has substantiated well-documented phenomena such as biofilm formation (DePas et al., 2014), upregulation of OmpT and mucoidy development (Nair et al., 2019), and overexpression of SPase II (Xiao et al., 2012). In the endeavor to identify genes in *Pseudomonas aeruginosa* that contribute to its susceptibility to *M. xanthus* predation, a cluster of prey-related proteins has

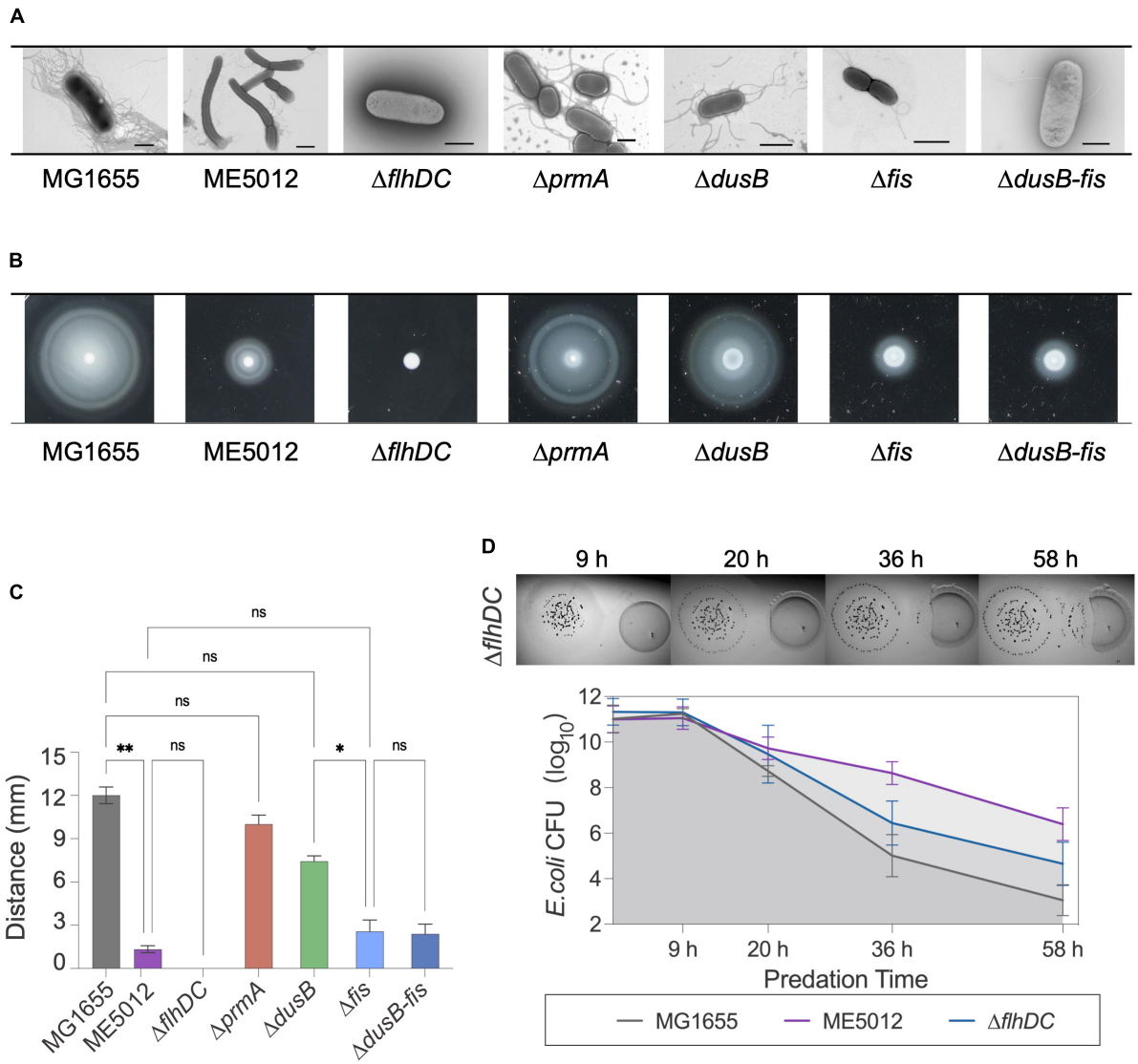

FIGURE 4
Flagellum-related phenotypes of *E. coli* strains. **(A)** Flagellar production of *E. coli* strains was observed through TEM. Scale bars are 1 μm for MG1655, 2 μm for ME5012, 1 μm for Δ*flhDC*, 2 μm for Δ*prmA*, 1 μm for Δ*dusB*, 1 μm for Δ*fis*, and 0.8 μm for Δ*dusB-fis*, respectively. **(B)** Motilities of *E. coli* strains in 0.2% agar. *E. coli* cells were spotted on LB plates with 0.2% agar and incubated at 37°C for 5 h, and the representative motility halos are shown. **(C)** The quantification of mobility halos in panel **(B)**. Error bars infer calculated standard deviations based on three replicates (*$P < 0.05$, **$P < 0.01$, ns > 0.05). **(D)** Visualization of colony invasion of *M. xanthus* DK1622 (left) into *E. coli* Δ*flhDC* mutant (right), and the quantitative analysis of surviving *E. coli* cells by CFU determination.

emerged, suggesting that its capacity to withstand predation relies on the effectiveness of metal/oxidative stress system, motility system, and mechanisms for detoxifying antimicrobial peptides (Sydney et al., 2021). This discovery underscores the potency of whole-genome screening as a robust methodology for elucidating predation resistance mechanisms. Therefore, we conducted a comprehensive screening of the *E. coli* large-scale chromosome deletion library, culminating in the identification of the mutant ME5012, which displayed remarkably reduced susceptibility to predation by *M. xanthus*. Subsequent investigation revealed the pivotal roles played by the *dusB* and *fis* genes in driving this observed phenotype. To the best of our knowledge, this represents the initial report detailing the involvement of the global regulator encoded by the *dusB-fis* operon (Crozat et al., 2010; Gerganova et al., 2015; Kasho et al., 2023) in the regulation of prey susceptibility in *E. coli*.

Fis is a highly abundant small DNA-binding protein within *E. coli*, playing a multifaceted role in regulating various biological processes, including transcription, recombination, replication reaction, nucleoid compaction, and chromosome conformation (Crozat et al., 2010; Nafissi et al., 2012; Duprey et al., 2014; Kasho et al., 2023). The expression profile of Fis is characterized by elevated levels during rapid growth under nutrient-rich conditions, while it diminishes during slow growth in nutrient-poor environments or in the stationary phase (Ali Azam et al., 1999). Positioned upstream of *fis* gene within the operon, the *dusB* gene encodes a tRNA synthase in *E. coli*, responsible for modifying tRNAs by converting uridine to 5,6-dihydrouridine within D loops

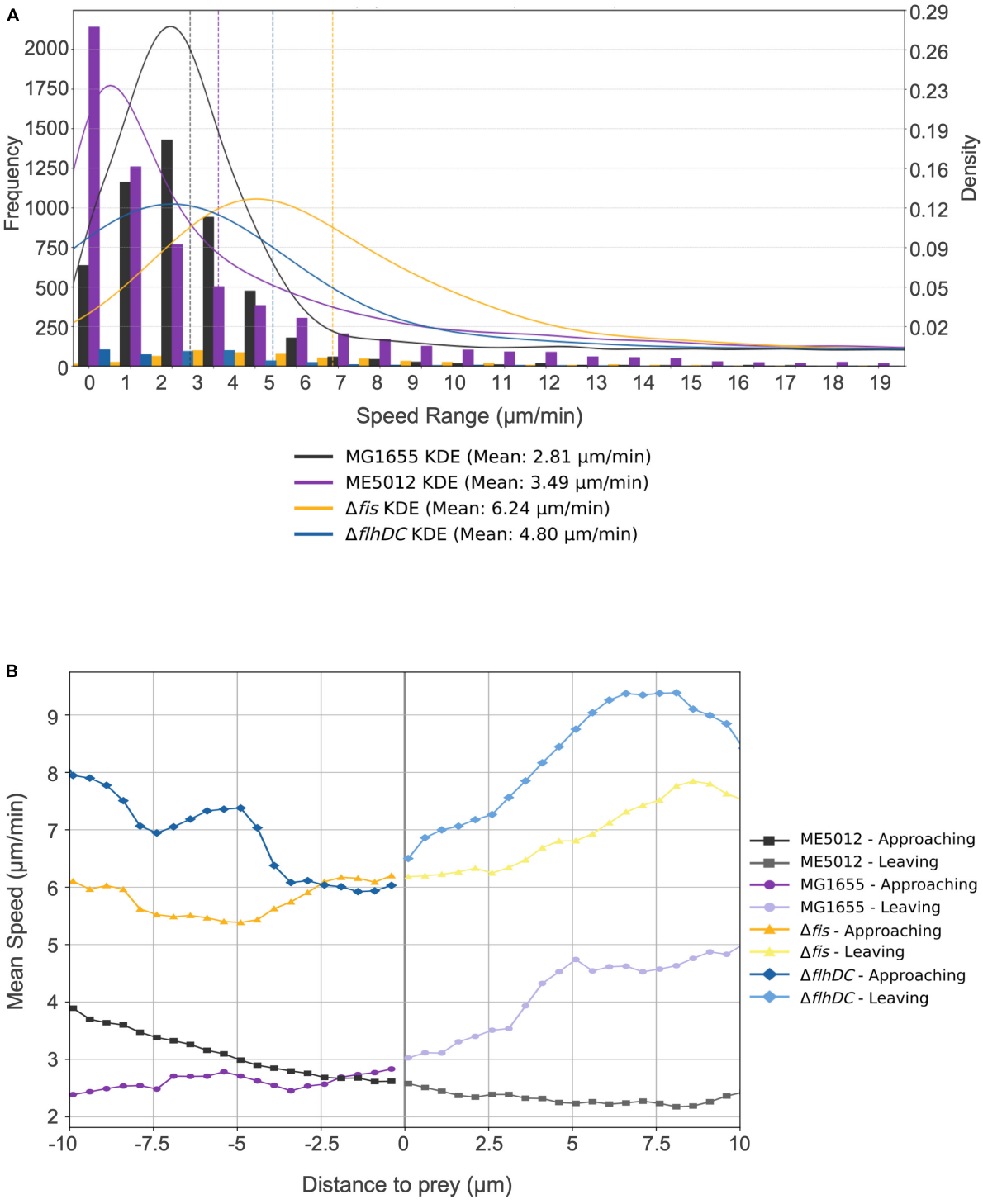

FIGURE 5
Motility characterization of *M. xanthus* DK1622 with the presence of various *E. coli* prey strains. **(A)** Frequency distribution of *M. xanthus* DK1622 cell movement speed with Kernel Density Estimation (KED) and mead speed. The set of four juxtaposed bar charts illustrates the frequency distribution of motility speeds of DK1622 cells mixed with different live *E. coli* prey cells, e.g., MG1655, ME5012, Δ*flhDC*, and Δ*fis*, respectively. The vertical dashed lines indicate the mean speed for each dataset. **(B)** The representative profile of the instantaneous speed of a *M. xanthus* DK1622 cell approaching and leaving a live *E. coli* prey cell. The *X*-axis represents the distance of a DK1622 cell to a prey cell, with negative values indicating the predator's approach to the prey, and positive values indicating the predator's leaving away from the prey. The zero point signifies the cell-cell contact between the predator and prey. The *Y*-axis represents the instantaneous velocity of the DK1622 cell.

(Bishop et al., 2002). The regulatory control of Fis synthesis is primarily exercised at the transcription initiation site of the *dusB-fis* operon (Cheng et al., 2000), and although translation of *dusB* is limited, it plays a key role in facilitating the robust translation of *fis* (Crozat et al., 2010; Nafissi et al., 2012; Burkhardt et al., 2017). Furthermore, the analyses of several mutations affecting

10.3389/fmicb.2023.1304874

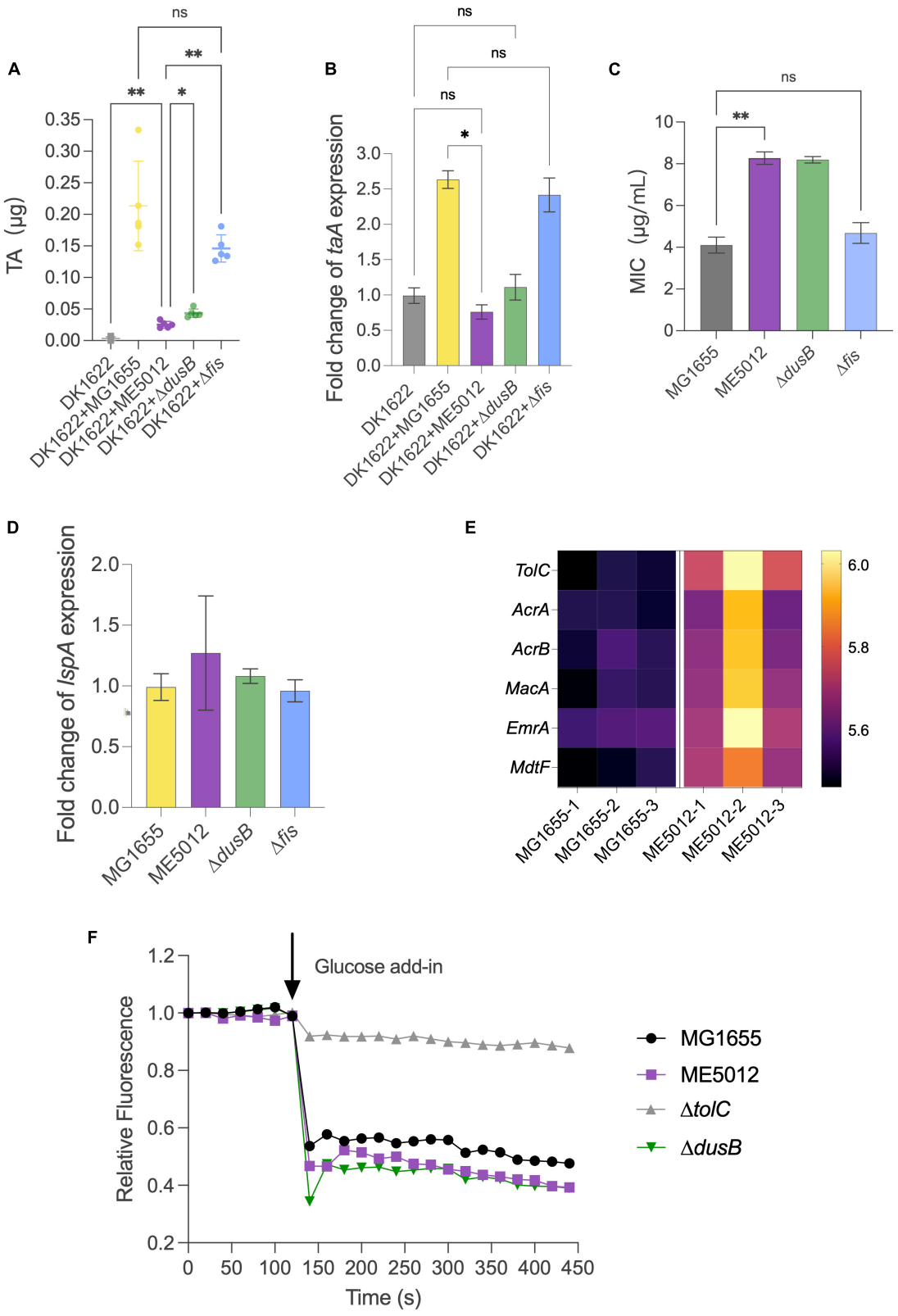

FIGURE 6
Inducibility of *M. xanthus* TA production and TA susceptibility of *E. coli* strains. **(A)** TA production by *M. xanthus* DK1622 with the presence of various *E. coli* prey strains was quantified by HPLC. **(B)** The expression of *taA* gene in DK1622 was quantified by qPCR with the presence of various E. coli prey strains. **(C)** MIC values of E. coli strains against TA (*$P < 0.05$, **$P < 0.01$, ns > 0.05). **(D)** Relative level of *lspA* gene expression in the *E. coli* mutants compared to that of MG1655. **(E)** Heatmap of some efflux pump proteins in MG1655 and ME5012 determined by the quantitative proteomic analysis. **(F)** Efflux activities in *E. coli* cells. Energy-depleted cells were loaded with Nile red and re-energized with glucose (arrow, 120 s), and efflux was measured as the decrease in Nile red fluorescence.

the transcription, translation, and protein activity of Fis in both *fis* and *dusB* genes have demonstrated substantial parallelism in the resulting phenotypic effects (Crozat et al., 2010). Our findings indicate that while the individual deletion of *dusB* and *fis* genes confers notable reduction in the sensitivity of *E. coli* to predation by *M. xanthus*, only the simultaneous deletion of both *dusB* and *fis* genes replicates the predation susceptibility observed in ME5012. This suggests that these two genes may play non-identical roles in the anti-predation process.

The quantitative proteomics analysis of ME5012 revealed a conspicuous alteration in the flagella assembly pathway, with 21 related genes showing significant downregulation compared to MG1655. In line with these findings, ME5012 exhibited markedly reduced motility in semi-solid agar compared to the WT, and a notable deficiency in flagellar production was observed through TEM. Strikingly, only the Δ*fis* and Δ*fis-dusB* strains displayed a significant reduction in motility, akin to the ME5012 strain. The Δ*fis* mutant nearly reached the flagellar production level of ME5012, while the Δ*dusB* mutant exhibited only a slight reduction in flagellar synthesis compared to the WT. Our observations align with previous reports, e.g., the *fis*:Km mutant of adherent-invasive *E. coli* (AIEC) failing to express flagellin (Miquel et al., 2010), implying a potential regulatory role of Fis in *E. coli* flagellar synthesis. In a Gram-negative plant pathogen *Dickeya dadantii* (formerly *Erwinia chrysanthemi*), Fis plays an essential role in the expression of the main virulence genes, and binds to the promoter regions of *fliC* to activate *fli* operon expression and flagella production (Lautier and Nasser, 2007; Duprey et al., 2014). Furthermore, the Δ*flhDC* mutant abolishing flagella production exhibited lower degree of predation susceptibility, albeit lower than that of ME5012, hinting at the possible involvement of *E. coli*'s flagellar structures in predation by *M. xanthus*. The analysis of *M. xanthus* DK1622 cell movement suggested that surface flagella on WT *E. coli* cells might be recognized by *M. xanthus* during the solitary predation, potentially trapping the predator cells and reducing their motility velocity, thus hindering their departure from the prey. Conversely, in cases where flagella were absent, as seen in the Δ*flhDC* mutant, DK1622 cells exhibited significantly higher movement speeds, diminishing their chances of contacting prey and reducing predation efficiency. Therefore, the deletion of the *fis* gene substantially curtails flagellum production in *E. coli*, resulting in a certain level of reduced susceptibility to *M. xanthus* predation. However, the distinct motility patterns observed in DK1622 cells when encountering ME5012 and the Δ*fis* mutant suggest a more intricate mechanism underpinning ME5012's predation resistance, despite the similarities in predation susceptibility and flagella production between ME5012 and the Δ*fis* mutant.

It is particularly interesting to note the up-regulation of TA production and the *taA* gene of DK1622 in response to direct contact with the specific live *E. coli* prey. When *M. xanthus* encounters MG1655 cells, there is a significant augmentation in TA secretion, thereby enhancing predation efficacy. This finding lends support to previous research indicating that antibiotic TA plays a pivotal role in the inhibition/killing effects when *M. xanthus* preys on live *E. coli* (Xiao et al., 2011). The inability to elicit the up-regulation of *M. xanthus* TA production by ME5012 suggests the requirement for specific genetic components in *E. coli*. Indeed, this inductive response diminishes significantly when Δ*dusB* cells are employed as prey, in contrast to Δ*fis* cells. However, the mechanism underlying this observed phenotype remains elusive, and the question of how *M. xanthus* can discern the presence of different prey and respond differentially presents an intriguing avenue for further exploration. Furthermore, both ME5012 and Δ*dusB* strains exhibited a MIC slightly higher than that of MG1655 and Δ*fis*, which cannot be attributed to the overexpression of *lspA*. Proteomic analysis revealed the up-regulation of several efflux pump proteins in ME5012 compared to MG1655. Both ME5012 and Δ*dusB* strains displayed slightly higher levels of active efflux activity than MG1655, which might contribute to their slight increase in resistance against TA. Nevertheless, establishing a direct connection between DusB and efflux pumps warrants further investigation.

In conclusion, our investigation sheds light on the complex interplay of genetic components within *E. coli* during its interaction with *M. xanthus* in a predator-prey context. The prominent parts of the *dusB* and *fis* genes in driving a reduced predation-susceptible phenotype underscore the multifaceted nature of the defense mechanisms employed by *E. coli*. Although the roles of these genes in governing flagellum production and responses related to TA have been proposed, the intricacies concerning the functions of the *dusB-fis* operon in *E. coli*'s reaction to *M. xanthus*'s tad-like (Seef et al., 2021) and type III-like (Thiery et al., 2022) apparatus-mediated contact-dependent killing require more in-depth examinations. Furthermore, our findings prompt further investigations into the nuances surrounding the functions of the *dusB-fis* operon in *E. coli*'s response to non-antibiotic substances, which also play an essential role in *M. xanthus* prey killing (Zwarycz et al., 2020), particularly in light of their potential facilitation by OMVs (Zwarycz et al., 2023). Unraveling the mechanisms underlying the interactions between *M. xanthus* and *E. coli* will provide deeper insights into the predator-prey dynamics and the broader ecological implications of such interactions.

Data availability statement

The data presented in the study are deposited in the ProteomeXchange Consortium via the PRODE partner repository with accession number PXD046017.

Author contributions

NZ: Conceptualization, Writing – original draft, Writing – review and editing, Data curation, Investigation, Methodology, Software, Validation, Visualization. TL: Data curation, Writing – review and editing. HP: Methodology, Writing – review and editing, Conceptualization, Data curation, Resources. YW: Writing – review and editing, Data curation, Methodology, Software, Visualization. QL: Writing – review and editing, Data curation. JL: Writing – review and editing, Data curation, Investigation. XH: Resources, Writing – review and editing. WS: Conceptualization, Writing – review and editing, Resources. YL: Writing – review and editing, Resources. CW: Data curation, Writing – review and editing, Writing – original draft, Funding

acquisition. FZ: Writing – review and editing, Supervision, Writing – original draft, Methodology. WH: Writing – review and editing, Conceptualization, Funding acquisition, Supervision, Writing – original draft.

Funding

The author(s) declare financial support was received for the research, authorship, and/or publication of this article. This research was supported by the National Natural Science Foundation of China (32070100, to WH), Shandong Provincial Natural Science Foundation (ZR2021QC087, to CW), and the National Key R&D Program of China (2021YFC2101000, to WH).

Acknowledgments

We would like to thank Sen Wang, Xiaoju Li, and Xiangmei Ren from the Core Facilities for Life and Environmental Sciences, State Key Laboratory of Microbial Technology of Shandong University for their help and guidance in HPLC, TEM, and LC-MS/MS experiments. We thank Dr. Barry Warner from National Institute of Genetics of Japan for providing all the *E. coli* mutant strains of their Large-scale Chromosome Deletion Library.

Conflict of interest

The authors declare that the research was conducted in the absence of any commercial or financial relationships that could be construed as a potential conflict of interest.

The authors declared that they were an editorial board member of Frontiers, at the time of submission. This had no impact on the peer review process and the final decision.

Publisher's note

Supplementary material

The Supplementary Material for this article can be found online at: https://www.frontiersin.org/articles/10.3389/fmicb.2023.1304874/full#supplementary-material

References

Ali Azam, T., Iwata, A., Nishimura, A., Ueda, S., and Ishihama, A. (1999). Growth phase-dependent variation in protein composition of the *Escherichia coli* nucleoid. *J. Bacteriol.* 181, 6361–6370. doi: 10.1128/JB.181.20.6361-6370.1999

Arend, K. I., Schmidt, J. J., Bentler, T., Luchtefeld, C., Eggerichs, D., Hexamer, H. M., et al. (2021). *Myxocaccus xanthus* predation of gram-positive or gram-negative bacteria is mediated by different bacteriolytic mechanisms. *Appl. Environ. Microbiol.* 87:e02382-20. doi: 10.1128/AEM.02382-20

Berleman, J. E., Allen, S., Danielewicz, M. A., Remis, J. P., Gorur, A., Cunha, J., et al. (2014). The lethal cargo of *Myxococcus xanthus* outer membrane vesicles. *Front. Microbiol.* 5:474. doi: 10.3389/fmicb.2014.00474

Berleman, J. E., and Kirby, J. R. (2007). Multicellular development in *Myxococcus xanthus* is stimulated by predator-prey interactions. *J. Bacteriol.* 189, 5675–5682. doi: 10.1128/JB.00544-07

Bishop, A. C., Xu, J., Johnson, R. C., Schimmel, P., and de Crecy-Lagard, V. (2002). Identification of the tRNA-dihydrouridine synthase family. *J. Biol. Chem.* 277, 25090–25095. doi: 10.1074/jbc.M203208200

Bohnert, J. A., Karamian, B., and Nikaido, H. (2010). Optimized Nile Red efflux assay of AcrAB-TolC multidrug efflux system shows competition between substrates. *Antimicrob. Agents Chemother.* 54, 3770–3775. doi: 10.1128/AAC.00620-10

Borges-Walmsley, M. I., and Walmsley, A. R. (2001). The structure and function of drug pumps. *Trends Microbiol.* 9, 71–79. doi: 10.1016/s0966-842x(00)01920-x

Burkhardt, D. H., Rouskin, S., Zhang, Y., Li, G. W., Weissman, J. S., and Gross, C. A. (2017). Operon mRNAs are organized into ORF-centric structures that predict translation efficiency. *Elife* 6:e22037. doi: 10.7554/eLife.22037

Campos, J. M., Geisselsoder, J., and Zusman, D. R. (1978). Isolation of bacteriophage MX4, a generalized transducing phage for *Myxococcus xanthus*. *J. Mol. Biol.* 119, 167–178. doi: 10.1016/0022-2836(78)90431-x

Cheng, Y. S., Yang, W. Z., Johnson, R. C., and Yuan, H. S. (2000). Structural analysis of the transcriptional activation region on Fis: crystal structures of six Fis mutants with different activation properties. *J. Mol. Biol.* 302, 1139–1151. doi: 10.1006/jmbi.2000.4123

Cormier, J., and Janes, M. (2014). A double layer plaque assay using spread plate technique for enumeration of bacteriophage MS2. *J. Virol. Methods* 196, 86–92. doi: 10.1016/j.jviromet.2013.10.034

Crozat, E., Winkworth, C., Gaffe, J., Hallin, P. F., Riley, M. A., Lenski, R. E., et al. (2010). Parallel genetic and phenotypic evolution of DNA superhelicity in experimental populations of *Escherichia coli*. *Mol. Biol. Evol.* 27, 2113–2128. doi: 10.1093/molbev/msq099

Cujova, S., Slaninova, J., Monincova, L., Fucik, V., Bednarova, L., Stokrova, J., et al. (2013). Panurgines, novel antimicrobial peptides from the venom of communal bee *Panurgus calcaratus* (Hymenoptera: *Andrenidae*). *Amino Acids* 45, 143–157. doi: 10.1007/s00726-013-1482-4

Cunrath, O., Meinel, D. M., Maturana, P., Fanous, J., Buyck, J. M., Saint Auguste, P., et al. (2019). Quantitative contribution of efflux to multi-drug resistance of clinical *Escherichia coli* and *Pseudomonas aeruginosa* strains. *EBioMedicine* 41, 479–487. doi: 10.1016/j.ebiom.2019.02.061

Datsenko, K. A., and Wanner, B. L. (2000). One-step inactivation of chromosomal genes in *Escherichia coli* K-12 using PCR products. *Proc. Natl. Acad. Sci. U.S.A.* 97, 6640–6645. doi: 10.1073/pnas.120163297

DePas, W. H., Syed, A. K., Sifuentes, M., Lee, J. S., Warshaw, D., Saggar, V., et al. (2014). Biofilm formation protects *Escherichia coli* against killing by *Caenorhabditis elegans* and *Myxococcus xanthus*. *Appl. Environ. Microbiol.* 80, 7079–7087. doi: 10.1128/AEM.02464-14

Duprey, A., Reverchon, S., and Nasser, W. (2014). Bacterial virulence and Fis: adapting regulatory networks to the host environment. *Trends Microbiol.* 22, 92–99. doi: 10.1016/j.tim.2013.11.008

Gerganova, V., Berger, M., Zaldastanishvili, E., Sobetzko, P., Lafon, C., Mourez, M., et al. (2015). Chromosomal position shift of a regulatory gene alters the bacterial phenotype. *Nucleic Acids Res.* 43, 8215–8226. doi: 10.1093/nar/gkv709

Gibson, D. G., Young, L., Chuang, R. Y., Venter, J. C., Hutchison, C. A. III, and Smith, H. O. (2009). Enzymatic assembly of DNA molecules up to several hundred kilobases. *Nat. Methods* 6, 343–345. doi: 10.1038/nmeth.1318

Hu, W., Gibiansky, M. L., Wang, J., Wang, C., Lux, R., Li, Y., et al. (2016). Interplay between type IV pili activity and exopolysaccharides secretion controls motility patterns in single cells of *Myxococcus xanthus*. *Sci. Rep.* 6:17790. doi: 10.1038/srep17790

Hungate, B. A., Marks, J. C., Power, M. E., Schwartz, E., van Groenigen, K. J., Blazewicz, S. J., et al. (2021). The functional significance of bacterial predators. *mBio* 12:e00466-21. doi: 10.1128/mBio.00466-21

Jeong, H., Mason, S. P., Barabasi, A. L., and Oltvai, Z. N. (2001). Lethality and centrality in protein networks. *Nature* 411, 41–42. doi: 10.1038/35075138

Kaimer, C., Weltzer, M. L., and Wall, D. (2023). Two reasons to kill: predation and kin discrimination in myxobacteria. *Microbiology (Reading)* 169:001372. doi: 10.1099/mic.0.001372

Kasho, K., Ozaki, S., and Katayama, T. (2023). IHF and Fis as *Escherichia coli* cell cycle regulators: activation of the replication origin oriC and the regulatory cycle of the DnaA initiator. *Int. J. Mol. Sci.* 24:11572. doi: 10.3390/ijms241411572

Kassim, A., Omuse, G., Premji, Z., and Revathi, G. (2016). Comparison of Clinical Laboratory Standards Institute and European Committee on Antimicrobial Susceptibility Testing guidelines for the interpretation of antibiotic susceptibility at a University teaching hospital in Nairobi, Kenya: a cross-sectional study. *Ann. Clin. Microbiol. Antimicrob.* 15:21. doi: 10.1186/s12941-016-0135-3

Kato, J., and Hashimoto, M. (2008). Construction of long chromosomal deletion mutants of *Escherichia coli* and minimization of the genome. *Methods Mol. Biol.* 416, 279–293. doi: 10.1007/978-1-59745-321-9_18

Kobayashi, N., Nishino, K., and Yamaguchi, A. (2001). Novel macrolide-specific ABC-type efflux transporter in *Escherichia coli*. *J. Bacteriol.* 183, 5639–5644. doi: 10.1128/JB.183.19.5639-5644.2001

Lautier, T., and Nasser, W. (2007). The DNA nucleoid-associated protein Fis coordinates the expression of the main virulence genes in the phytopathogenic bacterium *Erwinia chrysanthemi*. *Mol. Microbiol.* 66, 1474–1490. doi: 10.1111/j.1365-2958.2007.06012.x

Li, B., Yue, Y., Yuan, Z., Zhang, F., Li, P., Song, N., et al. (2017). *Salmonella* STM1697 coordinates flagella biogenesis and virulence by restricting flagellar master protein FlhD4C2 from recruiting RNA polymerase. *Nucleic Acids Res.* 45, 9976–9989. doi: 10.1093/nar/gkx656

Li, F., Wang, C., Xu, J., Wang, X., Cao, M., Wang, S., et al. (2023). Evaluation of the antibacterial activity of *Elsholtzia ciliate* essential oil against halitosis-related *Fusobacterium nucleatum* and *Porphyromonas gingivalis*. *Front. Microbiol.* 14:1219004. doi: 10.3389/fmicb.2023.1219004

Livingstone, P. G., Millard, A. D., Swain, M. T., and Whitworth, D. E. (2018). Transcriptional changes when *Myxococcus xanthus* preys on *Escherichia coli* suggest myxobacterial predators are constitutively toxic but regulate their feeding. *Microb. Genom.* 4:e000152. doi: 10.1099/mgen.0.000152

Livingstone, P. G., Morphew, R. M., and Whitworth, D. E. (2017). Myxobacteria are able to prey broadly upon clinically-relevant pathogens, exhibiting a prey range which cannot be explained by phylogeny. *Front. Microbiol.* 8:1593. doi: 10.3389/fmicb.2017.01593

Lloyd, D. G., and Whitworth, D. E. (2017). The myxobacterium *Myxococcus xanthus* can sense and respond to the quorum signals secreted by potential prey organisms. *Front. Microbiol.* 8:439. doi: 10.3389/fmicb.2017.00439

Majeed, A., and Mukhtar, S. (2023). Protein-protein interaction network exploration using cytoscape. *Methods Mol. Biol.* 2690, 419–427. doi: 10.1007/978-1-0716-3327-4_32

Miquel, S., Claret, L., Bonnet, R., Dorboz, I., Barnich, N., and Darfeuille-Michaud, A. (2010). Role of decreased levels of Fis histone-like protein in Crohn's disease-associated adherent invasive *Escherichia coli* LF82 bacteria interacting with intestinal epithelial cells. *J. Bacteriol.* 192, 1832–1843. doi: 10.1128/JB.01679-09

Moce-Llivina, L., Lucena, F., and Jofre, J. (2004). Double-layer plaque assay for quantification of enteroviruses. *Appl. Environ. Microbiol.* 70, 2801–2805. doi: 10.1128/AEM.70.5.2801-2805.2004

Muller, S., Strack, S. N., Hoefler, B. C., Straight, P. D., Kearns, D. B., and Kirby, J. R. (2014). Bacillaene and sporulation protect *Bacillus subtilis* from predation by *Myxococcus xanthus*. *Appl. Environ. Microbiol.* 80, 5603–5610. doi: 10.1128/AEM.01621-14

Munoz-Dorado, J., Marcos-Torres, F. J., Garcia-Bravo, E., Moraleda-Munoz, A., and Perez, J. (2016). Myxobacteria: moving, killing, feeding, and surviving together. *Front. Microbiol.* 7:781. doi: 10.3389/fmicb.2016.00781

Nafissi, M., Chau, J., Xu, J., and Johnson, R. C. (2012). Robust translation of the nucleoid protein Fis requires a remote upstream AU element and is enhanced by RNA secondary structure. *J. Bacteriol.* 194, 2458–2469. doi: 10.1128/JB.00053-12

Nagakubo, S., Nishino, K., Hirata, T., and Yamaguchi, A. (2002). The putative response regulator BaeR stimulates multidrug resistance of *Escherichia coli* via a novel multidrug exporter system, MdtABC. *J. Bacteriol.* 184, 4161–4167. doi: 10.1128/JB.184.15.4161-4167.2002

Nair, R. R., Vasse, M., Wielgoss, S., Sun, L., Yu, Y. N., and Velicer, G. J. (2019). Bacterial predator-prey coevolution accelerates genome evolution and selects on virulence-associated prey defences. *Nat. Commun.* 10:4301. doi: 10.1038/s41467-019-12140-6

Perez, J., Jimenez-Zurdo, J. I., Martinez-Abarca, F., Millan, V., Shimkets, L. J., and Munoz-Dorado, J. (2014). Rhizobial galactoglucan determines the predatory pattern of *Myxococcus xanthus* and protects *Sinorhizobium meliloti* from predation. *Environ. Microbiol.* 16, 2341–2350. doi: 10.1111/1462-2920.12477

Perez, J., Moraleda-Munoz, A., Marcos-Torres, F. J., and Munoz-Dorado, J. (2016). Bacterial predation: 75 years and counting! *Environ. Microbiol.* 18, 766–779. doi: 10.1111/1462-2920.13171

Rombouts, S., Mas, A., Le Gall, A., Fiche, J. B., Mignot, T., and Nollmann, M. (2023). Multi-scale dynamic imaging reveals that cooperative motility behaviors promote efficient predation in bacteria. *Nat. Commun.* 14:5588. doi: 10.1038/s41467-023-41193-x

Santos, S. B., Carvalho, C. M., Sillankorva, S., Nicolau, A., Ferreira, E. C., and Azeredo, J. (2009). The use of antibiotics to improve phage detection and enumeration by the double-layer agar technique. *BMC Microbiol.* 9:148. doi: 10.1186/1471-2180-9-148

Seef, S., Herrou, J., de Boissier, P., My, L., Brasseur, G., Robert, D., et al. (2021). A Tad-like apparatus is required for contact-dependent prey killing in predatory social bacteria. *Elife* 10:e72409. doi: 10.7554/eLife.72409

Simunovic, V., Zapp, J., Rachid, S., Krug, D., Meiser, P., and Muller, R. (2006). Myxovirescin A biosynthesis is directed by hybrid polyketide synthases/nonribosomal peptide synthetase, 3-hydroxy-3-methylglutaryl-CoA synthases, and trans-acting acyltransferases. *Chembiochem* 7, 1206–1220. doi: 10.1002/cbic.200600075

Sydney, N., Swain, M. T., So, J. M. T., Hoiczyk, E., Tucker, N. P., and Whitworth, D. E. (2021). The genetics of prey susceptibility to myxobacterial predation: a review, including an investigation into *Pseudomonas aeruginosa* mutations affecting predation by *Myxococcus xanthus*. *Microb. Physiol.* 31, 57–66. doi: 10.1159/000515546

Tas, H., Nguyen, C. T., Patel, R., Kim, N. H., and Kuhlman, T. E. (2015). An integrated system for precise genome modification in *Escherichia coli*. *PLoS One* 10:e0136963. doi: 10.1371/journal.pone.0136963

Teng, C. H., Tseng, Y. T., Maruvada, R., Pearce, D., Xie, Y., Paul-Satyaseela, M., et al. (2010). NlpI contributes to *Escherichia coli* K1 strain RS218 interaction with human brain microvascular endothelial cells. *Infect. Immun.* 78, 3090–3096. doi: 10.1128/IAI.00034-10

Thiery, S., and Kaimer, C. (2020). The predation strategy of *Myxococcus xanthus*. *Front. Microbiol.* 10:2. doi: 10.3389/fmicb.2020.00002

Thiery, S., Turowski, P., Berleman, J. E., and Kaimer, C. (2022). The predatory soil bacterium *Myxococcus xanthus* combines a Tad- and an atypical type 3-like protein secretion system to kill bacterial cells. *Cell Rep.* 40:111340. doi: 10.1016/j.celrep.2022.111340

von Mering, C., Jensen, L. J., Snel, B., Hooper, S. D., Krupp, M., Foglierini, M., et al. (2005). STRING: known and predicted protein-protein associations, integrated and transferred across organisms. *Nucleic Acids Res.* 33, D433–D437. doi: 10.1093/nar/gki005

Wang, C., Liu, X., Zhang, P., Wang, Y., Li, Z., Li, X., et al. (2019). *Bacillus licheniformis* escapes from *Myxococcus xanthus* predation by deactivating myxovirescin A through enzymatic glucosylation. *Environ. Microbiol.* 21, 4755–4772. doi: 10.1111/1462-2920.14817

Wang, Y., Hu, B., Du, S., Gao, S., Chen, X., and Chen, D. (2016). Proteomic analyses reveal the mechanism of *Dunaliella salina* Ds-26-16 gene enhancing salt tolerance in *Escherichia coli*. *PLoS One* 11:e0153640. doi: 10.1371/journal.pone.0153640

Wang, Y., Li, X., Zhang, W., Zhou, X., and Li, Y. Z. (2014). The groEL2 gene, but not groEL1, is required for biosynthesis of the secondary metabolite myxovirescin in *Myxococcus xanthus* DK1622. *Microbiology (Reading)* 160(Pt 3), 488–495. doi: 10.1099/mic.0.065862-0

Xiao, Y., and Wall, D. (2014). Genetic redundancy, proximity, and functionality of *lspA*, the target of antibiotic TA, in the *Myxococcus xanthus* producer strain. *J. Bacteriol.* 196, 1174–1183. doi: 10.1128/JB.01361-13

Xiao, Y., Gerth, K., Muller, R., and Wall, D. (2012). Myxobacterium-produced antibiotic TA (myxovirescin) inhibits type II signal peptidase. *Antimicrob. Agents Chemother.* 56, 2014–2021. doi: 10.1128/AAC.06148-11

Xiao, Y., Wei, X., Ebright, R., and Wall, D. (2011). Antibiotic production by myxobacteria plays a role in predation. *J. Bacteriol.* 193, 4626–4633. doi: 10.1128/JB.05052-11

Zhang, F., Li, B., Dong, H., Chen, M., Yao, S., Li, J., et al. (2020). YdiV regulates *Escherichia coli* ferric uptake by manipulating the DNA-binding ability of Fur in a SlyD-dependent manner. *Nucleic Acids Res.* 48, 9571–9588. doi: 10.1093/nar/gkaa696

Zhang, W., Wang, Y., Lu, H., Liu, Q., Wang, C., Hu, W., et al. (2020). Dynamics of solitary predation by *Myxococcus xanthus* on *Escherichia coli* observed at the single-cell level. *Appl. Environ. Microbiol.* 86:e02286-19. doi: 10.1128/AEM.02286-19

Zhao, K., Liu, M., and Burgess, R. R. (2007). Adaptation in bacterial flagellar and motility systems: from regulon members to 'foraging'-like behavior in *E. coli*. *Nucleic Acids Res.* 35, 4441–4452. doi: 10.1093/nar/gkm456

Zwarycz, A. S., Livingstone, P. G., and Whitworth, D. E. (2020). Within-species variation in OMV cargo proteins: the *Myxococcus xanthus* OMV pan-proteome. *Mol. Omics* 16, 387–397. doi: 10.1039/d0mo00027b

Zwarycz, A. S., Page, T., Nikolova, G., Radford, E. J., and Whitworth, D. E. (2023). Predatory strategies of *Myxococcus xanthus*: prey susceptibility to OMVs and moonlighting enzymes. *Microorganisms* 11:874. doi: 10.3390/microorganisms11040874

frontiers | Frontiers in Microbiology

TYPE Original Research
PUBLISHED 04 January 2024
DOI 10.3389/fmicb.2023.1320827

OPEN ACCESS

EDITED BY
Régis Grimaud,
Université de Pau et des Pays de l'Adour, France

REVIEWED BY
Wei Hu,
Shandong University, China
Paul Gladstone Livingstone,
Cardiff Metropolitan University, United Kingdom

*CORRESPONDENCE
Qing Yao
✉ yaoqscau@scau.edu.cn
Honghui Zhu
✉ zhuhh_gdim@163.com

RECEIVED 13 October 2023
ACCEPTED 04 December 2023
PUBLISHED 04 January 2024

CITATION
Zhou Y, Chen H, Jiang H, Yao Q and Zhu H (2024) Characteristics of a lipase ArEstA with lytic activity against drug-resistant pathogen from a novel myxobacterium, *Archangium lipolyticum* sp. nov. *Front. Microbiol.* 14:1320827. doi: 10.3389/fmicb.2023.1320827

Characteristics of a lipase ArEstA with lytic activity against drug-resistant pathogen from a novel myxobacterium, *Archangium lipolyticum* sp. nov.

Yang Zhou[1], Haixin Chen[1,2], Hongxia Jiang[2], Qing Yao[3]* and Honghui Zhu[1]*

[1]Key Laboratory of Agricultural Microbiomics and Precision Application (MARA), Guangdong Provincial Key Laboratory of Microbial Culture Collection and Application, Key Laboratory of Agricultural Microbiome (MARA), State Key Laboratory of Applied Microbiology Southern China, Institute of Microbiology, Guangdong Academy of Sciences, Guangzhou, China, [2]Guangdong Key Laboratory for Veterinary Pharmaceutics Development and Safety Evaluation, College of Veterinary Medicine, South China Agricultural University, Guangzhou, China, [3]College of Horticulture, Guangdong Province Key Laboratory of Microbial Signals and Disease Control, Guangdong Engineering Research Center for Litchi, South China Agricultural University, Guangzhou, China

Bacteriolytic myxobacteria are versatile micropredators and are proposed as potential biocontrol agents against diverse bacterial and fungal pathogens. Isolation of new myxobacteria species and exploration of effective predatory products are necessary for successful biocontrol of pathogens. In this study, a myxobacterium strain CY-1 was isolated from a soil sample of a pig farm using the *Escherichia coli* baiting method. Based on the morphological observation, physiological test, 16S rRNA gene sequence, and genomic data, strain CY-1 was identified as a novel species of the myxobacterial genus *Archangium*, for which the name *Archangium lipolyticum* sp. nov. was proposed. Subsequent predation tests indicated that the strain efficiently lysed drug-resistant pathogens, with a higher predatory activity against *E. coli* 64 than *Staphylococcus aureus* GDMCC 1.771 (MRSA). The lysis of extracellular proteins against ester-bond-containing substrates (tributyrin, tween 80, egg-yolk, and autoclaved drug-resistant pathogens) inspired the mining of secreted predatory products with lipolytic activity. Furthermore, a lipase ArEstA was identified from the genome of CY-1, and the heterologously expressed and purified enzyme showed bacteriolytic activity against Gram-negative bacteria *E. coli* 64 but not against Gram-positive MRSA, possibly due to different accessibility of enzyme to lipid substrates in different preys. Our research not only provided a novel myxobacterium species and a candidate enzyme for the development of new biocontrol agents but also reported an experimental basis for further study on different mechanisms of secreted predatory products in myxobacterial killing and degrading of Gram-negative and Gram-positive preys.

KEYWORDS

***Archangium lipolyticum* CY-1, myxobacterial predation, secreted proteins, lipase, biological agent**

Introduction

Myxobacteria are ubiquitous predatory bacteria with complicated multicellular morphogenesis and complex social behaviors. Compared to studies into their sophisticated social lifestyle, researches on cultured species and myxobacteria taxonomy are relatively lacking (Wang et al., 2022). Myxobacteria are presently classified as a phylum (Myxococcota) according to the genome analysis (Waite et al., 2020). Culture-independent methods have revealed a high diversity of myxobacteria in different environments (Wang et al., 2021; Zhang et al., 2023a). However, the number of currently cultured myxobacteria is still remarkably small because the usual dilution and plating techniques used for microorganism isolation are unlikely to reveal the presence of myxobacteria (Mohr, 2018). The baiting method for myxobacteria isolation and the repeated transfers for purification are time-consuming and difficult (Shimkets et al., 2006). Furthermore, the most recently identified new species of myxobacteria belong to the genera *Myxococcus* and *Corallococcus*, which are frequently isolated but not dominant in soil indicated by culture-independent methods (Chambers et al., 2020; Livingstone et al., 2020; Zhou et al., 2020; Petters et al., 2021), and relatively fewer members of less-studied myxobacteria species have been reported over the last decade (Ahearne et al., 2023). Therefore, more efforts are encouraged to explore and obtain the less-studied myxobacteria with an extended taxonomic range.

Another fascinating characteristic of most myxobacteria is their predation behavior, which involves killing other microbial species to consume their biomass. Their predation behavior on pathogens has wide application potential in biological control (Pérez et al., 2016). For example, the myxobacterium *Corallococcus* sp. EGB could inhibit the growth of different plant pathogenic fungi and showed good biological control against cucumber *Fusarium* wilt (Li et al., 2017). In fact, myxobacteria process certain features that make them effective biological agents, such as predation on other bacteria and fungi, formation of fruiting bodies with moderate resistance, and the ability to slide on solid surfaces for diffusion (Ye et al., 2020). These characteristics have made the application of myxobacteria in exploring new resources with excellent predation against various pathogens a hot research topic.

The predation process of myxobacteria includes using social gliding motility to search for prey and employing a series of synergetic predatory products to kill and decompose the prey cells. The ability of myxobacteria to kill prey is mostly attributed to the secretion of hydrolytic enzymes and secondary metabolites, which presumably lyse surrounding bacteria (Berleman and Kirby, 2009; Muñoz-Dorado et al., 2016; Pérez et al., 2016). Exploring predation factors and their mechanisms in predation is one of the important fields of myxobacteria predation. It has been reported that myxobacterial outer membrane vesicles loaded with various predation factors acted as predatory weapons (Berleman et al., 2014). Previous studies have indicated that myxobacteria produce diverse secondary metabolites involved in their predation (Xiao et al., 2011; Surup et al., 2014; Schulz et al., 2018). In contrast to secondary metabolites, the function of myxobacteria hydrolytic enzymes in predation has received less attention. The model myxobacterium *Myxococcus xanthus* produces a variety of hydrolytic enzymes such as proteases, peptidases, lipases, and glycoside hydrolases responsible for lysing prey biomass (Evans et al., 2012). Recently, Zhang et al. (2023b) reported three specialized glucanases from *Archangium* sp. AC19 that act as a cooperative consortium to efficiently decompose β-1,3-glucans of plant-pathogenic oomycetes *Phytophthora*.

Myxobacteria completely consume prey biomass with a group attack strategy to efficiently destroy the prey cell structures. Based on the prey structure, macromolecule components found in the cell wall, cytomembrane, and nucleus are targets of lytic weapons from myxobacteria. In fact, myxobacteria genomes encode numerous peptidases, glycoside hydrolases, polysaccharide lyases, and carbohydrate esterases (Schneiker et al., 2007; Zhou et al., 2021; Wang et al., 2022), which likely target the prey structure in the process of predation. For example, glycoside hydrolases from myxobacteria targeting peptidoglycan in Gram-positive bacteria or β-1,6-glucans in fungi cell walls have been characterized and shown to contribute to prey biomass disruption of predation (Li et al., 2019; Arend et al., 2021). However, it remains unknown whether myxobacteria lytic enzymes can target other components of prey cell structures and how to play roles in predation.

Here we reported a predatory myxobacterium strain CY-1 isolated from pig farm soil and the strain showed efficient lytic activity against drug-resistant pathogens. This promising biocontrol agent was identified as a potential new species and proposed as *Archangium lipolyticum* sp. nov. A secreted carbohydrate esterase (ArEstA) in the CY-1 genome was identified and expressed in *E. coli*. Furthermore, the enzyme activity, biochemical characteristics, and bacteriolytic activity against drug-resistant pathogens were evaluated.

Materials and methods

Isolation and purification of myxobacterium strain CY-1

Strain CY-1 was isolated from a soil sample collected at a pig farm (N 22°57′49″, E 115°19′23″) in the city of Shanwei, Guangdong Province, China. The *Escherichia coli* baiting method was used to isolate myxobacteria (Shimkets et al., 2006). The swarming predatory colonies or fruiting bodies were observed after incubation at 30°C for 7 days. Then the potential myxobacteria were purified by cutting the furthest swarm colony edge or fruiting body from soil samples and repeatedly transferring them onto fresh VY/2 agar (0.5% dried baker's yeast, 0.1% $CaCl_2{\cdot}2H_2O$, 1.5% agar). Strain CY-1 was finally purified and deposited at the Guangdong Microbial Culture Collection Center (GDMCC 1.3728^T).

Identification of strain CY-1

Morphological characterization was conducted to describe the isolated myxobacterium strain CY-1. Growth performance was tested on VY/2, MD1 (0.6% casein, 0.2% soluble starch, 0.2% $MgSO_4{\cdot}7H_2O$, 0.04% $CaCl_2{\cdot}2H_2O$), CTT (1% casein, 8 mM $MgSO_4$, 10 mM Tris–HCl, 1 mM KH_2PO_4, pH 7.6), and CYE (1% casein, yeast extract 0.05%, 8 mM $MgSO_4$, 10 mM Mops, pH 7.6) medium at 30°C. Morphogenesis was observed by stereomicroscope, phase contrast microscope (PCM), and transmission electron microscopy (TEM). The swarm and fruiting body were observed by stereomicroscope. For PCM, strain CY-1 was grown in MD1 broth for 3 days, centrifuged, washed, and responded

with TPM buffer (10 mM Tris–HCl, 1 mM KH_2PO_4, 8 mM $MgSO_4$, pH 7.6). The resuspended cells were pipped on the slide and observed using an Axioscope 5 PCM microscope with an oil lens (Carl Zeiss, Jena, Germany). For TEM, the centrifuged pellet was fixed with 3% glutaraldehyde, followed by a secondary fixative of 1% osmium tetroxide. Samples were resuspended in 100 µL 2% agar solution and left at 4°C overnight before sectioning. Sections were observed using a H7650 TEM microscope (Hitachi, Tokyo, Japan).

Utilization of peptone and carbohydrate resources was performed on minimal medium agar supplemented with a final concentration of 0.2% (w/v) as described by Garcia et al. (2014). The tested peptone and carbohydrate resources included casein, tryptone, yeast extract, beef extract, soy peptone, polypeptone, starch, galactose, lactose, fructose, glucose, sorbitol, mannitol, sucrose, maltose, trehalose, and xylose. Antibiotic sensitivity was tested on VY/2 agar supplemented with different antibiotics at a final concentration of 50 µg ml^{-1} at 30°C (Mohr et al., 2012). The tested antibiotics included ampicillin, apramycin, neomycin, bacitracin, gentamicin, tetracycline, erythromycin, chloramphenicol, nalidixic acid, streptomycin, rifampin, hygromycin, zeocin, and kanamycin.

Isolate CY-1 was initially identified by 16S rRNA gene sequencing using the primers set F27/1492R (Lane, 1991). Amplification and sequencing of the 16S rRNA gene were carried out as previously described (Lachnik et al., 2002). The 16S rRNA gene sequence was compared with the EzTaxon database (Yoon et al., 2017a) to identify the most similar species.

The genome-based method was further used to identify strain CY-1, which has been proposed as the new standard for sequence-based taxonomic assignment (Richter and Rosselló-Móra, 2009). The genome of strain CY-1 was sequenced and used for genome-based identification. Briefly, a swarm of strain CY-1 was inoculated in MD1 liquid medium and incubated in a shake flask at 30°C for 3 days. Genomic DNA was extracted from spin-down biomass and sequenced by Majorbio (Shanghai, China) on the Illumina Hiseq 4000 platform using PE250. After quality control, the high-quality reads were assembled to contigs using SPAdes 3.13.1 (Bankevich et al., 2012). Then the contigs file was input into CheckM to estimate the genome completeness and degree of contamination (Parks et al., 2015). Prodigal (Hyatt et al., 2010) and Prokka (Seemann, 2014) were used for gene prediction and genome annotation, respectively. Additionally, the whole-genome phylogeny of strain CY-1 and related species was generated using the UBCG pipeline 3.0 (Na et al., 2018). The genomic taxonomy based on overall genome-relatedness indices digital DNA–DNA hybridization (dDDH) and average nucleotide identity (ANI) of strain CY-1 and related species were also used to identify the isolate. The dDDH values were calculated using the Genome-to-Genome Distance Calculator GGDC 3.0 (Meier-Kolthoff et al., 2022), and the ANI values were estimated using the online ANI calculator[1] (Yoon et al., 2017b).

Predation of drug-resistant bacteria by CY-1

CY-1 was incubated on VY/2 medium at 30°C for 3 days. The drug-resistant pathogens (Methicillin-resistant *Staphylococcus aureus* GDMCC 1.771, extended-spectrum β-lactamase CTX-M-27-producing *Escherichia coli* 64, Zhao et al., 2021) were inoculated in nutrient broth and shaken at 180 rpm and 30°C, respectively. The overnight shaken cultures were collected by centrifugation and resuspended in TPM buffer to the optical density of $OD_{600} = 5$. Then, 200 µL of pathogen suspension was spotted in the center of the TPM solid medium. When the pathogen bacteria were air-dried to form lawns, a 5 mm diameter plug strain of CY-1 was inoculated on the center of the pathogen colony. Three biological replicates were set up for each treatment and incubated at 30°C for 4 days. The zones of predation were observed after 2 days (early stage) and 4 days (late stage) of co-culture using a stereomicroscope and the imaging software (Olympus SZX10, Olympus Corporation, Tokyo, Japan), and the viable prey cells from the TPM plates were scraped, washed, and counted on nutrient broth solid plates via serial dilution. The colony-forming units (CFU) were obtained after incubating the plates at 30°C overnight.

Lysis of biomacromolecules by CY-1

The WAT agar (0.1% $MgSO_4 \cdot 2H_2O$, 0.02% K_2HPO_4, 1.5% agar, pH 7.6) added with 0.5% substrate was used to determine the lytic actions of CY-1 toward starch, chitin, tween, cellulose, and skim milk. The strain CY-1 was inoculated on the substrate agar, and the lytic actions were recorded as described (Shimkets et al., 2006). Considering that hydrolytic enzymes involved in outside prey-lysis are one of the mechanisms of myxobacteria predation, the lytic action of CY-1 liquid culture supernatant was also evaluated. Briefly, cell-free VY/2 culture supernatant was obtained by centrifugation of 250 mL culture 2 times for 15 min at 8,000 rpm and sequential filtration using 0.45-µm and 0.22-µm pore size filters. The filtered supernatant was concentrated by ultrafiltration with the molecular cut-off of 10 kDa. Considering the lytic action of CY-1 on Tween 80, we also tested the lysis of CY-1 extracellular proteins on ester-bond substrates. The filter paper disk diffusion method on TPM agar mixed with the autoclaved drug-resistant pathogen suspension ($OD_{600} = 1$) or substrate (0.5% tween, egg-yolk, tributyrin) was used to evaluate the lytic activity of crude extracellular proteins, respectively. The filter paper disks (5 mm diameter) were loaded with 20 µL of concentrated supernatant and placed on the TPM agar. Then the agar plates were incubated at 30°C and the transparent zone formed along the filter paper disks was observed and noted. Three replicates were set for each treatment. Heated extracellular proteins were also included as controls.

Cloning, expression, and purification of the potential predatory factor ArEstA

We further focused on the alpha/beta hydrolases superfamily, which is one of the largest groups with diverse catalytic functions, such as hydrolysis of ester and peptide bonds. We searched for alpha/beta hydrolase domain protein in deduced amino acid sequences from the CY-1 genome based on the HMMER search using Pfam hidden Markov models (Eddy, 2009). An extracellular alpha-beta hydrolase (ArEstA) annotated to esterase in the CY-1 genome was identified in this study. As one of the potential predatory factors, the bacteriolytic activity of ArEstA against drug-resistant pathogens was evaluated.

1 https://www.ezbiocloud.net/tools/ani

The sequence of ArEstA was analyzed by the SignalP web server.[2] The gene of ArEstA without signal peptide was cloned into the pET28a(+) (Invitrogen) expression vector at EcoRI and HindIII restriction sites. The obtained plasmid was transformed in *E. coli* BL21(DE3) electrocompetent cells. *E. coli* BL21(DE3) carrying the recombinant plasmid was shaken overnight at 37°C in LB broth with 100 ng μl^{-1} kanamycin. The culture was then inoculated (2%) into fresh LB broth with kanamycin and grown at 37°C until OD_{600} reached 0.6. Then the IPTG was added at a final concentration of 0.1 mM and the culture was incubated overnight at 16°C, 180 rpm for the induction of the expression of ArEstA. The cells were harvested and washed twice in ice-cold lysis buffer (137 mM NaCl, 2.7 mM KCl, 10 mM Na_2HPO_4, 1.8 mM KH_2PO_4, pH 8.0) and resuspended in the same buffer. After ultrasonic disruption, lysates were centrifuged to remove cell debris. The supernatant was passed through a 0.45 μm filter and then applied to metal-chelating Ni-NTA affinity chromatography (P2233, Beyotime, China) equilibrated with lysis buffer. After being washed in washing buffer (50 mM KH_2PO_4, 300 mM NaCl, 2 mM imidazole, pH 8.0), the Ni-NTA bound ArEstA was eluted using elution buffer (50 mM KH_2PO_4, 300 mM NaCl, 150 mM imidazole, pH 8.0) and dialyzed against lysis buffer. Sodium dodecyl sulfate-polyacrylamide gel electrophoresis (12%) was performed to verify molecular weight and purity.

Characterization of ArEstA

Purified ArEstA was subjected to several biochemical assays including optimum temperature and pH, effects of metal ions on enzyme stability, and substrate specificity. The data were expressed as an average of the results from triplicate assays. Esterase activity was measured spectrophotometrically according to the method described (Cheng et al., 2011), using *p*-nitrophenyl (*p*NP) butyrate (C4) or *p*NP esters of other fatty acids (C2, C8, C12, and C16) as the substrates. The purified enzyme was incubated with a 200 μL reaction mixture containing 10 mM substrates, 1% ethanol, and 50 mM Tris–HCl (pH 8.0). The amount of *p*-nitrophenol released from *p*NP esters was monitored at 410 nm for 10 min by a Multiskan GO spectrophotometer. The activity was expressed as the release of 1 μmol of *p*-nitrophenol per minute. Protein concentration was determined by Bradford's method using bovine serum albumin as standard. The filter paper disk diffusion method described above was also used to test the lytic ability of ArEstA toward ester-bond substrates (0.5% tween, egg-yolk, and tributyrin). The optimal pH for enzyme activity was determined by measuring the activity at pH ranging from 4.0 to 10.0 (50 mM citric-phosphate buffer for pH 4.0–6.0, 50 mM phosphate buffer for pH 6.5–7.5, 50 mM Tris–HCl buffer for pH 8.0–10.0). The effect of temperature on the activity of ArEstA was examined in 50 mM Tris–HCl buffer (pH 8.5) ranging from 20°C to 65°C by measuring the activity as the above method. The effect of metal ions (5 mM Mg^{2+}, Mn^{2+}, Cu^{2+}, Zn^{2+}, Fe^{2+}, Fe^{3+}, Co^{2+}, Ni^{2+}, Ba^{2+}, Ca^{2+}, K^{+}, and Na^{+}) on enzymatic activity was assessed in 50 mM Tris–HCl buffer (pH 8.5) at 45°C.

Lytic action of ArEstA

The lytic action of ArEstA on the pathogen was performed by the filter paper disk diffusion method described above with some modification. The fresh drug-resistant pathogen suspension was used and the incubation time lasted for 48 h. Furthermore, the lytic action of ArEstA on the pathogen was also determined by the viable plate counting method. The pathogens at the mid-logarithmic phase were collected, washed, and resuspended in 50 mM phosphate buffer. The 200 μL reaction mixture contained ArEstA (0.5 mg/mL) and resuspended pathogen (final $OD_{600} = 0.1$). Controls were incubated in the absence of ArEstA. The mixture was incubated at 37°C for 2 h. Then the mixture was serially diluted and spread on nutrient agar plates. The CFU was obtained after incubating the agar plates at 30°C overnight. All assays were performed in triplicate and the results are the means of three independent experiments. Based on the results of the lytic activity of ArEstA against pathogens, the same mixture from *E. coli* 64 was obtained and used to indicate the lytic action using an H7650 TEM microscope (Hitachi, Tokyo, Japan).

Sequence analysis and homology modeling

The amino acid sequences of ArEstA and related esterases were aligned using the Clustal Omega web server[3] (Sievers and Higgins, 2018). The homology model structure was created by the SWISS-MODEL web server[4] (Waterhouse et al., 2018). Verify_3D (Luthy et al., 1992) was used to check the residue profiles of the 3D models obtained. PROCHECK (Laskowski et al., 1996) analysis was performed to assess the stereochemical qualities of the 3D models. Pymol software (DeLano and Bromberg, 2004) was used to view the structure and generate figures.

Results

Isolation and identification of strain CY-1

Strain CY-1 was isolated from pig farm soil by the *E. coli* baiting method for myxobacteria isolation. The colony expanded to form a swarm on VY/2, MD1, and CTT agar and formed fruiting bodies on VY/2 agar after starvation. A swarm of strain CY-1 showed yellow brown to purple color on VY/2 agar with a film-like appearance (Figure 1A) and significant veins and flares were observed on the periphery of the swarm (Figure 1B). The sessile fruiting bodies appeared on VY/2 agar for the 3-day cultivation and matured to dark brown and bean-shaped for 5 days (Figure 1C). The vegetative cells collected from MD1 agar were long slender, needle-shaped rods with rounded poles measuring 0.5 ~ 0.6 × 5.0 ~ 12.0 μm with a mean length of 6 ~ 8 μm indicated by phase contrast microscope and TEM (Figures 1D,E). Testing for growth at different temperatures (buffered VY/2 with pH 7.5) demonstrated that CY-1 grew at a temperature of 25 ~ 40°C. The optimum pH of CY-1 was 7.5. Substrate lytic action

2 https://services.healthtech.dtu.dk/services/SignalP-6.0/

3 https://www.ebi.ac.uk/Tools/msa/clustalo/

4 https://swissmodel.expasy.org/

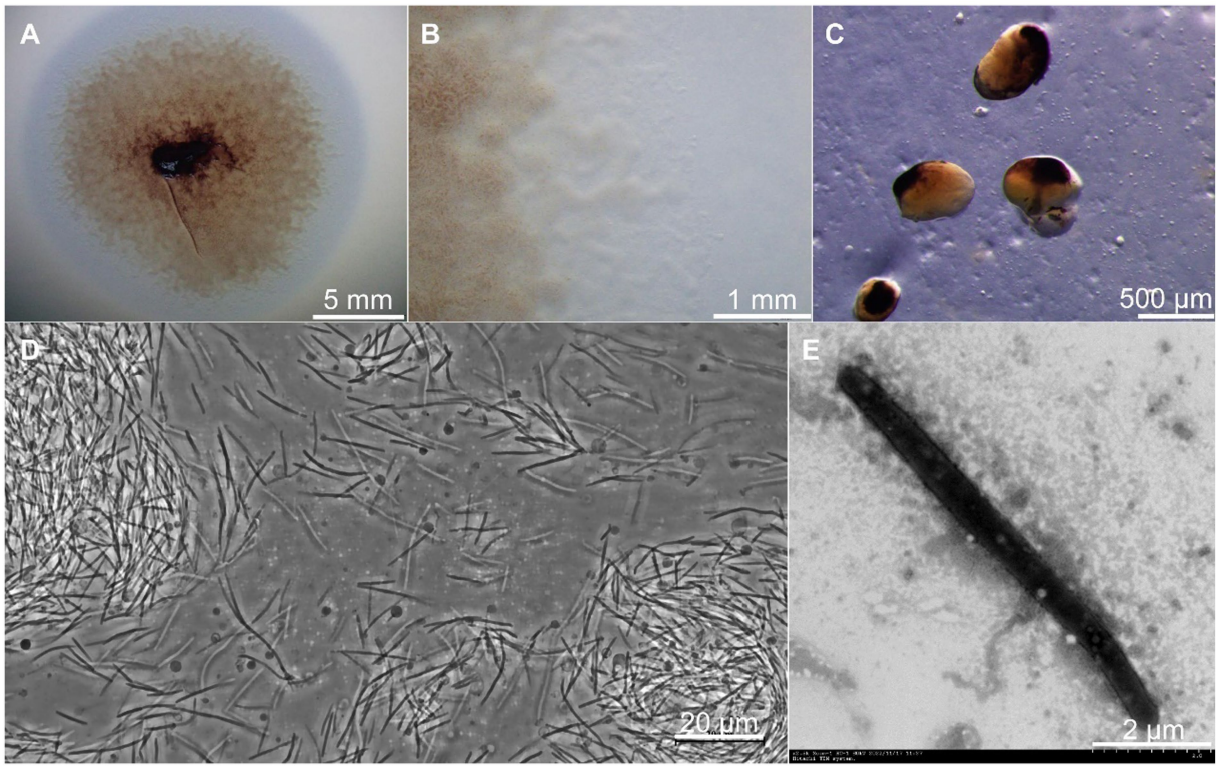

FIGURE 1
Growth and morphology of strain CY-1. **(A)** The spreading swarm colony of CY-1 on VY/2 agar after the 3-day cultivation. **(B)** Colony edge on VY/2 agar with defined veins and flared edges. **(C)** The dark brown and bean-shaped fruiting bodies formed on VY/2 agar. The long slender, needle-shaped rods of vegetative cells were observed using a phase contrast microscope **(D)** and transmission electron microscopy **(E)**. The scale bar was noted at the bottom right of each panel.

tests indicated that skim milk, starch, and Tween 80 were efficiently lysed by CY-1. This strain utilized all the tested peptone, starch, galactose, lactose, galactose, mannitol, sucrose, maltose, and lactose. The novel isolate was resistant to apramycin, hygromycin, gentamicin, ampicillin, kanamycin, and bacitracin, but was sensitive to zeocin, chloramphenicol, tetracycline, streptomycin, rifampicin, nalidixic acid, neomycin, and erythromycin.

The 16S rRNA gene of CY-1 showed closest similarity to *A. violaceum* Cb vi61^T (99.03%), *A. minus* Cb m2^T (98.61%), *A. disciforme* CMU 1^T (97.71%), and *A. gephyra* DSM 2261^T (97.64%), suggesting the relatedness to members of genus *Archangium*. To further identify strain CY-1, the draft genome of strain CY-1 was obtained. The draft genome of strain CY-1 was 12.6 M with a 68.5% GC content spread over 75 contigs, with an N50 of 332.6 kb and an L50 of 12. The Prokka-based annotation of the draft genome identified 10,017 protein-coding genes and 75 non-coding genes. The genome-based phylogenomic tree indicated that CY-1 showed the highest similarity to *Archangium*, and represented a new clade located in the genus *Archangium* (Figure 2A). *In silico* genome-to-genome comparisons unambiguously showed that strain CY-1 possessed 24.4 ~ 38.3% dDDH and 83.23 ~ 86.88% ANI values with other species of *Archangium*, which were below the cut-off values for novel species (<70% dDDH, <95% ANI) (Goris et al., 2007; Meier-Kolthoff et al., 2013). CY-1 showed the highest dDDH and ANI values to *A. violaceum* Cb vi61^T (Figures 2B,C). Based on genomic and phylogenetic differences, we proposed that the candidate strain described here represented a novel species of *Archangium*.

Predation and lytic action of strain CY-1 on drug-resistant pathogens

Strain CY-1 was able to prey on the tested drug-resistant bacteria in the plate assay, resulting in the lytic zone of the lawn of pathogen colonies (Figure 3A). After 4 days of co-culture, the pathogen colonies were lysed and overlaid by the growing cells of CY-1. The social predatory behaviors against different pathogens seemed to be different. Strain CY-1 extended fast with a thin and transparent swarm against MRSA but finally accumulated less biomass than the Gram-negative bacteria *E. coli* 64 (Figure 3A). The cell number of viable *E. coli* 64 and MRSA decreased after 2-day co-culture (early stage) and drastically decreased after 4-day co-culture (late stage). The cell number of viable *E. coli* 64 seemed less than that of MRSA but the variation was not significant (Figure 3B).

Then we focused on the secreted predatory products of strain CY-1 involved in the lysis of drug-resistant bacteria. In addition to the lysis of strain CY-1 against drug-resistant pathogens, the concentrated extracellular proteins collected from the fermentation supernatant of CY-1 also showed lytic activity toward autoclaved pathogens. Furthermore, the concentrated extracellular proteins of CY-1 lysed tween 80, egg-yolk, and tributyrin, suggesting that predatory

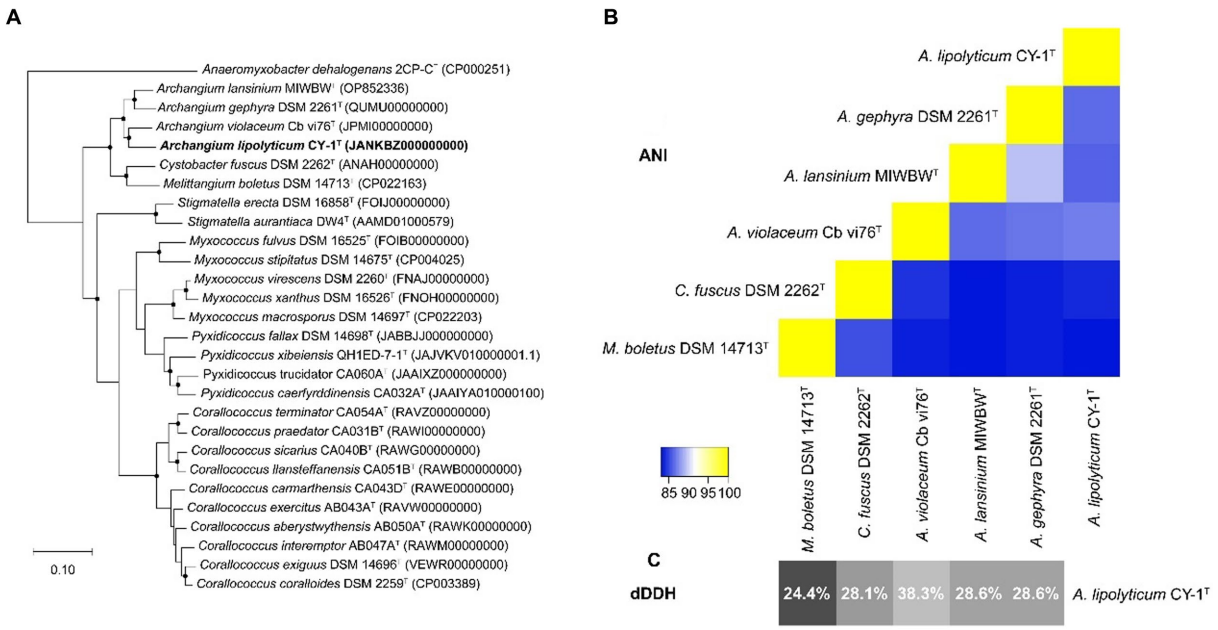

FIGURE 2
Genome-based identification of strain CY-1. **(A)** Phylogenetic tree based on genome sequence of strain CY-1 and the closely related type strains. Dots on branches indicate the bootstrap value >80%. *Anaeromyxobacter dehalogenans* 2CP-C^{T} was used as an outgroup to root the tree. The strain CY-1 was noted in bold font. **(B)** Heatmap generated from ANI values between CY-1 and the related species estimated using the online ANI calculator (https://www.ezbiocloud.net/tools/ani). **(C)** Grey-scale map generated from dDDH values between CY-1 and the related species calculated using the Genome-to-Genome Distance Calculator GGDC 3.0.

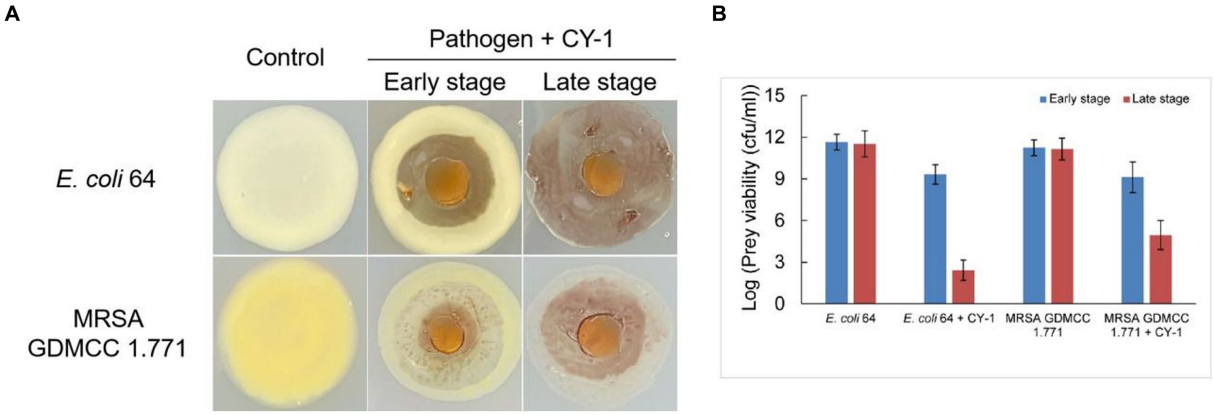

FIGURE 3
The predation behavior **(A)** and predatory activity [**(B)**, variable prey cell numbers after 2 days (early stage) and 4 days (late stage) co-incubation] of CY-1 against drug-resistant pathogens.

product(s) in the crude proteins likely break down ester bond substrates of prey cells during predation (Table 1).

Heterologous expression and biochemical characterization of ArEstA from strain CY-1

To explore the secreted predatory product(s) in the crude proteins of strain CY-1 with the ester-bond lytic activity and potential antibacterial activity, we analyzed its genome-encoded proteins that might act on ester or lipid. Because the superfamily of alpha/beta hydrolases is responsible for the hydrolysis of ester bonds, this conserved domain was explored along the genome of CY-1. The protein WP_257448299.1 assigned as ArEstA was chosen for further exploration as a putative extracellular esterase. The phylogenetic relationship between ArEstA and lipolytic enzymes representing the families proposed by Arpigny and Jaeger (1999) indicated that ArEstA was related to lipolytic enzymes from *Sulfolobus acidocaldarius* (accession number AAC67392.1), *Moraxella* sp. (accession number CAA37863.1) and *Psychrobacter immobilis* (accession number CAA47949.1), sharing 20, 18, and 17% amino acid sequence identity with ArEstA, respectively. According to Arpigny and Jaeger (1999),

these enzymes belong to family V of bacterial lipolytic enzymes (Figure 4A). Analysis of these ArEstA proteins by multiple sequence alignment and the homology model based on the AlphaFold DB model of carboxylesterase (A0A3E0AS93_9BACT) revealed that both the pentapeptide motif Gly114-Tyr115-Ser116-Met117-Gly118 and the catalytic triad Ser116-His256-Asp220 were conserved in ArEstA. The catalytic nucleophile Ser is located in the central portion of the conserved motif G-X-S-M-G-G (Figures 4B,C), which is a sequence pattern of family V (Arpigny and Jaeger, 1999). Based on the sequence and structure analysis, we speculated that ArEstA might represent a new member in family V of lipolytic enzymes.

The gene of ArEstA without signal peptide was cloned into the pET-28a vector and transformed into *E. coli* BL21(DE3) to express the enzyme protein. The purified ArEstA was a highly soluble protein of approximately 32 kDa (Figure 5A), consistent with the expected molecular weight. ArEstA showed lytic activity against *p*NP-C4 and *p*NP-C16 with a specific activity of 9.59 U/mg and 2.05 U/mg, respectively. ArEstA also showed hydrolysis toward tween 80, egg-yolk, and tributyrin.

Effects of pH on the enzymic activity of ArEstA were measured in a pH range from 4.0 to 10.0 with *p*NP butyrate as the substrate. The protein exhibited the maximum activity at pH 7.5–8.5 and the activity was almost completely lost at pH 5.5 (Figure 5B). The results suggested that ArEstA showed the optimum activity in alkalescent pH conditions. The protein showed the maximum activity at 35–45°C and the relativity still reached more than 70% at the temperature range from 30°C to 50°C. However, the activity was completely lost at 65°C (Figure 5C). These data indicated that ArEstA was a mesothermal enzyme. The enzyme activity was enhanced by the presence of 5 mM Na^+ to 1.2-fold. The enzyme activity was strongly inhibited by Cu^{2+}, Ba^{2+}, Fe^{2+}, Fe^{3+}, and Ni^+, and little or not affected by the presence of K^+, Zn^{2+}, Mn^{2+}, and Ca^{2+} (Figure 5D).

The substrate specificity of ArEstA against *p*NP fatty acyl esters with various lengths of the acyl chain was assayed at pH 8.5 and 30°C. The ArEstA exhibited high activity against short-chain fatty acids of *p*NP butyrate (C4) and *p*NP octanoate (C8) except *p*NP acetate (C2). The activity significantly decreased to 29.7 and 9.1% for *p*NP dodecanoate (C12) and *p*NP palmitate (C16), respectively (Figure 5E).

TABLE 1 The lysis of extracellular proteins on autoclaved drug-resistant bacteria and ester bond substrates.

Substrate	Extracellular proteins	Heated extracellular proteins
Autoclaved *E. coli* 64	++	–
Autoclaved MRSA GDMCC 1.771	+	–
Tween 80	+	–
Egg-yolk	+	–
Tributyrin	+	–

++, strong lysis; +, weak lysis; –, no lysis.

Lytic action of ArEstA against drug-resistant pathogen

Since the predatory product(s) in the concentrated extracellular proteins of CY-1 can break down ester bond of prey cell component during predation, we explored whether the lipolytic enzyme ArEstA show lytic activity against drug-resistant pathogen like the predator CY-1. As shown in Figure 6, significant bacteriolysis was only observed on the *E. coli* plate treated with ArEstA, which to some

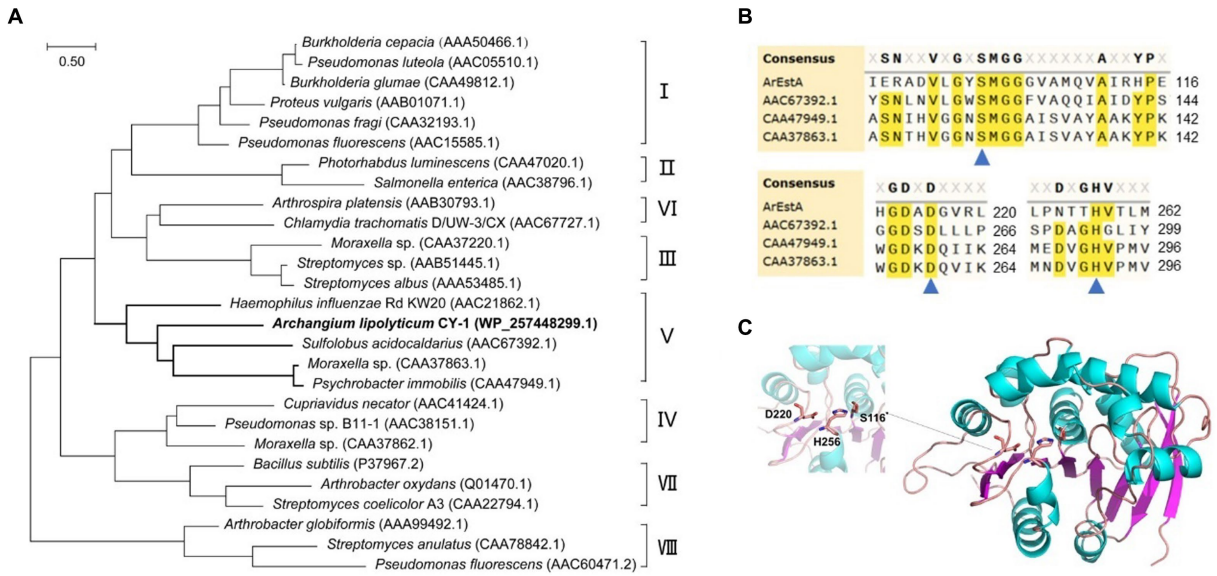

FIGURE 4
Sequence and structure analysis of ArEstA. **(A)** Phylogeny of ArEstA and the characterized lipolytic enzymes. ArEstA of myxobacterium *A. lipolyticum* CY-1 was noted in bold font. **(B)** Multiple sequence alignment of ArEstA and representative sequences from family V. The catalytic residues were indicated by blue triangles. **(C)** The model structure of ArEstA. The predicted catalytic residues of ArEstA were shown in sticks and labeled.

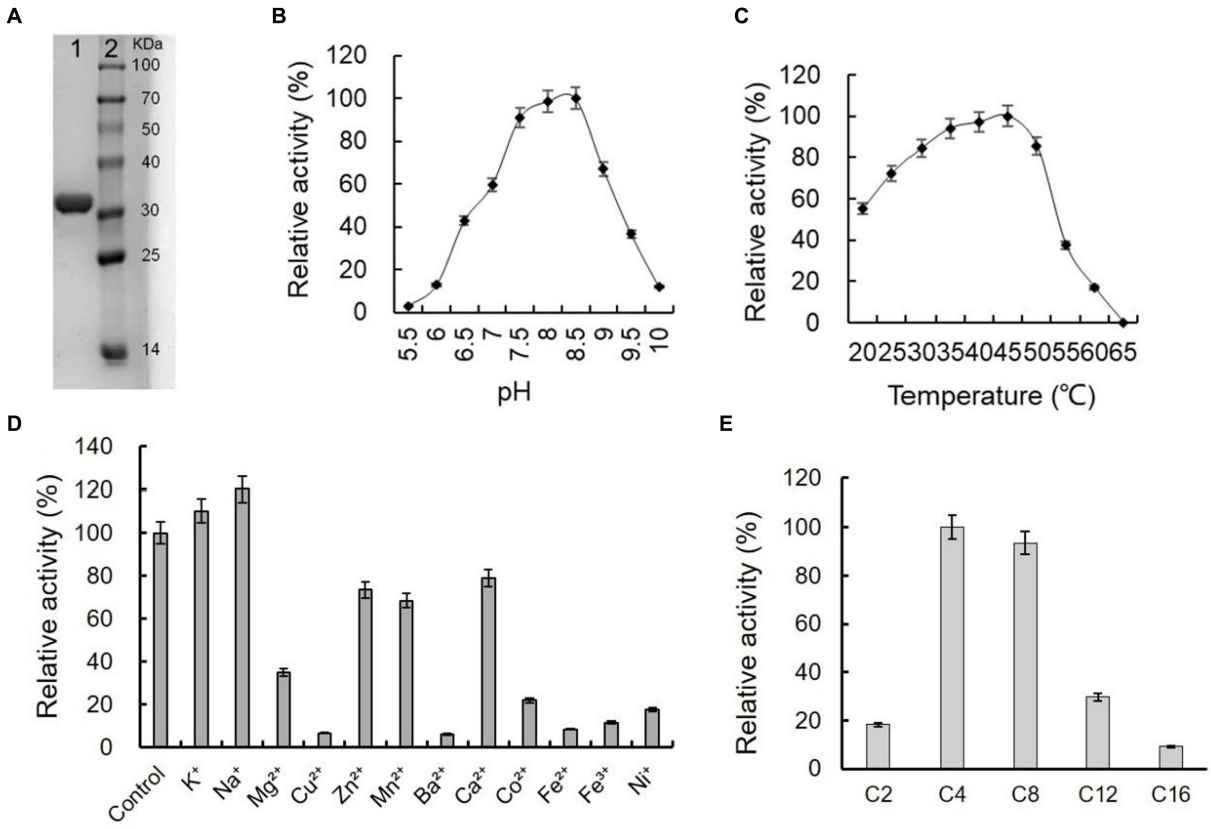

FIGURE 5
Purification and biochemical characterization of ArEstA. **(A)** SDS-PAGE analysis of the purified ArEstA. Lane 1, the purified protein of ArEstA protein, Lane 2, molecular weight marker. The effect of pH **(B)**, temperature **(C)**, and metal ions **(D)** on the activity of ArEstA. **(E)** Enzyme activities of ArEstA on different substrates.

extent was consistent with the strong lytic activity of extracellular proteins against *E. coli*. Then the antibacterial activity of ArEstA was further tested using viable plate counting assays. The number of viable *E. coli* cells treated with 0.5 mg mL^{-1} ArEstA was significantly decreased compared with control (Figure 6B), but ArEstA did not show antibacterial activity against MRSA. Furthermore, TEM showed the disruption and wrinkle of the cell envelope of *E. coli* treated with ArEstA (Figure 6C).

Discussion

Myxobacteria have been proposed as potential biocontrol agents and have shown effective biocontrol activity against bacterial and fungal pathogens (Pérez et al., 2016). Isolation of new myxobacteria species and exploration of effective predatory products are necessary for successful pathogen biocontrol. We reported a new myxobacterium isolation of the *Archangium* and provided a candidate hydrolase showing bacteriolytic activity against Gram-negative drug-resistant bacteria in this study. The genus *Archangium* belongs to the less well-studied group Archangiaceae of Myxococcales, which is sibling to the largest group Myxococcaceae of the recently classified phylum Myxococcota (Waite et al., 2020). Traditionally, colony and fruiting body morphology are important indicators for myxobacteria taxonomy; however, the phase variation in myxobacteria can result in colonies with differences in pigment, texture, and swarming capabilities, which may complicate myxobacteria morphological taxonomy (Furusawa et al., 2011). Recently, it has been increasingly appreciated that limitations of 16S rRNA phylogenetic-based taxonomic assignment can be overcome by considering more genes, ultimately considering every gene of the bacterial genome (Livingstone et al., 2020; Liu et al., 2021). The relatively high 16S rRNA gene similarity of CY-1 to its closest type strain (99.03%) suggested that more genes were needed for accurate identification of the isolate. In this study, the genome-based phylogenetic analysis along with the low values of genome-based indices (dDDH and ANI) indicated that CY-1 is a member of the described *Archangium* genus. The morphology of the vegetative cell, colony, fruiting body, and predatory behavior confirmed that CY-1 had the typical characteristics of myxobacteria.

The predatory products of myxobacteria, including secondary metabolites and hydrases showing promising antimicrobial activities, have been reported (Sasse et al., 2003; Zhou et al., 2021; Zhang et al., 2023b). While most studies have focused on antibiotic production by myxobacteria, there are only a few reports about their enzymatic potential. Due to the broad prey spectrum and the complete clearing of prey biomass, myxobacteria must possess a versatile set of predation mechanisms to access nutrients from different prey species and different kinds of lytic enzymes targeting different components of prey cells. Previous studies have reported that myxobacterial glycoside hydrolases were involved in prey disintegration and showed

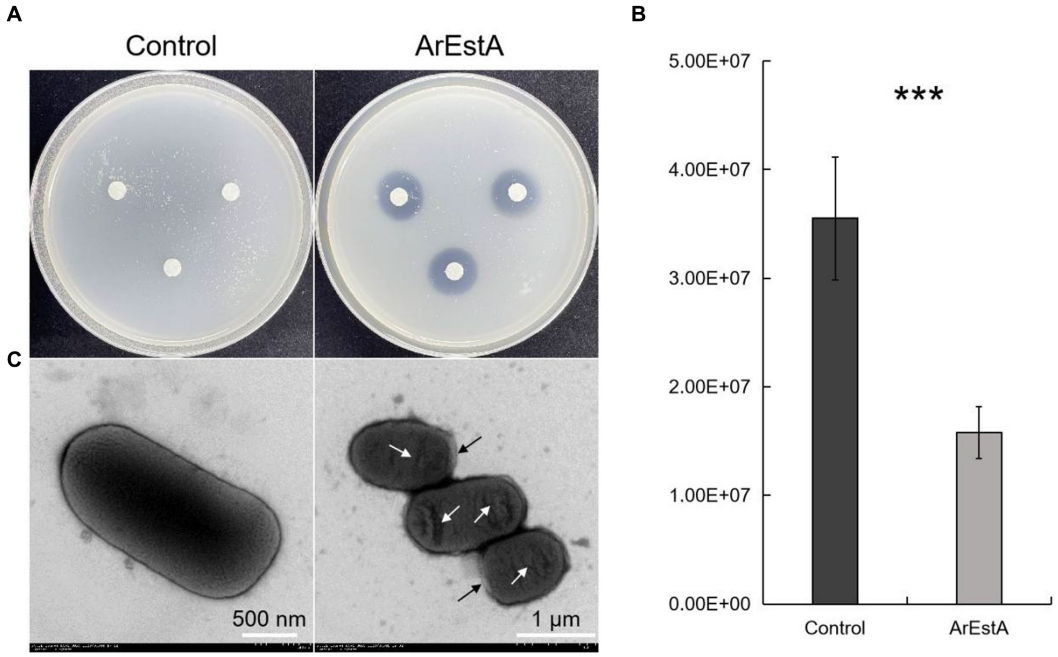

FIGURE 6
Bacteriolytic activity of ArEstA against *E. coli*. **(A)** Lytic activity of ArEstA on *E. coli* using the filter paper disk diffusion method. Plate count assays **(B)** and transmission electron microscopy observation **(C)** for the antimicrobial activity of ArEstA on *E. coli*. The black and white arrow indicated disruption and wrinkle of the cell envelope of *E. coli* treated with ArEstA, respectively. ***$p < 0.001$.

conspicuous biocontrol efficacy in the defense of phytopathogens (Li et al., 2019; Zhang et al., 2023b). In this study, we identified a lipolytic enzyme ArEstA with bacteriolytic activity against Grame-negative drug-resistant bacteria *E. coli* 64 from the novel myxobacterium CY-1. A cold-adapted lipase with high lytic activity to *p*NP acetate from a cellulolytic myxobacterium was previously reported, but the antimicrobial activity of this enzyme was beyond the focus of their study (Cheng et al., 2011). To the best of our knowledge, our study is the first to report on the identification of lipolytic enzymes in bacteriolytic myxobacterium and its antimicrobial activity.

Myxobacteria secrete enzymes with different functions that synergistically act in the degradation of prey biomass (Berleman et al., 2014; Arend et al., 2021). We speculate that CY-1 can secrete lipases to directly degrade compounds containing ester bonds in cellular components of prey, thereby disrupting the cellular structure and achieving killing and lysis of prey. This speculation can be partially supported by the lytic activity of ArEstA to Gram-negative bacteria *E. coli* but not Gram-positive bacteria MRSA. The thick cell wall of Gram-positive bacteria prevented the access of enzymes to substrates. However, for the Gram-negative prey, the lipoprotein in the outer membrane can be easily accessed by lipase, and partial destruction of their thinner cell wall may cause access to lips in the cell membrane. Furthermore, the disruption and wrinkle of the cell envelope of *E. coli* treated with ArEstA also supported its attack on prey cells. Additionally, the combined use of exogenous lipolytic enzymes and triacylglycerols containing medium-chain fatty acids (MCFA) is a promising alternative to in-feed antibiotics in piglets due to the strong antibacterial properties of MCFA (Decuypere and Dierick, 2003). Therefore, we speculated that the bactericidal activity of ArEstA may also be related to the antibacterial activity of its hydrolysate MCFA. However, the ArEstA and glyceride reaction solution with enzyme inactivation after overnight incubation did not show bacteriolysis to *E. coli*, which indicated that the effect of MCFA for the bacteriolytic activity may be very limited in this study.

Another interesting aspect of this study is how CY-1 itself avoids the damage of the lipolytic enzyme ArEstA in predation. It is certain that the production and release of myxobacterial attacking weapons are highly regulated. Both predation and fruiting body formation of myxobacteria involve lytic action (Varon et al., 1984; Berleman et al., 2014). While predation involves the lysis of prey cells but not myxobacterial cells, autolysis of some vegetative cells provides essential requirements for the surviving cells to induce myxospores formation (Wireman and Dworkin, 1977). These different lytic actions indicate various lytic strategies and regulation systems of myxobacteria, but how they protect themselves from predation remains to be explored. The compartmentalized outer membrane vesicles packed with predatory products may help myxobacteria resistant to their own weapons (Evans et al., 2012). However, ArEstA can be expressed heterologously in *E. coli* BL21(DE3) cells but showed a bacteriolytic effect on drug-resistant *E. coli* 64 *in vitro*. We thought that the level of ArEstA background expression was very low which did not affect the growth of host cells (Pan and Malcolm, 2000), and the low protein production caused by damage of soluble ArEstA to host cells during the induction stage was overcome by expanding the amount of fermentation to obtain sufficient protein. Nevertheless, the unknown intracellular regulatory mechanism of host cells may play a role in the heterologous expression of lytic enzymes, such as proteases, lipases, and glycoside hydrolases. The bactericidal activity of ArEstA *in vitro* was independent of intracellular regulation.

Description of *Archangium lipolyticum* sp. nov.

Archangium lipolyticum (li.po.ly'ti.*ca*. Gr. neut. n. *lipos*, fat; Gr. masc. adj. *lytikos*, dissolving; N.L. fem. adj. *lipolytica*, dissolving fat or lipid, referring to the property of being able to hydrolyze lipids).

Vegetative cells glide on solid media and a swarm of cells are yellow brown to purple color and film-like appearance with significant veins and flares on the periphery of the swarm. Vegetative cells are 0.5 ~ 0.6 × 5.0 ~ 12.0 μm in size with rounded poles. Sessile fruiting bodies appeared on VY/2 agar and matured to dark brown and bean-shaped. The optimal growth temperature is 30°C. The optimal pH is 7.0. Obvious growth appeared on VY/2, MD1, CTT, and CYE agar. The optimum growth temperature is 25 ~ 40°C and the optimum pH is 7.5. Skim milk, starch, and Tween 80 can be efficiently lysed. The type strain is CY-1^T (= GDMCC 1.3728^T), which is isolated from a soil sample collected at a pig farm in the city of Shanwei, Guangdong Province, China. The DNA G + C content of the type strain is 68.5%, calculated from its genome sequence. The 16S rRNA gene sequence and genome sequence accession numbers of strain CY-1 in GeneBank are OR649234 and JANKBZ000000000, respectively.

Data availability statement

The datasets presented in this study are deposited in the NCBI database under accession numbers OR649234 and JANKBZ000000000, and further inquiries can be directed to the corresponding authors.

Author contributions

YZ: Conceptualization, Data curation, Formal analysis, Funding acquisition, Investigation, Methodology, Project administration, Software, Visualization, Writing – original draft, Writing – review & editing. HC: Formal analysis, Methodology, Data curation, Investigation, Writing – original draft. HJ: Conceptualization, Supervision, Resources, Writing – review & editing. QY: Conceptualization, Formal analysis, Resources, Supervision, Writing – review & editing. HZ: Conceptualization, Data curation, Formal analysis, Funding acquisition, Resources, Supervision, Writing – review & editing.

Funding

The author(s) declare financial support was received for the research, authorship, and/or publication of this article. This research was funded by the National Natural Science Foundation of China (grant numbers 31900084 and 32370122), the Guangdong Basic and Applied Basic Research Foundation (grant numbers 2021A1515011150 and 2022A1515010314), the Guangdong Special Support Program (2021JC06N628), and the Guangzhou Basic and Applied Basic Research Foundation (grant number 202102021200).

Conflict of interest

The authors declare that the research was conducted in the absence of any commercial or financial relationships that could be construed as a potential conflict of interest.

Publisher's note

References

Ahearne, A., Phillips, K. E., Knehans, T., Hoing, M., Dowd, S. E., and Stevens, D. C. (2023). Chromosomal organization of biosynthetic gene clusters, including those of nine novel species, suggests plasticity of myxobacterial specialized metabolism. *Front. Microbiol.* 14:1227206. doi: 10.3389/fmicb.2023.1227206

Arend, K. I., Schmidt, J. J., Bentler, T., Lüchtefeld, C., Eggerichs, D., Hexamer, H. M., et al. (2021). *Myxococcus xanthus* predation of gram-positive or gram-negative bacteria is mediated by different bacteriolytic mechanisms. *Appl. Environ. Microbiol.* 87:e02382-20. doi: 10.1128/AEM.02382-20

Arpigny, J. L., and Jaeger, K. E. (1999). Bacterial lipolytic enzymes: classification and properties. *Biochem. J.* 343, 177–183.

Bankevich, A., Nurk, S., Antipov, D., Gurevich, A. A., Dvorkin, M., Kulikov, A. S., et al. (2012). SPAdes: a new genome assembly algorithm and its applications to single-cell sequencing. *J. Comput. Biol.* 19, 455–477. doi: 10.1089/cmb.2012.0021

Berleman, J. E., Allen, S., Danielewicz, M. A., Remis, J. P., Gorur, A., Cunha, J., et al. (2014). The lethal cargo of *Myxococcus xanthus* outer membrane vesicles. *Front. Microbiol.* 5:474. doi: 10.3389/fmicb.2014.00474

Berleman, J. E., and Kirby, J. R. (2009). Deciphering the hunting strategy of a bacterial wolfpack. *FEMS Microbiol. Rev.* 33, 942–957. doi: 10.1111/j.1574-6976.2009.00185.x

Chambers, J., Sparks, N., Sydney, N., Livingstone, P. G., Cookson, A. R., Whitworth, D. E., et al. (2020). Comparative genomics and pan-genomics of the myxococcaceae, including a description of five novel species: *Myxococcus eversor* sp. nov., *Myxococcus llanfairpwllgwyngyllgogerychwyrndrobwllllantysiliogogogochensis* sp. nov., *Myxococcus vastator* sp. nov., *Pyxidicoccus caerfyrddinensis* sp. nov., and *Pyxidicoccus trucidator* sp. nov. *Genome Biol. Evol.* 12, 2289–2302. doi: 10.1093/gbe/evaa212

Cheng, Y., Qian, Y., Li, Z., Wu, Z., Liu, H., and Li, Y. (2011). A novel cold-adapted lipase from *Sorangium cellulosum* strain So0157-2: gene cloning, expression, and enzymatic characterization. *Int. J. Mol. Sci.* 12, 6765–6780. doi: 10.3390/ijms12106765

Decuypere, J. A., and Dierick, N. A. (2003). The combined use of triacylglycerols containing medium-chain fatty acids and exogenous lipolytic enzymes as an alternative to in-feed antibiotics in piglets: concept, possibilities and limitations, an overview. *Nutr. Res. Rev.* 16, 193–210. doi: 10.1079/NRR200369

DeLano, W. L., and Bromberg, S. (2004) *PyMOL user's guide*. San Carlos, CA: DeLano Scientific LLC. 629.

Eddy, S. R. (2009). A new generation of homology search tools based on probabilistic inference. *Genome Inform.* 23, 205–211. doi: 10.1142/9781848165632_0019

Evans, A. G. L., Davey, H. M., Cookson, A., Currinn, H., Cooke-Fox, G., Stanczyk, P. J., et al. (2012). Predatory activity of *Myxococcus xanthus* outer-membrane vesicles and properties of their hydrolase cargo. *Microbiology* 158, 2742–2752. doi: 10.1099/mic.0.060343-0

Furusawa, G., Dziewanowska, K., Stone, H., Settles, M., and Hartzell, P. (2011). Global analysis of phase variation in *Myxococcus xanthus*. *Mol. Microbiol.* 81, 784–804. doi: 10.1111/j.1365-2958.2011.07732.x

Garcia, R., Gemperlein, K., and Müller, R. (2014). *Minicystis rosea* gen. nov. sp. nov. a polyunsaturated fatty acid-rich and steroid-producing soil myxobacterium. *Int. J. Syst. Evol. Microbiol.* 64, 3733–3742. doi: 10.1099/ijs.0.068270-0

Goris, J., Konstantinidis, K. T., Klappenbach, J. A., Coenye, T., Vandamme, P., Tiedje, J. M., et al (2007). DNA-DNA hybridization values and their relationship to

whole-genome sequence similarities. *Int. J. Syst. Evol. Microbiol.* 57, 81–91. doi: 10.1099/ijs.0.64483-0

Hyatt, D., Chen, G. L., Locascio, P. F., Land, M. L., Larimer, F. W., and Hauser, L. J. (2010). Prodigal: prokaryotic gene recognition and translation initiation site identification. *BMC Bioinformatics* 11:119. doi: 10.1186/1471-2105-11-119

Lachnik, J., Ackermann, B., Bohrssen, A., Maass, S., Diephaus, C., Punken, A., et al (2002). Rapid-cycle PCR and fluorimetry for detection of mycobacteria. *J. Clin. Microbiol.* 2002, 3364–3373. doi: 10.1128/JCM.40.9.3364-3373.2002

Lane, D. J. (1991). "16S/23S rRNA sequencing" in *Nucleic acid techniques in bacterial systematics*. eds. E. Stackebrandt and M. Goodfellow (Chichester: Wiley), 115–148.

Laskowski, R. A., Rullmannn, J. A., MacArthur, M. W., Kaptein, R., and Thornton, J. M. (1996). AQUA and PROCHECK-NMR: programs for checking the quality of protein structures solved by NMR. *J. Biomol. NMR* 8, 477–486. doi: 10.1007/BF00228148

Li, Z., Ye, X., Chen, P., Ji, K., Zhou, J., Wang, F., et al. (2017). Antifungal potential of *Corallococcus* sp. strain EGB against plant pathogenic fungi. *Biol. Control* 110, 10–17. doi: 10.1016/j.biocontrol.2017.04.001

Li, Z., Ye, X., Liu, M., Xia, C., Lei, Z., Xue, L., et al. (2019). A novel outer membrane β-1,6-glucanase is deployed in the predation of fungi by myxobacteria. *ISME J.* 13, 2223–2235. doi: 10.1038/s41396-019-0424-x

Liu, Y., Pei, T., Yi, S., Du, J., Zhang, X., Deng, X., et al. (2021). Phylogenomic analysis substantiates the *gyrB* gene as a powerful molecular marker to efficiently differentiate the most closely related genera *Myxococcus*, *Corallococcus*, and *Pyxidicoccus*. *Front. Microbiol.* 12:763359. doi: 10.3389/fmicb.2021.763359

Livingstone, P. G., Ingleby, O., Girdwood, S., Cookson, A. R., Morphew, R. M., Whitworth, D. E., et al. (2020). Predatory organisms with untapped biosynthetic potential: descriptions of novel corallococcus species *C. aberystwythensis* sp. nov., *C. carmarthensis* sp. nov., *C. exercitus* sp. nov., *C. interemptor* sp. nov., *C. llansteffanensis* sp. nov., *C. praedator* sp. nov., *C. sicarius* sp. nov., and *C. terminator* sp. nov. *Appl. Environ. Microbiol.* 86:19. doi: 10.1128/AEM.01931-19

Luthy, R., Bowie, J. U., and Eisenberg, D. (1992). Assessment of protein models with three-dimensional profiles. *Nature* 356, 83–85. doi: 10.1038/356083a0

Meier-Kolthoff, J. P., Auch, A. F., Klenk, H., and Göker, M. (2013). Genome sequence-based species delimitation with confidence intervals and improved distance functions. *BMC Bioinformatics.* 14, 1–14. doi: 10.1186/1471-2105-14-60

Meier-Kolthoff, J. P., Sardà Carbasse, J., Peinado-Olarte, R. L., and Göker, M. (2022). TYGS and LPSN: a database tandem for fast and reliable genome-based classification and nomenclature of prokaryotes. *Nucleic Acid Res.* 50, D801–D807. doi: 10.1093/nar/gkab902

Mohr, K. I. (2018). Diversity of myxobacteria-we only see the tip of the iceberg. *Microorganisms* 6:84. doi: 10.3390/microorganisms6030084

Mohr, K. I., Garcia, R., Gerth, K., Irschik, H., and Müller, R. (2012). *Sandaracinus mylolyticus* gen. nov. sp. nov. a starch-degrading soil myxobacterium, and description of Sandaracinaceae fam. nov. *Int. J. Syst. Evol. Microbiol.* 62, 1191–1198. doi: 10.1099/ijs.0.033696-0

Muñoz-Dorado, J., Marcos-Torres, F. J., García-Bravo, E., Moraleda-Muñoz, A., and Pérez, J. (2016). Myxobacteria: moving, killing, feeding, and surviving together. *Front. Microbiol.* 7:781. doi: 10.3389/fmicb.2016.00781

Na, S. I., Kim, Y. O., Yoon, S. H., Ha, S. M., Baek, I., and Chun, J. (2018). UBCG: up-to-date bacterial core gene set and pipeline for phylogenomic tree reconstruction. *J. Microbiol.* 56, 280–285. doi: 10.1007/s12275-018-8014-6

Pan, S. H., and Malcolm, B. A. (2000). Reduced background expression and improved plasmid stability with pET vectors in BL21 (DE3). *BioTechniques* 29, 1234–1238. doi: 10.2144/00296st03

Parks, D. H., Imelfort, M., Skennerton, C. T., Hugenholtz, P., and Tyson, G. W. (2015). CheckM: assessing the quality of microbial genomes recovered from isolates, single cells, and metagenomes. *Genome Res.* 25, 1043–1055. doi: 10.1101/gr.186072.114

Pérez, J., Moraleda-Muñoz, A., Marcos-Torres, F. J., and Muñoz-Dorado, J. (2016). Bacterial predation: 75 years and counting! *Environ. Microbiol.* 18, 766–779. doi: 10.1111/1462-2920.13171

Petters, S., Groß, V., Söllinger, A., Pichler, M., Reinhard, A., Bengtsson, M. M., et al. (2021). The soil microbial food web revisited: predatory myxobacteria as keystone taxa? *ISME J.* 15, 2665–2675. doi: 10.1038/s41396-021-00958-2

Richter, M., and Rosselló-Móra, R. (2009). Shifting the genomic gold standard for the prokaryotic species definition. *Proc. Natl. Acad. Sci. U. S. A.* 106, 19126–19131. doi: 10.1073/pnas.0906412106

Sasse, F., Leibold, T., Kunze, B., Höfle, G., and Reichenbach, H. (2003). Cyrmenins, new beta-methoxyacrylate inhibitors of the electron transport, production, isolation, physico-chemical and biological properties. *J. Antibiot.* 56, 827–831. doi: 10.7164/antibiotics.56.827

Schneiker, S., Perlova, O., Kaiser, O., Gerth, K., Alici, A., Altmeyer, M. O., et al. (2007). Complete genome sequence of the myxobacterium *Sorangium cellulosum*. *Nat. Biotechnol.* 25, 1281–1289. doi: 10.1038/nbt1354

Schulz, E., Goes, A., Garcia, R., Panter, F., Koch, M., and Müller, R. (2018). Biocompatible bacteria-derived vesicles show inherent antimicrobial activity. *J. Control. Release* 290, 46–55. doi: 10.1016/j.jconrel.2018.09.030

Seemann, T. (2014). Prokka: rapid prokaryotic genome annotation. *Bioinformatics* 30, 2068–2069. doi: 10.1093/bioinformatics/btu153

Shimkets, L. J., Dworkin, M., and Reichenbach, H. (2006). "The myxobacteria" in *The prokaryotes*. eds. M. Dworkin, S. Falkow, E. Rosenberg, K. H. Schleifer and E. Stackebrandt (New York: Springer), 31–115.

Sievers, F., and Higgins, D. G. (2018). Clustal omega for making accurate alignments of many protein sequences. *Protein Sci.* 27, 135–145. doi: 10.1002/pro.3290

Surup, F., Viehrig, K., Mohr, K. I., Herrmann, J., Jansen, R., and Müller, R. (2014). Disciformycins A and B: 12-membered macrolide glycoside antibiotics from the myxobacterium *Pyxidicoccus fallax* active against multiresistant staphylococci. *Angew. Chem. Int. Ed.* 53, 13588–13591. doi: 10.1002/anie.201406973

Varon, M., Cohen, S., and Rosenberg, E. (1984). Autocides produced by *Myxococcus xanthus*. *J. Bacteriol.* 160, 1146–1150. doi: 10.1128/jb.160.3.1146-1150.1984

Waite, D. W., Chuvochina, M., Pelikan, C., Parks, D. H., Yilmaz, P., Wagner, M., et al. (2020). Proposal to reclassify the proteobacterial classes Deltaproteobacteria and Oligoflexia, and the phylum Thermodesulfobacteria into four phyla reflecting major functional capabilities. *Int. J. Syst. Evol. Microbiol.* 70, 5972–6016. doi: 10.1099/ijsem.0.004213

Wang, C., Lv, Y., Zhou, L., Zhang, Y., Yao, Q., and Zhu, H. (2022). Comparative genomics of *Myxococcus* and *Pyxidicoccus*, including the description of four novel species: *Myxococcus guangdongensis* sp. nov., *Myxococcus qinghaiensis* sp. nov., *Myxococcus dinghuensis* sp. nov., and *Pyxidicoccus xibeiensis* sp. nov. front. Microbiol. 13, 995049 13:995049. doi: 10.3389/fmicb.2022.995049

Wang, J., Wang, J., Wu, S., Zhang, Z., and Li, Y. (2021). Global geographic diversity and distribution of the myxobacteria. *Microbiol. Spectr.* 9:e0001221. doi: 10.1128/Spectrum.00012-21

Waterhouse, A., Bertoni, M., Bienert, S., Studer, G., Tauriello, G., Gumienny, R., et al. (2018). SWISS-MODEL: homology modelling of protein structures and complexes. *Nucleic Acids Res.* 46, W296–W303. doi: 10.1093/nar/gky427

Wireman, J. W., and Dworkin, M. (1977). Developmentally induced autolysis during fruiting body formation by *Myxococcus xanthus*. *J. Bacteriol.* 129, 798–802. doi: 10.1128/jb.129.2.798-802.1977

Xiao, Y., Wei, X., Ebright, R., and Wall, D. (2011). Antibiotic production by myxobacteria plays a role in predation. *J. Bacteriol.* 193, 4626–4633. doi: 10.1128/JB.05052-11

Ye, X., Li, Z., Luo, X., Wang, W., Li, Y., Li, R., et al. (2020). A predatory myxobacterium controls cucumber fusarium wilt by regulating the soil microbial community. *Microbiome* 8:49. doi: 10.1186/s40168-020-00824-x

Yoon, S. H., Ha, S. M., Kwon, S., Lim, J., Kim, Y., Seo, H., et al. (2017a). Introducing EzBioCloud: a taxonomically united database of 16S rRNA gene sequences and whole-genome assemblies. *Int. J. Syst. Evol. Microbiol.* 67, 1613–1617. doi: 10.1099/ijsem.0.001755

Yoon, S. H., Ha, S. M., Lim, J. M., Kwon, S. J., and Chun, J. (2017b). A large-scale evaluation of algorithms to calculate average nucleotide identity. *Antonie Van Leeuwenhoek* 110, 1281–1286. doi: 10.1007/s10482-017-0844-4

Zhang, L., Dong, C., Wang, J., Liu, M., Wang, J., Hu, J., et al. (2023b). Predation of oomycetes by myxobacteria via a specialized CAZyme system arising from adaptive evolution. *ISME J.* 17, 1089–1103. doi: 10.1038/s41396-023-01423-y

Zhang, L., Huang, X., Zhou, J., and Ju, F. (2023a). Active predation, phylogenetic diversity, and global prevalence of myxobacteria in wastewater treatment plants. *ISME J.* 17, 671–681. doi: 10.1038/s41396-023-01378-0

Zhao, Q. Y., Li, W., Cai, R. M., Lu, Y. W., Zhang, Y., Cai, P., et al. (2021). Mobilization of Tn1721-like structure harboring blaCTX-M-27 between P1-like bacteriophage in *Salmonella* and plasmids in *Escherichia coli* in China. *Vet. Microbiol.* 253:108944. doi: 10.1016/j.vetmic.2020.108944

Zhou, Y., Yi, S., Zang, Y., Yao, Q., and Zhu, H. (2021). The predatory Myxobacterium Citreicoccus inhibens gen. nov. sp. nov. showed antifungal activity and Bacteriolytic property against Phytopathogens. *Microorganisms* 9:2137. doi: 10.3390/microorganisms9102137

Zhou, Y., Zhang, X., Yao, Q., and Zhu, H. (2020). Both soil bacteria and soil chemical property affected the micropredator myxobacterial community: evidence from natural forest soil and greenhouse rhizosphere soil. *Microorganisms* 8:1387. doi: 10.3390/microorganisms8091387

frontiers | Frontiers in Microbiology

TYPE Review
PUBLISHED 08 January 2024
DOI 10.3389/fmicb.2023.1294854

OPEN ACCESS

EDITED BY
Li Zhoukun,
Nanjing Agricultural University, China

REVIEWED BY
Yuqiang Zhao,
Jiangsu Province and Chinese Academy of Sciences, China
Orlando Borras-Hidalgo,
Qilu University of Technology, China

*CORRESPONDENCE
Huirong Liu,
✉ huirong_liu@imau.edu.cn

RECEIVED 15 September 2023
ACCEPTED 13 December 2023
PUBLISHED 08 January 2024

CITATION
Zhang L, Bao L, Li S, Liu Y and Liu H (2024) Active substances of myxobacteria against plant diseases and their action mechanisms. *Front. Microbiol.* 14:1294854. doi: 10.3389/fmicb.2023.1294854

Active substances of myxobacteria against plant diseases and their action mechanisms

Lele Zhang[1], Liangliang Bao[2], Songyuan Li[1], Yang Liu[1] and Huirong Liu[1]*

[1]College of Life Sciences, Inner Mongolia Agricultural University, Hohhot, Inner Mongolia, China, [2]College of Science, Inner Mongolia Agricultural University, Hohhot, Inner Mongolia, China

Myxobacteria have a complex life cycle and unique social behavior. They can prey on plant pathogenic fungi, bacteria, and oomycetes in the soil by producing some enzymes and small molecule compounds. The enzymes mainly include β-1,6-glucanase, β-1,3-glucanase, chitinase, protease, peptidase, and formaldehyde dismutase. β-1,6-glucanase, β-1,3-glucanase, and chitinase can degrade the glycosidic bonds in the cell wall of plant pathogen, causing some holes to form on the cell walls of the plant pathogen. Proteases and peptidases can break plant pathogenic cells into many small fragments and facilitate extracellular digestion of proteins during myxobacterial predation. Formaldehyde dismutase converts formaldehyde to formate and methanol, it can help myxobactria protect themselves in the process of predation. Small molecule substances produced by myxobacteria include isooctanol, di-isobutyl phthalate, myxovirescin, cystobactamid derivatives, hyalodione, argyrin derivatives, Methyl (2R)-2-azido-3-hydroxyl-2-methylpropanoate and N-(3-Amino-2-hydroxypropyl)-N-meth-ylsulfuric diamide, etc. Isooctanol destroyed the cell wall and cell membrane of plant pathogen, causing intracellular reactive oxygen species (ROS) to accumulate, leading to apoptosis and cell death. Di-isobutyl phthalate had biofilm inhibitory activity against bacteria. Myxovirescin could inhibit the incorporation of diamibopimelic acid and uridine diphosphate-Nacetylglucosamine intobacterial cell wall and interfered with the polymerizaton of the lipid-disacchar-pentapeptide. Cystobactamid derivatives exerted their natural antibacterial properties by inhibition of bacterial gyrases. Hyalodione had broad antibacterial and antifungal activity. Argyrin derivatives inhibited protein synthesis by interfering with the binding of elongation factor G (EF-G) to ribosomes. Methyl (2R)-2-azido-3-hydroxyl-2-methylpropanoate and N-(3-Amino-2-hydroxypropyl)-N-meth-ylsulfuric diamide reduced the content of soluble proteins and the activity of protective enzymes (PPO, POD, PAL, and SOD) in plant pathogen, increased oxidative damage and cell membrane permeability. Myxobacteria, as a new natural compound resource bank, can control plant pathogenic fungi, oomycetes and bacteria by producing some enzymes and small molecule compounds, so it has great potential in plant disease control.

KEYWORDS

myxobacteria, plant diseases, biological control, carbohydrate-active enzymes, small molecule compounds

1 Introduction

Myxobacteria are microorganisms of the phylum Myxococcota (Waite et al., 2020; Oren and Garrity, 2021), which are well known for their complex life cycles and unique social behaviors. Myxobacteria have a wide range of habitats, including soil rich in organic matter, rotting wood, animal dung and marine environment (Saggu et al., 2023). They can survive in high-salinity environments (Gemperlein et al., 2018). Some halophilic myxobacteria i.e., *Haliangium spp.* (Ryosuke et al., 2002), *Plesiocystis pacifica* (Iizuka et al., 2003a) and *Enhygromyxa salina* (Iizuka et al., 2003b) had been isolated from marine environment. Research over the past few decades has proven that myxobacteria have become a resource library of new natural compounds, ranking second only to *Actinomycetes* and *Bacillus* among prokaryotes (Arguelles-Arias et al., 2009; Weissman and Müller, 2010). Metabolites produced by myxobacteria often have structures that other microbial metabolites do not have, and40% of myxobacterial metabolites have novel chemical structures. For example, in contrast to Actinomycetes derivatives, most small molecules of myxobacteria are not glycosylated (Rix et al., 2002). It is currently unclear why myxobacteria produce large amounts of metabolites, but researchers generally believe that metabolites play an important role in regulating cell-to-cell interactions within a population (Davies et al., 2006) and in prey hunting (Xiao et al., 2011).

Myxobacteria can prey on plant pathogen and destroy pathogen's cell morphology and structure. When myxobacteria prey on pathogen, they can kill microorganisms and lyse cells by producing metabolites such as antibiotics, cell wall degrading enzymes, lipases, nucleases, polysaccharases, and proteases, thereby clearing the pathogens. The destroyed pathogenic cells are surrounded by many filamentous substances. The cell structure become loose and irregular, and the cell contents overflow, and eventually the pathogen lyse and die.

Therefore, myxobacteria can serve as biological control agents (BCAs) of plant diseases (Ye et al., 2020b). The BCAs in agricultural planting can reduce the use of pesticides, reduce the adverse effects caused by excessive use of chemicals and achieve the purpose of controlling soil-borne plant diseases. The BCAs are very effective in preventing and managing plant diseases and achieving ecological and economic benefits such as increasing agricultural output and reducing environmental pollution. Research on myxobacteria can provide new potential ways for biological control of plant diseases. This paper reviews the research progress on the active substances of myxobacteria against plant diseases and their action mechanisms.

2 Enzymes

Myxobacteria produce some enzymes playing important roles in preying on pathogens. These enzymes include carbohydrate-active enzymes (CAZymes), peptidases, lipases, etc. CAZymes include glycosyltransferases (GTs), glycoside hydrolases (GHs), carbohydrate esterases (CEs), auxiliary activities (AAs), carbohydrate-binding modules (CBMs), and polysaccharide lyases (PLs). CAZymes can modify the glycosidic bonds of carbohydrates and are important basic functional units in carbohydrate metabolism pathways (Dong et al., 2023). GHs hydrolyze glycosidic bonds and play an important role in the hydrolysis and synthesis of sugars and glycoconjugates in organisms (Kaushal and Singh, 2020). The enzymes produced by myxobacteria to control plant pathogens are shown in Figure 1 and Table 1.

2.1 β-1,6-Glucanase

β-1,6-glucan is a component of the fungal cell wall smaller than chitin and β-1,3-glucan. It can cross-link cell wall proteins to the chitin layer and β-1,3-glucan layer. Inhibiting the synthesis of β-1,6-glucan is conducive to the effective disintegration and further degradation of pathogen cell wall during the process of myxobacteria preying on plant pathogen. β-1,6-glucanase can hydrolyze the glycosidic bonds of β-1,6-glucan, thereby destroying the entire cell wall structure of fungi. β-1,6-glucanase GluM from the strain EGB of *Coralococcus* sp. is a novel family of outer membrane β-barrel proteins that can inhibit fungal embryonic tube development (Li et al., 2019b). β-1,6-glucanase GluM is essential in the initial sensing and efficient decomposition of fungi.

Electron microscopy observation of the hyphae of *Magnaporthe oryzae* treated with β-1,6-glucanase GluM showed that the hyphae were stretched and partially broken, and the hyphal cell wall changed from a dense structure to a loose structure. The spore folds of the treated *M. oryzae* were irregular. The density of spore decreased, and the morphology of spore showed a deformed state. The morphological and structural changes of *M. oryzae* were speculated to be due to the hydrolysis of the cell wall by β-1,6-glucanase GluM, resulting in incomplete cell structure and outflow of contents, ultimately leading to morphological changes. Therefore, β-1,6-glucanase GluM inhibited the infection of *M. oryzae* in rice by digesting the pathogen's cell wall (Zhou et al., 2019).

After treated with GluM, the hyphae and spores of *Fusarium oxysporum f.* sp. *cucumerinum* (FOC) shrank obviously. The cell wall of FOC appeared to be perforated and damaged, the cell wall structure was loose, and large vacuoles formed in the cells. The High Osmolarity Glycerol (HOG) in FOC cells was activated. The phosphorylation level of Hog1-likemitogenactivated proteinkinase (MAPK) was significantly increased and the glycerol content increased 2.6 times. The osmotic pressure in FOC cells increased, which accelerated cell lysis. When the strain EGB of *Corallococcus* sp. were inoculated with the potted cucumbers, the strain could adapt well to the soil environment and effectively reduced the abundance of soil-borne *F. oxysporum* and the occurrence of cucumber wilt disease (Ye et al., 2020b).

In the *GluM* transgenic experiment, the β-1,6-glucanase gene was transferred into japonica rice variety ZH11 to obtain transgenic japonica rice with overexpression of *GluM*. In the fungal disease resistance experiment, the rice blast area of *GluM* transgenic rice was reduced by 82.7%. The sheath blight disease was reduced by 35.76%–43.67% and the incidence of rice smut disease was reduced by 65.79%. The results showed that transgenic rice containing GluM protein could degrade fungal cell walls through specific hydrolysis and enhanced resistance to fungal diseases (Shen et al., 2023).

The β-1,6-glucanase produced by myxobacteria inhibits not only the growth of pathogenic fungus, but also the growth of oomycetes. The fermentation products of *C. coralliformis* strain CMC0606 had a strong inhibitory effect on *Phytophthora capsici*, and the diameter of inhibition zone was 16mm (Bader et al., 2022). The strain EGB had a

10.3389/fmicb.2023.1294854

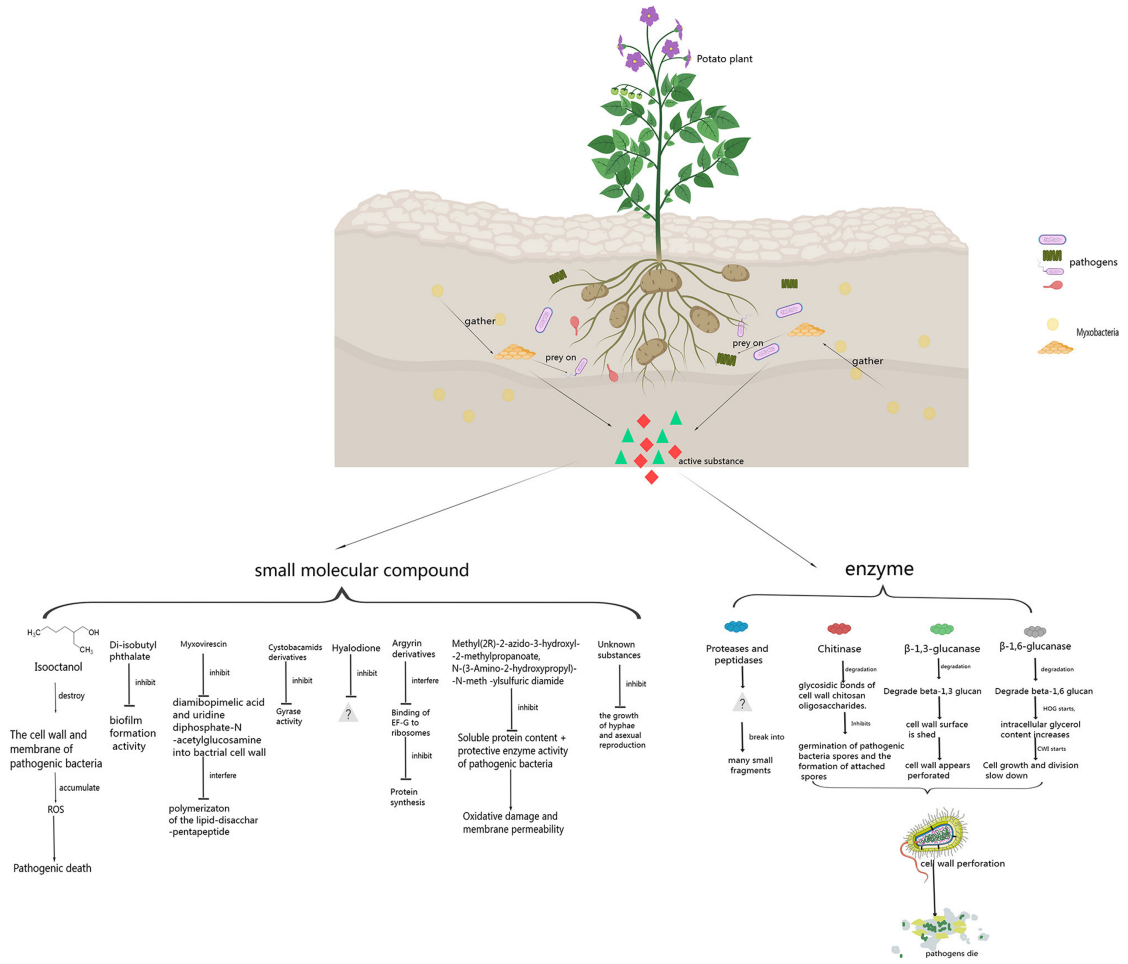

FIGURE 1
Control principle of myxobacteria against pathogens.

strong inhibitory effect on the growth of *P. capsica*. The mycelium of *P. capsica* collapsed and the growth of the pathogen was obviously inhibited. The results showed that β-1,6-glucanase in the fermentation supernation of strain EGB was effective in inhibiting oomycetes (Zhang et al., 2023).

2.2 β-1,3-Glucanase

β-1,3-glucan is a component of the fungal cell wall. Extensive hydrolysis of fungal cell wall polymer chains by β-1,3-glucanase can reduce the mechanical strength of the cell wall, leading to the final lysis of the fungal cell. β-1,3-glucanase IamC from strain EGB can cleave β-1,3- or β-1,6-glucan substrates by exo-hydrolysis. Cu^{2+}, Co^{2+}, Mg^{2+}, and Cr^{3+} inhibit the activity of IamC, while Mn^{2+} is an effective activator of IamC, indicating that IamC is a metal ion-dependent hydrolase. After exposure of *M. oryzae* to IamC, the germ tube and appressorium formation rates were significantly reduced from 94 and 97% to 59 and 51%. The hyphae of *M. oryzae* was enlarged and deformed, and more granular contents appeared inside the hyphae. There was a large accumulation of reactive oxygen species (ROS) in the spores and hyphae of *M. oryzae* and the distribution of chitin in the cell wall of pathogen changed. The β-1,3-glucanase IamC derived from strain EGB acted on different β-glycosidic bonds in the cell wall of *M. oryzae*. β-glycosidic bonds of polysaccharides from different sites of cell wall of pathogen were hydrolyzed, ultimately leading to cell lysis of *M. oryzae* (Zhou et al., 2019).

Archangium strain AC19 showed strong predatory activity gainst *Phytophthora sojae* P6497 and protected soybeans from stem rot disease. Strain AC19 was observed to prey on *P. sojae*, and the hyphal cell wall of *P. sojae* P6497 showed perforation. The fermentation supernatant of strain AC19 significantly inhibited the growth and infection of *P. sojae*. The active substances that digested *P. sojae* were the CAZymes secreted by strain AC19. The cell wall-acting CAZymes in strain AC19 were specialized β-1,3-glucanases (AcGlu13.1,–13.2, and–13.3). These β-1,3-glucanases targeted β-1,3-glucan from the cell wall of *Phytophthora*. AcGlu13.1 caused cell wall surface shedding through its degradative activity. AcGlu13.2 and AcGlu13.3 could cause perforated structures in the cell wall (Zhang et al., 2023).

TABLE 1 Control principle of myxobacteria against pathogens.

Antagonistic substances	Antagonistic principle	References
Enzymes		
β-1,6-Glucanase	Degrades β-1,6-glucan. When HOG is activated, the intracellular glycerol content increases and the osmotic pressure increases; when CWI is activated, cell growth and division slow down.	Zhou et al. (2019) and Ye et al. (2020a)
β-1,3-Glucanase	Hydrolyzesβ-1,3-glucan. The cell wall surface falls off and a perforated structure appears in the cell wall.	Zhou et al. (2019) and Zhang et al. (2023)
Chitinase	Degrades the glycosidic bonds of cell wall chitosan oligosaccharides. Inhibits the germination of pathogenic bacteria spores and the formation of attached spores.	Li et al. (2019a)
Proteases and peptidases	The morphology of R. solanacearum changed significantly, and the cells were broken into many small fragments	Dong et al. (2023)
Formaldehyde dismutase	Decompose the formaldehyde produced by pathogenic bacteria to prey on them.	Willsey et al. (2016) and Sutton et al. (2019)
Small molecule compounds		
Isooctanol	Destroy the cell wall and cell membrane of pathogenic bacteria, accumulate ROS, and cause cell death.	Ye et al. (2020a)
Di-isobutyl phthalate	Exhibits biofilm formation inhibitory activity against pathogenic bacteria.	Sharma et al. (2021)
Myxovirescin	Inhibits the incorporation of diamibopimelic acid and uridine diphosphate-N-acetylglucosamine into bactrial cell wall, and interferes with the polymerizaton of the lipid-disacchar-pentapeptide	Rosenberg et al. (1982) and Paitan et al. (1999)
Cystobacamids derivatives	Inhibits bacterial gyrase to exert antibacterial activity	Kim et al. (2019) and Solga et al. (2024)
Hyalodione	Strongly inhibits the activity of pathogenic bacteria.	Okanya et al. (2012)
Argyrin derivatives	Participate in the non-ribosomal peptide synthase pathway and inhibit protein synthesis by interfering with the binding of elongation factor G (EF-G) to ribosomes	Pogorevc et al. (2019) and Wieland et al. (2022)
Methyl(2R)-2-azido-3-hydroxyl-2-methylpropanoate, N-(3-Amino-2-hydroxypropyl)-N-meth-ylsulfuric diamide	Reduce the content of soluble proteins and activity of protective enzymes in pathogenic bacteria, and increase oxidative damage and cell membrane permeability.	Wu (2018)
Some unknown substances	Inhibits the growth of hyphae and asexual reproduction of Phytophthora infestans	Ren et al. (2016), Ding (2017), Wu (2018) and Zhao (2018)

2.3 Chitinase

The fungal cell wall is mainly composed of chitin, β-1,3-glucan and β-1,6-glucan. The chitin accounts for 22%–40% of the fungal cell wall (Bowman and Free, 2006). Chitinase ofGHs family can hydrolyze chitin in fungal cell walls, so chitinase is regarded as an antifungal factor for biocontrol of fungal diseases (Shehata et al., 2018; Li et al., 2019a). Strain EGB can synthesize the endo-chitinase CcCti1 which belongs to the GHs family 18 (GH18) and has potential antifungal activity. CcCti1 can not only degrade chitosan oligosaccharide, but also hydrolyze chitin into N-acetylated chitohexaose (GlcNAc)6. CcCti1 had biological control activity against the plant pathogen *M. oryzae*, inhibiting the germination of conidia and the formation of appressoria of *M. oryzae* at a concentration of 0.08 mg/mL (Li et al., 2019a). Rice blast caused by *M. oryzae* is the main limiting factor in global rice production and is one of the most destructive diseases in cultivated rice in the world (Talbot, 2003). The transgenic plants with chitinase genes showed strong resistance to rice blast. The reason may be that the cell wall integrity of pathogen changed, leading to significant internal expansion pressure and lysis of fungal cells (Selitrennikoff, 2001). Therefore, transgenic plants with chitinase genes were more resistant to the *M. oryzae*.

2.4 Proteases and peptidases

Tomato bacterial wilt (TBW) caused by *Ralstonia solanacearum* is one of the most destructive soilborne diseases, and tomato production has suffered huge losses due to the epidemic of TBW (Mansfield et al., 2012). *M. xanthus* R31 had good biological control potential against TBW, and the biocontrol efficiency against TBW in pot experiments was as high as 81.9%. The MEROPS database of strain R31 genome had annotated 274 proteins, including 132 metalloproteases and 107 serine proteases. Three M36 metalloproteases were identified in the R31 genome that may contribute to the extracellular digestion of proteins during predatory behavior (Dong et al., 2023). Proteins of the M23 family were endopeptidases that cleaved bacterial cell wall peptidoglycan by degrading the peptide bonds of cross-linked peptides (Odintsov et al., 2004). Proteases and peptidases, such as the M36 metalloprotease MepA secreted by *M. xanthus* strain DK1622, may promote the predation of prey by degrading proteins of prey cells (Berleman et al., 2014).

2.5 Formaldehyde dismutase

When *Pseudomonas aeruginosa* was preyed on, it secreted toxic formaldehyde to resist predation. Fomaldehyde can be converted into formate and methanol by formaldehyde detoxifying enzymes, such as formaldehyde dismutase (Fdm), produced by *P. aeruginosa* to protect itself (Willsey et al., 2016). It was shown that myxobacteria could produce formaldehyde dismutase. Therefore, myxobacteria had the ability to prey on *P. aeruginosa* by converting toxic formaldehyde secreted by *P. aeruginosa* into non-toxic substances (Sutton et al., 2019). *Myxobacteria* may also be able to prey on similar plant pathogens by a similar way.

3 Small molecule compounds

The biological control activity of *myxobacteria* against pathogen depends on not only enzymes, but also some small molecule compounds. These compounds include isooctanol, di-isobutyl phthalate, myxovirescin, cystobactamid derivatives, hyalodione, argyrin derivatives, Methyl (2R)-2-azido-3-hydroxyl-2-methylpropanoate, and N-(3-Amino-2-hydroxypropyl)-N-meth-ylsulfuric diamide, etc. Some small molecule compounds produced by myxobacteria to control plant pathogens are shown in Figure 1 and Table 1.

3.1 Isooctanol

Strain EGB exhibited superior biological control activity against *F. oxysporum*. *F. oxysporum* is a ubiquitous soil-borne plant pathogen that can cause vascular wilt in a variety of crops (Pietro et al., 2003). A total of 32 volatile compounds produced by strain EGB were identified, and isooctanol had the highest antifungal activity. The mycelia of *F. oxysporum* treated with isooctanol showed severely shrinkage and collapse. The hyphae of *F. oxysporum* treated by isooctanol, the transcript levels of many genes related to the cell wall integrity (CWI) pathway and redox reactions were significantly increased by 15-to 40-fold. The transcription levels of chitin synthase (FOXG_12345, FOXG_10443 and FOXG_04179), chitinase (FOXG_19879 and FOXG_17332), endo-1,3 (4)-β-glucanase (FOXG_22849, FOXG_10637 and FOXG_03928) were upregulated after the mycelia of *F. oxysporum* were treated with isooctanol. The transcription levels of genes related to components corresponding to cell wall integrity (FOXG_09228), programmed cell death control protein (FOXG_03587) and cell division control protein (FOXG_00362) increased, slowing down the growth and division rate of cells, and activating cell apoptosis. Isooctanol destroyed the cell wall and cell membrane of *F. oxysporum*, causing intracellular reactive oxygen species (ROS) to accumulate, leading to apoptosis and cell death. A dose of only 3.75 μL/plate of isooctanol was sufficient to inhibit *F. oxysporum* (Ye et al., 2020a).

3.2 Diisobutyl phthalate

M. fulvus strain ST/P/71 had obvious antibacterial activity against *B. subtilis*, and the extract from the strain ST/P/71 mainly showed inhibition activity against *B. subtilis*. During seperating by Reverse Phase High Performance Liquid Chromatography (RP-HPLC), two pure compounds were eluted at RT 54.24 (Ra2) and RT 71.27 (Ra3). Ra2 was identified as di-isobutyl phthalate. This substance showed biofilm formation inhibitory activity against *B. subtilis*, with an MBIC50 of 2.703 μg/mL (Sharma et al., 2021). Di-isobutyl phthalate had biofilm formation inhibitory activity against *B. subtilis*, so it could have similar functions to plant pathogenic bacteria. Therefore, diisobutyl phthalate may have great potential in the prevention and control of plant pathogenic bacteria.

3.3 Myxovirescin

One of the 18 metabolites of *M. xanthus* strain DK1622 is polyketide *myxovirescin* (antibiotic TA), which had antibacterial activity. *Myxovirescin* played an important role in killing *Escherichia coli*, including lysis and subsequent predation (Xiao et al., 2011). The antibiotic TA was produced and named after *M. vanthits* strain TA(ATCC31046) (Rosenberg et al., 1982). The antibiotic TA could inhibit the incorporation of diamibopimelic acid and uridine diphosphate-N-acetylglucosamine into *E. coli* cell wall, and antibiotic TA interfered with the polymerizaton of the lipid-disacchar-pentapeptide (Rosenberg et al., 1982; Paitan et al., 1999). Myxobacteria encode a variety of substances to attack prey cells, with antibiotics serving as a front line weapon. Antibiotics can act as small molecule weapons to penetrate and kill or neutralize the metabolism of prey. The prevention and control principle of myxovirescin against bacterial pathogens has been relatively clear. This substance can be applied to research on prevention and control of plant pathogenic bacteria.

3.4 Cystobactamid derivatives

Myxobacteria produce specialized metabolites when preying, the production of specialized metabolites and lytic proteins of *myxobacteria* is related to their predation (Akbar and Stevens, 2021). Müller et al. found that the target compound inhibiting *P. aeruginosa* and other bacterial pathogens had a UV absorption spectrum similar to that of cystobactamides. Cystobacamids are aromatic oligoamides that exert their natural antibacterial properties by inhibition of bacterial gyrases (Solga et al., 2024). The improved orthogonally functionalized methoxyaspartate of cystobactamides could expand the synthesis of new cystobactamides. At present, four new types of cystobactamides 919-1 (1), 919-2 (2), 920-1 (3), 920-2 (4) and cystobactamides 861-2 (5) had been successfully synthesized and measured. Moeller et al. (2019) compared the antibacterial properties of this class of substanaces, the cyano derivative of cystobactamide 861-2(5) had antimicrobial activity against Gram-negative bacteria and its activity was higher than that of any natural cystobactamide tested so far.

Culture isolation of *C. coralline* strain M23 yielded coralmycin A (1), B (2) and another derivative, cystobactin 919-2. Coralmycin A had the strongest antibacterial activity against Gram-negative bacteria and had a wide antibacterial spectrum. Coralmycin A and B were cystobactamid derivatives (Kim et al., 2016). Seven new coralmycin derivatives and three known compounds were also isolated from the another culture of strain M23. The coralmycin derivatives are C (1), D (2), E (3), F (4), G (5), H (6), and I (7), the known compounds are cystobactamide 891-2(8), 905-2(9), and 507(10). The compounds had DNA gyrase inhibitory activity and antibacterial activity. The β-methoxyasparagine structure of

coralmycin may affect prey ingestion (Kim et al., 2019). Research on the structure of cystobactamides can be used to develop new structural substances with more antibacterial activity. Therefore, this type of substances may also have great potential in the prevention and control of Gram-negative plant pathogenic bacteria.

3.5 Hyalodione

Hyalodione isolated from the extract of the *Hyalangium minutum* strain NOCB-2T had antibacterial activity against *P. aeruginosa*. Hyalodione is a novel S-methyl cyclohexadiene-dione, which belongs to the class qinone (Herrmann et al., 2017). Hyaladione had broad antibacterial and antifungal activity. The tested strains included *P. aeruginosa*, *Rhodotorula glutarum* and *Staphylococcus aureus* (Okanya et al., 2012). Research on how hyalodione control bacteria and fungi need to be continued. Hyalodione also has great potential in controlling plant pathogenic bacteria and fungi.

3.6 Argyrin derivatives

The culture medium of the strains of *Archangium gephyra* contained a group of cyclic peptides composed of naturally produced octapeptides, which exhibited strong antibiotic effects against *P. aeruginosa* (Nickeleit et al., 2008; Stauch et al., 2010; Wieland et al., 2022). Among them, argyrin participates in the non-ribosomal peptide synthetase pathway, combining with elongation factor G (EF-G) as its target (Pogorevc et al., 2019). Argyrins inhibit protein synthesis by interfering with EF-G binding to the ribosome (Wieland et al., 2022). Several derivatives of argyrin A could be obtained by modifying the methoxytry ptophan residue. The methoxy group of this residue was crucial for its antibacterial activity and its activity will be lost if the position is replaced by other substituents (Siebert et al., 2019). Argyrin has antibacterial activity against bacteria, so there is great practical value to study its antibacterial activity against plant pathogenic bacteria.

3.7 Methyl (2R)-2-azido-3-hydroxyl-2-methylpropanoate and N-(3-amin o-2-hydroxypropyl)-N-meth-ylsulfuric diamide

The predation of bacteria and fungi by predatory *myxobacteria* has been mostly studied, but the predation of oomycetes has received little attention. *P. infestans* is the pathogen that causes potato late blight, which is one of the most serious diseases of potato (Rix et al., 2002). Wu collected *myxobacteria* isolated from soil samples in central Inner Mongolia. Eighty-three percent of the myxobacterial strains were resistant to *P. infestans*, among which the strains of *Myxococcus* and *Coralococcus* accounted for a higher proportion. The strains with the most significant antibacterial activity were *M. xanthus* B25-I-1, *M. fulvus* B25-I-3 and *M. stipitatus* X6-II-1. Strain B25-I-1 exhibited antagonistic activity against a variety of fungi and bacteria, and its active substances reduced the content of soluble proteins and the activity of protective enzymes (PPO, POD, PAL, and SOD) in *P. infestans*, increased oxidative damage and cell membrane permeability. It had a strong inhibitory effect on the hyphae, asexual reproduction and sexual reproduction of *P. infestans* (Wu, 2018). The active substance of strain B25-I-3 showed a strong inhibitory effect on the growth of *P. infestans*, inhibited the growth of mycelium and asexual reproduction, and reduced the infection ability of pathogens (Wu, 2018; Wu Z. et al., 2021; Wu Z. H. et al., 2021). After the fermentation products of B25-I-1 and B25-I-3 were separated, it was found that the components that had antagonistic effects on *P. infestans* contained Methyl(2R)-2-azido-3-hydroxyl-2-methylpropanoate and N-(3-Amino-2-hydroxypropyl)-N-meth-ylsulfuricdiamide.

3.8 Some unknown substances

P. infestans causes devastating diseases by invading the leaves, stems and tubers of potato plants (Berleman and Kirby, 2009). *M. xanthus* YR-7 isolated from soil samples in Bayannur area of Inner Mongolia had significant resistance to *P. infestans*. The growth inhibition rate of strain YR-7 against *P. infestans* hyphae was as high as 96.67%. The fermentation product of YR-7 was tested in isolated leaves. The experimental results proved that the active substance against *P. infestans* is a non-protein substance (Ren et al., 2016). About 72% of the myxobacteria isolated from soil samples in Ordos and Wuhai areas of Inner Mongolia had varying degrees of antagonistic effects on the growth of *P. infestans*. The ones with stronger ability to inhibit oomycetes were *C. exiguous* E10, *M. fallax* E11 and *C. coralloides* E12. The diameters of the inhibition zones were 26 mm, 24 mm and 24 mm (Ding, 2017; Wu, 2018). About 78.75% of the myxobacteria isolated from soil samples in Alxa area of Inner Mongolia had varying degrees of activity against *P. infestans*. The resistance of *Myxococcus fulvus* AL-24 and *Anqiococcu* AL-10 was outstanding. The fermentation products of strain AL-24 and strain AL-10 had good infection prevention activity and weak infection treatment activity on detached potato leaves (Zhao, 2018). Myxobacteria isolated from Indian soil samples, the extracts of *Coralococcus parvum* S104 and S145 showed broad-spectrum antibacterial activity. The water extract (WE) and DMSO extract (DE) of GNDU172 showed obvious activity against *B. subtilis*, and the DE of strain S213 and strain S223 showed similar activity. The DE of S223 has activity against *Pseudomonas syringae* and *B. cereus* (Kumar et al., 2017). However, all of these active substances are unknow and need to be seperated and identified in the future.

4 Discussion

Plant pathogen is a major threat to crops worldwide, not only reducing crop yields but also causing significant damage to crop quality. In order to control or avoid excessive economic losses caused by plant pathogens, synthetic agrochemicals are often used in agricultural production as the most common method to control plant pathogens and improve crop yield quality. However, excessive use can cause adverse effects on the environment and human health.

Myxobacteria feed on bacteria and fungi in the soil and obtain nutrients by preying on other microorganisms. The cell wall of plant pathogens protects cells from external invasion and is a key barrier between predatory myxobacteria and prey cells (Berleman and Kirby, 2009). In order to break through the cell wall barrier, Myxobacteria have evolved targeted preying methods. One method is to degrade the cell wall or increase the permeability of the cell membrane through antibacterial metabolites and cell wall degrading enzymes. The other

one is a targeted, contactdependent killing mechanism through the Tad-like system and protein secretion system (Thiery et al., 2022). The Tad-like system mediates the contact-dependent killing of myxobacteria on prey cells (Seef et al., 2021).

The general method for myxobacteria to control plant pathogenic bacteria is the first method mentioned above. During the interaction between myxobacteria and prey cells, antibiotics, lytic enzymes, hydrolases, etc. involved in the process. This review summarizes the prevention and control principles of myxobacteria in plant pathogenic fungi, oomycetes, and bacterial disasters (Table 1). Myxobacteria secrete enzymes that can degrade cell wall components. Myxobacteria produce small molecule compounds that inhibit the normal growth and proliferation of pathogens. The enzymes secreted by myxobacteria are mainly chitinase, β-1,6-glucanase and β-1,3-glucanase, etc, which increase intracellular osmotic pressure by degrading the cell wall of prey cells, promoting cell lysis and death. Some small molecule compounds produced by myxobacteria affect the normal growth and reproduction of prey cells or changing their permeability, thereby inducing apoptosis of prey cells.

In the process of preventing and controlling plant diseases, it is possible to use myxobacteria to develop a certain BCAs that inhibits pathogens efficiently, which will be helpful to reduce the cost increase and environmental pollution caused by excessive use of pesticides, and maximize economic and environmental benefits.

In addition to preventing and controlling plant diseases in agriculture, myxobacteria can also be used to increase production, storage, and transportation of agricultural and sideline products. For example, myxobacteria-mediated paper impregnated with silver nanoparticles (AgNPs) is used in fruit packaging to extend the shelf life to 15 days (Bhople et al., 2016).

At present, there are only relevant reports on the prevention and control of plant diseases by myxobacteria on fungi, oomycetes and bacteria. There are no reports on the prevention and control of plant virus damage. The principle of prevention and treatment of animal viruses by myxobacteria is to inhibit the activity of RNA-dependent RNA polymerase complex, ion channel inhibitor, and signal pathway inhibition. Myxobacteria are also very likely to inhibit RNA synthesis or inhibit signaling pathways in the prevention and control of plant virus damage. Therefore, myxobacteria also have great research value in the prevention and control of plant virus damage.

Author contributions

LZ: Conceptualization, Investigation, Software, Writing – original draft. LB: Methodology, Writing – review & editing. SL: Data curation, Formal analysis, Writing – original draft. YL: Resources, Writing – review & editing. HL: Project administration, Supervision, Writing – review & editing.

Funding

The author(s) declare financial support was received for the research, authorship, and/or publication of this article. This study was supported by the National Natural Science Foundation of China (no. 32260696) and the Science and Technology Plan Project of Inner Mongolia Autonomous Region (no. 2021GG0079).

Acknowledgments

The authors appreciate the support of the National Natural Science Foundation of China and the Science and Technology Program of Inner Mongolia Autonomous region and the help of College of Life Sciences of Inner Mongolia Agricultural University and other members in the lab.

Conflict of interest

The authors declare that the research was conducted in the absence of any commercial or financial relationships that could be construed as a potential conflict of interest.

Publisher's note

Supplementary material

The Supplementary material for this article can be found online at: https://www.frontiersin.org/articles/10.3389/fmicb.2023.1294854/full#supplementary-material

References

Akbar, S., and Stevens, D. C. (2021). Functional genomics study of *Pseudomonas putida* to determine traits associated with avoidance of a myxobacterial predator. *Sci. Rep.* 11:16445. doi: 10.1038/s41598-021-96046-8

Arguelles-Arias, A., Ongena, M., Halimi, B., Lara, Y., Brans, A., Joris, B., et al. (2009). *Bacillus amyloliquefaciens* GA1 as a source of potent antibiotics and other secondary metabolites for biocontrol of plant pathogens. *Microb. Cell Factories* 8:63. doi: 10.1186/1475-2859-8-63

Bader, C. D., Panter, F., Garcia, R., Tchesnokov, E. P., Haid, S., Walt, C., et al. (2022). Sandacrabins - structurally unique antiviral RNA polymerase inhibitors from a rare myxobacterium. *Chem. Eur. J.* 28:e202104484. doi: 10.1002/chem.202104484

Berleman, J. E., Allen, S., Danielewicz, M. A., Remis, J. P., Gorur, A., Cunha, J., et al. (2014). The lethal cargo of Myxococcus xanthus outer membrane vesicles. *Front. Microbiol.* 5:474. doi: 10.3389/fmicb.2014.00474

Berleman, J. E., and Kirby, J. R. (2009). Deciphering the hunting strategy of a bacterial wolfpack. *FEMS Microbiol. Rev.* 33, 942–957. doi: 10.1111/j.1574-6976.2009.00185.x

Bhople, S., Gaikwad, S., Deshmukh, S., Bonde, S., Gade, A., Sen, S., et al. (2016). Myxobacteria-mediated synthesis of silver nanoparticles and their impregnation in wrapping paper used for enhancing shelf life of apples. *IET Nanobiotechnol.* 10, 389–394. doi: 10.1049/iet-nbt.2015.0111

Bowman, S. M., and Free, S. J. (2006). The structure and synthesis of the fungal cell wall. *Bio Essays* 28, 799–808. doi: 10.1002/bies.20441

Davies, J., Spiegelman, G. B., and Yim, G. (2006). The world of subinhibitory antibiotic concentrations. *Curr. Opin. Microbiol.* 9, 445–453. doi: 10.1016/j.mib.2006.08.006

Ding, Y. (2017). Isolation and Identification of Myxobacteria from the Ordos Plateau Area and Preliminary Analysis of Their Antagonistic Activity Against Phytophthora infestans. *Master, Innebr Mongolia Agricultural University*. Available online at: https://wap.cnki.net/touch/web/Dissertation/Article/10129-1017211855.nh.html (Accessed January 23, 2024).

Dong, H., Gao, R., Dong, Y., Yao, Q., and Zhu, H. (2023). Whole-genome sequencing of a biocontrol *Myxococcus xanthus* R31 isolate and comparative genomic analysis. *Gene* 863:147286. doi: 10.1016/j.gene.2023.147286

Gemperlein, K., Zaburannyi, N., Garcia, R., La Clair, J., and Müller, R. (2018). Metabolic and biosynthetic diversity in marine myxobacteria. *Mar. Drugs* 16:314. doi: 10.3390/md16090314

Herrmann, J., Fayad, A. A., and Müller, R. (2017). Natural products from myxobacteria: novel metabolites and bioactivities. *Nat. Prod. Rep.* 34, 135–160. doi: 10.1039/c6np00106h

Iizuka, T., Jojima, Y., Fudou, R., Hiraishi, A., Ahn, J.-W., and Yamanaka, S. (2003a). Plesiocystis pacifica gen. nov., sp. nov., a marine myxobacterium that contains dihydrogenated menaquinone, isolated from the Pacific coasts of Japan. *Int. J. Syst. Evol. Microbiol.* 53, 189–195. doi: 10.1099/ijs.0.02418-0

Iizuka, T., Jojima, Y., Fudou, R., Tokura, M., Hiraishi, A., and Yamanaka, S. (2003b). Enhygromyxa salina gen. nov., sp. nov., a slightly halophilic myxobacterium isolated from the coastal areas of Japan. *Syst. Appl. Microbiol.* 26, 189–196. doi: 10.1078/072320203322346038

Kaushal, G., and Singh, S. P. (2020). Comparative genome analysis provides shreds ofmolecular evidence for reclassification of LeuconostocmesenteroidesMTCC 10508 as a strain of Leu. suionicum. *Genomics* 112, 4023–4031. doi: 10.1016/j.ygeno.2020.06.040

Kim, B.-M., Minh, N. V., Choi, H.-Y., and Kim, W.-G. (2019). Coralmycin derivatives with potent anti-gram negative activity produced by the myxobacteria *Corallococcus coralloides* M23. *Molecules* 24:1390. doi: 10.3390/molecules24071390

Kim, Y. J., Kim, H.-J., Kim, G.-W., Cho, K., Takahashi, S., Koshino, H., et al. (2016). Isolation of Coralmycins a and B, potent anti-gram negative compounds from the Myxobacteria *Corallococcus coralloides* M23. *J. Nat. Prod.* 79, 2223–2228. doi: 10.1021/acs.jnatprod.6b00294

Kumar, S., Yadav, A. K., Chambel, P., and Kaur, R. (2017). Molecular and functional characterization of myxobacteria isolated from soil in India. *3 Biotech* 7:112. doi: 10.1007/s13205-017-0722-9

Li, Z., Xia, C., Wang, Y., Li, X., Qiao, Y., Li, C., et al. (2019a). Identification of an endo-chitinase from Corallococcus sp. EGB and evaluation of its antifungal properties. *Int. J. Biol. Macromol.* 132, 1235–1243. doi: 10.1016/j.ijbiomac.2019.04.056

Li, Z., Ye, X., Liu, M., Xia, C., Zhang, L., Luo, X., et al. (2019b). A novel outer membrane ß-1,6-glucanase is deployed in the predation of fungi by myxobacteria. *ISME J.* 13, 2223–2235. doi: 10.1038/s41396-019-0424-x

Mansfield, J., Genin, S., Magori, S., Citovsky, V., Sriariyanum, M., Ronald, P., et al. (2012). Top 10 plant pathogenic bacteria in molecular plant pathology. *Mol. Plant Pathol.* 13, 614–629. doi: 10.1111/j.1364-3703.2012.00804.x

Moeller, M., Norris, M. D., Planke, T., Cirnski, K., Herrmann, J., Müller, R., et al. (2019). Scalable syntheses of methoxyaspartate and preparation of the antibiotic cystobactamid 861-2 and highly potent derivatives. *Organ. Lett.* 21, 8369–8372. doi: 10.1021/acs.orglett.9b03143

Nickeleit, I., Zender, S., Sasse, F., Geffers, R., Brandes, G., Sörensen, I., et al. (2008). Argyrin A reveals a critical role for the tumor suppressor protein p27kip1 in mediating antitumor activities in response to proteasome inhibition. *Cancer Cell* 14, 23–35. doi: 10.1016/j.ccr.2008.05.016

Odintsov, S. G., Sabala, I., Marcyjaniak, M., and Bochtler, M. (2004). Latent LytMat 1.3Å resolution. *J. Mol. Biol.* 335, 775–785. doi: 10.1016/j.jmb.2003.11.009

Okanya, P. W., Mohr, K. I., Gerth, K., Steinmetz, H., Huch, V., Jansen, R., et al. (2012). Hyaladione, an S-methyl Cyclohexadiene-dione from *Hyalangium minutum*. *J. Nat. Prod.* 75, 768–770. doi: 10.1021/np200776v

Oren, A., and Garrity, G. M. (2021). Valid publication of the[[Inline Image]] names of forty-two phyla of prokaryotes. *Int. J. Syst. Evol. Microbiol.* 71:4. doi: 10.1099/ijsem.0.005056

Paitan, Y., Orr, E., Ron, E. Z., and Rosenberg, E. (1999). A nonessential signal peptidase II (Lsp) of Myxococcus xanthus might be involved in biosynthesis of the polyketide antibiotic TA. *J. Bacteriol.* 181, 5644–5651. doi: 10.1128/JB.181.18.5644-5651.1999

Pietro, A. D., Madrid, M. P., Caracuel, Z., Delgado-Jarana, J., and Roncero, M. I. G. (2003). Fusarium oxysporum: exploring the molecular arsenal of a vascular wilt fungus. *Mol. Plant Pathol.* 4, 315–325. doi: 10.1046/j.1364-3703.2003.00180.x

Pogorevc, D., Tang, Y., Hoffmann, M., Zipf, G., Bernauer, H. S., Popoff, A., et al. (2019). Biosynthesis and heterologous production of argyrins. *ACS Synth. Biol.* 8, 1121–1133. doi: 10.1021/acssynbio.9b00023

Ren, X. (2016). *Isolation and Identification of Myxobacteria from Soil in Bayannaoer Area and Preliminary Study on their Antibiotic Activities Against Phytophthora Infestans* Master, Inner Mongolia Agricultural University. Available at: https://cdmd.cnki.com.cn/Article/CDMD-10129-1016249574.htm

Rix, U., Fischer, C., Remsing, L. L., and Rohr, J. (2002). Modification of post-PKS tailoring steps through combinatorial biosynthesis. *Nat. Prod. Rep.* 19, 542–580. doi: 10.1039/b103920m

Rosenberg, E., Fytlovitch, S., Carmeli, S., and Kashman, Y. (1982). Chemical properties of Myxococcus xanthus antibiotic TA. *J. Antibiot.* 35, 788–793. doi: 10.7164/antibiotics.35.788

Ryosuke, F., Yasuko, J., Takashi, I., and Yamanaka, S. (2002). Haliangium ochraceum gen. nov., sp. nov. and Haliangium tepidum sp. nov.: novel moderately halophilic myxobacteria isolated from coastal saline environments. *J. Gen. Appl. Microbiol.* 48, 109–116. doi: 10.2323/jgam.48.109

Saggu, S. K., Nath, A., and Kumar, S. (2023). Myxobacteria: biology and bioactive secondary metabolites. *Res. Microbiol.* 174:104079. doi: 10.1016/j.resmic.2023.104079

Seef, S., Herrou, J., de Boissier, P., My, L., Brasseur, G., Robert, D., et al. (2021). A Tad-like apparatus is required for contact-dependent prey killing in predatory social bacteria. *eLife* 10:e72409. doi: 10.7554/eLife.72409

Selitrennikoff, C. P. (2001). Antifungal Proteins. *Appl. Environ. Microbiol.* 67, 2883–2894. doi: 10.1128/aem.67.7.2883-2894.2001

Sharma, A., Kumar, A., Babu, V., Ali, A., and Katoch, M. (2021). Myxobacteria from animal dung pellets collected from northwestern Himalayas: a new source of di-isobutyl phthalate. *J. Basic Microbiol.* 62, 162–173. doi: 10.1002/jobm.202100518

Shehata, A. N., Abd El Aty, A. A., Darwish, D. A., Abdel Wahab, W. A., and Mostafa, F. A. (2018). Purification, physicochemical and thermodynamic studies of antifungal chitinase with production of bioactive chitosan-oligosaccharide from newly isolated aspergillus griseoaurantiacus KX010988. *Int. J. Biol. Macromol.* 107, 990–999. doi: 10.1016/j.ijbiomac.2017.09.071

Shen, E., Wang, X., Lu, Z., Zhou, F., Ma, W., Cui, Z., et al. (2023). Overexpression of a beta-1, 6-glucanase gene GluM in transgenic rice confers high resistance to rice blast, sheath blight and false smut. *Pest Manag. Sci.* 79, 2152–2162. doi: 10.1002/ps.7394

Siebert, D. C. B., Sommer, R., Pogorevc, D., Hoffmann, M., Wenzel, S. C., Müller, R., et al. (2019). Chemical synthesis of tripeptide thioesters for the biotechnological incorporation into the myxobacterial secondary metabolite argyrin via mutasynthesis. *Beilstein J. Org. Chem.* 15, 2922–2929. doi: 10.3762/bjoc.15.286

Solga, D., Wieske, L. H. E., Wilcox, S., Zeilinger, C., Jansen-Olliges, L., Cirnski, K., et al. (2024). Is simultaneous binding toDNA and gyrase important for the antibacterial activity of cystobactamids? *Chemistry* 13:e202303796. doi: 10.1002/chem.202303796

Stauch, B., Simon, B., Basile, T., Schneider, G., Malek, N. P., Kalesse, M., et al. (2010). Elucidation of the structure and intermolecular interactions of a reversible cyclicpeptide inhibitor of the proteasome by NMR spectroscopy and molecular modeling. *Angew. Chem. Int. Ed.* 49, 3934–3938. doi: 10.1002/anie.201000140

Sutton, D., Livingstone, P. G., Furness, E., Swain, M. T., and Whitworth, D. E. (2019). Genome-wide identification of myxobacterial predation genes and demonstration of formaldehyde secretion as a potentially predation-resistant trait of Pseudomonas aeruginosa. *Front. Microbiol.* 10:2650. doi: 10.3389/fmicb.2019.02650

Talbot, N. J. (2003). On the trail of a cereal killer: exploring the biology of Magnaporthe grisea. *Annu. Rev. Microbiol.* 57, 177–202. doi: 10.1146/annurev.micro.57.030502.090957

Thiery, S., Turowski, P., Berleman, J. E., and Kaimer, C. (2022). The predatory soil bacterium Myxococcus xanthus combines a Tad- and an atypical type 3-like protein secretion system to kill bacterial cells. *Cell Rep.* 40:111340. doi: 10.1016/j.celrep.2022.111340

Waite, D. W., Chuvochina, M., Pelikan, C., Parks, D. H., Yilmaz, P., Wagner, M., et al. (2020). Proposal to reclassify the proteobacterial classes Deltaproteobacteria and Oligoflexia, and the phylum Thermodesulfobacteria into four phyla reflecting major functional capabilities. *Int. J. Syst. Evol. Microbiol.* 70, 5972–6016. doi: 10.1099/ijsem.0.004213

Weissman, K. J., and Müller, R. (2010). Myxobacterial secondary metabolites: bioactivities and modes-of-action. *Nat. Prod. Rep.* 27, 1276–1295. doi: 10.1039/c001260m

Wieland, M., Holm, M., Rundlet, E. J., Morici, M., Koller, T. O., Maviza, T. P., et al. (2022). The cyclic octapeptide antibiotic argyrin B inhibits translation by trapping EFG on the ribosome during translocation. *Proc. Natl. Acad. Sci. U.S.A.* 119:e2114214119. doi: 10.1073/pnas.2114214119

Willsey, G. G., Wargo, M. J., and O'Toole, G. A. (2016). Sarcosine catabolism in Pseudomonas aeruginosa is transcriptionally regulated by SouR. *J. Bacteriol.* 198, 301–310. doi: 10.1128/jb.00739-15

Wu, Z. (2018). *Isolation of Myxobacteria from the Central Region of Inner Mongolia and their Activity and Components Against Potato Late Blight Pathogen* Doctor, Inner Mongolia Agricultural University. Available at: https://cdmd.cnki.com.cn/Article/CDMD-10129-1018881788.htm

Wu, Z., Cui, H., Sun, Z., and Liu, H. (2021). Biocontrol mechanism of *Myxococcus xanthus* B25-I-1 against *Phytophthora infestans*. *Pestic. Biochem. Physiol.* 175:104832. doi: 10.1016/j.pestbp.2021.104832

Wu, Z. H., Ma, Q., Sun, Z. N., Cui, H. C., and Liu, H. R. (2021). Biocontrol mechanism of *Myxococcus fulvus* B25-I-3 against Phytophthora infestans and its control efficiency on potato late blight. *Folia Microbiol.* 66, 555–567. doi: 10.1007/s12223-021-00865-1

Xiao, Y., Wei, X., Ebright, R., and Wall, D. (2011). Antibiotic production by Myxobacteria plays a role in predation. *J. Bacteriol.* 193, 4626–4633. doi: 10.1128/jb.05052-11

Ye, X., Chen, Y., Ma, S., Yuan, T., Wu, Y., Li, Y., et al. (2020a). Biocidal effects of volatile organic compounds produced by the myxobacterium *Corrallococcus* sp. EGB against fungal phytopathogens. *Food Microbiology* 91:103502. doi: 10.1016/j.fm.2020.103502

Ye, X., Li, Z., Luo, X., Wang, W., Li, Y., Li, R., et al. (2020b). A predatory myxobacterium controls cucumber fusarium wilt by regulating the soil microbial community. *Microbiome* 8:49. doi: 10.1186/s40168-020-00824-x

Zhang, L., Dong, C., Wang, J., Liu, M., Wang, J., Hu, J., et al. (2023). Predation of oomycetes by myxobacteria via a specialized CAZyme system arising from adaptive evolution. *ISME J.* 17, 1089–1103. doi: 10.1038/s41396-023-01423-y

Zhao, P. (2018). *Isolation and Identification of Myxobacteria in Alashan Area and Preliminary Study on their Antibiotic Activity Against Phytophthora infestans* Master, Inner Mongolia Agricultural University. Available at: https://cdmd.cnki.com.cn/Article/CDMD-10129-1018882358.htm

Zhou, J., Chen, J., Li, Z., Ye, X., Dong, W., Jiang, M., et al. (2019). Enzymatic properties of a multi-specific β-(1,3)-glucanase from Corallococcus sp. EGB and its potential antifungal applications. *Protein Expr. Purif.* 164:105481. doi: 10.1016/j.pep.2019.105481

frontiers | Frontiers in Microbiology

TYPE Correction
PUBLISHED 13 March 2024
DOI 10.3389/fmicb.2024.1392109

OPEN ACCESS

APPROVED BY
Frontiers Editorial Office,
Frontiers Media SA, Switzerland

*CORRESPONDENCE
Huirong Liu
huirong_liu@imau.edu.cn

RECEIVED 27 February 2024
ACCEPTED 27 February 2024
PUBLISHED 13 March 2024

CITATION
Zhang L, Bao L, Li S, Liu Y and Liu H (2024) Corrigendum: Active substances of myxobacteria against plant diseases and their action mechanisms.
Front. Microbiol. 15:1392109.
doi: 10.3389/fmicb.2024.1392109

Corrigendum: Active substances of myxobacteria against plant diseases and their action mechanisms

Lele Zhang[1], Liangliang Bao[2], Songyuan Li[1], Yang Liu[1] and Huirong Liu[1]*

[1]College of Life Sciences, Inner Mongolia Agricultural University, Hohhot, Inner Mongolia, China, [2]College of Science, Inner Mongolia Agricultural University, Hohhot, Inner Mongolia, China

KEYWORDS

myxobacteria, plant diseases, biological control, carbohydrate-active enzymes, small molecule compounds

A corrigendum on

Active substances of myxobacteria against plant diseases and their action mechanisms

by Zhang, L., Bao, L., Li, S., Liu, Y., and Liu, H. (2024). *Front. Microbiol.* 14:1294854. doi: 10.3389/fmicb.2023.1294854

In the published article, there was an error in the article title. Instead of "Substances derived from myxobacteria that prevent and control plant pathogenic diseases and their prevention and control principles," it should be "Active substances of myxobacteria against plant diseases and their action mechanisms."

1. In the published article, some references were not cited. The missing references are listed below. In the published article [Berleman, J.E., Allen, S., Danielewicz, M.A., Remis, J.P., Gorur, A., Cunha, J., et al. (2014). The lethal cargo of Myxococcus xanthus outer membrane vesicles. Frontiers in Microbiology 5. doi: 10.3389/fmicb.2014.00474] was not cited in the article. The citation has now been inserted in [2 Enzymes], [2.4 Proteases and peptidases], [Paragraph 1] and should read:

   "[Proteases and peptidases, such as the M36 metalloprotease MepA secreted by *M. xanthus* strain DK1622, may promote the predation of prey by degrading proteins of prey cells (Berleman et al., 2014).]"

2. In the published article [Ding, Y. (2017). Isolation and Identification of Myxobacteria from the Ordos Plateau Area and Preliminary Analysis of Their Antagonistic Activity Against Phytophthora Infestans. Master, Inner Mongolia Agricultural University. https://wap.cnki.net/touch/web/Dissertation/Article/10129-1017211855.nh.html] was not cited in the article. The citation has now been inserted in [3 Small molecule compounds], [3.8 Some unknown substances], [Paragraph 1] and should read:

   "[The diameters of the inhibition zones were 26 mm, 24 mm and 24 mm (Ding, 2017; Wu, 2018).]"

3. In the published article [Herrmann, J., Fayad, A.A., and Müller, R. (2017). Natural products from myxobacteria: novel metabolites and bioactivities. Natural Product Reports 34(2), 135-160. doi: 10.1039/c6np00106h], was not cited in the article. The citation has now been inserted in [3 Small molecule compounds], [3.5 *Hyalodione*], [Paragraph 1] and should read:

"[Hyalodione is a novel S-methyl cyclohexadiene-dione, which belongs to the class qinone (Herrmann et al., 2017).]"

4. In the published article [Iizuka, T., Jojima, Y., Fudou, R., Hiraishi, A., Ahn, J.-W., and Yamanaka, S. (2003a). Plesiocystis pacifica gen. nov., sp. nov., a marine myxobacterium that contains dihydrogenated menaquinone, isolated from the Pacific coasts of Japan. International Journal of Systematic and Evolutionary Microbiology 53(1), 189-195. doi: 10.1099/ijs.0.02418-0] was not cited in the article. The citation has now been inserted in [1 Introduction], [Paragraph 1] and should read:

"[Some halophilic myxobacteria i.e., *Haliangium* spp. (Ryosuke et al., 2002), *Plesiocystis pacifica* (Iizuka et al., 2003a) and *Enhygromyxa salina* (Iizuka et al., 2003b) had been isolated from marine environment.]"

5. In the published article [Iizuka, T., Jojima, Y., Fudou, R., Tokura, M., Hiraishi, A., and Yamanaka, S. (2003b). Enhygromyxa salina gen. nov., sp. nov., a Slightly Halophilic Myxobacterium Isolated from the Coastal Areas of Japan. Systematic and Applied Microbiology 26(2), 189-196. doi: 10.1078/072320203322346038] was not cited in the article. The citation has now been inserted in [1 Introduction], [Paragraph 1] and should read:

"[Some halophilic myxobacteria i.e., *Haliangium spp.* (Ryosuke et al., 2002), *Plesiocystis pacifica* (Iizuka et al., 2003a) and *Enhygromyxa salina* (Iizuka et al., 2003b) had been isolated from marine environment.]"

6. In the published article [Kaushal, G., and Singh, S.P. (2020). Comparative genome analysis provides shreds of molecular evidence for reclassification of Leuconostoc mesenteroides MTCC 10508 as a strain of Leu. suionicum. Genomics 112(6), 4023-4031. doi: 10.1016/j.ygeno.2020.06.040] was not cited in the article. The citation has now been inserted in [2. Enzymes], [Paragraph 1] and should read:

"[GHs hydrolyze glycosidic bonds and play an important role in the hydrolysis and synthesis of sugars and glycoconjugates in organisms (Kaushal and Singh, 2020).]"

7. In the published article [Mansfield, J., Genin, S., Magori, S., Citovsky, V., Sriariyanum, M., Ronald, P., et al. (2012). Top 10 plant pathogenic bacteria in molecular plant pathology. Molecular Plant Pathology 13(6), 614-629. doi: 10.1111/j.1364-3703.2012.00804.x.] was not cited in the article. The citation has now been inserted in [2. Enzymes], [2.4 Proteases and peptidases], [Paragraph 1] and should read:

"[Tomato bacterial wilt (TBW) caused by *Ralstonia solanacearum* is one of the most destructive soil-borne diseases, and tomato production has suffered huge losses due to the epidemic of TBW (Mansfield et al., 2012).]"

8. In the published article [Moeller, M., Norris, M.D., Planke, T., Cirnski, K., Herrmann, J., Müller, R., et al. (2019). Scalable Syntheses of Methoxyaspartate and Preparation of the Antibiotic Cystobactamid 861-2 and Highly Potent Derivatives. Organic Letters 21(20), 8369-8372. doi: 10.1021/acs.orglett.9b03143] was not cited in the article. The citation has now been inserted in [3 Small molecule compounds], [3.4 Cystobactamid derivatives], [Paragraph 1] and should read:

"[Moeller et al. (2019) compared the antibacterial properties of this class of substanaces, the cyano derivative of cystobactamide 861-2(5) had antimicrobial activity against Gram-negative bacteria and its activity was higher than that of any natural cystobactamide tested so far.]"

9. In the published article [Nickeleit, I., Zender, S., Sasse, F., Geffers, R., Brandes, G., Sörensen, I., et al. (2008). Argyrin A Reveals a Critical Role for the Tumor Suppressor Protein p27kip1 in Mediating Antitumor Activities in Response to Proteasome Inhibition. Cancer Cell 14(1), 23-35. doi: 10.1016/j.ccr.2008.05.016] was not cited in the article. The citation has now been inserted in [3 Small molecule compounds], [3.6 Argyrin derivatives], [Paragraph 1] and should read:

"[The culture medium of the strains of *Archangium gephyra* contained a group of cyclic peptides composed of naturally produced octapeptides, which exhibited strong antibiotic effects against *P. aeruginosa* (Nickeleit et al., 2008; Stauch et al., 2010; Wieland et al., 2022).]"

10. In the published article [Odintsov, S.G., Sabala, I., Marcyjaniak, M., and Bochtler, M. (2004). Latent LytM at 1.3Å Resolution. Journal of Molecular Biology 335(3), 775-785. doi: 10.1016/j.jmb.2003.11.009] was not cited in the article. The citation has now been inserted in [2. Enzymes], [2.4 Proteases and peptidases], [Paragraph 1] and should read:

"[Proteins of the M23 family were endopeptidases that cleaved bacterial cell wall peptidoglycan by degrading the peptide bonds of cross-linked peptides (Odintsov et al., 2004).]"

11. In the published article [Oren, A., and Garrity, G. M. (2021). Valid publication of the names of forty-two phyla of prokaryotes. International Journal of Systematic and Evolutionary Microbiology 71(10). doi: 10.1099/ijsem.0.005056] was not cited in the article. The citation has now been inserted in [1 Introduction], [Paragraph 1] and should read:

"[Myxobacteria are microorganisms of the phylum Myxococcota (Waite et al., 2020; Oren and Garrity, 2021), which are well known for their complex life cycles and unique social behaviors.]"

12. In the published article [Paitan Y, Orr E, Ron EZ, and E., R. (1999). A nonessential signal peptidase II (Lsp) of Myxococcus xanthus might be involved in biosynthesis of the polyketide antibiotic TA. Journal of Bacteriology 181(18), 5644-5651. doi: 10.1128/JB.181.18.5644-5651.1999] was not cited in the article. The citation has now been inserted in [3

Small molecule compounds], [3.3 Myxovirescin], [Paragraph 1] and should read:

"[The antibiotic TA could inhibit the incorporation of diamibopimelic acid and uridine diphosphate-N-acetylglucosamine into *E. coli* cell wall, and antibiotic TA interfered with the polymerizaton of the lipid-disacchar-pentapeptide (Rosenberg et al., 1982; Paitan et al., 1999).]"

13. In the published article [Pogorevc, D., Tang, Y., Hoffmann, M., Zipf, G., Bernauer, H.S., Popoff, A., et al. (2019). Biosynthesis and Heterologous Production of Argyrins. ACS Synthetic Biology 8(5), 1121-1133. doi: 10.1021/acssynbio.9b00023] was not cited in the article. The citation has now been inserted in [3 Small molecule compounds], [3.6 Argyrin derivatives], [Paragraph 1] and should read:

"[Among them, argyrin participates in the non-ribosomal peptide synthetase pathway, combining with elongation factor G (EF-G) as its target (Pogorevc et al., 2019).]"

14. In the published article [Ren, X., Wu, Z., Cui, H., Gao, X., and Feng, F. (2016). Isolation and identification of antagonistic strain YR-7 of Phytophthora infestans and its active substances. Bulletin of Microbiology 43(07), 1513-1523. doi: 10.13344/j.microbiol.china.150617] was not cited in the article. The citation has now been inserted in [3 Small molecule compounds], [3.8 Some unknown substances], [Paragraph 1] and should read:

"[The experimental results proved that the active substance against *P. infestans* is a non-protein substance (Ren et al., 2016).]"

15. In the published article [Rix, U., Fischer, C., Remsing, L.L., and Rohr, J.r. (2002). Modification of post-PKS tailoring steps through combinatorial biosynthesis. Natural Product Reports 19(5), 542-580. doi: 10.1039/b103920m.] was not cited in the article. The citation has now been inserted in [1 Introduction], [Paragraph 1] and should read:

"[For example, in contrast to Actinomycetes derivatives, most small molecules of myxobacteria are not glycosylated (Rix et al., 2002).]"

16. In the published article [Rosenberg E, Fytlovitch S, Carmeli S, and Y., K. (1982). Chemical properties of Myxococcus xanthus antibiotic TA. The Journal of Antibiotics 35(7), 788-793. doi: 10.7164/antibiotics.35.788] was not cited in the article. The citation has now been inserted in [3 Small molecule compounds], [3.3 Myxovirescin], [Paragraph 1] and should read:

"[The antibiotic TA was produced and named after M. vanthits strain TA(ATCC31046) (Rosenberg et al., 1982). The antibiotic TA could inhibit the incorporation of diamibopimelic acid and uridine diphosphate-N-acetylglucosamine into E. coli cell wall, and antibiotic TA interfered with the polymerizaton of the lipid-disacchar-pentapeptide (Rosenberg et al., 1982; Paitan et al., 1999).]"

17. In the published article [Ryosuke Fudou, Yasuko Jojima, Takashi Iizuka, and Yamanaka, S. (2002). Haliangium ochraceum gen. nov., sp. nov. and Haliangium tepidum sp. nov.: novel moderately halophilic myxobacteria isolated from coastal saline environments. The Journal of general and applied microbiology 48(2), 109-116. doi: 10.2323/jgam.48.109] was not cited in the article. The citation has now been inserted in [1 Introduction], [Paragraph 1] and should read:

"[Some halophilic myxobacteria i.e., *Haliangium spp.* (Ryosuke et al., 2002), *Plesiocystis pacifica* (Iizuka et al., 2003a) and *Enhygromyxa salina* (Iizuka et al., 2003b) had been isolated from marine environment.]"

18. In the published article [Saggu, S.K., Nath, A., and Kumar, S. (2023). Myxobacteria: biology and bioactive secondary metabolites. Research in Microbiology 174(7), 104079. doi: 10.1016/j.resmic.2023.104079] was not cited in the article. The citation has now been inserted in [1 Introduction], [Paragraph 1] and should read:

"[Myxobacteria have a wide range of habitats, including soil rich in organic matter, rotting wood, animal dung and marine environment (Saggu et al., 2023).]"

19. In the published article [Seef, S., Herrou, J., de Boissier, P., My, L., Brasseur, G., Robert, D., et al. (2021). A Tad-like apparatus is required for contact-dependent prey killing in predatory social bacteria. eLife 10. doi: 10.7554/eLife.] was not cited in the article. The citation has now been inserted in [4 Discussion], [Paragraph 2] and should read:

"[The Tad-like system mediates the contact-dependent killing of myxobacteria on prey cells (Seef et al., 2021).]"

In the published article, there was an error in the Figure 1 and in the legend for Figure 1 as published. In the small molecule substances, we changed change mucin to myxovirescin, cyclosporamiade analogues to cystobacamids derivatives, we deleted coralmycin A hyaluronic acid dione protocystin A and enhygromic acid(1), deoxyenhygrolides A(2), deoxyenhygrolides B(3), and added hyalodione and argyrin derivatives, unknown substances. Furthermore, we changed pathogens to plant pathogens. The corrected Figure 1 and its caption appears below.

In the published article, there was an error in the Table 1 as published. Antagonistic substances are divided into two categories, namely enzymes and small molecule substances. Enzymes contain β-1,6-glucanase, β-1,3-glucanase, Chitinase, Proteases and peptidases, Formaldehyde dismutase. Small molecule compounds contain Isooctanol, Di-isobutyl phthalate, Myxovirescin, Cystobacamids derivatives, Hyalodione, Argyrin derivatives. The corrected table appears below.

In the published article, there was an error in [Table 1] as published. The corrected [Table 1 Active substances of myxobacteria against plant diseases and their action mechanisms] and its caption ** [Table 1 Active substances of myxobacteria against plant diseases and their action mechanisms] appear below.

In the published article, there was **31** errors.

1. [The relevant content was added to the text, the abstract also made corresponding changes.] A correction has been made to [Abstract].

This sentence previously stated: "[Myxobacteria have a complex life cycle and unique social behavior, and obtain nutrients by preying on bacteria and fungi in soil. Chitinase, β-1,3 glucanase and β-1,6 glucanase produced by myxobacteria can degrade the glycosidic bond of cell wall of some plant pathogenic fungi, resulting in a perforated structure in the cell wall. In addition, isooctanol produced by myxobacteria can lead to the accumulation of intracellular reactive oxygen species in some pathogenic fungi and induce cell apoptosis. Myxobacteria can also perforate the cell wall of some plant pathogenic oomycetes by β-1,3 glucanase, reduce the content of intracellular soluble protein and protective enzyme activity, affect the permeability of oomycete cell membrane, and aggravate the oxidative damage of pathogen cells. Small molecule compounds such as diisobutyl phthalate and myxovirescin produced by myxobacteria can inhibit the formation of biofilm and lipoprotein of bacteria, and cystobactamids can inhibit the activity of DNA gyrase, thus changing the permeability of bacterial cell membrane. Myxobacteria, as a new natural compound resource bank, can control plant pathogenic fungi, oomycetes and bacteria by producing carbohydrate active enzymes and small molecular compounds, so it has great potential in plant disease control.]" The corrected sentence appears below: "[Myxobacteria have a complex life cycle and unique social behavior. They can prey on plant pathogenic fungi, bacteria, and oomycetes in the soil by producing some enzymes and small molecule compounds. The enzymes mainly include β-1,6-glucanase, β-1,3-glucanase, chitinase, protease, peptidase, and formaldehyde dismutase. β-1,6-glucanase, β-1,3-glucanase, and chitinase can degrade the glycosidic bonds in the cell wall of plant pathogen, causing some holes to form on the cell walls of the plant pathogen. Proteases and peptidases can break plant pathogenic cells into many small fragments and facilitate extracellular digestion of proteins during myxobacterial predation. Formaldehyde dismutase converts formaldehyde to formate and methanol, it can help myxobactria protect themselves in the process of predation. Small molecule substances produced by myxobacteria include isooctanol, di-isobutyl phthalate, myxovirescin, cystobactamid derivatives, hyalodione, argyrin derivatives, Methyl (2R)-2-azido-3-hydroxyl-2-methylpropanoate and N-(3-Amino-2-hydroxypropyl)-N-meth-ylsulfuric diamide, etc. Isooctanol destroyed the cell wall and cell membrane of plant pathogen, causing intracellular reactive oxygen species (ROS) to accumulate, leading to apoptosis and cell death. Di-isobutyl phthalate had biofilm inhibitory activity against bacteria. Myxovirescin could inhibit the incorporation of diamibopimelic acid and uridine diphosphate-N-acetylglucosamine intobacterial cell wall, and interfered with the polymerizaton of the lipid-disacchar-pentapeptide. Cystobactamid derivatives exerted their natural antibacterial properties by inhibition of bacterial gyrases. Hyalodione had broad antibacterial and antifungal activity. Argyrin derivatives inhibited protein synthesis by interfering with the binding of elongation factor G (EF-G) to ribosomes. Methyl (2R)-2-azido-3-hydroxyl-2-methylpropanoate and N-(3-Amino-2-hydroxypropyl)-N-meth-ylsulfuric diamide reduced the content of soluble proteins and the activity of protective enzymes (PPO, POD, PAL, and SOD) in plant pathogen, increased oxidative damage and cell membrane permeability. Myxobacteria, as a new natural compound resource bank, can control plant pathogenic fungi, oomycetes and bacteria by producing some enzymes and small molecule compounds, so it has great potential in plant disease control.]."

2. [There are two opinions on the species of myxobacteria, it is not yet certain which one is correct]. A correction has been made to [1 Introduction], [Paragraph 1].

This sentence previously stated: "[Myxobacteria are a type of deltaproteobacteria with rod-shaped vegetative cells (Velicer and Vos, 2009), which are well known for their complex life cycles and unique social behaviors. Myxobacteria have a wide range of life, and most of them live in soil, especially on land rich in microorganisms and organic matter. Recent studies have found that they can survive in high-salinity environments (Gemperlein et al., 2018). Research over the past few decades has proven that myxobacteria have become a resource library of new natural compounds, ranking second only to Actinomycetes and Bacillus among prokaryotes (Arguelles-Arias et al., 2009; Weissman and Müller, 2010). Metabolites produced by myxobacteria often have structures that other microbial metabolites do not have, and approximately 40% of myxobacterial metabolites have novel chemical structures. For example, in contrast to actinomycete derivatives, most small molecules of myxobacterial origin are not glycosylated (Rix et al., 2002). It iscurrently unclear why myxobacteria produce large amounts of metabolites, but researchers generally believe that metabolites play an important role in regulating cell–cell interactions within the colony (Davies et al., 2006) and in prey hunting (Xiao et al., 2011).]" The corrected sentence appears below: "[Myxobacteria are microorganisms of the phylum Myxococcota (Waite et al., 2020; Oren and Garrity, 2021), which are well known for their complex life cycles and unique social behaviors. Myxobacteria have a wide range of habitats, including soil rich in organic matter, rotting wood, animal dung and marine environment (Saggu et al., 2023). They can survive in high-salinity environments (Gemperlein et al., 2018). Some halophilic myxobacteria i.e., *Haliangium* spp. (Ryosuke et al., 2002), *Plesiocystis pacifica* (Iizuka et al., 2003a) and *Enhygromyxa salina* (Iizuka et al., 2003b) had been isolated from marine environment. Research over the past few decades has proven that myxobacteria have become a resource library of new natural compounds, ranking second only to *Actinomycetes* and *Bacillus* among prokaryotes (Arguelles-Arias et al., 2009; Weissman and Müller, 2010). Metabolites produced by myxobacteria often have structures that other microbial metabolites do not have, and ~40% of myxobacterial metabolites have novel chemical structures. For example, in contrast to *Actinomycetes* derivatives, most small molecules of myxobacteria are not glycosylated (Rix et al., 2002). It is currently unclear why myxobacteria produce large amounts of metabolites, but researchers generally believe that metabolites play an important role in regulating cell-to-cell interactions

within a population (Davies et al., 2006) and in prey hunting (Xiao et al., 2011).]"

3. A correction has been made to [1 Introduction], [Paragraph 2].

This sentence previously stated: "[Myxobacteria prey on plant pathogen and destroy pathogen's cell morphology and structure. The destroyed pathogenic cells are surrounded by many filamentous substances. The cell structure is loose and irregular, and the cell contents overflow, effectively lysing the pathogenic cells. Myxobacteria produce extracellular enzymes with carbohydrate-active enzymes (CAZymes), mainly glycosyltransferases (GTs), glycoside hydrolases (GHs), carbohydrate-binding modules (CBMs) and polysaccharide (PLs), etc. CAZymes can modify the glycosidic bonds of carbohydrates and are important basic functional units in carbohydrate metabolism pathways, while GHs can degrade the glycosidic bonds of peptidoglycan in the cell wall (Dong et al., 2023). When myxobacteria prey on prey, they can kill microorganisms and lyse cells by producing metabolites such as antibiotics, cell wall degrading enzymes, lipases, nucleases, polysaccharases, and proteases, thereby clearing biological macromolecules.]" The corrected sentence appears below: "[Myxobacteria can prey on plant pathogen and destroy pathogen's cell morphology and structure. When myxobacteria prey on pathogen, they can kill microorganisms and lyse cells by producing metabolites such as antibiotics, cell wall degrading enzymes, lipases, nucleases, polysaccharases, and proteases, thereby clearing the pathogens. The destroyed pathogenic cells are surrounded by many filamentous substances. The cell structure become loose and irregular, and the cell contents overflow, and eventually the pathogen lyse and die.]"

4. A correction has been made to [1 Introduction], [Paragraph 3].

This sentence previously stated: "[Myxobacteria are abundant in surface soils, but only a few studies have reported their role in agricultural soils. Myxobacteria are potential biocontrol agents. The application of biological control agents (BCAs) in agricultural planting can reduce the use of pesticides, reduce the adverse effects caused by excessive use of chemicals and achieve the purpose of controlling soil-borne plant diseases. BCAs are very effective in preventing and managing plant diseases, achieve ecological and economic benefits such as increasing agricultural output and reducing environmental pollution. Myxobacteria are potential BCAs, but their mode of action has been less studied at the molecular level. Their research can provide new potential ways for biological control of plant diseases and insect pests.]" The corrected sentence appears below: "[Therefore, myxobacteria can serve as biological control agents (BCAs) of plant diseases (Ye et al., 2020b). The BCAs in agricultural planting can reduce the use of pesticides, reduce the adverse effects caused by excessive use of chemicals and achieve the purpose of controlling soil-borne plant diseases. The BCAs are very effective in preventing and managing plant diseases and achieving ecological and economic benefits such as increasing agricultural output and reducing environmental pollution. Research on myxobacteria can provide new potential ways for biological control of plant diseases. This paper reviews the research progress on the active substances of myxobacteria against plant diseases and their action mechanisms.]"

5. A correction has been made to [2 Enzymes], [Paragraph 1].

This sentence previously stated: "[At present, the mechanism by which myxobacteria inhibit the growth of pathogenic bacteria has not been thoroughly studied. Some studies have only been conducted to the extent that myxobacteria inhibit the growth of plant pathogen. There is still great research value and space in the future. Research on the active enzymes of myxobacteria that prey on plant pathogens is mainly divided into three categories: β-1,6-glycosidase, β-1,3-glycosidase and chitinase. In addition, there are a few studies on Proteases, lipases and formaldehyde dismutase. Active enzymes produced by myxobacteria to control plant pathogens are shown in Figure 1 and Table 1.]" The corrected sentence appears below: "[Myxobacteria produce some enzymes playing important roles in preying on pathogens. These enzymes include carbohydrate-active enzymes (CAZymes), peptidases, lipases, etc. CAZymes include glycosyltransferases (GTs), glycoside hydrolases (GHs), carbohydrate esterases (CEs), auxiliary activities (AAs), carbohydrate-binding modules (CBMs), and polysaccharide lyases (PLs). CAZymes can modify the glycosidic bonds of carbohydrates and are important basic functional units in carbohydrate metabolism pathways (Dong et al., 2023). GHs hydrolyze glycosidic bonds and play an important role in the hydrolysis and synthesis of sugars and glycoconjugates in organisms (Kaushal and Singh, 2020). The enzymes produced by myxobacteria to control plant pathogens are shown in Figure 1 and Table 1.]"

6. A correction has been made to [2 Enzymes], [2.1 β-1,6-glucanase], [Paragraph 1].

This sentence previously stated: "[β-1,6-Glucan is a component of the fungal cell wall that is smaller than chitin and β-1,3-glucan and can cross-link cell wall proteins to the chitin layer and β-1, 3-Glucan layer. Inhibiting the synthesis of β-1,6-glucan is conducive to the effective disintegration and further degradation of the cell wall during the process of myxobacteria preying on plant pathogen. Coralococcus EGB-derived β-1,6-glucanase GluM is a novel family of outer membrane β-barrel proteins that can inhibit fungal embryonic tube development. β-1,6-Glucanase GluM preys on it is essential in the initial sensing and efficient decomposition of fungi and can also inhibit the growth of oomycetes.]" The corrected sentence appears below: "[β-1,6-glucan is a component of the fungal cell wall smaller than chitin and β-1,3-glucan. It can cross-link cell wall proteins to the chitin layer and β-1,3-glucan layer. Inhibiting the synthesis of β-1,6-glucan is conducive to the effective disintegration and further degradation of pathogen cell wall during the process of myxobacteria preying on plant pathogen. β-1,6-glucanase can hydrolyze the glycosidic bonds of β-1,6-glucan, thereby destroying the entire cell wall structure of fungi. β-1,6-glucanase GluM from the strain EGB of *Coralococcus* sp. is a novel family of outer membrane β-barrel proteins that can inhibit fungal embryonic tube development (Li et al., 2019b). β-1,6-glucanase GluM is

essential in the initial sensing and efficient decomposition of fungi.]"

7. A correction has been made to [2 Enzymes], [2.1 β-1,6-glucanase], [Paragraph 2].

   This sentence previously stated: "[Electron microscopy of the hyphae of Magnaporthe oryzae treated with β-1,6-glucanase GluM showed that the hyphae were stretched and partially broken, and the hyphal cell wall changed from a dense structure to a loose structure. The spore folds of the treated rice blast fungus were irregular, the density decreased, and the spore morphology showed a deformed state. The morphological and structural changes of M. oryzae are speculated to be due to the hydrolysis of the cell wall by β-1,6-glucanase GluM, resulting in incomplete cell structure and outflow of contents, ultimately leading to morphological changes. β-1,6-glucanase GluM limits the infection of rice by digesting the cell wall of M. oryzae (Zhou et al., 2019).]" The corrected sentence appears below: "[Electron microscopy observation of the hyphae of *Magnaporthe oryzae* treated with β-1,6-glucanase GluM showed that the hyphae were stretched and partially broken, and the hyphal cell wall changed from a dense structure to a loose structure. The spore folds of the treated *M. oryzae* were irregular. The density of spore decreased, and the morphology of spore showed a deformed state. The morphological and structural changes of *M. oryzae* were speculated to be due to the hydrolysis of the cell wall by β-1,6-glucanase GluM, resulting in incomplete cell structure and outflow of contents, ultimately leading to morphological changes. Therefore, β-1,6-glucanase GluM inhibited the infection of *M. oryzae* in rice by digesting the pathogen's cell wall (Zhou et al., 2019).]"

8. A correction has been made to [2 Enzymes], [2.1 β-1,6-glucanase], [Paragraph 3].

   This sentence previously stated: "[After GluM treated the hyphae and spores of F. oxysporumf. sp. cucumerinum (FOC), there was obvious shrinkage. The cell wall of FOC appears to be perforated and damaged, the structure is loose, and large vacuoles are formed in the cells. The high osmolarity glycerol (HOG) is activated, the phosphorylation level of Hog1-likemitogen-activated proteinkinase (MAPK) in FOC cells increases significantly, and the intracellular glycerol content increases 2.6 times. The osmotic pressure in FOC cells increased, which accelerated cell lysis. The cell wall integrity (CWI) initiates the transcription of genes related to the synthesis of cell wall components, chitin synthase genes (FOX-04163), chitinase genes (FOXG-19879, FOXG-19525, FOXG-12882), the transcript levels of β-glucanase gene (FOXG-03928) and β-glucan synthase gene (FOXG-03721) increased. The transcription levels of genes related to components corresponding to cell wall integrity (FOXG-09228), programmed cell death control protein (FOXG-03587) and cell division control protein (FOXG-00362) increased, slowing down the growth and division rate of cells and activating cell apoptosis. After inoculation of Coralococcus EGB into cucumbers, it can adapt well to the soil environment, effectively reduce the abundance of soil-borne F. oxysporum, and significantly reduce the occurrence of cucumber wilt disease (Ye et al., 2020b).]" The corrected sentence appears below: "[After treated with GluM, the hyphae and spores of *Fusarium oxysporum* f. sp. *cucumerinum* (FOC) shrank obviously. The cell wall of FOC appeared to be perforated and damaged, the cell wall structure was loose, and large vacuoles formed in the cells. The High Osmolarity Glycerol (HOG) in FOC cells was activated. The phosphorylation level of Hog1-likemitogen-activated proteinkinase (MAPK) was significantly increased and the glycerol content increased 2.6 times. The osmotic pressure in FOC cells increased, which accelerated cell lysis. When the strain EGB of *Corallococcus* sp. were inoculated with the potted cucumbers, the strain could adapt well to the soil environment and effectively reduced the abundance of soil-borne *F. oxysporum* and the occurrence of cucumber wilt disease (Ye et al., 2020b).]"

9. A correction has been made to [2 Enzymes], [2.1 β-1,6-glucanase], [Paragraph 4].

   This sentence previously stated: "[In the GluM transgenic experiment, the β-1,6-glucanase gene GluM was transferred into japonica rice ZH11 to obtain transgenic japonica rice with overexpression of GluM. In the fungal disease resistance experiment, the rice blast area of GluM transgenic rice was reduced by 82.7%, the sheath blight disease was reduced by 35.76–43.67%, and the incidence of rice smut disease was reduced by 65.79%. The results show that transgenic rice containing GluM protein can degrade fungal cell walls through specific hydrolysis and enhance resistance to fungal diseases (Shen et al., 2023).]" The corrected sentence appears below: "[In the *GluM* transgenic experiment, the β-1,6-glucanase gene was transferred into japonica rice variety ZH11 to obtain transgenic japonica rice with overexpression of *GluM*. In the fungal disease resistance experiment, the rice blast area of *GluM* transgenic rice was reduced by 82.7%. The sheath blight disease was reduced by 35.76%—43.67% and the incidence of rice smut disease was reduced by 65.79%. The results showed that transgenic rice containing GluM protein could degrade fungal cell walls through specific hydrolysis and enhanced resistance to fungal diseases (Shen et al., 2023).]"

10. A correction has been made to [2 Enzymes], [2.1 β-1,6-glucanase], [Paragraph 5].

    This sentence previously stated: "[The β-1,6-glucanase produced by myxobacteria not only inhibits the growth of fungal pathogens, but also plays a certain role in oomycetes. The fermentation product of Coralococcus coralliformis CMC0606 has a strong inhibitory effect on Phytophthora capsici, and the diameter of its inhibition zone is 16mm (Bader et al., 2022). Coralococcus EGB has a good inhibitory effect on the growth of P. capsici, which is mainly manifested by the collapse of mycelium and the growth is obviously inhibited. Preliminary research on the disease resistance mechanism of strain EGB suggests that there may be an antibacterial protein of β-1,6-glucanase in the extracellular fermentation supernatant of EGB (Zhang et al., 2023).]" The corrected sentence appears below: "[The β-1,6-glucanase produced by myxobacteria inhibits not only the growth of pathogenic fungus, but also the growth of oomycetes. The fermentation

products of *C. coralliformis* strain CMC0606 had a strong inhibitory effect on *Phytophthora capsici*, and the diameter of inhibition zone was 16 mm (Bader et al., 2022). The strain EGB had a strong inhibitory effect on the growth of *P. capsica*. The mycelium of *P. capsica* collapsed and the growth of the pathogen was obviously inhibited. The results showed that β-1,6-glucanase in the fermentation supernation of strain EGB was effective in inhibiting oomycetes (Zhang et al., 2023).]"

11. A correction has been made to [2 Enzymes], [2.2 β-1,3-glucanase], [Paragraph 1].

    This sentence previously stated: "[β-1,3-Glucan is the most abundant component of the fungal cell wall. Extensive hydrolysis of fungal cell wall polymer chains by β-1,3-glucanase can reduce the mechanical strength of the cell wall, leading to the final lysis of the fungal cell. β-1,3-glucanase IamC derived from Coralococcus EGB can cleave β-1,3- or β-1,6-glucan substrates by exo-hydrolysis and hydrolyze β by endo-hydrolysis.−1,4-glucan or xylan substrate is a type of glucanase with multifunctional activity. Cu2+, Co2+, Mg2+, and Cr3+ inhibit the activity of IamC, while Mn2+ is an effective activator of IamC, indicating that IamC is a metal ion-dependent hydrolase. After exposure of M. oryzae to IamC, the germ tube and appressorium formation rates were significantly reduced from 94 and 97% to 59 and 51%. The hyphae are enlarged and deformed, and more granular contents appear inside the hyphae. A large amount of reactive oxygen species (ROS) accumulation and changes in chitin distribution can be observed in the spores and hyphae of M. oryzae. The β-1,3-glucanase IamC derived from Coralococcus EGB acts on different β-glycosidic bonds in the cell wall of M. oryzae. It is hydrolyzed from different sites of cell wall polysaccharides to exert solubilization and antibacterial activity against M. oryzae (Zhou et al., 2019).]" The corrected sentence appears below: "[β-1,3-glucan is a component of the fungal cell wall. Extensive hydrolysis of fungal cell wall polymer chains by β-1,3-glucanase can reduce the mechanical strength of the cell wall, leading to the final lysis of the fungal cell. β-1,3-glucanase IamC from strain EGB can cleave β-1,3- or β-1,6-glucan substrates by exo-hydrolysis. Cu^{2+}, Co^{2+}, Mg^{2+}, and Cr^{3+} inhibit the activity of IamC, while Mn^{2+} is an effective activator of IamC, indicating that IamC is a metal ion-dependent hydrolase. After exposure of *M. oryzae* to IamC, the germ tube and appressorium formation rates were significantly reduced from 94 and 97% to 59 and 51%. The hyphae of *M. oryzae* was enlarged and deformed, and more granular contents appeared inside the hyphae. There was a large accumulation of reactive oxygen species (ROS) in the spores and hyphae of *M. oryzae* and the distribution of chitin in the cell wall of pathogen changed. The β-1,3-glucanase IamC derived from strain EGB acted on different β-glycosidic bonds in the cell wall of *M. oryzae*. β-glycosidic bonds of polysaccharides from different sites of cell wall of pathogen were hydrolyzed, ultimately leading to cell lysis of *M. oryzae* (Zhou et al., 2019).]"

12. A correction has been made to [2 Enzymes], [2.2 β-1,3-glucanase], [Paragraph 2].

    This sentence previously stated: "[Archangium AC19 showed strong predatory activity against Phytophthora sojae P6497 and protected soybeans from stem rot. Strain AC19 was observed to prey on P. sojae, and the hyphal cell wall of P. sojae P6497 showed perforation. The results of the indoor biological control test of strain AC19 showed that strain AC19 showed significant biological control effect on soybean hypocotyls, and the supernatant significantly reduced the growth of P. sojae and inhibited infection. Experimental results show that strain AC19 is a myxobacteria that can secrete CAZymes that inhibit P. sojae. The active substance that preys on and digests P. sojae is a cell wall hydrolase. The cell wall-acting CAZymes in strain AC19 are specialized β-1,3-glucanases (AcGlu13.1, −13.2, and−13.3) that target β-1,3-glucans from Phytophthora spp. AcGlu13.1 causes cell wall surface shedding, showing degradative activity. AcGlu13.2 and AcGlu13.3 can cause perforated structures in the cell wall (Zhang et al., 2023).]" The corrected sentence appears below: "[*Archangium* strain AC19 showed strong predatory activity against *Phytophthora sojae* P6497 and protected soybeans from stem rot disease. Strain AC19 was observed to prey on *P. sojae*, and the hyphal cell wall of *P. sojae* P6497 showed perforation. The fermentation supernatant of strain AC19 significantly inhibited the growth and infection of *P. sojae*. The active substances that digested *P. sojae* were the CAZymes secreted by strain AC19. The cell wall-acting CAZymes in strain AC19 were specialized β-1,3-glucanases (AcGlu13.1,−13.2, and−13.3). These β-1,3-glucanases targeted β-1,3-glucan from the cell wall of *Phytophthora*. AcGlu13.1 caused cell wall surface shedding through its degradative activity. AcGlu13.2 and AcGlu13.3 could cause perforated structures in the cell wall (Zhang et al., 2023).]"

13. A correction has been made to [2 Enzymes], [2.3 Chitinase], [Paragraph 1].

    This sentence previously stated: "[β-1,6-glucan, and chitin accounts for 22–40% of the fungal cell wall (Bowman and Free, 2006). Chitinase can hydrolyze chitin in fungal cell walls, so chitinase is regarded as an antifungal factor for biocontrol of fungal diseases and has great potential in the enzymatic synthesis and hydrolysis of chitin (Shehata et al., 2018). Coraliococcus EGB can synthesize the endochitinase CcCti1, which belongs to the glycoside hydrolase family 18 (GH18) and has potential antifungal activity. CcCti1 can not only degrade chitosan oligosaccharide, but also hydrolyze chitin into N-acetylated chitohexaose (GlcNAc)6. CcCti1 has biological control activity against the plant pathogen Magnaporthe oryzae, inhibiting the germination of conidia and the formation of appressoria of M. oryzae at a concentration of 0.08 mg/mL (Li et al., 2019a). Rice blast caused by M. oryzae is the main limiting factor in global rice production and one of the most destructive diseases in cultivated rice in the world (Talbot, 2003). Experiments on resistance to rice blast fungus have shown that transgenic plants with chitinase genes show strong resistance to rice blast. The reason may be that fungi have significant internal expansion pressure, and slight changes in cell wall integrity

can cause lysis of fungal cells (Selitrennikoff, 2001). Therefore, transgenic plants with chitinase genes are more resistant to the rice blast fungus.]" The corrected sentence appears below: "[The fungal cell wall is mainly composed of chitin, β-1,3-glucan and β-1,6-glucan. The chitin accounts for 22%−40% of the fungal cell wall (Bowman and Free, 2006). Chitinase of GHs family can hydrolyze chitin in fungal cell walls, so chitinase is regarded as an antifungal factor for biocontrol of fungal diseases (Shehata et al., 2018; Li et al., 2019a). Strain EGB can synthesize the endo-chitinase CcCti1 which belongs to the GHs family 18 (GH18) and has potential antifungal activity. CcCti1 can not only degrade chitosan oligosaccharide, but also hydrolyze chitin into N-acetylated chitohexaose (GlcNAc)6. CcCti1 had biological control activity against the plant pathogen *M. oryzae*, inhibiting the germination of conidia and the formation of appressoria of *M. oryzae* at a concentration of 0.08 mg/mL (Li et al., 2019a). Rice blast caused by *M. oryzae* is the main limiting factor in global rice production and is one of the most destructive diseases in cultivated rice in the world (Talbot, 2003). The transgenic plants with chitinase genes showed strong resistance to rice blast. The reason may be that the cell wall integrity of pathogen changed, leading to significant internal expansion pressure and lysis of fungal cells (Selitrennikoff, 2001). Therefore, transgenic plants with chitinase genes were more resistant to the *M. oryzae*.]"

14. A correction has been made to [2 Enzymes], [2.4 Proteases and peptidases], [Paragraph 1].

    This sentence previously stated: "[Tomato bacterial wilt (TBW) caused by Ralstonia solanacearum is one of the most destructive soil-borne diseases, and tomato production has suffered huge losses due to the epidemic of TBW (Mansfield et al., 2012). M. xanthus R31 has good biological control potential against TBW, and the biocontrol efficiency against TBW in pot experiments was as high as 81.9%. In the experiment of preying on R. solanacearum, M. xanthus GDMCC801043 appeared to prey on the bacteria on the third day. In a pot experiment on biological control of R. solanacearum, the incidence rate dropped to 38.8%, the disease index dropped to 18.0%, and the biocontrol efficiency reached 81.9%. When strain CDMCC80143 preyed on R. solanacearum, the morphology of R. solanacearum changed significantly, and the cells were broken into many small fragments. Myxobacteria secrete a large amount of filamentous extracellular substances that surround R. solanacearum. Experiments have shown that the extracellular substances may be proteases, cellulases and lipases.]" The corrected sentence appears below: "[Tomato bacterial wilt (TBW) caused by *Ralstonia solanacearum* is one of the most destructive soil-borne diseases, and tomato production has suffered huge losses due to the epidemic of TBW (Mansfield et al., 2012). *M. xanthus* R31 had good biological control potential against TBW, and the biocontrol efficiency against TBW in pot experiments was as high as 81.9%. The MEROPS database of strain R31 genome had annotated 274 proteins, including 132 metalloproteases and 107 serine proteases. Three M36 metalloproteases were identified in the R31 genome that may contribute to the extracellular digestion of proteins during predatory behavior (Dong et al., 2023). Proteins of the M23 family were endopeptidases that cleaved bacterial cell wall peptidoglycan by degrading the peptide bonds of cross-linked peptides (Odintsov et al., 2004). Proteases and peptidases, such as the M36 metalloprotease MepA secreted by *M. xanthus* strain DK1622, may promote the predation of prey by degrading proteins of prey cells (Berleman et al., 2014).]"

15. A correction has been made to [2 Enzymes], [2.5 Formaldehyde dismutase], [Paragraph 1].

    This sentence previously stated: "[When Pseudomonas aeruginosa is captured, it secretes toxic formaldehyde to resist predation and produces formaldehyde detoxifying enzymes, such as formaldehyde dismutase (Fdm). Therefore, myxobacteria that have the ability to prey on P. aeruginosawill also protect themselves by producing Fdm to achieve the purpose of preying on P. aeruginosa.]" The corrected sentence appears below: "[When *Pseudomonas aeruginosa* was preyed on, it secreted toxic formaldehyde to resist predation. Fomaldehyde can be converted into formate and methanol by formaldehyde detoxifying enzymes, such as formaldehyde dismutase (Fdm), produced by *P. aeruginosa* to protect itself (Willsey et al., 2016). It was shown that myxobacteria could produce formaldehyde dismutase. Therefore, myxobacteria had the ability to prey on *P. aeruginosa* by converting toxic formaldehyde secreted by *P. aeruginosa* into non-toxic substances (Sutton et al., 2019). Myxobacteria may also be able to prey on similar plant pathogens by a similar way.]"

16. A correction has been made to [3 Small molecule compounds], [2.5 Formaldehyde dismutase], [Paragraph 1].

    This sentence previously stated: "[The biological control activity of myxobacteria against pathogenic bacteria is not only active extracellular protease, but also produce volatile compounds (VOCs). These substances include isooctanol, diisobutyl phthalate, mucin, cystobactamide analogues, coral A, hyalurondione, protosin A, methyl (2R)-2-azido-3-hydroxyl-2-methylpropanoate and N-(3-amino-2-hydroxypropyl)-N-meth-ylsulfuric diamide. Small molecule compounds produced by myxobacteria to control plant pathogens are shown in Figure 1 and Table 1.]" The corrected sentence appears below: "[The biological control activity of myxobacteria against pathogen depends on not only enzymes, but also some small molecule compounds. These compounds include isooctanol, di-isobutyl phthalate, myxovirescin, cystobactamid derivatives, hyalodione, argyrin derivatives, Methyl (2R)-2-azido-3-hydroxyl-2-methylpropanoate, and N-(3-Amino-2-hydroxypropyl)-N-meth-ylsulfuric diamide, etc. Some small molecule compounds produced by myxobacteria to control plant pathogens are shown in Figure 1 and Table 1.]"

17. A correction has been made to [3 Small molecule compounds], [3.1 Isooctanol], [Paragraph 1].

    This sentence previously stated: "[Coraliococcus EGB exhibits superior biological control activity against F. oxysporum. F. oxysporum is a ubiquitous soil-borne plant pathogen that can cause vascular wilt in a variety of crops (Pietro et al., 2003). A total of 32 volatile compounds produced by strain EGB were identified, and isooctanol had the highest

antifungal activity. Isooctanol destroys the cell wall and cell membrane of F. oxysporum, causing intracellular reactive oxygen species (ROS) to accumulate, leading to apoptosis and cell death. A dose of only 3.75μL/plate of isooctanol is sufficient to inhibit F. oxysporum. VOCs are also suitable for controlling plant pathogens during the postharvest storage stage because VOCs are biodegradable and have no toxic residues on the product surface (Ye et al., 2020a).]" The corrected sentence appears below: "[Strain EGB exhibited superior biological control activity against *F. oxysporum. F. oxysporum* is a ubiquitous soil-borne plant pathogen that can cause vascular wilt in a variety of crops (Pietro et al., 2003). A total of 32 volatile compounds produced by strain EGB were identified, and isooctanol had the highest antifungal activity. The mycelia of *F. oxysporum* treated with isooctanol showed severely shrinkage and collapse. The hyphae of *F. oxysporum* treated by isooctanol, the transcript levels of many genes related to the cell wall integrity (CWI) pathway and redox reactions were significantly increased by 15-to 40-fold. The transcription levels of chitin synthase (FOXG_12345, FOXG_10443 and FOXG_04179), chitinase (FOXG_19879 and FOXG_17332), endo-1,3 (4)-β-glucanase (FOXG_22849, FOXG_10637 and FOXG_03928) were upregulated after the mycelia of *F. oxysporum* were treated with isooctanol. The transcription levels of genes related to components corresponding to cell wall integrity (FOXG_09228), programmed cell death control protein (FOXG_03587) and cell division control protein (FOXG_00362) increased, slowing down the growth and division rate of cells, and activating cell apoptosis. Isooctanol destroyed the cell wall and cell membrane of *F. oxysporum*, causing intracellular reactive oxygen species (ROS) to accumulate, leading to apoptosis and cell death. A dose of only 3.75 μL/plate of isooctanol was sufficient to inhibit *F. oxysporum* (Ye et al., 2020a).]"

18. A correction has been made to [3 Small molecule compounds], [3.2 Isooctanol], [Paragraph 1].

    This sentence previously stated: "[Myxobacterium strain ST/P/71 has obvious antibacterial activity against Bacillus subtilis, and the ST/P/71 extract shows inhibition against B. subtilis. The secondary metabolites of strain ST/P/71 were separated and purified, and two pure compounds were obtained at RT54.24 (Ra2) and RT71.27 (Ra3). Ra2 was identified as diisobutyl phthalate. This substance shows biofilm formation inhibitory activity against B. subtilis, with an MBIC50 of 2.702μg/mL. Currently, there are few studies on myxobacteria inhibiting bacterial biofilm formation (Sharma et al., 2021).]" The corrected sentence appears below: "[*M. fulvus* strain ST/P/71 had obvious antibacterial activity against *B. subtilis*, and the extract from the strain ST/P/71 mainly showed inhibition activity against *B. subtilis*. During seperating by Reverse Phase High Performance Liquid Chromatography (RP-HPLC), two pure compounds were eluted at RT 54.24 (Ra2) and RT 71.27 (Ra3). Ra2 was identified as di-isobutyl phthalate. This substance showed biofilm formation inhibitory activity against *B. subtilis*, with an $MBIC_{50}$ of 2.703 μg/mL (Sharma et al., 2021). Di-isobutyl phthalate had biofilm formation inhibitory activity against *B. subtilis*, so it could have similar functions to plant pathogenic bacteria. Therefore, di-isobutyl phthalate may have great potential in the prevention and control of plant pathogenic bacteria.]"

19. A correction has been made to [3 Small molecule compounds], [3.2 Isooctanol], [Paragraph 2], delete the paragraph.

20. A correction has been made to [3 Small molecule compounds], [3.3 Myxovirescin], [Paragraph 1].

    This sentence previously stated: "[Bacterial biofilms protect microbial communities from predation, and B. subtilis biofilm formation is triggered by thiopeptide antibiotics. Soil bacteria interact with each other in a competitive and cooperative manner. Most bacteria tested under laboratory conditions are unable to resist Myxococcus xanthus, but Bacillus subtilis NCIB3610 (Zeigler et al., 2008) can temporarily resist the predation of M. xanthus. This short-term protection Special metabolite protection is required (Müller et al., 2014). One of the 18 metabolites of M. xanthus DK1622 is mucin, which has antibacterial activity and can inhibit the production of lipoproteins to meet the needs of preying on bacteria (Xiao et al., 2011).]" The corrected sentence appears below: "[One of the 18 metabolites of *M. xanthus* strain DK1622 is polyketide myxovirescin (antibiotic TA), which had antibacterial activity. Myxovirescin played an important role in killing *Escherichia coli*, including lysis and subsequent predation (Xiao et al., 2011). The antibiotic TA was produced and named after *M. vanthits* strain TA(ATCC31046) (Rosenberg et al., 1982). The antibiotic TA could inhibit the incorporation of diamibopimelic acid and uridine diphosphate-N-acetylglucosamine into *E. coli* cell wall, and antibiotic TA interfered with the polymerizaton of the lipid-disacchar-pentapeptide (Rosenberg et al., 1982; Paitan et al., 1999). Myxobacteria encode a variety of substances to attack prey cells, with antibiotics serving as a front line weapon. Antibiotics can act as small molecule weapons to penetrate and kill or neutralize the metabolism of prey. The prevention and control principle of myxovirescin against bacterial pathogens has been relatively clear. This substance can be applied to research on prevention and control of plant pathogenic bacteria.]"

21. A correction has been made to [3 Small molecule compounds], [3.4 Cystobactamid derivatives], [Paragraph 1].

    Divide "[Myxobacteria produce specialized metabolites when antimicrobial and exhibit cooperative, swarming predatory strategies, and the production of specialized metabolites and lytic proteins of myxobacteria is related to their predation (Akbar and Stevens, 2021). During the biological screening process of new myxobacterial extracts, substances that inhibit Pseudomonas aeruginosa were obtained. The target compound has a UV absorption spectrum similar to cystobactamide (Hüttel et al., 2017). Seven new coralmycin derivatives and three known compounds were isolated from the culture of C. coralline M23. The coralmycin derivatives are C (1), D (2), E (3), and F (4), G (5), H (6) and I (7), the known compounds are cystobactamide 891-2 (8), 905-2 (9), and 507 (10). Based on the structure–activity relationship of the antibacterial and DNA gyrase inhibitory activities of the obtained compound, the principle

of its action in inhibiting Pseudomonas was analyzed. The structure of p-nitrobenzoic acid is crucial for inhibiting DNA gyrase and the growth of bacteria, while the nitro part of p-nitrobenzoic acid and the C-4 position of the nitro part of the isopropyl chain are important for certain Gram-negative bacteria. The permeability of bacteria (e.g., Pseudomonas aeruginosa, Klebsiella pneumoniae) is of great significance. The β-methoxyasparagine structure may affect bacterial cellular prey uptake (Kim et al., 2019). Another culture isolation of strain M23 also yielded coralmycin A (1), B (2) and another derivative, cystobactin 919-2. Coralmycin A has the strongest antibacterial activity against Gram-negative bacteria and has a wide antibacterial spectrum. Research data shows that the hydroxyl groups of the β-methoxyasparagine unit and the benzoic acid unit are extremely important for antibacterial activity (Kim et al., 2016).]" into 2 paragraphs, the first paragraph is "[Myxobacteria produce specialized metabolites when preying, the production of specialized metabolites and lytic proteins of myxobacteria is related to their predation (Akbar and Stevens, 2021). Müller et al. found that the target compound inhibiting *P. aeruginosa* and other bacterial pathogens had a UV absorption spectrum similar to that of cystobactamides. Cystobacamids are aromatic oligoamides that exert their natural antibacterial properties by inhibition of bacterial gyrases (Solga et al., 2024). The improved orthogonally functionalized methoxyaspartate of cystobactamides could expand the synthesis of new cystobactamides. At present, four new types of cystobactamides 919-1 (1), 919-2 (2), 920-1 (3), 920-2 (4) and cystobactamides 861-2 (5) had been successfully synthesized and measured. Moller et al. (2019) compared the antibacterial properties of this class of substanaces, the cyano derivative of cystobactamide 861-2(5) had antimicrobial activity against Gram-negative bacteria and its activity was higher than that of any natural cystobactamide tested so far.]." The second paragraph is "[Culture isolation of *C. coralline* strain M23 yielded coralmycin A (1), B (2) and another derivative, cystobactin 919-2. Coralmycin A had the strongest antibacterial activity against Gram-negative bacteria and had a wide antibacterial spectrum. Coralmycin A and B were cystobactamid derivatives (Kim et al., 2016). Seven new coralmycin derivatives and three known compounds were also isolated from the another culture of strain M23. The coralmycin derivatives are C (1), D (2), E (3), F (4), G (5), H (6), and I (7), the known compounds are cystobactamide 891-2(8), 905-2(9), and 507(10). The compounds had DNA gyrase inhibitory activity and antibacterial activity. The β-methoxyasparagine structure of coralmycin may affect prey ingestion (Kim et al., 2019). Research on the structure of cystobactamides can be used to develop new structural substances with more antibacterial activity. Therefore, this type of substances may also have great potential in the prevention and control of Gram-negative plant pathogenic bacteria.]"

22. A correction has been made to [3 Small molecule compounds], [3.5 Hyalodione], [Paragraph 1].

    This sentence previously stated: "[Myxobacteria isolated from Indian soil samples, the extracts of Coralococcus parvum S104 and S145 showed broad-spectrum antibacterial activity. The WE and DE of GNDU172 showed obvious activity against B. subtilis, and the DE of strain S213 and strain S223 showed similar activity. Antibacterial activity spectrum, active against Pseudomonas syringae, while DE of S223 has strong activity against B. cereus (Kumar et al., 2017). Hyalodione was isolated from the extract of the myxobacterium hyalangiumminutum NOCB-2T and has antibacterial activity against Pseudomonas aeruginosa with a MIC value of 8.5μg/mL (Okanya et al., 2012).]" The corrected sentence appears below: "[Hyalodione isolated from the extract of the *Hyalangium minutum* strain NOCB-2T had antibacterial activity against *P. aeruginosa*. Hyalodione is a novel S-methyl cyclohexadiene-dione, which belongs to the class qinone (Herrmann et al., 2017). Hyaladione had broad antibacterial and antifungal activity. The tested strains included *P. aeruginosa*, *Rhodotorula glutarum* and *Staphylococcus aureus* (Okanya et al., 2012). Research on how hyalodione control bacteria and fungi need to be continued. Hyalodione also has great potential in controlling plant pathogenic bacteria and fungi.]"

23. A correction has been made to [3 Small molecule compounds], [3.6 Argyrin derivatives], [Paragraph 1]. This sentence previously stated: "[The culture medium of Archangiumgephyra strains contains a group of cyclic peptides composed of 8 amino acid residues, namely protocystins A-H, which exhibit good antibiotic effects against Pseudomonas aeruginosa (Stauch et al., 2010). Among them, protocystin A combines with elongation factor G (EF-G) as its target. Several derivatives of protocystin A can be obtained by modifying the methoxytryptophan residue, and the methoxy group is located the antibacterial activity will be lost if the position is replaced by other substituents (Siebert et al., 2019).]" The corrected sentence appears below: "[The culture medium of the strains of *Archangium gephyra* contained a group of cyclic peptides composed of naturally produced octapeptides, which exhibited strong antibiotic effects against *P. aeruginosa* (Nickeleit et al., 2008; Stauch et al., 2010; Wieland et al., 2022). Among them, argyrin participates in the non-ribosomal peptide synthetase pathway, combining with elongation factor G (EF-G) as its target (Pogorevc et al., 2019). Argyrins inhibit protein synthesis by interfering with EF-G binding to the ribosome (Wieland et al., 2022). Several derivatives of argyrin A could be obtained by modifying the methoxytry ptophan residue. The methoxy group of this residue was crucial for its antibacterial activity and its activity will be lost if the position is replaced by other substituents (Siebert et al., 2019). Argyrin has antibacterial activity against bacteria, so there is great practical value to study its antibacterial activity against plant pathogenic bacteria.]"

24. A correction has been made to [3 Small molecule compounds], [3.7 Methyl (2R)-2-azido-3-hydroxyl-2-methylpropanoate and N-(3-Amino-2-hydroxypropyl)-N-meth-ylsulfuric diamide.], [Paragraph 1].

    This sentence previously stated: "[83% of the myxobacteria had antibacterial activity against P. infestans, among which Myxococcus and Coralococcus had a higher antibacterial proportion. The strains with the most significant antibacterial activity of the isolated myxobacteria were M. xanthusB25-I-1, Myxococcus fulvus B25-I-3 and Myxococcus stipitatus

X6-II-1. M. xanthus B25-I-1 exhibits antagonistic activity against a variety of fungi and bacteria, and its active extract reduces the content of soluble proteins and the activity of protective enzymes (PPO, POD, PAL and SOD) in P. infestans, Increased oxidative damage and cell membrane permeability. It has a strong inhibitory effect on the hyphae, asexual reproduction and sexual reproduction of P. infestans (Wu, 2018). The active substance of M. fulvus B25-I-3 shows a strong inhibitory effect on the growth of P. infestans, inhibits the growth of mycelium and other asexual reproduction, and reduces the reinfection ability of pathogenic bacteria (Wu, 2018; Wu Z. et al., 2021; Wu Z. H. et al., 2021). After the fermentation products of B25-I-1 and B25-I-3 were separated, it was found that the components that had antagonistic effects on P. infestanscontained methyl (2R)-2-azido-3-hydroxyl-2-methylpropanoate and N- (3-amino-2-hydroxypropyl)-N-meth-ylsulfuricdiamide.]" The corrected sentence appears below: "[Eighty-three percent of the myxobacterial strains were resistant to *P. infestans*, among which the strains of *Myxococcus* and *Coralococcus* accounted for a higher proportion. The strains with the most significant antibacterial activity were *M. xanthus* B25-I-1, *M. fulvus* B25-I-3 and *M. stipitatus* X6-II-1. Strain B25-I-1 exhibited antagonistic activity against a variety of fungi and bacteria, and its active substances reduced the content of soluble proteins and the activity of protective enzymes (PPO, POD, PAL, and SOD) in *P. infestans*, increased oxidative damage and cell membrane permeability. It had a strong inhibitory effect on the hyphae, asexual reproduction and sexual reproduction of *P. infestans* (Wu, 2018). The active substance of strain B25-I-3 showed a strong inhibitory effect on the growth of *P. infestans*, inhibited the growth of mycelium and asexual reproduction, and reduced the infection ability of pathogens (Wu, 2018; Wu Z. et al., 2021; Wu Z. H. et al., 2021). After the fermentation products of B25-I-1 and B25-I-3 were separated, it was found that the components that had antagonistic effects on *P. infestans* contained Methyl(2R)-2-azido-3-hydroxyl-2-methylpropanoate and N- (3-Amino-2-hydroxypropyl)-N-meth-ylsulfuricdiamide.]"

25. A correction has been made to [3 Small molecule compounds], [3.7 Methyl (2R)-2-azido-3-hydroxyl-2-methylpropanoate and N-(3-Amino-2-hydroxypropyl)-N-meth-ylsulfuric diamide.], deleted the second paragraph. The second paragraph has little connect with [3.7 Methyl (2R)-2-azido-3-hydroxyl-2-methylpropanoate and N-(3-Amino-2-hydroxypropyl)-N-meth-ylsulfuric diamide.]
26. [Some substance that cannot be determined is defined as somes unknown substanes].

    A correction has been made to [3 Small molecule compounds], [3.8 Some unknown substances], [Paragraph 1].

    The corrected sentence appears below: "[*P. infestans* causes devastating diseases by invading the leaves, stems and tubers of potato plants (Berleman and Kirby, 2009). *M. xanthus* YR-7 isolated from soil samples in Bayannur area of Inner Mongolia had significant resistance to *P. infestans*. The growth inhibition rate of strain YR-7 against *P. infestans* hyphae was as high as 96.67%. The fermentation product of YR-7 was tested in isolated leaves. The experimental results proved that the active substance against *P. infestans* is a non-protein substance (Ren et al., 2016). About 72% of the myxobacteria isolated from soil samples in Ordos and Wuhai areas of Inner Mongolia had varying degrees of antagonistic effects on the growth of *P. infestans*. The ones with stronger ability to inhibit oomycetes were *C. exiguous* E10, *M. fallax* E11 and *C. coralloides* E12. The diameters of the inhibition zones were 26 mm, 24 mm and 24 mm (Ding, 2017; Wu, 2018). About 78.75% of the myxobacteria isolated from soil samples in Alxa area of Inner Mongolia had varying degrees of activity against *P. infestans*. The resistance of *Myxococcus fulvus* AL-24 and *Anqiococcu* AL-10 was outstanding. The fermentation products of strain AL-24 and strain AL-10 had good infection prevention activity and weak infection treatment activity on detached potato leaves (Zhao, 2018). Myxobacteria isolated from Indian soil samples, the extracts of *Coralococcus parvum* S104 and S145 showed broad-spectrum antibacterial activity. The water extract (WE) and DMSO extract (DE) of GNDU172 showed obvious activity against *B. subtilis*, and the DE of strain S213 and strain S223 showed similar activity. The DE of S223 has activity against *Pseudomonas syringae* and *B. cereus* (Kumar et al., 2017). However, all of these active substances are unknow and need to be seperated and identified in the future.]"
27. A correction has been made to [4 Discussion], [Paragraph 1].

    [Delete the last sentence of the first paragraph.]
28. A correction has been made to [4 Discussion], [Paragraph 2].

    This sentence previously stated: "[One is to degrade the cell wall or increase the permeability of the cell membrane through antibacterial metabolites and cell wall degrading enzymes; the other one is a targeted, contact-dependent killing mechanism through the Tad-like system and protein secretion system.]" The corrected sentence appears below: "[One method is to degrade the cell wall or increase the permeability of the cell membrane through antibacterial metabolites and cell wall degrading enzymes. The other one is a targeted, contact-dependent killing mechanism through the Tad-like system and protein secretion system (Thiery et al., 2022). The Tad-like system mediates the contact-dependent killing of myxobacteria on prey cells (Seef et al., 2021).]"
29. A correction has been made to [4 Discussion], [Paragraph 3].

    This sentence previously stated: "[During the interaction between myxobacteria and prey cells, antibiotics, lytic enzymes, hydrolases, etc. may be involved in the process. This review summarizes the prevention and control principles of myxobacteria in plant pathogenic fungi, oomycetes, and bacterial disasters, which can be divided into two categories (Table 1). Myxobacteria secrete carbohydrate-active enzymes that can degrade cell wall components and degrade the components of the cell wall. Myxobacteria produce small molecule compounds that enter the cells of pathogens and inhibit the normal growth and proliferation of pathogens. The CAZymes secreted by myxobacteria are mainly chitinase, β-1,6-glucanase and β-1,3-glucanase, which increase intracellular osmotic pressure by degrading the cell wall of prey cells, promote cell lysis and death. Small molecule compounds produced by myxobacterial fermentation enter prey cells,

affecting their normal growth and reproduction or changing their permeability, thereby inducing apoptosis of prey cells.]" The corrected sentence appears below: "[During the interaction between myxobacteria and prey cells, antibiotics, lytic enzymes, hydrolases, etc. involved in the process. This review summarizes the prevention and control principles of myxobacteria in plant pathogenic fungi, oomycetes, and bacterial disasters (Table 1). Myxobacteria secrete enzymes that can degrade cell wall components. Myxobacteria produce small molecule compounds that inhibit the normal growth and proliferation of pathogens. The enzymes secreted by myxobacteria are mainly chitinase, β-1,6-glucanase and β-1,3-glucanase, etc, which increase intracellular osmotic pressure by degrading the cell wall of prey cells, promoting cell lysis and death. Some small molecule compounds produced by myxobacteria affect the normal growth and reproduction of prey cells or changing their permeability, thereby inducing apoptosis of prey cells.]"

30. A correction has been made to [4 Discussion], [Paragraph 4].

This sentence previously stated: "[In the process of preventing and controlling plant diseases with myxobacteria, it is possible to develop a certain biological control agent that inhibits pathogens efficiently, quickly and targetedly, reducing the cost increase and environmental pollution caused by excessive use of pesticides, and maximizing economic and environmental benefits.]" The corrected sentence appears below: "[In the process of preventing and controlling plant diseases, it is possible to use myxobacteria to develop a certain BCAs that inhibits pathogens efficiently, which will be helpful to reduce the cost increase and environmental pollution caused by excessive use of pesticides, and maximize economic and environmental benefits.]"

31. A correction has been made to [4 Discussion], [Paragraph 5].

This sentence previously stated: "[For example, myxobacteria-mediated nanosilver ion paper is used in fruit packaging to extend the shelf life to 15days (Bhople et al., 2016).]" The corrected sentence appears below: "[For example, myxobacteria-mediated paper impregnated with silver nanoparticles (AgNPs) is used in fruit packaging to extend the shelf life to 15 days (Bhople et al., 2016).]"

In the published article, there was an error in the name of Section. Instead of "*[2 Active enzymes]*," it should be "*[2 Enzymes]*."

In the published article, there was four errors in the name of Sub-Section. Instead of "*[2.4 Proteases and lipases]*," it should be "*[2.4 Proteases and peptidases]*." Instead of "*[3.3 Mucin]*," it should be "*[3.3 Myxovirescin]*." Instead of "*[3.4 Cystobactamide analogues and coralmycin A]*," it should be "*[3.4 Cystobactamid derivatives]*." Instead of "*[3.6 Protocystin A*,]" it should be "*[3.6 Argyrin derivatives]*."

In the published article [3.8 Some unknown substances] was not listed in the article.

In the published article, the following 4 citations were deleted in the article, [Müller, S., Strack, S. N., Hoefler, B. C., Straight, P. D., Kearns, D. B., Kirby, J. R., et al. (2014). Bacillaene and sporulation protect Bacillus subtilis from predation by Myxococcus xanthus. Appl. Environ. Microbiol. 80, 5603–5610. doi: 10.1128/aem.01621-14], [Tomura, T., Nagashima, S., Yamazaki, S., Iizuka, T., Fudou, R., and Ojika, M. (2017). An unusual diterpene—enhygromic acid and deoxyenhygrolides from a marine myxobacterium, Enhygromyxa sp. Mar. Drugs 15:109. doi: 10.3390/md15040109], [Velicer, G. J., and Vos, M. (2009). Sociobiology of the myxobacteria. Annu. Rev. Microbiol. 63, 599–623. doi: 10.1146/annurev.micro.091208.073158], [Zeigler, D. R., Pragai, Z. N., Rodriguez, S., Chevreux, B., Muffler, A., Albert, T., et al. (2008). The origins of 168, W23, and other Bacillus subtilis legacy strains. J. Bacteriol.190, 6983–6995. doi: 10.1128/jb.00722-08.]

The authors apologize for these errors and state that this does not change the scientific conclusions of the article in any way. The original article has been updated.

Publisher's note

References

Akbar, S., and Stevens, D. C. (2021). Functional genomics study of *Pseudomonas putida* to determine traits associated with avoidance of a myxobacterial predator. *Sci. Rep.* 11:16445. doi: 10.1038/s41598-021-96046-8

Arguelles-Arias, A., Ongena, M., Halimi, B., Lara, Y., Brans, A., Joris, B., et al. (2009). *Bacillus amyloliquefaciens* GA1 as a source of potent antibiotics and other secondary metabolites for biocontrol of plant pathogens. *Microb. Cell Factories* 8:63. doi: 10.1186/1475-2859-8-63

Bader, C. D., Panter, F., Garcia, R., Tchesnokov, E. P., Haid, S., Walt, C., et al. (2022). Sandacrabins - structurally unique antiviral RNA polymerase inhibitors from a rare myxobacterium. *Chem. Eur. J.* 28:e202104484. doi: 10.1002/chem.202104484

Berleman, J. E., Allen, S., Danielewicz, M. A., Remis, J. P., Gorur, A., Cunha, J., et al. (2014). The lethal cargo of *Myxococcus xanthus* outer membrane vesicles. *Front. Microbiol.* 5:474. doi: 10.3389/fmicb.2014.00474

Berleman, J. E., and Kirby, J. R. (2009). Deciphering the hunting strategy of a bacterial wolfpack. *FEMS Microbiol. Rev.* 33, 942–957. doi: 10.1111/j.1574-6976.2009.00185.x

Bhople, S., Gaikwad, S., Deshmukh, S., Bonde, S., Gade, A., Sen, S., et al. (2016). Myxobacteria-mediated synthesis of silver nanoparticles and their impregnation in wrapping paper used for enhancing shelf life of apples. *IET Nanobiotechnol.* 10, 389–394. doi: 10.1049/iet-nbt.2015.0111

Bowman, S. M., and Free, S. J. (2006). The structure and synthesis of the fungal cell wall. *Bio Essays* 28, 799–808. doi: 10.1002/bies.20441

Davies, J., Spiegelman, G. B., and Yim, G. (2006). The world of subinhibitory antibiotic concentrations. *Curr. Opin. Microbiol.* 9, 445–453. doi: 10.1016/j.mib.2006.08.006

Ding, Y. (2017). *Isolation and Identification of Myxobacteria from the Ordos Plateau Area and Preliminary Analysis of Their Antagonistic Activity Against Phytophthora infestans*. Master, Innebr Mongolia Agricultural University. Available online at: https://wap.cnki.net/touch/web/Dissertation/Article/10129-1017211855.nh.html (accessed January 23, 2024).

Dong, H., Gao, R., Dong, Y., Yao, Q., and Zhu, H. (2023). Whole-genome sequencing of a biocontrol *Myxococcus xanthus* R31 isolate and

comparative genomic analysis. *Gene* 863:147286. doi: 10.1016/j.gene.2023.147286

Gemperlein, K., Zaburannyi, N., Garcia, R., La Clair, J., and Müller, R. (2018). Metabolic and biosynthetic diversity in marine myxobacteria. *Mar. Drugs* 16:314. doi: 10.3390/md16090314

Herrmann, J., Fayad, A. A., and Müller, R. (2017). Natural products from myxobacteria: novel metabolites and bioactivities. *Nat. Prod. Rep.* 34, 135–160. doi: 10.1039/c6np00106h

Hüttel, S., Testolin, G., Herrmann, J., Planke, T., Gille, F., Moreno, M., et al. (2017). Discovery and total synthesis of natural cystobactamid derivatives with superior activity against gram-negative pathogens. *Angew. Chem. Int. Ed.* 56, 12760–12764. doi: 10.1002/anie.201705913

Iizuka, T., Jojima, Y., Fudou, R., Hiraishi, A., Ahn, J.-W., and Yamanaka, S. (2003a). *Plesiocystis pacifica gen.* nov., sp. nov., a marine myxobacterium that contains dihydrogenated menaquinone, isolated from the Pacific coasts of Japan. *Int. J. Syst. Evol. Microbiol.* 53, 189–195. doi: 10.1099/ijs.0.02418-0

Iizuka, T., Jojima, Y., Fudou, R., Tokura, M., Hiraishi, A., and Yamanaka, S. (2003b). *Enhygromyxa salina gen.* nov., sp. nov., a slightly halophilic myxobacterium isolated from the coastal areas of Japan. *Syst. Appl. Microbiol.* 26, 189–196. doi: 10.1078/072320203322346038

Kaushal, G., and Singh, S. P. (2020). Comparative genome analysis provides shreds of molecular evidence for reclassification of *Leuconostoc mesenteroides* MTCC 10508 as a strain of *Leu. suionicum*. *Genomics* 112, 4023–4031. doi: 10.1016/j.ygeno.2020.06.040

Kim, B.-M., Minh, N. V., Choi, H.-Y., and Kim, W.-G. (2019). Coralmycin derivatives with potent anti-gram negative activity produced by the myxobacteria *Corallococcus coralloides* M23. *Molecules* 24:1390. doi: 10.3390/molecules24071390

Kumar, S., Yadav, A. K., Chambel, P., and Kaur, R. (2017). Molecular and functional characterization of myxobacteria isolated from soil in India. *3 Biotech* 7:112. doi: 10.1007/s13205-017-0722-9

Li, Z., Xia, C., Wang, Y., Li, X., Qiao, Y., Li, C., et al. (2019a). Identification of an endo-chitinase from Corallococcus sp. EGB and evaluation of its antifungal properties. *Int. J. Biol. Macromol.* 132, 1235–1243. doi: 10.1016/j.ijbiomac.2019.04.056

Li, Z., Ye, X., Liu, M., Xia, C., Zhang, L., Luo, X., et al. (2019b). A novel outer membrane ß-1,6-glucanase is deployed in the predation of fungi by myxobacteria. *ISME J.* 13, 2223–2235. doi: 10.1038/s41396-019-0424-x

Mansfield, J., Genin, S., Magori, S., Citovsky, V., Sriariyanum, M., Ronald, P., et al. (2012). Top 10 plant pathogenic bacteria in molecular plant pathology. *Mole. Plant Pathol.* 13, 614–629. doi: 10.1111/j.1364-3703.2012.00804.x

Moeller, M., Norris, M. D., Planke, T., Cirnski, K., Herrmann, J., Müller, R., et al. (2019). Scalable syntheses of methoxyaspartate and preparation of the antibiotic cystobactamid 861-2 and highly potent derivatives. *Organ. Lett.* 21, 8369–8372. doi: 10.1021/acs.orglett.9b03143

Nickeleit, I., Zender, S., Sasse, F., Geffers, R., Brandes, G., Sörensen, I., et al. (2008). Argyrin A reveals a critical role for the tumor suppressor protein p27kip1 in mediating antitumor activities in response to proteasome inhibition. *Cancer Cell* 14, 23–35. doi: 10.1016/j.ccr.2008.05.016

Odintsov, S. G., Sabala, I., Marcyjaniak, M., and Bochtler, M. (2004). Latent LytM at 1.3Å resolution. *J. Mol. Biol.* 335, 775–785. doi: 10.1016/j.jmb.2003.11.009

Okanya, P. W., Mohr, K. I., Gerth, K., Steinmetz, H., Huch, V., Jansen, R., et al. (2012). Hyaladione, an S-methyl Cyclohexadiene-dione from *Hyalangium minutum*. *J. Nat. Prod.* 75, 768–770. doi: 10.1021/np200776v

Oren, A., and Garrity, G. M. (2021). Valid publication of the[[Inline Image]] names of forty-two phyla of prokaryotes. *Int. J. Syst. Evol. Microbiol.* 71:4. doi: 10.1099/ijsem.0.005056

Paitan, Y., Orr, E., Ron, E. Z., and Rosenberg, E. (1999). A nonessential signal peptidase II (Lsp) of *Myxococcus xanthus* might be involved in biosynthesis of the polyketide antibiotic TA. *J. Bacteriol.* 181, 5644–5651. doi: 10.1128/JB.181.18.5644-5651.1999

Pietro, A. D., Madrid, M. P., Caracuel, Z., Delgado-Jarana, J., and Roncero, M. I. G. (2003). Fusarium oxysporum: exploring the molecular arsenal of a vascular wilt fungus. *Mol. Plant Pathol.* 4, 315–325. doi: 10.1046/j.1364-3703.2003.00180.x

Pogorevc, D., Tang, Y., Hoffmann, M., Zipf, G., Bernauer, H. S., Popoff, A., et al. (2019). Biosynthesis and heterologous production of argyrins. *ACS Synth. Biol.* 8, 1121–1133. doi: 10.1021/acssynbio.9b00023

Ren, X., Wu, Z., Cui, H., Gao, X., and Feng, F. (2016). Isolation and identification of antagonistic strain YR-7 of *Phytophthora infestans* and its active substances. *Bull. Microbiol.* 43, 1513–1523. doi: 10.13344/j.microbiol.china.150617

Rix, U., Fischer, C., Remsing, L. L., and Rohr, J. (2002). Modification of post-PKS tailoring steps through combinatorial biosynthesis. *Nat. Prod. Rep.* 19, 542–580. doi: 10.1039/b103920m

Rosenberg, E., Fytlovitch, S., Carmeli, S., and Kashman, Y. (1982). Chemical properties of *Myxococcus xanthus* antibiotic TA. *J. Antibiot.* 35, 788–793. doi: 10.7164/antibiotics.35.788

Ryosuke, F., Yasuko, J., Takashi, I., and Yamanaka, S. (2002). *Haliangium ochraceum gen.* nov., sp. nov. and *Haliangium tepidum* sp. nov.: novel moderately halophilic myxobacteria isolated from coastal saline environments. *J. Gen. Appl. Microbiol.* 48, 109–116. doi: 10.2323/jgam.48.109

Saggu, S. K., Nath, A., and Kumar, S. (2023). Myxobacteria: biology and bioactive secondary metabolites. *Res. Microbiol.* 174:104079. doi: 10.1016/j.resmic.2023.104079

Seef, S., Herrou, J., de Boissier, P., My, L., Brasseur, G., Robert, D., et al. (2021). A Tad-like apparatus is required for contact-dependent prey killing in predatory social bacteria. *eLife* 10:e72409. doi: 10.7554/eLife.72409

Selitrennikoff, C. P. (2001). Antifungal Proteins. *Appl. Environ. Microbiol.* 67, 2883–2894. doi: 10.1128/aem.67.7.2883-2894.200

Sharma, A., Kumar, A., Babu, V., Ali, A., and Katoch, M. (2021). Myxobacteria from animal dung pellets collected from northwestern Himalayas: a new source of di-isobutyl phthalate. *J. Basic Microbiol.* 62, 162–173. doi: 10.1002/jobm.202100518

Shehata, A. N., Abd El Aty, A. A., Darwish, D. A., Abdel Wahab, W. A., and Mostafa, F. A. (2018). Purification, physicochemical and thermodynamic studies of antifungal chitinase with production of bioactive chitosan-oligosaccharide from newly isolated aspergillus griseoaurantiacus KX010988. *Int. J. Biol. Macromol.* 107, 990–999. doi: 10.1016/j.ijbiomac.2017.09.071

Shen, E., Wang, X., Lu, Z., Zhou, F., Ma, W., Cui, Z., et al. (2023). Overexpression of a beta-1, 6-glucanase gene GluM in transgenic rice confers high resistance to rice blast, sheath blight and false smut. *Pest Manag. Sci.* 79, 2152–2162. doi: 10.1002/ps.7394

Siebert, D. C. B., Sommer, R., Pogorevc, D., Hoffmann, M., Wenzel, S. C., Müller, R., et al. (2019). Chemical synthesis of tripeptide thioesters for the biotechnological incorporation into the myxobacterial secondary metabolite argyrin via mutasynthesis. *Beilstein J. Org. Chem.* 15, 2922–2929. doi: 10.3762/bjoc.15.286

Solga, D., Wieske, L. H. E., Wilcox, S., Zeilinger, C., Jansen-Olliges, L., Cirnski, K., et al. (2024). Is simultaneous binding to DNA and gyrase important for the antibacterial activity of cystobactamids? *Chemistry* 13:e202303796. doi: 10.1002/chem.202303796

Stauch, B., Simon, B., Basile, T., Schneider, G., Malek, N. P., Kalesse, M., et al. (2010). Elucidation of the structure and intermolecular interactions of a reversible cyclic-peptide inhibitor of the proteasome by NMR spectroscopy and molecular modeling. *Angew. Chem. Int. Ed.* 49, 3934–3938. doi: 10.1002/anie.201000140

Sutton, D., Livingstone, P. G., Furness, E., Swain, M. T., and Whitworth, D. E. (2019). Genome-wide identification of myxobacterial predation genes and demonstration of formaldehyde secretion as a potentially predation-resistant trait of Pseudomonas aeruginosa. *Front. Microbiol.* 10:2650. doi: 10.3389/fmicb.2019.02650

Talbot, N. J. (2003). On the trail of a cereal killer: exploring the biology of Magnaporthe grisea. *Annu. Rev. Microbiol.* 57, 177–202. doi: 10.1146/annurev.micro.57.030502.090957

Thiery, S., Turowski, P., Berleman, J. E., and Kaimer, C. (2022). The predatory soil bacterium Myxococcus xanthus combines a Tad- and an atypical type 3-like protein secretion system to kill bacterial cells. *Cell Rep.* 40:111340. doi: 10.1016/j.celrep.2022.111340.

Waite, D. W., Chuvochina, M., Pelikan, C., Parks, D. H., Yilmaz, P., Wagner, M., et al. (2020). Proposal to reclassify the proteobacterial classes Deltaproteobacteria and Oligoflexia, and the phylum Thermodesulfobacteria into four phyla reflecting major functional capabilities. *Int. J. Syst. Evol. Microbiol.* 70, 5972–6016. doi: 10.1099/ijsem.0.004213

Weissman, K. J., and Müller, R. (2010). Myxobacterial secondary metabolites: bioactivities and modes-of-action. *Nat. Prod. Rep.* 27, 1276–1295. doi: 10.1039/c001260m

Wieland, M., Holm, M., Rundlet, E. J., Morici, M., Koller, T. O., Maviza, T. P., et al. (2022). The cyclic octapeptide antibiotic argyrin B inhibits translation by trapping EF-G on the ribosome during translocation. *Proc. Natl. Acad. Sci. U.S.A.* 119:e2114214119. doi: 10.1073/pnas.2114214119

Willsey, G. G., Wargo, M. J., and O'Toole, G. A. (2016). Sarcosine catabolism in Pseudomonas aeruginosa is transcriptionally regulated by SouR. *J. Bacteriol.* 198, 301–310. doi: 10.1128/jb.00739-15

Wu, Z. (2018). *Isolation of Myxobacteria from the Central Region of Inner Mongolia and their Activity and Components Against Potato Late Blight Pathogen* Doctor, Inner Mongolia Agricultural University. Available online at: https://cdmd.cnki.com.cn/Article/CDMD-10129-1018881788.htm

Wu, Z., Cui, H., Sun, Z., and Liu, H. (2021). Biocontrol mechanism of *Myxococcus xanthus* B25-I-1 against *Phytophthora infestans*. *Pestic. Biochem. Physiol.* 175:104832. doi: 10.1016/j.pestbp.2021.104832

Wu, Z. H., Ma, Q., Sun, Z. N., Cui, H. C., and Liu, H. R. (2021). Biocontrol mechanism of *Myxococcus fulvus* B25-I-3 against Phytophthora infestans and its control efficiency on potato late blight. *Folia Microbiol.* 66, 555–567. doi: 10.1007/s12223-021-00865-1

Xiao, Y., Wei, X., Ebright, R., and Wall, D. (2011). Antibiotic production by Myxobacteria plays a role in predation. *J. Bacteriol.* 193, 4626–4633. doi: 10.1128/jb.05052-11

Ye, X., Chen, Y., Ma, S., Yuan, T., Wu, Y., Li, Y., et al. (2020a). Biocidal effects of volatile organic compounds produced by the myxobacterium *Corrallococcus* sp. EGB against fungal phytopathogens. *Food Microbiology* 91:103502. doi: 10.1016/j.fm.2020.103502

Ye, X., Li, Z., Luo, X., Wang, W., Li, Y., Li, R., et al. (2020b). A predatory myxobacterium controls cucumber fusarium wilt by regulating the soil microbial community. *Microbiome* 8:49. doi: 10.1186/s40168-020-00824-x

Zhang, L., Dong, C., Wang, J., Liu, M., Wang, J., Hu, J., et al. (2023). Predation of oomycetes by myxobacteria via a specialized CAZyme system arising from adaptive evolution. *ISME J.* 17, 1089–1103. doi: 10.1038/s41396-023-01423-y

Zhao, P. (2018). *Isolation and Identification of Myxobacteria in Alashan Area and Preliminary Study on their Antibiotic Activity Against Phytophthora infestans* Master, Inner Mongolia Agricultural University. Available at: https://cdmd.cnki.com.cn/Article/CDMD-10129-1018882358.htm

Zhou, J., Chen, J., Li, Z., Ye, X., Dong, W., Jiang, M., et al. (2019). Enzymatic properties of a multi-specific β-(1,3)-glucanase from *Corallococcus* sp. EGB and its potential antifungal applications. *Protein Expr. Purif.* 164:105481. doi: 10.1016/j.pep.2019.105481

TABLE 1 Control principle of myxobacteria against pathogens.

Antagonistic substances	Antagonistic principle	References
Enzymes		
β-1,6-glucanase	Degrades β-1,6-glucan. When HOG is activated, the intracellular glycerol content increases and the osmotic pressure increases; when CWI is activated, cell growth and division slow down	Zhou et al. (2019) and Ye et al. (2020a)
β-1,3-glucanase	Hydrolyzesβ-1,3-glucan. The cell wall surface falls off and a perforated structure appears in the cell wall	Zhou et al. (2019) and Zhang et al. (2023)
Chitinase	Degrades the glycosidic bonds of cell wall chitosan oligosaccharides. Inhibits the germination of pathogenic spores and the formation of attached spores	Li et al. (2019a)
Proteases and peptidases	The morphology of *R. solanacearum* changed significantly, and the cells were broken into many small fragments	Dong et al. (2023)
Formaldehyde dismutase	Formaldehyde is concerted into formate and methanol to protect myxobactria	Willsey et al. (2016) and Sutton et al. (2019)
Small molecule compounds		
Isooctanol	Destroy the cell wall and cell membrane of pathogenic bacteria, accumulate ROS, and cause cell death	Ye et al. (2020a)
Di-isobutyl phthalate	Exhibits biofilm formation inhibitory activity against bacteria	Sharma et al. (2021)
Myxovirescin	Inhibits the incorporation of diamibopimelic acid and uridine diphosphate-N-acetylglucosamine into bactrial cell wall, and interferes with the polymerizaton of the lipid-disacchar-pentapeptide	Rosenberg et al. (1982) and Paitan et al. (1999)
Cystobacamids derivatives	Inhibits bacterial gyrase to exert antibacterial activity	Kim et al. (2019) and Solga et al. (2024)
Hyalodione	Strongly inhibits the activity of pathogenic bacteria.	Okanya et al. (2012)
Argyrin derivatives	Participate in the non-ribosomal peptide synthase pathway and inhibit protein synthesis by interfering with the binding of elongation factor G (EF-G) to ribosomes	Pogorevc et al. (2019) and Wieland et al. (2022)
Methyl(2R)-2-azido-3-hydroxyl-2-methylpropanoate, N-(3-Amino-2-hydroxypropyl)-N-meth -ylsulfuric diamide	Reduce the content of soluble proteins and activity of protective enzymes in pathogenic bacteria, and increase oxidative damage and cell membrane permeability	Wu (2018)
Some unknown substances	Inhibits the growth of hyphae and asexual reproduction of *Phytophthora infestans*	Ren et al. (2016), Ding (2017), Wu (2018), and Zhao (2018)

10.3389/fmicb.2024.1392109

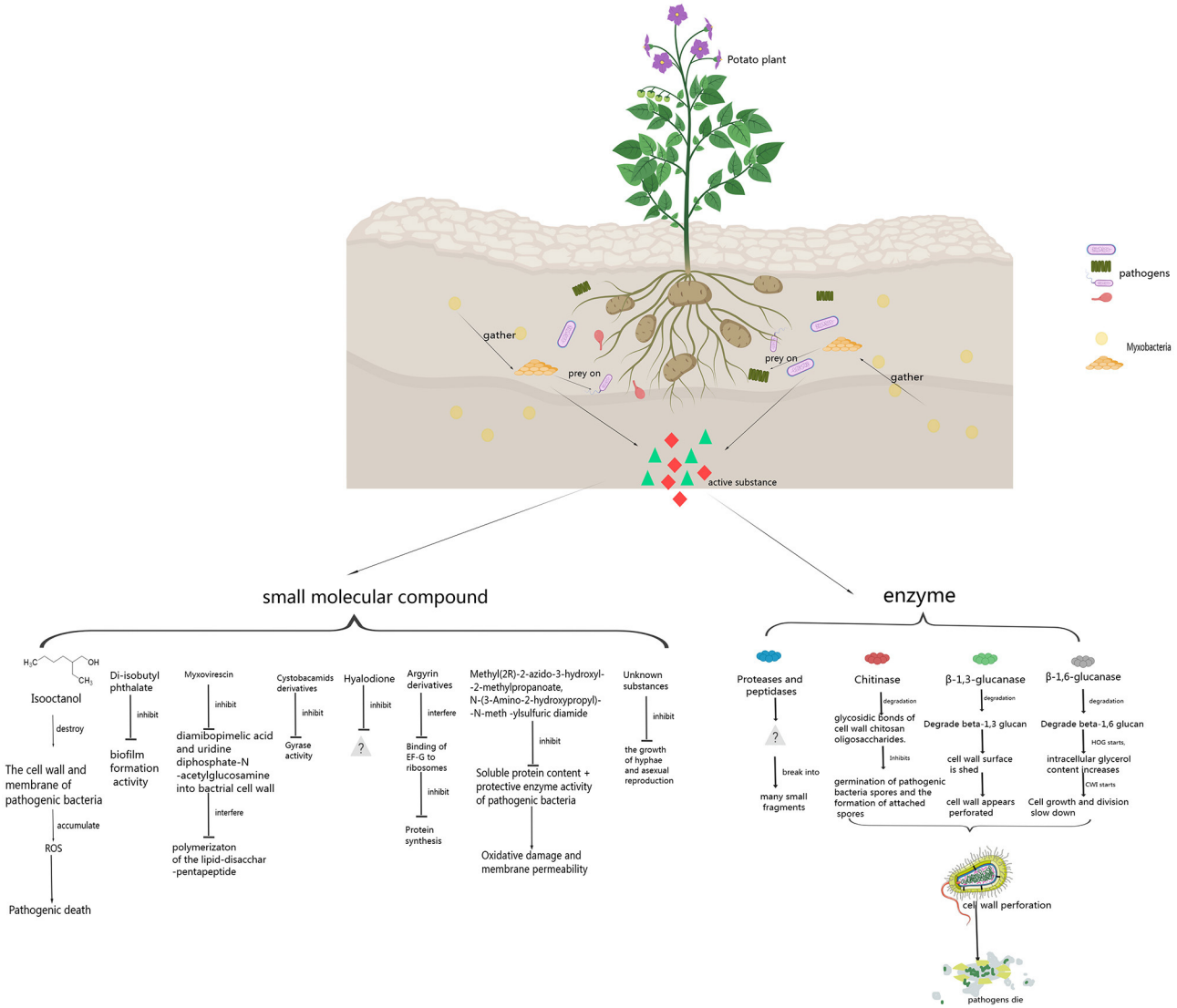

FIGURE 1
Control principle of myxobacteria against plant pathogens.

frontiers | Frontiers in Microbiology

TYPE Original Research
PUBLISHED 08 January 2024
DOI 10.3389/fmicb.2023.1294631

OPEN ACCESS

EDITED BY
David Edward Whitworth,
Aberystwyth University, United Kingdom

REVIEWED BY
Emilia Mauriello,
UMR7283 Laboratoire de Chimie Bactérienne (LCB), France
Shogo Yoshimoto,
Nagoya University, Japan

*CORRESPONDENCE
Jing Chen
✉ chenjing@vt.edu

RECEIVED 15 September 2023
ACCEPTED 11 December 2023
PUBLISHED 08 January 2024

CITATION
Chen Y, Topo EJ, Nan B and Chen J (2024) Mathematical modeling of mechanosensitive reversal control in *Myxococcus xanthus*. *Front. Microbiol.* 14:1294631. doi: 10.3389/fmicb.2023.1294631

Mathematical modeling of mechanosensitive reversal control in *Myxococcus xanthus*

Yirui Chen[1,2], Elias J. Topo[3], Beiyan Nan[3] and Jing Chen[1,4,5]*

[1]Department of Biological Sciences, Virginia Tech, Blacksburg, VA, United States, [2]Genetics, Bioinformatics and Computational Biology Graduate Program, Virginia Tech, Blacksburg, VA, United States, [3]Department of Biology, Texas A&M University, College Station, TX, United States, [4]Fralin Life Sciences Institute, Virginia Tech, Blacksburg, VA, United States, [5]Center for Soft Matter and Biological Physics, Virginia Tech, Blacksburg, VA, United States

Adjusting motility patterns according to environmental cues is important for bacterial survival. *Myxococcus xanthus*, a bacterium moving on surfaces by gliding and twitching mechanisms, modulates the reversal frequency of its front-back polarity in response to mechanical cues like substrate stiffness and cell-cell contact. In this study, we propose that *M. xanthus*'s gliding machinery senses environmental mechanical cues during force generation and modulates cell reversal accordingly. To examine our hypothesis, we expand an existing mathematical model for periodic polarity reversal in *M. xanthus*, incorporating the experimental data on the intracellular dynamics of the gliding machinery and the interaction between the gliding machinery and a key polarity regulator. The model successfully reproduces the dependence of cell reversal frequency on substrate stiffness observed in *M. xanthus* gliding. We further propose reversal control networks between the gliding and twitching motility machineries to explain the opposite reversal responses observed in wild type *M. xanthus* cells that possess both motility mechanisms. These results provide testable predictions for future experimental investigations. In conclusion, our model suggests that the gliding machinery in *M. xanthus* can function as a mechanosensor, which transduces mechanical cues into a cell reversal signal.

KEYWORDS

mechanosensing, bacterial motility, gliding motility, polarity regulation, myxobacteria, mathematical modeling

Introduction

The ability to sense the environment and adapt their behaviors accordingly is crucial for survival and propagation of bacteria. For motile bacteria, their motility is often highly adaptable to environmental cues. A well-studied example is chemotaxis in *Escherichia coli* swimming: the bacterium decreases its tumbling frequency when it senses an increase of nutrient concentration, and vice versa (Berg and Brown, 1972). Over a long time scale, this response amounts to biased cell movements toward nutrient-dense areas (Wadhams and Armitage, 2004; Sourjik and Wingreen, 2012). Besides diffusive chemical signals, bacteria can also adapt their motility (and other behaviors) to mechanical cues (Persat et al., 2015; Colin et al., 2019; Gordon and Wang, 2019; Dufrene and Persat, 2020). For instance, increasing the load on an *E. coli* flagellum stabilizes the stator units in the flagellar motor, leading to an increased power output and recovery of the rotation

frequency of the flagellum (Lele et al., 2013; Tipping et al., 2013; Wadhwa et al., 2019). Moreover, Type IV pilus, an appendage driving twitching motility in a broad range of bacteria, switches from extension to retraction rapidly and nearly exclusively upon touching a surface with its tip, suggesting that it can sense physical contacts (Tala et al., 2019; Dufrene and Persat, 2020). Because bacteria experience constantly fluctuating forces, especially when they live on inhomogeneous surfaces or in complex biofilms, their ability to respond to mechanical cues plays a critical role in their survival.

In this work, we focus on the cellular mechanism for mechanosensing in the motility of a soil-dwelling bacterium, *Myxococcus xanthus*. *M. xanthus* is a model organism for studying bacterial social behaviors, as it features complex spatial patterns and structures at the population level, such as streams, rippling waves, aggregation and fruiting bodies (Welch and Kaiser, 2001; Zhang et al., 2012a; Keane and Berleman, 2016). These spatial patterns and structures play important roles in "social" collaboration during predation and sporulation (Berleman and Kirby, 2009; Velicer and Vos, 2009; Zhang et al., 2012a; Munoz-Dorado et al., 2016). Formation of the spatial patterns and structures hinges on the *M. xanthus* cells' ability to modulate their motility in response to external stimuli (Berleman and Kirby, 2007). Specifically, *M. xanthus* frequently reverses its direction of motion (Mauriello et al., 2010a; Schumacher and Sogaard-Andersen, 2017) and its reversal frequency is influenced by both chemical and mechanical cues (Igoshin et al., 2001, 2004; Borner et al., 2002; Kaimer et al., 2012). For the latter, the reversal frequency changes upon physical contact with other *M. xanthus* cells (Shi et al., 1996; Welch and Kaiser, 2001) or prey cells (Mcbride and Zusman, 1996; Zhang et al., 2020), and varies with substrates stiffness (Zhou and Nan, 2017). In this work, as a starting point to dissect the cellular mechanism of *M. xanthus* mechanosensing, we focused on investigating the dependence of the cell reversal frequency on substrate stiffness.

M. xanthus moves on surfaces through social (S)-motility favored by cells in large groups and adventurous (A)-motility favored by isolated cells (Shi and Zusman, 1993). S-motility, also known as twitching motility, is driven by Type IV pili (Sun et al., 2000; Mauriello et al., 2010a; Zhang et al., 2012a), the same cellular appendage that drives the twitching motility in *Pseudomonas aeruginosa* (Burrows, 2012). A-motility, also known as gliding motility, is powered by multi-subunit Agl-Glt complexes, which actively travel along helical intracellular trajectories and generate propulsion as they aggregate in the so-called focal adhesion sites that contact the underlying substrate (Nan et al., 2011, 2013, 2014; Islam and Mignot, 2015; Faure et al., 2016). Both the S- and A-motility machineries are activated at the leading pole of the cell (Schumacher and Sogaard-Andersen, 2017; Carreira et al., 2022). The polarity of the cell is defined by asymmetric concentration of polarity regulators. Particularly, the Ras-like GTPase MglA (Mauriello et al., 2010b) concentrates at the leading pole, while its cognate GTPase activating protein, the MglB/RomY complex (Miertzschke et al., 2011; Szadkowski et al., 2022), and cognate guanine nucleotide exchange factor, the RomR/RomX complex (Szadkowski et al., 2019), concentrate at the trailing pole (Leonardy et al., 2007, 2010; Patryn et al., 2010; Zhang et al., 2010; Bulyha et al., 2011). These polarity regulators form feedback loops that amount to a spatial oscillator where the regulators periodically switch between the two cell poles and reverse the cell's polarity and direction of motion (Zhang et al., 2010, 2012b; Treuner-Lange et al., 2015; Schumacher and Sogaard-Andersen, 2017; Guzzo et al., 2018; Szadkowski et al., 2019; Carreira et al., 2022). Surprisingly, wild type *M. xanthus* cells reverse on hard, 1.5% agar almost twice as frequently as they do on soft, 0.5% agar (Zhou and Nan, 2017), while the opposite trend was observed in *M. xanthus* mutants without the S-motility (S^- cells) (this work).

Although the molecular mechanisms for force generation (Sun et al., 2000, 2011; Mignot et al., 2007; Nan et al., 2011, 2013; Faure et al., 2016) and polarity switching (Zhang et al., 2010, 2012b; Guzzo et al., 2018; Galicia et al., 2019; Szadkowski et al., 2019, 2022) have been intensively studied in *M. xanthus*, it remains unknown how mechanosensing regulates cell reversal. Mechanosensing relies on molecules capable of converting external mechanical cues into intracellular signals. Among the most promising candidates playing this role are motility machineries, which, by the nature of their function, form mechanical links between the cell and external substrates. In eukaryotes, for example, the focal adhesion mechanism (macromolecular structures that dynamically assemble and drive cell migration) indeed mediates mechanosensing through mechanical connection to the extracellular matrix (Cheng et al., 2017; Tao et al., 2017; Martino et al., 2018). In *M. xanthus*, the polarity regulator MglA is also an essential subunit of the active A-motility machinery (Patryn et al., 2010; Zhang et al., 2010; Treuner-Lange et al., 2015; Faure et al., 2016). We hence hypothesize that the A-motility machinery may influence the polarity pathway and modulate cell reversal in response to external mechanical cues.

To investigate our hypothesis, we expanded an existing mathematical model for periodic polarity switch in *M. xanthus* (Guzzo et al., 2018), and incorporated the experimental data on the subcellular dynamics of A-motility machineries and the interaction between MglA and the A-motility machinery. The model-predicted relationship between substrate stiffness and cell reversal frequency is consistent with the experimental observation in S^- mutant cells with only A-motility. To elucidate the opposite dependence of reversal frequency on substrate stiffness observed in wild type cells with both A-and S-motility, we further examined extended pathways in which the S-motility machinery influences cell reversal as well. Because direct link between the S-motility machinery and the polarity pathway is yet missing and the reversal frequency of cells that moves with S-motility alone is insensitive to substrate stiffness (Zhou and Nan, 2017), we assumed that the S-motility machinery affects cell reversal indirectly through the A-motility machinery, and only examined generic pathways within this category. For each candidate pathway, we combined its topology with our model results and qualitatively predicted the dependence of cell reversal frequency on substrate stiffness in both genetic backgrounds. The qualitative predictions suggest that promotion of the activation of A-motility machinery by S-motility is necessary to reconcile the opposite reversal responses in wild type cells vs. S^- mutants. Our model proposes a mechanosensing mechanism through A-motility in *M. xanthus* and provides testable predictions for future experimental study.

Results

Modeling the coupling between polarity control and A-motility

We constructed a model (Figure 1) that incorporates the following key experimental observations. For short, we refer to the multi-subunit A-motility machinery as the "A-motor."

1 An A-motor can assume three possible states: inactive, active, or engaged. An inactive motor, which likely represents disassembled parts of the motor (Nan et al., 2015; Faure et al., 2016; Nan, 2017), only diffuses in the cell.
2 An active motor travels along the helical track towards either the leading or trailing pole. The directionality of an active motor randomly switches (Nan et al., 2015), probably due to the lack of polarity in the short patches of MreB filaments (Kim et al., 2006; Van Den Ent et al., 2014; Errington, 2015; Billaudeau et al., 2017), on which the A-motor moves along (Mauriello et al., 2010b; Nan et al., 2011; Treuner-Lange et al., 2015; Fu et al., 2018).
3 As an active A-motor passes through a focal adhesion site, it can engage with the focal adhesion site and generate thrust. The engagement of a motor at the focal adhesion site likely represents coupling between the inner-membrane energy-harvesting subunits and the periplasmic and outer-membrane subunits (Islam et al., 2023).
4 Activation and deactivation of A-motors occur at the cell poles, where the polarity regulators are concentrated (Zhang et al., 2010, 2012b; Treuner-Lange et al., 2015; Guzzo et al., 2018; Galicia et al., 2019; Szadkowski et al., 2019, 2022). The motor is activated upon binding with MglA, which is reversed by MglB, the cognate GTPase activating protein for MglA (Miertzschke et al., 2011).
5 The polarity pathway follows a recent model (Guzzo et al., 2018). Specifically, MglA and MglB antagonize each other in polar localization; MglB promotes polar localization of RomR and its own polar localization; finally, RomR promotes polar localization of MglA. Strong mutual inhibition between MglA and MglB breaks the symmetry and makes them concentrate at opposite poles. The negative feedback loop, MglA ⊣ MglB → RomR → MglA, causes periodic switching in their polar localization.

With the equations and parameters given in Supplementary Methods (Supplementary Equations S1–S32; Supplementary Tables S1–S3), our model recapitulates key motility characteristics, including:

1 The cell reverses periodically every ~12 min (Figure 2A) (Kaimer and Zusman, 2016; Guzzo et al., 2018; Szadkowski et al., 2019).
2 MglA concentrates at the leading pole, and MglB and RomR concentrate at the trailing pole (Figure 2B) (Zhang et al., 2010, 2012b; Treuner-Lange et al., 2015; Guzzo et al., 2018; Szadkowski et al., 2019).
3 MglA forms a concentration gradient between the leading and trailing cell poles (Figures 2D,E), and about half of the MglA molecules are localized outside the polar regions (Figure 2C) (Nan et al., 2015).
4 Active motors form a concentration gradient that decreases from the leading pole to the trailing pole (Figures 2D,E) (Mignot et al., 2007).

Interaction between MglA and A-motors predicts dependence of cell reversal frequency on substrate stiffness in A$^+$S$^-$ cells

Next, we used the model to predict how substrate stiffness affects cell reversal frequency through the connection between the A-motor and the polarity pathway. Previous observations showed that harder substrates induce more intense clustering of A-motors at the cell-substrate interface (Nan et al., 2010). Because clustered A-motors at the substrate interface engage in force generation (Nan et al., 2013; Faure et al., 2016), this phenomenon indicates that harder substrates increase the number of engaged motors. This implication was confirmed by single-molecule tracking of AglR, a protein component of the energy-harvesting unit in A-motors: the number of fast-moving AglR molecules—representing motors that are not engaged in force generation—decreased as substrate stiffness increased (Nan et al., 2013). In light of these experimental observations, in the model we represented substrate stiffness by the motor engagement rate [conversion from an active motor (M_{a+} or M_{a-} in Figure 1) to an engaged motor (M_{e+} or M_{e-} in Figure 1)]. Particularly, a harder substrate corresponds to a higher engagement

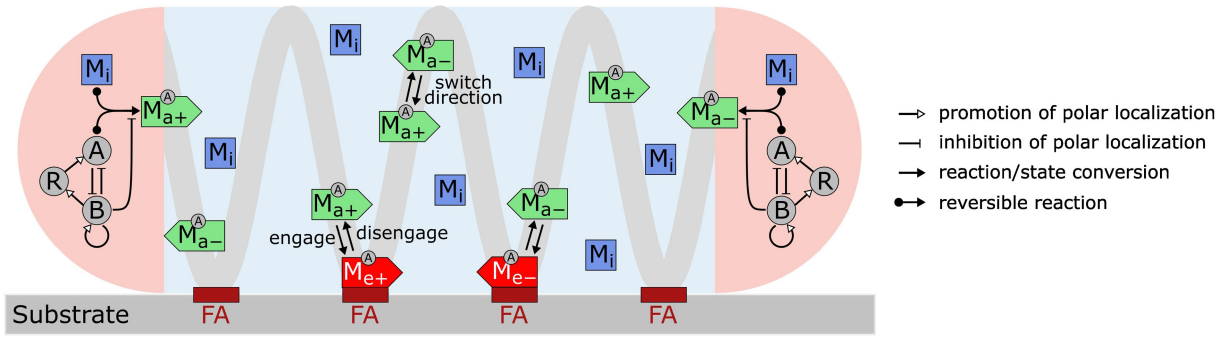

FIGURE 1
Model for *M. xanthus* reversal control with mechanosensing through A-motors. A-motors are present in three states in the cell: inactive (M_i), active (M_{a+}, M_{a-}) and engaged (M_{e+}, M_{e-}). Inactive motors diffuse in the cell. Active motors move directionally along the helical trajectory (light gray line) and randomly switch directions (+: moving to the right; −: moving to the left). When active motors pass a focal adhesion site (maroon bars labeled as "FA"), they can become engaged in force generation. Activation and deactivation of motors only occur at the cell poles (pink areas). A motor is activated through binding with MglA (A) and is inactivated by MglB (B). Feedback loops among MglA (A), MglB (B) and RomR (R), as proposed by Guzzo et al. (2018), control periodic polarity switch.

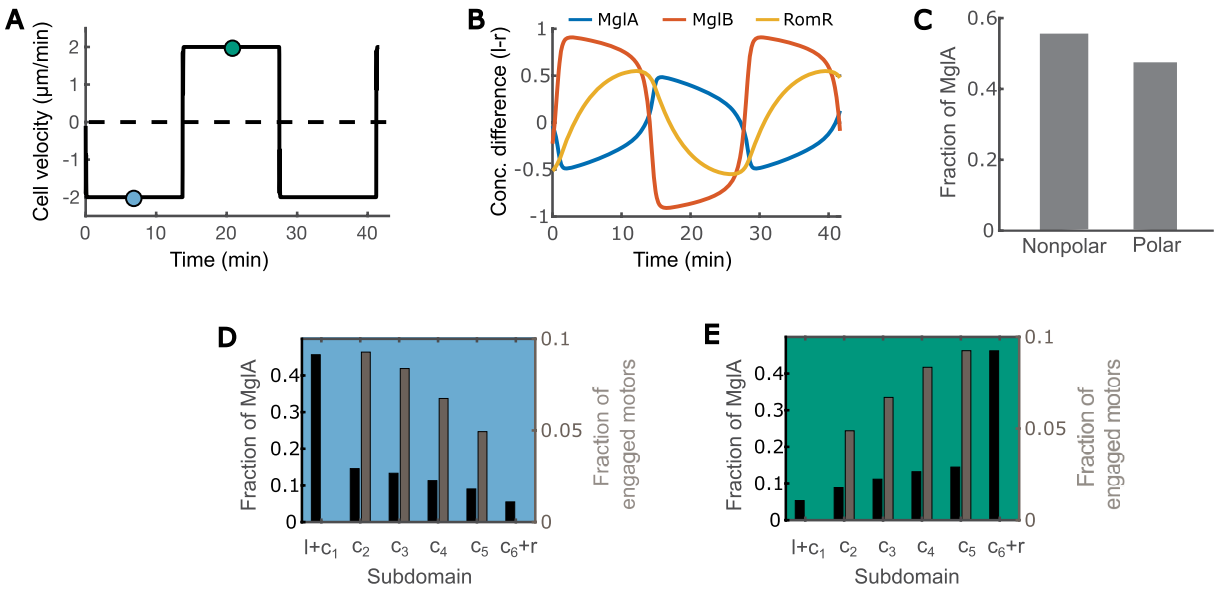

FIGURE 2
The model recapitulates key characteristics of *M. xanthus* motility. **(A)** Time course of the cell velocity. Positive and negative velocities correspond to motion towards the right and left, respectively. **(B)** Time courses of the concentration difference of MglA (A), MglB (B) and RomR (R) between the left (l) and right (r) poles. Positive and negative values indicate concentrations of the molecules at the left and right poles, respectively. **(C)** Distribution of MglA in the polar vs. nonpolar domains at the steady phase of the reversal cycle. Data sampled at the teal and/or blue points in **(A)**. **(D,E)** Spatial distribution of engaged motors and MglA along the cell when the cell is heading right **(D)** vs. left **(E)**. Subdomain labels: l: bound to the left pole. r: bound to the right pole. c_1: unbound, in cytoplasmic domain at the left pole. c_6: unbound, in cytoplasmic domain at the right pole. $c_{2\sim5}$: in cytoplasmic subdomains between poles. **(D,E)** present data sampled at the teal and blue time points, respectively, in **(A)**.

rate, and vice versa (Figure 3A). We tuned the model parameters such that the fraction of engaged motors falls in a similar range as the experimental measurements on 0.8–5% agar (Nan et al., 2013) (Figure 3A).

Our model predicts that the reversal frequency decreases as the motor engagement rate increases (i.e., as substrate stiffness increases) (Figure 3B). This prediction was validated by the experimental observation in A^+S^- (*pilA*$^-$) cells (Figure 3C). Note that as the production of pilin, the subunit of type IV pilus that drives S-motility, was disabled in these mutant cells, motility-mediated mechanosensing can only be attributed to the A-motility machinery, and hence these cells are more closely related to the model than wild type cells.

The above model prediction can be understood in the following way. Recall that MglA binds to the active and engaged motors. An active motor can quickly reach either cell pole [~2.5 s to traverse the typical cell length of 5 μm with the typical speed of 2 μm/s (Nan et al., 2015)]. If it reaches the trailing pole, the motor is inactivated and releases MglA. In contrast, an engaged motor moves towards the trailing pole at a much slower speed [roughly the cell speed, ~2 μm/min, as the engaged motors are nearly stationary relative to the substrate (Mignot et al., 2007; Nan et al., 2010, 2013)]. Therefore, the engaged motors effectively sequester MglA in nonpolar regions. The higher motor engagement rate on a stiffer substrate boosts the number of engaged motors and hence sequesters MglA more strongly away from cell poles. The reduction of MglA at the poles, in turn, decreases the cell reversal frequency (Supplementary Figure S1). Taken together, increased motor engagement on harder substrates sequesters MglA away from cell poles and thus reduces cell reversal frequency.

Activation of A-motors affects cell reversal frequency

Next, we thoroughly explored the effect of A-motor dynamics on cell reversal frequency. The engagement and disengagement of A-motors are reverse reactions, and hence the effects of varying their rates are just inversed. Similar relation is true between activation and deactivation of A-motors. For these reverse reactions, we only need to investigate the effect of one reaction out of a pair. In the last section we explored the effect of engagement rate. Here we focused on the activation rate of A-motors, which refers to the conversion from a diffusive inactive motor (M_i in Figure 1) to a directional active motor (M_{a+} or M_{a-} in Figure 1). Interestingly, we found a biphasic relationship between A-motor activation and cell reversal: as the activation rate rises, the cell reversal frequency first increases and then decreases (Figure 4A).

The above prediction can be understood as follows. On the one hand, boosting the A-motor activation rate increases the proportion of active motors (Figure 4B), which enhances directed transport of active (GTP-bound) MglA towards the trailing pole, and thus promotes polarity switching. Note that MglA can also diffuse from one pole to the other, but because most diffusive MglA molecules are inactive (GDP-bound), active MglA cannot be efficiently transported by diffusion. On the other hand, enhanced motor activation also increases the proportion of engaged motors (Figure 4C), because the ratio between active and engaged motors are roughly constant when the engagement rate is fixed (Supplementary Figure S2C). As reasoned in the previous section, the engaged motors effectively sequester MglA in nonpolar regions and consequently reduce the reversal frequency. The effect of increasing active motors dominates when the A-motor

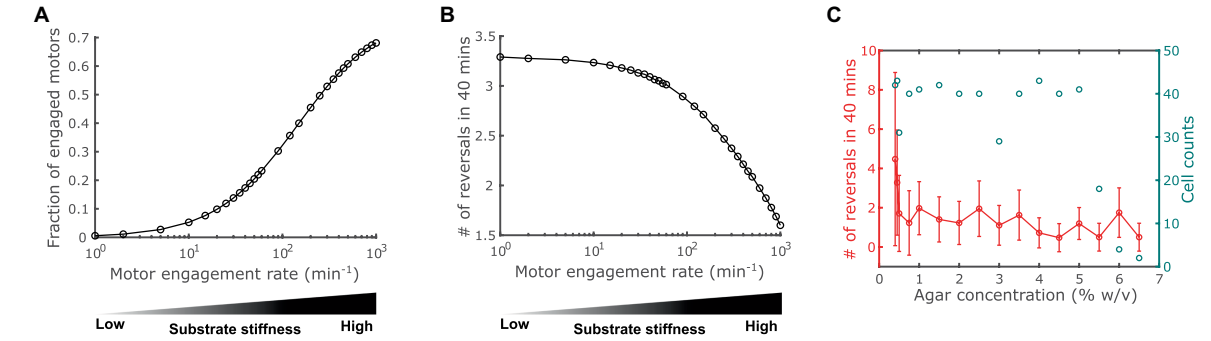

FIGURE 3
Impact of substrate stiffness on cell reversal frequency. **(A)** Using A-motor engagement rate as a proxy for substrate stiffness in the model. Harder substrates are represented by higher engagement rates, which result in higher fractions of engaged A-motors. The model parameters are tuned such that the range of the fraction of engaged A-motors is consistent with the experimental observation in Nan et al. (2013). **(B)** Model predicted dependence of the cell reversal frequency on substrate stiffness. **(C)** Experimentally observed cell reversal frequencies in A^+S^- (*pilA*$^-$) cells on surfaces with various stiffness tuned by agar concentration (% w/v). Blue circles and the right axis show the number of cells measured for each agar concentration.

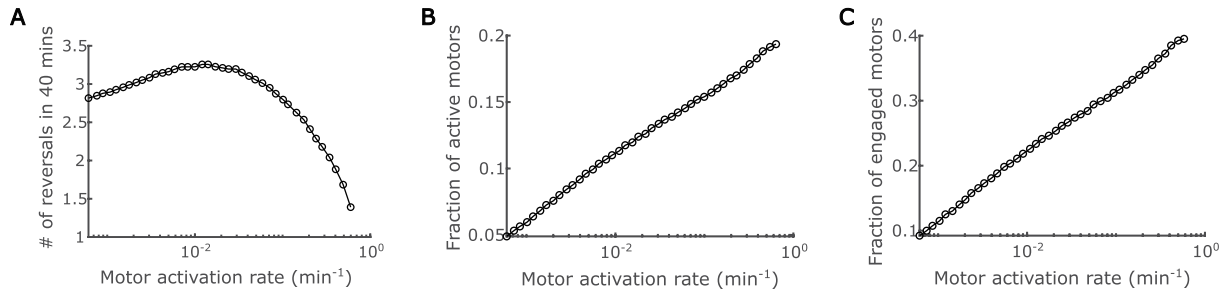

FIGURE 4
Impact of regulation of A-motor activation. **(A)** Predicted dependence of the cell reversal frequency on the activation rate of A-motors. **(B)** Predicted dependence of the fraction of active A-motors on the motor activation rate. **(C)** Predicted dependence of the fraction of engaged A-motors on the motor activation rate.

activation rate is low, while the effect of increasing engaged motors dominates when A-motor activation rate is high. The transition happens presumably because enhanced transport of active MglA has an immediate influence on the polar MglA/MglB/RomR dynamics, while the sequestration of MglA only has significant impact when a substantial fraction of MglA is sequestered. Together, these amount to a biphasic dependence of cell reversal frequency on the activation rate of A-motors.

Proper reversal control networks can explain disparities in mechanosensing behaviors in A^+S^- vs. wild type cells

Our model has predicted how mechanosensing regulates cell reversal through A-motility alone, which matches the observation in A^+S^- cells. Different from A^+S^- cells, however, wild type cells that move by both A- and S-motility reverse more frequently on harder surfaces (Zhou and Nan, 2017). This observation suggests that type IV pili that drive S-motility also mediate mechanosensing. However, direct control of cell reversal by the S-motility machinery seems unlikely. Although MglA interacts with certain S-motility proteins, such as FrzS and SgmX (Mercier et al., 2020; Potapova et al., 2020; Bautista et al., 2023), these proteins function downstream of MglA; none of them were reported to transport MglA like the A-motility machinery does or directly regulate its activity. Furthermore, the reversal frequency of cells that move by S-motility alone does not change in response to substrate stiffness (Zhou and Nan, 2017), suggesting that A-motility may be required for S-motility mediated mechanosensing. Therefore, we hypothesize that the A-motility machinery serves as the hub of mechanosensing, and the S-motility machinery only mediates an indirect control of cell reversal through the A-motility machinery.

To test the hypothesis, we combined the predicted dependence of cell reversal frequency on both the engagement and activation rates of A-motors (Supplementary Figure S2), and used the combined model prediction to screen various reversal control networks for those that can qualitatively explain the experimentally observed cell reversal frequencies in wild type and A^+S^- cells on 0.5 and 1.5% agar surfaces (Figure 5A). To focus on our hypothesis, we only examined networks where the S-motility machinery regulates cell reversal indirectly through the A-motility machinery. The candidate networks consist of several certain and uncertain controls. Certain controls include the positive dependence of the A-motor engagement rate on substrate stiffness (Nan et al., 2010), the model-predicted inhibition of cell reversal by A-motor engagement, and the negative dependence of S-motility on substrate stiffness [S-motility is more effective on soft

substrates (Shi and Zusman, 1993)] (Figure 5A). Uncertain controls include (i) the possibility that S-motility could influence the engagement and activation of A-motors, each in three possible ways: no effect, promotion, or inhibition (Figure 5A); and (ii) the cell reversal frequency either increases with stronger motor activation in the region of low activation rate, or decreases in the region of high activation rate (Figure 4A and Supplementary Figure S2A). Combination of the above possibilities gave rise to 18 possible networks (Figures 5C–T). Reversal frequencies of the wild type and A^+S^- cells on 0.5 and 1.5% agar surfaces for each network were estimated from the predicted 2D phase diagram for the dependence of cell reversal frequency on the engagement and activation rates of A-motors (same as Supplementary Figure S2A). According to these estimates, none of the 18 networks qualitatively explained the intertwined dependence of cell reversal frequency on substrate stiffness in both genetic backgrounds.

We then considered additional networks in which the wild type and A^+S^- cells reside in different regions of the phase diagram in terms of the A-motor activation rate (Figures 5U–Z). Particularly, if S-motility promotes A-motor activation, then wild type cells should have high rate of A-motor activation and increasing the activation rate in this region inhibits cell reversal (Figures 5U–W). In contrast, due to the lack of S-motility, A^+S^- cells should have low rate of A-motor activation and increasing the activation rate in this region promotes cell reversal (Figures 5U–W). Following the same logic, opposite predictions are yielded if S-motility inhibits A-motor activation, i.e., A-motor activation promotes cell reversal in wild type cells, and inhibits it in A^+S^- cells (Figures 5X–Z). The possibility that S-motility does not affect A-motor activation was not considered, because in this case the wild type and A^+S^- cells cannot have different A-motor activation rates. Among the six additional networks, we found three (Figures 5U–W) that qualitatively reproduced the experimental data on different agar surfaces in both genetic backgrounds (Supplementary Figure S3). In all the three viable networks, S-motility promotes A-motor activation. In contrast, whether and how S-motility regulates A-motor engagement does not affect the qualitative outputs of these networks. In summary, promotion of A-motor activation by S-motility is necessary to reconcile the seemingly contradictory mechanosensing behaviors in wild type vs. A^+S^- cells.

Discussion

Mechanosensing is an important function of bacteria, which allows them to 'perceive' the properties of the surfaces in contact and adjust behaviors accordingly. Through mechanosensing, *M. xanthus* regulates its cell reversal frequency in response to external mechanical cues, such as substrate stiffness and physical contacts with colony mates or prey cells. These responses are crucial for complex pattern formation in *M. xanthus* populations (Igoshin et al., 2001, 2004). Here we developed the first mathematical model for mechanosensing-based reversal control in *M. xanthus* in response to substrate stiffness. The model highlights the interplay between the polarity pathway and the A-motor, particularly incorporating the experimentally established dynamics of A-motors and their binding to polarity regulator MglA (Figure 1). Based on the previously observed intensification of A-motor clustering on hard substrates (Nan et al., 2010), the model uses the A-motor engagement rate to represent substrate stiffness. The model predicts a dependence of cell reversal frequency on substrate stiffness that is consistent with that found in cells that move with A-motility alone (A^+S^-) (Figure 3). Furthermore, the model predicts a biphasic dependence of the reversal frequency on the activation rate of A-motors (Figure 4). Finally, we tested the hypothesis that the S-motility machinery mediates reversal control indirectly through the A-motility machinery, and found that an additional promotion of A-motor activation by S-motility can explain why the wild type and A^+S^- cells show opposite responses to substrate stiffness (Zhou and Nan, 2017) (Figure 5). This model prediction awaits future experimental validation. Overall, our model suggests that the A-motility machinery of *M. xanthus* serves as a hub of mechanosensing-based reversal control, which modulates cell reversal in response to environmental mechanical cues.

Note that our model predictions are qualitative, as the model was built upon simplified mechanism of the A-motility machinery and polarity pathway, both of which comprise many molecules that dynamically interact with each other, but the details of these interactions are yet elusive. For instance, the observed spatial dynamics of Agl proteins that constitute the energy-harvesting core of the A-motility machinery and the MreB molecules that constitute the intracellular track for A-motility switch between immotile, directed motion, and diffusion (Nan et al., 2013, 2015; Fu et al., 2018). However, their population distributions do not exhibit three clearly distinct peaks that correspond to these three movement patterns, indicating that the dynamics of the A-motility machinery is more intricate than the three states assumed in the model. Moreover, even though the cast of molecular players constituting the A-motility machinery is increasingly clear (Luciano et al., 2011; Faure et al., 2016; Islam et al., 2023), how exactly A-motors interact with the substrate is not known (Wong et al., 2021; Chen and Nan, 2022). In the model, we resorted to a generic and simplistic assumption that the motor engagement rate depends on substrate stiffness, based on the observed relationship between the motor clustering intensity and substrate stiffness (Nan et al., 2010). These simplifications could cause the quantitative difference between the model prediction and experimental observation, e.g., in Figure 3. Furthermore, for the polarity pathway, we simply adopted the model from (Guzzo et al., 2018). Details of this core regulatory pathway would certainly affect the model prediction quantitatively. As future experiments disclose more mechanistic and quantitative details about these pathways, we will be able to refine our model and make more accurate predictions. On a side note, here we compared the measured reversal frequencies of wild type cells that we previously published (Zhou and Nan, 2017) with those of A^+S^- cells that we collected in this work. This comparison is warranted, because the reversal frequency assay does not involve any labeling or other perturbations to the cell, and hence the results, especially the qualitative trends, are very robust. These data are sufficient for comparison with the qualitative predictions of our current model. With a more precise model in the future, a more tightly controlled experiment and more detailed analysis of the experimental data (e.g., comparing the distribution of reversal frequencies rather than just the average) could become necessary.

In the last part of our work where we theorize about the opposite reversal responses observed in A^+S^- vs. wild type cells, we chose to confine our choices of regulatory networks to those in which S-motility controls mechanosensing indirectly through the A-motility machinery. This assumption was made mainly because

10.3389/fmicb.2023.1294631

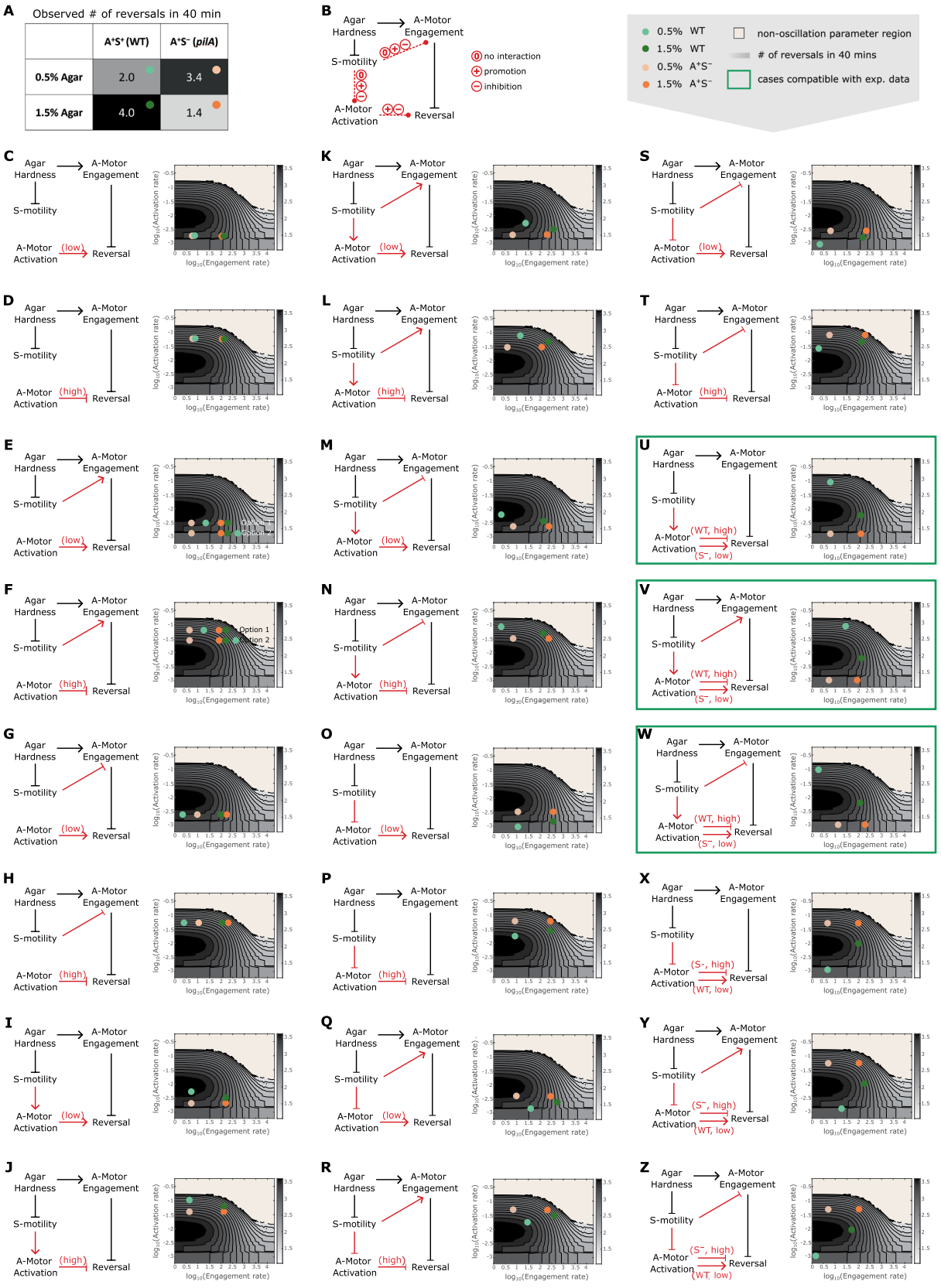

FIGURE 5
Reversal control networks that reconcile the contrasting mechanosensing responses in wild type vs. A^+S^- cells. **(A)** Experimentally observed cell reversal frequencies of wild type and A^+S^- cells on soft (0.5%) and hard (1.5%) agar surfaces. The observed reversal frequencies are visually represented by the shade of the corresponding cells of the table, where darker colors indicate higher reversal frequencies. **(B)** Summary of all generic reversal control networks in which the S-motility machinery controls cell reversal indirectly through the A-motility machinery. Black arrows: controls of

(Continued)

FIGURE 5 (Continued)
certainty. Red arrows: controls with uncertainty. **(C–Z)** Examination of individual networks for their qualitative compatibility with the experimental data. Representative parameter points for wild type and A^+S^- cells on 0.5 and 1.5% agar surfaces for each network (left) were chosen according to the expected relations among the four cases of interest in terms of their A-motor engagement and activation rates, and are shown on the 2D phase diagram (right, same as Supplementary Figure S2B). Note that due to the higher activity of S-motility on soft substrates, its influence on A-motors is expected to be more pronounced on 0.5% agar compared to 1.5% agar. Hence, the parameter point representing the wild type cell on 0.5% agar (light green dots) must be located in a similar direction relative to the parameter point for the A^+S^- cell on 0.5% agar (light orange dots) as the parameter point for the wild type cell on 1.5% agar (dark green dots) is relative to the parameter point for the A^+S^- cell on 1.5% agar (bright orange dots), except that the former pair of dots (light green vs. light orange) are separated by a greater distance. For example, in panel (K), because S-motility promotes both activation and engagement of A-motors, the dark green and light green dots are located northeast of the bright orange and light orange dots, respectively; but the distance between the light green and light orange dots is larger than that between the dark green and bright orange dots. Green boxes highlight networks that can explain the qualitative relationship among the experimental data points shown in **(A)**.

M. xanthus cells moving by S-motility alone exhibit similar reversal frequency on soft and hard agar surfaces (Zhou and Nan, 2017), suggesting that S-motility probably does not respond to mechanical cues directly. Recently, MglA was found to activate the S-motility machinery at the leading cell pole (Mercier et al., 2020; Potapova et al., 2020; Bautista et al., 2023). A feedback may exist between the S-motility machinery and MglA, which could be incorporated in future revision of the model.

The mechanical cues sensed by *M. xanthus* are more than just substrate stiffness. Previous experiments show that *M. xanthus* cells can also sense physical contacts with colony mates or preys and modulate the frequency and timing of cell reversals accordingly (Hodgkin and Kaiser, 1977; Welch and Kaiser, 2001; Lobedanz and Sogaard-Andersen, 2003; Kaiser and Welch, 2004; Sogaard-Andersen, 2007). Such cellular responses are key to rippling wave formation (Igoshin et al., 2001, 2004), cooperative predation (Berleman et al., 2006, 2008; Keane and Berleman, 2016) and fruiting body formation (Jelsbak and Sogaard-Andersen, 2003; Kaiser and Welch, 2004; Sozinova et al., 2006; Sliusarenko et al., 2007; Thutupalli et al., 2015) in *M. xanthus* populations. Furthermore, exopolysaccharides (EPS), which comprise the majority of the extracellular matrix of *M. xanthus*, inhibit *M. xanthus* reversal in a dosage-dependent manner (Zhou and Nan, 2017). Meanwhile, methylcellulose has the same effect on *M. xanthus* reversal (Zhou and Nan, 2017). As a synthetic polysaccharide that does not exist naturally, methylcellulose is unlikely to trigger chemically specific signals in *M. xanthus*. Hence, the cell probably senses both EPS and methylcellulose mechanically. It is possible that all these mechanosensing behaviors are mediated by the A-motility machinery. For example, the extracellular polysaccharides may promote or mediate engagement of A-motors, which is predicted by our model to inhibit cell reversal (Figure 3).

Mechanoresponses have been studied in various other cellular systems, such as load-dependent recruitment of stator subunits to the bacterial flagellar motor (Nord et al., 2017; Wadhwa et al., 2019), frequency-dependent alignment of muscle cell stress fiber in response to cyclic mechanical stress (Liu et al., 2008; Hsu et al., 2009), and thickening of arterial walls induced by hypertension (Hahn and Schwartz, 2009). While each system employs its own set of molecules for mechanoresponses, certain general principles are shared. Notably, the components responsible for sensing the force are typically force-generating or force-bearing by themselves (Hoffman et al., 2011). Moreover, mechanical forces are often transduced into biochemical signals that influence downstream pathways (Hoffman et al., 2011). These principles are evident in our mechanosensing model. The force-generating A-motility machinery of *M. xanthus* is proposed to transduce the mechanical cues it senses into a cell reversal signal, through its coupling with the reversal regulator MglA. However, unlike the signals in most well studied mechanoresponse mechanisms, the biochemical signal in our model does not arise from force-induced protein conformational changes, but rather from a motor-driven intracellular spatial regulation.

Elucidating the mechanisms of mechanosensing and mechanoresponse is challenging due to the complexity and dynamic nature of these processes. Mathematical modeling provides a useful tool to coherently combine segregated pieces of experimental observations, and generate hypotheses and testable predictions for future experimental studies. Ultimately, integration of modeling and experimentation will provide the best tool to uncover mysteries in bacterial mechanosensing/response and shed light on the intricate interplay between bacterial motility and environmental stimuli.

Data availability statement

The original contributions presented in the study are included in the article/Supplementary material, and further inquiries can be directed to the corresponding author.

Author contributions

YC: Data curation, Formal analysis, Investigation, Methodology, Visualization, Writing – original draft, Writing – review & editing, Software. ET: Investigation, Methodology, Writing – original draft. BN: Funding acquisition, Resources, Supervision, Validation, Writing – review & editing, Data curation. JC: Conceptualization, Formal analysis, Funding acquisition, Investigation, Project administration, Resources, Supervision, Validation, Writing – review & editing, Methodology, Visualization.

Funding

The author(s) declare financial support was received for the research, authorship, and/or publication of this article. This work was supported by NIH 1R35GM138370 to JC and 1R01GM129000 to BN.

Acknowledgments

We acknowledge members of the Chen lab for helpful discussion.

Conflict of interest

The authors declare that the research was conducted in the absence of any commercial or financial relationships that could be construed as a potential conflict of interest.

Publisher's note

All claims expressed in this article are solely those of the authors and do not necessarily represent those of their affiliated organizations, or those of the publisher, the editors and the reviewers. Any product that may be evaluated in this article, or claim that may be made by its manufacturer, is not guaranteed or endorsed by the publisher.

Supplementary material

The Supplementary material for this article can be found online at: https://www.frontiersin.org/articles/10.3389/fmicb.2023.1294631/full#supplementary-material

References

Bautista, S., Schmidt, V., Guiseppi, A., Mauriello, E. M. F., Attia, B., Elantak, L., et al. (2023). Frz S acts as a polar beacon to recruit SgmX, a central activator of type IV pili during *Myxococcus xanthus* motility. *EMBO J.* 42:e111661. doi: 10.15252/embj.2022111661

Berg, H. C., and Brown, D. A. (1972). Chemotaxis in *Escherichia coli* analysed by three-dimensional tracking. *Nature* 239, 500–504. doi: 10.1038/239500a0

Berleman, J. E., Chumley, T., Cheung, P., and Kirby, J. R. (2006). Rippling is a predatory behavior in *Myxococcus xanthus*. *J. Bacteriol.* 188, 5888–5895. doi: 10.1128/JB.00559-06

Berleman, J. E., and Kirby, J. R. (2007). Multicellular development in *Myxococcus xanthus* is stimulated by predator-prey interactions. *J. Bacteriol.* 189, 5675–5682. doi: 10.1128/JB.00544-07

Berleman, J. E., and Kirby, J. R. (2009). Deciphering the hunting strategy of a bacterial wolfpack. *FEMS Microbiol. Rev.* 33, 942–957. doi: 10.1111/j.1574-6976.2009.00185.x

Berleman, J. E., Scott, J., Chumley, T., and Kirby, J. R. (2008). Predataxis behavior in *Myxococcus xanthus*. *Proc. Natl. Acad. Sci. U. S. A.* 105, 17127–17132. doi: 10.1073/pnas.0804387105

Billaudeau, C., Chastanet, A., Yao, Z., Cornilleau, C., Mirouze, N., Fromion, V., et al. (2017). Contrasting mechanisms of growth in two model rod-shaped bacteria. *Nat. Commun.* 8:15370. doi: 10.1038/ncomms15370

Borner, U., Deutsch, A., Reichenbach, H., and Bar, M. (2002). Rippling patterns in aggregates of myxobacteria arise from cell-cell collisions. *Phys. Rev. Lett.* 89:078101. doi: 10.1103/PhysRevLett.89.078101

Bulyha, I., Hot, E., Huntley, S., and Sogaard-Andersen, L. (2011). GTPases in bacterial cell polarity and signalling. *Curr. Opin. Microbiol.* 14, 726–733. doi: 10.1016/j.mib.2011.09.001

Burrows, L. L. (2012). *Pseudomonas aeruginosa* twitching motility: type IV pili in action. *Annu. Rev. Microbiol.* 66, 493–520. doi: 10.1146/annurev-micro-092611-150055

Carreira, L. A. M., Szadkowski, D., Muller, F., and Sogaard-Andersen, L. (2022). Spatiotemporal regulation of switching front-rear cell polarity. *Curr. Opin. Cell Biol.* 76:102076. doi: 10.1016/j.ceb.2022.102076

Chen, J., and Nan, B. (2022). Flagellar motor transformed: biophysical perspectives of the *Myxococcus xanthus* gliding mechanism. *Front. Microbiol.* 13:891694. doi: 10.3389/fmicb.2022.891694

Cheng, B., Lin, M., Huang, G., Li, Y., Ji, B., Genin, G. M., et al. (2017). Cellular mechanosensing of the biophysical microenvironment: a review of mathematical models of biophysical regulation of cell responses. *Phys Life Rev* 22-23, 88–119. doi: 10.1016/j.plrev.2017.06.016

Colin, R., Drescher, K., and Sourjik, V. (2019). Chemotactic behaviour of *Escherichia coli* at high cell density. *Nat. Commun.* 10:5329. doi: 10.1038/s41467-019-13179-1

Dufrene, Y. F., and Persat, A. (2020). Mechanomicrobiology: how bacteria sense and respond to forces. *Nat. Rev. Microbiol.* 18, 227–240. doi: 10.1038/s41579-019-0314-2

Errington, J. (2015). Bacterial morphogenesis and the enigmatic Mre B helix. *Nat. Rev. Microbiol.* 13, 241–248. doi: 10.1038/nrmicro3398

Faure, L. M., Fiche, J. B., Espinosa, L., Ducret, A., Anantharaman, V., Luciano, J., et al. (2016). The mechanism of force transmission at bacterial focal adhesion complexes. *Nature* 539:530-+. doi: 10.1038/nature20121

Fu, G., Bandaria, J. N., Le Gall, A. V., Fan, X., Yildiz, A., Mignot, T., et al. (2018). MotAB-like machinery drives the movement of MreB filaments during bacterial gliding motility. *Proc. Natl. Acad. Sci. U. S. A.* 115, 2484–2489. doi: 10.1073/pnas.1716441115

Galicia, C., Lhospice, S., Varela, P. F., Trapani, S., Zhang, W., Navaza, J., et al. (2019). MglA functions as a three-state GTPase to control movement reversals of *Myxococcus xanthus*. *Nat. Commun.* 10:5300. doi: 10.1038/s41467-019-13274-3

Gordon, V. D., and Wang, L. (2019). Bacterial mechanosensing: the force will be with you, always. *J. Cell Sci.* 132:jcs227694. doi: 10.1242/jcs.227694

Guzzo, M., Murray, S. M., Martineau, E., Lhospice, S., Baronian, G., My, L., et al. (2018). A gated relaxation oscillator mediated by FrzX controls morphogenetic movements in *Myxococcus xanthus*. *Nat. Microbiol.* 3, 948–959. doi: 10.1038/s41564-018-0203-x

Hahn, C., and Schwartz, M. A. (2009). Mechanotransduction in vascular physiology and atherogenesis. *Nat. Rev. Mol. Cell Biol.* 10, 53–62. doi: 10.1038/nrm2596

Hodgkin, J., and Kaiser, D. (1977). Cell-to-cell stimulation of movement in nonmotile mutants of Myxococcus. *Proc. Natl. Acad. Sci. U. S. A.* 74, 2938–2942. doi: 10.1073/pnas.74.7.2938

Hoffman, B. D., Grashoff, C., and Schwartz, M. A. (2011). Dynamic molecular processes mediate cellular mechanotransduction. *Nature* 475, 316–323. doi: 10.1038/nature10316

Hsu, H. J., Lee, C. F., and Kaunas, R. (2009). A dynamic stochastic model of frequency-dependent stress fiber alignment induced by cyclic stretch. *PLoS One* 4:e4853. doi: 10.1371/journal.pone.0004853

Igoshin, O. A., Mogilner, A., Welch, R. D., Kaiser, D., and Oster, G. (2001). Pattern formation and traveling waves in myxobacteria: theory and modeling. *Proc. Natl. Acad. Sci. U. S. A.* 98, 14913–14918. doi: 10.1073/pnas.221579598

Igoshin, O. A., Welch, R., Kaiser, D., and Oster, G. (2004). Waves and aggregation patterns in myxobacteria. *Proc. Natl. Acad. Sci. U. S. A.* 101, 4256–4261. doi: 10.1073/pnas.0400704101

Islam, S. T., Jolivet, N. Y., Cuzin, C., Belgrave, A. M., My, L., Fleuchot, B., et al. (2023). Unmasking of the von Willebrand A-domain surface adhesin CglB at bacterial focal adhesions mediates myxobacterial gliding motility. *Sci. Adv.* 9:eabq0619. doi: 10.1126/sciadv.abq0619

Islam, S. T., and Mignot, T. (2015). The mysterious nature of bacterial surface (gliding) motility: a focal adhesion-based mechanism in *Myxococcus xanthus*. *Semin. Cell Dev. Biol.* 46, 143–154. doi: 10.1016/j.semcdb.2015.10.033

Jelsbak, L., and Sogaard-Andersen, L. (2003). Cell behavior and cell-cell communication during fruiting body morphogenesis in *Myxococcus xanthus*. *J. Microbiol. Methods* 55, 829–839. doi: 10.1016/j.mimet.2003.08.007

Kaimer, C., Berleman, J. E., and Zusman, D. R. (2012). Chemosensory signaling controls motility and subcellular polarity in *Myxococcus xanthus*. *Curr. Opin. Microbiol.* 15, 751–757. doi: 10.1016/j.mib.2012.10.005

Kaimer, C., and Zusman, D. R. (2016). Regulation of cell reversal frequency in *Myxococcus xanthus* requires the balanced activity of CheY-like domains in FrzE and FrzZ. *Mol. Microbiol.* 100, 379–395. doi: 10.1111/mmi.13323

Kaiser, D., and Welch, R. (2004). Dynamics of fruiting body morphogenesis. *J. Bacteriol.* 186, 919–927. doi: 10.1128/JB.186.4.919-927.2004

Keane, R., and Berleman, J. (2016). The predatory life cycle of *Myxococcus xanthus*. *Microbiology (Reading)* 162, 1–11. doi: 10.1099/mic.0.000208

Kim, S. Y., Gitai, Z., Kinkhabwala, A., Shapiro, L., and Moerner, W. E. (2006). Single molecules of the bacterial actin MreB undergo directed treadmilling motion in *Caulobacter crescentus*. *Proc. Natl. Acad. Sci. U. S. A.* 103, 10929–10934. doi: 10.1073/pnas.0604503103

Lele, P. P., Hosu, B. G., and Berg, H. C. (2013). Dynamics of mechanosensing in the bacterial flagellar motor. *Proc. Natl. Acad. Sci. U. S. A.* 110, 11839–11844. doi: 10.1073/pnas.1305885110

Leonardy, S., Freymark, G., Hebener, S., Ellehauge, E., and Sogaard-Andersen, L. (2007). Coupling of protein localization and cell movements by a dynamically localized response regulator in *Myxococcus xanthus*. *EMBO J.* 26, 4433–4444. doi: 10.1038/sj.emboj.7601877

Leonardy, S., Miertzschke, M., Bulyha, I., Sperling, E., Wittinghofer, A., and Sogaard-Andersen, L. (2010). Regulation of dynamic polarity switching in bacteria by a Ras-like G-protein and its cognate GAP. *EMBO J.* 29, 2276–2289. doi: 10.1038/emboj.2010.114

Liu, B., Qu, M. J., Qin, K. R., Li, H., Li, Z. K., Shen, B. R., et al. (2008). Role of cyclic strain frequency in regulating the alignment of vascular smooth muscle cells *in vitro*. *Biophys. J.* 94, 1497–1507. doi: 10.1529/biophysj.106.098574

Lobedanz, S., and Sogaard-Andersen, L. (2003). Identification of the C-signal, a contact-dependent morphogen coordinating multiple developmental responses in *Myxococcus xanthus*. *Genes Dev.* 17, 2151–2161. doi: 10.1101/gad.274203

Luciano, J., Agrebi, R., Le Gall, A. V., Wartel, M., Fiegna, F., Ducret, A., et al. (2011). Emergence and modular evolution of a novel motility machinery in bacteria. *PLoS Genet.* 7:e1002268. doi: 10.1371/journal.pgen.1002268

Martino, F., Perestrelo, A. R., Vinarsky, V., Pagliari, S., and Forte, G. (2018). Cellular Mechanotransduction: from tension to function. *Front. Physiol.* 9:824. doi: 10.3389/fphys.2018.00824

Mauriello, E. M., Mignot, T., Yang, Z., and Zusman, D. R. (2010a). Gliding motility revisited: how do the myxobacteria move without flagella? *Microbiol. Mol. Biol. Rev.* 74, 229–249. doi: 10.1128/MMBR.00043-09

Mauriello, E. M., Mouhamar, F., Nan, B., Ducret, A., Dai, D., Zusman, D. R., et al. (2010b). Bacterial motility complexes require the actin-like protein, MreB and the Ras homologue, MglA. *EMBO J.* 29, 315–326. doi: 10.1038/emboj.2009.356

Mcbride, M. J., and Zusman, D. R. (1996). Behavioral analysis of single cells of *Myxococcus xanthus* in response to prey cells of *Escherichia coli*. *FEMS Microbiol. Lett.* 137, 227–231. doi: 10.1111/j.1574-6968.1996.tb08110.x

Mercier, R., Bautista, S., Delannoy, M., Gibert, M., Guiseppi, A., Herrou, J., et al. (2020). The polar Ras-like GTPase MglA activates type IV pilus via SgmX to enable twitching motility in *Myxococcus xanthus*. *Proc. Natl. Acad. Sci. U. S. A.* 117, 28366–28373. doi: 10.1073/pnas.2002783117

Miertzschke, M., Koerner, C., Vetter, I. R., Keilberg, D., Hot, E., Leonardy, S., et al. (2011). Structural analysis of the Ras-like G protein MglA and its cognate GAP MglB and implications for bacterial polarity. *EMBO J.* 30, 4185–4197. doi: 10.1038/emboj.2011.291

Mignot, T., Shaevitz, J. W., Hartzell, P. L., and Zusman, D. R. (2007). Evidence that focal adhesion complexes power bacterial gliding motility. *Science* 315, 853–856. doi: 10.1126/science.1137223

Munoz-Dorado, J., Marcos-Torres, F. J., Garcia-Bravo, E., Moraleda-Munoz, A., and Perez, J. (2016). Myxobacteria: moving, killing, feeding, and surviving together. *Front. Microbiol.* 7:781. doi: 10.3389/fmicb.2016.00781

Nan, B. (2017). Bacterial gliding motility: rolling out a consensus model. *Curr. Biol.* 27, R154–R156. doi: 10.1016/j.cub.2016.12.035

Nan, B. Y., Bandaria, J. N., Guo, K. Y., Fan, X., Moghtaderi, A., Yildiz, A., et al. (2015). The polarity of myxobacterial gliding is regulated by direct interactions between the gliding motors and the Ras homolog MglA. *Proc. Natl. Acad. Sci. U. S. A.* 112, E186–E193. doi: 10.1073/pnas.1421073112

Nan, B. Y., Bandaria, J. N., Moghtaderi, A., Sun, I. H., Yildiz, A., and Zusman, D. R. (2013). Flagella stator homologs function as motors for myxobacterial gliding motility by moving in helical trajectories. *Proc. Natl. Acad. Sci. U. S. A.* 110, E1508–E1513. doi: 10.1073/pnas.1219982110

Nan, B., Chen, J., Neu, J. C., Berry, R. M., Oster, G., and Zusman, D. R. (2011). Myxobacteria gliding motility requires cytoskeleton rotation powered by proton motive force. *Proc. Natl. Acad. Sci. U. S. A.* 108, 2498–2503. doi: 10.1073/pnas.1018556108

Nan, B., Mauriello, E. M., Sun, I. H., Wong, A., and Zusman, D. R. (2010). A multi-protein complex from *Myxococcus xanthus* required for bacterial gliding motility. *Mol. Microbiol.* 76, 1539–1554. doi: 10.1111/j.1365-2958.2010.07184.x

Nan, B., Mcbride, M. J., Chen, J., Zusman, D. R., and Oster, G. (2014). Bacteria that glide with helical tracks. *Curr. Biol.* 24, R169–R173. doi: 10.1016/j.cub.2013.12.034

Nord, A. L., Gachon, E., Perez-Carrasco, R., Nirody, J. A., Barducci, A., Berry, R. M., et al. (2017). Catch bond drives stator mechanosensitivity in the bacterial flagellar motor. *Proc. Natl. Acad. Sci. U. S. A.* 114, 12952–12957. doi: 10.1073/pnas.1716002114

Patryn, J., Allen, K., Dziewanowska, K., Otto, R., and Hartzell, P. L. (2010). Localization of MgIA, an essential gliding motility protein in *Myxococcus xanthus*. *Cytoskeleton* 67, 322–337. doi: 10.1002/cm.20447

Persat, A., Nadell, C. D., Kim, M. K., Ingremeau, F., Siryaporn, A., Drescher, K., et al. (2015). The mechanical world of Bacteria. *Cells* 161, 988–997. doi: 10.1016/j.cell.2015.05.005

Potapova, A., Carreira, L. A. M., and Sogaard-Andersen, L. (2020). The small GTPase MglA together with the TPR domain protein SgmX stimulates type IV pili formation in *M. xanthus*. *Proc. Natl. Acad. Sci. U. S. A.* 117, 23859–23868. doi: 10.1073/pnas.2004722117

Schumacher, D., and Sogaard-Andersen, L. (2017). Regulation of cell polarity in motility and cell division in *Myxococcus xanthus*. *Annu. Rev. Microbiol.* 71, 61–78. doi: 10.1146/annurev-micro-102215-095415

Shi, W., Ngok, F. K., and Zusman, D. R. (1996). Cell density regulates cellular reversal frequency in *Myxococcus xanthus*. *Proc. Natl. Acad. Sci. U. S. A.* 93, 4142–4146. doi: 10.1073/pnas.93.9.4142

Shi, W., and Zusman, D. R. (1993). The two motility systems of *Myxococcus xanthus* show different selective advantages on various surfaces. *Proc. Natl. Acad. Sci. U. S. A.* 90, 3378–3382. doi: 10.1073/pnas.90.8.3378

Sliusarenko, O., Zusman, D. R., and Oster, G. (2007). Aggregation during fruiting body formation in *Myxococcus xanthus* is driven by reducing cell movement. *J. Bacteriol.* 189, 611–619. doi: 10.1128/JB.01206-06

Sogaard-Andersen, L. (2007). "Contact-dependent signaling in *Myxococcus xanthus*: the function of the C-signal in fruiting body morphogenesis" in *Myxobacteria: Multicellularity and differentiation*, 77–91.

Sourjik, V., and Wingreen, N. S. (2012). Responding to chemical gradients: bacterial chemotaxis. *Curr. Opin. Cell Biol.* 24, 262–268. doi: 10.1016/j.ceb.2011.11.008

Sozinova, O., Jiang, Y., Kaiser, D., and Alber, M. (2006). A three-dimensional model of myxobacterial fruiting-body formation. *Proc. Natl. Acad. Sci. U. S. A.* 103, 17255–17259. doi: 10.1073/pnas.0605555103

Sun, M., Wartel, M., Cascales, E., Shaevitz, J. W., and Mignot, T. (2011). Motor-driven intracellular transport powers bacterial gliding motility. *Proc. Natl. Acad. Sci. U. S. A.* 108, 7559–7564. doi: 10.1073/pnas.1101101108

Sun, H., Zusman, D. R., and Shi, W. Y. (2000). Type IV pilus of *Myxococcus xanthus* is a motility apparatus controlled by the frz chemosensory system. *Curr. Biol.* 10, 1143–1146. doi: 10.1016/S0960-9822(00)00705-3

Szadkowski, D., Carreira, L. A. M., and Sogaard-Andersen, L. (2022). A bipartite, low-affinity roadblock domain-containing GAP complex regulates bacterial front-rear polarity. *PLoS Genet.* 18:e1010384. doi: 10.1371/journal.pgen.1010384

Szadkowski, D., Harms, A., Carreira, L. A. M., Wigbers, M., Potapova, A., Wuichet, K., et al. (2019). Spatial control of the GTPase MglA by localized RomR-RomX GEF and MglB GAP activities enables *Myxococcus xanthus* motility. *Nat Microbiol* 4, 1344–1355. doi: 10.1038/s41564-019-0451-4

Tala, L., Fineberg, A., Kukura, P., and Persat, A. (2019). *Pseudomonas aeruginosa* orchestrates twitching motility by sequential control of type IV pili movements. *Nat. Microbiol.* 4, 774–780. doi: 10.1038/s41564-019-0378-9

Tao, J., Li, Y., Vig, D. K., and Sun, S. X. (2017). Cell mechanics: a dialogue. *Rep. Prog. Phys.* 80:036601. doi: 10.1088/1361-6633/aa5282

Thutupalli, S., Sun, M., Bunyak, F., Palaniappan, K., and Shaevitz, J. W. (2015). Directional reversals enable *Myxococcus xanthus* cells to produce collective one-dimensional streams during fruiting-body formation. *J. R. Soc. Interface* 12:20150049. doi: 10.1098/rsif.2015.0049

Tipping, M. J., Delalez, N. J., Lim, R., Berry, R. M., and Armitage, J. P. (2013). Load-dependent assembly of the bacterial flagellar motor. *MBio* 4:4. doi: 10.1128/mBio.00551-13

Treuner-Lange, A., Macia, E., Guzzo, M., Hot, E., Faure, L. M., Jakobczak, B., et al. (2015). The small G-protein MglA connects to the MreB actin cytoskeleton at bacterial focal adhesions. *J. Cell Biol.* 210, 243–256. doi: 10.1083/jcb.201412047

Van Den Ent, F., Izore, T., Bharat, T. A., Johnson, C. M., and Lowe, J. (2014). Bacterial actin MreB forms antiparallel double filaments. *elife* 3:e02634. doi: 10.7554/eLife.02634

Velicer, G. J., and Vos, M. (2009). Sociobiology of the myxobacteria. *Annu. Rev. Microbiol.* 63, 599–623. doi: 10.1146/annurev.micro.091208.073158

Wadhams, G. H., and Armitage, J. P. (2004). Making sense of it all: bacterial chemotaxis. *Nat. Rev. Mol. Cell Biol.* 5, 1024–1037. doi: 10.1038/nrm1524

Wadhwa, N., Phillips, R., and Berg, H. C. (2019). Torque-dependent remodeling of the bacterial flagellar motor. *Proc. Natl. Acad. Sci. U. S. A.* 116, 11764–11769. doi: 10.1073/pnas.1904577116

Welch, R., and Kaiser, D. (2001). Cell behavior in traveling wave patterns of myxobacteria. *Proc. Natl. Acad. Sci. U. S. A.* 98, 14907–14912. doi: 10.1073/pnas.261574598

Wong, G. C. L., Antani, J. D., Lele, P., Chen, J., Nan, B., Kühn, M. J., et al. (2021). Roadmap on emerging concepts in the physical biology of bacterial biofilms: from surface sensing to community formation. *Phys. Biol.* 18:051501. doi: 10.1088/1478-3975/abdc0e

Zhang, Y., Ducret, A., Shaevitz, J., and Mignot, T. (2012a). From individual cell motility to collective behaviors: insights from a prokaryote, *Myxococcus xanthus*. *FEMS Microbiol. Rev.* 36, 149–164. doi: 10.1111/j.1574-6976.2011.00307.x

Zhang, Y., Franco, M., Ducret, A., and Mignot, T. (2010). A bacterial Ras-like small GTP-binding protein and its cognate GAP establish a dynamic spatial polarity Axis to control directed motility. *PLoS Biol.* 8:e1000430.

Zhang, Y., Guzzo, M., Ducret, A., Li, Y. Z., and Mignot, T. (2012b). A dynamic response regulator protein modulates G-protein-dependent polarity in the bacterium *Myxococcus xanthus*. *PLoS Genet.* 8:e1002872. doi: 10.1371/journal.pgen.1002872

Zhang, W., Wang, Y., Lu, H., Liu, Q., Wang, C., Hu, W., et al. (2020). Dynamics of solitary predation by *Myxococcus xanthus* on *Escherichia coli* observed at the single-cell level. *Appl. Environ. Microbiol.* 86, e2286–19. doi: 10.1128/AEM.02286-19

Zhou, T., and Nan, B. (2017). Exopolysaccharides promote *Myxococcus xanthus* social motility by inhibiting cellular reversals. *Mol. Microbiol.* 103, 729–743. doi: 10.1111/mmi.13585

frontiers | Frontiers in Microbiology

TYPE Mini Review
PUBLISHED 24 January 2024
DOI 10.3389/fmicb.2024.1339696

OPEN ACCESS

EDITED BY
Li Zhoukun,
Nanjing Agricultural University, China

REVIEWED BY
Wei Hu,
Microbial Technology Institute/Shandong University, China

*CORRESPONDENCE
Aurelio Moraleda-Muñoz
✉ aureliom@ugr.es
Francisco Javier Marcos-Torres
✉ fjmarcos@ugr.es

RECEIVED 16 November 2023
ACCEPTED 15 January 2024
PUBLISHED 24 January 2024

CITATION
Contreras-Moreno FJ, Pérez J, Muñoz-Dorado J, Moraleda-Muñoz A and Marcos-Torres FJ (2024) *Myxococcus xanthus* predation: an updated overview. *Front. Microbiol.* 15:1339696. doi: 10.3389/fmicb.2024.1339696

Myxococcus xanthus predation: an updated overview

Francisco Javier Contreras-Moreno, Juana Pérez, José Muñoz-Dorado, Aurelio Moraleda-Muñoz* and Francisco Javier Marcos-Torres*

Departamento de Microbiología, Facultad de Ciencias, Universidad de Granada, Granada, Spain

Bacterial predators are widely distributed across a variety of natural environments. Understanding predatory interactions is of great importance since they play a defining role in shaping microbial communities in habitats such as soils. *Myxococcus xanthus* is a soil-dwelling bacterial predator that can prey on Gram-positive and Gram-negative bacteria and even on eukaryotic microorganisms. This model organism has been studied for many decades for its unusual lifecycle, characterized by the formation of multicellular fruiting bodies filled with myxospores. However, less is known about its predatory behavior despite being an integral part of its lifecycle. Predation in *M. xanthus* is a multifactorial process that involves several mechanisms working synergistically, including motility systems to efficiently track and hunt prey, and a combination of short-range and contact-dependent mechanisms to achieve prey death and feed on them. In the short-range attack, *M. xanthus* is best known for the collective production of secondary metabolites and hydrolytic enzymes to kill prey and degrade cellular components. On the other hand, contact-dependent killing is a cell-to-cell process that relies on Tad-like and type III secretion systems. Furthermore, recent research has revealed that metals also play an important role during predation, either by inducing oxidative stress in the prey, or by competing for essential metals. In this paper, we review the current knowledge about *M. xanthus* predation, focusing on the different mechanisms used to hunt, kill, and feed on its prey, considering the most recent discoveries and the transcriptomic data available.

KEYWORDS

myxobacteria, bacterial predation, bacterial interaction, predator-prey interactions, motility, secondary metabolites, hydrolytic enzymes, metals

Introduction

Myxococcus xanthus is a soil-dwelling bacterial predator renowned for its social and multicellular behavior, which is evident along its complex lifecycle. When nutrients are scarce, *M. xanthus* cells coordinate to form multicellular structures known as fruiting bodies, where some of them differentiate into resistant myxospores. Depending on external cues, such as nutrient levels or the presence of prey microorganisms, *M. xanthus* must decide whether to initiate this developmental cycle or to activate its predatory mechanisms to feed (Muñoz-Dorado et al., 2016).

Coordinating these two facets of its lifecycle has led to an extensive coevolution between both stages. Indeed, mutations in genes involved in early stages of the developmental cycle, where cells are still to commit to this process, have been found to negatively impact predation.

By contrast, genes required in later stages of the development, where cells are fully committed to fruiting-body formation, do not seem to play a role in predation (Pham et al., 2005; Berleman et al., 2008; Pérez et al., 2022). Furthermore, some predator–prey interactions can stimulate fruiting bodies formation even during predation, although cells within the fruiting bodies are unable to differentiate into myxospores (Berleman and Kirby, 2007).

When conditions are favorable again, myxospores from a fruiting body will germinate into a population of vegetative cells known as swarm, which will actively hunt for prey to feed on them. Cells within the swarm will cooperate in an attempt to prey with different degrees of success on a great diversity of Gram-negative and Gram-positive bacteria (Figure 1), including nitrogen-fixing bacteria and some human and plant pathogens, as well as fungi and nematodes (Mendes-Soares and Velicer, 2013; Livingstone et al., 2017; Petters et al., 2021; Sydney et al., 2021).

M. xanthus predation is a multifactorial task that combines a broad arsenal of resources to ensure prey death. This process starts with tracking of prey in the environment driven by its motility systems and signal-transduction mechanisms. Upon encountering a suitable prey, *M. xanthus* uses a combination of short-range and contact-dependent mechanisms to kill and lyse prey cells. While short-range killing mainly involves the production of a battery of secondary metabolites (SMs) such as antibiotics, and of hydrolytic enzymes to degrade and feed on the cellular components of the prey (Muñoz-Dorado et al., 2016), contact-dependent lysis is mediated by secretion systems (Seef et al., 2021; Thiery et al., 2022). Moreover, recent studies have shown that metals are also involved in *M. xanthus* predation either by using metals to provoke oxidative stress or by outcompeting prey for possession of essential metals (Contreras-Moreno et al., 2020; Lee et al., 2020; Dong et al., 2022b; Pérez et al., 2022).

While the developmental stage of *M. xanthus* has been thoroughly studied, less attention has been paid to its predatory behavior. This is, however, not an isolated facet of its lifestyle, but is heavily interconnected to the other traits of *M. xanthus* biology to shape its lifecycle (Volz et al., 2012; Pérez et al., 2022). In fact, there is mounting evidence that predation has played a major role in the selection of *M. xanthus* biological features via coevolution with its prey (Nair et al., 2019; La Fortezza et al., 2022). In this minireview we will discuss the state-of-the-art of the toolset used by *M. xanthus* to prey, including the most recent findings derived from transcriptomic analyses during predation.

Motility systems

M. xanthus cells must actively search for prey in the soil to obtain nutrients. To approach the prey, they use two types of motility systems: an individual gliding movement, known as adventurous (A) motility, and a collective twitching-type movement, known as social (S) motility. A-motility relies on a Agl-Glt multiprotein outer-membrane complex that attaches the substrate at fixed sites of focal adhesion. These Agl-Glt complexes move directionally across the inner membrane toward the anterior pole of the cell, following a helical trajectory (Islam et al., 2023). Gliding occurs over an exopolysaccharide slime produced by the bacterium, which facilitates cells to follow the trail of previous cells rather than creating a new one, which enables exploration and prey foraging (Rombouts et al., 2023). On the other hand, S-motility is driven by type-IV pili, which pull the cells forward by extending, attaching to surfaces (or other cells), and then retracting (Chang et al., 2016). In *M. xanthus*, this is a collective movement where the cells must be in contact with each other, allowing them to coordinate the swarm's movement (Skotnicka and Søgaard-Andersen, 2017).

A study using mutants impaired in these two motility systems clearly showed that both are required to efficiently prey on

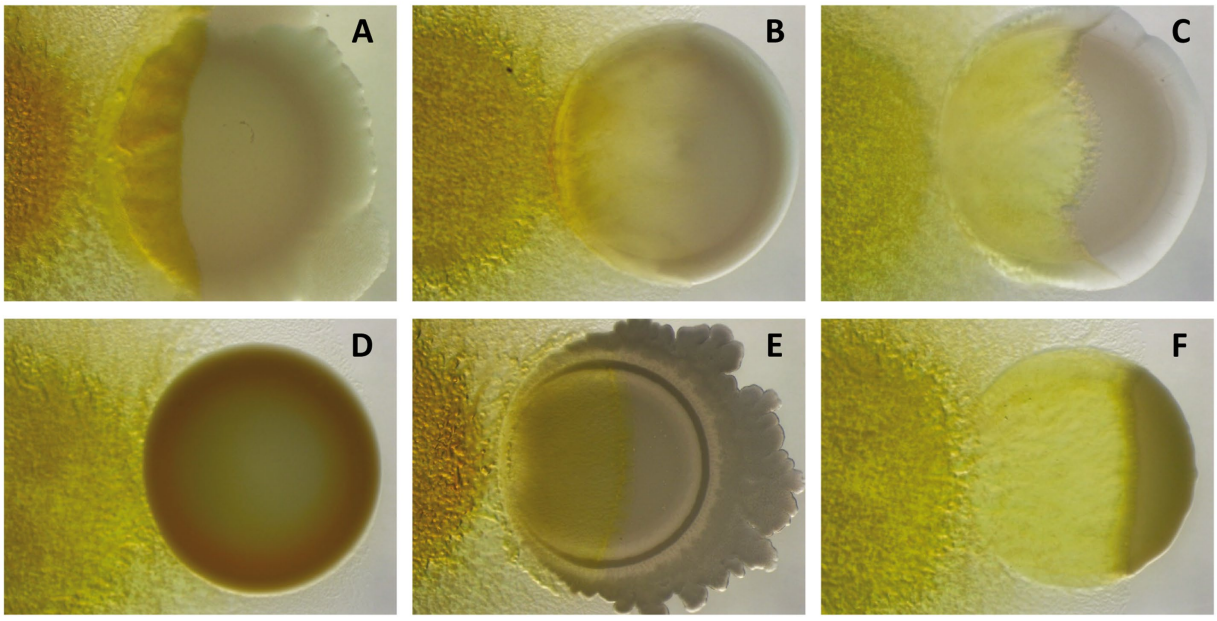

FIGURE 1
Predation assays of *M. xanthus* DK1622 (left) against different Gram-negative [**(A)** *Pseudomonas putida*; **(B)** *Sinorhizobium meliloti*; **(C)** *Escherichia coli*] and Gram-positive bacteria [**(D)** *Staphylococcus aureus*; **(E)** *Bacillus subtilis*; **(F)** *Micrococcus* sp.] after 72 h of interaction, showing its different capabilities to kill and consume prey.

Sinorhizobium meliloti (Pérez et al., 2014). In fact, transcriptomic analyses of *M. xanthus* during predation (predatosomes) have shown upregulation of some genes required for both motility systems as well as some regulators involved in motility, such as the sigma factor SigF (Lee et al., 2020; Pérez et al., 2022). Both types of motility occur simultaneously or alternate in different subpopulations of the swarm to adapt to different prey local distribution (Rombouts et al., 2023).

While scouting the area in search for prey, *M. xanthus* seems to detect some prey molecules such as acyl homoserine lactones, that stimulate motility and facilitate their encounter (Lloyd and Whitworth, 2017; Akbar et al., 2022). Once the predator finds its prey, it must stay in close vicinity to activate its attack mechanisms and then feed on their cellular by-products. Therefore, upon detection, *M. xanthus* cells "stop" by repeatedly reversing their trajectory to optimize prey lysis (Zhang et al., 2020; Thiery and Kaimer, 2022). These repeated reversals are also important to feed on prey, as mutant predator cells defective in this mechanism tend to abandon prey colonies after lysis, without consuming their cellular remains (McBride and Zusman, 1996; Zhang et al., 2020).

Secondary metabolites

M. xanthus induces prey cell death and lysis by cooperative production of different lytic factors, acting either in isolation or synergistically (Figure 2A). Among them, SMs play an important role in prey killing, especially those with antimicrobial activity. *M. xanthus* genome holds an outstanding biosynthetic capacity for SM production, including at least 18 nonribosomal peptide synthetases (NRPS), 22 polyketide synthases (PKS), and 6 mixed PKS/NRPS, making a total of 14.5% of its genome (Goldman et al., 2006). Antimicrobial compounds so far isolated from *M. xanthus* have shown to be more efficient against Gram-positive bacteria (Xiao et al., 2011; Hoffmann et al., 2018), which could be due to the protective role of the Gram-negative outer membrane and/or a potential facilitation for the intracellular delivery of outer membrane vesicles (OMVs) cargo molecules (Zwarycz et al., 2023). To date, only 2 *M. xanthus* SMs have been directly implicated in predation: (i) myxovirescin, a macrocyclic SM able to block bacterial growth by inhibiting type a II signal peptidase (Xiao et al., 2011, 2012), and (ii) myxoprincomide, a SM required for effective predation against *Bacillus subtilis* (Cortina et al., 2012; Müller et al., 2016). However, the most recent predatosome data suggest that SM production is prey specific. Thus, while genes coding for myxoprincomide, myxovirescin, and myxalamide have been reported as being upregulated against *Micrococcus luteus* and *Escherichia coli*, only myxalamide is upregulated when preying on *S. meliloti*. However, against *S. meliloti*, additional clusters probably involved in the biosynthesis of unidentified bio-products are also upregulated (Pérez et al., 2022; Wang et al., 2023).

Hydrolytic enzymes

Besides SMs, *M. xanthus* requires a battery of hydrolytic enzymes to degrade prey cell components and feed on them (Figure 2A). To induce lysis of Gram-positive bacteria, this myxobacterium needs to degrade prey cell-walls via peptidoglycan-lysing enzymes (Hart and

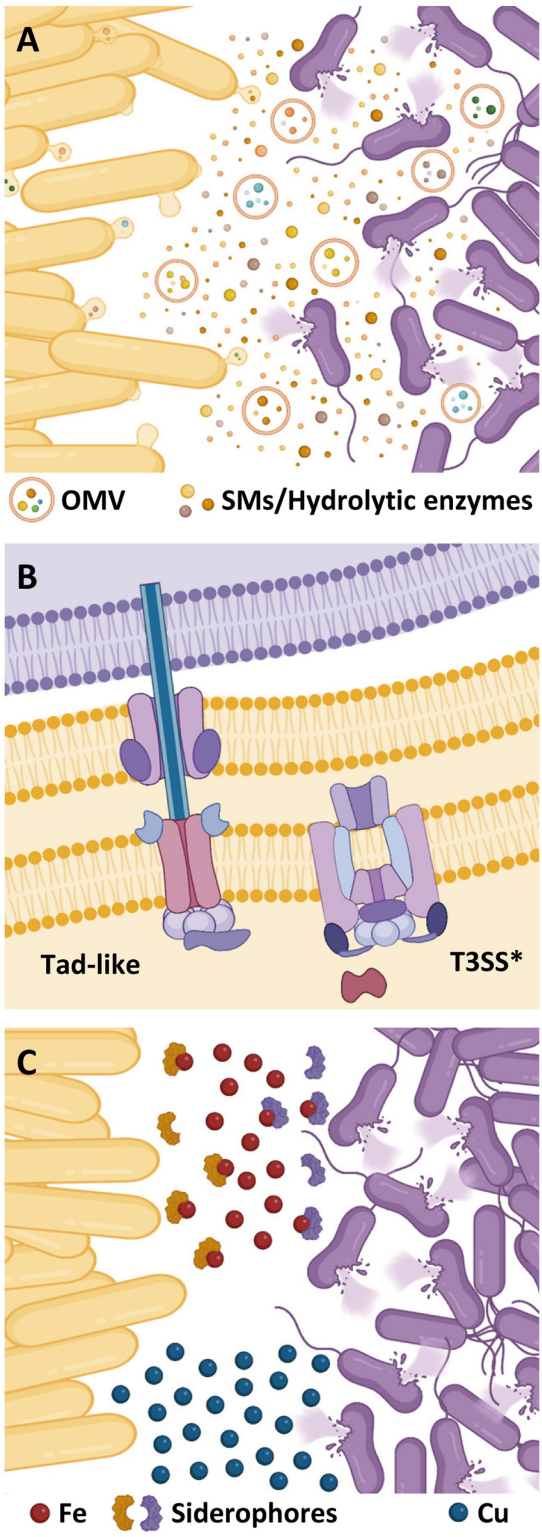

FIGURE 2
Different resources used by *M. xanthus* (yellow cells) to kill prey (purple cells). **(A)** Secondary metabolites (SMs) and hydrolytic enzymes are secreted into the extracellular medium or delivered via outer membrane vesicles (OMVs). **(B)** Contact-dependent killing mechanisms of *M. xanthus*. **(C)** Role of metals during bacterial predation. Competition for iron mediated by siderophores and accumulation of copper at the predator–prey interphase.

Zahler, 1966; Sudo and Dworkin, 1972; Arend et al., 2021). A protein with lysozyme-like-activity (LlpM) able to induce cell lysis has been identified, although it is not essential for this process, reinforcing the idea that cell-wall lytic activity of the *M. xanthus* secretome is a multifactorial process with several hydrolytic enzymes involved (Arend et al., 2021). In fact, secretion of hydrolytic enzymes has shown to drive predation in natural isolates with genomes specially enriched in this type of enzymes (Dong et al., 2022a, 2023).

Transcriptomic studies against different prey have revealed upregulation of several *M. xanthus* genes coding cell-wall lysing proteins. Thus, when the Gram-negative *S. meliloti* and the Gram-positive *Streptomyces coelicolor* were used as prey, two genes coding N-acetylmuramoyl-L-alanine amidases were upregulated (Lee et al., 2020; Pérez et al., 2022). Moreover, five genes coding for proteins with LysM-domains were overexpressed against *S. meliloti* and two of them were also upregulated in co-cultures with *E. coli* (Livingstone et al., 2018; Pérez et al., 2022). However, during predation on *Pseudomonas aeruginosa* or *M. luteus*, no gene involved in cell-wall lysis was differentially expressed (Wang et al., 2023). These discrepancies may be due to characteristics of the prey, but also to variances in the methodology used on each assay.

In addition to cell-walls, *M. xanthus* must also hydrolyze prey proteins and lipids to use them as nutrients or as building blocks for metabolic processes. Until now, only the peptidase MepA has been experimentally studied and it seems to contribute to predation by degrading proteins released from lysed cells (Berleman et al., 2014). Indeed, *mepA* is upregulated in co-culture with *S. meliloti* and with *S. coelicolor*, supporting its role in predation (Lee et al., 2020; Pérez et al., 2022). *M. xanthus* predatosomes against different bacteria indicate that, to achieve full prey lysis, the predator needs to induce a plethora of hydrolytic enzymes. In fact, besides those aforementioned, *M. xanthus* genes coding for several hydrolytic enzymes are transcriptionally upregulated in co-culture with *S. meliloti*, *E. coli*, or *M. luteus*, including peptidases, metalloproteases, alpha/beta fold hydrolases, lipases, and nucleases (Pérez et al., 2022; Wang et al., 2023).

The delivery of this lethal cocktail to the prey is facilitated by OMVs, which include in their cargo many putative hydrolytic proteins and molecules associated with antibiotic activities (Kahnt et al., 2010; Berleman et al., 2014; Remis et al., 2014). In fact, isolated *M. xanthus* OMVs can kill Gram-positive and Gram-negative bacteria (Evans et al., 2012; Remis et al., 2014; Livingstone et al., 2018; Zwarycz et al., 2023). Moreover, it has been proved that OMV killing activity against different bacteria correlates with the predatory activity of *M. xanthus*. However, the absence of correlation between OMV killing activity and their ability to fuse with different prey cell-walls reinforces the idea that the composition of the OMVs cargo is more critical than their delivery for the predatory activity (Zwarycz et al., 2023).

Contact-dependent killing

Although the predatory strategy of *M. xanthus* is usually described as a cooperative process, single myxobacteria can kill individual prey cells (Zhang et al., 2020; Arend et al., 2021; Seef et al., 2021).

This one-to-one interaction requires a contact-dependent mechanism (Figure 2B). In this sense, many bacteria have evolved specialized nanomachines to export proteins and/or virulence factors across the cell envelope into the surroundings, or to inject them into eukaryotic or prokaryotic cells (Costa et al., 2015; Galán and Waksman, 2018).

Although analyses of the *M. xanthus* genome have revealed a large potential for secretion (Konovalova et al., 2010), only two secretion systems have been so far related to cell contact-dependent prey killing: a degenerate type III-like system (T3SS*) and a tight adherence (Tad) secretion apparatus, also known as "Kil complex" (Seef et al., 2021; Thiery et al., 2022).

T3SSs are multiprotein complexes encoded by a broad range of bacteria with pathogenic or interbacterial antagonism (Galán and Waksman, 2018). While several pathogenic enterobacteria use specialized T3SS to deliver effector proteins into eukaryotic cells (Wagner et al., 2018), other species have adapted flagella-type T3SS for cytotoxin export (Dongre et al., 2018; Halte and Erhardt, 2021). However, *M. xanthus* T3SS* lacks a dedicated outer membrane secretin and any homologs to needle and translocon components (Figure 2B), thus being classified as "non-flagellar, needle-less" T3SS (Konovalova et al., 2010; Abby and Rocha, 2012; Diepold and Armitage, 2015).

On the other hand, Tad-like secretion systems are considered members of the type IV filament superfamily, and are related to bacterial adhesion, biofilm stabilization, and contact-dependent regulation of adhesion (Ellison et al., 2017; Denise et al., 2019; Seef et al., 2021).

M. xanthus T3SS* and Tad-like components have been shown to be interdependently, but coordinately, accumulated at the predator–prey interface for killing *E. coli* prey cells, exhibiting a functional interplay and different functions during the predatory interaction. Thus, while the Tad-like apparatus is instrumental in prey cell death (but does not cause prey disintegration), the T3SS* is required for cell lysis (Thiery et al., 2022). Nevertheless, both systems are required for utilizing live prey as a nutrient source, although they are not directly involved in the degradation or uptake of dead prey biomass (Thiery et al., 2022).

Homologous genes encoding Tad-like complexes have been identified in different genera of bacterial predators (Seef et al., 2021; Wang et al., 2023). However, the co-occurrence of T3SS* and Tad complexes is restricted to the sub-order *Cystobacterineae* of the *Myxococcales*, suggesting a specialized function of these secretion systems in myxobacterial predation (Abby and Rocha, 2012; Wang et al., 2023).

Gram-negative and Gram-positive prey elicit similar responses by *M. xanthus* regarding the formation of Tad and T3SS* foci, since both can lead to aggregation of these multiprotein complexes (Wang et al., 2023). Thus, the transcriptomic analysis of the co-culture of *M. xanthus* with *E. coli* and *M. luteus* revealed that part of the genes encoding the T3SS*, as well as part of one of the two clusters encoding the Tad-like apparatus, were significantly upregulated in both cases (Wang et al., 2023). A similar result was reported from the interaction between *M. xanthus* and *S. meliloti*, although in this case the upregulation of genes from both clusters coding the Tad-like complex was detected (Pérez et al., 2022). However, during co-culture with *S. coelicolor*, transcriptomic data indicated that only some genes coding the T3SS*, but not those coding the Tad-like apparatus, were upregulated (Lee et al., 2020). Similarly, *P. aeruginosa* failed to induce accumulation of Tad complexes, turning out to be resistant to

M. xanthus predation (Seef et al., 2021). Interestingly, the coordinated accumulation of the T3SS*/Tad complexes has not been observed during contact with other *M. xanthus* cells, but only during the interaction with prey cells, which implies that contact-dependent killing mechanisms discriminate between kin and prey cells (Wall, 2016; Seef et al., 2021; Thiery et al., 2022).

Role of metals in the predatory interaction

The use of metals by bacterial predators has gained relevance in the recent years as a new mechanism of inducing prey death. Two metals have been reported to be involved in the predatory behavior of *M. xanthus*: copper and iron (Figure 2C). These two metals exhibit a dual role on living cells since they are cofactors of enzymes that are essential for vital functions, but toxic at high concentrations (Rensing and McDevitt, 2013; Ladomersky and Petris, 2015; Li et al., 2021).

In the case of copper, it has been shown that *M. xanthus* utilizes this metal to poison *S. meliloti*. This metal accumulates inside the cells at the interface where predator collides with the prey, provoking changes in both partners of the interaction and helping the predator to penetrate in the prey colony (Contreras-Moreno et al., 2020). While *M. xanthus* upregulates the expression of copper detoxification genes such as those coding for the P1B-ATPase CopA, the multicopper oxidase CuoA, and the copper efflux pumps Cus2 and Cus3 (Sánchez-Sutil et al., 2007; Moraleda-Muñoz et al., 2010a,b; Pérez et al., 2018), *S. meliloti* produces a brown pigment that has been identified as melanin (Contreras-Moreno et al., 2020). Predatory analyses have revealed that melanin is overproduced by the prey during predation, indicating that copper is being used to generate oxidative stress and that the pigment functions as a defensive shield for the prey (Contreras-Moreno et al., 2020). However, it remains to be elucidated how the predator achieves accumulation of copper in the prey to kill it by generating reactive oxygen species.

Iron also seems to play an important role during myxobacterial predation. Several transcriptomes of *M. xanthus* against diverse prey have been published, and in all of them siderophore biosynthesis is upregulated in both predator and prey (Lee et al., 2020; Pérez et al., 2022; Soto et al., 2023; Wang et al., 2023; Whitworth et al., 2023). Moreover, the same result has been observed during predation of another myxobacterium, *Cystobacter ferrugineus*, against *Pseudomonas putida* (Akbar and Stevens, 2021), indicating that competition for iron may be a general predatory mechanism among myxobacteria.

Experimentally, it has been demonstrated that depletion of iron triggers the biosynthesis of the antibiotic actinorhodin in *S. coelicolor* to prevent predation from *M. xanthus* (Lee et al., 2020). Moreover, a mutant of *M. xanthus* that produces less siderophores (myxochelins) is defective in predation against *P. aeruginosa* (Dong et al., 2022b). Similarly, mutants in a putative TonB-dependent transporter for ferrimyxochelins and in components of the ABC transporter that introduces ferrimyxochelins into the cytoplasm also exhibit less efficient predation on this prey (Dong et al., 2022b). All these data seem to indicate that competition for iron plays a decisive role in the myxobacterial predatory interaction with the prey.

Concluding remarks

Bacterial predation is a key factor in shaping ecosystems and establishing microbial diversity in soils. Understanding these interactions will contribute to improve soil conditions in agriculture. Moreover, some bacterial predators are considered "microfactories" of SMs that can be used to overcome the current antibiotic crisis (Pérez et al., 2016, 2020).

Predation is an integral part of *M. xanthus* biology and, therefore, this bacterium has developed a diverse toolset to adapt to its predatory lifestyle. Among the best-understood facets of its predatory activity are the mechanisms used to kill and lyse their prey. The cooperative production of SMs and hydrolytic enzymes along with cell-to-cell contact killing via T3SS* and Tad-like complexes, are well-established predatory mechanisms. Future research in this topic will provide new information about less known aspects of *M. xanthus* predation and uncover new tools used by this microorganism to kill prey. In fact, recent studies have led to the identification of metals as additional weapons used by myxobacteria to kill their prey. Since fluctuations in metal concentration may occur in the habitats because of several activities, it is expected that they determine which population will predominate in the myxobacterial predatory interaction, which may have a significant impact on the environment and agriculture.

Author contributions

FC-M: Writing – original draft, Writing – review & editing. JP: Writing – original draft, Writing – review & editing. JM-D: Writing – original draft, Writing – review & editing, Funding acquisition. AM-M: Writing – original draft, Writing – review & editing, Funding acquisition. FM-T: Conceptualization, Writing – original draft, Writing – review & editing, Funding acquisition.

Funding

The author(s) declare financial support was received for the research, authorship, and/or publication of this article. This work has been supported by grant PID2020-112634GBI00 funded by MCIN/AEI/10.13039/501100011033 (to AM-M and JM-D) and by the Marie Skłodowska-Curie Action (MSCA) grant LysM Ref. 101106411 (to FM-T and JM-D).

Conflict of interest

The authors declare that the research was conducted in the absence of any commercial or financial relationships that could be construed as a potential conflict of interest.

Publisher's note

References

Abby, S. S., and Rocha, E. P. C. (2012). The non-flagellar type III secretion system evolved from the bacterial flagellum and diversified into host-cell adapted systems. *PLoS Genet.* 8:e1002983. doi: 10.1371/journal.pgen.1002983

Akbar, S., Phillips, K. E., Misra, S. K., Sharp, J. S., and Stevens, D. C. (2022). Differential response to prey quorum signals indicates predatory specialization of myxobacteria and the ability to predate *Pseudomonas aeruginosa*. *Environ. Microbiol.* 24, 1263–1278. doi: 10.1111/1462-2920.15812

Akbar, S., and Stevens, D. C. (2021). Functional genomics study of *Pseudomonas putida* to determine traits associated with avoidance of a myxobacterial predator. *Sci. Rep.* 11:16445. doi: 10.1038/s41598-021-96046-8

Arend, K. I., Schmidt, J. J., Bentler, T., Lüchtefeld, C., Eggerichs, D., Hexamer, H. M., et al. (2021). *Myxococcus xanthus* predation of gram-positive or gram-negative bacteria is mediated by different bacteriolytic mechanisms. *Appl. Environ. Microbiol.* 87, e02382–e02320. doi: 10.1128/aem.02382-20

Berleman, J. E., Allen, S., Danielewicz, M. A., Remis, J. P., Gorur, A., Cunha, J., et al. (2014). The lethal cargo of *Myxococcus xanthus* outer membrane vesicles. *Front. Microbiol.* 5:574. doi: 10.3389/fmicb.2014.00474

Berleman, J. E., and Kirby, J. R. (2007). Multicellular development in *Myxococcus xanthus* is stimulated by predator-prey interactions. *J. Bacteriol.* 189, 5675–5682. doi: 10.1128/JB.00544-07

Berleman, J. E., Scott, J., Chumley, T., and Kirby, J. R. (2008). Predataxis behavior in *Myxococcus xanthus*. *Proc. Natl. Acad. Sci. U. S. A.* 105, 17127–17132. doi: 10.1073/pnas.0804387105

Chang, Y. W., Rettberg, L. A., Treuner-Lange, A., Iwasa, J., Søgaard-Andersen, L., and Jensen, G. J. (2016). Architecture of the type IVa pilus machine. *Science* 351:aad2001. doi: 10.1126/science.aad2001

Contreras-Moreno, F. J., Muñoz-Dorado, J., García-Tomsig, N. I., Martínez-Navajas, G., Pérez, J., and Moraleda-Muñoz, A. (2020). Copper and melanin play a role in *Myxococcus xanthus* predation on *Sinorhizobium meliloti*. *Front. Microbiol.* 11:94. doi: 10.3389/fmicb.2020.00094

Cortina, N. S., Krug, D., Plaza, A., Revermann, O., and Müller, R. (2012). Myxoprincomide: a natural product from *Myxococcus xanthus* discovered by comprehensive analysis of the secondary metabolome. *Angew. Chem. Int. Ed. Engl.* 51, 811–816. doi: 10.1002/anie.201106305

Costa, T. R., Felisberto-Rodrigues, C., Meir, A., Prevost, M. S., Redzej, A., Trokter, M., et al. (2015). Secretion systems in gram-negative bacteria: structural and mechanistic insights. *Nat. Rev. Microbiol.* 13, 343–359. doi: 10.1038/nrmicro3456

Denise, R., Abby, S. S., and Rocha, E. P. C. (2019). Diversification of the type IV filament superfamily into machines for adhesion, protein secretion, DNA uptake, and motility. *PLoS Biol.* 17:e3000390. doi: 10.1371/journal.pbio.3000390

Diepold, A., and Armitage, J. P. (2015). Type III secretion systems: the bacterial flagellum and the injectisome. Philos. *Philos. Trans. R. Soc. Lond. B Biol. Sci.* 370, 20150020–20150119. doi: 10.1098/rstb.2015.0020

Dong, Y., Dong, H., Feng, Z., Wang, X., Yao, Q., and Zhu, H. (2022b). A disturbed siderophore transport inhibits myxobacterial predation. *Cell* 11:3718. doi: 10.3390/cells11233718

Dong, H., Gao, R., Dong, Y., Yao, Q., and Zhu, H. (2023). Whole-genome sequencing of a biocontrol *Myxococcus xanthus* R31 isolate and comparative genomic analysis. *Gene* 863:147286. doi: 10.1016/j.gene.2023.147286

Dong, H., Xu, X., Gao, R., Li, Y., Li, A., Yao, Q., et al. (2022a). *Myxococcus xanthus* R31 suppresses tomato bacterial wilt by inhibiting the pathogen *Ralstonia solanacearum* with secreted proteins. *Front. Microbiol.* 12:801091. doi: 10.3389/fmicb.2021.801091

Dongre, M., Singh, B., Aung, K. M., Larsson, P., Miftakhova, R., Persson, K., et al. (2018). Flagella-mediated secretion of a novel *Vibrio cholerae* cytotoxin affecting both vertebrate and invertebrate hosts. *Commun. Biol.* 1:59. doi: 10.1038/s42003-018-0065-z

Ellison, C. K., Kan, J., Dillard, R. S., Kysela, D. T., Ducret, A., Berne, C., et al. (2017). Obstruction of pilus retraction stimulates bacterial surface sensing. *Science* 358, 535–538. doi: 10.1126/science.aan5706

Evans, A. G., Davey, H. M., Cookson, A., Currinn, H., Cooke-Fox, G., Stanczyk, P. J., et al. (2012). Predatory activity of *Myxococcus xanthus* outer-membrane vesicles and properties of their hydrolase cargo. *Microbiology* 158, 2742–2752. doi: 10.1099/mic.0.060343-0

Galán, J. E., and Waksman, G. (2018). Protein-injection machines in bacteria. *Cell* 172, 1306–1318. doi: 10.1016/j.cell.2018.01.034

Goldman, B. S., Nierman, W. C., Kaiser, D., Slater, S. C., Durkin, A. S., Eisen, J. A., et al. (2006). Evolution of sensory complexity recorded in a myxobacterial genome. *Proc. Natl. Acad. Sci. U. S. A.* 103, 15200–15205. doi: 10.1073/pnas.0607335103

Halte, M., and Erhardt, M. (2021). Protein export via the type III secretion system of the bacterial flagellum. *Biomol. Ther.* 11, 186–219. doi: 10.3390/biom11020186

Hart, B. A., and Zahler, S. A. (1966). Lytic enzyme produced by *Myxococcus xanthus*. *J. Bacteriol.* 92, 1632–1637. doi: 10.1128/JB.92.6.1632-1637.1966

Hoffmann, M., Auerbach, D., Panter, F., Hoffmann, T., Dorrestein, P. C., and Müller, R. (2018). Homospermidine lipids: a compound class specifically formed during fruiting body formation of *Myxococcus xanthus* DK1622. *ACS Chem. Biol.* 13, 273–280. doi: 10.1021/acschembio.7b00816

Islam, S. T., Jolivet, N. Y., Cuzin, C., Belgrave, A. M., My, L., Fleuchot, B., et al. (2023). Unmasking of the von Willebrand A-domain surface adhesin CglB at bacterial focal adhesions mediates myxobacterial gliding motility. *Sci. Adv.* 9:eabq0619. doi: 10.1126/sciadv.abq0619

Kahnt, J., Aguiluz, K., Koch, J., Treuner-Lange, A., Konovalova, A., Huntley, S., et al. (2010). Profiling the outer membrane proteome during growth and development of the social bacterium *Myxococcus xanthus* by selective biotinylation and analyses of outer membrane vesicles. *J. Proteome Res.* 9, 5197–5208. doi: 10.1021/pr1004983

Konovalova, A., Petters, T., and Søgaard-Andersen, L. (2010). Extracellular biology of *Myxococcus xanthus*. *FEMS Microbiol. Rev.* 34, 89–106. doi: 10.1111/j.1574-6976.2009.00194.x

La Fortezza, M., Rendueles, O., Keller, H., and Velicer, G. J. (2022). Hidden paths to endless forms most wonderful: ecology latently shapes evolution of multicellular development in predatory bacteria. *Commun. Biol.* 5:977. doi: 10.1038/s42003-022-03912-w

Ladomersky, E., and Petris, M. J. (2015). Copper tolerance and virulence in bacteria. *Metallomics* 7, 957–964. doi: 10.1039/c4mt00327f

Lee, N., Kim, W., Chung, J., Lee, Y., Cho, S., Jang, K. S., et al. (2020). Iron competition triggers antibiotic biosynthesis in *Streptomyces coelicolor* during coculture with *Myxococcus xanthus*. *ISME J.* 14, 1111–1124. doi: 10.1038/s41396-020-0594-6

Li, Y. P., Ben Fekih, I., Chi Fru, E., Moraleda-Muñoz, A., Li, X., Rosen, B. P., et al. (2021). Antimicrobial activity of metals and metalloids. *Annu. Rev. Microbiol.* 75, 175–197. doi: 10.1146/annurev-micro-032921-123231

Livingstone, P. G., Millard, A. D., Swain, M. T., and Whitworth, D. E. (2018). Transcriptional changes when *Myxococcus xanthus* preys on *Escherichia coli* suggest myxobacterial predators are constitutively toxic but regulate their feeding. *Microb. Genom.* 4:e000152. doi: 10.1099/mgen.0.000152

Livingstone, P. G., Morphew, R. M., and Whitworth, D. E. (2017). Myxobacteria are able to prey broadly upon clinically-relevant pathogens, exhibiting a prey range which cannot be explained by phylogeny. *Front. Microbiol.* 8:1593. doi: 10.3389/fmicb.2017.01593

Lloyd, D. G., and Whitworth, D. E. (2017). The Myxobacterium *Myxococcus xanthus* can sense and respond to the quorum signals secreted by potential prey organisms. *Front. Microbiol.* 8:439. doi: 10.3389/fmicb.2017.00439

McBride, M. J., and Zusman, D. R. (1996). Behavioral analysis of single cells of *Myxococcus xanthus* in response to prey cells of *Escherichia coli*. *FEMS Microbiol. Lett.* 137, 227–231. doi: 10.1111/j.1574-6968.1996.tb08110.x

Mendes-Soares, H., and Velicer, G. J. (2013). Decomposing predation: testing for parameters that correlate with predatory performance by a social bacterium. *Microb. Ecol.* 65, 415–423. doi: 10.1007/s00248-012-0135-6

Moraleda-Muñoz, A., Pérez, J., Extremera, A. L., and Muñoz-Dorado, J. (2010b). Differential regulation of six heavy metal efflux systems in the response of *Myxococcus xanthus* to copper. *Appl. Environ. Microbiol.* 76, 6069–6076. doi: 10.1128/AEM.00753-10

Moraleda-Muñoz, A., Pérez, J., Extremera-León, A. L., and Muñoz-Dorado, J. (2010a). Expression and physiological role of three *Myxococcus xanthus* copper-dependent P1B-type ATPases during bacterial growth and development. *Appl. Environ. Microbiol.* 76, 6077–6084. doi: 10.1128/AEM.00755-10

Müller, S., Strack, S. N., Ryan, S. E., Shawgo, M., Walling, A., Harris, S., et al. (2016). Identification of functions affecting predator-prey interactions between *Myxococcus xanthus* and *Bacillus subtilis*. *J. Bacteriol.* 198, 3335–3344. doi: 10.1128/JB.00575-16

Muñoz-Dorado, J., Marcos-Torres, F. J., García-Bravo, E., Moraleda-Muñoz, A., and Pérez, J. (2016). Myxobacteria: moving, killing, feeding, and surviving together. *Front. Microbiol.* 7:781. doi: 10.3389/fmicb.2016.00781

Nair, R. R., Vasse, M., Wielgoss, S., Sun, L., Yu, Y. N., and Velicer, G. J. (2019). Bacterial predator-prey coevolution accelerates genome evolution and selects on virulence-associated prey defences. *Nat. Commun.* 10:4301. doi: 10.1038/s41467-019-12140-6

Pérez, J., Contreras-Moreno, F. J., Marcos-Torres, F. J., Moraleda-Muñoz, A., and Muñoz-Dorado, J. (2020). The antibiotic crisis: how bacterial predators can help. *Comput. Struct. Biotechnol. J.* 18, 2547–2555. doi: 10.1016/j.csbj.2020.09.010

Pérez, J., Contreras-Moreno, F. J., Muñoz-Dorado, J., and Moraleda-Muñoz, A. (2022). Development versus predation: transcriptomic changes during the lifecycle of *Myxococcus xanthus*. *Front. Microbiol.* 13:1004476. doi: 10.3389/fmicb.2022.1004476

Pérez, J., Jiménez-Zurdo, J. I., Martínez-Abarca, F., Millán, V., Shimkets, L. J., and Muñoz-Dorado, J. (2014). Rhizobial galactoglucan determines the predatory pattern of *Myxococcus xanthus* and protects *Sinorhizobium meliloti* from predation. *Environ. Microbiol.* 16, 2341–2350. doi: 10.1111/1462-2920.12477

Pérez, J., Moraleda-Muñoz, A., Marcos-Torres, F. J., and Muñoz-Dorado, J. (2016). Bacterial predation: 75 years and counting! *Environ. Microbiol.* 18, 766–779. doi: 10.1111/1462-2920.13171

Pérez, J., Muñoz-Dorado, J., and Moraleda-Muñoz, A. (2018). The complex global response to copper in the multicellular bacterium *Myxococcus xanthus*. *Metallomics* 10, 876–886. doi: 10.1039/c8mt00121a

Petters, S., Groß, V., Söllinger, A., Pichler, M., Reinhard, A., Bengtsson, M. M., et al. (2021). The soil microbial food web revisited: predatory myxobacteria as keystone taxa? *ISME J.* 15, 2665–2675. doi: 10.1038/s41396-021-00958-2

Pham, V. D., Shebelut, C. W., Diodati, M. E., Bull, C. T., and Singer, M. (2005). Mutations affecting predation ability of the soil bacterium *Myxococcus xanthus*. *Microbiology* 151, 1865–1874. doi: 10.1099/mic.0.27824-0

Remis, J. P., Wei, D., Gorur, A., Zemla, M., Haraga, J., Allen, S., et al. (2014). Bacterial social networks: structure and composition of *Myxococcus xanthus* outer membrane vesicle chains. *Environ. Microbiol.* 16, 598–610. doi: 10.1111/1462-2920.12187

Rensing, C., and McDevitt, S. F. (2013). The copper metallome in prokaryotic cells. *Met. Ions Life Sci.* 12, 417–450. doi: 10.1007/978-94-007-5561-1_12

Rombouts, S., Mas, A., Le Gall, A., Fiche, J. B., Mignot, T., and Nollmann, M. (2023). Multi-scale dynamic imaging reveals that cooperative motility behaviors promote efficient predation in bacteria. *Nat. Commun.* 14:5588. doi: 10.1038/s41467-023-41193-x

Sánchez-Sutil, M. C., Gómez-Santos, N., Moraleda-Muñoz, A., Martins, L. O., Pérez, J., and Muñoz-Dorado, J. (2007). Differential expression of the three multicopper oxidases from *Myxococcus xanthus*. *J. Bacteriol.* 189, 4887–4898. doi: 10.1128/JB.00309-07

Seef, S., Herrou, J., de Boissier, P., My, L., Brasseur, G., Robert, D., et al. (2021). A tad-like apparatus is required for contact-dependent prey killing in predatory social bacteria. *elife* 10:e72409. doi: 10.7554/elife.72409

Skotnicka, D., and Søgaard-Andersen, L. (2017). Type IV pili-dependent motility as a tool to determine the activity of c-di-GMP modulating enzymes in *Myxococcus xanthus*. *Methods Mol. Biol.* 1657, 157–165. doi: 10.1007/978-1-4939-7240-1_13

Soto, M. J., Pérez, J., Muñoz-Dorado, J., Contreras-Moreno, F. J., and Moraleda-Muñoz, A. (2023). Transcriptomic response of *Sinorhizobium meliloti* to the predatory attack of *Myxococcus xanthus*. *Front. Microbiol.* 14:1213659. doi: 10.3389/fmicb.2023.1213659

Sudo, S., and Dworkin, M. (1972). Bacteriolytic enzymes produced by *Myxococcus xanthus*. *J. Bacteriol.* 110, 236–245. doi: 10.1128/JB.110.1.236-245.1972

Sydney, N., Swain, M. T., So, J. M. T., Hoiczyk, E., Tucker, N. P., and Whitworth, D. E. (2021). The genetics of prey susceptibility to Myxobacterial predation: a review, including an investigation into *Pseudomonas aeruginosa* mutations affecting predation by *Myxococcus xanthus*. *Microb. Physiol.* 31, 57–66. doi: 10.1159/000515546

Thiery, S., and Kaimer, C. (2022). The predation strategy of *Myxococcus xanthus*. *Front. Microbiol.* 11:2. doi: 10.3389/fmicb.2020.00002

Thiery, S., Turowski, P., Berleman, J. E., and Kaimer, C. (2022). The predatory soil bacterium *Myxococcus xanthus* combines a tad -and an atypical type 3-like protein secretion system to kill bacterial cells. *Cell Rep.* 40:111340. doi: 10.1016/j.celrep.2022

Volz, C., Kegler, C., and Müller, R. (2012). Enhancer binding proteins act as hetero-oligomers and link secondary metabolite production to myxococcal development, motility, and predation. *Chem. Biol.* 19, 1447–1459. doi: 10.1016/j.chembiol.2012.09.010

Wagner, S., Grin, I., Malmsheimer, S., Singh, N., Torres-Vargas, C. E., and Westerhausen, S. (2018). Bacterial type III secretion systems: a complex device for the delivery of bacterial effector proteins into eukaryotic host cells. *FEMS Microbiol. Lett.* 365, 1–13. doi: 10.1093/femsle/fny201

Wall, D. (2016). Kin recognition in bacteria. *Annu. Rev. Microbiol.* 70, 143–160. doi: 10.1146/annurev-micro-102215-095325

Wang, C., Xiao, Y., Wang, Y., Liu, Y., Yao, Q., and Zhu, H. (2023). Comparative genomics and transcriptomics insight into myxobacterial metabolism potentials and multiple predatory strategies. *Front. Microbiol.* 14:1146523. doi: 10.3389/fmicb.2023.1146523

Whitworth, D. E., Pérez, J., Mitchell, R. J., and Pande, S. (2023). Editorial: mechanisms of prokaryotic predation, volume II. *Front. Microbiol.* 14:1256252. doi: 10.3389/fmicb.2023.1256252

Xiao, Y., Gerth, K., Müller, R., and Wall, D. (2012). Myxobacterium-produced antibiotic TA (myxovirescin) inhibits type II signal peptidase. *Antimicrob. Agents Chemother.* 56, 2014–2021. doi: 10.1128/AAC.06148-11

Xiao, Y., Wei, X., Ebright, R., and Wall, D. (2011). Antibiotic production by myxobacteria plays a role in predation. *J. Bacteriol.* 193, 4626–4633. doi: 10.1128/jb.05052-11

Zhang, W., Wang, Y., Lu, H., Liu, Q., Wang, C., Hu, W., et al. (2020). Dynamics of solitary predation by *Myxococcus xanthus* on *Escherichia coli* observed at the single-cell level. *Appl. Environ. Microbiol.* 86:e02286-19-13. doi: 10.1128/AEM.02286-19

Zwarycz, A. S., Page, T., Nikolova, G., Radford, E. J., and Whitworth, D. E. (2023). Predatory strategies of *Myxococcus xanthus*: prey susceptibility to OMVs and moonlighting enzymes. *Microorganisms* 11:874. doi: 10.3390/microorganisms11040874

frontiers | Frontiers in Microbiology

TYPE Original Research
PUBLISHED 05 February 2024
DOI 10.3389/fmicb.2024.1324153

OPEN ACCESS

EDITED BY
Renaud Berlemont,
California State University, Long Beach, United States

REVIEWED BY
Yuqiang Zhao,
Jiangsu Province and Chinese Academy of Sciences, China
Jinfang Zheng,
Institute of Artificial Intelligence, China

*CORRESPONDENCE
Honghui Zhu
✉ zhuhh_gdim@163.com

RECEIVED 19 October 2023
ACCEPTED 15 January 2024
PUBLISHED 05 February 2024

CITATION
Zhou X, Zhou X, Zhang X, Dong H, Dong Y and Zhu H (2024) Secretory CAZymes profile and GH19 enzymes analysis of *Corallococcus silvisoli* c25j21. *Front. Microbiol.* 15:1324153. doi: 10.3389/fmicb.2024.1324153

Secretory CAZymes profile and GH19 enzymes analysis of *Corallococcus silvisoli* c25j21

Xiaoli Zhou, Xianmin Zhou, Xianjiao Zhang, Honghong Dong, Yijie Dong and Honghui Zhu*

Key Laboratory of Agricultural Microbiomics and Precision Application (MARA), Key Laboratory of Agricultural Microbiome (MARA), State Key Laboratory of Applied Microbiology Southern China, Guangdong Provincial Key Laboratory of Microbial Culture Collection and Application, Institute of Microbiology, Guangdong Academy of Sciences, Guangzhou, China

Extracellular enzymes play important roles in myxobacteria degrading macromolecules and preying on other microorganisms. Glycoside hydrolases 19 (GH19) are widely present in myxobacteria, but their evolution and biological functions have not been fully elucidated. Here we investigated the comparative secretory proteome of *Corallococcus silvisoli* c25j21 in the presence of cellulose and chitin. A total of 313 proteins were detected, including 16 carbohydrate-active enzymes (CAZymes), 7 of which were induced by cellulose or chitin, such as GH6, GH13, GH19, AA4, and CBM56. We further analyzed the sequence and structural characteristics of its three GH19 enzymes to understand their potential functions. The results revealed that myxobacterial GH19 enzymes are evolutionarily divided into two clades with different appended modules, and their different amino acid compositions in the substrate binding pockets lead to the differences in molecular surface electrostatic potentials, which may, in turn, affect their substrate selectivity and biological functions. Our study is helpful for further understanding the biological functions and catalytic mechanisms of myxobacterial CAZymes.

KEYWORDS

GH19, myxobacteria, CAZyme, lysozyme, secretory proteome

1 Introduction

Myxobacteria are a class of bacteria with the ability to degrade biomass and prey on a variety of other microorganisms (Munoz-Dorado et al., 2016). They have good application potential and research value in the fields of biomass waste utilization, pathogen biocontrol, and drug development. Extracellular enzymes have long been considered to be important factors in macromolecular degradation and microbial predation by myxobacteria (Sudo and Dworkin, 1972; Berleman and Kirby, 2009; Konovalova et al., 2010), but the specific enzyme functions and mechanisms remain to be clarified.

In recent years, several extracellular carbohydrate-active enzymes (CAZymes) have been characterized as macromolecular degradation activities. In terms of macromolecular degradation, there are several research reports on amylase, such as AmyM, CoMA, and IsoM from *Corallococcus* sp. EGB, which have been well characterized (Li et al., 2015, 2017; Zhou et al., 2018; Chen X. et al., 2020). Fewer studies on myxobacterial cellulose-active enzymes have been reported. Two enzymes from *Myxobacter* sp. AL-1, Cel9 and chitosanase-cellulase, were biochemically characterized as endoglucanases and bifunctional chitosanase-cellulase, respectively (Pedraza-Reyes and Gutierrez-Corona, 1997;

Tellez-Valencia et al., 2003). We have previously characterized two lytic polysaccharide monooxygenases ViLPMO10A and ViLPMO10B from *Vitiosangium* sp. GDMCC 1.1324 and found that they have chitin- and cellulose- activities, respectively. The synergistic activity of ViLPMO10B and cellulase for straw degradation was also investigated (Zhou et al., 2020).

CAZymes have also been found to participate in the process of myxobacteria preying on other microorganisms. The outer membrane β-1,6-glucanase GluM was found to be essential for EGB to prey on phytopathogenic fungi *Magnaporthe oryzae* due to its ability to target and degrade fungal cell wall glucans (Li et al., 2019b). A secreted cocktail of β-1,3-glucanases was confirmed to be a major contributor of *Archangium* sp. AC19 during predation on oomycetes *Phytophthora* (Zhang et al., 2023). Besides, an endochitinase CcCti1 belonging to the glycoside hydrolase 18 (GH18) family was characterized to show biocontrol activity against the plant pathogen fungus *M. oryzae in vitro* (Li et al., 2019a). The cell wall composition of bacteria and fungi is different, and the myxobacterial enzymes that target them may also be different. As for CAZymes involved in the process of myxobacteria preying on bacteria, the GH19 family enzymes have been reported. LlpM from *M. xanthus* has been characterized as a lysozyme and has lytic activity against Gram-positive bacteria e.g., *Micrococcus luteus* and *Bacillus subtilis* (Arend et al., 2021). We previously identified lysozyme C25GH19B from *C. silvisoli* c25j21, which showed bacteriolytic activity against both Gram-positive and Gram-negative pathogenic bacteria (Li et al., 2022). The GH19 family contains enzymes that are biochemically characterized as chitinases and lysozymes (or endolysins). Among them, chitinases come mainly from plants, and a few from *Streptomyces*, and lysozymes mainly come from phages. GH19 enzyme genes are widespread in myxobacteria, and some strains have more than one GH19 gene, such as *C. silvisoli* c25j21, which has three redundant GH19 genes in its genome. However, apart from the two enzymes mentioned above, little is known about the GH19 enzymes derived from myxobacteria.

In this study, to understand the biological functions of myxobacterial CAZymes, especially the GH19 enzymes, we performed a comparative secretory proteomic analysis of *C. silvisoli* c25j21 in the presence of cellulose and chitin. In addition, we investigated the sequence and structural characteristics of its three GH19 enzymes and their myxobacterial homologous proteins. Our study will provide the basis for further understanding and research on the biological functions and enzymatic mechanisms of myxobacterial CAZymes.

2 Materials and methods

2.1 Culture of *C. silvisoli* c25j21 and protein preparation

Three culture media were used to study the secretory proteome of *C. silvisoli* c25j21. For Blank group, MD1 liquid medium (Casein peptone 0.6%, soluble starch 0.2%, $MgSO_4 \cdot 7H_2O$ 0.2%, $CaCl_2 \cdot 2H_2O$ 0.04%, pH 7.2) was used. For the Cel and Chi groups, 1% (w/v) rice straw powder or α-chitin was added to the MD1 medium containing half of the casein peptone and half of the soluble starch, respectively. The swarms of c25j21 grown on VY/2 agar were taken and inoculated into the above medium and cultured at 30°C with shaking at 180 rpm for 1 week. Each group had three replicates. After the culture, the culture supernatant was separated by centrifugation at 12,000 *g* and frozen in liquid nitrogen.

Protein preparation and proteomic analysis were performed by Shanghai Applied Protein Technology Co., Ltd., China. SDT (4% SDS, 100 mM Tris-HCl, 1 mM DTT, pH 7.6) buffer was used for protein extraction. The amount of protein was quantified with the BCA Protein Assay Kit (Bio-Rad, USA). Protein was digested by trypsin and the peptides of each sample were desalted, concentrated, and reconstituted in 0.1% (v/v) formic acid.

2.2 LC-MS/MS and data analysis

LC-MS/MS analysis was performed on a Q exactive mass spectrometer (Thermo Scientific) that was coupled to Easy nLC (Proxeon Biosystems, now Thermo Fisher Scientific, Inc., Waltham, USA). The peptides were loaded onto a reverse phase trap column (Thermo Scientific Acclaim PepMap100, 100 μm × 2 cm, nanoViper C18) connected to the C18-reversed phase analytical column (Thermo Scientific Easy Column, 10 cm long, 75 μm inner diameter, 3 μm resin) in buffer A (0.1% Formic acid) and separated with a linear gradient of buffer B (84% acetonitrile and 0.1% Formic acid) at a flow rate of 300 nl/min. The mass spectrometer was operated in positive ion mode. The MS raw data for each sample were combined and searched using the MaxQuant 1.5.3.17 software for identification and quantitation analysis.

2.3 Annotation of CAZymes

The protein sequences of c25j21 were submitted to the dbCAN3 webserver[1] and annotated using HMMER (Zheng et al., 2023).

2.4 Multiple sequence alignment and phylogenetic tree construction

The protein sequences of C25GH19A (WP_143898266) and C25GH19B (WP_161664743) were used as queries to blast against the NCBI non-redundant protein sequences database through the blastp algorithm. The max target sequences and the expected threshold were set as 100 and 0.05, respectively. The obtained amino acid sequences were conducted with multiple sequence alignment using the Clustal Omega web server[2] (Sievers and Higgins, 2018) (**Supplementary Table 1**). The results were rendered by ESPript 3.0 (Robert and Gouet, 2014). The neighbor-joining phylogenetic trees were created by MEGA-X (Kumar et al., 2018), and the figure was generated by the iTOL web server[3] (Letunic and Bork, 2019). The domain compositions of the proteins were predicted by the NCBI batch CD-search tool (Lu et al., 2020).

1 https://bcb.unl.edu/dbcan2/
2 https://www.ebi.ac.uk/tools/msa/clustalo/
3 https://itol.embl.de/

TABLE 1 Templates for homology modeling in this study.

Proteins (NCBI entry)	Templates (PDB or AlphaFold entry)
WP_239013920	AF-A0A1L9B4N1-F1
WP_143898266	AF-A0A3A8TK71-F1
WP_147439293	4OK7
WP_163999114	AF-A0A1H7SNC6-F1
MCA2980842	AF-A0A848L6Y9-F1
WP_161664743	4OK7
NBD12723	AF-A0A1H7SNC6-F1

The amino acid sequences were searched against Pfam database with an expected value threshold of 0.01 (Mistry et al., 2021). The integrated figures of the phylogenetic trees and the conserved domains were generated by TBtools (Chen C. et al., 2020).

2.5 Homology modeling

The homology model structures of the proteins were created by the SWISS-MODEL web server[4] (Waterhouse et al., 2018), and the templates are listed in **Table 1**. Verify_3D (Luthy et al., 1992) was used to check the residue profiles of the 3D models obtained. PROCHECK (Laskowski et al., 1996) analysis was performed to assess the stereochemical qualities of the 3D models. PyMOL software (The PyMOL Molecular Graphics System, Version 1.8 Schrödinger, LLC, De Lano Scientific, San Carlos, CA, USA) was used to view the structures and generate figures.

2.6 Protein sequence conservation analysis

The multiple sequence alignment files of the proteins in Clade I and Clade II were submitted to the AL2CO online server (Pei and Grishin, 2001), respectively, and residue conservation analysis were performed using the default parameters. The results were mapped onto the model structures of C25GH19A and C25GH19B using PyMOL, respectively.

2.7 Substrate binding pocket prediction

The substrate binding pockets of C25GH19A and C25GH19B, without any ligand, were calculated by the CavityPlus web server with default parameters[5] (Wang et al., 2023).

2.8 Electrostatic potential and pKa value calculation

Electrostatic potentials of the protein surfaces were calculated using the program APBS (Jurrus et al., 2018). The PQR file and the pKa values were calculated via PDB2PQR specifying the pH at 7 (Dolinsky et al., 2007). The figures were generated by PyMOL software.

2.9 Molecular docking

The peptidoglycan disaccharide substrate NAGNAM (N2) was extracted from the complex structure of PGRP-IBETAC (PDB entry: 2EAX) (Cho et al., 2007). The chitin trisaccharide substrate (N3) was extracted from the complex structure of OfChtIII (PDB entry: 5WV9) (Liu et al., 2018). AutoDock 4.2.6 (The Scripps Research Institute, La Jolla, CA, USA) was used for the molecular docking study (Morris et al., 2009). The AutoDock Tools 1.5.6 was used to prepare the protein and ligands for the docking procedure. Kollman charges and polar hydrogens were added. AutoGrid was used to generate the grid maps. Each grid was centered at the substrate binding pockets of the enzymes. The grid dimensions were 126 points in each dimension separated by 0.375 Å. The files were generated in PDBQT format. For ligands, random starting positions and orientations were used. The genetic algorithm was used with 2,500,000 energy evaluations and a population of 150 individuals, and 50 runs were carried out.

3 Results

3.1 The comparative secretory proteome of *C. silvisoli* c25j21 in the presence of cellulose and chitin

We previously isolated a myxobacterium strain, *C. silvisoli* c25j21 (Zhang et al., 2022), whose genome encodes 7197 proteins, 180 of which are annotated as CAZymes, including 20 auxiliary activities (AA), 11 separate carbohydrate-binding modules (CBM), 19 carbohydrate esterases (CE), 60 glycoside hydrolases (GH), 66 glycosyltransferases (GT), and 4 polysaccharide lyases (PL) (**Figure 1A**). To understand the roles of these CAZymes in polysaccharides metabolism, we investigated the secretory proteome of c25j21 when grown in the presence of cellulose or chitin, or neither, respectively. A total of 313 proteins were detected, of which 16 CAZymes were identified, including 2 AAs, 4 individual CBMs, 2 CEs, 7 GHs, and 1 PL (**Figure 1B** and **Supplementary Tables 2, 3**). There were 153 constitutively expressed proteins, including 9 CAZymes, such as GH13, PL20, CE1, CE4, AA5, CBM32, CBM13, etc (**Figure 1C**). Cellulose induced the expression of 57 proteins, including 5 CAZymes, namely GH13, GH6, AA4, CBM56, etc. Chitin induced the expression of 66 proteins, three of which were CAZymes, including GH13, GH19, and CBM56.

Consistent with previous studies showing that c25j21 has good starch utilization ability, in this study, it was found that this strain can secrete a variety of amylases, including the members of the subfamily GH13_6, GH13_10, GH13_11, and GH13_13. Interestingly, although c25j21 did not show cellulose and chitin hydrolytic activities in our previous plate experiments, the addition of lignocellulose or α-chitin to MD1 medium with reduced carbon sources could induce the secretion of related enzymes in the present study. Rice straw induced the secretion of two enzymes

4 https://swissmodel.expasy.org/

5 http://pkumdl.cn:8000/cavityplus/

10.3389/fmicb.2024.1324153

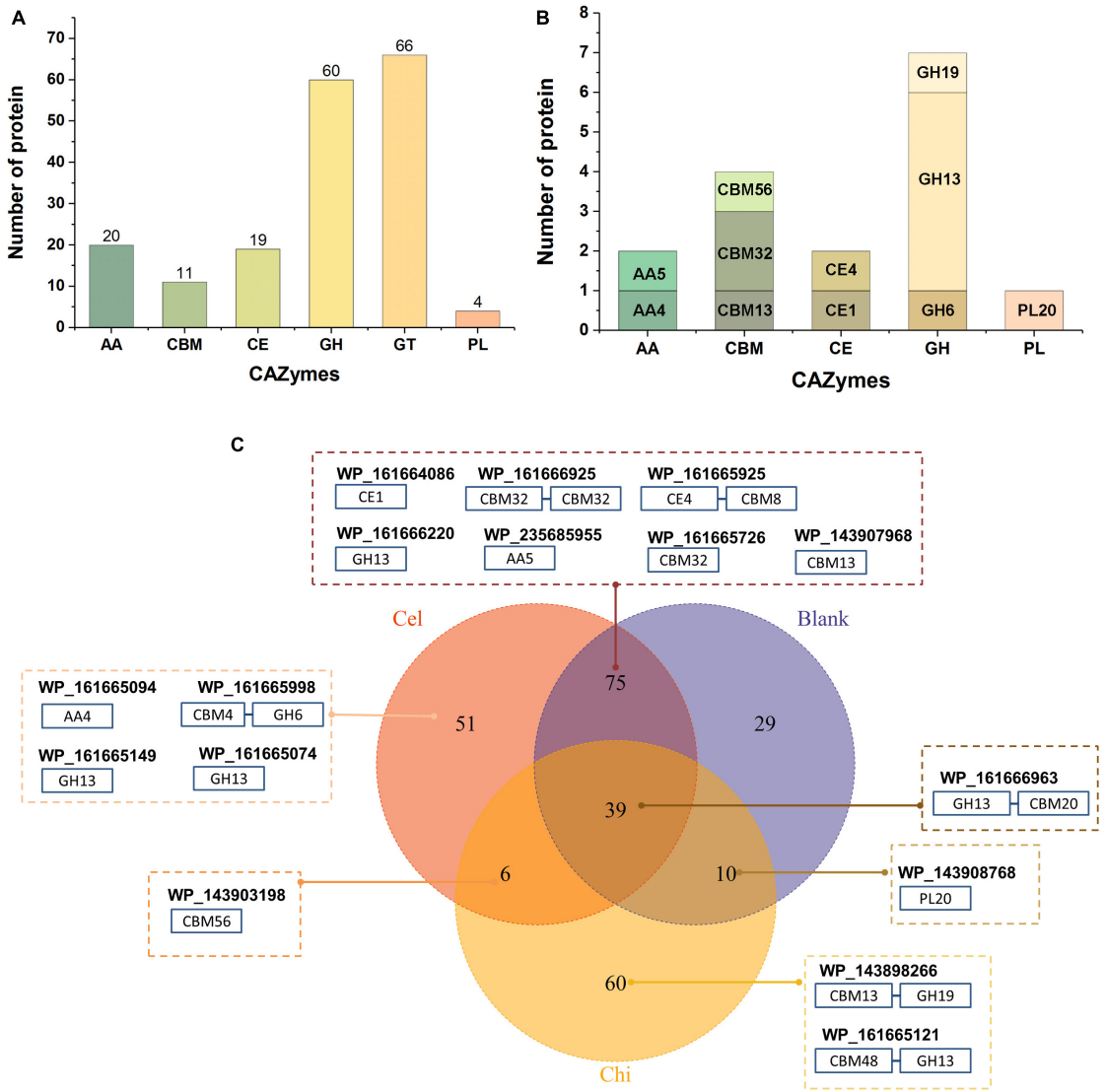

FIGURE 1
Secretory proteomic analysis of the CAZymes of c25j21. **(A)** CAZymes encoded by the genome of c25j21 annotated by dbCAN. **(B)** CAZymes detected by secretory proteomic analysis. **(C)** Venn plots of secreted proteins under different growth conditions. Numbers indicate the amount of protein detected. Cel, medium added cellulose; Chi, medium added α-chitin; Blank, medium without cellulose and chitin. In the dashed boxes are the NCBI IDs of the annotated CAZymes along with the schematic representation of their domain compositions.

belonging to the lignin-active AA4 and cellulose-active GH6 family, respectively. At the same time, α-chitin induced the secretion of a GH19 family enzyme, presumably with chitinase activity. Both of these added substrates induced the secretion of a CBM56 family protein, which may assist in polysaccharide degradation. In general, c25j21 has a large number of CAZyme genes, but relatively few of them are secreted. These results suggest that not many of the CAZymes encoded in the genome are involved in polysaccharide metabolism, and they may have other functions.

3.2 Three distinct GH19 enzymes from *C. silvisoli* c25j21

There are three GH19 enzymes encoded in the genome of c25j21, designated as C25GH19A (WP_143898266), C25GH19B (WP_161664743), and C25GH19C (NBD12723) (Figure 2A), of which only C25GH19A is induced by chitin, suggesting that they may have different biological functions. In our previous work, we have recombinantly expressed the C25GH19B in *E. coli* and characterized its enzymatic activity. C25GH19B was shown to be a lysozyme with bacteriolytic activity against both Gram-positive and Gram-negative plant pathogenic bacteria (Li et al., 2022). Both C25GH19A and C25GH19B have an N-terminal signal peptide, while C25GH19C without a signal peptide is predicted to be secreted by a non-classical pathway, indicating that they are extracellular enzymes. Unlike C25GH19B, which has only the catalytic GH19 module, both C25GH19A and C26GH19C have appended modules. A carbohydrate-binding module family 13 (CBM13) and lysin motif (LysM) modules located at the N-terminal of C25GH19A and C25GH19C, respectively, may play an important role in their substrate binding.

10.3389/fmicb.2024.1324153

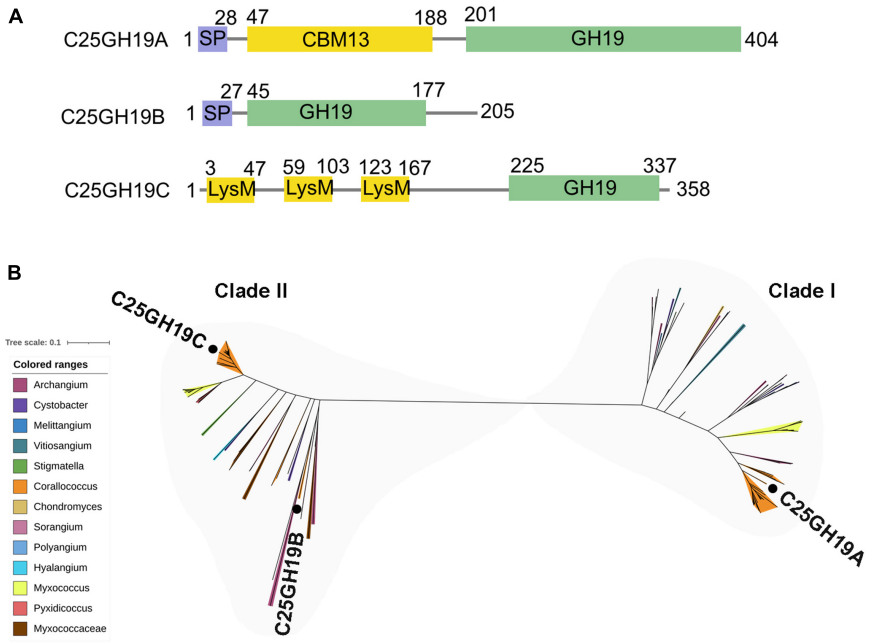

FIGURE 2
Protein sequences analysis of C25GH19s. **(A)** Module composition of C25GH19A, C25GH19B, and C25GH19C. **(B)** Phylogenetic tree of the GH19 modules of C25GH19s and their homologous proteins. Proteins from different myxobacteria genera are represented by different colors. C25GH19A, C25GH19B, and C25GH19C are labeled. The phylogenetic tree was created by MEGA-X, and the figure was generated by iTOL.

Multiple sequence alignment of the GH19 modules of the three enzymes revealed a 66% sequence identity between C25GH19B and C25GH19C, whereas C25GH19A shared less homology with them, with only 37 to 38% sequence identity. Comparing the protein sequences of these three GH19 modules against NCBI-nr protein database showed that their homologous proteins were widely distributed in several genera of myxobacteria (Figure 2B). Phylogenetic analysis revealed that these proteins clustered into two clades, with C25GH19B and C25GH19C in the same clade (clade II) and C25GH19A in the other clade (clade I). These results suggest that the two types of GH19 modules may have evolved different catalytic functions.

3.3 Phylogeny of myxobacterial GH19 enzymes

The enzymes of clade I are derived from the orders *Myxococcales* and *Polyangiales*. Phylogenetic analysis of GH19 modules revealed that these members clustered into three groups (Figure 3A). Group Ia includes enzymes derived from the genera *Corallococcus* and *Archangium*. All members of this group have a CBM13 module, except for three proteins with incomplete sequences. In addition to the genus *Myxococcus*, group Ib also includes enzymes derived from the genera *Polyangium*, *Sorangium*, and *Chondromyces*, belonging to the order *Polyangiale*, whose additional modules could not be annotated. The enzymes in the group Ic are derived from six genera of myxobacteria in the *Myxococcaceae* family, namely *Vitiosangium*, *Archangium*, *Stigmatella*, *Cystobacter*, *Hyalangium*, and *Melittangium*, and more than half of them have an appended module of unknown function.

Unlike clade I, the members of clade II are all derived from the order *Myxococcales*, covering seven genera, e.g., *Corallococcus*, *Pyxidicoccus*, *Myxococcus*, *Stigmatella*, *Hyalangium*, *Cystobacter*, and *Archangium* (Figure 3B). In the phylogenetic tree, the members of the basal branches near the root position mostly contain no additional modules, while the members of the terminal branches mostly have one to three LysM modules. It is speculated that they may have acquired appended modules through gene transfer and duplication during evolution.

More than 75% of clade I members have CBM13 modules, which are also known as Ricin-like lectin modules, were first identified in plant lectins such as ricin, and have been found in a number of glycoside hydrolases and glycosyltransferases, which function in binding to a variety of polysaccharides. About 60% of the clade II members have LysM modules, which are also known as CBM50. LysM was initially discovered in the lysozyme of a bacteriophage as a peptidoglycan binding module. Later, it was gradually found that LysM modules were widely present in plants and pathogenic fungi, and regulated plant immune response by binding to chitin in the cell wall of pathogenic fungi. The different composition of additional modules among the myxobacterial GH19 enzymes suggests that they may have different substrate selectivity.

3.4 Structural characteristics of the two types of GH19 enzymes

To understand the differences in amino acid composition and structural characteristics between the enzymes of the two clades, we performed multiple sequence alignment (MSA) and structural alignment of them. MSA showed that the catalytic center residues

10.3389/fmicb.2024.1324153

of the two clade enzymes were conserved (Figure 4A). One significant difference between them is that the enzymes in clade I have three longer loops compared to those in clade II. Among them, loops II and III are spatially located near the catalytic center and may influence the shape of the substrate binding pockets and participate in substrate binding (Figure 4B). Meanwhile, there are some conserved sites within the two clades, but these sites are significantly different between the two clades (Figure 4A, wavy lines). These sites contain more positively charged amino acids such as Arg and Lys in members of clade II compared to clade I. Amino acid conservation analysis of enzymes in both clades was performed separately, and the results were mapped to the 3D model structures of C25GH19A and C25GH19B, respectively (Figure 4C). The results showed that the most conserved sites of enzymes in both clades are located near the catalytic center, at the domain interface, that is, the substrate-binding pockets. These results suggest that the two types of GH19 enzymes may have different substrate recognition modes and catalytic functions.

Since these significant differences in amino acid composition are located in the substrate binding pocket region, to further understand the impact of these differences on enzyme structures as well as catalytic functions, we analyzed the substrate binding pockets of the three C25GH19s (Figure 5A). The results showed that the substrate binding pockets of all three enzymes are

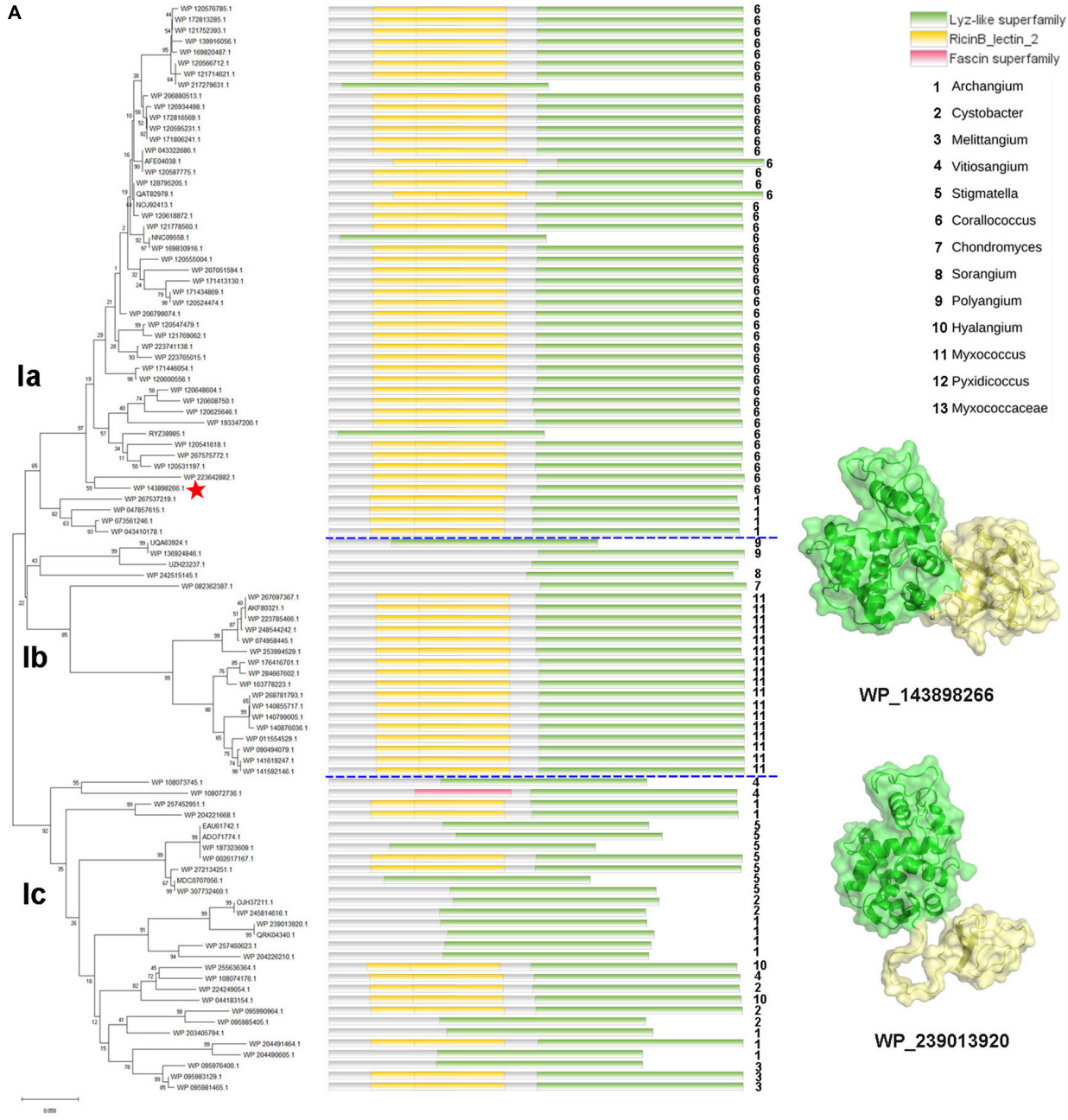

FIGURE 3
(Continued)

10.3389/fmicb.2024.1324153

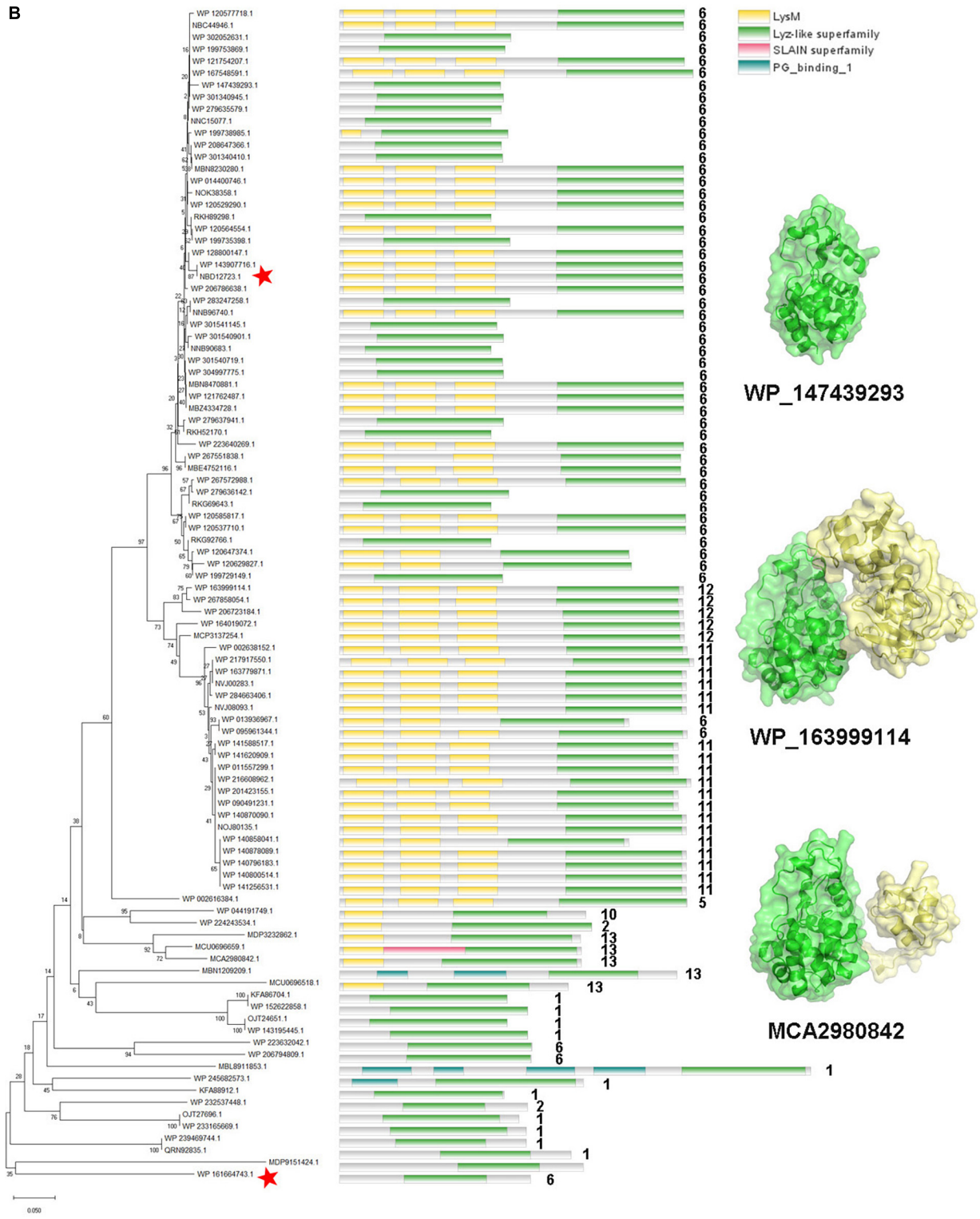

FIGURE 3
Phylogeny and module composition of the proteins in clade I **(A)** and clade II **(B)**. The tree was generated using the GH19 modules only. Appended modules that are present in the full protein sequence are indicated in the conserved module composition column but were not included in the calculation of the tree. Model structures of the representative members with different module compositions are mapped onto the tree, with colors representing the different modules. C25GH19s are indicated by red stars.

relatively wide open regions located at domain interfaces, which are suitable for binding of large polysaccharide substrates. The protein surface electrostatic potentials of these enzymes at pH 7.0 were calculated. As shown in Figure 5B, the substrate binding pocket of C25GH19A is negatively charged, which is favorable for enzymes binding to polysaccharides with positive charge, such as chitin.

10.3389/fmicb.2024.1324153

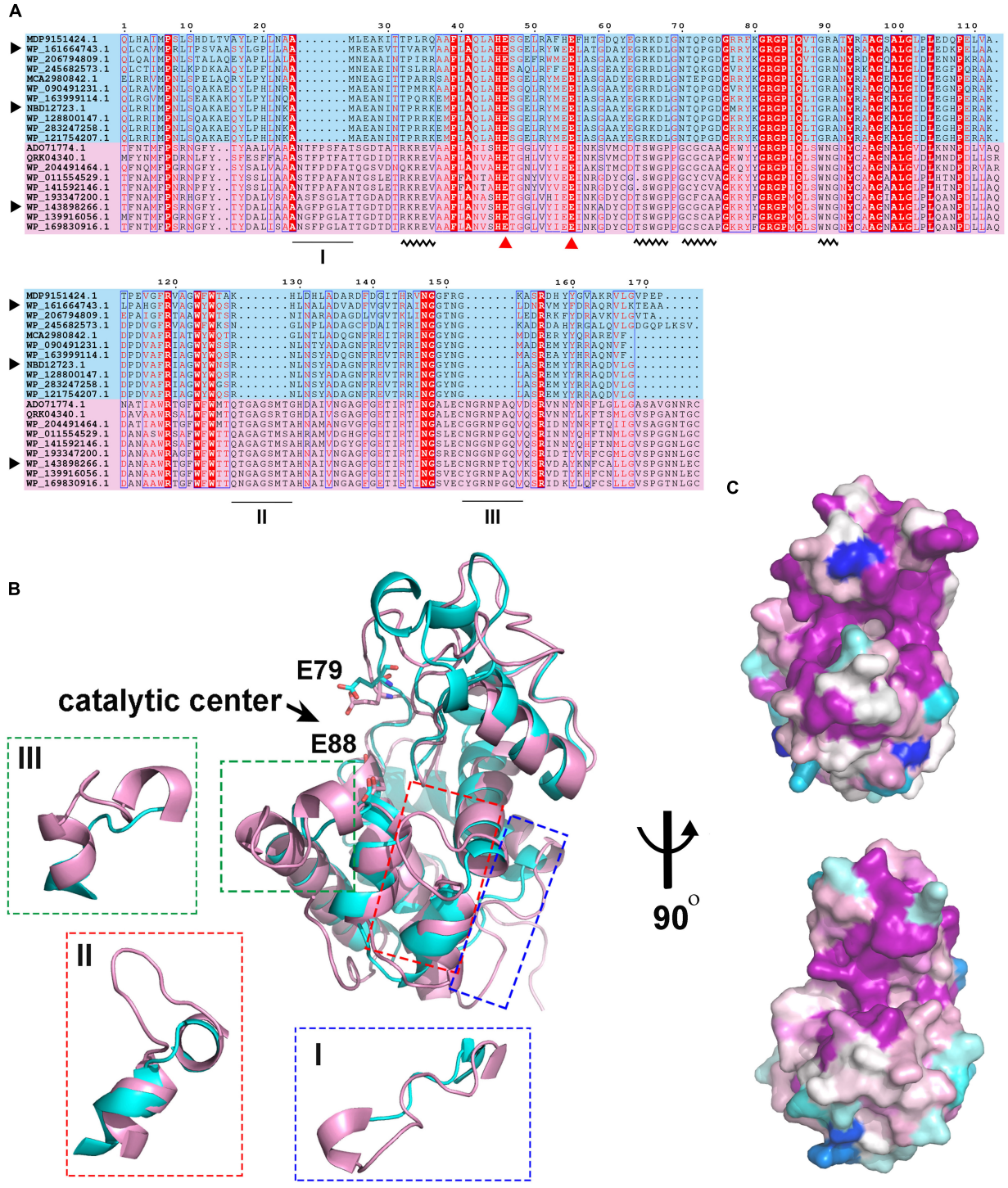

FIGURE 4
Sequence and structure alignment of C25GH19s. **(A)** Multiple sequence alignment of C25GH19s and their homologs. The pink and blue background indicate the proteins in Clade I and Clade II. The catalytic residues are indicated by red triangles. The black triangle indicates C25GH19A (WP_143898266), C25GH19B (WP_161664743), and C25GH19C (NBD12723). The black underlines indicate loops of significantly different lengths. The black wavy lines indicate conserved sites that differ significantly between the two clades. **(B)** Superposition of the model structures of C25GH19A (magenta) and C25GH19B (cyan). The catalytic residues are shown in sticks and labeled according to C25GH19B. The three loops of remarkably different lengths are circled and shown in the enlarged diagrams. **(C)** Conservation of residues across the Clade I (up) and Clade II (down) calculated by AL2CO and mapped onto C25GH19A and C25GH19B, respectively. Colors range from variable (blue) to conserved (purple).

The substrate binding pockets of C25GH19B and C25GH19C are positively charged, which may be more suitable for the binding of negatively charged polysaccharides, such as peptidoglycan. This is consistent with our previous findings, that is, C25GH19B has peptidoglycan hydrolysis activity but cannot hydrolyze chitin (Li et al., 2022).

10.3389/fmicb.2024.1324153

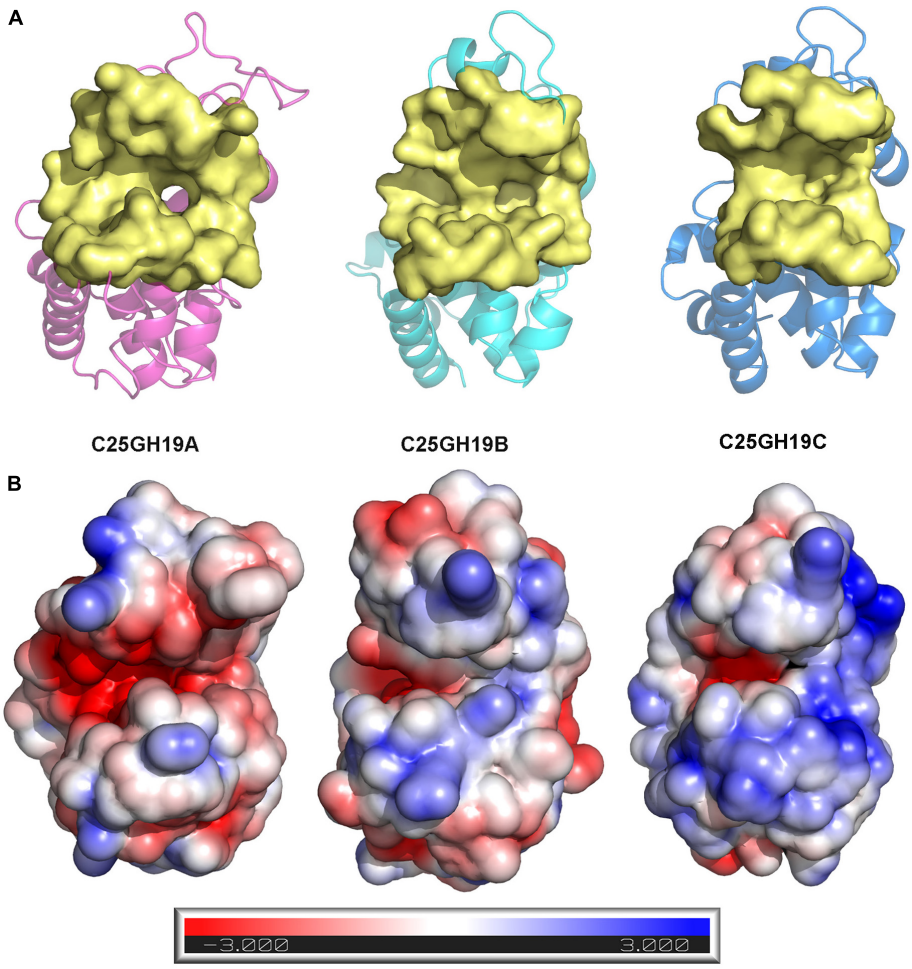

FIGURE 5
Structural comparison between C25GH19s. **(A)** The substrate binding pockets (yellow) of C25GH19A (magenta), C25GH19B (cyan), and C25GH19C (blue) predicted by CavityPlus. **(B)** The electrostatic potentials of protein surfaces. The electrostatic potential ranges from −3 to +3. Red indicates negatively charged, blue indicates positively charged, and white indicates uncharged.

3.5 Substrate binding modes of C25GH19s

The above findings inspired us to further explore the binding modes of these enzymes to different polysaccharide substrates. To analyze the possible interaction of C25GH19A with chitin substrates, the chitin trisaccharide $(GlcNAc)_3$ was extracted from the oligosaccharide-complexed crystal structure of the chitinase OfChtI and docked into the model structure of C25GH19A (**Figures 6A, B**). The chitin trisaccharide binds well in the substrate binding pocket of C25GH19A with a binding free energy of −2.32 kcal/mol. The residues M297, N304, Q341, Q298, L299, and G343 form hydrogen bonds with $(GlcNAc)_3$, while residues N269, E267, E258, I366, S369, A344, S300, W301, W336, and F337 interact with the chitin trisaccharide through van der Waals. Disaccharide NAGNAM was extracted from the complex crystal structure of the protein PGRP-Iβ and docked into the model structures of C25GH19B and C25GH19C, respectively, to analyze their potential binding modes to peptidoglycan substrates (**Figures 6C–F**). The binding free energies of C25GH19B or C25GH19C complexes with NAGNAM obtained by molecular docking were −5.64 and −5.81 kcal/mol, respectively. In C25GH19B, residues T121, Q119, E79, R98, and D100 form hydrogen bonds with the substrate NAGNAM; residues I179, Y95, N180, I118, L101, N125, and L120 participate in van der Waals interactions; in addition, Y157 forms Pi-alky interaction with NAGNAM (**Figure 6D**). C25GH19C also interacts with NAGNAM via hydrogen bonds and van der Waals interactions, and the residues involved include I275, Y252, T278, N282, R318, N337, Q276, Y314, E236, L277, L258, G338, and I336 (**Figure 6F**). Since both chitin and peptidoglycan are natural polymers, the use of disaccharides and trisaccharides as model substrates here only indicates the possible binding modes between them, and further studies on the activities and intermolecular interactions of these enzymes on these natural substrates are still needed in future work.

4 Discussion

Myxobacteria generally have larger genomes than other bacteria, and the large number of extracellular enzymes encoded

10.3389/fmicb.2024.1324153

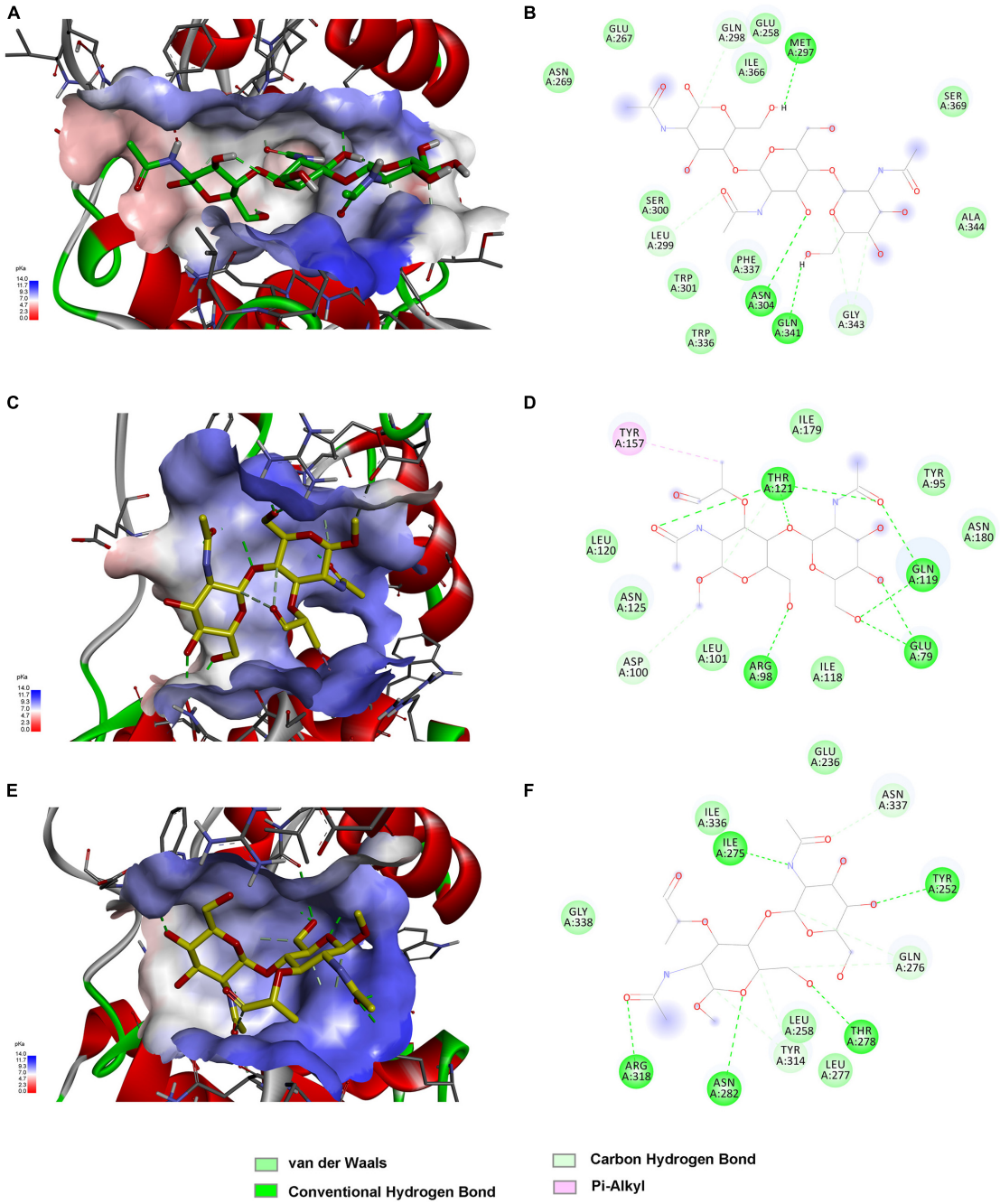

FIGURE 6
Substrate binding modes of C25GH19s predicted by molecular docking. **(A)** C25GH19A-chitin trisaccharide $(GlcNAc)_3$ complex. **(B)** The interactions between $(GlcNAc)_3$ and the residues of C25GH19A. **(C)** C25GH19B-NAGNAM complex. **(D)** The interactions between NAGNAM and the residues of C25GH19B. **(E)** C25GH19C-NAGNAM complex. **(F)** The interactions between NAGNAM and the residues of C25GH19C.

by them are considered to be major contributors to their powerful biomass degradation ability and important weapons for preying on other microorganisms. In this study, we performed a comparative secretory proteomic analysis of a previously isolated myxobacterium *C. silvisoli* c25j21. The results showed that the number of CAZymes induced by chitin and cellulose was not large. On the one hand, we found that a considerable number of secreted proteins induced by chitin and cellulose could not be annotated and predicted, and there may be some novel CAZymes that need more biochemical experiments to explore. On the other hand, these results also suggested that most CAZymes of c25j21 may have other biological functions than biomass degradation. As with its three redundant GH19 enzymes, only C25GH19A can be induced by chitin, while C25GH19B, which is not induced by chitin, has previously been characterized by lysozyme activity.

Sequence and structural analysis of these GH19enzymes and their homologous proteins from myxobacteria showed that

these proteins have evolved into two clades, in which clade I, where C25GH19A is located, is distributed in the two families of *Myxococcaceae* and *Polyangiaceae*, while clade II, where C25GH19B and C25GH19C are located, is distributed only in the family of *Myxococcaceae*. This difference in the distribution of these enzymes among myxobacteria species may be related to their biological functions.

The substrate binding pocket is the most important region affecting substrate recognition, binding, and catalysis of enzymes. From the multiple sequence alignments and structural comparisons, it can be seen that the amino acid composition of this region is the most conserved within each clade, but the difference between the two clades is significant. Although both clades of GH19s have wide, open substrate binding pockets suitable for binding large polysaccharide substrates, their substrate binding pockets have different molecular surface electrostatic potentials, which makes them suitable for the accommodation of polysaccharides with different properties, such as positively charged chitin or negatively charged peptidoglycan.

Most CAZymes are multi-module enzymes, and in addition to the catalytic modules, appended modules generally have substrate binding ability, thus affecting the substrate selectivity of the enzymes. The appended modules of these two clades of myxobacterial GH19s in this study are also distinct. More than 75% of the enzymes of clade I carry the CBM13 module, while about 60% of the enzymes of clade II carry one or more LysM modules. Meanwhile, phylogenetic analysis showed that these enzymes may have acquired appended modules through gene transfer and duplication during evolution. These results suggest that although the myxobacteria, such as c25j21, have redundant GH19 genes, they have evolved different enzyme properties and may have non-redundant biological functions.

In summary, this study provides a better understanding of the secreted proteome of *C. silvisoli* c25j21 in the presence of cellulose and chitin, as well as its three redundant GH19 enzymes. These results will lay a theoretical and experimental foundation for further study of the physiological functions of CAZymes in the process of myxobacteria predation and polysaccharides metabolism, as well as their development and application.

Data availability statement

The original contributions presented in this study are included in this article/**Supplementary materials**, further inquiries can be directed to the corresponding author.

Author contributions

XiaolZ: Conceptualization, Funding acquisition, Investigation, Methodology, Writing – original draft, Writing – review & editing. XianmZ: Writing – review & editing. XianjZ: Writing – review & editing. HD: Writing – review & editing. YD: Writing – review & editing. HZ: Funding acquisition, Project administration, Writing – review & editing.

Funding

The authors declare financial support was received for the research, authorship, and/or publication of this article. This work was funded by the Guangdong Basic and Applied Basic Research Foundation (2022A1515011013); Seed Industry Revitalization Project of Special Funds for Provincial Rural Revitalization Strategy in 2022 (2022-440000-4301030403-9538); Guangdong Special Support Program (2021JC06N628); and the Natural Science Foundation of Guangdong Province (2022A1515012440).

Conflict of interest

The authors declare that the research was conducted in the absence of any commercial or financial relationships that could be construed as a potential conflict of interest.

Publisher's note

Supplementary material

The Supplementary Material for this article can be found online at: https://www.frontiersin.org/articles/10.3389/fmicb.2024.1324153/full#supplementary-material

SUPPLEMENTARY TABLE 1
Protein sequences in this study.

SUPPLEMENTARY TABLE 2
Data for the venn plots of secreted proteins under different growth conditions.

SUPPLEMENTARY TABLE 3
The secretory proteome sequencing data.

References

Arend, K. I., Schmidt, J. J., Bentler, T., Luchtefeld, C., Eggerichs, D., Hexamer, H. M., et al. (2021). Myxococcus xanthus predation of Gram-positive or Gram-negative bacteria is mediated by different bacteriolytic mechanisms. *Appl. Environ. Microbiol.* 87:e2382-20.

Berleman, J. E., and Kirby, J. R. (2009). Deciphering the hunting strategy of a bacterial wolfpack. *FEMS Microbiol. Rev.* 33, 942–957. doi: 10.1111/j.1574-6976.2009.00185.x

Chen, C., Chen, H., Zhang, Y., Thomas, H. R., Frank, M. H., He, Y., et al. (2020). TBtools: an integrative toolkit developed for interactive analyses of big biological data. *Mol. Plant* 13, 1194–1202. doi: 10.1016/j.molp.2020.06.009

Chen, X., Zhang, L., Li, X., Qiao, Y., Zhang, Y., Zhao, Y., et al. (2020). Impact of maltogenic alpha-amylase on the structure of potato starch and its retrogradation properties. *Int. J. Biol. Macromol.* 145, 325–331. doi: 10.1016/j.ijbiomac.2019.12.098

Cho, S., Wang, Q., Swaminathan, C. P., Hesek, D., Lee, M., Boons, G. J., et al. (2007). Structural insights into the bactericidal mechanism of human peptidoglycan recognition proteins. *Proc. Natl. Acad. Sci. U S A.* 104, 8761–8766.

Dolinsky, T. J., Czodrowski, P., Li, H., Nielsen, J. E., Jensen, J. H., Klebe, G., et al. (2007). PDB2PQR: expanding and upgrading automated preparation of biomolecular structures for molecular simulations. *Nucleic Acids Res.* 35, W522–W525. doi: 10.1093/nar/gkm276

Jurrus, E., Engel, D., Star, K., Monson, K., Brandi, J., Felberg, L. E., et al. (2018). Improvements to the APBS biomolecular solvation software suite. *Protein Sci.* 27, 112–128. doi: 10.1002/pro.3280

Konovalova, A., Petters, T., and Sogaard-Andersen, L. (2010). Extracellular biology of Myxococcus xanthus. *FEMS Microbiol. Rev.* 34, 89–106.

Kumar, S., Stecher, G., Li, M., Knyaz, C., and Tamura, K. (2018). MEGA X: molecular evolutionary genetics analysis across computing platforms. *Mol. Biol. Evol.* 35, 1547–1549. doi: 10.1093/molbev/msy096

Laskowski, R. A., Rullmannn, J. A., MacArthur, M. W., Kaptein, R., and Thornton, J. M. (1996). AQUA and PROCHECK-NMR: programs for checking the quality of protein structures solved by NMR. *J. Biomol. NMR* 8, 477–486. doi: 10.1007/BF00228148

Letunic, I., and Bork, P. (2019). Interactive Tree Of Life (iTOL) v4: recent updates and new developments. *Nucleic Acids Res.* 47, W256–W259. doi: 10.1093/nar/gkz239

Li, Y., Zhou, X., Zhang, X., Xu, Z., Dong, H., Yu, G., et al. (2022). A myxobacterial GH19 lysozyme with bacteriolytic activity on both Gram-positive and negative phytopathogens. *AMB Express* 12:54. doi: 10.1186/s13568-022-01393-y

Li, Z., Ji, K., Zhou, J., Ye, X., Wang, T., Luo, X., et al. (2017). A debranching enzyme IsoM of Corallococcus sp. strain EGB with potential in starch processing. *Int. J. Biol. Macromol.* 105(Pt 1), 1300–1309. doi: 10.1016/j.ijbiomac.2017.07.153

Li, Z., Wu, J., Zhang, B., Wang, F., Ye, X., Huang, Y., et al. (2015). AmyM, a novel Maltohexaose-forming alpha-Amylase from Corallococcus sp. strain EGB. *Appl. Environ. Microbiol.* 81, 1977–198714. doi: 10.1128/AEM.03934-14

Li, Z., Xia, C., Wang, Y., Li, X., Qiao, Y., Li, C., et al. (2019a). Identification of an endo-chitinase from Corallococcus sp. EGB and evaluation of its antifungal properties. *Int. J. Biol. Macromol.* 132, 1235–1243. doi: 10.1016/j.ijbiomac.2019.04.056

Li, Z., Ye, X., Liu, M., Xia, C., Zhang, L., Luo, X., et al. (2019b). A novel outer membrane beta-1,6-glucanase is deployed in the predation of fungi by myxobacteria. *ISME J.* 13, 2223–2235. doi: 10.1038/s41396-019-0424-x

Liu, T., Zhu, W., Wang, J., Zhou, Y., Duan, Y., Qu, M., et al. (2018). The deduced role of a chitinase containing two nonsynergistic catalytic domains. *Acta Crystallogr. D Struct. Biol.* 74(Pt 1), 30–40. doi: 10.1107/S2059798317018289

Lu, S., Wang, J., Chitsaz, F., Derbyshire, M. K., Geer, R. C., Gonzales, N. R., et al. (2020). CDD/SPARCLE: the conserved domain database in 2020. *Nucleic Acids Res.* 48, D265–D268.

Luthy, R., Bowie, J. U., and Eisenberg, D. (1992). Assessment of protein models with three-dimensional profiles. *Nature* 356, 83–85.

Mistry, J., Chuguransky, S., Williams, L., Qureshi, M., Salazar, G. A., Sonnhammer, E. L. L., et al. (2021). Pfam: the protein families database in 2021. *Nucleic Acids Res.* 49, D412–D419.

Morris, G. M., Huey, R., Lindstrom, W., Sanner, M. F., Belew, R. K., Goodsell, D. S., et al. (2009). AutoDock4 and AutoDockTools4: automated docking with selective receptor flexibility. *J. Comput. Chem.* 30, 2785–2791. doi: 10.1002/jcc.21256

Munoz-Dorado, J., Marcos-Torres, F. J., Garcia-Bravo, E., Moraleda-Munoz, A., and Perez, J. (2016). Myxobacteria: moving, killing, feeding, and surviving together. *Front. Microbiol.* 7:781. doi: 10.3389/fmicb.2016.00781

Pedraza-Reyes, M., and Gutierrez-Corona, F. (1997). The bifunctional enzyme chitosanase-cellulase produced by the gram-negative microorganism Myxobacter sp. AL-1 is highly similar to Bacillus subtilis endoglucanases. *Arch. Microbiol.* 168, 321–327. doi: 10.1007/s002030050505

Pei, J., and Grishin, N. V. (2001). AL2CO: calculation of positional conservation in a protein sequence alignment. *Bioinformatics* 17, 700–712. doi: 10.1093/bioinformatics/17.8.700

Robert, X., and Gouet, P. (2014). Deciphering key features in protein structures with the new ENDscript server. *Nucleic Acids Res.* 42, W320–W324. doi: 10.1093/nar/gku316

Sievers, F., and Higgins, D. G. (2018). Clustal Omega for making accurate alignments of many protein sequences. *Protein Sci.* 27, 135–145.

Sudo, S., and Dworkin, M. (1972). Bacteriolytic enzymes produced by Myxococcus xanthus. *J. Bacteriol.* 110, 236–245.

Tellez-Valencia, A., Sandoval, A. A., and Pedraza-Reyes, M. (2003). The non-catalytic amino acid Asp446 is essential for enzyme activity of the modular endocellulase Cel9 from Myxobacter sp. AL-1. *Curr. Microbiol.* 46, 307–310. doi: 10.1007/s00284-002-3862-y

Wang, S., Xie, J., Pei, J., and Lai, L. (2023). CavityPlus 2022 update: an integrated platform for comprehensive protein cavity detection and property analyses with user-friendly tools and cavity databases. *J. Mol. Biol.* 435:168141. doi: 10.1016/j.jmb.2023.168141

Waterhouse, A., Bertoni, M., Bienert, S., Studer, G., Tauriello, G., Gumienny, R., et al. (2018). SWISS-MODEL: homology modelling of protein structures and complexes. *Nucleic Acids Res.* 46, W296–W303.

Zhang, L., Dong, C., Wang, J., Liu, M., Wang, J., Hu, J., et al. (2023). Predation of oomycetes by myxobacteria via a specialized CAZyme system arising from adaptive evolution. *ISME J.* 17, 1089–1103. doi: 10.1038/s41396-023-01423-y

Zhang, X. J., Feng, G. D., Liu, Y., Zhou, Y., Deng, X., Yao, Q., et al. (2022). Corallococcus silvisoli sp. nov., a novel myxobacterium isolated from subtropical forest soil. *Arch. Microbiol.* 204:141. doi: 10.1007/s00203-021-02725-5

Zheng, J., Ge, Q., Yan, Y., Zhang, X., Huang, L., and Yin, Y. (2023). dbCAN3: automated carbohydrate-active enzyme and substrate annotation. *Nucleic Acids Res.* 51, W115–W121. doi: 10.1093/nar/gkad328

Zhou, J., Li, Z., Zhang, H., Wu, J., Ye, X., Dong, W., et al. (2018). Novel Maltogenic Amylase CoMA from Corallococcus sp. strain EGB catalyzes the conversion of maltooligosaccharides and soluble starch to maltose. *Appl. Environ. Microbiol.* 84:e00152-18. doi: 10.1128/AEM.00152-18

Zhou, X., Xu, Z., He, J., Li, Y., Pan, C., Wang, C., et al. (2020). A myxobacterial LPMO10 has oxidizing cellulose activity for promoting biomass enzymatic saccharification of agricultural crop straws. *Bioresour. Technol.* 318:124217. doi: 10.1016/j.biortech.2020.124217

frontiers | Frontiers in Microbiology

TYPE Original Research
PUBLISHED 08 March 2024
DOI 10.3389/fmicb.2024.1369499

OPEN ACCESS

EDITED BY
Maria Fátima Carvalho,
University of Porto, Portugal

REVIEWED BY
Aslihan Kurt-Kizildogan,
Ondokuz Mayıs University, Türkiye
Lasse van Geelen,
Heinrich Heine University of Düsseldorf, Germany

*CORRESPONDENCE
Honghui Zhu
✉ zhuhh_gdim@163.com
Qing Yao
✉ yaoqscau@scau.edu.cn

†These authors have contributed equally to this work

RECEIVED 12 January 2024
ACCEPTED 22 February 2024
PUBLISHED 08 March 2024

CITATION
Zang Y, Zhang X, Wang Z, Tong Q, Zhou Y, Yao Q and Zhu H (2024) *Hyalangium ruber* sp. nov, characterization of a novel myxobacterium strain s54d21 and their secondary metabolites.
Front. Microbiol. 15:1369499.
doi: 10.3389/fmicb.2024.1369499

Hyalangium ruber sp. nov, characterization of a novel myxobacterium strain s54d21 and their secondary metabolites

Yi Zang[1†], Xianjiao Zhang[1,2†], Zhe Wang[1], Qingyi Tong[3], Yang Zhou[1], Qing Yao[2*] and Honghui Zhu[1*]

[1]Key Laboratory of Agricultural Microbiomics and Precision Application (MARA), Guangdong Provincial Key Laboratory of Microbial Culture Collection and Application, Key Laboratory of Agricultural Microbiome (MARA), State Key Laboratory of Applied Microbiology Southern China, Institute of Microbiology, Guangdong Academy of Sciences, Guangzhou, China, [2]College of Horticulture, South China Agriculture University, Guangzhou, China, [3]School of Pharmacy, Tongji Medical College, Huazhong University of Science and Technology, Wuhan, China

Myxobacteria are special bacteria with wide adaptability, which are rich sources of structurally diverse natural products with intriguing biological properties. Here, a gram-negative myxobacterium strain s54d21^T was isolated from the sediment of a wetland park in China using the *Escherichia coli* baiting method. Based on 16S rRNA gene sequence and genomic data, the strain was demonstrated to be a novel species of a rare genus *Hyalangium*, designated *Hyalangium ruber* sp. nov (type strain s54d21^T = GDMCC 1.1945^T = JCM 39263^T). The subsequent chemical investigation of the strain s54d21^T led to the isolation of three rare 3,5,6-trisubstituted 2(1*H*)-pyrazinones, namely, hyalanones A–C (**1**–**3**), together with a known macrolactin A (**4**). Those new structures and their absolute configurations were unambiguously assigned by extensive analyses of spectroscopic data and density functional theory (DFT) calculations. In biological assays, compound **4** exhibited moderate cytotoxic activities against human cell lines RKO, A549, and NCM460 with IC_{50} values ranging from 27.21 to 32.14 μM.

KEYWORDS

myxobacteria, *Hyalangium ruber*, secondary metabolite, structure elucidation, cytotoxicity

1 Introduction

Myxobacteria are a class of gram-negative eubacteria widely found in terrestrial and aquatic ecosystem. They are known for their complex lifecycle and social behavior that are probably mediated through secondary metabolites (Kaiser, 2003; Shrivastava and Sharma, 2021; Saggu et al., 2023). In past four decades, numbers of natural products from myxobacteria have been characterized with novel and complex structures, including polyketides, non-ribosomal peptides, and hybrids (Wenzel and Müller, 2009; Herrmann et al., 2017; Bader et al., 2020; Saggu et al., 2023). These secondary metabolites exhibit diverse biological properties, such as cytotoxic, antifungal, antibacterial, antiviral, antimalarial, and immunosuppressive effects (Wenzel and Müller, 2009; Schäberle et al., 2014; Dehhaghi et al., 2018; Bhat et al., 2021). Hence, myxobacteria are considered as important and enormous sources for structurally diverse and bioactive natural products that can be explored for drug discovery.

Although amount of myxobacteria have been identified in past two decades, there are numerous undiscovered or uncultivated myxobacteria. The genus *Hyalangium* belonging to Myxococcaceae family was initially established by Reichenbach (2005), while the only member *H. minutum* was isolated from a mountain soil with decayed plants before 2023. Continuous chemical research studies of *H. minutum* found a series of bioactive compounds, including hyaladione with significant cytotoxic and antimicrobial activities and unusual siderophores, namely, hyalachelins A–C (Okanya et al., 2012; Nadmid et al., 2014; Okanya et al., 2014; Surup et al., 2018). Until recently, two novel species of *H. versicolor* and *H. gracilis* were characterized and reclassified by Zhang et al. (2023).

In this study, the strain s54d21^T was isolated from a sample of wetland sediment as a novel member of *Hyalangium* classified by using the polyphasic approach. To search for novel and bioactive natural products from this strain, the chemical investigation of the culture broth of *Hyalangium ruber* sp. nov was performed, leading to the identification of three 2(1*H*)-pyrazinone derivatives, namely, hyalanones A–C (**1**–**3**), along with a known compound macrolactin A (**4**). The planar structures and absolute stereochemistry of those new isolates were unambiguously established by extensive spectroscopic methods and theoretical electronic circular dichroism (ECD) calculations with time-dependent DFT (TDDFT) methods. Hyalanones A–C (**1**–**3**) were assigned as rare 3,5,6-trisubstituted 2(1*H*)-pyrazinone analogs that were probably biosynthesized from valine and alanine or threonine, respectively. The known compound **4** was determined by comparing of NMR data and HRESIMS spectrum with literatures (Gustafson et al., 1989; He et al., 2013). Herein, we report the identification of the myxobacterium strain, isolation and structure elucidation of new compounds, and their biological assay.

2 Materials and methods

2.1 Isolation and cultivation of the myxobacteria strain

Strain s54d21^T was isolated from a sediment sample collected from Xinghu National Wetland Park (N 23°4′54″, E 112°28′17″) in Guangdong Province of China. The strain was isolated following the baiting approach with *E. coli* as prey on water agar (0.1% $CaCl_2$•$2H_2O$, 20 mM HEPES, 1.5% agar), where small portions of soil samples were placed adjacent to the *E. coli* spot. Until swarming colonies or fruiting bodies observed after incubation at 30°C, purification of the isolate was subsequently completed by repeatedly transferring onto fresh VY/2 agar (0.5% dried baker's yeast, 0.1% $CaCl_2$•$2H_2O$, 1.5% agar). Finally, the pure strain characterized orange-pigment fruiting bodies on agar and was deposited in Guangdong Microbial Culture Collection Center (GDMCC, No. 1.1945) and Japan Collection of Microorganisms (JCM, no. 39263).

2.2 Morphological and physiological analyses

The swarm morphology was observed under a stereomicroscope (Olympus SZX10, Japan). The vegetative cells and myxospores were investigated by using scanning electron microscope (SEM, Hitachi S-3000 N, Japan) and the phase contrast microscope (ZEISS Axioscope 5, Germany), respectively. The Gram reaction was determined using a Gram staining kit (Huankai, China), while Conga red staining was performed as described by McCurdy (1969). The oxidase test was determined using a commercial strip (Huankai, China), while the catalase test was performed using 3% (v/v) H_2O_2. The growth temperature range was determined on VY/2 agar at different temperatures (4, 10, 15, 20, 25, 30, 37, 40, and 42°C). The pH range (4.0–10.0, at intervals of 1 pH unit) for growth was tested on VY/2 agar at 30°C for 14 days and buffered with 100 mM citrate/sodium citrate (pH 4.0–5.0), HEPES (pH 6.0–8.0), and Tris (pH 9.0–10.0). Salt tolerance was evaluated by growing the isolated on VY/2 agar plates supplemented with NaCl to concentrations of 0.5, 1, 1.5, 2, and 3% (m/v). Susceptibility to antibiotics was investigated on VY/2 agar supplemented with various antibiotics at the final concentration of 50 μg/mL at 30°C for 14 days. Sixteen antibiotics were selected for strain s54d21^T: ampicillin, apramycin, spectinomycin, polymyxin B, neomycin, bacitracin B, gentamicin, tetracycline, erythromycin, oxytetracycline, chloramphenicol, nalidixic acid, trimethoprim, streptomycin, rifampin, and kanamycin. Anaerobic growth was tested on VY/2 agar plates in an anaerobic jar at 30°C for 14 days. Hydrolysis of starch, skimmed milk, colloidal chitin, and carboxymethycelluose (CMC) was assessed on tryptone agar (0.2% tryptone, 0.05% $MgSO_4$, 0.01% $CaCl_2$•$2H_2O$, 1.5% agar; pH 7.2) at the final concentration of 1.0% (m/v), respectively. Hydrolysis of Tween 20 and 80 was tested on tryptone agar supplemented with 1.0% (v/v) Tween 20 and 80, respectively. Additional enzyme activities were tested using the API ZYM and 20NE kits (bioMérieux, France), according to the manufacturer's instructions.

2.3 16S RNA analysis identification and phylogenetic analysis

Genomic DNA of strain s54d21^T was extracted by using Genomic DNA Isolation Kit (Magen, China). The 16S rRNA gene sequence was amplified using the universal primers 27F/1492R (Weisburg et al., 1991). The PCR products were sequenced by Shanghai Majorbio Biopharm Technology Co., Ltd. Sequence alignment was performed at online EZBioCloud server (Yoon et al., 2017a) and NCBI. Phylogenetic tree based on the 16S rRNA gene sequences was reconstructed using software MEGA X (Kumar et al., 2018) with the maximum likelihood (ML) method (Felsenstein, 1981) under the Kimura's two-parameter model (Kimura, 1980). Bootstrap analysis was conducted based on 1,000 replicates (Hoang et al., 2018).

2.4 Genome sequencing and bioinformatics analysis

Genomic sequencing was carried out using an Illumina Hiseq platform at Shanghai Majorbio Biopharm Technology Co., Ltd. The obtained reads were assembled into contigs using SPAdes v3.11.1 (Bankevich et al., 2012). Genome contamination and completeness were assessed using CheckM tool (Parks et al., 2015). Genome was annotated using the Prokka (Seemann, 2014) and RAST server (Aziz et al., 2008). The biosynthetic gene clusters of secondary metabolites

were predicted using antiSMASH 6.0 with the default settings (Blin et al., 2021). The carbohydrate activities were identified using the dbCAN2 meta server (Zhang et al., 2018). Average nucleotide identity (ANI) and digital DNA–DNA hybridization (dDDH) values among strain s54d21^T and the closely related type strains were calculated using an online ANI calculator and the Genome-to-Genome Distance Calculator 3.0 (Meier-Kolthoff et al., 2013; Yoon et al., 2017b). Phylogenomic tree was constructed using the up-to-data bacterial core gene (UBCG) pipeline based on 92 core housekeeping genes (Na et al., 2018).

2.5 Chemotaxonomic characterization

Respiratory quinones of the strain s54d21^T were extracted and analyzed as previously described using HPLC (Agilent 1260) (Collins et al., 1977). For the fatty acid detection, strain s54d21^T and its closely related type strains were incubated on VY/2 agar plates at 30°C for a week. Fatty acids were extracted and identified according to the described protocol using a gas chromatography mass spectrometry (GCMS, Agilent 7890B-5977B) (Gemperlein et al., 2014).

2.6 Chemical investigation of the myxobacteria strain

2.6.1 General experimental procedures

The UV, IR, and ECD spectra were obtained on a Jobin Yvon LabRAM HR800 instrument, a Bruker Vertex 70 instrument, and a JASCO-810 ECD spectrometer, respectively. Optical rotation values of new compounds were tested with a Rudolph Autopol IV automatic polarimeter. NMR spectra were recorded on a Bruker Ascend 600 MHz spectrometer, with ^{1}H and ^{13}C NMR chemical shifts referenced to the solvent or solvent impurity peaks for CD_3OD (δ_H 3.31 and δ_C 49.0). HRESIMS data were acquired using electrospray ionization (ESI) with a Thermo Fisher Orbitraq Exploris 120 mass spectrometer. Semi-preparative HPLC utilized a SHIMADZU Prominence LC-20AT quaternary system with a UV–VIS detector using a YMC-pack ODS-A column (5 μm, 10 × 250 mm). Column chromatography (CC) was performed using ODS (50 μm, YMC, Japan). Thin-layer chromatography (TLC) was performed with silica gel 60 GF254 (Yantai Chemical Industry Research Institute, China).

2.6.2 Fermentation, extraction, and isolation

2.6.2.1 Extraction and isolation

The strain was maintained on VY/2 agar at 30°C for 5 days, which was used as the seed culture. The strain was cultured in 10 L MD1G liquid medium (0.3% tryptone, 5.0% starch, 0.02% $MgSO_4$•$2H_2O$, 0.07% $CaCl_2$•$2H_2O$) on a rotary shaker (180 rpm) at 30°C for 10 days. Amberliter XAD-16 (2%, v/v) was added to the liquid medium on the fourth day (Okanya et al., 2012, 2014). After incubation, XAD and cell mass were harvested by centrifugation and filtration, which was washed using 10 L acetone and 10 L methanol sequentially at room temperature to yield 600 mg of crude extract.

The crude extract was fractioned by column chromatography (CC) over ODS with a gradient elution using MeOH/H_2O gradient (25 to 100%, v/v) to afford 9 fractions (Fr.1–Fr.9). Compound **1** (6.4 mg) was isolated from Fr.3–3 via semi-preparative HPLC (25% MeCN/H_2O for 45 min; flow rate: 3.0 mL/min; **1**: t_R = 38.0 min). Compounds **2** (0.9 mg) and **3** (1.0 mg) were further purified from Fr.3–1-3 by HPLC (20% MeCN/H_2O for 30 min; flow rate: 3.0 mL/min; **2**: t_R = 9.9 min; **3**: t_R = 24.6 min). Fr.4–4 was further purified by HPLC (40% MeCN/H_2O for 35 min; flow rate: 3.0 mL/min; **4**: t_R = 29.8 min) to get compound **4** (3.5 mg).

2.6.3 Spectroscopic data of new compounds

Hyalanone A (**1**): amorphous solid; UV (MeOH) λ_{max} nm (log ε): 231 (4.2), 331 (4.0); IR (NaCl) ν_{max} cm^{-1}: 3364, 2,966, 2,923, 2,869, 2,852, 1,648, 1,533, 1,466, 1,389, 1,347, 1,294, 1,212, 1,083, 1,036, 960, 816, 650, 623, 546, and 522; ^{1}H and ^{13}C NMR data (CD_3OD) (see Table 1); HRESIMS m/z 203.1155 $[M+Na]^+$ (calcd for $C_{10}H_{16}N_2ONa$, 203.1160).

Hyalanone B (**2**): amorphous solid; $[\alpha]^{25}_D$ −20 (*c* 0.1, MeOH); UV (MeOH) λ_{max} nm (log ε): 232 (4.0), 326 (3.8); IR (NaCl) ν_{max} cm^{-1}: 3364, 2,969, 2,922, 2,851, 1,649, 1,537, 1,468, 1,385, 1,335, 1,217, 1,077,

TABLE 1 Differential phenotypic and physiological characteristics of the strain s54d21^T and the closely related type strains.

Characteristics	1	2	3	4
Temperature growth range (°C)	20–40	15–40	20–42	20–37
pH tolerance	4.0–10.0	5.0–10.0	4.0–10.0	4.0–10.0
β-Galactosidase	–	+	–	–
Cystine arylamidase	–	+	+	+
Trypsin	–	–	+	+
α-Chymotrypsin	–	–	+	+
β-Glucosidase	+	–	+	+
Antibiotic resistance (50 μg/mL)				
Gentamicin	+	+	+	–
Kanamycin	+	–	–	–
Apramycin	–	–	+	+
Neomycin	–	–	+	–

1. s54d21^T; 2. *H. minutum* DSM 14724^T; 3. *H. gracilis* DSM 14753^T; 4. *H. versicolor* H56D21^T. All data were obtained from this study under the same conditions. +, positive; –, negative.

1,017, 900, 814, 643, and 574; ^{1}H and ^{13}C NMR data (CD_3OD) (see Table 1); HRESIMS m/z 219.1105 $[M+Na]^+$ (calcd for $C_{10}H_{16}N_2O_2Na$, 219.1104).

Hyalanone C (**3**): amorphous solid; $[\alpha]^{25}_{D}$ −11 (*c* 0.1, MeOH); UV (MeOH) λ_{max} nm (log ε): 232 (3.9), 318 (3.6); IR (NaCl) ν_{max} cm^{-1}: 3363, 2,969, 2,923, 2,852, 1,650, 1,537, 1,468, 1,384, 1,359, 1,338, 1,217, 1,116, 1,088, 619, and 577; ^{1}H and ^{13}C NMR data (CD_3OD) (see Table 1); HRESIMS *m/z* 233.1262 $[M+Na]^+$ (calcd for $C_{11}H_{18}N_2O_2Na$, 233.1260).

2.6.4 Theoretical computation method for structural identification

In general, conformational analyses were carried out via random searching in the Sybyl-X 2.0 (2013) using the MMFF94S force field with an energy cutoff of 5.0 kcal/mol. The results showed 15 lowest energy conformers. Subsequently, geometry optimizations and frequency analyses were implemented at the B3LYP-D3 (BJ)/6-31G* level in CPCM acetonitrile using ORCA5.0.1 (Neese, 2012, 2017). All conformers used for property calculations in this study were characterized to be stable point on potential energy surface (PES) with no imaginary frequencies. The excitation energies, oscillator strengths, and rotational strengths (velocity) of the first 60 excited states were calculated using the TD-DFT methodology at the PBE0/def2-TZVP level in CPCM acetonitrile using ORCA5.0.1. The ECD spectra were simulated by the overlapping Gaussian function (half the bandwidth at 1/e peak height, sigma = 0.30 for all) (Stephens and Harada, 2010). Gibbs free energies for conformers were determined by using thermal correction at B3LYP-D3 (BJ)/6-31G* level, and electronic energies were evaluated at the wB97M-V/def2-TZVP level in CPCM methanol using ORCA5.0.1. To get the final spectra, the simulated spectra of the conformers were averaged according to the Boltzmann distribution theory and their relative Gibbs free energy (ΔG).

2.6.5 Cytotoxicity assay

The cytotoxicity was determined by the MTS method as reported in our previous studies (Zang et al., 2020, 2022). Colorimetric assays were performed to evaluate the activity of each compound. A549 (human lung cancer cells), HepG-2 (human hepatocellular carcinoma cells), MCF-7 (human breast adenocarcinoma cells), RKO (human colon cells), and NCM460 (normal human colon mucosal epithelial cells) were purchased from the National Collection of Authenticated Cell Cultures of China. All cells were cultured in RPMI-1640 or DMEM medium (Hyclone, Logan, UT) supplemented with 10% fetal bovine serum (Hyclone) at 37°C in a humidified atmosphere with 5% CO_2. Cell viability was assessed by conducting colorimetric measurements of the amount of insoluble formazan formed in living cells based on the reduction in 3-(4,5-dimethylthiazol-2-yl)-5(3-carboxymethoxyphenyl)-2-(4-sulfopheny)-2H-tetrazolium (MTS) (Sigma, St. Louis, MO). In brief, 100 μL of suspended adherent cells were seeded into each well of a 96-well cell culture plate and allowed to adhere for 12–24 h before the addition of a drug. In addition, suspended cells were seeded just before the addition of a drug, with an initial density of 1×10^5 cells/ml in 100 μL of medium. Each cell line was exposed to each test compound at various concentrations in triplicate for 48 h. After the incubation, MTS solution (20 μL) was added to each well, and the incubation was continued for 2–4 h at 37°C. The optical density of the lysate was measured at 492 nm in a 96-well microtiter plate reader (MULTISKAN FC). The IC_{50} value of each compound was calculated by Reed and Muench's method.

2.6.6 Antimicrobial assay

The antimicrobial effect was determined following the method as reported in the previous study (Zang et al., 2016). Reference strains of *Staphylococcus aureus* (ATCC43300), *Escherichia coli* (ATCC11229), *Pseudomonas aeruginosa* (ATCC9027), and *Enterococcus faecalis* (ATCC29212) were cultivated for 24 h in Luria–Bertani medium (LB) at 37°C. Precultures of the tested microorganisms were made by inoculating 50 mL of LB medium and incubated for 24 h at 37°C. A culture suspension was made by 1/1000 dilution (OD600 0.01) from preculture and seeded in 96-well microtitration plates. In total, 1 μL of two-fold serial dilutions of each compound (40 mM) was prepared in 200 μL of medium. After 24 h, the optical density of the bacterial suspension of each well was measured at 595 nm using a multiplate reader (MULTISKAN FC). The MIC, which is the minimal concentration of a compound resulting in a 90% decrease in the number of microbial cultures compared with a control (DMSO only), was determined by curve fitting for bacteria. Vancomycin (Sigma–aldrich, Merck) was used as positive control.

2.6.7 Anti-inflammatory assay

RAW 264.7 cells were obtained from National Collection of Authenticated Cell Cultures (Shanghai, China) and maintained in DMEM containing 10% fetal bovine serum (FBS) (Gibco BRL Co, Grand Island, NY, United States) at 37°C in humidified incubator containing 5% CO_2. All tested compounds were dissolved in DMSO (the final concentration of DMSO was less than 0.25% in assay). Cell viability was evaluated by the CCK-8 method after 24 h of incubation with test compounds of 40 μM. RAW 264.7 cells were seeded into 96-well plates (2.5×10^5 cells/well) for 24 h and then pretreated with test compounds. After being incubated for 3 h, the cells were stimulated with 100 ng/mL LPS (final concentration) for another 24 h. Celastrol (Sigma–aldrich, Merck) was used as the positive control. NO content in the supernatant was measured using Griess reagent. The absorbance at 540 nm was measured on a microplate reader (MULTISKAN FC).

3 Results and discussion

3.1 Phylogenetic analysis based on 16S rRNA gene sequence

The nearly complete 16S rRNA gene sequence of the strain s54d21^T was obtained with the length of 1,536 bp (GenBank accession number: OR885464). Pairwise comparison of 16S rRNA gene revealed that the strain s54d21^T shared the highest similarity to *H. minutum* DSM 14724^T (98.2%), followed by *H. versicolor* H56D21^T (97.8%) and *H. gracilis* DSM 14753^T (97.7%). Phylogenetic analysis based on 16S rRNA gene sequence showed that the strain s54d21^T located in the genus *Hyalangium* and formed an individual branch containing all type strains of *Hyalangium* genus (Figure 1).

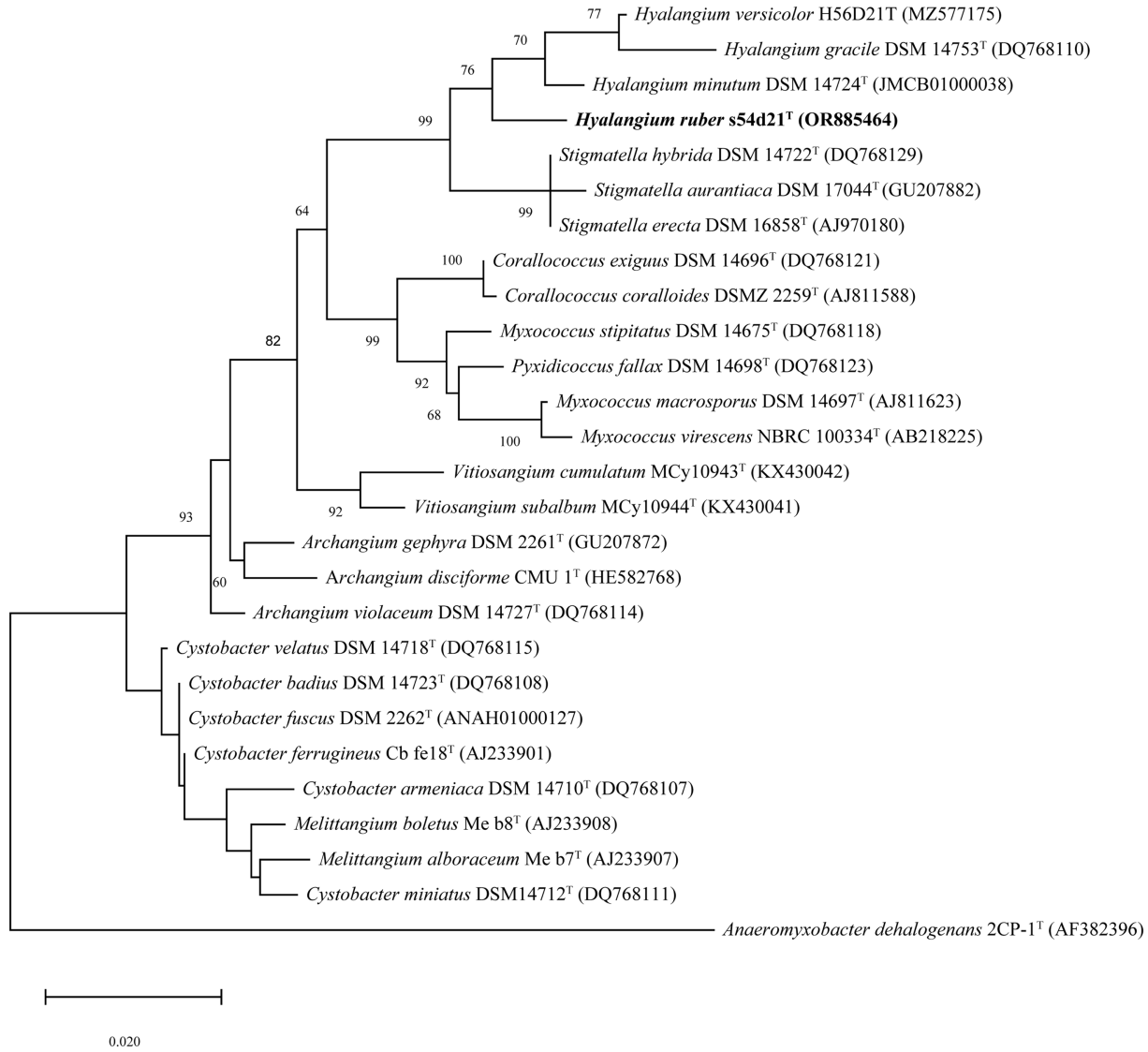

FIGURE 1
Maximum likelihood phylogenetic tree based on 16S rRNA gene sequences showing the relationships between strain s54d21^T and the closely related taxa. Bootstrap values were expressed as percentages of 1,000 replicates. More than 50% bootstrap values are shown. Bar, 0.02 the number of substitutions per site. The outgroup of the tree is *Anaeromyxobacter dehalogenans* 2CP-1^T.

3.2 Genome sequencing and phylogenomic analysis

The draft genome of the strain s54d21^T was 10.77 Mb in size with 43 contigs, the N50 of 586,569 bp, and the DNA G + C content of 68.5 mol% (Supplementary Table S1). The genome contained 8,621 protein-coding sequences, 70 tRNAs, and 3 rRNAs genes. The UBCG-based phylogenomic tree showed that the strain s54d21^T was closely related to all type species of *Hyalangium* (Figure 2), which was consistent with the tree topology based on the 16S rRNA genes. The calculated genome similarity values between the strain s54d21^T and other type species in the genus *Hyalangium* were in the ranges of 81.3–82.7% for ANI and 24.4–25.7% for dDDH (Supplementary Table S2), which were all below the threshold values for species delineation (95.0–96.0% for ANI and 70.0% for dDDH) (Goris et al., 2007; Richter and Rosselló-Móra, 2009). These results suggested that the strain s54d21^T should be considered as a novel species in the genus *Hyalangium*, for which the name *Hyalangium ruber* sp. nov was proposed.

The RAST annotation result showed that almost 81.0% of coding sequences in the strain s54d21^T were not assigned to subsystems. The general feature of subsystem category distribution in the strain s54d21^T genome was similar to those in its closest phylogenetic neighbor. No genes involved in motility and chemotaxis were found to be encoded by the strain s54d21^T genome and in the genomes of closely related type strains. However, genes associated with iron acquisition and metabolism were found in the strain s54d21^T more than these in the three closely related strain genomes (Supplementary Figure S1). Based on CAZy database annotation, the genome of the strain s54d21^T contained 23 carbohydrate-binding modules, 33 carbohydrate esterases, 78 glycoside hydrolases, 61 glycosyl transferases, 6 polysaccharide lyases, and 15 auxiliary activities (Supplementary Figure S1). There were most types of carbohydrate enzymes involved in glycoside hydrolases, which can

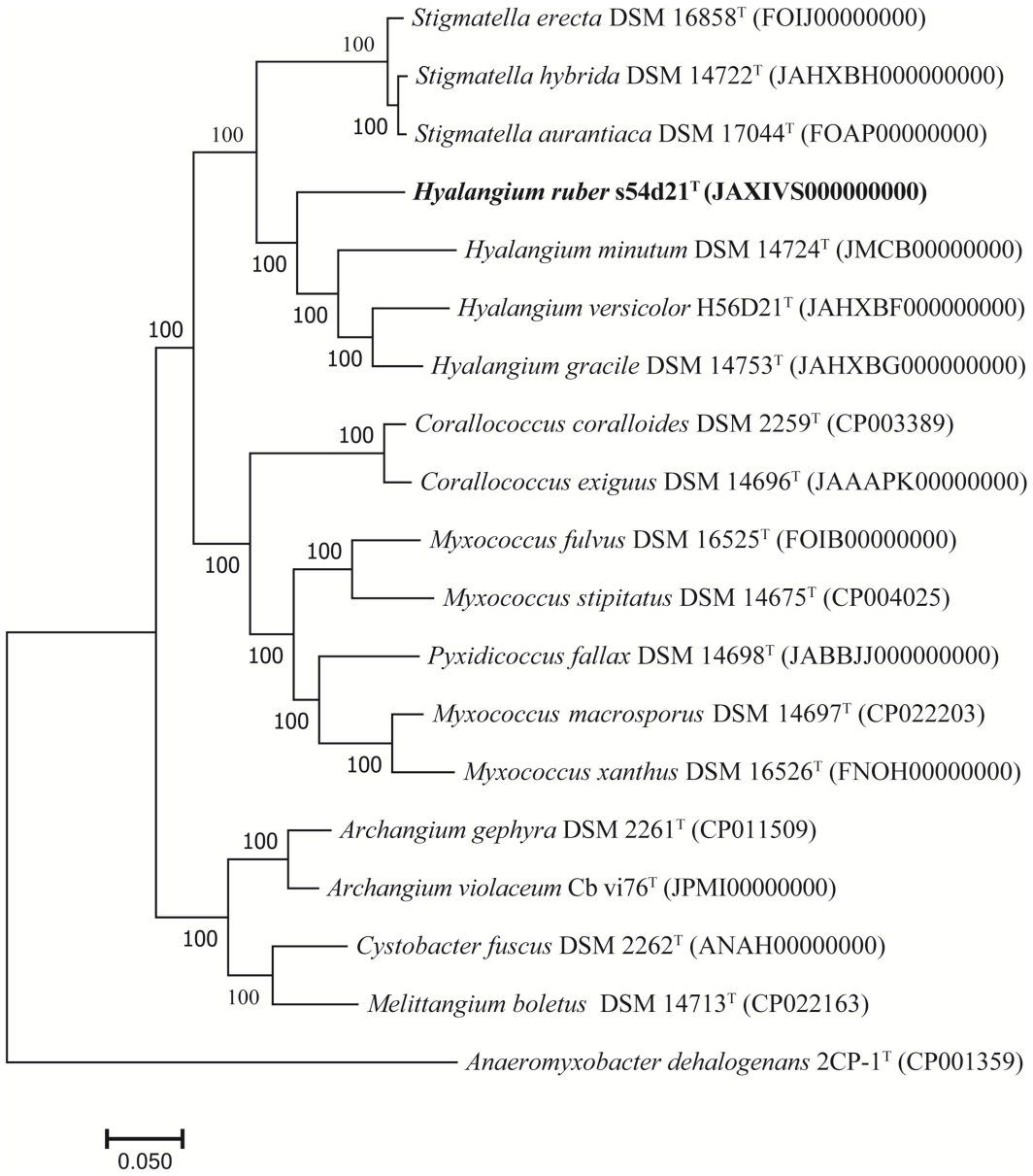

FIGURE 2
Phylogenomic tree reconstructed by the UBCG platform based on 92 core genes showing the relationships between strain s54d21^T and some closely related type strains. Bar, 0.05 represents the number of substitutions per site.

hydrolyze polysaccharides such as starch and peptidoglycan. A total of 32 biosynthetic gene clusters (BGCs) were identified in the strain s54d21^T genome, including three NRPS-like fragments, a PKS-type cluster, four hybrid PKS/NRPS-type cluster, nine RiPP-type clusters, five terpenes-type clusters, two lanthipeptides-type clusters, and others (Supplementary Figure S1).

3.3 Morphological, physiological, and biochemical characteristics

The swarms of the strain s54d21^T exhibited circular, red, thin film with wavy flared edges on VY/2 agar (Figure 3A). Vegetative cells were slender rods with tapered ends measuring 0.5–0.7 × 3–7 μm (Figure 3B). Sporangioles were spherical, some of which were empty and transparent (Figure 3C). Myxospores were irregular spherical (Figure 3C). Strain s54d21^T showed positive to oxidase, catalase, starch, aesculin hydrolysis, gelatin hydrolysis, alkaline phosphatase, esterase (C4), esterase lipase (C8), lipase (C14), leucine arylamidase, valine arylamidase, acid phosphatase, naphtol-AS-Bl-phosphoamidase, *β*-glucosidase, and *N*-acetyl-*β*-glucosaminidase. The differentiating characteristics with other type strains in the genus *Hyalangium* are shown in Table 1. Strain s54d21^T could be distinguished from its closely related type strains in temperature for growth, *β*-galactosidase, cystine arylamidase, trypsin, *α*-chymotrypsin, *β*-glucosidase and several antibiotic sensitivities.

The major respiratory quinone detected in the strain s54d21^T was menaquinone-8 (MK-8). The major fatty acids (>5% of the total

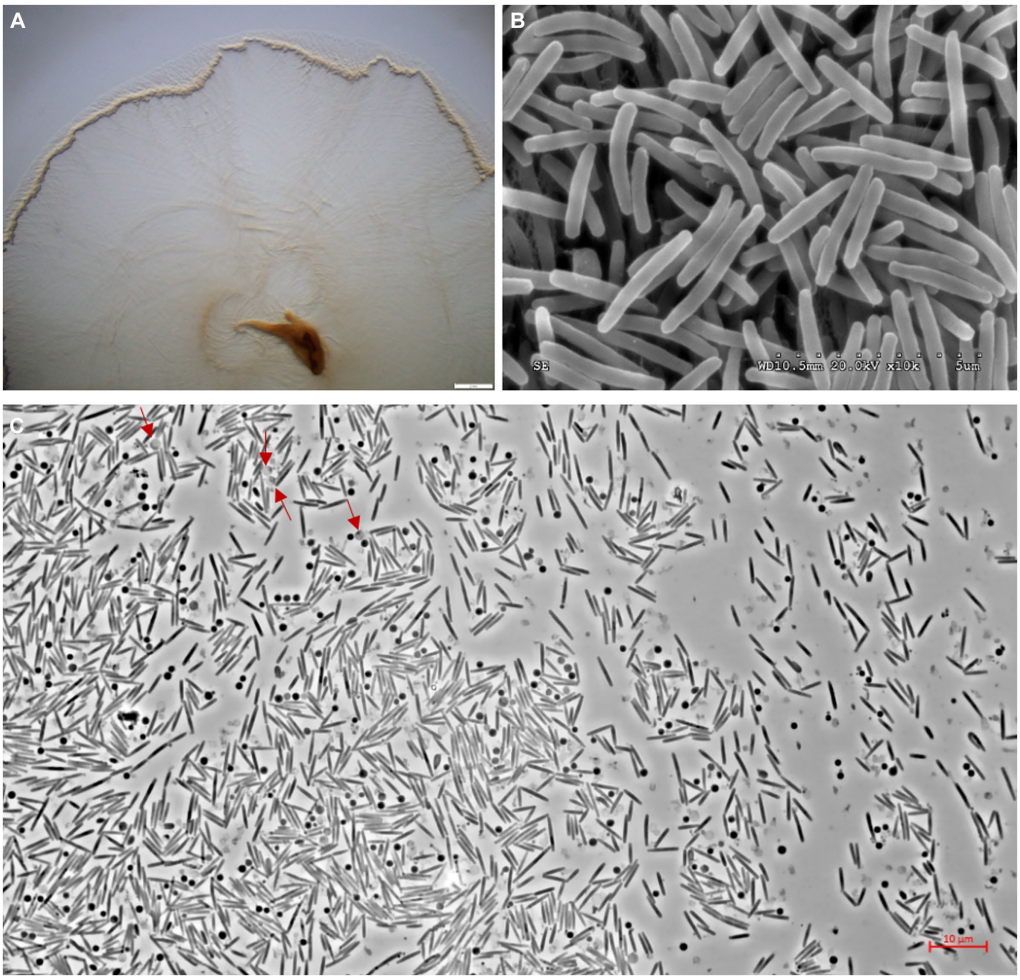

FIGURE 3
Photographs showing colonies and cell morphology of the strain s54d21^T. **(A)** The stereoscopic photographs of swarming colonies on VY/2 agar after 5 days of incubation at 30°C (bar, 2 mm). **(B)** The transmission electron microscopic photographs of vegetative cells (bar, 5 μm). **(C)** The phase contract microscopic photograph of rod-shaped vegetative cells, spherical sporangioles (red arrow), and spherical myxospores (bar, 10 μm).

amounts) contained iso-$C_{17:0}$ 2-OH (27.8%), iso-$C_{15:0}$ (17.4%), iso-$C_{15:0}$ DMA (8.2%), iso-$C_{16:0}$ (6.8%), $C_{16:1}\omega5c$ (6.6%), and iso-$C_{15:0}$ 3-OH (6.2%) (Supplementary Table S3). The high levels of iso-$C_{15:0,}$ $C_{16:1}\omega5c$, and iso-$C_{15:0}$ DMA were found in all type strains in the genus *Hyalangium* and seemed to be the major fatty acid in this genus. Moreover, the remarkably high amount of iso-$C_{17:0}$ 2-OH and the low proportions of $C_{16:1}\omega5c$, $C_{16:0,}$ $C_{16:1}\omega7c$, and iso-$C_{17:0}$ in the strain s54d21^T could distinguish the strain s54d21^T form its neighbor-type species in the genus *Hyalangium*.

3.4 Description of *Hyalangium ruber* sp. nov

Hyalangium ruber (ru'ber. L. masc. Adj. ruber red, referring to the color of the colonies).

Cells are gram-negative. Growth occurred at 20–40°C, pH 4.0–10.0 with the NaCl tolerance of 0–0.5% (m/v). Resistant to ampicillin, gentamicin, kanamycin, polymyxin B, and bacitracin B, sensitive to erythromycin, nalidixic acid, rifampin, spectinomycin, streptomycin, tetracycline, apramycin, chloramphenicol, neomycin, trimethoprim, and oxytetracycline. Major cellular fatty acids are iso-$C_{17:0}$ 2-OH, iso-$C_{15:0}$, iso-$C_{15:0}$ DMA, iso-$C_{16:0}$, $C_{16:1}\omega5c$, and iso-$C_{15:0}$ 3-OH. Predominant respiratory quinone is MK-8. The genomic DNA G + C content of the type strain is 68.5 mol%.

The type strain s54d21^T (= GDMCC 1.1945^T = JCM 39263^T) was isolated from the sediment sampled from Xinghu National Wetland Park located in Guangdong Province, China. The GenBank accession numbers for the 16S rRNA gene and whole genome sequences of the type strain are OR885464 and JAXIVS000000000, respectively.

3.5 Structure elucidation of new compounds

The gene sequence analyses of the strain s54d21^T supposed the production of polyketides and peptides in terms of the presence of PKS and NRPS BGCs. Therefore, the chemical investigation of the culture broth of the strain was performed as described. Here, the

10.3389/fmicb.2024.1369499

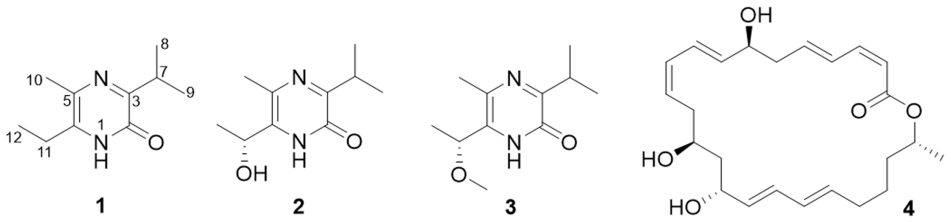

FIGURE 4
Chemical structures of isolated compounds (1–4).

TABLE 2 ^{1}H (150 MHz) and ^{13}C (600 MHz) NMR data of compounds 1–3 recorded in CD_3OD (δ in ppm; J in Hz).

Pos.	1		2		3	
	δ_H	δ_C	δ_H	δ_C	δ_H	δ_C
2	–	157.3	–	157.5	–	157.4
3	–	160.9	–	161.0	–	161.5
5	–	131.3	–	132.8	–	132.8
6	–	135.8	–	135.3	–	134.2
7	3.34 m	30.9	3.33 m	31.5	3.33 m	30.9
8	1.20 d 6.8	20.5	1.22 d 6.8	20.5	1.20 d 6.8	20.4
9	1.20 d 6.8	20.5	1.22 d 6.8	20.5	1.20 d 6.8	20.5
10	2.22 s	15.2	2.29 s	14.8	2.29 s	14.8
11	2.57 q 7.5	26.1	4.89 q 6.5	66.6	4.52 q 6.5	76.6
12	1.17 t 7.5	13.7	1.44 d 6.5	22.5	1.47 t 6.5	19.5
11-OCH_3	–	–	–	–	3.22 s	55.9

structure including absolute configurations of three new compounds (**1**–**3**) was elucidated (Figure 4).

Compound **1** was obtained as an amorphous solid, and the molecular formula of $C_{10}H_{16}N_2O$ was determined by the positive mode HRESIMS with a $[M+Na]^+$ ion peak at *m/z* 203.1150, indicating four degrees of unsaturation. The 1D NMR data (Table 2) and HSQC spectrum presented signals of ten carbons, including four methyls (a singlet at δ_H 2.22, two doublets at δ_H 1.20, and a triplet at δ_H 1.17), a methylene at δ_H 2.57 (q, J = 7.5 Hz) and δ_C 26.1, a methine at δ_H 3.34 (m) and δ_C 30.9, and four unprotonated carbons. ^{1}H–^{1}H COSY correlations demonstrated the existence of two spin systems of an ethyl group and an isopropyl moiety (Figure 5). Combination analyses of the chemical formula and HMBC correlations (Figure 5) revealed that four unprotonated carbons (C-2, C-3, C-5, and C-6) and two nitrogens were assigned to the 2(1*H*)-pyrazinone ring. The comparison of those spectroscopic data suggested that structure of **1** was such close to those knowns featuring a 3,5,6-substitued 2(1*H*)-pyrazinone core structure (Motohashi et al., 2011; Ma et al., 2020). The differences between **1** and known compounds were three substituent groups located at C-3, C-6, and C-5, including an abovementioned ethyl group, an isopropyl group, and a methyl (Me-10), respectively. Subsequent analyses of HMBC spectrum supported those assignments for structure **1**, where key HMBC correlations from H-7/Me-8 to C-2, H-7/Me-8/Me-10 to C-3, Me-10/H-11 to C-5, and Me-10/Me-12 to C-6 were observed (Figure 5). Hence, compound **1** was unambiguously determined as a 3,5,6-trisubstituted 2(1*H*)-pyrazinone and designated as hyalanone A.

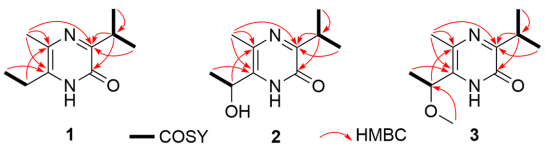

FIGURE 5
Key ^{1}H-^{1}H COSY and HMBC correlations of compounds (1–3).

Hyalanone B (**2**) was also isolated as an amorphous solid. The molecular formula was demonstrated to be $C_{10}H_{16}N_2O_2$ via a positive HRESIMS ion peak at *m/z* 219.1105 $[M+Na]^+$. The ^{1}H and ^{13}C NMR data of **2** was such close to those of **1,** except for an oxygenated methine at δ_H 4.89 (q, J = 6.5 Hz, H-11) and δ_C 66.6 (C-11) (Table 2), suggesting a similar 2(1*H*)-pyrazinone skeleton. A hydroxyethyl group replaced the ethyl at C-6 of **1**, which was further confirmed by H–^{1}H COSY cross-peaks and key HMBC correlations from Me-12 to C-6/C-11 and H-11 to C-5 (Figure 5). There is not enough compound **2** for Mosher's method to determine the absolute configuration of the chiral center C-11. Therefore, it was inferred from theoretical ECD calculation by using TDDFT methodology at PBE0/def2-TZVP level in CPCM acetonitrile using ORCA5.0.1 (Neese, 2012, 2017). As shown in Figure 6, the experimental ECD curve of **2** was well matched with the calculated one that concluded the absolute configuration of C-11 to be *R*.

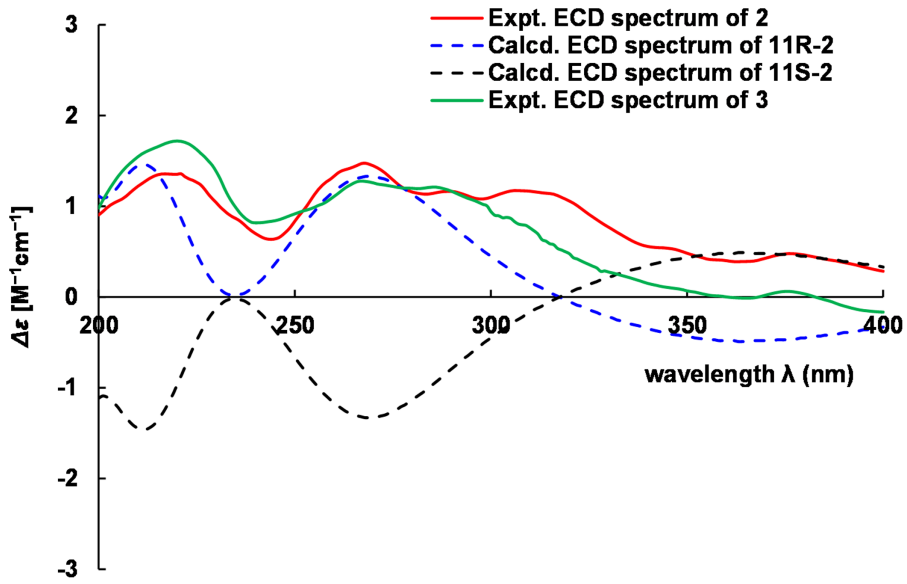

FIGURE 6
Comparison of experimental and calculated ECD of 2 and 3.

The molecular formula $C_{11}H_{18}N_2O_2$ of **3** was deduced from a HRESIMS spectrum. Analyses of 1D NMR data (Table 2) and HMBC correlations (Figure 5) of **3** exhibited a highly similarity with those of **2**, where the unique difference between them was an extra methoxyl at δ_H 3.22 and δ_C 55.9 (11-OMe) in **3**. Moreover, key HMBC correlation from 11-OMe to C-11 indicated the location of a methoxyl at C-11 of **3** rather than a hydroxyl in **2** (Figure 5). By comparing of experimental ECD curves of **2** and **3** (Figure 6), the absolute configuration of C-11 was still approved to be *R*. Therefore, compound **3** was established and given the name hyalanone C.

2(1*H*)-Pyrazinones are a type of natural products originally biosynthesized by NRPS gene cluster with two amino acids (Wyatt et al., 2010; Zimmermann and Fischbach, 2010; Wyatt et al., 2012). Based on biosynthetic pathways of pyrazinone analogs, three new compounds are proposed to be derived from the valine and alanine or threonine building blocks. Analyses of the genome sequence of strain s54d21^T by antiSMASH showed three NRPS-like and three PKS-NRPS BGCs. Among them, the NRPS (Region 1.3) and PKS-NRPS (Region 5.2) gene clusters containing a *Val* module are potent BGCs related to the biosynthesis of those new pyrazinones (Supplementary Figure S2).

3.6 Biological assays

The previous report of pyrazinone derivatives described their remarkable cytotoxicity against human cancer cell lines and antimicrobial activity (Jansen et al., 2014). Therefore, cytotoxic activities against human cancer cell lines and antimicrobial and anti-inflammatory effects of all isolates were tested in this study. The cytotoxicity evaluation of compounds **1**–**4** was performed using the MTS method, where taxol was used as the positive control. Among them, compound **4** displayed moderate cytotoxicity against A549, RKO, and NCM460 with IC_{50} values at 32.14 ± 2.25, 27.31 ± 8.96, and 31.33 ± 1.71 μM (positive control with IC_{50} values <0.008 μM), respectively. In addition, their inhibition of NO production in LPS-induced RAW 264.7 cells was tested. All compounds showed weak inhibitory effect (< 10.0%) of NO production at the concentration of 40 μM. The evaluation of their antimicrobial activities against *S. aureus*, *E. coli*, *P. aeruginosa*, and *E. faecalis* did not show obvious inhibition at the concentration of 200 μM.

Pyrazinones are previously reported to regulate phenotypic changes in the pathogen (e.g., quorum sensing) or act directly on the host (e.g., virulence factors), such as tyrvalin and phevalin are used as regulators of virulence factor gene expression (Wyatt et al., 2010; Secor et al., 2012). Thus, although three new pyrazinones do not exhibit obvious effects in the evaluation of cytotoxic, antimicrobial, and anti-inflammatory activities, the discovery of new molecules provides potential for further research studies of relationships between the small molecule and microorganisms as well as the role of myxobacteria in nature.

4 Conclusion

In this study, a novel myxobacterium s54d21^T belonging to a rare *Hyalangium* genus, designated *Hyalangium ruber* sp. nov, was purified from a wetland sediment using the *E. coli* baiting method. Uncovered by analysis of the gene sequence, the further chemical investigation of bioactive secondary metabolites from culture broth of *H. ruber* led to the production of three unprecedented 3,5,6-trisubstituted 2(1*H*)-pyrazinone derivatives, namely, hyalanones A–C (**1**–**3**), together with a known macrolactin A (**4**). In biological assay, compound **4** exhibited modest cytotoxic activities against human cell lines A549, RKO, and NCM460 with IC_{50} values between 27.31 and 32.14 μM. Although three new compounds have not exhibited significant activities in biological assays, their structures enrich the chemical diversity of 2(1*H*)-pyrazinones from myxobacteria.

Data availability statement

The datasets presented in this study can be found in online repositories. The names of the repository/repositories and accession number(s) can be found at: NCBI, OR885464 and JAXIVS000000000.

Author contributions

YZa: Supervision, Writing – review & editing, Writing – original draft, Project administration, Funding acquisition, Formal analysis, Data curation, Conceptualization. XZ: Writing – original draft, Methodology, Funding acquisition, Formal analysis, Data curation, Conceptualization. ZW: Writing – original draft, Methodology, Investigation, Data curation. QT: Writing – review & editing, Methodology. YZh: Writing – review & editing, Conceptualization. QY: Writing – review & editing, Supervision, Conceptualization. HZ: Writing – review & editing, Supervision, Funding acquisition, Conceptualization.

Funding

The author(s) declare that financial support was received for the research, authorship, and/or publication of this article. This study was funded by National Natural Science Foundation of China (No. 32000007), Guangdong special support program (No. 2021JC06N628), The Guangdong Strategic Special Fund for Rural Revitalization (2022-440000-43010104-9463), and GDAS's project for science and technology development (No. 2021GDASYL-20210102009).

Acknowledgments

The authors thank Prof. Yonghui Zhang, Prof. Hucheng Zhu, and the Analytical and Testing Center at Huazhong University of Science and Technology for assistance in testing of ECD, UV, and IR spectra.

Conflict of interest

The authors declare that the research was conducted in the absence of any commercial or financial relationships that could be construed as a potential conflict of interest.

Publisher's note

All claims expressed in this article are solely those of the authors and do not necessarily represent those of their affiliated organizations, or those of the publisher, the editors and the reviewers. Any product that may be evaluated in this article, or claim that may be made by its manufacturer, is not guaranteed or endorsed by the publisher.

Supplementary material

The Supplementary material for this article can be found online at: https://www.frontiersin.org/articles/10.3389/fmicb.2024.1369499/full#supplementary-material

References

Aziz, R. K., Bartels, D., Best, A. A., DeJongh, M., Disz, T., Edwards, R. A., et al. (2008). The RAST server: rapid annotations using subsystems technology. *BMC Genomics* 9:75. doi: 10.1186/1471-2164-9-75

Bader, C. D., Panter, F., and Müller, R. (2020). In depth natural product discovery - Myxobacterial strains that provided multiple secondary metabolites. *Biotechnol. Adv.* 39:107480. doi: 10.1016/j.biotechadv.2019.107480

Bankevich, A., Nurk, S., Antipov, D., Gurevich, A. A., Dvorkin, M., Kulikov, A. S., et al. (2012). SPAdes: a new genome assembly algorithm and its applications to single-cell sequencing. *J. Comput. Biol.* 19, 455–477. doi: 10.1089/cmb.2012.0021

Bhat, M. A., Mishra, A. K., Bhat, M. A., Banday, M. I., Bashir, O., Rather, I. A., et al. (2021). Myxobacteria as a source of new bioactive compounds: a perspective study. *Pharmaceutics* 13:1265. doi: 10.3390/pharmaceutics13081265

Blin, K., Shaw, S., Kloosterman, A. M., Charlop-Powers, Z., Weezel, G. P. V., Medema, M. H., et al. (2021). Anti SMASH 6.0: improving cluster detection and comparison capabilities. *Nucleic Acids Res.* 49, W29–W35. doi: 10.1093/nar/gkab335

Collins, M. D., Pirouz, T., Goodfellow, M., and Minnikin, D. E. (1977). Distribution of menaquinones in actinomycetes and corynebacteria. *J. Gen. Microbiol.* 100, 221–230. doi: 10.1099/00221287-100-2-221

Dehhaghi, M., Mohammadipanah, F., and Guillemin, G. J. (2018). Myxobacterial natural products: an under-valued source of products for drug discovery for neurological disorders. *Neurotoxicology* 66, 195–203. doi: 10.1016/j.neuro.2018.02.017

Felsenstein, J. (1981). Evolutionary trees from DNA sequences: a maximum likelihood approach. *J. Mol. Evol.* 17, 368–376. doi: 10.1007/BF01734359

Gemperlein, K., Rachid, S., Garcia, R. O., Wenzel, S. C., and Müller, R. (2014). Polyunsaturated fatty acid biosynthesis in myxobacteria: different PUFA synthases and their product diversity. *Chem. Sci.* 5, 1733–1741. doi: 10.1039/c3sc53163e

Goris, J., Konstantinidis, K. T., Klappenbach, J. A., Coenye, T., Vandamme, P., and Tiedje, J. M. (2007). DNA-DNA hybridization values and their relationship to whole-genome sequence similarities. *Int. J. Syst. Evol. Microbiol.* 57, 81–91. doi: 10.1099/ijs.0.64483-0

Gustafson, K., Roman, M., and William, F. (1989). The macrolactins, a novel class of antiviral and cytotoxic macrolides from a deep-sea marine bacterium. *J. Am. Chem. Soc.* 111, 7519–7524. doi: 10.1021/ja00201a036

He, S., Wang, H. Q., Yan, X. J., Zhu, P., Chen, J. J., and Yang, R. (2013). Preparative isolation and purification of macrolactin antibiotics from marine bacterium *Bacillus amyloliquefaciens* using high-speed counter-current chromatography in stepwise elution mode. *J. Chromatogr. A* 1272, 15–19. doi: 10.1016/j.chroma.2012.11.029

Herrmann, J., Fayad, A. A., and Müller, R. (2017). Natural products from myxobacteria: novel metabolites and bioactivities. *Nat. Prod. Rep.* 34, 135–160. doi: 10.1039/c6np00106h

Hoang, D. T., Chernomor, O., von Haeseler, A., Minh, B. Q., and Vinh, L. S. (2018). UFBoot2: improving the ultrafast bootstrap approximation. *Mol. Biol. Evol.* 35, 518–522. doi: 10.1093/molbev/msx281

Jansen, R., Sood, S., Mohr, K. I., Kunze, B., Irschik, H., Stadler, M., et al. (2014). Nannozinones and sorazinones, unprecedented pyrazinones from myxobacteria. *J. Nat. Prod.* 77, 2545–2552. doi: 10.1021/np500632c

Kaiser, D. (2003). Coupling cell movement to multicellular development in myxobacteria. *Nat. Rev. Microbiol.* 1, 45–54. doi: 10.1038/nrmicro733

Kimura, M. (1980). A simple method for estimating evolutionary rates of base substitutions through comparative studies of nucleotide sequences. *J. Mol. Evol.* 16, 111–120. doi: 10.1007/BF01731581

Kumar, S., Stecher, G., Li, M., Knyaz, C., and Tamura, K. (2018). MEGA X: molecular evolutionary genetics analysis across computing platforms. *Mol. Biol. Evol.* 35, 1547–1549. doi: 10.1093/molbev/msy096

Ma, X. Y., Zhang, Z. X., Wang, L., Hu, X. J., Liu, X. Y., and Huang, S. X. (2020). Two new 2(1H)-Pyrazinone derivatives from the plant endophyte streptomyces sp. KIB-H1992. Rec. Nat. *Prod.* 14, 196–200. doi: 10.25135/rnp.154.1907.1355

McCurdy, H. D. (1969). Studies on the taxonomy of the Myxobacterales. I. Record of Canadian isolates and survey of method. *Can. J. Microbiol.* 15, 1453–1461. doi: 10.1139/m69-259

Meier-Kolthoff, J. P., Auch, A. F., Klenk, H.-P., and Göker, M. (2013). Genome sequence-based species delimitation with confidence intervals and improved distance functions. *BMC Bioinformatics* 14:60. doi: 10.1186/1471-2105-14-60

Motohashi, K., Inaba, K., Fuse, S., Doi, T., Izumikawa, M., Khan, S. T., et al. (2011). JBIR-56 and JBIR-57, 2(1H)-pyrazinones from a marine sponge-derived streptomyces sp. SpD081030SC-03. *J. Nat. Prod.* 74, 1630–1635. doi: 10.1021/np200386c

Na, S. I., Kim, Y. O., Yoon, S. H., Ha, S. M., Baek, I., and Chun, J. (2018). UBCG: up-to-date bacterial core gene set and pipeline for phylogenomic tree reconstruction. *J. Microbiol.* 56, 280–285. doi: 10.1007/s12275-018-8014-6

Nadmid, S., Plaza, A., Lauro, G., Garcia, R., Bifulco, G., and Müller, R. (2014). Hyalachelins A-C, unusual siderophores isolated from the terrestrial myxobacterium *Hyalangium minutum*. *Org. Lett.* 16, 4130–4133. doi: 10.1021/ol501826a

Neese, F. (2012). The ORCA program system. *Wiley Interdiscip. Rev. Comput. Mol. Sci.* 2, 73–78. doi: 10.1002/wcms.81

Neese, F. (2017). Software update: the ORCA program system, version 4.0. *Wiley Interdiscip. Rev. Comput. Mol. Sci.* 8:e1327. doi: 10.1002/wcms.1327

Okanya, P. W., Mohr, K. I., Gerth, K., Kessler, W., Jansen, R., Stadler, M., et al. (2014). Hyafurones, hyapyrrolines, and hyapyrones: polyketides from *Hyalangium minutum*. *J. Nat. Prod.* 77, 1420–1429. doi: 10.1021/np500145f

Okanya, P. W., Mohr, K. I., Gerth, K., Steinmetz, H., Huch, V., Jansen, R., et al. (2012). Hyaladione, an S-methyl cyclohexadiene-dione from *Hyalangium minutum*. *J. Nat. Prod.* 75, 768–770. doi: 10.1021/np200776v

Parks, D. H., Imelfort, M., Skennerton, C. T., Hugenholtz, P., and Tyson, G. W. (2015). Check M: assessing the quality of microbial genomes recovered from isolates, single cells, and metagenomes. *Genome Res.* 25, 1043–1055. doi: 10.1101/gr.186072.114

Reichenbach, H. (2005). "Genus III. Hyalangium gen.nov" in *Bergey's manual of systematic bacteriology (the proteobacteria) part C (the alpha-, Beta-, Delta-, and Epsilonproteobacteria)*. eds. N. R. Krieg, D. J. Brenner, J. T. Staley and G. M. Garrity (New York: Springer), 1099–1101.

Richter, M., and Rosselló-Móra, R. (2009). Shifting the genomic gold standard for the prokaryotic species definition. *Proc. Natl. Acad. Sci. USA* 106, 19126–19131. doi: 10.1073/pnas.0906412106

Saggu, S. K., Nath, A., and Kumar, S. (2023). Myxobacteria: biology and bioactive secondary metabolites. *Res. Microbiol.* 174:104079. doi: 10.1016/j.resmic.2023.104079

Schäberle, T. F., Lohr, F., Schmitz, A., and König, G. M. (2014). Antibiotics from myxobacteria. *Nat. Prod. Rep.* 31, 953–972. doi: 10.1039/c4np00011k

Secor, P. R., Jennings, L. K., James, G. A., Kirker, K. R., Pulcini, E. D., McInnerney, K., et al. (2012). Phevalin (aureusimine B) production by *Staphylococcus aureus* biofilm and impacts on human keratinocyte gene expression. *PLoS One* 7:e40973. doi: 10.1371/journal.pone.0040973

Seemann, T. (2014). Prokka: rapid prokaryotic genome annotation. *Bioinformatics* 30, 2068–2069. doi: 10.1093/bioinformatics/btu153

Shrivastava, A., and Sharma, R. K. (2021). Myxobacteria and their products: current trends and future perspectives in industrial applications. *Folia Microbiol. (Praha)* 66, 483–507. doi: 10.1007/s12223-021-00875-z

Stephens, P. J., and Harada, N. (2010). ECD cotton effect approximated by the gaussian curve and other methods. *Chirality* 22, 229–233. doi: 10.1002/chir.20733

Surup, F., Chauhan, D., Niggemann, J., Bartok, E., Herrmann, J., Keck, M., et al. (2018). Activation of the NLRP3 inflammasome by Hyaboron, a new asymmetric boron-containing macrodiolide from the myxobacterium *Hyalangium minutum*. *ACS Chem. Biol.* 13, 2981–2988. doi: 10.1021/acschembio.8b00659

Sybyl-X 2.0 (2013). *"Sybyl software" version X 2.0 ed.* St. Louis, MO, USA: Tripos Associates Inc.

Weisburg, W. G., Barns, S. M., Pelletier, D. A., and Lane, D. J. (1991). 16S ribosomal DNA amplification for phylogenetic study. *J. Bacteriol.* 173, 697–703. doi: 10.1128/jb.173.2.697-703

Wenzel, S. C., and Müller, R. (2009). Myxobacteria--'microbial factories' for the production of bioactive secondary metabolites. *Mol. BioSyst.* 5, 567–574. doi: 10.1039/b901287g

Wyatt, M. A., Mok, M. C., Junop, M., and Magarvey, N. A. (2012). Heterologous expression and structural characterisation of a pyrazinone natural product assembly line. *Chembiochem* 13, 2408–2415. doi: 10.1002/cbic.201200340

Wyatt, M. A., Wang, W., Roux, C. M., Beasley, F. C., Heinrichs, D. E., Dunman, P. M., et al. (2010). *Staphylococcus aureus* nonribosomal peptide secondary metabolites regulate virulence. *Science* 329, 294–296. doi: 10.1126/science.1188888

Yoon, S. H., Ha, S. M., Kwon, S., Lim, J., Kim, Y., Seo, H., et al. (2017a). Introducing EzBioCloud: a taxonomically united database of 16S rRNA gene sequences and whole-genome assemblies. *Int. J. Syst. Evol. Microbiol.* 67, 1613–1617. doi: 10.1099/ijsem.0.001755

Yoon, S. H., Ha, S. M., Lim, J., Kwon, S., and Chun, J. (2017b). A large-scale evaluation of algorithms to calculate average nucleotide identity. *Antonie Van Leeuwenhoek* 110, 1281–1286. doi: 10.1007/s10482-017-0844-4

Zang, Y., Genta-Jouve, G., Escargueil, A. E., Larsen, A. K., Guedon, L., Nay, B., et al. (2016). Antimicrobial Oligophenalenone dimers from the soil fungus Talaromyces stipitatus. *J. Nat. Prod.* 79, 2991–2996. doi: 10.1021/acs.jnatprod.6b00458

Zang, Y., Gong, Y. H., Gong, J. J., Liu, J. J., Chen, C. M., Gu, L. H., et al. (2020). Fungal polyketides with three distinctive ring skeletons from the fungus penicillium canescens uncovered by OSMAC and molecular networking strategies. *J. Org. Chem.* 85, 4973–4980. doi: 10.1021/acs.joc.0c00147

Zang, Y., Zhou, B. P., Wei, M. S., Shi, Z. Y., Feng, G. D., Deng, M. R., et al. (2022). Aureoterrolides B–M: Eremophilane-type sesquiterpenoids isolated from aspergillus aureoterreus and their cytotoxicity. *Phytochemistry* 202:113294. doi: 10.1016/j.phytochem.2022.113294

Zhang, X. J., Feng, G. D., Liu, Y., Li, J. L., Deng, X. Q., Yao, Q., et al. (2023). Characterization of phytopathogen-preying Hyalangium versicolor sp. nov., and proposal for the reclassification of Cystobacter gracilis as Hyalangium gracile comb. *Nov. Arch. Microbiol.* 205:198. doi: 10.1007/s00203-023-03512-0

Zhang, H., Yohe, T., Huang, L., Entwistle, S., Wu, P., Yang, Z., et al. (2018). dbCAN2: a meta server for automated carbohydrate-active enzyme annotation. *Nucleic Acids Res.* 46, W95–W101. doi: 10.1093/nar/gky418

Zimmermann, M., and Fischbach, M. A. (2010). A family of pyrazinone natural products from a conserved nonribosomal peptide synthetase in *Staphylococcus aureus*. *Chem. Biol.* 17, 925–930. doi: 10.1016/j.chembiol.2010.08.006

frontiers | Frontiers in Microbiology

TYPE Original Research
PUBLISHED 08 April 2024
DOI 10.3389/fmicb.2024.1378288

OPEN ACCESS

EDITED BY
Li Zhoukun,
Nanjing Agricultural University, China

REVIEWED BY
Wenhui Wang,
Anhui Agricultural University, China
Yang Liu,
Guangdong Academy of Science, China
David Cole Stevens,
University of Mississippi, United States

*CORRESPONDENCE
Jian Han
✉ hjwjemail@163.com
Benzhong Fu
✉ benzhongf@yahoo.com

RECEIVED 29 January 2024
ACCEPTED 25 March 2024
PUBLISHED 08 April 2024

CITATION
Han J, Dong Z, Ji W, Lv W, Luo M and Fu B (2024) From predator to protector: *Myxococcus fulvus* WCH05 emerges as a potent biocontrol agent for fire blight. *Front. Microbiol.* 15:1378288. doi: 10.3389/fmicb.2024.1378288

From predator to protector: *Myxococcus fulvus* WCH05 emerges as a potent biocontrol agent for fire blight

Jian Han[1,2]*, Zhiming Dong[1,2], Wenbo Ji[1,2], Wen Lv[1,2], Ming Luo[1,2] and Benzhong Fu[1,2]*

[1]Department of Plant Pathology, College of Agronomy, Xinjiang Agriculture University/Key Laboratory of the Pest Monitoring and Safety Control of Crops and Forests of Xinjiang Uygur Autonomous Region, Urumqi, China, [2]Key Laboratory of Prevention and Control of Invasive Alien Species in Agriculture and Forestry of the North-western Desert Oasis (Co-construction by Ministry and Province), Ministry of Agriculture and Rural Affairs, Urumqi, China

Fire blight, caused by the Gram-negative bacterium *Erwinia amylovora*, poses a substantial threat to pome fruit production worldwide. Despite existing control strategies, a pressing need remains for sustainable and environmentally friendly fire blight management. Myxobacteria, renowned for their predatory behavior and potent enzymes, emerge as a groundbreaking biocontrol approach with significant potential. Here, we report the biocontrol potential of a novel *Myxococcus fulvus* WCH05, against *E. amylovora*. Using various *in vitro* and planta assays, we demonstrated the multifaceted biocontrol abilities of strain WCH05. In plate predation assays, strain WCH05 exhibited not only strong predation against *E. amylovora* but also broad-spectrum activities against other plant pathogenic bacteria. Pre-treatment with strain WCH05 significantly decreased pear blossom blight incidence in detached inflorescence assays, achieving a controlled efficacy of 76.02% that rivaled the antibiotic streptomycin (79.79%). In greenhouse trials, strain WCH05 effectively reduced the wilting rate and disease index in young pear seedlings, exhibiting both protective (73.68%) and curative (68.66%) control. Further investigation revealed that the biocontrol activity of strain WCH05 relies on both direct contact and extracellular enzyme secretion. While cell extracts lacked inhibitory activity, ammonium sulfate-precipitated secreted proteins displayed potent lytic activity against *E. amylovora*. Substrate spectrum analysis identified peptidases, lipases, and glycosidases among the secreted enzymes, suggesting their potential roles in pathogen degradation and biocontrol efficacy. This study presents the first evidence of *Myxococcus fulvus* WCH05 as a biocontrol agent against fire blight. Its potent predatory abilities and enzymatic arsenal highlight its potential for sustainable disease management in pome fruit production. Future research will focus on identifying and characterizing specific lytic enzymes and optimizing strain WCH05 application strategies for field efficacy.

KEYWORDS

***Myxococcus fulvus* WCH05, *Erwinia amylovora*, predation, biocontrol, extracellular proteins, fire blight**

1 Introduction

Fire blight, caused by the bacterium *Erwinia amylovora*, stands as one of the most devastating bacterial diseases affecting pome fruit trees within the *Rosaceae* family (Malnoy et al., 2012). This disease poses a significant threat to pear, apple, hawthorn, and quince trees, with a particularly rapid spread observed in pear fields (Momol et al., 2000). The bacterium can infect the blossoms of fruit trees and serve as a source of infection for leaves, young shoots, and immature fruit. Additionally, wounded branches represent a major way for bacterial invasion. Once the pathogen infiltrates the plant, it establishes lifelong colonization, leading to dissemination throughout the entire plant, rapid proliferation, and challenging control and eradication (Huang et al., 2022). In 2016, fire blight was first diagnosed in Yili region of Xinjiang Autonomous Region, located in northwestern China. Subsequently, in 2017, a widespread outbreak occurred in the Korla region of Xinjiang, resulting in an overall production reduction of approximately 30 to 50%. The disease later spread to most pear-producing areas in Xinjiang and some regions in Gansu Province, causing severe damage (Sun et al., 2023).

Management measures for the control of fire blight disease include quarantine, pruning, and removal of diseased plants, chemical control, biological control, and breeding of resistant varieties (Johnson and Stockwell, 1998). However, there is currently a lack of fire-blight-resistant fruit tree varieties in production. Removing diseased branches can effectively prevent the spread of fire blight, but it severely affects fruit yield. The widespread use of chemical pesticides has led to increasing problems of pathogen resistance, environmental pollution, and pesticide residues (Russo et al., 2008; Tancos et al., 2016).

Biocontrol of the fire blight is a promising alternative way in orchard disease management. Currently, there are some commercial biocontrol agents available in the market (Mikiciński et al., 2019). These beneficial strains used for disease management mainly rely on their antibiotic substances (Temple et al., 2004), nutrient and niche competition, and induced host resistance (Van Wees et al., 1997; Pieterse et al., 2014).

Fire blight is a newly emerging plant disease in China, and research on its biocontrol has not accomplished much. Though there are few reports on endophytic bacteria *Klebsiella* sp. TN50, *Paenibacillus* sp. HN89 and *Pseudomonas* sp. SN37, *Bacillus velezensis* JE4 and FX1 with the potential for the disease control (Xu et al., 2021; Huang et al., 2022; Lv et al., 2022).

Myxobacteria are a group of higher-order prokaryotes with multicellular group behavior and complex life history. They can obtain nutrients by using living microbial cells or other macromolecules as food (Munoz-Dorado et al., 2016), and can also produce a variety of enzymes and secondary metabolites with antibacterial activity (Thiery and Kaimer, 2020). In addition, myxobacteria can form stress-resistant fruiting bodies and myxospores, making them have strong environmental adaptability and colonization ability (Dawid, 2000). These characteristics of myxobacteria make them a new type of biocontrol microbial resource. The current research and application of myxobacteria in the biological control of fire blight have not been reported.

In recent years, some greenhouse and field experiments have shown that the application of myxobacteria can significantly reduce the damage of seedling wilt of forest trees (Dahm et al., 2015), cucumber wilt (Li et al., 2017), pepper anthracnose (Yun, 2014), and rice blast (Shen et al., 2023). However, there are only a few research on plant bacterial diseases. Such as on carrot soft rot caused by *Pectobacterium carotovorum* subsp. *carotovorum* (Li et al., 2018) and tomato bacterial wilt caused by *Ralstonia solanacearum* (Dong et al., 2021). However, these studies are currently limited to soil-borne bacterial diseases, and there are no reports on bacterial diseases that spread mainly on the aboveground parts of plants, such as fire blight. This study aimed to evaluate the biocontrol potential of *Myxococcus fulvus* WCH05 (Dong et al., 2024) obtained in previous research with strong predatory activity against *E. amylovora* and to preliminarily explore its biocontrol mechanism.

2 Materials and methods

2.1 Bacteria and culture conditions

The phytopathogen bacterial strains employed in this study included six bacterial pathogens. *Dickeya fangzhongdai* (Df; GMCC 1.15464) and *Pectobacterium carotovorum* subsp. *carotovorum* (Pcc; Eu 678364) were kindly provided by Associate Professor Li Zhoukun from Nanjing Agricultural University. *Acidovorax citrulli* (Ac; FC440) (Chen et al., 2023) was generously donated by Professor Liu Jun from Xinjiang Agricultural University. *P. syringae* pv. *syringae* (Pss; ATCC 19310) and *Clavibacter michiganensis* subsp. *michiganensis* (Cmm; SHBCC D10416) were gifts from Researcher Zhang Xianglin at the Urumqi Customs. *Erwinia amylovora* (Ea; E.a001) (Lü et al., 2023) was isolated, identified, and preserved by our laboratory from pear tree branches infected with fire blight in a pear orchard in Korla City, Xinjiang, and has been determined to be a highly virulent strain. All strains were routinely cultured on Luria-Bertani (LB) broth (5 g/L yeast extract, 10 g/L tryptone, 10 g/L NaCl, pH 7.0) at 30°C. The strain WCH05 was isolated from the unvegetated desert soil (soil type: brown calcareous soil) in Manas County, Xinjiang, China (N: 44°53′48.06″, E: 89°01′54.77″). Sampling was conducted in August 2020. It was identified as belonging to the *Myxococcus fulvus* in our previous work (Dong et al., 2024). Myxobacteria strains were maintained on VY/2 (5 g/L yeast, 1 g/L $CaCl_2{\cdot}2H_2O$, 15 g/L agar, pH 7.2) (Zhang et al., 2013) or Casitone-Tris (CTT) (10 g/L casitone, 1.97 g/L $MgSO_4$, 1.21 g/L Tris–HCl, 0.21 g/L K_2HPO_4, 15 g/L agar, pH 7.6) (Nair et al., 2019) medium at 30°C. TPM (10 mM/L Tris–HCl, 1 mM/L KH_2PO_4, 8 mM/L $MgSO_4$, pH 7.6), LBS (7 g/L soluble starch, 5 g/L yeast extract, 1 g/L casitone, 1 g/L $MgSO_4{\cdot}7H_2O$, pH 7.0).

2.2 Predatory activity against plant pathogens

The predatory capabilities of strain WCH05 were evaluated against above mentioned six bacterial pathogens. Target bacteria suspensions (50 µL, $OD_{600} = 1.0$) were spread onto TPM plates to form prey lawns, followed by drying. A 3 µL droplet of strain WCH05 suspension was then placed 2 mm from the prey's edge, initiating the encounter. Plates were incubated at 30°C for 5 days. Predatory expansion of the strain WCH05 swarm was visually monitored to assess its success in consuming and conquering the prey territory (Berleman et al., 2006).

To quantify the predatory performance, the bacterial lawn was removed using a sterile inoculating loop and suspended in 1 mL of sterile water. The dilution plating method was employed to enumerate the colonies of the six pathogenic bacteria, and the remaining viable cell count was calculated to assess the predatory capacity. It is noteworthy that strain WCH05 is unable to proliferate on LB medium. Images were captured in each case to visually document the predatory process. An SM7 Motic microscope was used for the image. Furthermore, co-cultures of strain WCH05 and *E. amylovora* on TPM plates were visualized using scanning electron microscopy (SEM, SUPRA55 VP, Zeiss).

2.3 Biological assay of strain WCH05 against fire blight

2.3.1 Preparation of the inoculum of myxobacteria and pathogenic bacteria

The strain WCH05 was activated and inoculated into 3 mL of LBS liquid medium at 30°C and 160 rpm for 2 days. It was then inoculated into 200 mL of VY/2 medium at 30°C and 160 rpm for 3 days. The bacterial pellet at the bottom of the bottle was fully dispersed with a pipette to obtain the myxobacteria inoculum.

The *E. amylovora* was activated by picking a single colony into LB liquid medium. It was then cultured in a shaker at 28°C and 160 rpm for 24 h until the OD_{600} of the culture reached 1.0. It was then diluted with sterile water to a concentration of 10^7 cfu·mL^{-1} as the inoculum.

2.3.2 Assay on pear inflorescences

Pear (*Pyrus sinkiangensis*) inflorescences were collected from a pear orchard (Xinjiang Korla City) and inserted into 0.05% NaCl solution to keep them moist and prevent decay. The strain WCH05 bacterial suspension was sprayed onto the pear inflorescences using a hand-held sprayer. After incubating for 24 h in a chamber at 28°C and 70% relative humidity, *E. amylovora* bacterial suspension was sprayed onto the inflorescences. Disease development was observed and recorded at 3- and 5-days post-inoculation. Flower rot rate and efficacy were calculated. 4,000-fold diluted streptomycin (Huabei Pharmaceutical Factory, with an active ingredient content of 72%), strain WCH05, and sterile water were used as positive and negative control treatments, respectively.

$$\text{Flower rot rate}(\%) = \left(\frac{\text{number of diseased flowers}}{\text{total number of flowers}}\right) \times 100\%.$$

$$\text{Efficacy}(\%) = \left(\frac{\text{negative control flower rot rate} - \text{treatment flower rot rate}}{\text{negative control flower rot rate}}\right) \times 100\%.$$

2.3.3 Assay on potted pear seedlings

2.3.3.1 Protective assay

The experiment was conducted in a greenhouse using 2-year-old potted pear seedlings (*P. betulifolia*) as the test material. The strain WCH05 bacterial suspension was sprayed onto the leaves and branches of the seedlings using a hand sprayer until they were completely wet (30 mL/plant). After 24 h, *E. amylovora* suspension was sprayed onto the seedlings. A control treatment of 4,000-fold diluted streptomycin and a control treatment of strain WCH05, and sterile water were also used. Three pots of each treatment were sprayed three times. The inoculated pear seedlings were incubated in a greenhouse at 28–30°C and 70% relative humidity. Disease development was observed daily. The number of diseased branches, the length of diseased branches, the ratio of diseased branch length to the length of the inoculated branches, and the disease severity level were recorded. Disease incidence and disease index were calculated, and efficacy was determined.

2.3.3.2 Therapeutic efficacy

In the therapeutic assay, the inoculation order of myxobacteria and the pathogen was reversed from the protective assay. That means the Ea bacterial suspension was sprayed onto the pear seedlings 24 h after the strain WCH05 bacterial suspension was sprayed. The experimental materials, incubation conditions, and efficacy evaluation were the same as above. The disease scale of fire blight was referred to Li et al. (2021).

2.4 Real-time quantitative PCR

The abundances of strain WCH05 in pear (*P. betulifolia*) leaf and pear (*P. sinkiangensis*) flower tissues were quantified using RT-qPCR. Specific primers for RT-qPCR were designed targeting the *lepA* gene (Accession number: ON313804) of strain WCH05, which encodes leader peptidase, a GTP binding membrane protein (Stackebrandt et al., 2007). The primers, *lepA*-F (5′-GGTGTTC GACTCCTGGTACG-3′) and *lepA*-R (5′-CTGAAGACACCCAG CTCCTG-3′) were designed using Primer3Plus online primer design software.[1] The amplicon size was 141 bp. The *lepA* gene fragment was cloned into T-Vector pMD™19 (Beijing Takara Biomedical Technology Co., Ltd., China) to obtain plasmid pMD19-lepA. Real-time fluorescence quantitative PCR was performed using gradient dilutions of plasmid pMD19-lepA as a template to establish a standard curve ($y = -3.2512x + 41.696$). RT-qPCR was conducted using a Bio-Rad CFX96 Touch Real-Time PCR Detection System (Bio-Rad, Hercules City, CA, United States) and Takara TB Green® Premix DimerEraser™ (Takara, China).

2.5 Scanning electron microscopy

The spatial distribution of myxobacteria strain WCH05 within pear flower and leaf tissues following inoculation was meticulously examined using scanning electron microscopy (SEM). Thin sections of the plant material were visualized under a SUPRA55 VP SEM microscope (Zeiss).

1 https://www.primer3plus.com/index.html

2.6 Secretome of strain WCH05

To understand strain WCH05's predatory prowess, we focused on its potent extracellular secretions. The strain WCH05 cultures (incubation 3 days) were centrifuged (12,000 rpm, 10 min), harvest the sterile supernatant with a 0.22 μm filter. The aforementioned supernatant was subsequently applied to cultures of Ea for a duration of 48 h, and samples were obtained at 12, 24, and 48 h post co-culturing to determine the viable cell count of Ea. Further probing their impact, we constructed a unique arena in a petri dish: a membrane-divided battlefield allowing extracellular metabolite infiltration but no cell contact. Here, the strain WCH05 and Ea are separated by this barrier.

2.7 Assay of strain WCH05 organic extracts

The strain WCH05 was introduced into the VY/2 culture medium, with the addition of 2% macroporous resin XAD-16. The culture was incubated at 30°C and 180 rpm for 4 days. The macroporous resin was collected by filtration with gauze, and twice the volume of methanol was added to the extraction. The crude extract was obtained by rotary evaporation. Then dissolved in dimethyl sulfoxide DSMO: H_2O (v/v 1 : 1). After co-culturing of extract with Ea for 24 h, the number of residual living Ea cells was determined by serial dilution plating. DMSO was used as the control.

2.8 Assay of strain WCH05 extracellular proteins

The strain WCH05 was cultured in VY/2 broth at 30°C for 4 days in a 180-rpm shaker. Following centrifugation at 12,000 rpm, 10 min the supernatant was harvested. Protein in the spent culture was precipitated with ammonium sulfate at various saturations (Li et al., 2019b). Dissolved in PBS buffer (NaCl 8.0 g/L, KCl 0.2 g/L, Na_2HPO_4 1.44 g/L, KH_2PO_4 0.24 g/L, pH 7.2) and cleansed of residual salts via dialysis. Fresh cultured Ea cells (OD_{600} 1.0) were then challenged with this protein arsenal. After 24 h of incubation at 37°C, the battlefield was surveyed. To virtualize the predatory results, transmission electron microscopy (TEM, Hitachi HT7800) was carried out with different scenarios.

2.9 Polysaccharide lyase and lipase activity assay

The polysaccharide lyase activity of the extracellular protein was evaluated using pustulan, chitin, xylan, carboxymethyl cellulose, laminarin, yeast glucan, and β-1,3-glucan as substrates. Enzyme activity was quantified using the 3,5-dinitrosalicylic acid (DNS) method with a commercially available DNS assay kit (Beijing Solarbio Science Technology Co., Ltd., China) following the manufacturer's instructions. Lipase activity was determined using p-nitrophenyl palmitate as a substrate, as described by Zheng et al. (2011). A standard curve was generated using a series of diluted p-nitrophenol solutions. Inactivated crude enzyme solution served as a negative control. Each experiment was performed in triplicate.

2.10 Statistical analysis

Statistical analysis was performed using a standard analysis of variance (ANOVA) followed by Duncan's multiple comparison test to identify significant differences among treatments. A significance level of $p < 0.05$ was considered statistically significant. To assess the variability within the data, standard deviations were calculated for all mean values. The ANOVA analysis was conducted using SPSS Statistics 19.0 software.

3 Results

3.1 *Myxococcus fulvus* WCH05 exhibits active predation against six plant pathogenic bacteria

In this study, we investigated the ability of *Myxococcus fulvus* WCH05 to prey on six plant pathogenic bacteria. We found that strain WCH05 exhibited strong chemotaxis towards all six pathogens, migrating towards and ultimately covering their bacterial lawns (Figure 1A). Co-culture for 5 days resulted in significant reductions in viable cell counts for all pathogens. Ea, for instance, its viable cells declined 5×10^3 times, while the remaining pathogens experienced reductions from 10^9 cfu·mL^{-1} to 10^7 cfu·mL^{-1} (Figure 1B). These findings demonstrate strain WCH05's broad predatory range ability against plant pathogenic bacteria.

Scanning electron microscopy revealed the intricacies of strain WCH05's predation on Ea cells. Upon sensing Ea-derived signals, strain WCH05 cells aggregated and moved in a coordinated manner towards Ea colonies (Figure 2C). They subsequently penetrated the Ea clusters (Figures 2E,F), causing morphological disruption and cell shrinkage/rupture (Figure 2F). Notably, damaged Ea cells were enveloped in a network of filamentous material (Figure 2F), likely representing strain WCH05's extracellular metabolites involved in Ea cell lysis. These results solidify strain WCH05's potential as a promising candidate for biocontrol development against diverse plant pathogens.

3.2 Efficacy of biological control on fire blight

We conducted greenhouse trials to assess the protective and therapeutic efficacy of strain WCH05 against fire blight. The results showed that strain WCH05 was able to significantly reduce the incidence and severity of Ea-induced fire blight.

Observations showed that spraying with the viscous bacterium treatment could reduce the flower rot rate. The effective rate on the 5th day was 76.02%, which was close to the effective rate of agricultural streptomycin (79.79%) ($p = 0.66$) (Figures 3A–D). To further study the effect of the viscous bacterium strain WCH05, we used greenhouse potted pear seedlings as the inoculation material and measured the protective and therapeutic effects of strain WCH05. The results of the protective experiment showed that pre-spraying strain WCH05 on pear seedlings could significantly reduce the incidence and disease index of pear seedlings. The protective effect on the 14th day was 73.68%, which was slightly

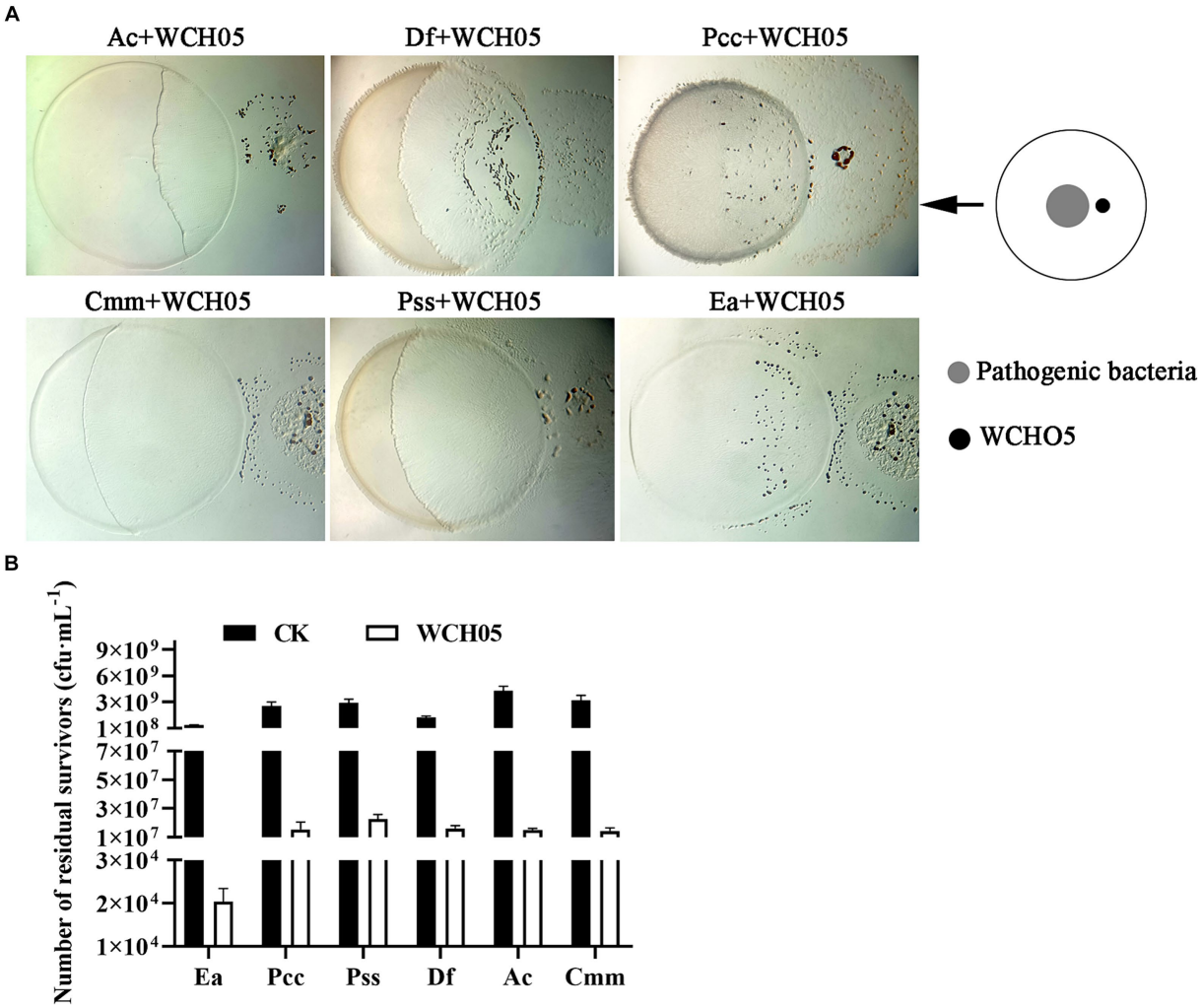

FIGURE 1
Predatory activity of *Myxococcus fulvus* WCH05 against diverse plant pathogenic bacteria. **(A)** Predation assay setup. Top-down schematic visualization illustrating a 50 μL inoculum of plant pathogenic bacteria placed on TPM plates, followed by a 3 μL spot of strain WCH05 suspension positioned 2 mm away. **(B)** Quantification of predation efficiency. Viable cell counts of various plant pathogenic bacteria after exposure to strain WCH05 on TPM plates.

lower than the efficacy of agricultural streptomycin (78.22%) ($p = 0.96$) (Figures 3B,E). The results of the therapeutic experiment showed that spraying strain WCH05 bacterial solution had a significant therapeutic effect on the branch wilt of pear seedlings, but the effective rate decreased. The therapeutic effect on the 14th day was 68.66%, which was slightly lower than the efficacy of agricultural streptomycin (71.57%) ($p = 0.31$) (Figures 3C,F).

SEM observations showed that strain WCH05 was able to colonize pear leaves and flower clusters. The cells were able to form a dense network on the leaf surface and produce extracellular metabolites that could inhibit the growth of pathogenic bacteria (Figure 4A).

Further quantitative detection found that after strain WCH05 was inoculated into pear flower clusters and pear leaves for up to 5 days, the biomass of strain WCH05 in each treatment did not significantly decrease compared with the first day after inoculation (Figures 4B,C). However, on the 14th day after inoculation on pear leaves, the biomass of strain WCH05 in the treatment group that only inoculated strain WCH05 decreased significantly ($p < 0.05$), while the biomass of strain WCH05 in the WCH05 + Ea treatment group did not change significantly (Figure 4C).

3.3 *Myxococcus fulvus* WCH05 predation on Ea relies on direct physical contact

The cell-free fermentation filtrate of strain WCH05 was co-cultured with Ea, and samples were taken at 12 h, 24 h, and 48 h. The number of viable Ea cells was determined by the dilution plating method. The results showed (Figure 5A) that the cell-free fermentation filtrate of strain WCH05 had no inhibitory effect on Ea during co-culture for 12–24 h. There was no significant difference in the number of viable cells remaining compared to the control. At 48 h, the number of viable Ea cells in the cell-free fermentation filtrate was even significantly higher than that in the control ($p < 0.05$) (Figure 5A). This lack of inhibition was mirrored in a separate bacterial membrane isolation experiment, where Ea exposed only to strain WCH05's

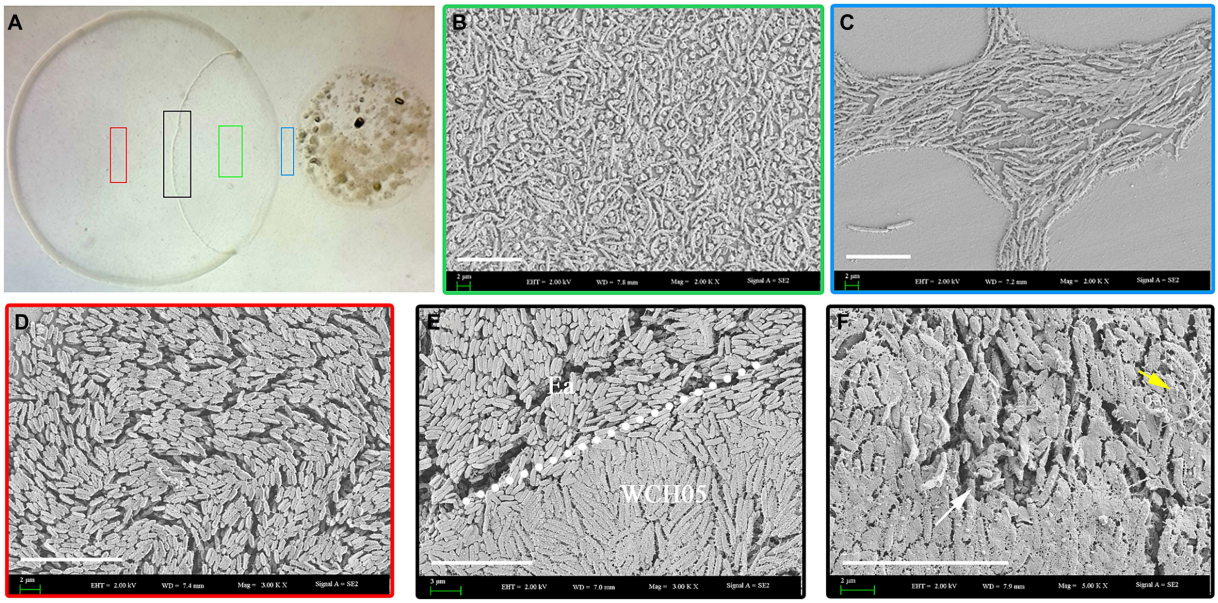

FIGURE 2
Predation of Ea by *Myxococcus fulvus* WCH05 revealed by scanning electron microscopy (SEM). **(A)** SEM image of strain WCH05 predation on Ea bacteria on a TPM plate. Samples were collected from areas marked by green, blue, black and red boxes in subsequent panels. **(B)** Magnified view of the green box in panel **A**, showing strain WCH05 transformed into numerous myxospores after predation. **(C)** Blue box magnification from panel A reveals strain WCH05 exhibiting tropism towards Ea cells. **(D)** Normal Ea cells with intact morphology, densely distributed on the TPM plate. **(E)** Predation interface where strain WCH05, Ea cells, and intact Ea coexist. The dashed white line delineates the boundary between Ea cells and strain WCH05 cells. **(F)** Close-up view of contact between strain WCH05 and Ea. Ea cells exhibit disrupted morphology and fragmentation. Yellow arrows highlight strain WCH05 secreting a reticulate extracellular substance entangling Ea cells. Scale bars represent 10 μm.

secreted metabolites displayed no reduction in viability (Figures 5B,C). Taken together, these results underscore the crucial role of direct bacterial contact in maximizing strain WCH05's predatory activity against Ea.

3.4 Activity of extracellular proteins of strain WCH05

Secondary metabolites extracted from the supernatant fermentation broth of strain WCH05 using a large-pore resin were diluted to different concentrations and co-cultured with Ea cells for 24 h to determine their inhibitory activity. The results revealed that the crude extract exhibited significant inhibitory activity against strain Ea only at a concentration of 200 mg/mL compared to the control. However, the viable cell counts of Ea decreased only slightly from the control 3.5×10^9 cfu·mL^{-1} to 3.0×10^9 cfu·mL^{-1}. Therefore, it is inferred that the secondary metabolites secreted by strain WCH05 cells did not play a major role (Figure 6A).

Furthermore, this study extracted the extracellular crude protein of strain WCH05 and determined its inhibitory activity against Ea. The results showed that the protein component treated with saturated ammonium sulfate at 60–80% led to a 1-log decrease in the viable cell number of Ea, while the protein component obtained by saturated ammonium sulfate at 80–100% led to a 2-log decrease in the viable cell number of Ea. The antibacterial activity of protein fractions precipitated by 20–40% and 40–60% saturated ammonium sulfate exhibited relatively low potency (Figure 6B).

Transmission electron microscopy observations revealed that the cell structure of Ea was loose and irregular, the cell contents were overflowing, and the integrity was destroyed (Figures 6C–H). These results suggest that effective proteins may exist in the components of saturated ammonium sulfate at 60–100%.

Further detection of the changes in the number of viable Ea cells before and after extracellular protein treatment was carried out using the plate gradient dilution method. The results showed that the number of viable cells significantly decreased with the prolongation of time after treatment with the extracellular protein of strain WCH05 (Figure 6I).

3.5 Activities of various enzymes

We investigated the lytic activity of strain WCH05 towards various substrates. The results demonstrated its ability to degrade starch, skimmed milk, sodium carboxymethyl cellulose, tributyrin, and glucan (Figures 7A,E). Notably, chitin proved resistant to degradation (Figure 7F).

To further characterize the substrate spectrum of its lytic extracellular proteins, we conducted additional analyses. The proteins readily hydrolyzed xylan with β-1,4-xylopyranosyl bonds, carboxymethyl cellulose with β-1,4 glycosidic bonds, laminarin with β-1,3–1,6 glycosidic bonds, Yeast glucan with β-1,3–1,6 glycosidic bonds, β-1,3-glucan with β-1,3 glycosidic bonds, and the lipase substrate p-nitrophenyl palmitate (Table 1). Conversely, they exhibited no activity towards pustulan with β-1,6-glycosidic bonds or chitin.

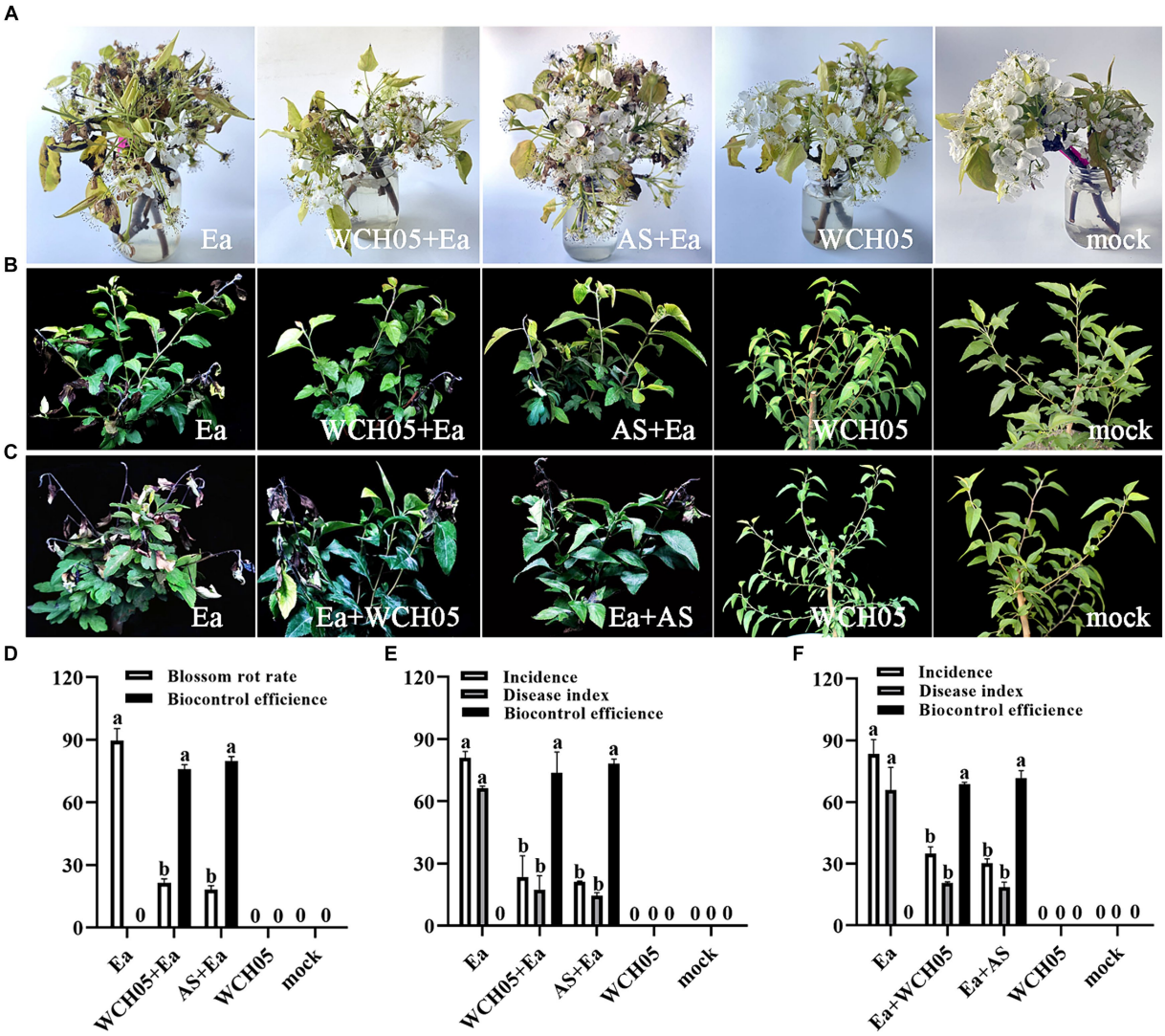

FIGURE 3
Bioassay of *Myxococcus fulvus* WCH05 for controlling pear fire blight. **(A)** *Ex vivo* pear inflorescence assay for strain WCH05 efficacy against pear fire blight. Protective **(B)** and therapeutic **(C)** assays were conducted to evaluate the efficacy of strain WCH05 against fire blight on pear seedlings. **(D)** Biocontrol efficacy of strain WCH05 against pear blossom rot. **(E)** Protective control effect of the strain WCH05 to fire blight of *Pyrus betulifolia*. **(F)** Therapeutic control effect of strain WCH05 to fire blight of *P. betulifolia*. Mock: Control with sterile water. Ea: Inoculated only with *Erwinia amylovora* (Ea). WCH05, Inoculated only with strain WCH05. WCH05 + Ea, Pre-treated with strain WCH05 24 h before Ea inoculation. AS+Ea, Pre-treated with streptomycin 24 h before Ea inoculation. Ea + WCH05, Inoculated with Ea, then treated with strain WCH05 24 h later. Ea + AS, Inoculated with Ea, then treated with streptomycin 24 h later.

These findings suggest that the extracellular proteins of strain WCH05 likely possess lipase, cellulase, and glycoside hydrolase activity specifically targeting β-1,3-glycosidic bonds.

4 Discussion

The invasion of fire blight poses a severe threat to China's fruit industry, particularly imposing significant risks on the pear industry in Xinjiang. In recent years, the role of beneficial microorganisms as biocontrol agents in the biological control of fire blight has received considerable attention and has shown promising results. While numerous microorganisms have been employed for the biological control of fire blight, research, and application of myxobacteria in this context remain largely unexplored. Extensive studies in recent years have highlighted the significant potential of myxobacteria in the biological control of plant diseases. In the field of combating plant pathogenic fungi, *Corallococcus* (Zhou et al., 2019; Li et al., 2019a; Xia et al., 2023), *Myxococcus* (Dong et al., 2021; Wu et al., 2021), *Nannocystis exedens* (Taylor and Draughon, 2001), *Cochliobolus miyabeanus* (Homma, 1984), and other predatory myxobacteria (Taylor and Draughon, 2001; Meliah et al., 2020), have demonstrated effective biocontrol against various plant pathogenic fungi. Notably, myxobacteria exhibit superior predation and antagonistic effects against bacteria, showcasing broad prospects in the biological control of bacterial plant diseases. For instance, *Myxococcus* sp. BS effectively

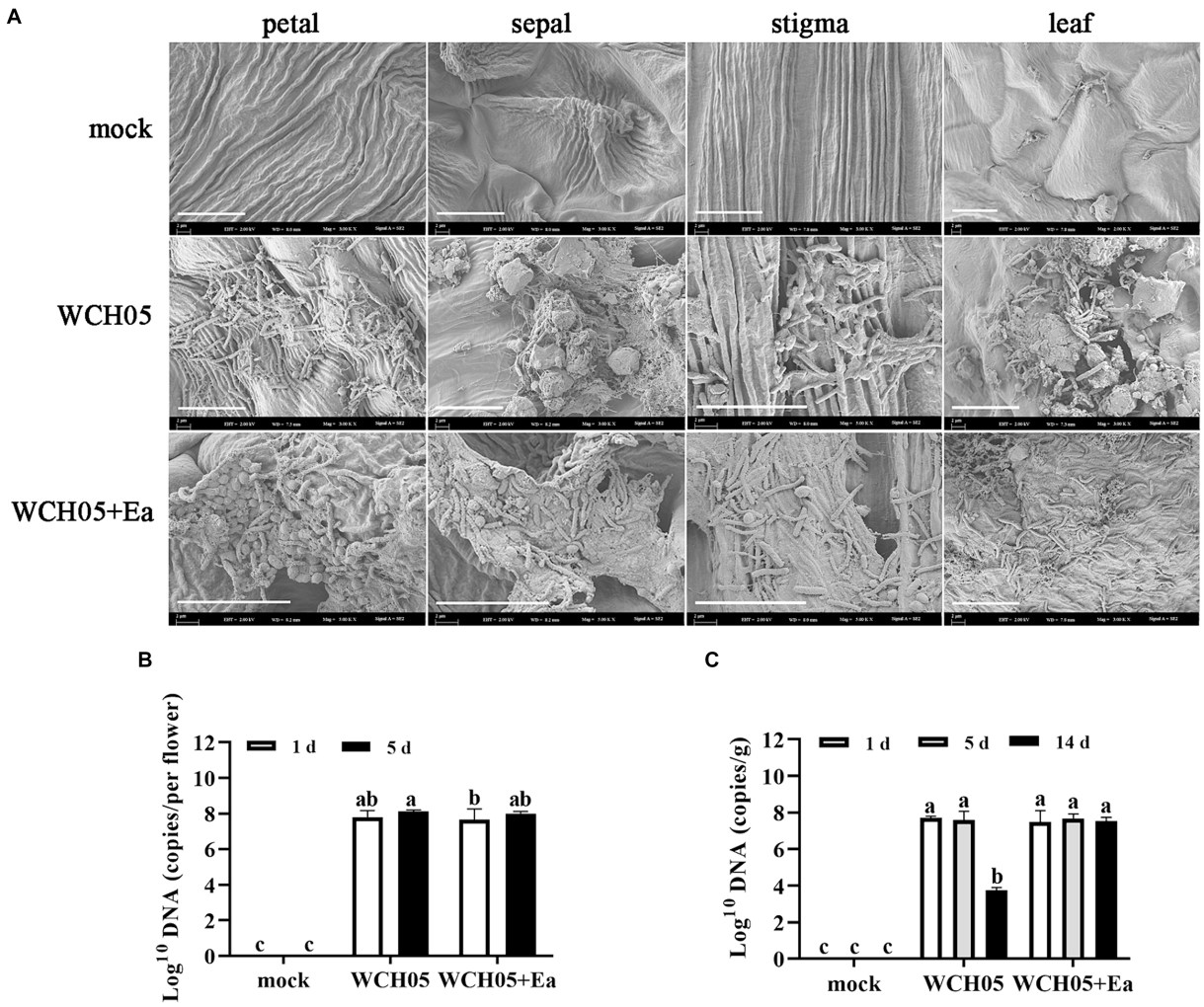

FIGURE 4
Colonization and quantification of *Myxococcus fulvus* WCH05 on pear inflorescence and leaves. **(A)** Scanning electron microscopy (SEM) images of strain WCH05 colonization on pear flower petals, sepals, stigma, and leaf surfaces. Images were taken 5 days after strain WCH05 inoculation on pear inflorescence and 14 days after strain WCH05 inoculation on pear leaves. **(B)** Quantitative analysis of strain WCH05 DNA copy number on pear inflorescence surfaces 1 and 5 days after strain WCH05 inoculation. **(C)** Quantitative analysis of strain WCH05 DNA copy number on pear leaf surfaces 1, 5, and 14 days after strain WCH05 inoculation. Mock, Control with sterile water; WCH05, Inoculated only with strain WCH05; WCH05 + Ea, Pre-treated with strain WCH05 24 h before Ea inoculation. Scale bars represent 10 μm. Error bars represent standard errors of the mean (±SD) from three independent replicates. Statistical comparisons were performed using Duncan's multiple range test ($p < 0.05$). Groups marked with the same letter do not differ significantly, while those with different letters show statistically significant differences.

inhibits the infection of carrot soft rot *Pectobacterium carotovorum* subsp. *carotovorum* on calla lily (Li et al., 2018). *M. xanthus* R31 exhibits significant biocontrol efficacy against tomato bacterial wilt (Dong et al., 2021). However, there are no report on fire blight using the predatory myxobacteria. To our knowledge, this is the first report of fire blight biocontrol using predatory myxobacteria.

This study, through detached flower cluster and potted Chinese pear seedling inoculation experiments, provides the first evidence of the potential application of myxobacteria in the biological control of fire blight. The findings not only offer new microbial resources for the biological control of fire blight but also lay the foundation for further research and development of myxobacterial biocontrol agents in the context of fire blight.

To date, the isolation and application of antagonistic bacteria for the biological control of plant pathogens remain a highly active research area. Researchers have identified numerous antagonistic strains with inhibitory effects against plant pathogens, including *Bacillus*, *Pseudomonas*, *Streptomyces*, *Lysobacter*, and *Trichoderma*, among others (Law et al., 2017; Fira et al., 2018; Sallam et al., 2019; Lin et al., 2021). The biocontrol mechanisms of these strains primarily involve the production of various antibiotic-like substances, toxins, bacteriocins, and proteinaceous antimicrobial substances during their growth metabolism, leading to the inhibition or elimination of plant pathogens. Myxobacteria, through their unique wolf-pack collective behavior and gliding motion, actively prey on bacteria, fungi, and yeast microorganisms (Mohr et al., 2016). However, effective predation by myxobacteria appears to involve direct cell-to-cell contact. Previous observations have demonstrated that myxobacterial strains, such as *Nannocystis exedens*, exert inhibitory effects on *Aspergillus flavus* and *A. parasiticus* by direct contact via the bacterial membrane, lysing the

10.3389/fmicb.2024.1378288

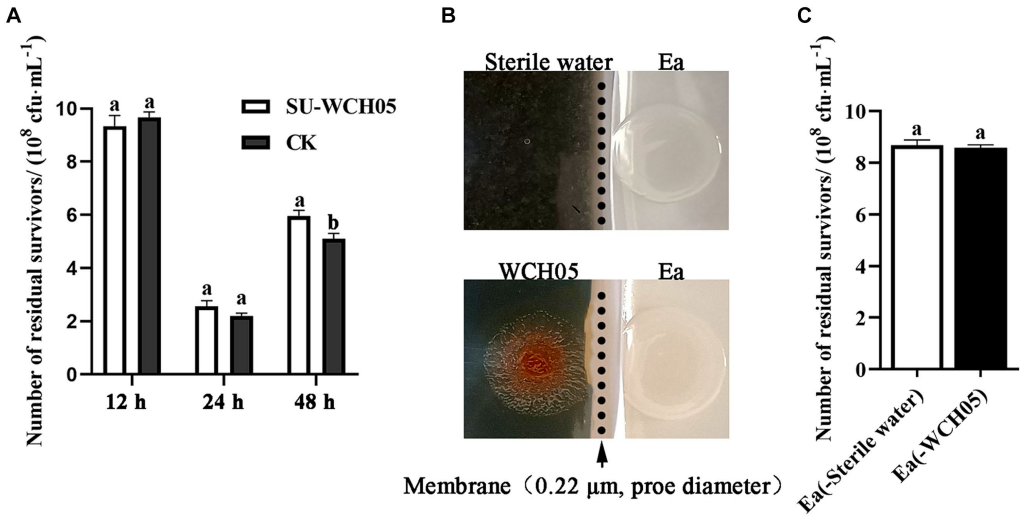

FIGURE 5
Survival of *Erwinia amylovora* (Ea) under different exposures to *Myxococcus fulvus* WCH05. **(A)** Viable cell counts of Ea after treatment with sterile supernatant of strain WCH05 (SU-WCH05). **(B)** Schematic illustration of strain WCH05 separation from VY/2 medium using a 0.22 μm pore diameter membrane (indicated by the arrow and dotted line). **(C)** Viable cell counts of Ea isolated from the culture were obtained after strain WCH05 separation. Error bars represent standard errors of the mean (±SD) from three independent replicates. Statistical comparisons were performed using Duncan's multiple range test ($p < 0.05$). Groups marked with the same letter do not differ significantly, while those with different letters show statistically significant differences.

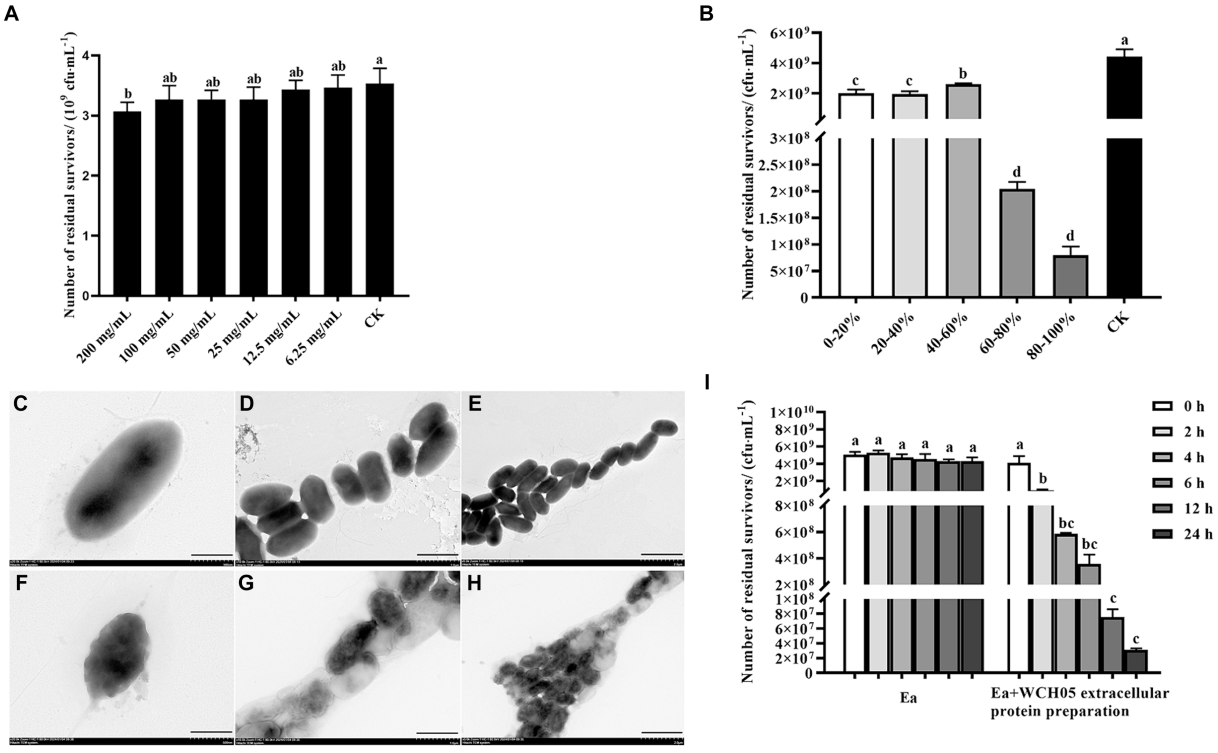

FIGURE 6
Unveiling the multifaceted attack of *Myxococcus fulvus* WCH05 secretions on Ea. **(A)** Dose-Dependent inhibition of Ea activity by strain WCH05 secondary metabolites. **(B)** Targeting Ea with strain WCH05 extracellular proteins: saturation precipitation strategy. **(C–E)** Transmission electron microscopy of Ea cells exposed to PBS control buffer. **(F–H)** Transmission electron microscopy of Ea cells treated with strain WCH05 extracellular proteins. **(I)** Time-Dependent effect of Ea extracellular proteins on strain WCH05 cell viability. Scale bars: 500 nm for panels C and F, 1 μm for panels **(D,G)**, 2 μm for panels **(E,H)**. Error bars represent standard errors of the mean (±SD) from three independent replicates. Statistical comparisons were performed using Duncan's multiple range test ($p < 0.05$). Groups marked with the same letter do not differ significantly, while those with different letters show statistically significant differences.

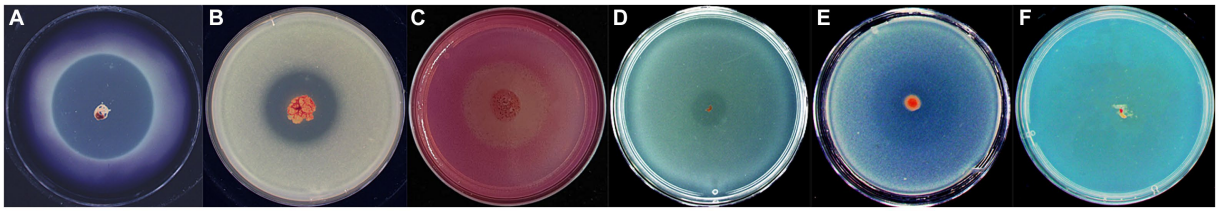

FIGURE 7
Assay of *Myxococcus fulvus* WCH05 degradation of various polymers. Each panel **(A–F)** shows a CTT plate containing 0.5% of a specific polymer: **(A)** starch, **(B)** skimmed milk, **(C)** sodium carboxymethyl cellulose, **(D)** tributyrin, **(E)** β-glucan, and **(F)** colloidal chitin. An exponential culture of strain WCH05 was spotted on each plate and incubated at 30°C for 5 days. The images shown are representative of triplicate experiments.

TABLE 1 Substrate specificity of extracellular crude enzymes of strain WCH05.

Substrate	Bond types	Enzyme activity ($U \cdot mL^{-1}$)
Pustulan	β-1,6-(Glucose)	0
Chitin	β-1, 4-*N*-Acetylaminoglycoside bond	0
p-Nitrophenyl palmitate	Ester linkage	82.24 ± 2.87
Xylan	β-1,4-(Xylopyranosyl)	21.02 ± 0.41
Carboxymethyl cellulose	β-1,4-(Glucose)	8.97 ± 0.39
Laminarin	β-1,3-β-1,6-(Glucose)	6.68 ± 0.61
Yeast glucan	β-1,3-β-1,6-(Glucose)	6.17 ± 0.55
β-1,3-glucan	β-1,3-(Glucose)	6.14 ± 0.10

spores, hyphae, and nuclei of the predatory fungi (Taylor and Draughon, 2001). Similarly, in this study, myxobacterial strain WCH05 exhibited efficient predatory capabilities upon contact with the *E. amylovora* on solid agar plates. However, the activity of Ea cells remained unaffected in co-culture experiments using sterile fermentation filtrate and membrane-separated co-culture experiments, reaffirming that the effective killing of prey cells by myxobacteria depends on direct cell-to-cell contact.

Currently, the predation mechanisms of myxobacteria primarily involve secondary metabolites, lytic enzymes, outer membrane vesicles (OMVs), and others (Berleman and Kirby, 2009; Evans et al., 2012; Mohr et al., 2016). Among these, the secondary metabolites produced by myxobacteria are considered small-molecule weapons capable of penetrating prey cells, halting their metabolism, or causing cell death (Xiao et al., 2011). For instance, the antibiotic TA produced by *M. xanthus* DK1622 exhibits potent antibacterial activity against *E. coli* MG1655 but lacks inhibitory activity against the Gram-positive bacterium *Micrococcus luteus*, suggesting a selective antibacterial effect. Furthermore, the efficacy of TA is influenced by the physiological state of prey cells, with reduced activity observed in metabolically inactive cells (Goldman et al., 2006; Xiao et al., 2011). Corallopyronin produced by *Corallococcus coralloides* exerts antibacterial effects by inhibiting bacterial RNA synthesis, predominantly inhibiting Gram-positive bacteria while having no impact on Gram-negative bacteria, yeast, and molds (Irschik et al., 1985). Recent advancements have elucidated the predatory mechanisms of myxobacteria, particularly highlighting the role of the type III and IV secretion systems. Seef et al. (2021) demonstrated that the integration of A-motility with contact-dependent killing serves as the primary predatory strategy for efficient invasion and consumption of prey colonies on surfaces. This process is mediated at the molecular level by a novel type IV filament-like apparatus (Kil), which facilitates both the immobilization of the predator and the plasmolysis of prey cells. Further investigations by Thiery et al. (2022) into the molecular mechanisms underlying contact-dependent killing in *M. xanthus* focused on the analysis of four protein secretion systems. Their research on the predation dynamics of mutant strains over various timescales revealed that a Tad-like and a type 3-like secretion system (Tad and T3SS) play pivotal roles in prey interaction. Specifically, the Tad-like system is crucial for inducing prey cell death, whereas the T3SS, despite lacking a needle structure, is responsible for initiating prey cell lysis.

In this study, we found that the sterile fermentation filtrate of strain WCH05 showed no inhibitory activity against Ea, although it cannot be ruled out that this may be due to a low content of secondary metabolites. Therefore, we further extracted secondary metabolites from the sterile fermentation filtrate using macroporous resin, The results revealed that secondary metabolites did not play a major role in the antibacterial activity. Consequently, we speculate that the secondary metabolites produced by strain WCH05 may not play a major role in the biological control of fire blight. Similarly, Dong et al. (2021) found that secondary metabolites secreted by *M. xanthus* R31 showed no inhibitory activity against *R. solanacearum*.

Myxobacteria can produce various enzymes, including proteases, amylases, cellulases, lipases, chitinases, xylanases, and others (Munoz-Dorado et al., 2016), forming the material basis for their predation. Previous studies suggested that myxobacteria secrete proteases or peptidases, lysozymes, and other lytic enzymes that may participate in their predation, but direct evidence has been lacking thus far (Ensign and Wolfe, 1966; Berleman and Kirby, 2009). Arend et al. (2021) demonstrated that *M. xanthus* employs different antibacterial mechanisms for predating Gram-positive or Gram-negative bacteria. For Gram-positive bacteria, *M. xanthus* secretes proteins that degrade peptidoglycan layers, leading to cell lysis, while outer membrane vesicles (OMVs) play a crucial role against Gram-negative bacteria.

Transcriptome analysis of myxobacteria predation on *Escherichia coli* revealed the activation of thousands of genes, suggesting that the bacterial cell wall and proteins are primary targets of myxobacterial attack (Livingstone et al., 2018). In the predation process of *Corallococcus* sp. EGB on fungi, the strain disrupts the fungal cell wall by secreting GluM and CcCti1 (Li et al., 2019a,b). These findings suggest that the enzymes secreted by myxobacteria during predation may be related to the composition of the prey cell wall. In this study, we observed that the extracellular enzymes produced by strain WCH05 exhibited lytic activity against Ea. Thus, we speculate that some of the extracellular enzymes, especially peptidases, lipases, glycoside hydrolases, etc., produced by strain WCH05 play a crucial role in its predation on Ea and contribute to the biological control of fire blight. However, the types of lytic enzymes secreted by myxobacteria during predation and their modes of action on prey cells require further investigation through transcriptomic and proteomic analyses. Future studies on the interactions between myxobacteria, prey, and plants will help elucidate the predation mechanisms of myxobacteria.

Myxobacteria are widely distributed in soil (Zhou et al., 2014), exhibiting strong adaptability to soil environments, making them more prone to colonization in soil. This is likely one of the reasons why research and application of myxobacteria in biological control have primarily focused on soil-borne diseases. In contrast to soil environments, the leaf surface represents a more challenging survival environment for microorganisms, with limited available nutrients and significant fluctuations in temperature, humidity, and UV radiation, all of which can profoundly impact microbial survival (Vorholt, 2012). As indigenous soil bacteria, whether myxobacteria can establish residency on the phyllosphere of plants remains unexplored.

SEM observation revealed that after strain WCH05 was inoculated onto pear leaf and inflorescence surfaces, it appeared to be able to adhere to the leaf and inflorescence surfaces via a large number of extracellular metabolites secreted by the cells (Figure 4A). Further detection by real-time quantitative PCR showed that strain WCH05 was able to maintain stable biomass on both pear inflorescence and *P. calleryana* leaf surfaces for the first 5 days after inoculation. This may be due to the broad-spectrum predatory activity of myxobacteria, simple nutrient requirements, and the fact that the epiphytic microorganisms and nutrients on the surface of plant tissues can meet the nutrient requirements of myxobacteria in a short period (Figures 4B,C). By the 14th day, with the gradual depletion of nutrients, coupled with the autolysis characteristics of myxobacteria growth, the biomass of strain WCH05 on the Ea-uninoculated *P.calleryana* leaf surface decreased significantly. However, on the Ea-inoculated *P. calleryana* leaf surface, strain WCH05 was able to continuously obtain nutrients through predation, thus maintaining the stability of the bacterial community (Figure 4C).

Similarly, Eisner et al. (2023) found that the wheat pathogenic fungus *Zymoseptoria tritici* on wheat straw could promote the growth of *M. xanthus*, suggesting potential reasons such as direct predation, release of carbon sources by *Z. tritici*, and alteration of environmental conditions favoring *M. xanthus* growth. However, the specific mechanisms underlying this growth promotion need further investigation for confirmation.

Although this study confirmed the significant biocontrol effect of myxobacteria against fire blight under greenhouse conditions and their ability to colonize the surfaces of pear flowers and leaves, their resistance, colonization efficiency, and control efficacy in the natural field environment need further confirmation in subsequent work. Additionally, some bottleneck issues limit the practical application of myxobacteria in the biological control of fire blight. For instance, the inherent autolytic characteristics of myxobacteria directly constrain the large-scale preparation and shelf life of myxobacterial agents. The tendency of myxobacteria to aggregate during growth in liquid culture severely hampers spray application. Therefore, addressing how to enhance cell dispersion during the growth process, establishing and optimizing myxobacterial fermentation processes, and overcoming these challenges require in-depth investigation in future studies.

5 Conclusion

Fire blight, a devastating bacterial disease of pome fruits, demands innovative control strategies. This study introduces *Myxococcus fulvus* WCH05, a potent biocontrol agent with a multifaceted attack against the fire blight pathogen, *E. amylovora*. The strain WCH05 exhibits broad-spectrum activity against plant pathogens through direct predation via a direct contact method. Additionally, extracellular enzyme proteins secreted by strain WCH05, especially certain peptidases, lipases, and glycoside hydrolases, play significant roles in the predation process. *In vivo* assays demonstrated strain WCH05's efficacy in protecting pear blossoms and young seedlings, rivaling the antibiotic oxytetracycline. This eco-friendly approach offers promising potential for sustainable fire blight management.

However, challenges like large-scale production and application remain. Future research will focus on characterizing strain WCH05's enzymes and optimizing application methods to translate this exciting biocontrol potential into practical solutions. The strain WCH05 represents a significant step towards sustainable fire blight control and highlights the vast potential of microbial resources for safeguarding crop health and promoting environmentally friendly agriculture.

Data availability statement

The original contributions presented in the study are included in the article/supplementary material, further inquiries can be directed to the corresponding authors.

Author contributions

JH: Writing – original draft, Writing – review & editing, Conceptualization, Data curation, Formal analysis, Funding acquisition, Investigation, Project administration, Resources, Supervision. ZD: Data curation, Writing – original draft, Formal analysis, Investigation. WJ: Data curation, Writing – original draft, Formal analysis, Investigation. WL: Data curation, Formal analysis, Writing – original draft. ML: Conceptualization, Funding acquisition, Resources, Supervision, Writing – review & editing. BF: Data curation, Formal analysis, Writing – original draft, Writing – review & editing.

Funding

The author(s) declare financial support was received for the research, authorship, and/or publication of this article. This work was supported by National Key R&D Program of China (grant no. 2021YFD1400200); Natural Science Foundation of Xinjiang Uygur Autonomous Region (2021D01A97); Key Project of Natural Science Foundation of Xinjiang Uygur Autonomous Region (2021D01D12).

Acknowledgments

We would like to thank Zhongli Cui and Zhoukun Li of the College of Life Sciences, Nanjing Agricultural University, for their technical guidance during this study.

Conflict of interest

The authors declare that the research was conducted in the absence of any commercial or financial relationships that could be construed as a potential conflict of interest.

Publisher's note

All claims expressed in this article are solely those of the authors and do not necessarily represent those of their affiliated organizations, or those of the publisher, the editors and the reviewers. Any product that may be evaluated in this article, or claim that may be made by its manufacturer, is not guaranteed or endorsed by the publisher.

References

Arend, K. I., Schmidt, J. J., Bentler, T., Luchtefeld, C., Eggerichs, D., Hexamer, H. M., et al. (2021). *Myxococcus xanthus* predation of gram-positive or gram-negative bacteria is mediated by different bacteriolytic mechanisms. *Appl. Environ. Microbiol.* 87:e02382-20. doi: 10.1128/AEM.02382-20

Berleman, J. E., Chumley, T., Cheung, P., and Kirby, J. R. (2006). Rippling is a predatory behavior in *Myxococcus xanthus*. *J. Bacteriol.* 188, 5888–5895. doi: 10.1128/JB.00559-06

Berleman, J. E., and Kirby, J. R. (2009). Deciphering the hunting strategy of a bacterial wolfpack. *FEMS Microbiol. Rev.* 33, 942–957. doi: 10.1111/j.1574-6976.2009.00185.x

Chen, B., Ma, B., Li, Y., Naibi, Y., Jind, S., and Liu, J. (2023). Preliminary functional analysis of the typeIII secreted effector gene aopW in *Acidovorax citrulli*. *Microbiology China* 50, 1973–1987. doi: 10.13344/j.microbiol.china.220662

Dahm, H., Brzezińska, A. J., Wrótniak-Drzewiecka, W., Golińska, P., Różycki, H., and Rai, M. (2015). Myxobacteria as a potential biocontrol agent effective against pathogenic fungi of economically important forest trees. *Dendrobiology* 74, 13–24. doi: 10.12657/denbio.074.002

Dawid, W. (2000). Biology and global distribution of myxobacteria in soils. *FEMS Microbiol. Rev.* 24, 403–427. doi: 10.1111/j.1574-6976.2000.tb00548.x

Dong, Z., Bai, X., Dou, X., Luo, M., Lü, W., and Han, J. (2024). Screening and biocontrol potential of myxobacteria preying on pathogenic bacteria causing pear fire blight. *J. Fruit Sci.* 41, 143–154. doi: 10.13925/j.cnki.gsxb.20230305

Dong, H., Xu, X., Gao, R., Li, Y., Li, A., Yao, Q., et al. (2021). *Myxococcus xanthus* R31 suppresses tomato bacterial wilt by inhibiting the pathogen *Ralstonia solanacearum* with secreted proteins. *Front. Microbiol.* 12:801091. doi: 10.3389/fmicb.2021.801091

Eisner, S. A., Fiegna, F., McDonald, B. A., and Velicer, G. J. (2023). Bacterial predation of a fungal wheat pathogen: prelude to experimental evolution of enhanced biocontrol agents. *Plant Pathol.* 72, 1059–1068. doi: 10.1111/ppa.13716

Ensign, J. C., and Wolfe, R. S. (1966). Characterization of a small proteolytic enzyme which lyses bacterial cell walls. *J. Bacteriol.* 91, 524–534. doi: 10.1128/jb.91.2.524-534.1966

Evans, A. G. L., Davey, H. M., Cookson, A., Currinn, H., Cooke-Fox, G., Stanczyk, P. J., et al. (2012). Predatory activity of *Myxococcus xanthus* outer-membrane vesicles and properties of their hydrolase cargo. *Microbiology (Reading)* 158, 2742–2752. doi: 10.1099/mic.0.060343-0

Fira, D., Dimkic, I., Beric, T., Lozo, J., and Stankovic, S. (2018). Biological control of plant pathogens by Bacillus species. *J. Biotechnol.* 285, 44–55. doi: 10.1016/j.jbiotec.2018.07.044

Goldman, B. S., Nierman, W. C., Kaiser, D., Slater, S. C., Durkin, A. S., Eisen, J. A., et al. (2006). Evolution of sensory complexity recorded in a myxobacterial genome. *Proc. Natl. Acad. Sci. USA* 103, 15200–15205. doi: 10.1073/pnas.0607335103

Homma, Y. (1984). Perforation and lysis of hyphae of Rhizoctonia solani and conidia of Cochliobolus miyabeanus by soil myxobacteria. *Phytopathology* 74:1234. doi: 10.1094/Phyto-74-1234

Huang, W., Sheng, Q., Luo, M., Ma, D. Y., and Zhang, C. Z. (2022). Occurrence status of fire blight on Korla fragrant pear in Xinjiang and the control proposals. *Plant Protect. Sinica* 48:7. doi: 10.16688/j.zwbh.2022407

Irschik, H., Jansen, R., Hofle, G., Gerth, K., and Reichenbach, H. (1985). The corallopyronins, new inhibitors of bacterial RNA synthesis from Myxobacteria. *J. Antibiot. (Tokyo)* 38, 145–152. doi: 10.7164/antibiotics.38.145

Johnson, K. B., and Stockwell, V. O. (1998). Management of fire blight: a case study in microbial ecology. *Annu. Rev. Phytopathol.* 36, 227–248. doi: 10.1146/annurev.phyto.36.1.227

Law, J. W.-F., Ser, H.-L., Khan, T. M., Chuah, L.-H., Pusparajah, P., Chan, K.-G., et al. (2017). The potential of Streptomyces as biocontrol agents against the Rice blast fungus, Magnaporthe oryzae (Pyricularia oryzae). *Front. Microbiol.* 8:3. doi: 10.3389/fmicb.2017.00003

Li, Y., Li, H., Ye, L., Zhou, J., and Luo, M. (2021). Biological characteristics of *Pseudomonas syringae* pv. Syringae causing shoot dieback disease on apple and screening of bactericides. *Chinese Agricultural Science Bulletin* 37, 112–119. doi: 10.11924/j.issn.1000-6850.casb2020-0471

Li, Z., Wang, T., Luo, X., Li, X., Xia, C., Zhao, Y., et al. (2018). Biocontrol potential of Myxococcus sp. strain BS against bacterial soft rot of calla lily caused by *Pectobacterium carotovorum*. *Biol. Control* 126, 36–44. doi: 10.1016/j.biocontrol.2018.07.004

Li, Z., Xia, C., Wang, Y., Li, X., Qiao, Y., Li, C., et al. (2019a). Identification of an endo-chitinase from Corallococcus sp. EGB and evaluation of its antifungal properties. *Int. J. Biol. Macromol.* 132, 1235–1243. doi: 10.1016/j.ijbiomac.2019.04.056

Li, Z., Ye, X., Chen, P., Ji, K., Zhou, J., Wang, F., et al. (2017). Antifungal potential of Corallococcus sp. strain EGB against plant pathogenic fungi. *Biol. Control* 110, 10–17. doi: 10.1016/j.biocontrol.2017.04.001

Li, Z., Ye, X., Liu, M., Xia, C., Zhang, L., Luo, X., et al. (2019b). A novel outer membrane β-1,6-glucanase is deployed in the predation of fungi by myxobacteria. *ISME J.* 13, 2223–2235. doi: 10.1038/s41396-019-0424-x

Lin, L., Xu, K., Shen, D., Chou, S. H., Gomelsky, M., and Qian, G. (2021). Antifungal weapons of Lysobacter, a mighty biocontrol agent. *Environ. Microbiol.* 23, 5704–5715. doi: 10.1111/1462-2920.15674

Livingstone, P. G., Millard, A. D., Swain, M. T., and Whitworth, D. E. (2018). Transcriptional changes when *Myxococcus xanthus* preys on *Escherichia coli* suggest myxobacterial predators are constitutively toxic but regulate their feeding. *Microb. Genom.* 4:e000152. doi: 10.1099/mgen.0.000152

Lü, T., Xu, L., Xi, H., Han, J., and Luo, M. (2023). Characterization of the infectious colonization and expansion with GFP tagged strain of *Erwinia amylovora* in Kuerlexiangli pear (Pyrus sinkiangensis Yu) shoots. *J. Fruit Sci.* 40, 1692–1702. doi: 10.13925/j.cnki.gsxb.20230056

Lv, T., He, X., Luo, M., Han, J., Bao, H., and Huang, W. (2022). Optimization of culture medium and flask fermentation conditions for *Bacillus velezensis* FX1 against *Erwinia amylovora*. *Chin. J. Biol. Cont.* 38, 1553–1565. doi: 10.16409/j.cnki.2095-039x.2022.08.002

Malnoy, M., Martens, S., Norelli, J. L., Barny, M. A., Sundin, G. W., Smits, T. H., et al. (2012). Fire blight: applied genomic insights of the pathogen and host. *Annu. Rev. Phytopathol.* 50, 475–494. doi: 10.1146/annurev-phyto-081211-172931

Meliah, S., Kusumawati, D. I., and Ilyas, M. (2020). Preliminary study of myxobacteria as biocontrol agents for Panama disease pathogen, tropical race 4 fusarium odoratissimum. *IOP Conf. Ser. Earth Environ. Sci.* 457:012060. doi: 10.1088/1755-1315/457/1/012060

Mikiciński, A., Puławska, J., Molzhigitova, A., and Sobiczewski, P. (2019). Bacterial species recognized for the first time for its biocontrol activity against fire blight (*Erwinia amylovora*). *Eur. J. Plant Pathol.* 156, 257–272. doi: 10.1007/s10658-019-01885-x

Mohr, K. I., Stechling, M., Wink, J., Wilharm, E., and Stadler, M. (2016). Comparison of myxobacterial diversity and evaluation of isolation success in two niches: Kiritimati Island and German compost. *Microbiology* 5, 268–278. doi: 10.1002/mbo3.325

Momol, M. T., Momol, E. A., and Dankers, W. (2000). A severe outbreak of fire blight in Woody ornamental Rosaceae plants in North Florida and South Georgia. *Plant Dis.* 84:1153. doi: 10.1094/PDIS.2000.84.10.1153C

Munoz-Dorado, J., Marcos-Torres, F. J., Garcia-Bravo, E., Moraleda-Munoz, A., and Perez, J. (2016). Myxobacteria: moving, killing, feeding, and surviving together. *Front. Microbiol.* 7:781. doi: 10.3389/fmicb.2016.00781

Nair, R. R., Vasse, M., Wielgoss, S., Sun, L., Yu, Y. N., and Velicer, G. J. (2019). Bacterial predator-prey coevolution accelerates genome evolution and selects on virulence-associated prey defences. *Nat. Commun.* 10:4301. doi: 10.1038/s41467-019-12140-6

Pieterse, C. M., Zamioudis, C., Berendsen, R. L., Weller, D. M., Van Wees, S. C., and Bakker, P. A. (2014). Induced systemic resistance by beneficial microbes. *Annu. Rev. Phytopathol.* 52, 347–375. doi: 10.1146/annurev-phyto-082712-102340

Russo, N. L., Burr, T. J., Breth, D. I., and Aldwinckle, H. S. (2008). Isolation of streptomycin-resistant isolates of *Erwinia amylovora* in New York. *Plant Dis.* 92, 714–718. doi: 10.1094/PDIS-92-5-0714

Sallam, N. M. A., Eraky, A. M. I., and Sallam, A. (2019). Effect of Trichoderma spp. on fusarium wilt disease of tomato. *Mol. Biol. Rep.* 46, 4463–4470. doi: 10.1007/s11033-019-04901-9

Seef, S., Herrou, J., de Boissier, P., My, L., Brasseur, G., Robert, D., et al. (2021). A tad-like apparatus is required for contact-dependent prey killing in predatory social bacteria. *eLife* 10:e72409. doi: 10.7554/eLife.72409

Shen, E., Wang, X., Lu, Z., Zhou, F., Ma, W., Cui, Z., et al. (2023). Overexpression of a beta-1,6-glucanase gene GluM in transgenic rice confers high resistance to rice blast, sheath blight and false smut. *Pest Manag. Sci.* 79, 2152–2162. doi: 10.1002/ps.7394

Stackebrandt, E., Pauker, O., Steiner, U., Schumann, P., Straubler, B., Heibei, S., et al. (2007). Taxonomic characterization of members of the genus Corallococcus: molecular divergence versus phenotypic coherency. *Syst. Appl. Microbiol.* 30, 109–118. doi: 10.1016/j.syapm.2006.03.002

Sun, W., Gong, P., Zhao, Y., Ming, L., Zeng, Q., and Liu, F. (2023). Current situation of fire blight in China. *Phytopathology* 113, 2143–2151. doi: 10.1094/PHYTO-05-23-0170-RVW

Tancos, K. A., Villani, S., Kuehne, S., Borejsza-Wysocka, E., Breth, D., Carol, J., et al. (2016). Prevalence of streptomycin-resistant *Erwinia amylovora* in New York apple orchards. *Plant Dis.* 100, 802–809. doi: 10.1094/PDIS-09-15-0960-RE

Taylor, W. J., and Draughon, F. A. (2001). *Nannocystis exedens*: a potential biocompetitive agent against aspergillus flavus and aspergillus parasiticus. *J. Food Prot.* 64, 1030–1034. doi: 10.4315/0362-028x-64.7.1030

Temple, T. N., Stockwell, V. O., Loper, J. E., and Johnson, K. B. (2004). Bioavailability of Iron to *Pseudomonas fluorescens* strain A506 on flowers of pear and apple. *Phytopathology* 94, 1286–1294. doi: 10.1094/PHYTO.2004.94.12.1286

Thiery, S., and Kaimer, C. (2020). The predation strategy of *Myxococcus xanthus*. *Front. Microbiol.* 11:2. doi: 10.3389/fmicb.2020.00002

Thiery, S., Turowski, P., Berleman, J. E., and Kaimer, C. (2022). The predatory soil bacterium *Myxococcus xanthus* combines a tad- and an atypical type 3-like protein secretion system to kill bacterial cells. *Cell Rep.* 40:111340. doi: 10.1016/j.celrep.2022.111340

Van Wees, S. C., Pieterse, C. M., Trijssenaar, A., Van't Westende, Y. A., Hartog, F., and Van Loon, L. C. (1997). Differential induction of systemic resistance in Arabidopsis by biocontrol bacteria. *Mol. Plant-Microbe Interact.* 10, 716–724. doi: 10.1094/MPMI.1997.10.6.716

Vorholt, J. A. (2012). Microbial life in the phyllosphere. *Nat. Rev. Microbiol.* 10, 828–840. doi: 10.1038/nrmicro2910

Wu, Z., Cui, H., Sun, Z., and Liu, H. (2021). Biocontrol mechanism of *Myxococcus xanthus* B25-I-1 against *Phytophthora infestans*. *Pestic. Biochem. Physiol.* 175:104832. doi: 10.1016/j.pestbp.2021.104832

Xia, C., Zhao, Y., Zhang, L., Li, X., Cheng, Y., Wang, D., et al. (2023). Myxobacteria restrain Phytophthora invasion by scavenging thiamine in soybean rhizosphere via outer membrane vesicle-secreted thiaminase I. *Nat. Commun.* 14:5646. doi: 10.1038/s41467-023-41247-0

Xiao, Y., Wei, X., Ebright, R., and Wall, D. (2011). Antibiotic production by myxobacteria plays a role in predation. *J. Bacteriol.* 193, 4626–4633. doi: 10.1128/JB.05052-11

Xu, L., Gulizzier, M., Han, J., Huang, W., and Luo, M. (2021). Screening of endophytic antagonistic bacteria from 'kuerlexiangli' pear and their biocontrol potential against fire blight disease. *Acta Botan. Boreali-Occiden. Sin.* 41, 132–141. doi: 10.7606/j.issn.1000-4025.2021.01.0132

Yun, S. C. (2014). Selection and a 3-year Field trial of *Sorangium cellulosum* KYC 3262 against anthracnose in hot pepper. *Plant Pathol. J.* 30, 279–287. doi: 10.5423/PPJ.OA.01.2014.0002

Zhang, X., Yao, Q., Cai, Z., Xie, X., and Zhu, H. (2013). Isolation and identification of myxobacteria from saline-alkaline soils in Xinjiang, China. *PLoS One* 8:e70466. doi: 10.1371/journal.pone.0070466

Zheng, X., Chu, X., Zhang, W., Wu, N., and Fan, Y. (2011). A novel cold-adapted lipase from Acinetobacter sp. XMZ-26: gene cloning and characterisation. *Appl. Microbiol. Biotechnol.* 90, 971–980. doi: 10.1007/s00253-011-3154-1

Zhou, J., Chen, J., Li, Z., Ye, X., Dong, W., Jiang, M., et al. (2019). Enzymatic properties of a multi-specific beta-(1,3)-glucanase from Corallococcus sp. EGB and its potential antifungal applications. *Protein Expr. Purif.* 164:105481. doi: 10.1016/j.pep.2019.105481

Zhou, X. W., Li, S. G., Li, W., Jiang, D. M., Han, K., Wu, Z. H., et al. (2014). Myxobacterial community is a predominant and highly diverse bacterial group in soil niches. *Environ. Microbiol. Rep.* 6, 45–56. doi: 10.1111/1758-2229.12107

Frontiers in Microbiology

Explores the habitable world and the potential of microbial life

The largest and most cited microbiology journal which advances our understanding of the role microbes play in addressing global challenges such as healthcare, food security, and climate change.

Discover the latest Research Topics

See more →

Frontiers

Avenue du Tribunal-Fédéral 34
1005 Lausanne, Switzerland
frontiersin.org

Contact us

+41 (0)21 510 17 00
frontiersin.org/about/contact